A STUDY OF THE STRENGTH AND BEHAVIOUR OF CONCRETE BLOCKWORK MASONRY UNDER ECCENTRIC LOADS WITH SPECIAL REFERENCE TO REINFORCED COLUMNS

by

NART M. NAGHOJ

A thesis submitted for the degree of

Doctor of Philosophy

Department of Civil Engineering and Building Science

University of Edinburgh

July 1994



DECLARATION

The author wishes to declare that this thesis has been composed by himself and that all the work and the results included have been carried out by himself under the supervision of Dr. D.R. Fairbairn and Dr. R. Royles, and has not been submitted to any other University or Institution.

Edinburgh, July 1994

Nart Naghoj

ACKNOWLEDGEMENT

The author wishes to thank Dr. D.R. Fairbairn for his kindness, supervision, encouragement and assistance and to Dr. R. Royles for his supervision and assistance in the final stages of this work. The author wishes to express his gratitude to Professor and Head of the Engineering Planning Unit J.M. Rotter and to Professor and Head of the Department of Civil Engineering M.C. Forde for their attention and continuous support.

Thanks are also due to Professor A.W. Hendry for his valuable advice during the preparation of the research program, to Dr. S.R. Davies and to Dr. F.M. Khalaf for his continuous assistance. The author would also like to express his gratitude to the following people: Mrs. B. McWilliam, Mrs. G. Temple for her great patience in typing the entire manuscript, Mrs. C. Corsie, Mr. J. Hutcheson, Mr. N. McWilliam and the department technical staff.

Finally, many thanks to my friends Khaled and Nabeel for their encouragement and support.

ABSTRACT

This thesis presents a comprehensive experimental and theoretical investigation carried out to study the behaviour and to determine the ultimate compressive strength, f'_m, of blockwork masonry prisms. The enhancing effect of strain gradient on f'_m caused by eccentricity was studied in some detail.

The thesis also presents the results of an experimental and theoretical investigation carried out to study the strength and behaviour of reinforced blockwork masonry built with different percentages of vertical reinforcement and subjected to various eccentricities in order to establish the load-moment strength interaction diagrams.

On the basis of the test results gathered from the experimental part of this study and the basic assumptions used in the design of reinforced concrete columns using ultimate limit state principles, a theoretical method was suggested to predict the ultimate strength of reinforced blockwork masonry columns subjected to axial and eccentric loads.

CONTENTS

			Page
Acknowledgements			iii
Abstract			iv
Contents			v
List of Tables			x
List of Figures			xiii
Notation			xxxx
Chapter	1	Introduction	1
Chapter	2	Literature Review	4
	2.2	Masonry Columns	4
	2.2.1	Brickwork Masonry Columns	4
	2.2.2	Blockwork Masonry Columns	14
	2.2.3	Enhancement of Compressive Strength, f'_m, for Eccentrically Loaded Blockwork Prisms	29
	2.2.4	Summary and conclusions	33
Chapter	3	Material Mechanical Properties	40
	3.1	Introduction	40
	3.2	Concrete Block	40
	3.3	Mortar	42
	3.4	Concrete Infill	43
	3.5	Steel Reinforcement	44
	3.6	Single Blocks	44
	3.7	Three Block Prisms	45
	3.8	Summary and Discussion of Test Results	47
Chapter	4	Concentrically & Eccentrically Loaded Blockwork Masonry Prisms	62

4.1	Introduction	62
4.2	Experimental Programme	62
4.2	Experimental Programme	62
4.2.1	Specimen Construction	62
4.2.2	Strain Measurements	63
4.2.3	Capping	64
4.2.4	Testing Procedure	64
4.3	Theoretical Programme	66
4.3.1	Introduction	66
4.3.2	Three Dimensional Finite Element Model	66
4.4	Discussion of Experimental Results	69
4.4.1	Modes of Failure	69
4.4.1.1	Concentrically Loaded Prisms	69
4.4.1.2	Eccentrically Loaded Prisms with an Eccentricity of t/6	70
4.4.1.3	Eccentrically Loaded Prisms with an Eccentricity of t/3	71
4.4.2	Experimental Results	71
4.5	Discussion of Theoretical Results	76
4.5.1	General	76
4.5.2	Analysis of Axially Loaded Prisms	76
4.5.2.1	Axially Loaded Unfilled Full-Block Prism	77
4.5.2.2	Axially Loaded Filled Full-Block Prism	78
4.5.2.3	Axially Loaded Unfilled Half-Block Prism	81
4.5.2.4	Axially Loaded Filled Half-Block Prism	83
4.5.3	Analysis of Eccentrically Loaded Prisms	86

	4.5.3.1	Unfilled Full-Block Prism Compressed Under Eccentric Load at t/6	86
	4.5.3.2	Filled Full-Block Prism Compressed Under Eccentric Load at t/6	88
	4.5.3.3	Unfilled Half-Block Prism Compressed Under Eccentric Load at t/6	91
	4.5.3.4	Filled Half-Block Prism Compressed Under Eccentric Load at t/6	93
	4.5.3.5	Unfilled Full-Block Prism Compressed Under Eccentric Load at t/3	95
	4.5.3.6	Filled Full-Block Prism Compressed Under Eccentric Load at t/3	97
	4.5.3.7	Unfilled Half-Block Prism Compressed Under Eccentric Load at t/3	99
	4.5.3.8	Filled Half-Block Prism Compressed Under Eccentric Load at t/3	101
	4.6	A Brief Discussion on the Effect of the Eccentricity on Enhancing the Compressive strength, f'_m, of Blockwork prisms	103
	4.7	Conclusions	104
Chapter	5	Concentrically and Eccentrically Loaded Reinforced Blockwork Masonry Columns	190
	5.1	Introduction	190
	5.2	Experimental Study	191
	5.2.1	Programme Variables	191
	5.2.2	Geometry of Columns	193
	5.2.3	Test Procedure and Equipment	193

	5.2.4	Building Test Specimens	194
	5.2.5	Measurements of Strains and Deflections	198
	5.3	Theoretical Analysis	200
	5.3.1	Introduction	200
	5.3.2	Three Dimensional Non-linear Finite Element Model	200
	5.3.3	Two Dimensional Non-linear Finite Element Model	201
	5.4	Applying Reinforced Concrete N/M Interaction Curves to Blockwork Masonry Columns Using Different Stress Blocks	201
Chapter	6	Comparison of Experimental and Theoretical Results	223
	6.1	Introduction	223
	6.2	Axially Loaded Blockwork Columns	223
	6.2.1	Modes of Failure	223
	6.2.1.1	Unreinforced Columns	223
	6.2.1.2	Reinforced Columns	224
	6.2.3	Modulus of Elasticity of Blockwork Masonry Columns	224
	6.2.4	Column Strength	230
	6.2.5	Strain Measurements	231
	6.3	Eccentrically Loaded Blockwork Columns with an Eccentricity of t/6	233
	6.3.1	Modes of Failure	233
	6.3.1.1	Unreinforced Columns	233
	6.3.1.2	Reinforced Columns	233

	6.3.2	Ultimate Strain	234
	6.3.3	Strain Distribution	234
	6.3.4	Load-Deflection Relationship (e = t/6)	235
	6.4	Blockwork Columns Loaded with an e > t/6 Eccentricity	235
	6.4.1	Modes of Failure	235
	6.4.2	Strain Distribution	236
	6.4.3	Column Lateral Deflections for e > t/6	236
	6.4.4	Column Cracking Loads	237
	6.5	Load-Moment Interaction Diagrams	238
	6.5.1	Introduction	238
	6.5.2	Experimental Results and Comparison with Theoretical Load/Moment Curves	238
	6.6	General Discussion	241
	6.7	Conclusions	244
Chapter	7	General Summary, Conclusions and Suggestions for Further Work	351
	7.1	General Summary	351
	7.2	Conclusions	352
	7.3	Suggestions for Further Work	355
References			357
Appendix A			364
Appendix B			390
Appendix C			393
Appendix D			396

LIST OF TABLES

The tables for a chapter are arranged in sequence at the end of a chapter.

Chapter 3

Table 3.1 Dimensions of typical concrete block.

Table 3.2 Sieve analysis of mortar sand.

Table 3.3 Sieve analysis of concrete sand.

Table 3.4 Sieve analysis of 10 mm single size crushed aggregate.

Table 3.5 Mechanical properties of steel reinforcement.

Table 3.6 Compressive strength of single block compressed normal to bed face.

Table 3.7 Compressive strength of 3-course high prisms.

Table 3.8 Mechanical properties of materials.

Chapter 4

Table 4.1 The material properties used in developing the non-linear three dimensional finite element model.

Table 4.2 Compressive strength of 4-course high full-block prisms.

Table 4.3 Compressive strength of 4-course high half-block prisms.

Chapter 5

Table 5.1 The material properties for steel reinforcement used in developing the non-linear two and three dimensional finite element models.

Table 5.2 The material properties used in developing the non-linear two dimensional finite element model.

Table 5.3 Values of the parabolic stress factors for different $\varepsilon_u/\varepsilon_m$.

Chapter 6

Table 6.1 Test results for concentrically loaded blockwork masonry columns.

Table 6.2 Ultimate axial load of blockwork masonry columns.

Table 6.3 Test results for eccentrically loaded columns with an eccentricity of t/6.

Table 6.4 Test results for eccentrically loaded columns (the case of E_1 eccentricity).

Table 6.5 Test results for eccentrically loaded columns (the case of E_2 eccentricity).

Table 6.6 Load-crack width experimental results for the FCE_1 (No Steel) column.

Table 6.7 Load-crack width experimental results for the FCE_1 (10 mm) column.

Table 6.8 Load-crack width experimental results for the FCE_1 (20 mm) column.

Table 6.9 Load-crack width experimental results for the HCE_1 (No Steel) column.

Table 6.10 Load-crack width experimental results for the HCE_1 (8 mm) column.

Table 6.11 Load-crack width experimental results for the HCE_1 (20 mm) column.

Table 6.12 Load-crack width experimental results for the FCE_2 (No Steel) column.

Table 6.13 Load-crack width experimental results for the FCE_2 (10 mm) column.

Table 6.14 Load-crack width experimental results for the FCE_2 (20 mm) column.

Table 6.15 Load-crack width experimental results for the HCE_2 (No Steel) column.

Table 6.16 Load-crack width experimental results for the HCE_2 (8 mm) column.

Table 6.17 Load-crack width experimental results for the HCE_2 (20 mm) column.

Table 6.18 Stress results of the FEA study for concentrically loaded full-block masonry columns.

Table 6.19 Stress results of the FEA study for concentrically loaded half-block masonry columns.

Table 6.20 Compressive strength of concentrically and t/6 eccentrically loaded full and half-block masonry columns.

Appendix C

Table C.1 Designation of the blockwork columns

LIST OF FIGURES

The figures for a chapter are arranged in sequence at the end of a chapter.

Chapter 2

Fig. 2.1 Typical details of columns tested by Withey (13).

Fig. 2.2 Typical pier in Davey and Thomas (14) tests.

Fig. 2.3 Typical test setup for columns tested by Eltraify (19).

Fig. 2.4 Typical interaction diagrams obtained by Eltraify(19) for a typical rectangular section.

Fig. 2.5 Typical details of columns tested by Khalaf (26).

Chapter 3

Fig. 3.1 Three unfilled half-blocks separated and capped with 1 - 2 mm dental plaster joints.

Fig. 3.2 Three steel moulded mortar cubes separated and capped with 1 - 2 mm dental plaster joints.

Fig. 3.3 Compressive stress-strain curves for block material.

Fig. 3.4 Lateral strain-vertical strain curves for block material.

Fig. 3.5 Compressive stress-strain curves for concrete.

Fig. 3.6 Lateral strain-vertical strain curve for concrete.

Fig. 3.7 Compressive stress-strain curves for mortar.

Fig. 3.8 Lateral strain-vertical strain curves for mortar.

Chapter 4

Fig. 4.1 Test setup for eccentrically loaded prisms.

Fig. 4.2 Typical FEA mesh used to model the concentrically loaded prisms.

Fig. 4.3 Typical FEA mesh used to model the eccentrically loaded prisms.

Fig. 4.4 Typical mode of failure for concentrically loaded unfilled full-block prism.

Fig. 4.5 Typical mode of failure for concentrically loaded filled half-block prism.

Fig. 4.6 Typical mode of failure for concentrically loaded unfilled half-block prism.

Fig. 4.7 Typical mode of failure for concentrically loaded filled half-block prism.

Fig. 4.8 Typical mode of failure for eccentrically loaded filled full-block prism compressed at t/6.

Fig. 4.9 Typical mode of failure for eccentrically loaded unfilled half-block prism compressed at t/6.

Fig. 4.10 Typical mode of failure for eccentrically loaded filled half-block prism compressed at t/6.

Fig. 4.11 Typical mode of failure for eccentrically loaded filled full-block prism compressed at t/3.

Fig. 4.12 Typical mode of failure for eccentrically loaded unfilled half-block prism compressed at t/3.

Fig. 4.13 Typical mode of failure for eccentrically loaded filled half-block prism compressed at t/3.

Fig. 4.14 Stress-strain curves for unfilled full-block axially loaded prism.

Fig. 4.15 Stress-strain curves for filled full-block axially loaded prism.

Fig. 4.16 Stress-strain curves for unfilled half-block axially loaded prism.

Fig. 4.17 Stress-strain curves for filled half-block axially loaded prism.

Fig. 4.18 Load-strain curves for unfilled full-block prism compressed under eccentric load at e = t/6.

Fig. 4.19 Load-strain curves for filled full-block prism compressed under eccentric load at e = t/6.

Fig. 4.20 Load-strain curves for unfilled half-block prism compressed under eccentric load at e = t/6.

Fig. 4.21 Load-strain curves for filled half-block prism compressed under eccentric load at e = t/6.

Fig. 4.22 Load-strain curves for unfilled full-block prism compressed under eccentric load at e = t/3.

Fig. 4.23 Load-strain curves for filled full-block prism compressed under eccentric load at e = t/3.

Fig. 4.24 Load-strain curves for unfilled half-block prism compressed under eccentric load at e = t/3.

Fig. 4.25 Load-strain curves for filled half-block prism compressed under eccentric load at e = t/3.

Fig. 4.26 Load-moment interaction diagram for blockwork masonry prisms.

Fig. 4.27 Idealised stress-strain relationship for confined 10 mm mortar joint (based on a suggestion by Khalaf[39]).

Fig. 4.28 Deformation of axially loaded unfilled full-block prism, in the Y-direction.

Fig. 4.29 Deformation of axially loaded unfilled full-block prism, in the X-direction.

Fig. 4.30 Deformation of axially loaded unfilled full-block prism, in the Z-direction.

Fig. 4.31 Major principal stress in the block material, for an axially loaded unfilled full-block prism.

Fig. 4.32 Minor principal stress 1 in the block material for an axially loaded unfilled full-block prism.

Fig. 4.33 Minor principal stress 2 in the block material for an axially loaded unfilled full-block prism.

Fig. 4.34 Shear stress in the block material for an axially loaded unfilled full-block prism.

Fig. 4.35 Major principal stress in the mortar material for an axially loaded unfilled full-block prism.

Fig. 4.36 Minor principal stress 1 in the mortar material for an axially loaded unfilled full-block prism.

Fig. 4.37 Minor principal stress 2 in the mortar material for an axially loaded unfilled full-block prism.

Fig. 4.38 Shear stress in the mortar material for an axially loaded unfilled full-block prism.

Fig. 4.39 Deformation of axially loaded filled full-block prism, in the Y-direction.

Fig. 4.40 Deformation of axially loaded filled full-block prism, in the X-direction.

Fig. 4.41 Deformation of axially loaded filled full-block prism, in the Z-direction.

Fig. 4.42 Major principal stress in the block material for an axially loaded filled full-block prism.

Fig. 4.43 Minor principal stress 1 in the block material for an axially loaded filled full-block prism.

Fig. 4.44 Minor principal stress 2 in the block material for an axially loaded filled full-block prism.

Fig. 4.45 Shear stress in the block material for an axially loaded filled full-block prism.

Fig. 4.46 Major principal stress in the mortar material for an axially loaded filled full-block prism.

Fig. 4.47 Minor principal stress 1 in the mortar material for an axially loaded filled full-block prism.

Fig. 4.48 Minor principal stress 2 in the mortar material for an axially loaded filled full-block prism.

Fig. 4.49 Shear stress in the mortar material for an axially loaded filled full-block prism.

Fig. 4.50 Major principal stress in the concrete infill for an axially loaded filled full-block prism.

Fig. 4.51 Minor principal stress 1 in the concrete infill for an axially loaded filled full-block prism.

Fig. 4.52 Minor principal stress 2 in the concrete infill for an axially loaded filled full-block prism.

Fig. 4.53 Shear stress in the concrete infill for an axially loaded filled full-block prism.

Fig. 4.54 Deformation of axially loaded unfilled half-block prism, in the Y-direction.

Fig. 4.55 Deformation of axially loaded unfilled half-block prism, in the X-direction.

Fig. 4.56 Deformation of axially loaded unfilled half-block prism, in the Z-direction.

Fig. 4.57 Major principal stress in the block material for an axially loaded unfilled half-block prism.

Fig. 4.58 Minor principal stress 1 in the block material for an axially loaded unfilled half-block prism.

Fig. 4.59 Minor principal stress 2 in the block material for an axially loaded unfilled half-block prism.

Fig. 4.60 Shear stress in the block material for an axially loaded unfilled half-block prism.

Fig. 4.61 Major principal stress in the mortar material for an axially loaded unfilled half-block prism.

Fig. 4.62 Minor principal stress 1 in the mortar material for an axially loaded unfilled half-block prism.

Fig. 4.63 Minor principal stress 2 in the mortar material for an axially loaded unfilled half-block prism.

Fig. 4.64 Shear stress in the mortar material for an axially loaded unfilled half-block prism.

Fig. 4.65 Deformation of axially loaded filled half-block prism, in the Y-direction.

Fig. 4.66 Deformation of axially loaded filled half-block prism, in the X-direction.

Fig. 4.67 Deformation of axially loaded filled half-block prism, in the Z-direction.

Fig. 4.68 Major principal stress in the block material for an axially loaded filled half-block prism.

Fig. 4.69 Minor principal stress 1 in the block material for an axially loaded filled half-block prism.

Fig. 4.70 Minor principal stress 2 in the block material for an axially loaded filled half-block prism.

Fig. 4.71 Shear stress in the block material for an axially loaded filled half-block prism.

Fig. 4.72 Major principal stress in the mortar material for an axially loaded filled half-block prism.

Fig. 4.73 Minor principal stress 1 in the mortar material for an axially loaded filled half-block prism.

Fig. 4.74 Minor principal stress 2 in the mortar material for an axially loaded filled half-block prism.

Fig. 4.75 Shear stress in the mortar material for an axially loaded filled half-block prism.

Fig. 4.76 Major principal stress in the concrete infill for an axially loaded filled half-block prism.

Fig. 4.77 Minor principal stress 1 in the mortar material for an axially loaded filled half-block prism.

Fig. 4.78 Minor principal stress 2 in the mortar material for an axially loaded filled half-block prism.

Fig. 4.79 Shear stress in the concrete infill for an axially loaded filled half-block prism.

Fig. 4.80 Deformation in the Y-direction of unfilled full-block prism compressed under eccentric load for e = t/6.

Fig. 4.81 Deformation in the X-direction of unfilled full-block prism compressed under eccentric load for e = t/6.

Fig. 4.82 Deformation in the Z-direction of unfilled full-block prism compressed under eccentric load for e = t/6.

Fig. 4.83 Major principal stress in the block material of unfilled full-block prism compressed under eccentric load for e = t/6.

Fig. 4.84 Minor principal stress 1 in the block material of unfilled full-block prism compressed under eccentric load for e = t/6.

Fig. 4.85 Minor principal stress 2 in the block material of unfilled full-block prism compressed under eccentric load for e = t/6.

Fig. 4.86 Shear stress in the block material of unfilled full-block prism compressed under eccentric load for e = t/6.

Fig. 4.87 Major principal stress in the mortar material of unfilled full-block prism compressed under eccentric load for e = t/6.

Fig. 4.88 Minor principal stress 1 in the mortar material of unfilled full-block prism compressed under eccentric load for e = t/6.

Fig. 4.89 Minor principal stress 2 in the mortar material of unfilled full-block prism compressed under eccentric load for e = t/6.

Fig. 4.90 Shear stress in the mortar material of unfilled full-block prism compressed under eccentric load for e = t/6.

Fig. 4.91 Deformation in the Y-direction of filled full-block prism compressed under eccentric load for e = t/6.

Fig. 4.92 Deformation in the X-direction of filled full-block prism compressed under eccentric load for e = t/6.

Fig. 4.93 Deformation in the Z-direction of filled full-block prism compressed under eccentric load for e = t/6.

Fig. 4.94 Major principal stress in the block material of filled full-block prism compressed under eccentric load for e = t/6.

Fig. 4.95 Minor principal stress 1 in the block material of filled full-block prism compressed under eccentric load for e = t/6.

Fig. 4.96 Minor principal stress 2 in the block material of filled full-block prism compressed under eccentric load for e = t/6.

Fig. 4.97 Shear stress in the block material of filled full-block prism compressed under eccentric load for e = t/6.

Fig. 4.98 Major principal stress in the mortar material of filled full-block prism compressed under eccentric load for e = t/6.

Fig. 4.99 Minor principal stress 1 in the mortar material of filled full-block prism compressed under eccentric load for e = t/6.

Fig. 4.100 Minor principal stress 2 in the mortar material of filled full-block prism compressed under eccentric load for e = t/6.

Fig. 4.101 Shear stress in the mortar material of filled full-block prism compressed under eccentric load for e = t/6.

Fig. 4.102 Major principal stress in the concrete infill of filled full-block prism compressed under eccentric load for e = t/6.

Fig. 4.103 Minor principal stress 1 in the concrete infill of filled full-block prism compressed under eccentric load for e = t/6.

Fig. 4.104 Minor principal stress 2 in the concrete infill of filled full-block prism compressed under eccentric load for e = t/6.

Fig. 4.105 Shear stress in the concrete infill of filled full-block prism compressed under eccentric load for e = t/6.

Fig. 4.106 Deformation in the Y-direction of unfilled half-block prism compressed under eccentric load for e = t/6.

Fig. 4.107 Deformation in the X-direction of unfilled half-block prism compressed under eccentric load for e = t/6.

Fig. 4.108 Deformation in the Z-direction of unfilled half-block prism compressed under eccentric load for e = t/6.

Fig. 4.109 Major principal stress in the block material of unfilled half-block prism compressed under eccentric load for e = t/6.

Fig. 4.110 Minor principal stress 1 in the block material of unfilled half-block prism compressed under eccentric load for e = t/6.

Fig. 4.111 Minor principal stress 2 in the block material of unfilled half-block prism compressed under eccentric load for e = t/6.

Fig. 4.112 Shear stress in the block material of unfilled half-block prism compressed under eccentric load for e = t/6.

Fig. 4.113 Major principal stress in the mortar material of unfilled half-block prism compressed under eccentric load for e = t/6.

Fig. 4.114 Minor principal stress 1 in the mortar material of unfilled half-block prism compressed under eccentric load for e = t/6.

Fig. 4.115 Minor principal stress 2 in the mortar material of unfilled half-block prism compressed under eccentric load for e = t/6.

Fig. 4.116 Shear stress in the mortar material of unfilled half-block prism compressed under eccentric load for e = t/6.

Fig. 4.117 Deformation in the Y-direction of filled half-block prism compressed under eccentric load for e = t/6.

Fig. 4.118 Deformation in the X-direction of filled half-block prism compressed under eccentric load for e = t/6.

Fig. 4.119 Deformation in the Z-direction of filled half-block prism compressed under eccentric load for e = t/6.

Fig. 4.120 Major principal stress in the block material of filled half-block prism compressed under eccentric load for e = t/6.

Fig. 4.121 Minor principal stress 1 in the block material of filled half-block prism compressed under eccentric load for e = t/6.

Fig. 4.122 Minor principal stress 2 in the block material of filled half-block prism compressed under eccentric load for e = t/6.

Fig. 4.123 Shear stress in the block material of filled half-block prism compressed under eccentric load for e = t/6.

Fig. 4.124 Major principal stress in the mortar material of filled half-block prism compressed under eccentric load for e = t/6.

Fig. 4.125 Minor principal stress 1 in the mortar material of filled half-block prism compressed under eccentric load for e = t/6.

Fig. 4.126 Minor principal stress 2 in the mortar material of filled half-block prism compressed under eccentric load for e = t/6.

Fig. 4.127 Shear stress in the mortar material of filled half-block prism compressed under eccentric load for e = t/6.

Fig. 4.128 Major principal stress in the concrete infill of filled half-block prism compressed under eccentric load for e = t/6.

Fig. 4.129 Minor principal stress 1 in the concrete infill of filled half-block prism compressed under eccentric load for e = t/6.

Fig. 4.130 Minor principal stress 2 in the concrete infill of filled half-block prism compressed under eccentric load for e = t/6.

Fig. 4.131 Shear stress in the concrete infill of filled half-block prism compressed under eccentric load for e = t/6.

Fig. 4.132 State of stresses at the mortar and the block interface near failure.

Chapter 5

Fig. 5.1 Typical cross-sections of full-block masonry columns.

Fig. 5.2 Typical cross-sections of half-block masonry columns.

Fig. 5.3 Test setup for the concentrically and eccentrically loaded full-block masonry columns.

Fig. 5.4 Test setup for the concentrically and eccentrically loaded half-block masonry columns.

Fig. 5.5 Typical FEA mesh used to model full-block masonry columns under axial loads.

Fig. 5.6 Typical FEA mesh used to model half-block masonry columns under axial loads.

Fig. 5.7 Typical FEA mesh used to model full-block masonry columns under load eccentricities = t/6.

Fig. 5.8 Typical FEA mesh used to model half-block masonry columns under load eccentricities = t/6.

Fig. 5.9 Typical FEA mesh used to model full-block masonry columns under load eccentricities > t/6.

Fig. 5.10 Typical FEA mesh used to model half-block masonry columns under load eccentricities > t/6.

Fig. 5.11 Conditions at failure for reinforced blockwork masonry columns under different cases of loading.

Fig. 5.12 Stress-strain relationship for concrete (BS 8110 [37]).

Fig. 5.13 Short term stress-strain design curve for reinforcement (BS 8110 [37]).

Fig. 5.14 Simplified design stress block (BS 8110 [37]).

Fig. 5.15 Methods used to simplify the active stress-strain parabolic area for brickwork masonry.

Fig. 5.16 Load-moment interaction diagrams for full-block masonry columns.

Fig. 5.17 Load-moment interaction diagrams for half-block masonry columns.

Chapter 6

Fig. 6.1 Typical mode of failure for an unreinforced full-block masonry column compressed under axial load.

Fig. 6.2 Typical mode of failure for an unreinforced full-block masonry column compressed under axial load.

Fig. 6.3 Full-block masonry column's elastic modulus.

Fig. 6.4 Half-block masonry column's elastic modulus.

Fig. 6.5 Average masonry strains measured by electrical strain gauges and LVDT strains for the FCA (No Steel) column.

Fig. 6.6 Average vertical reinforcement strains and LVDT strains for the HCA (No Steel) column.

Fig. 6.7 Average vertical reinforcement strains and LVDT strains for the FCA (10 mm) column.

Fig. 6.8 Average masonry strains measured by electrical strain gauges and LVDT strains for the FCA (20 mm) column.

Fig. 6.9 Average vertical reinforcement strains and LVDT strains for the FCA (8 mm) column.

Fig. 6.10 Average vertical reinforcement strains and LVDT strains for the HCA (20 mm) column.

Fig. 6.11 Experimental and predicted modulus of elasticity for full-block masonry columns using equation 6.8 [24].

Fig. 6.12 Experimental and predicted modulus of elasticity for half-block masonry columns using equation 6.8 [24].

Fig. 6.13 Experimental and predicted modulus of elasticity for full-block masonry columns.

Fig. 6.14 Experimental and predicted modulus of elasticity for half-block masonry columns.

Fig. 6.15 Theoretical and experimental results for the FCA (10 mm) column.

Fig. 6.16 Theoretical and experimental results for the FCA (20 mm) column.

Fig. 6.17 Theoretical and experimental results for the HCA (8 mm) column.

Fig. 6.18 Theoretical and experimental results for the HCA (20 mm) column.

Fig. 6.19 Typical mode of failure for an unreinforced full-block masonry column compressed with an eccentricity of t/6.

Fig. 6.20 Mode of failure for the $FCE_{t/6}$ (20 mm) column.

Fig. 6.21 Mode of failure for the $HCE_{t/6}$ (8 mm) column.

Fig. 6.22 Mode of failure for the $HCE_{t/6}$ (20 mm) column.

Fig. 6.23 Strain distribution for the $FCE_{t/6}$ (No Steel) column cross-section.

Fig. 6.24 Strain distribution across the $FCE_{t/6}$ (10 mm) column cross-section.

Fig. 6.25 Strain distribution across the $FCE_{t/6}$ (20 mm) column cross-section.

Fig. 6.26 Strain distribution for the $HCE_{t/6}$ (No Steel) column cross-section.

Fig. 6.27 Strain distribution across the $HCE_{t/6}$ (8 mm) column cross-section.

Fig. 6.28 Strain distribution across the $HCE_{t/6}$ (20 mm) column cross-section.

Fig. 6.29 Load-deflection relationship for the $FCE_{t/6}$ (No Steel) column.

Fig. 6.30 Load-deflection relationship for the $FCE_{t/6}$ (10 mm) column.

Fig. 6.31 Load-deflection relationship for the $FCE_{t/6}$ (20 mm) column.

Fig. 6.32 Load-deflection relationship for the $HCE_{t/6}$ (No Steel) column.

Fig. 6.33 Load-deflection relationship for the $HCE_{t/6}$ (8 mm) column.

Fig. 6.34 Load-deflection relationship for the $HCE_{t/6}$ (20 mm) column.

Fig. 6.35 Theoretical and experimental results for deflections at mid-height of column $FCE_{t/6}$ (No Steel).

Fig. 6.36 Theoretical and experimental results for deflections at mid-height of column $FCE_{t/6}$ (10 mm).

Fig. 6.37 Theoretical and experimental results for deflections at mid-height of column $FCE_{t/6}$ (20 mm).

Fig. 6.38 Theoretical and experimental results for deflections at mid-height of column $HCE_{t/6}$ (No Steel).

Fig. 6.39 Theoretical and experimental results for deflections at mid-height of column $HCE_{t/6}$ (8 mm).

Fig. 6.40 Theoretical and experimental results for deflections at mid-height of column $HCE_{t/6}$ (20 mm).

Fig. 6.41 Mode of failure for the FCE_1 (No steel) column.

Fig. 6.42 Mode of failure for the FCE_1 (10 mm) column.

Fig. 6.43 Mode of failure for the FCE_1 (20 mm) column.

Fig. 6.44 Mode of failure for the HCE_1 (No steel) column.

Fig. 6.45 Mode of failure for the HCE_1 (20 mm) column.

Fig. 6.46 Mode of failure for the FCE_2 (No Steel) column.

Fig. 6.47 Mode of failure for the FCE_2 (10 mm) column.

Fig. 6.48 Mode of failure for the FCE_2 (20 mm) column.

Fig. 6.49 Mode of failure for the HCE_2 (No Steel) column.

Fig. 6.50 Mode of failure for the HCE_2 (8 mm) column.

Fig. 6.51 Mode of failure for the HCE_2 (20 mm) column.

Fig. 6.52 Strain distribution for the FCE_1 (No steel) column.

Fig. 6.53 Strain distribution across the FCE_1 (10 mm) column cross-section.

Fig. 6.54 Strain distribution across the FCE_1 (20 mm) column cross-section.

Fig. 6.55 Strain distribution for the HCE_1 (No steel) column.

Fig. 6.56 Strain distribution across the HCE_1 (8 mm) column cross-section.

Fig. 6.57 Strain distribution across the HCE_1 (20 mm) column cross-section.

Fig. 6.58 Strain distribution for the FCE_2 (No steel) column.

Fig. 6.59 Strain distribution across the FCE_2 (10 mm) column cross-section.

Fig. 6.60 Strain distribution across the FCE_2 (20 mm) column cross-section.

Fig. 6.61 Strain distribution for the HCE_2 (No steel) column.

Fig. 6.62 Strain distribution across the HCE_2 (8 mm) column cross-section.

Fig. 6.63 Strain distribution across the HCE_2 (20 mm) column cross-section.

Fig. 6.64 Load-deflection relationship for the FCE_1 (No Steel) column.

Fig. 6.65 Load-deflection relationship for the FCE_1 (10 mm) column.

Fig. 6.66 Load-deflection relationship for the FCE_1 (20 mm) column.

Fig. 6.67 Load-deflection relationship for the HCE_1 (No Steel) column.

Fig. 6.68 Load-deflection relationship for the HCE_2 (8 mm) column.

Fig. 6.69 Load-deflection relationship for the HCE_2 (20 mm) column.

Fig. 6.70 Load deflection relationship for the FCE_2 (No Steel) column.

Fig. 6.71 Load-deflection relationship for the FCE_2 (No Steel) column.

Fig. 6.72 Load-deflection relationship for the FCE_2 (20 mm) column.

Fig. 6.73 Load-deflection relationship for the HCE_2 (No Steel) column.

Fig. 6.74 Load-deflection relationship for the HCE_2 (8 mm) column.

Fig. 6.75 Load-deflection relationship for the HCE_2 (20 mm) column.

Fig. 6.76 Theoretical and experimental results for deflections at mid-height of column FCE_1 (No Steel).

Fig. 6.77 Theoretical and experimental results for deflections at mid-height of column FCE_1 (10 mm).

Fig. 6.78 Theoretical and experimental results for deflections at mid-height of column FCE_1 (20 mm).

Fig. 6.79 Theoretical and experimental results for deflections at mid-height of column HCE_1 (No Steel).

Fig. 6.80 Theoretical and experimental results for deflections at mid-height of column HCE_1 (8 mm).

Fig. 6.81 Theoretical and experimental results for deflections at mid-height of column HCE_1 (20 mm).

Fig. 6.82 Theoretical and experimental results for deflections at mid-height of column FCE_2 (No Steel).

Fig. 6.83 Theoretical and experimental results for deflections at mid-height of column FCE_2 (10 mm).

Fig. 6.84 Theoretical and experimental results for deflections at mid-height of column FCE_2 (20 mm).

Fig. 6.85 Theoretical and experimental results for deflections at mid-height of column HCE_2 (No Steel).

Fig. 6.86 Theoretical and experimental results for deflections at mid-height of column HCE_2 (8 mm).

Fig. 6.87 Theoretical and experimental results for deflections at mid-height of column HCE_2 (20 mm).

Fig. 6.88 Load-moment interaction diagrams for full-block masonry columns.

Fig. 6.89 Load-moment interaction diagrams for half-block masonry columns.

Fig. 6.90 Relationship between failure strain and load eccentricity for full-block masonry columns.

Fig. 6.91 Relationship between failure strain and load eccentricity for half-block masonry columns.

Appendix A

Fig. A.1 Deformation in the Y-direction of unfilled full-block prism compressed under eccentric load for e = t/3.

Fig. A.2 Deformation in the X-direction of unfilled full-block prism compressed under eccentric load for e = t/3.

Fig. A.3 Deformation in the Z-direction of unfilled full-block prism compressed under eccentric load for e = t/3.

Fig. A.4 Major principal stress in the block material of unfilled full-block prism compressed under eccentric load for e = t/3.

Fig. A.5 Minor principal stress 1 in the block material of unfilled full-block prism compressed under eccentric load for e = t/3.

Fig. A.6 Minor principal stress 2 in the block material of unfilled full-block prism compressed under eccentric load for e = t/3.

Fig. A.7 Shear stress in the block material of unfilled full-block prism compressed under eccentric load for e = t/3.

Fig. A.8 Major principal stress in the mortar material of unfilled full-block prism compressed under eccentric load for e = t/3.

Fig. A.9 Minor principal stress 1 in the mortar material of unfilled full-block prism compressed under eccentric load for e = t/3.

Fig. A.10 Minor principal stress 2 in the mortar material of unfilled full-block prism compressed under eccentric load for e = t/3.

Fig. A.11 Shear stress in the mortar material of unfilled full-block prism compressed under eccentric load for e = t/3.

Fig. A.12 Deformation in the Y-direction of filled full-block prism compressed under eccentric load for e = t/3.

Fig. A.13 Deformation in the X-direction of filled full-block prism compressed under eccentric load for e = t/3.

Fig. A.14 Deformation in the Z-direction of filled full-block prism compressed under eccentric load for e = t/3.

Fig. A.15 Major principal stress in the block material of filled full-block prism compressed under eccentric load for e = t/3.

Fig. A.16 Minor principal stress 1 in the block material of filled full-block prism compressed under eccentric load for e = t/3.

Fig. A.17 Minor principal stress 2 in the block material of filled full-block prism compressed under eccentric load for e = t/3.

Fig. A.18 Shear stress in the block material of filled full-block prism compressed under eccentric load for e = t/3.

Fig. A.19 Major principal stress in the mortar material of filled full-block prism compressed under eccentric load for e = t/3.

Fig. A.20 Minor principal stress 1 in the block material of filled full-block prism compressed under eccentric load for e = t/3.

Fig. A.21 Minor principal stress 2 in the block material of filled full-block prism compressed under eccentric load for e = t/3.

Fig. A.22 Shear stress in the mortar material of filled full-block prism compressed under eccentric load for e = t/3.

Fig. A.23 Major principal stress in the concrete infill of filled full-block prism compressed under eccentric load for e = t/3.

Fig. A.24 Minor principal stress 1 in the concrete infill of filled full-block prism compressed under eccentric load for e = t/3.

Fig. A.25 Minor principal stress 2 in the concrete infill of filled full-block prism compressed under eccentric load for e = t/3.

Fig. A.26 Shear stress in the concrete infill of filled full-block prism compressed under eccentric load for e = t/3.

Fig. A.27 Deformation in the Y-direction of unfilled half-block prism compressed under eccentric load for e = t/3.

Fig. A.28 Deformation in the X-direction of unfilled half-block prism compressed under eccentric load for e = t/3.

Fig. A.29 Deformation in the Z-direction of unfilled half-block prism compressed under eccentric load for e = t/3.

Fig. A.30 Major principal stress in the block material of unfilled half-block prism compressed under eccentric load for e = t/3.

Fig. A.31 Minor principal stress 1 in the block material of unfilled half-block prism compressed under eccentric load for e = t/3.

Fig. A.32 Minor principal stress 2 in the block material of unfilled half-block prism compressed under eccentric load for e = t/3.

Fig. A.33 Shear stress in the block material of unfilled half-block prism compressed under eccentric load for e = t/3.

Fig. A.34 Major principal stress in the mortar material of unfilled half-block prism compressed under eccentric load for e = t/3.

Fig. A.35 Minor principal stress 1 in the block material of unfilled half-block prism compressed under eccentric load for e = t/3.

Fig. A.36 Minor principal stress 2 in the block material of unfilled half-block prism compressed under eccentric load for e = t/3.

Fig. A.37 Shear stress in the mortar material of unfilled half-block prism compressed under eccentric load for e = t/3.

Fig. A.38 Deformation in the Y-direction of filled half-block prism compressed under eccentric load for e = t/3.

Fig. A.39 Deformation in the X-direction of filled half-block prism compressed under eccentric load for e = t/3.

Fig. A.40 Deformation in the Z-direction of filled half-block prism compressed under eccentric load for e = t/3.

Fig. A.41 Major principal stress in the block material of filled half-block prism compressed under eccentric load for e = t/3.

Fig. A.42 Minor principal stress 1 in the block material of filled half-block prism compressed under eccentric load for e = t/3.

Fig. A.43 Minor principal stress 2 in the block material of filled half-block prism compressed under eccentric load for e = t/3.

Fig. A.44 Shear stress in the block material of filled half-block prism compressed under eccentric load for e = t/3.

Fig. A.45 Major principal stress in the mortar material of filled half-block prism compressed under eccentric load for e = t/3.

Fig. A.46 Minor principal stress 1 in the mortar material of filled half-block prism compressed under eccentric load for e = t/3.

Fig. A.47 Minor principal stress 2 in the mortar material of filled half-block prism compressed under eccentric load for e = t/3.

Fig. A.48 Shear stress in the mortar material of filled half-block prism compressed under eccentric load for e = t/3.

Fig. A.49 Major principal stress in the concrete infill of filled half-block prism compressed under eccentric load for e = t/3.

Fig. A.50 Minor principal stress 1 in the concrete infill of filled half-block prism compressed under eccentric load for e = t/3.

Fig. A.51 Minor principal stress 2 in the concrete infill of filled half-block prism compressed under eccentric load for e = t/3.

Fig. A.52 Shear stress in the concrete infill of filled half-block prism compressed under eccentric load for e = t/3.

Appendix B

Fig. B.1 Parabolic stress-block

NOTATION

The symbols listed below are those employed in this investigation. The notations for other previous works are defined in the text where necessary.

A_c = Cross-sectional area of concrete, mm^2

A_g = Cross-sectional area of specimen, mm^2

A_m = Cross-sectional area of masonry, mm^2

A_s = Total area of vertical reinforcement, mm^2

A_{s1} = Area of reinforcement near the more highly compressed face of the column section, mm^2

A_{s2} = Area of reinforcement near the less compressed face of the column section, mm^2

A_{shell} = Blockwork masonry shell area, mm^2

b = Width of column section, mm

d = Effective depth of tension reinforcement, mm

d_1 = Depth to centroid of reinforcement A_{s1}, mm

d_2 = Depth to centroid of reinforcement A_{s2}, mm

e = Eccentricity of applied load, mm

E_{bs} = Secant modulus of elasticity of concrete block derived from testing three unfilled half-blocks prism as described in chapter 3, N/mm^2

E_{cs} = Secant modulus of elasticity of concrete derived from testing three cubes prism as described in chapter 3, N/mm^2

E_{js} = Secant modulus of elasticity of mortar joint derived experimentally as described in chapter 3, N/mm^2

E_m = Short term static modulus of elasticity of masonry, N/mm^2

E_{mrs} = Secant modulus of elasticity of mortar derived from testing three cubes prism as described in chapter 3, N/mm^2

E_s = Modulus of elasticity of steel, kN/mm^2

f = Compressive stress, N/mm^2

f_c = Compressive cube strength of concrete, N/mm^2 .

f_k = Characteristic compressive strength of masonry, N/mm^2

f'_m = Ultimate compressive strength of blockwork masonry, N/mm^2

f_{s1} = Stress in the reinforcement near the more highly compressed face of the column section, N/mm^2

f_{s2} = Stress in the reinforcement near the less compressed face of the column section, N/mm^2

f_y = Yield stress of reinforcement, N/mm^2

h = Height of specimen, mm

h_b = Height of block, mm

k = Neutral axis depth factor

k_m, k_s = Failure strain factor for masonry and steel.

k_1, k_2, k_3 = Characteristic ratios of stress-block

l = Length of specimen, mm

M_u = Ultimate bending moment capacity of column, kN m

N_u = Ultimate axial load capacity of column, kN

P_u = Ultimate axial force, kN

t = Overall depth of column section, or thickness of prism, mm

x = Neutral axis depth, mm

Γ = The contribution of concrete infill to the blockwork masonry column elastic modulus

Δ = Lateral deflection of column, mm

ε_m = Strain at maximum stress

ε_1 = Compressive strain in column reinforcement A_{s1}

ε_2 = Compressive strain in column reinforcement A_{s2}

ε_u = Ultimate strain

ϕ = Bar diameter, mm

ρ = Steel ratio

μ = Poisson's ratio

CHAPTER 1
INTRODUCTION

Masonry is one of the oldest permanent construction materials used by mankind. Its origin has been traced back 20,000 years. The Summerians were the first people to manufacture masonry and used sun-baked clay bricks some 5500 years ago(1). Other ancient civilisations such as the ancient Egyptians, Greeks, Chinese and Romans utilised masonry in a wide variety of structures. The Pyramids, the Acropolis, the Great Wall, and the Coliseum are notable examples of masonry structures still standing today.

Concrete was also used by the early civilisations. The oldest known concrete was discovered during excavations on the banks of the River Danube in Yugoslavia (2), and dates back to 5600 BC.

Although concrete has a long history, it was not until 1835 that an all concrete house was built in Kent, England.

The first concrete blocks were made in the United Kingdom in about 1850 by Joseph Gibbs (3). The blocks were hollow with moulded faces to imitate the dressed stone of that period. A significant growth in production did not occur until 1910.

After the First World War, a major growth took place. Many concrete block houses were built with the establishment of many small block manufacturers throughout the United Kingdom. After the Second World War the demand for concrete blocks increased rapidly and both solid and hollow blocks

became widely acceptable. The low cost and ease of handling made masonry the most popular building material. At the same time, masonry development was taking place in the United States of America with the evolution of high quality facing concrete masonry, and machines associated with its production. The seismic problems, associated with certain areas of the country, also fostered the development of reinforced masonry [4][5][6].

Reinforced blockwork masonry consists of four component materials: concrete blocks, mortar, concrete infill and steel reinforcement. These four materials give masonry its non-homogeneous properties compared to those of concrete. The strength and behaviour of masonry structural elements is influenced by the different mechanical properties of the four components, and by the different shapes and geometry of the block units.

Columns subjected to a combination of axial load and uni-axial bending moments are common, a typical example being external columns in framed structures. The reinforced blockwork load capacity for specific values of eccentricity is determined by such factors as the dimensions of the cross-section, the percentage of reinforcement, the strength of the blockwork and the depth of the reinforcement cover. The parabolic shape of the compression zone and the non-linear stress distribution in the blockwork introduces complications in the design of eccentrically loaded blockwork columns.

The working stress method which is based on elastic theory is still recommended by most masonry reference books [7][54][55][56], and current Codes of Practice [8][9]. The British Code of Practice for masonry,

BS 5628: Parts 1, 2 and 3 [10] is one of the minority of masonry codes which adopted the use of limit state design philosophy, where the degree of risk is varied according to the choice of partial safety factors.

The main objectives and scope of this study are:

(1) To review current understanding of the behaviour of reinforced brickwork and blockwork masonry columns and the methods used to determine their ultimate strength.

(2) To determine the mechanical properties of the materials used in the construction of blockwork masonry.

(3) To study experimentally and theoretically the compressive strength and behaviour of blockwork masonry prisms under axial and eccentric loads.

(4) To determine the effect of changing the percentage of vertical reinforcement on the strength and behaviour of axially and eccentrically loaded reinforced blockwork columns.

(5) To develop a new method of predicting the ultimate strength of reinforced blockwork masonry columns subjected to axial compression or combined bending and axial compression.

The units used throughout this study are SI units.

CHAPTER 2
LITERATURE REVIEW

2.1 INTRODUCTION

This chapter presents a summary of previous research studies on brickwork and blockwork masonry columns. It also provides a review of previous work carried out on eccentrically loaded blockwork masonry prisms to study the compressive strength, f'_m.

2.2 MASONRY COLUMNS

2.2.1 Brickwork Masonry Columns

Earlier attempts at testing brick piers were carried out at Watertown Arsenal (11) U.S.A. in 1882 to establish a relationship between the compressive strength of plain brickwork piers and the compressive strength of brick units. The test variables were column height, column cross section and mortar types. By 1886, an inversely proportional relationship between brickwork column strength and column height to thickness ratio had been proposed.

In 1900, research conducted at Cornell University (11) showed that the compressive strength of brick piers, with horizontal reinforcement consisting either of wire netting or mesh in every joint, was significantly greater than that of plain brick piers. The same conclusion was obtained by research carried out by The Bureau of Standards Laboratory in Pittsburgh, Pennsylvania in 1915 (11).

In 1923, Brebner (12) tested reinforced brickwork prisms with circular and square cross-sections, for which all the prisms were 6-courses in height. Small percentages of vertical reinforcement and large amounts of horizontal

reinforcement were used. The results showed that the compressive strength of square cross-section prisms with circular 5 mm stirrups was 62% greater compared to that of unreinforced prisms. The results also showed a decrease of 16% in prism strength when square cross-sections were reinforced with 0.8% vertical reinforcement compared to those reinforced with horizontal circular stirrups, and an increase of 36% over those with no reinforcement. The compressive strength of circular prisms increased by an average of 36% when the prisms were reinforced with circular stirrups compared to that of unreinforced prisms. The compressive strength of circular prisms with circular stirrups increased by 19% compared to those with horizontal reinforcement only and 62% compared to those with no reinforcement.

In 1908 research carried out on brickwork piers at the University of Illinois[11] was the first to study the effect of changing the mortar type on the pier compressive strength and its modulus of elasticity.

In 1916 researchers at the Swedish Technical Institute [11] were the first to study the compressive strength of eccentrically loaded brickwork piers. The results showed that the eccentricity of loading decreased the strength considerably.

Lyse [11] in 1933 tested thirty three reinforced columns in vertical compression. All were 3 m in height and 317.5 mm square in cross-section. The test variables were brick type, mortar type, vertical reinforcement, lateral reinforcement, and both lateral and vertical reinforcement.

Lyse found that the strength of the brick had a marked effect upon the strength of the column and that the strength of the mortar affected the strength of the column. The strength of a column with vertical reinforcement is a combination of the effective strength of the bricks and the yield strength of the vertical reinforcement. The strength of a reinforced brickwork column was given by the following equation:-

$$S = A(k f'_b + \rho f'_s) \qquad .....(2.1)$$

where

S = Column strength, N

A = Column cross-sectional area, mm^2

k = Ratio of masonry strength to brick strength

f'_b = Ultimate strength of the brick, N/mm^2

ρ = Ratio of area of longitudinal steel to cross-sectional area of column

f'_s = Yield point of the vertical reinforcement, N/mm^2.

Lyse recommended that the value of k should be determined experimentally by testing small plain brick columns containing the same type of brick and mortar, and using the same workmanship and other conditions as that used in the actual structure.

In 1934 Withey [13] tested thirty two reinforced brickwork columns under concentric load. Each column was 318 mm square and 1.8 m high with a slenderness ratio of 5.8. Figure 2.1 shows details of the tested columns. The test results indicated that the column strength varies directly with the strength of the masonry and the percentage of longitudinal steel, and is

increased by using lateral reinforcement. The equation proposed by Withey to calculate the capacity of reinforced blockwork columns was as follows:

$$P/A = f_b(1 - \rho) + \rho f_s + K\rho' f'_s \qquad .....(2.2)$$

where

P = Maximum load, N

A = Gross area of cross-section, mm^2

f_b = Unit stress of a plain brick column, N/mm^2

ρ = Longitudinal steel ratio in terms of gross area

ρ' = Lateral steel ratio in terms of gross area

f_s = Yield point of longitudinal steel, N/mm^2.

f'_s = Yield point of lateral hoops, N/mm^2.

K = Constant assumed to depend on the ratio of gross area to core area, and possibly on the kind of brick.

In 1950 Davey and Thomas [14] carried out concentric and eccentric compression tests on plain and reinforced brickwork piers. The variables considered in the plain piers were: mortar type, brick type, the cross-sectional area and pier height which was varied from 0.30 m to 3.60 m in order to study the slenderness effects. The piers were loaded at eccentricities which ranged from t/12 to t/3. The results showed that the effect of slenderness varies according to the eccentricity of loading.

Other tests were carried out on reinforced brickwork piers, 2.74 m high, with variable cross-sectional area. The slenderness ratio was varied with between 4 and 6.

The piers were loaded through knife-edges with the eccentricity varying from t/13 to 14t/15. The percentage of vertical reinforcement ranged from 0.1% to

0.2%. Failure of the tested columns resulted either from crushing in the compression face or by yielding of the vertical reinforcement. Figure 2.2 shows a typical pier.

Unfortunately, the authors did not propose a failure theory or design method for plain and reinforced brickwork columns.

In 1967 Anderson and Hoffman [15] tested reinforced brickwork masonry columns. All the columns were 3.05 m high and 305 mm x 405 mm in cross-section, hinged at the top and fixed at the bottom. The load eccentricities varied between 0 and 34% of their depth. The purpose of the research was to compare test data with values of ultimate strength obtained by the Design Method of the American Concrete Institute (ACI 318-63) for reinforced brickwork masonry columns. The authors concluded that the ACI USD method for reinforced concrete could be applied to reinforced brickwork masonry columns provided that more data was obtained from tests to establish the true shape of the stress-strain curve for brickwork masonry, the ultimate strain at ultimate strength, and the effect of using different percentages of vertical reinforcement on the behaviour of brickwork masonry.

In 1970 Brettle [16] proposed a computer aided ultimate strength design procedure which could be applied to reinforced brickwork piers under axial compression and bi-axial bending. The program was used to compare values with the experimental results provided by Davey and Thomas. The results showed that the experimental failure loads for a plain column were, on average 30% higher than those computed using the proposed program, and 34% lower for reinforced columns.

Armstrong and Hendry [17] in 1973 tested full-size and model brickwork prisms with various amounts of reinforcement in each mortar joint. The prisms were 6-courses in height. Test results showed that the strength of the reinforced specimens were 30% to 40% higher than the unreinforced specimens. The authors pointed out that the surface area and the number of reinforcement wires rather than cross-sectional area were more significant in determining the effectiveness of the reinforcement on the compressive strength of the prism. Therefore the bond force that can be transmitted from the mortar to the reinforcement should control the increase in the prism's compressive strength.

Ohler and Gopfert [18] in 1982 tested a number of piers of both sand, lime and concrete masonry. The piers were 1.75 m in height and had a slenderness ratio of 7.3. The horizontal reinforcement which was placed in every bed joint consisted of either 6 mm diameter rectangular stirrups, 6 mm diameter hooped stirrups or 3 mm diameter mesh. The strengths reported were obtained for testing piers consisting of sand lime brickwork and mesh type reinforcement.

The reinforcement was found to be less effective in enhancing the strength of piers made of concrete blocks. Reinforcing the mortar joint had the effect of changing the pier 's mode of failure and so confirmed the conclusions of Lyse [11] and Withey [13] that the horizontal reinforcement was effective in localising failure, but had little effect on the strength of the column.

In 1983 Eltraify [19] conducted an experimental study on columns constructed with half scale brickwork which were subjected to axial load and

bi-axial bending. He presented a theoretical study based on a computer program which gave a comparison between the more exact theory and approximate methods developed originally for reinforced concrete. The theoretical study also included the uniaxial bending case.

Only one type of brick, with a compressive strength of 43.2 N/mm^2, and one type of mortar mix 1:¼:3 (cement:lime:sand) were used throughout. Two percentages of reinforcement were used. The concrete grout mix used was 1:0.1:3:2 (cement:lime:sand:aggregate) with an average compressive cube strength of 17.6 N/mm^2. No lateral reinforcement was used due to the use of half scale bricks in building the columns. All the columns tested were of 283 mm x 168 mm, cross-section, with a slenderness ratio ranging from 8 to 20 simplifying the method of representing the problem mathematically, a pin ended column was chosen. The typical test setup is shown in Fig. 2.3. The axial force was applied through steel balls placed at both ends of the column, using a 60 ton hydraulic jack fixed to a steel frame at the column top end. The flexural force was applied by two 4 ton hydraulic tension jacks. The axial load was applied in small increments up to a certain level of thrust then kept constant. The flexural force was then applied in increments until failure.

The experimental results indicated that the mid-height moments were larger than the end moments. According to the author this was due to the lateral deformation of the specimens after the bending moments were applied. The ratio of mid-height moment to ends moment increased as the bending moment increased. A ratio up to 2.6 was observed for bending about the weak axis, while the ratio for bending about the major axis was 1.2. The author noted that for slender columns, the ultimate strength is strongly

affected by the weak axis flexibility which usually leads to a buckling type of failure. Deflections up to 19 mm were observed about the minor axis, and up to 8 mm about the major axis.

Two types of non-linearity were considered in the theoretical study. First, material non-linearity due to the non-linear behaviour of the materials used i.e. brickwork, grout, concrete and steel. The second type was geometrical non-linearity which is due to the effect of lateral deflection on the total bending moment. Both the geometrical and the material non-linearities were used to determine the strain and curvature distributions in a cross-section subjected to axial compressive force and bi-axial bending moments. The effect of both non-linearities on the overall ultimate strength of the member was also considered. The author described the theoretical procedure as very tedious, and difficult to perform manually. Therefore a computer program was presented by the author to carry out the iterative processes.

Mx-My interaction diagrams obtained using the computer program were derived by the author. Figure 2.4 shows a typical rectangular section for which d1 = 0.9t and d2 = 0.85b. It was assumed that the grout and brickwork have identical stress-strain characteristics. The partial safety factors used in the derivation were 2.5 for brickwork and 1.15 for steel. In considering the effect of slenderness ratio, it was found that the ratio of the mid-height moment to the end moment was greater about the minor axes and that ultimate failure was expected to occur about the weaker axis.

With regard to the effect of the stress-strain relationship in reinforced brickwork sections subjected to bi-axial bending, the author assumed three types of stress-strain relationships, viz. linear, parabolic without a falling

branch and a parabolic with a falling branch. Ultimate compressive strain was assumed to be either 0.002, 0.003 or 0.004 giving a total of nine different stress-strain curves. The ultimate axial force increased from 0.05 to 0.2t. Also between types two and three, there is an increase of 4 to 10% as the eccentricity increases. The main reason for this difference in axial force was the increase in area under the stress-block as the stress-strain relationship changed from type one to type three.

When the ultimate strain was increased from 0.002 to 0.004, the axial load increased from 1 to 8 %. This percentage was increased with increase in eccentricity and the amount of reinforcement.

The author proposed a modified CP 110 approach based on the derivation of bi-axial design charts. The area of reinforcement required a section where the values of Nu, Mx and My are known and can easily be found from the appropriate design chart by the intersection of Mx and My without going into a trial area as adopted by CP 110. The author presented three theoretical methods of analysis for the design of bi-axially loaded brickwork columns. These were:

- An iterative approach;
- The CP 110 approach; and,
- A modified CP 110 approach.

The modified CP 110 approach can be used as an alternative to the iterative approach and will give results which are conservative. With the modified approach, either the parabolic stress-block or the rectangular stress-block can be used but the results showed that the maximum stress for the rectangle would be $0.3f_k$.

In 1985 Edgell and Templeton [20] tested one storey high axially loaded reinforced brickwork masonry columns of square 327 mm cross-section (one and a half bricks) with a central hole, 108 mm square (half brick) kept unfilled. Two types of bricks were used, high and low strength, with a mortar mix, 1:¼:3 (cement:lime:sand). 6 mm diameter stirrups were included in every first, second, or fourth course of the brickwork constructed. Two additional columns were constructed where welded rectangular stirrups were placed in every fourth course.

Compared with unreinforced brickwork, the column strength increased by 31.2% and 20% for the low and high strength columns respectively when square stirrups were included in every fourth joint. The mode of failure of the unreinforced columns was by splitting at the perpendicular joints over the full height of the column. The mode of failure of the reinforced columns was by spalling of the brickwork outside the stirrups. Columns tested with hooped stirrup reinforcement achieved a strength enhancement of 35%. The column containing expanded metal achieved a strength enhancement of 31.2% and those with 50 mm mesh achieved 18.7%. A different mode of failure was observed for the columns containing mesh and expanded metal compared with the unreinforced columns and those columns with stirrups. A number of vertical cracks was observed across the width of the columns containing expanded metal and 25 mm mesh reinforcement. Columns with hooped stirrup reinforcement failed by spalling of the brickwork outside the stirrups leaving the core clearly defined.

In 1990 Davies [61] showed that the number of interaction diagrams developed for the design of short reinforced masonry columns subjected to

vertical loading and uniaxial bending, could be kept to a minimum by a careful selection of non-dimensional groups of parameters.

2.2.2 Blockwork Masonry Columns

In 1931, Shank and Foster [21] studied the behaviour of plain concrete blockwork pilasters when subjected to eccentric loads. The variables in their study included block type, cross-sectional area, and pilaster height. The results showed that the pilaster ultimate compressive strength was half of the unit strength, was inversely proportional to the block absorption and directly proportional to the pilaster's modulus of elasticity.

Thirty seven concrete masonry columns were tested in 1979 by Feeg et al [22] at the University of Alberta to establish the effect of reinforcement detailing on their strength and behaviour. All the columns were 1.62 m high and all had a nominal 400 mm square cross-section. Thirty four columns were constructed using 400 x 200 x 200 mm lightweight, plain corner blocks, with an average unit net area strength of 17.03 N/mm^2. The cross-section of the column consisted of two such units laid in running bond. The remaining three columns were built using 400 x 400 x 200 mm single core lightweight autoclaved pilaster units with an average unit net area strength of 16.89 N/mm^2 laid in stacked bond. Face shell bedding was used throughout and a 10 mm joint thickness was maintained. All columns were constructed with a mortar mix having volume proportions of 1:½:4 (cement:lime:sand) and average 28 day compressive strength of 13.07 N/mm^2, using cubes cured under wet burlap, and 4.57 N/mm^2 when the cubes were cured under laboratory conditions. All the columns were filled with grout having volume proportions of 1:3:2 (cement:sand:gravel) and an average compressive strength of 18.84 N/mm^2, determined from tests on standard moist cured

cylinders. The vertical reinforcement was placed coincident with the core centroid. The block unit shape restricted placement of all tie reinforcement in the joints between courses. A 200 mm spacing between ties was maintained. Ties with diameters of 3.77, 4.76, and 6.35 mm were used.

The variables investigated were:

(1) Tie diameter and location; ties were positioned either in the mortar joint between the block and outer shells or in contact with the vertical reinforcement.

(2) The vertical reinforcement area varied between 0.7% and 1.3% of the total column cross-sectional area.

(3) The distribution of the vertical reinforcement. Columns with identical percentages of vertical reinforcement, but with different bar sizes were compared.

(4) Two types of vertical reinforcement with yield strengths of 275 N/mm^2 and 415 N/mm^2 were used.

Three modes of failure were observed. The first mode was by overall vertical splitting of the column; the second mode was by overall splitting similar to the first one but buckling was not confined to within the tie spacing; and the third mode was by simultaneous crushing of the masonry and buckling of the vertical reinforcement within the tie spacing.

The average elastic modulus was found to be about 800 times the masonry prism strength. The column's ultimate strain was doubled by adding grout and was increased further by increasing the amount of reinforcement. The ultimate strain however showed no definite trends with variation of the percentage of vertical reinforcement. It was also observed that increasing

the tie diameter increased the column ultimate strength. This was accompanied by a decrease in the amount of vertical cracking at failure. No significant difference in strength was found between columns having ties in contact with the vertical reinforcement and those with no contact. It was observed that the columns with ties in contact with the vertical reinforcement provided more restraint against buckling of the vertical reinforcement. The column strength decreased when the diameter of the vertical bars was increased. This was due to the stress developed in the masonry surrounding the bars which increased with increase in bar diameter. It was noticed that the grout did not fill completely the vertical spaces between the block units. This created a weak plane which contributed to the vertical splitting of the columns when loaded. It was also observed that the column strength decreased significantly when mortar droppings were not removed from the interior base of the column. After failure of the columns, rust was noted on ungalvanised ties which had been placed in the mortar joints. The mortar placed on top of the ties did not completely surround the tie. It was noted that the use of high slump grout in the columns constructed from pilaster units resulted in a large amount of shrinkage cracking.

Unfortunately equations to predict the ultimate load and deformations were not presented in the Feeg et al study.

In 1980 Salim [23] tested blockwork masonry prisms with helical confinement reinforcement at the prism core. All the specimens were built from block units, 200 mm square and 200 mm high. The unit net average strength was 36.0 N/mm^2. The units were horizontally laid and built with mortar with an average compressive strength of 23.7 N/mm^2. All the joints were 9.5 mm in thickness. A helical mild steel wire, 5.2 mm in diameter, with

a core diameter of 108 mm centre to centre, was placed inside the prism core and the prism was grouted with grout having an average compressive strength of 21.1 N/mm^2.

The results obtained showed that the compressive strength of helical reinforced prisms were 30% to 38% higher than that of unreinforced prisms. The failure mode of the ungrouted prisms was by tensile splitting which initiated in the centre of the block. The unreinforced grout prisms displayed a failure mode which was similar to that of ungrouted prisms but less explosive. It was observed that the grouted prism began to crack at loads of between 70% to 75% of ultimate load.

The observed failure mode of prisms reinforced with confinement wire was by long cracks which started in the top or bottom blocks at about 45% to 55% of ultimate load. Unlike the sudden failure of the ungrouted and unreinforced grouted prism, the failure of prisms built with helical confinement was more ductile.

In 1980 Sturgeon et al [24] carried out an investigation of reinforced concrete block masonry columns at the University of Alberta. Forty three concentrically loaded, sixteen eccentrically loaded columns and forty seven prisms were manufactured and tested up to failure. The columns were 1.83 m high and 400 mm square in cross-section. The columns were constructed using 400 x 400 x 200 mm single core pilaster units and tested under three different eccentricities of t/12, t/6 and t/3.

The mortar mix used in constructing all the columns and prisms was 1:¼:4 (cement:lime:sand) mix by volume. Full mortar bedding was used and a joint

of 10 mm was maintained throughout. Five concrete mixes with 28 day moist cured cylinder design compressive strengths of 35, 28, 17.5, 17.5 and 10.5 N/mm^2, and slumps of 150, 125, 100, 225 and 100 mm were used. The effect of slump on the behaviour and strength of masonry columns was evaluated by testing two columns grouted with a mix designed with the same strength of 17.57 N/mm^2 and a different slump of 100 mm and 225 mm.

The columns were designed to have three percentages of longitudinal reinforcement, 0.76, 1.3 and 2.6% based on the gross cross-sectional area of the column. Where longitudinal steel was required, lateral ties were wired directly to the steel and all the reinforcement was then placed in the column unit. For those columns constructed without vertical reinforcement but with grout and lateral ties, the horizontal reinforcement was placed within the mortar joint of the cross-section. Five different types of lateral ties were used, with all ties fabricated from 6 mm diameter plain steel. The longitudinal steel varied between two grades, viz. 400 and 600 N/mm^2 yield stress.

The mode of failure of the ungrouted columns was sudden, complete and explosive. Vertical cracks were only observed at the block face centres at the top of the specimen. These propagated down several courses just prior to column collapse.

The failure of grouted columns containing no lateral reinforcement was similar to ungrouted columns. Vertical splitting of the shell originated at block face centres in the upper courses well in advance of column collapse. Subsequent loading elongated and widened these cracks until overall splitting of the shell and crushing of the concrete core occurred. Fewer

grouted columns failed by simultaneous overall vertical splitting of the masonry shell and concrete core. In general columns containing a high strength concrete core failed explosively and those with a low strength concrete core settled gradually under the load. In the grouted columns containing lateral reinforcement in the mortar joints, vertical cracking occurred just prior to failure originating in the upper courses at the column corners rather than at the block centres. In addition, the lateral ties tended to confine the block shell and prevent explosive spalling of the shell at failure. In general, in all the grouted unreinforced columns tested, the shell-core interface bonding in the failure zone was completely broken, and the masonry shell could be easily removed in order to view the concrete core. The reinforced columns with lateral ties having 90^{o} hooks and 65 mm extensions were constructed with 0.76% vertical reinforcement. The failure of these columns was characterised by simultaneous splitting of the shell, crushing of the core, and buckling of the vertical reinforcement between the tie spacing. In these failures the tie hooks did not pull. The ties provided adequate support for the vertical reinforcement and prevented buckling from occurring over more than one course. In contrast to this behaviour, these ties did not adequately restrain buckling for the higher percentages of vertical reinforcement. The tie hooks were pulled to form an angle of about 120^{o} and in extreme cases a number of tie hooks were pulled out completely allowing bars to buckle over as many as five courses. This resulted in rather explosive failures for these columns regardless of concrete core strengths. Columns constructed with lateral ties using 135^{o} hooks and 100 mm extensions did not pull out even for the higher percentages of longitudinal reinforcement, and restricted buckling to the lateral tie spacing. Because of this, confinement failure was not as sudden and distress to the core and shell was not as extensive in the failure zones.

In all the reinforced columns, cracking originated at the column corners in the upper courses in advance of column failure and extended down vertically as loading continued. The authors reported that failure in all the columns occurred within the upper half of the column. To establish whether or not this was due to the end conditions, six columns were selected at random and tested in an inverted position. Five of these six columns failed in their lower half. It was therefore concluded that the location of the failure zone in the column upper region was due to the presence of weaker concrete in the upper core as a result of bleeding and segregation during pouring and vibration. In view of the observations reported, the authors suggested use of the following tie details for masonry columns:

(1) For concrete block masonry columns constructed with 400 x 400 x 200 mm pilaster units, 6 mm diameter plain steel should be avoided for fabrication of the lateral ties. Not less than 10 mm diameter deformed lateral ties were recommended where 32 mm diameter plain bars are used as recommended in ACI 318-77 for reinforced concrete.

(2) Where 6 mm diameter plain bars are used it is recommended that 135^{o} bends plus a minimum of 100 mm extensions be employed. If 90^{o} bends plus 65 mm extensions are used, the overlapping extensions should be tack welded to prevent pulling out. In order to reduce distress to the column shell, mortar joint lateral reinforcement should be provided to assist those ties in contact with the vertical reinforcement in confining lateral expansion of the core and maintaining concrete core and shell integrity.

(3) A vertical tie spacing of 200 mm is insufficient to prevent buckling of the vertical reinforcement before yield is attained, and is

recommended for masonry columns constructed with units which permit a reduced spacing.

(4) It is suggested that lateral tie hooks should be positioned at different corner bars. Positioning lateral tie hooks along one vertical reinforcement bar creates a line of structural weakness in the column.

The increase in ultimate strength of the concentrically loaded columns was found to be directly proportional to the increase in concrete strength. The authors presented the following theoretical equation:

$$P_{uc} = \frac{[0.85f'_c A_c + 0.7f'_{mpn} A_{shell}]}{1000} \qquad .....(2.3)$$

where

P_{uc} = Column ultimate load, kN

f'_c = Standard concrete cylinder compressive strength, N/mm^2

f'_{mpn} = Plain prism net area compressive strength, N/mm^2

A_{shell} = Masonry shell area, mm^2

The strength of grouted columns containing lateral reinforcement was 8% to 28% greater than equivalent ungrouted columns. The strength of columns fabricated with a longitudinal reinforcement percentage of 0.76% and steel of grade 400 N/mm^2 yield were consistently higher than those with the same longitudinal percentage but a steel grade of 600 N/mm^2 yield. This suggests that the deformational characteristics of grade 400 N/mm^2 yield steel are more compatible with the masonry shell and concrete core. Other steel grades were not examined for higher percentages of longitudinal reinforcement. The yield strain in the longitudinal reinforcement was reached in only one of the columns tested. The contribution of the vertical

reinforcement to the ultimate strength of masonry columns was generally expressed as:

$$P_S = \frac{E_S A_S}{700} \qquad .....(2.4)$$

where

P_S = Load carried by vertical reinforcement, kN

E_S = Elastic modulus of steel reinforcement, kN/mm^2

A_S = Cross-sectional area of longitudinal reinforcement, mm^2

The authors suggested the following empirical equation to predict the ultimate strength of concentrically loaded, short, reinforced concrete block masonry columns fabricated with materials, dimensions, and workmanship similar to those used in their study:

$$P_{uc} = \frac{0.85\, f'_C(A_C - A_S)}{1000} + \frac{E_S A_S}{700} \qquad .....(2.5)$$

For eccentrically loaded columns, the failure mode characterised by explosive removal of the column block shell on the compression face was peculiar to columns with eccentricities of t/12 and t/3, regardless of concrete strength, grade and percentage of vertical reinforcement. This mode was characterised by an explosive removal of the column block shell on the compression face, with subsequent crushing of the concrete core and buckling of the compression longitudinal steel. Columns loaded with an eccentricity of t/3 all failed by local crushing either in the bottom or the top course. The loading plates for the large eccentricities did not provide an adequate transfer of load to the tension face of the column. The authors proposed an ultimate strength design procedure for eccentrically loaded

masonry columns similar to the one recommended by the ACI 318-77 for eccentrically loaded reinforced concrete columns. The column was analysed as a reinforced concrete column of strength and dimensions equal to the core.

In 1986 Al-sarraf, Faiyadh and Khalaf [25] tested a total of seventeen short reinforced block masonry columns 1.27 m in height, constructed of 400 x 200 x 200 mm low strength 2-core concrete hollow blocks. The columns, axially loaded to failure, were divided into two series, viz. one block and two block cross-sections with vertical reinforcement which varied from 0.6% to 4.26%. Two different lateral ties were used, 6 mm diameter plain and 10 mm diameter deformed bars. The block strength was 9.90 N/mm^2, the mortar strength was 13.65 N/mm^2 and the grout strength, 17.25 N/mm^2, respectively.

The general mode of failure for all the masonry columns was essentially by compression. At 40% to 50% of the ultimate failure load, cracking occurred at different locations in the column. The cracks continued to propagate in both the mortar and the blocks. Failure resulted from crushing with outward deflection of the masonry shell at different positions in the column accompanied by outward buckling of the vertical reinforcement between the lateral ties. The core remained in position with high internal disruption. The masonry compressive strength, f'_m, was calculated using methods A and B in the ACI Standard Code for Masonry Structures (ACI-531R-79). Method A evaluates f'_m on the basis of the strength of the block unit and the type of mortar, method B relates the value of f'_m to the actual prism test.

The results showed that columns reinforced with plain ties 6 mm in diameter and 10 mm deformed bars showed a reduction of 40% in the ($P_{test}/P_{cal.}$) ratio of experimental and calculated failure load. Results also showed that columns reinforced with three bars in each bundle gave much lower ($P_{test}/P_{cal.}$) ratios than the two bar-bundled columns. The authors concluded that the minimum diameter of lateral steel tie used in reinforced masonry columns should be 10 mm diameter which is exactly the value recommended by the ACI Standards for reinforced concrete. So the range of diameters for vertical reinforcement recommended by the ACI Standards (ACI 318M-83) for reinforced concrete can be used for reinforced masonry columns. Due to difficulties in the compaction of 2-core concrete blocks, it is practical to lower the 4% maximum steel ratio for concrete to 3% for blockwork masonry.

In 1991 Khalaf [26] tested forty one axially loaded short blockwork masonry columns to determine their strength and study the mechanism of failure. The columns were constructed from full-block 390 x 190 mm and half-block 190 x 190 mm cross-sections and all were six courses high with a slenderness ratio of 6.26. Details of a typical masonry column are shown in Fig. 2.5.

One type of mortar 1:¼:3 (cement:lime:sand) and one type of concrete infill 1:3:2 (cement:sand:aggregate) were used, with a mortar joint of 10 mm. The block at the base of each column was a bond beam type in which the end shells and mid-web had been removed to make it possible to clear the mortar droppings after construction, and to assist in fixing the vertical reinforcement to the first lateral tie under the column. The full-blocks had 20 mm wide by 20 mm deep grooves to accommodate the lateral ties. Ties were placed in every course during construction of the columns.

Twelve of the forty one full and half-block columns were unreinforced. These were tested either unfilled or filled under axial load to determine the short term static modulus of elasticity. The remaining columns were divided into the following four series for both full and half-block columns: first, a series with three different lateral ties, 6, 8 and 10 mm in diameter, with no vertical reinforcement, to study the effect of lateral tie confinement on the strength and behaviour of masonry columns. Second, a series of columns reinforced with different percentages of vertical reinforcement, 1.7% and 5.3% for the full-block; and 1.98% and 5.4% for the half-block and with different lateral ties 6, 8 and 10 mm in diameter, to assess the most efficient lateral tie to be used in blockwork masonry columns. Fourth a series of columns with 8 mm lateral ties and different percentages of vertical reinforcement, 0.42%, 1.7%, 3.4% and 5.3% for the full-block columns; and 0.56%, 1.3%, 1.8%, 3.5% and 5.4% for the half-block columns, to study the effect of changing the percentage of vertical reinforcement on the strength and behaviour of masonry columns.

The unfilled prisms showed a greater tendency to split longitudinally along the block end shells. In most of the filled columns, crushing of concrete at one of the mortar joints occurred after failure. The mode of failure was less abrupt than for the unfilled columns. Some signs of cracking were observed at the block end and side shells at 80% and 90% of the ultimate load.

The columns reinforced with 6 mm and 8 mm diameter lateral ties only displayed a different mode of failure to the filled unreinforced columns. The concrete core remained intact even after the block shells crushed and had deformed outward. The failure was more ductile, without complete collapse

at ultimate load, as in the case of unreinforced columns. Some signs of block shell cracking was observed at 80% to 90% of the ultimate load. Full-block columns reinforced with 10 mm diameter lateral ties showed premature splitting of the block side shells and crushing of the concrete cores. This may have been caused by some stress concentration as a result of using ties of larger diameter. Columns, reinforced with different percentages of vertical reinforcement only, displayed an abrupt mode of failure at ultimate load with buckling of the vertical bars. This caused an explosive failure of the block shells followed by complete disintegration of the columns.

Columns reinforced with the same percentage of vertical reinforcement and different diameters of lateral ties showed similar modes of failure for the three diameters of lateral ties used. The failure was dominated by localised block shell crushing and outward deformation at one or two courses and not throughout the column height as with the other columns. This was due to the constraint on the vertical bars buckling between the lateral ties. The concrete core remained intact despite the fact that all the blocks crushed and deformed outward. The failure was more ductile with no complete collapse at ultimate load. The vertical bars buckled to the outside between the lateral ties at the final stage of loading. Block shell cracking was observed at 80% to 90% of the ultimate load.

The columns, reinforced with 8 mm lateral ties and different percentages of vertical reinforcement, showed the same mode of failure as those reinforced with different diameters of lateral tie and the same percentage of vertical reinforcement as discussed previously.

The full-block columns, reinforced with 6 mm and 8 mm lateral ties and with no vertical bars, showed increases in the strains recorded over 4-courses of 25.1% and 19.1% compared to those for filled unreinforced columns. The strains recorded over 4-courses for columns reinforced with 10 mm lateral ties showed a decrease of 17%, compared to those for filled unreinforced columns. The decrease in strain may be due to the high tensile splitting stresses concentrated around the lateral ties near the block mid-webs. This resulted in premature splitting of the column side shells. These high splitting stresses are the result of the size of the lateral ties used.

The major conclusions derived by the author from the results of strain measurements for both full and half-block columns were:

(1) All columns reinforced with hot rolled deformed high yield 8 mm diameter lateral ties, recorded higher strain values than those columns reinforced with 6 and 10 mm diameter lateral ties.

(2) The values of the average strain recorded on the vertical bars for all the columns tested are almost half the yield strain of the vertical bars.

(3) The values of the average strain recorded on the horizontal ties are small compared to the yield strain of the ties.

The results showed that the compressive strength of the unreinforced half and full-block columns based on gross area decreased by 12.9% and 33.5% compared to unfilled columns based on net area. The strength of the unfilled, full-block columns showed a decrease of 25.2% compared to the half-block columns. This was due to differences in the aspect ratio, l/t, and the mortar bedded area between the full-block columns. The results showed that the compressive strength of full-block columns, reinforced with 6 and 8 mm lateral ties and vertical bars, increased by 17.7% and 17.6%

respectively compared to the filled unreinforced columns. The columns reinforced with 10 mm diameter lateral ties failed at a compressive strength which was 8.3% less than that for filled unreinforced columns. The increase in column strength can be attributed to the confinement of the concrete infill by the lateral ties. These confinement stresses cause a reduction in the harmful tensile stresses exerted on the block shells by the concrete and are not a result of an increase in the concrete strength.

The results showed that for columns reinforced with the same vertical reinforcement and 8 mm lateral ties, the experimental values of ultimate load gave the most consistent increases in strength compared to filled unreinforced columns. Columns reinforced with different vertical reinforcement and ties 8 mm in diameter also showed a steady increase in the column ultimate load, P_u, as the percentage of vertical reinforcement increased. This behaviour is similar to that for reinforced concrete columns.

In order to calculate the ultimate load of block masonry columns the author proposed the following formula:

$$P_u = \frac{\left(f'_m (A_g - A_s) + \frac{f_y}{2} \times A_s\right)}{1000} \qquad .....(2.6)$$

where

P_u = Ultimate load of blockwork masonry column, kN

f'_m = Ultimate compressive strength of blockwork masonry, N/mm^2

A_g = Gross cross-sectional area of specimen, mm^2

A_s = Area of vertical reinforcement, mm^2

f_y = Yield strength of reinforcement, N/mm^2

The contribution of the vertical reinforcement to the ultimate load of blockwork masonry columns was assumed to be based on half the yield strength of the vertical bars, f_y. The contribution of the lateral ties, which were 17.6% and 4.4% in the cases of full and half-block columns respectively, was ignored in this calculation.

2.2.3 Enhancement of Compressive Strength f'_m for Eccentrically Loaded Blockwork Prisms

In 1983 Drysdale and Hamid [27] tested two hundred and twenty block masonry prisms under eccentric compressive loads, where the eccentricity was varied from 0 to $\frac{5t}{12}$. The objective was to study the effects of grouting, percentage of solid, block size and strength on the relative capacity of masonry prisms.

The concrete blocks used to construct the test specimens were selected from eight different types of blocks. The compressive strength was determined by testing sulphur capped half-blocks. One mortar type, with 1:½:4 (cement:lime:sand) proportions, and three types of grout: weak, normal and strong with block moulded compressive strengths of 13.7, 21.1 and 41.0 N/mm^2, were used.

Small walls 790 x 1590 mm were constructed using only face shell mortar joints. The blocks were grouted with grouts with a slump of 250 mm. Three block high prisms were made from parts of the walls using a diamond saw cut at each head joint. Three specimens were produced each one a half-

block long with a height to thickness ratio of 3. The specimens were tested under eccentric loads with pin/pin end conditions.

The ungrouted specimens tested with 0 and t/6 eccentricities showed splitting of the webs prior to face shell splitting. The grouted specimen tested with a t/6 eccentricity, failed by crushing on the compression side along with tensile debonding of the mortar at the tension side. With eccentricities of t/3 and $\frac{5t}{12}$ cracking occurred along the mortar joint on the tension side prior to compression failure on the opposite side. The specimen tested with an eccentricity of t/3, failed by spalling on the compression face of the block.

The test results indicated that block strength was not a significant factor in the relative decrease in capacity with increased eccentricity of loading. The change in type of grout did not result in significant changes in relative strengths. An increase of nearly 200% in grout strength produced an increase 6 to 17% in the ultimate load depending on the eccentricity.

In studying the effects that changes in the percentage of solid area of block have on the relationship between strength capacity and eccentricity it was found that this variable was an important factor.

The decrease in capacity with increase in eccentricity was similar for solid and for grouted masonry. It was found that the size of the unit, with similar proportions, is not a significant factor when the eccentricity ratio of loading is varied.

The ultimate compressive stress at the extreme fibre of a concrete block masonry unit increased slightly indicating that the strain gradient has little or no effect on the failure of the relatively thin face shells of a hollow block. Solid units, on the other hand, showed significant increases in the extreme fibre ultimate compressive stress with increased eccentricity indicating an increased strain gradient.

In 1987, Khalaf [39] conducted an experimental and analytical investigation using two and three dimensional finite element analyses for axially and eccentrically loaded single block specimens, also two block prisms loaded in a direction parallel to the unit bed face. Approximate methods were recommended to determine values of f'_m, and ultimate strain, ε_m, to be used in the design of masonry elements.

Five concrete filled single block and eleven two block prisms with different mortar type and concrete infill were tested axially under a load applied parallel to the unit bed face. The observed mode of failure for the single blocks was first, by local crushing at the inner face of the block legs, followed by shearing near the legs, with lateral deformation of the block shells, and finally by complete disintegration of the specimen. The axially loaded two block prisms showed two modes of failure. The first mode was by local crushing at the inner face of the mortar joints, followed by shearing and lateral deflection of the block shells at the mortar joints. The second mode was similar to the first mode, but serious tensile cracks were observed at the centre of the webs near the unfilled void between the blocks. The mode of failure depends on the mortar compressive strength. Test results showed that the single block specimens failed at loads which were 34% less than those for the block material. This reduction was attributed to

differences in the deformation characteristics of the concrete infill block material. The concrete infill is subjected to large lateral expansion due to the increase in Poisson's Ratio towards ultimate strength.

Four concrete filled two block prisms were tested under eccentric loading with an eccentricity of t/6 and using pin/pin end conditions. The mode of failure was essentially by crushing and lateral deflection of the block shell at the mortar joint. There was little evidence of tensile cracks at the centre of the webs near the mortar joints. Vertical cracks were observed between the masonry and the concrete infill.

The eccentrically loaded two block prisms constructed with mortar of lower strength, 17.8 N/mm^2, failed at a load 17% below the average strength of prisms built with a mortar of higher strength, 23.6 N/mm^2. The author suggested that the mortar has an important role in determining the strength of prisms loaded in a direction parallel to the bed face. On the other hand no difference was found in the strength of prisms constructed using concrete infills the strengths of which differed by 45%.

The maximum compressive strength for the eccentrically loaded prisms was calculated using an idealised compressive stress distribution for the 10 mm mortar joint obtained from the average stress-strain curves for the axially loaded prisms. The stress on the tension side was assumed to be zero. Plain sections were assumed to remain plane. The prisms show a 4% increase in strength compared to axially loaded prisms with high mortar strengths. This increase was attributed to the strain gradient effect.

The results from the three dimensional stress analysis agreed with the test results for the eccentrically loaded prism, but gave higher elastic vertical stresses at the inner face of the mortar joints rather than the outer face.

2.2.4 Summary and conclusions

A certain amount of research has been carried out on reinforced masonry columns in order to study the strength and behaviour of brickwork and blockwork masonry columns. From this work it is apparent that the strength and type of column failure of brickwork masonry columns was affected by factors such as the properties of mortar, the strength of unit brick, the percentage of vertical reinforcement, the shape and position of lateral ties, the slenderness ratio and the load eccentricity.

On the other hand relatively little research work has been conducted on blockwork masonry columns using one or two core hollow blocks. The detailing of lateral ties, diameter, type and location of the ties within the columns, the type, the percentage and distribution of vertical reinforcement as well as the strength of both mortar and concrete infill were found to be significant factors affecting the strength and type of failure of blockwork masonry short columns. Additionally load eccentricity had a marked influence on these characteristics.

Quite recently it was established that the contribution of vertical reinforcement to the ultimate load of reinforced blockwork masonry columns was achieved by developing no more than half the yield strength of the vertical bars.

In previously published work on solid, unfilled and filled hollow block prisms tested under eccentric compressive loads it was found that the compressive strength at the extreme fibre of solid and filled masonry prisms increased significantly indicating an amplification of strain gradient. However the strain gradient was found to have little or no effect on the failure of the unfilled prisms.

Against this background it was felt that further investigations should be undertaken to establish:

(a) The compressive strength and behaviour of blockwork masonry prisms.

(b) A new method of predicting the ultimate strength of reinforced blockwork masonry columns subjected to axial and eccentric loads.

The main objectives of this study have already been outlined in more detail in chapter 1.

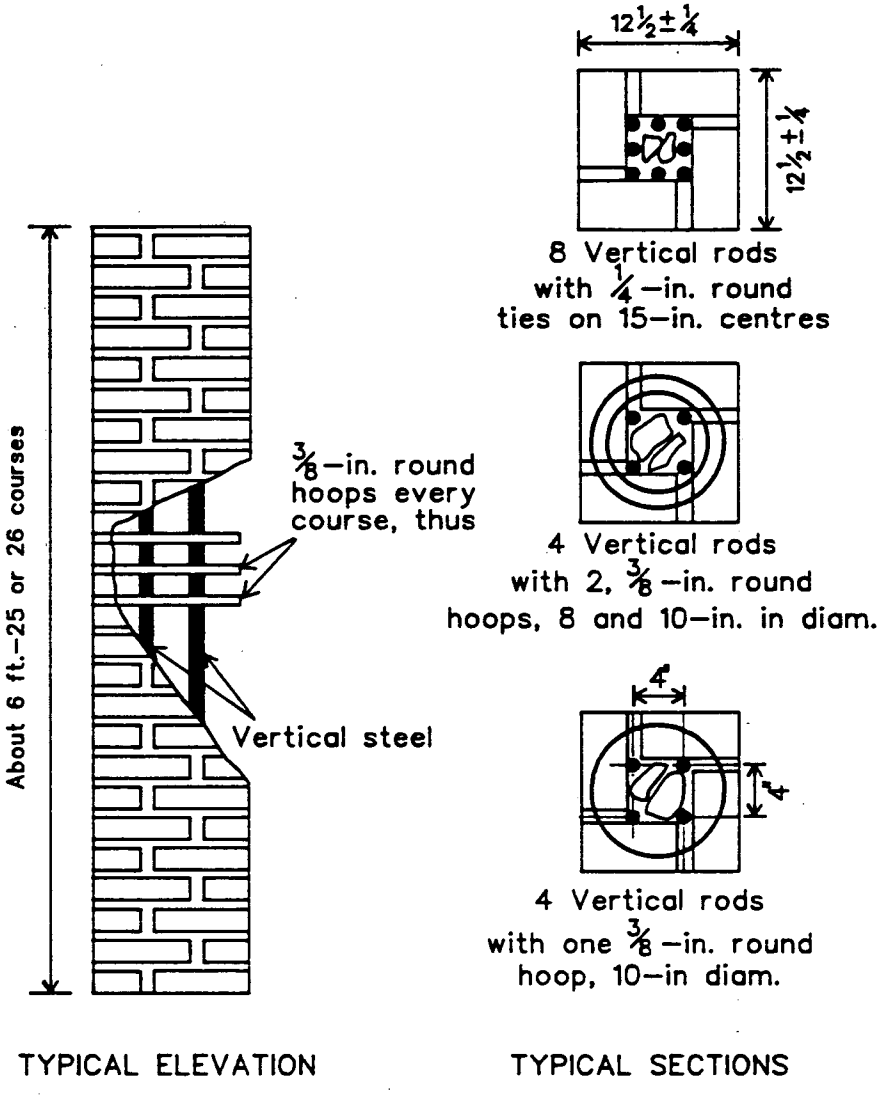


Fig. 2.1 Typical details of columns tested by Withey (13)

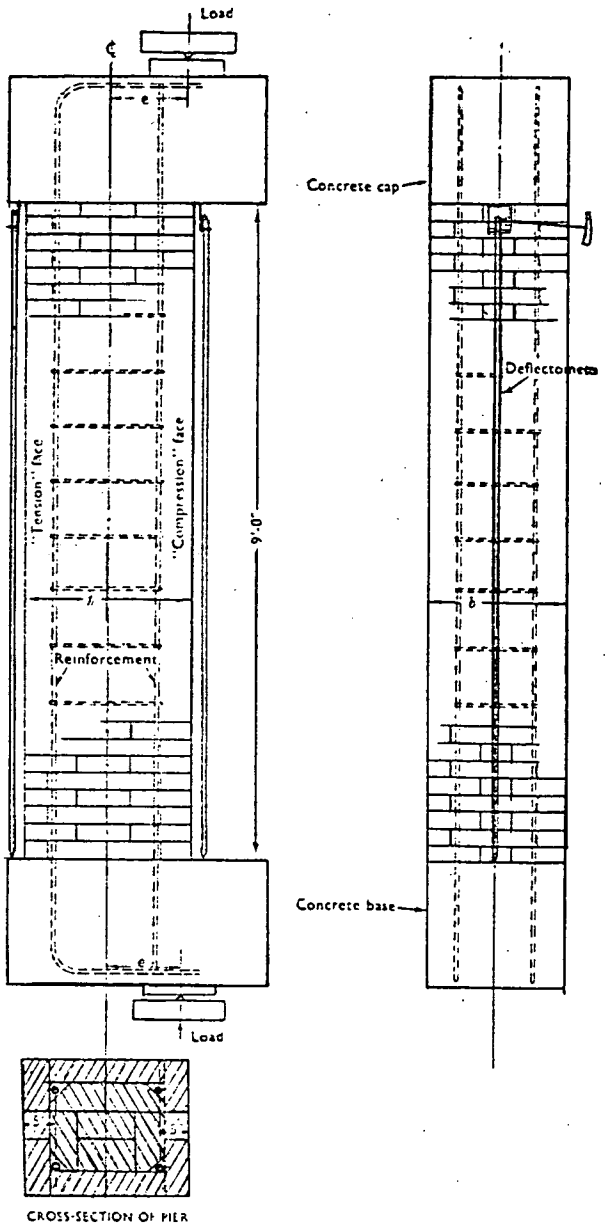


Fig. 2.2 Typical pier in Davey and Thomas [14] tests

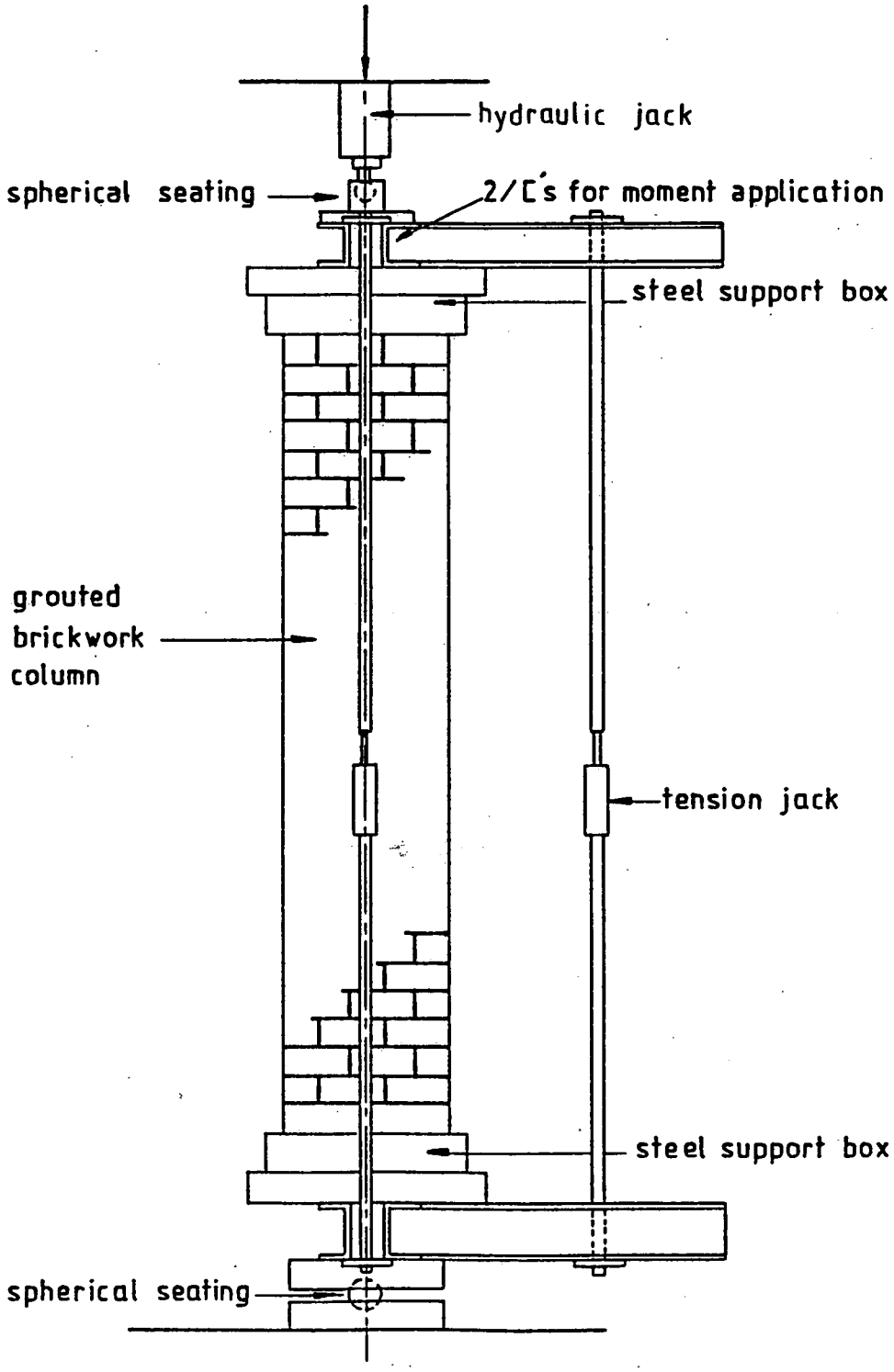


Fig. 2.3 Typical test setup for columns tested by Eltraify (19)

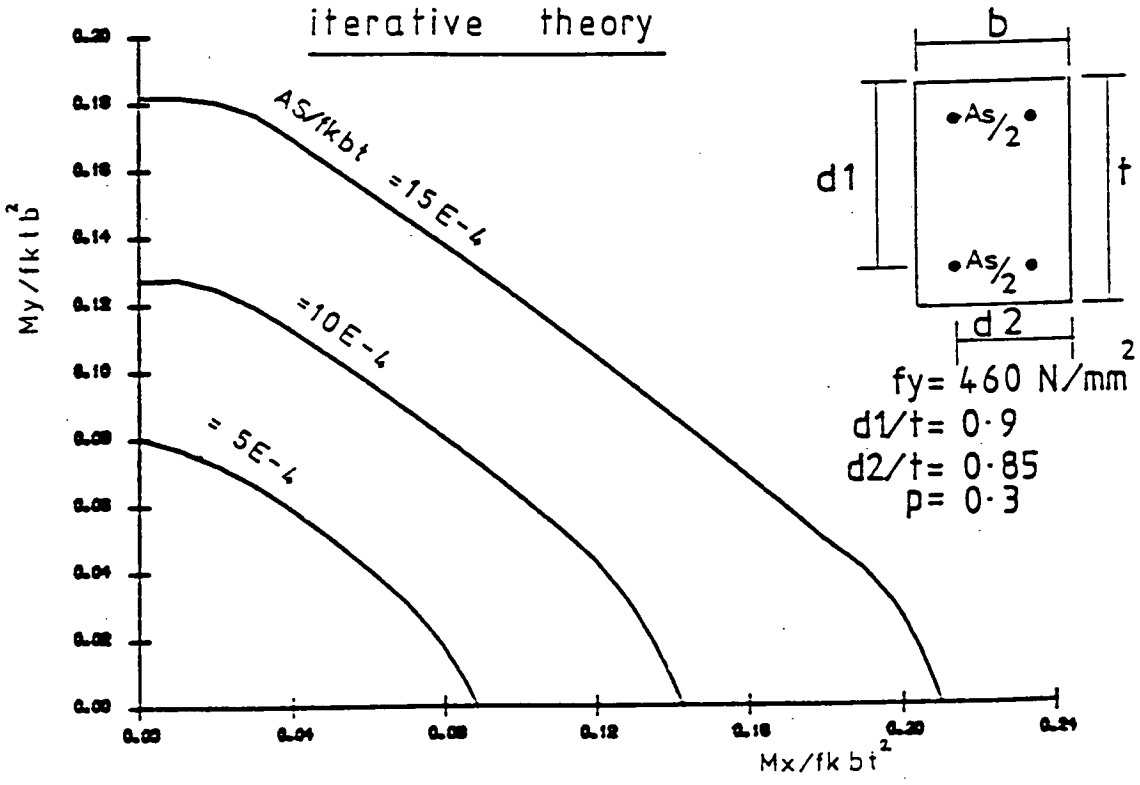


Fig. 2.4 Typical interaction diagrams obtained by Eltraify [19] for a typical rectangular section

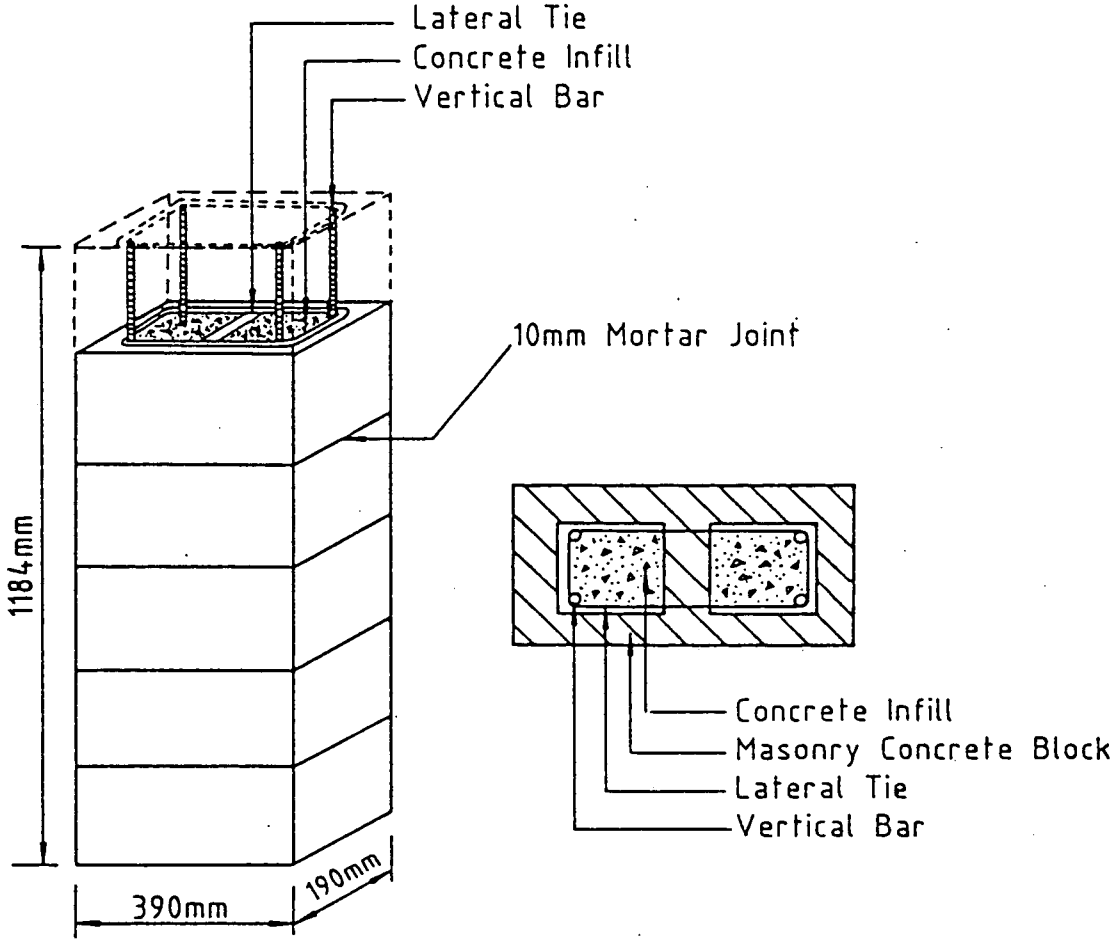


Fig. 2.5 Typical details of columns tested by Khalaf (26)

CHAPTER 3
MATERIAL MECHANICAL PROPERTIES

3.1 INTRODUCTION

This chapter deals with the determination of the mechanical properties of all the materials used in constructing the prisms and the columns. The mechanical properties obtained were used in the theoretical analysis of this study. The materials used in this investigation consist of four component materials: concrete blocks, concrete infill, mortar and steel reinforcement. Only one type of each component was used throughout this study. British Standard BS 5628: Part 2: 1985 [10] specifies that when masonry is built with hollow concrete blocks and the vertical cavities are filled completely with in-situ concrete, the value of f_K should be obtained as if the blocks were solid, provided that the characteristic cube strength of the infill is not less than the compressive strength of the blocks, assessed on their net area. Where the infill concrete is less strong than the concrete in the block, the characteristic compressive strength of the masonry should be obtained as if the blocks were solid and of compressive strength equal to the cube strength of the infill concrete. Both the American and Canadian Masonry Codes [8] [9] specify that the grout strength should not be less than the strength of the block unit.

3.2 CONCRETE BLOCK

The dimensions of the hollow concrete blocks used in this study are given in Table 3.1. The supplied blocks were manufactured from two batches having the same mix proportions. A number of solid blocks cast from the same batch having the same dimensions as the hollow blocks were also

supplied. Solid blocks from the same mix as the hollow blocks were sawn to produce 190 x 190 x 190 mm cubes. The cubes were then tested in compression and the average compressive strength of the cubes adjusted to specimen size [30]. The cube strength of the block material , f_b, was then determined. To determine the mechanical properties of the hollow block, three hollow block prisms were tested. Each prism consisted of three half-block units with 1 - 2 mm dental plaster joints inserted between the half-blocks as well as the machine plates and the prism. The dental plaster mix was achieved by mixing dental plaster with water in plastic bags to the required workability. The area of each bag was chosen to be slightly larger than the area of the specimen. The specimen was adjusted using a building level and four pieces of wood between the testing machine and its spherical head to prevent the machine head from rotating. The soft dental plaster was pressed by the machine head to accomplish the desired thickness. After 10 -15 minutes setting of the plaster occurred and the four pieces of wood were removed. The strains on the vertical and horizontal axis of the specimen were measured using two axis 20 mm electrical strain gauges mounted on two opposite sides at the prism-mid height. The stress-strain relationship was recorded by a data logger up to prism failure. Figure 3.1 shows a three unfilled half-block prism separated and capped by a thin layers of dental plaster joints.

The mechanical properties of the solid blocks were determined by testing a solid full-block cast from the same mix as the hollow block. The solid block was compressed parallel to the bed face. Two axis (vertical and horizontal) 20 mm electrical strain gauges were mounted on two opposite faces at the mid-height of the block to measure the strains on the vertical and the horizontal axis. The stress-strain relationship was then recorded by a strain

data logger throughout the test up to block failure.

3.3 MORTAR

A high strength mortar, with 1:¼:3 (cement:lime:sand) proportions batched by volume and mixed with water to a suitable workability, was used in the construction of all the prisms and columns used in this study. Portland cement was used throughout. The mortar mix was designed to confirm to designation (i) in BS 5628. The sieve analysis was carried out in accordance with BS 812: Part 1: 1975 [31], and is given in Table 3.2. The mortar sand falls within the grading conforming to BS 1200: 1976 [33] requirements. Three 102 x 102 x 102 mm and three 200 x 100 mm cylinders were cast with each batch, cured in a water tank and tested in compression after 28 days.

The mechanical properties of the mortar were determined by testing three 102 x 102 x 102 mm steel moulded cubes stacked vertically separated by a thin layer (1 - 2 mm) of dental plaster using the same method as for the hollow blocks. Figure 3.2 shows a three mortar cubes prism separated and capped by thin layers of dental plaster joints.

In order to compare the results for the three 102 mm cubes, mortar cylinders were tested to determine their mechanical properties. The strains were measured using 20 mm electrical strain gauges and recorded by a data logger.

Another method of determining the mechanical properties of the mortar was to test two block prisms constructed with a 10 mm mortar joint between, as employed by Khalaf [26][58]. Three prisms were constructed from two half-

blocks left under polythene sheeting for 14 days to allow the mortar to gain in strength, then cured further under laboratory conditions. After 28 days two of the specimens were tested in axial compression.

Two axis (vertical and horizontal) 10 mm electrical strain gauges were mounted on the mortar joint at two opposite sides of the third prism. The gauge positions were first marked, cleaned, filled with concrete adhesive, then left for 24 hours. The surface was then levelled, cleaned and the gauges bonded and wired. The vertical and horizontal strains were recorded using a computer strain logger throughout the test until failure.

3.4 CONCRETE INFILL

One type of concrete infill was used to fill all the hollow blocks of the columns and prisms investigated in this study. A medium strength mix, 1:3:2 (cement:sand:aggregate) batched by volume, was used. The water content was adjusted to provide a concrete of high slump, 150 mm. Ordinary Portland cement was used in all mixes.

The sieve analyses for the sand and 10 mm single size crushed aggregate used in the concrete mix were performed in accordance with BS 812: Part 1: 1975 [31] and are given in Tables 3.3 and 3.4 respectively. The results are in agreement with the requirements of BS 882: 1983 [32]. With each batch of concrete more than three 102 x 102 x 102 mm cubes and 200 x 100 mm cylinders were cast, cured in water and tested in compression after 28 days.

The mechanical properties for the concrete infill were determined by testing three 102 x 102 x 102 mm steel moulded cubes. The cubes were stacked vertically and separated by a thin layer (1 - 2 mm) of dental plaster. These

were prepared by the same method used for determining the mechanical properties of the mortar and hollow blocks. The strains were measured by two axis (vertical and horizontal) 10 mm electrical strain gauges mounted on two opposite sides of the middle cube. A strain data logger was used to record the vertical and horizontal strains throughout the test up to failure.

3.5 STEEL REINFORCEMENT

Hot rolled deformed high yield steel bars conforming to BS 4449: 1978 [34] were used to construct the reinforced blockwork columns. A uniaxial tension test was conducted to determine the yield and ultimate tensile strength of the reinforcement. Three samples of the steel bars were tested for each diameter. The strains were measured using post-yield electrical strain gauges fixed at the mid-length of the bars, and recorded by a computer strain logger. Table 3.5 shows the values of Young's Modulus, yield strength, yield strain and ultimate tensile strength obtained for each bar diameter.

3.6 SINGLE BLOCKS

Full and half-block filled and unfilled specimens were tested up to failure to determine their compressive strength. Two high slump concrete infills with a mix of 1:3:2 and 1:2:2 (cement:sand:aggregate) proportions were used to fill the blocks. The concrete was placed in two layers.

Each layer was compacted by a steel rod, as used in compacting concrete cubes and cylinders. Three 102 x 102 x 102 mm cubes and three cylinders were cast from the same mix and left in a water tank. Ordinary Portland cement was used throughout. The filled concrete blocks were left under polythene sheets for 14 days to cure, then removed and left to cure under

ambient laboratory conditions. After 28 days, the cubes, cylinders and filled blocks were tested in axial compression until failure. The mechanical properties of the single block filled and half-block filled and unfilled were determined by testing specimens with two axis (vertical and horizontal) 20 mm electrical strain gauges mounted on two opposite faces of the blocks. The positions of the gauges were first marked, cleaned, filled with concrete adhesive, then left for 24 hours. They were then bonded and wired. The specimens were capped with a thin layer (1 - 2 mm) of dental plaster, then prepared by the method used to determine the mechanical properties of the hollow blocks. A strain data logger was used to record the vertical and horizontal strains throughout the test. The rate of loading was in accordance with BS 6073: Part 1: 1981 [36]. The load pattern was in accordance with BS: 1881 Part 121: 1983 [35] to enable the determination of the static modulus of elasticity.

Table 3.6 summarises the results of the compressive strengths of single full and half-blocks compressed normal to the bed face.

3.7 THREE BLOCK PRISMS

A total of eighteen 3-course high prisms, nine full and nine half-block prisms were tested using one type of mortar and two types of concrete infill. In each set of nine prisms three were filled with a medium strength concrete mix, 1:3:2 (cement:sand:aggregate) proportions, three with a high strength concrete mix, 1:2:2 (cement:sand:aggregate) proportions and three prisms were left unfilled.

All the prisms were constructed by an experienced mason using a high strength mortar mix, 1:¼:3 (cement:lime:sand) proportions with 10 mm

horizontal mortar joints. The prisms were cured under polythene sheeting to enable the mortar joints to gain strength. A concrete mix of high slump, 150 mm, was used to fill the prisms. The concrete was placed in two layers, each of which was compacted using a 25 mm poker vibrator until full compaction was achieved. The prisms were then left to cure under polythene sheeting for 14 days. The polythene was then removed and the specimens were then cured for a further 14 days under ambient temperature in the laboratory. Steel moulded cubes and cylinders were cast from the same mixes, cured in a water tank, then tested in compression after 28 days. The mechanical properties of the concrete infill and the mortar were determined by testing three 102 x 102 x 102 mm steel moulded cubes stacked vertically. These were prepared and tested by the same method as described in sections 3.3 and 3.4 for the mortar and concrete materials respectively.

All the prisms were loaded axially to determine their ultimate compressive strength. The filled and unfilled full-block specimens were tested in a steel rig. The load was applied by two 2MN capacity jacks through a 150 mm thick steel bearing plate. The filled and unfilled half-block specimens were tested in an Avery Universal testing machine with a capacity of 1MN.

For each set of three specimens, one was tested with no strain gauges, one fitted with demec points and one fitted with electrical strain gauges. Demec points and electrical strain gauges were glued in identical positions both sides of the specimen 24 hours prior to testing.

Prior to testing, the specimens were capped with a thin layer, (1 - 2 mm) of dental plaster [28], prepared by the same method as used in section 3.2.

The loading rate was in accordance with BS 6073: Part 1: 1981 [36]. The load pattern was in accordance with BS: 1881 Part 121: 1983 [35] to enable the determination of the static modulus of elasticity.

Table 3.7 summarises the results of the compressive strengths for all unfilled and filled full and half-block 3-course high prisms.

3.8 SUMMARY AND DISCUSSION OF TEST RESULTS

Table 3.8 summarises the mechanical properties of the material used in constructing both the prisms and the columns.

The compressive stress-strain curves for three unfilled half-block prisms separated and capped with 1 - 2 mm dental plaster layer are shown in Fig. 3.3. The figure also shows the three compressive stress-strain curves for the single unfilled half-block curve, the solid block compressed parallel to the bed face curve, and the idealised curve for the concrete block which was derived from the following equations given by BS 8110: Part 2 [37] for rigorous analysis of non-critical sections as:

$$f = 0.8 f_{cu} \left(\frac{kn - n^2}{1 + (k-2)n} \right) \qquad \text{.....(3.1)}$$

$$n = \frac{\varepsilon}{\varepsilon_{c,1}} = \frac{\varepsilon}{0.0022} \qquad \text{..... (3.2)}$$

$$k = \frac{1.4 \varepsilon_{c,1} E_o}{f_{cu}} = \frac{3E_o}{f_{cu}} \qquad \text{..... (3.3)}$$

where

f = Compressive stress in concrete or block material, N/mm^2

f_{cu} = Characteristic cube strength of concrete or block material, N/mm^2

E_o = Modulus of Elasticity of the concrete, kN/mm^2

ε = Strain in the concrete or block material

$\varepsilon_{c,1}$ = Strain in the concrete or block material at maximum stress

The above equations were applied to establish the idealised compressive stress-strain curve for the concrete infill shown in Fig. 3.5. Figure 3.5 also shows the stress-strain curves for a concrete cube, obtained by testing three cubes separated by (1 - 2 mm) thick layers of dental plaster, and for a concrete cylinder.

The vertical-lateral strain curves for the concrete blocks and concrete infill are given in Figs 3.4 and 3.6 respectively.

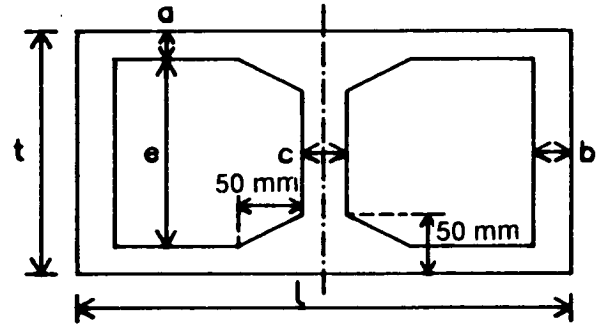
Figure 3.7 shows the compressive stress-strain curve of a confined 10 mm mortar joint, as well as the curves for three mortar cubes separated by (1 - 2 mm) thick dental plaster layers, and for a mortar cylinder. The vertical-lateral strain curves for mortar are given in Fig. 3.8.

The stress-strain curves for high strength mortar show that the cylinders and cubes reached higher strength values than the unfilled 2-course high half-block prism constructed with a 10 mm high strength mortar joint.

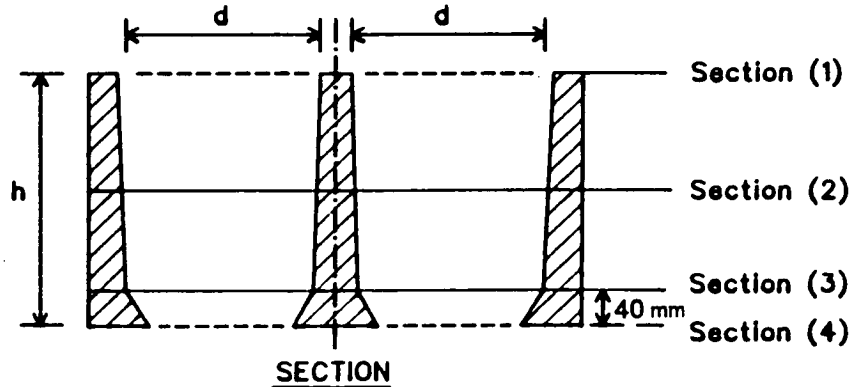
Table 3.1 Dimensions of typical concrete block

Section	Length l (mm)	Thickness t (mm)	a (mm)	b (mm)	c (mm)	d (mm)	e (mm)
(1)	390 (190)	190	33	30	55 (22.5)	124	137.5
(2)	390 (190)	190	35	33	59 (24.5)	120	132.5
(3)	390 (190)	190	36	34	61 (25.5)	118	130.5
(4)	390 (190)	190	47	47	81 (35.5)	96	107.5

Values in brackets are for a half-block.
Block height h = 189 mm



TOP VIEW



SECTION

Table 3.2 Sieve analysis of mortar sand

Test Sieve	% by weight passing BS Sieve	
	Test Results	BS:1200 Limit Table (1) type S Sand
6.30 mm	100	100
5.00 mm	100	98 -100
2.36 mm	98	90 -100
1.18 mm	94	70 -100
600 μm	87	40 -100
300 μm	51	5 -70
150 μm	12	0 -15
75 μm	3	0 - 5

Table 3.3 Sieve analysis of concrete sand

Test Sieve	% by weight passing BS Sieve	
	Test Results	BS:882 Limit Table 5
10.0 mm	100	100
5.00 mm	98	89 -100
2.36 mm	93	60 -100
1.18 mm	87	30 -100
600 μm	83	15 -100
300 μm	49	5 -70
150 μm	10	0 -15

Table 3.4 Sieve analysis of 10 mm single size crushed aggregate

Test Sieve	% by weight passing BS Sieve	
	Test Results	BS:882 Limit Table 4
14.00 mm	100	100
10.00 mm	96	85 -100
5.00 mm	18	0 -25
2.36 mm	1	0 - 5

Table 3.5 Mechanical properties of steel reinforcement

Bar Diameter (mm)	Area (mm^2)	Yield Strength (N/mm^2)	Yield Strain (%)	Ultimate Strength (N/mm^2)	Young's Modulus (kN/mm^2)
8	50.27	527.1	0.26	622.6	204
10	78.54	520.7	0.27	637.8	204
20	314.16	534.7	0.28	647.1	196

All bars are hot rolled deformed high yield steel bars conforming to BS4449:1978.



Table 3.6 Compressive strength of single blocks compressed normal to bed face

Block Type	Mix Proportions by Volume	Number of Tests	Average Compressive Strength (N/mm^2)		Infill Average Cube Strength (N/mm^2)
			Net Area	Gross Area	
		Single Full-Block*			
Unfilled	-	3	28.64	16.11	-
Filled	1:3:2	3	-	18.29	21.25
Filled	1:2:2	5	-	22.22	26.66
		Single Half-Block**			
Unfilled	-	3	30.78	16.96	-
Filled	1:3:2	3	-	19.89	21.25
Filled	1:2:2	5	-	24.29	26.66

*Net area = 41700 mm^2 (Area at section 1, Table 3.1)
Gross area = 74100 mm^2 (390 x 190 mm)
**Net area = 19900 mm^2 (Area at section 1, Table 3.1)
Gross area = 36100 mm^2 (190 x 190 mm)

Table 3.7 Compressive strength of 3-course high prisms

Prism Type	Mix Proportions by Volume	Number of Tests	Average Compressive Strength (N/mm^2)		Average Cube Compressive Strength (N/mm^2)	
			Net Area	Gross Area	Mortar	Concrete Infill
			Full-Block Prisms*			
Unfilled	-	3	21.91	12.33	22.40	-
Filled	1:3:2	3	-	13.71	22.40	21.25
Filled	1:2:2	3	-	14.69	22.40	26.66
			Half-Block Prisms**			
Unfilled	-	3	25.93	14.29	22.40	-
Filled	1:3:2	3	-	14.73	22.40	21.25
Filled	1:2:2	3	-	16.60	22.40	26.66

*Net area = 41700 mm^2 (Area at section 1, Table 3.1)
Gross area = 74100mm^2 (390 x 190 mm)
**Net area = 19900mm^2 (Area at section 1, Table 3.1)
Gross area = 36100mm^2 (190 x 190 mm)

Table 3.8 Mechanical properties of material

Material	Specimens or Cube Strength (N/mm^2)	Cylinder Strength (N/mm^2)	Three Cubes Specimen Strength (N/mm^2)	Tangent Modulus of Elasticity (N/mm^2)	Secant** Modulus of Elasticity (N/mm^2)	Poisson's Ratio	
						Zero Stress	Maximum Stress
Solid block	24.69	-	-	18160	15410	0.18	0.25
Prism+	19.09	-	-	35340	29050	0.14	0.19
Unfilled Single Half-Block	29.14	-	-	37446	37012	0.14	0.18
Mortar 1:¼:3	27.20	26.05	23.50	14814 13539*	11718 11034*	0.18	0.25
10mm Mortar Joint 1:¼:3	-	-	-	6129	4054	-	-
Concrete Infill 1:3:2	22.75	17.18	16.40	17379 17248*	13529 14766*	0.16	0.24
Steel	-	-	-	See Table 3.5	-	0.30	-

**The secant modulus of elasticity at 2/3rd the maximum compressive strength of specimens.
*Modulus of Elasticity obtained from cylinder tests.
+Unfilled three half-block prism with 1 - 2 mm dental plaster joints.



Fig. 3.1 Three unfilled half-blocks separated and capped with 1- 2 mm dental plaster joints

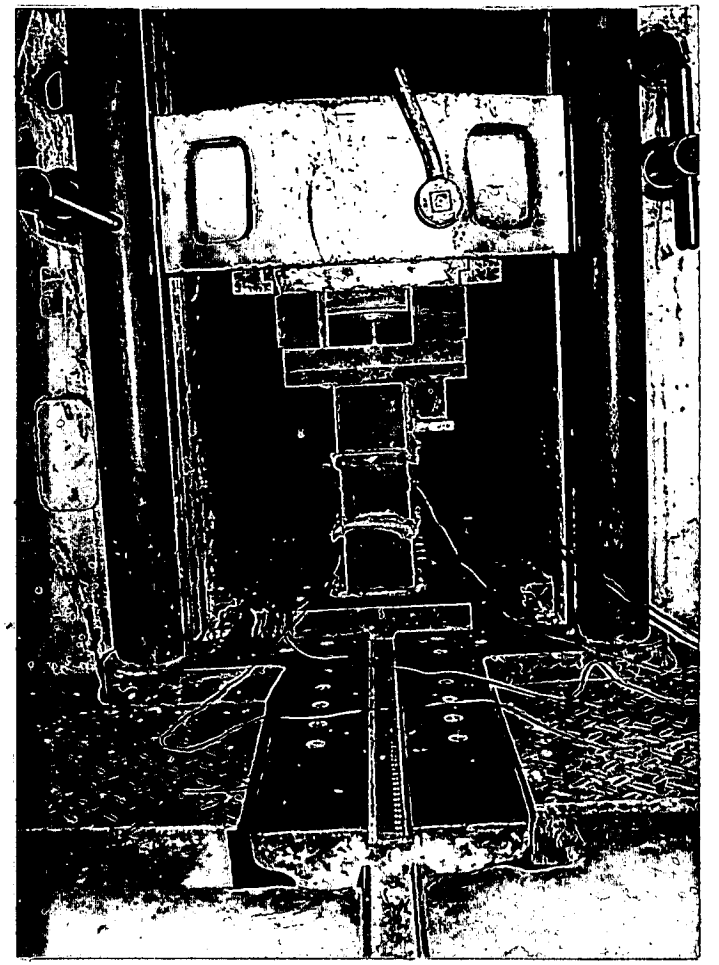


Fig. 3.2 Three steel moulded mortar cubes separated and capped with 1- 2 mm dental plaster joints

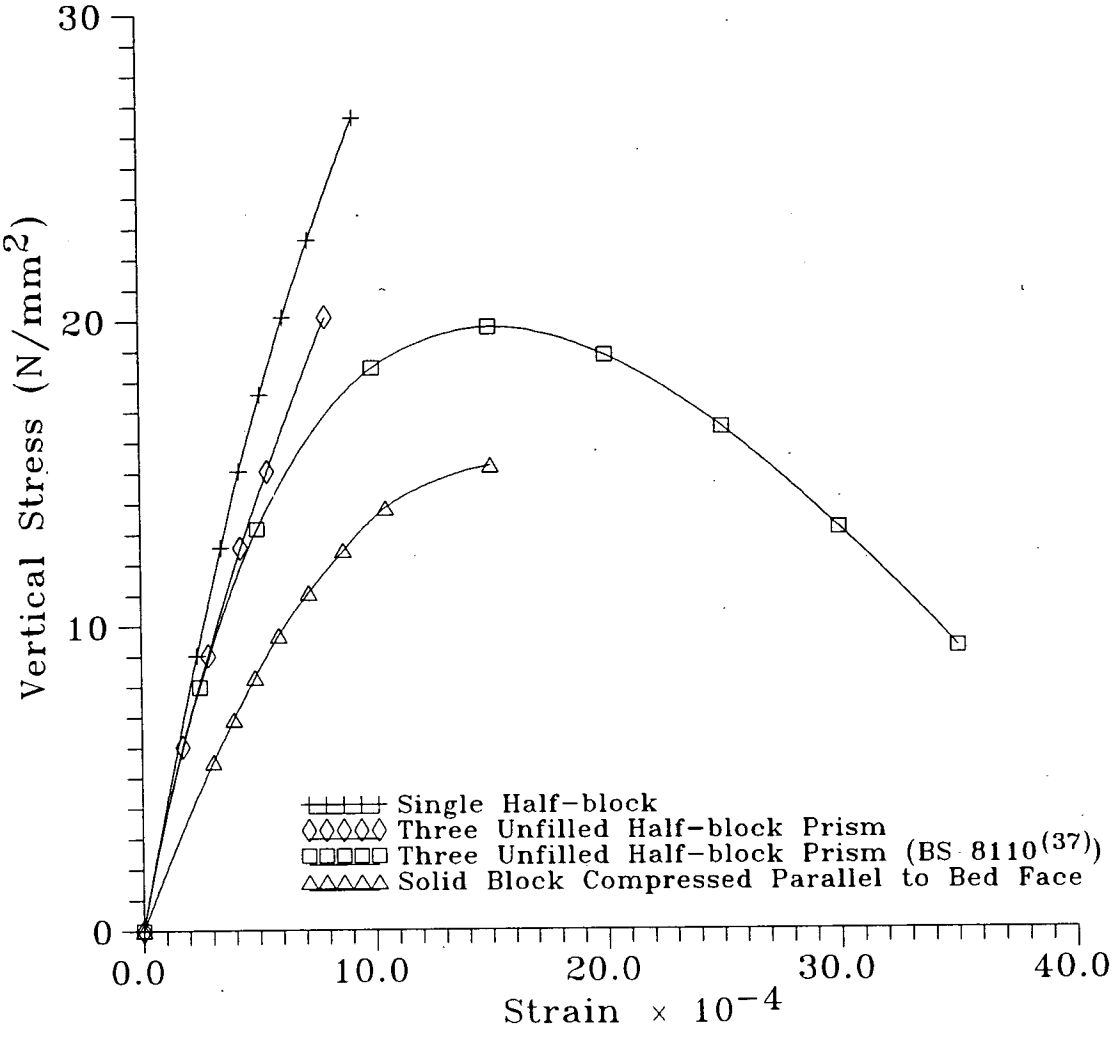


Fig. 3.3 Compressive stress-strain curves for block material

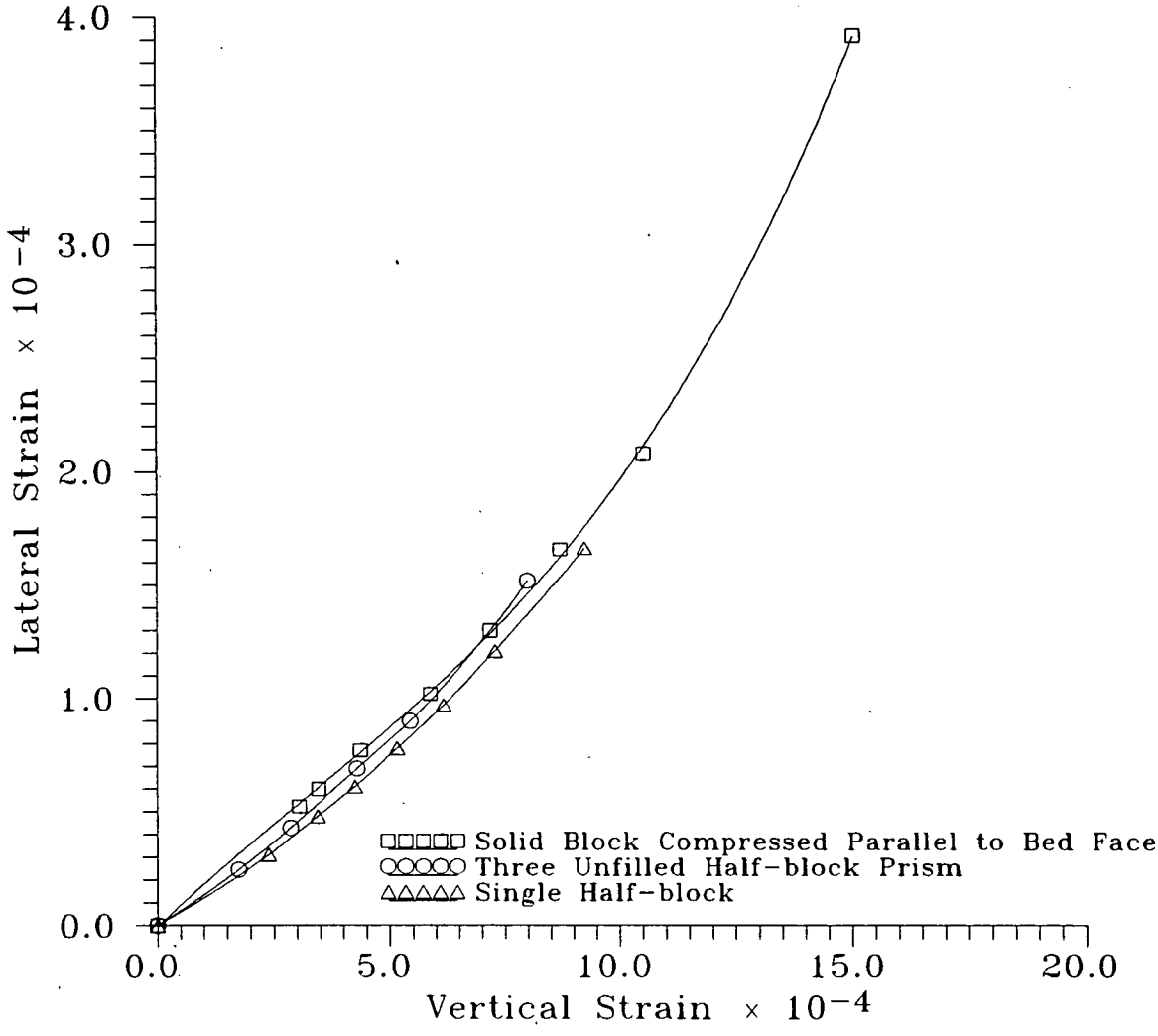


Fig. 3.4 Lateral strain–vertical strain curves for block material

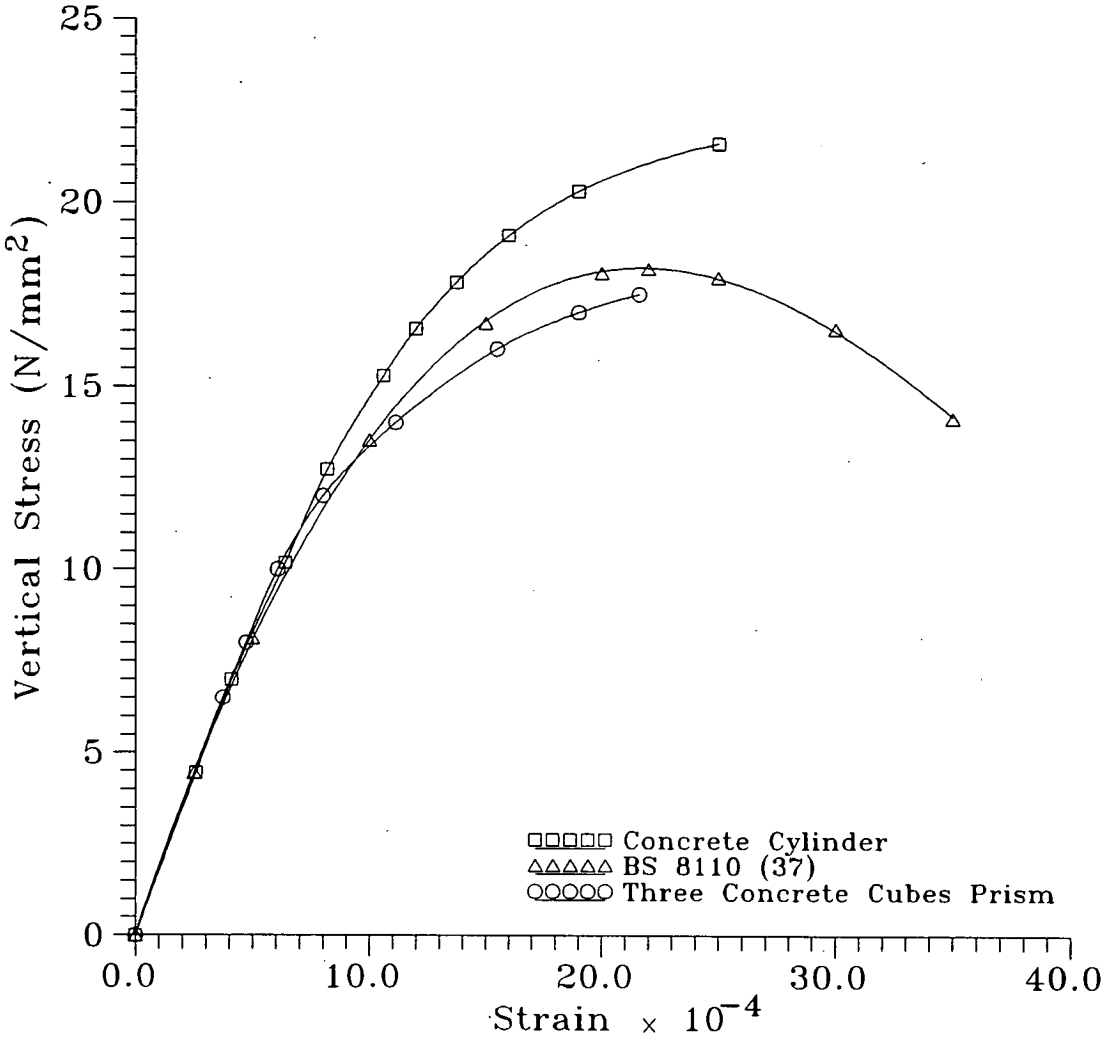


Fig. 3.5 Compressive stress strain curves for concrete

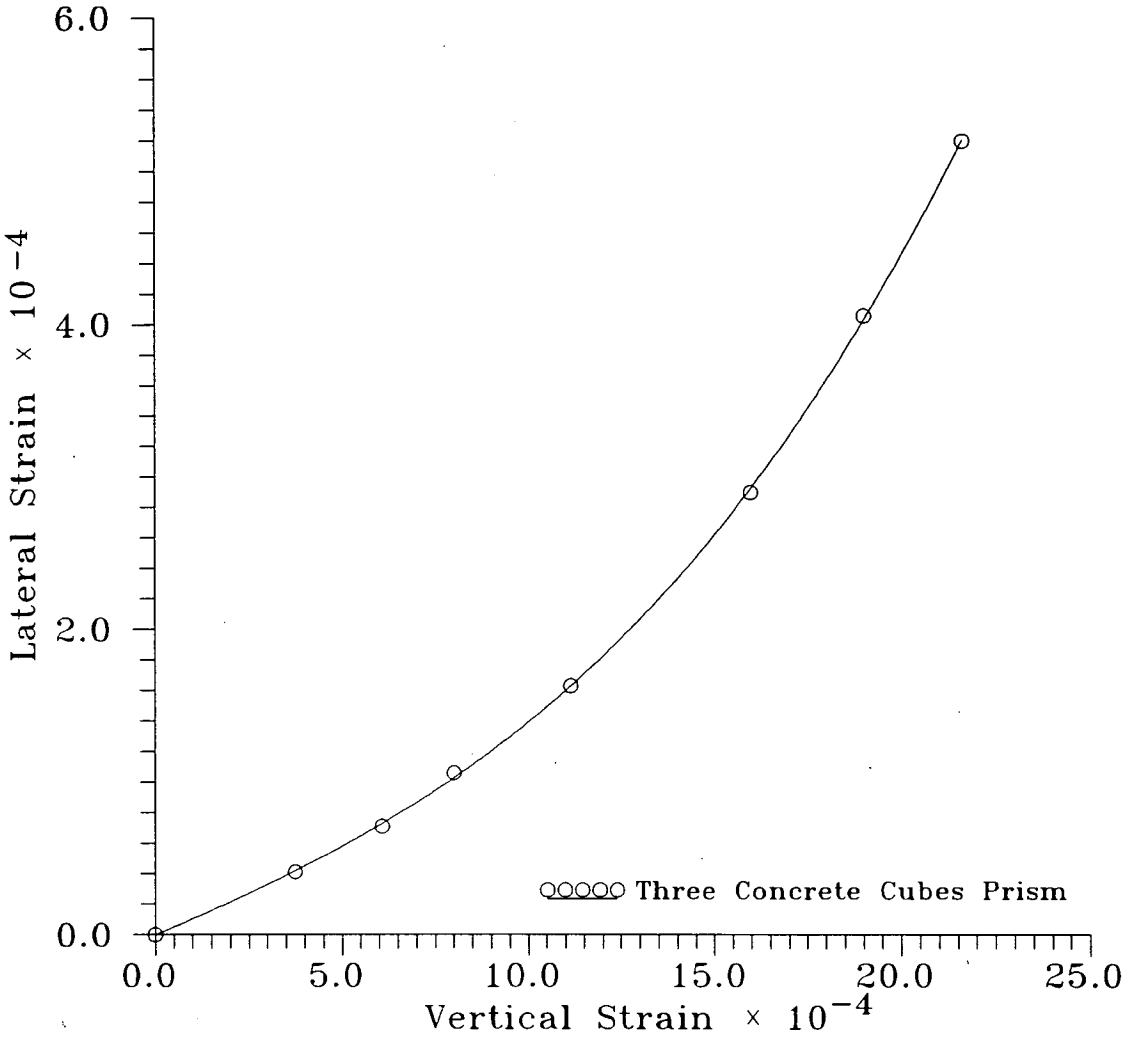


Fig. 3.6 Lateral strain–vertical strain curve for concrete

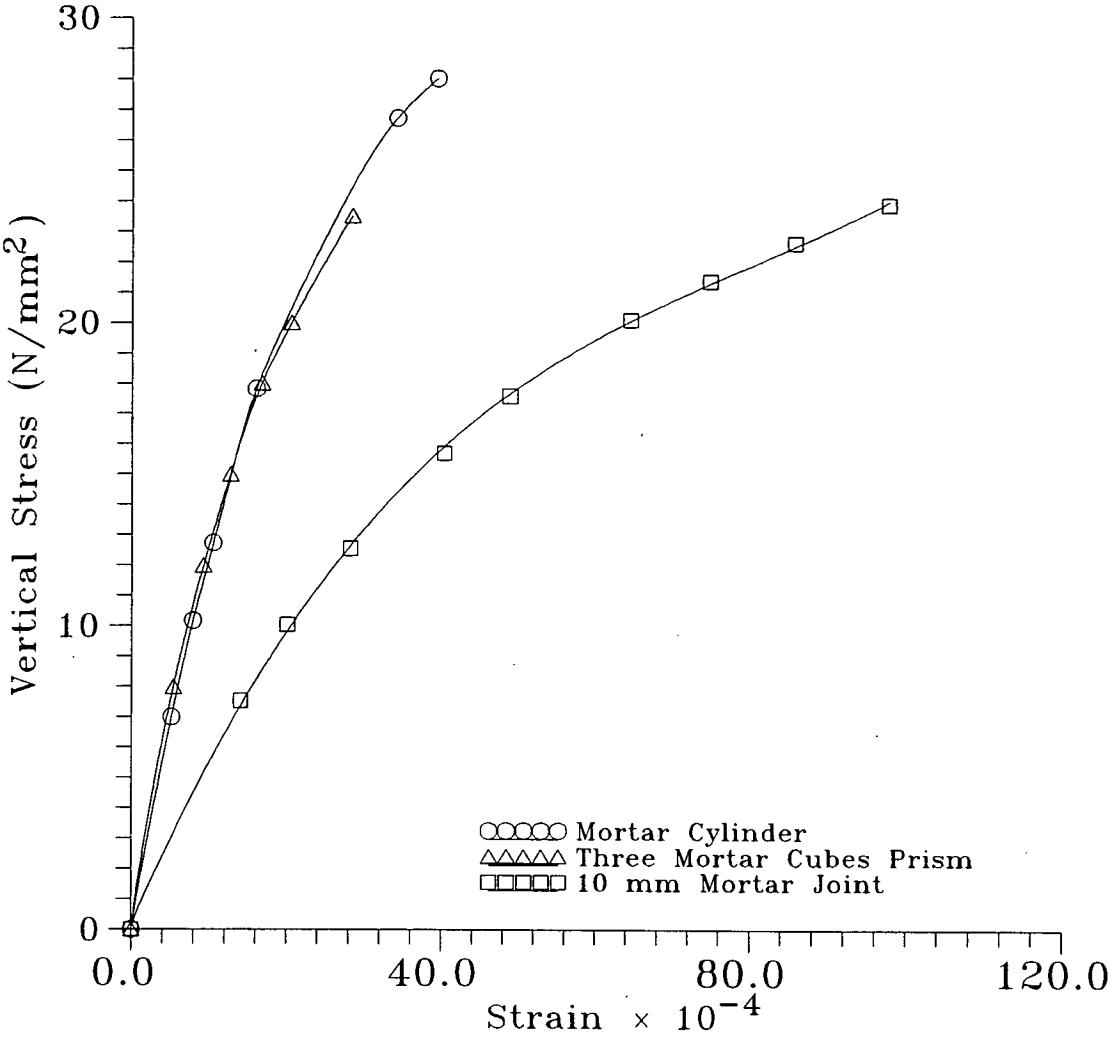


Fig. 3.7 Compressive stress–strain curves for mortar

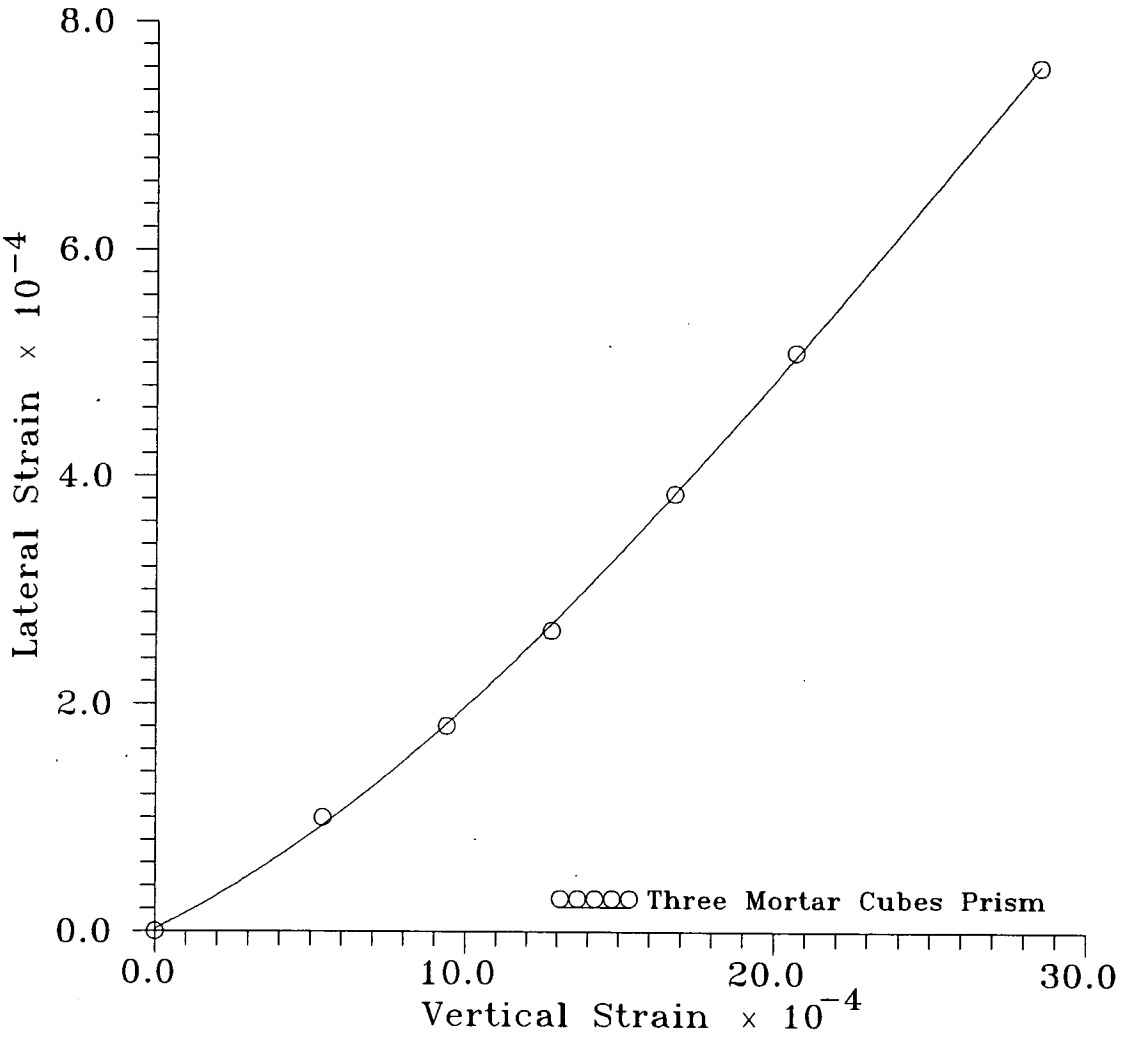


Fig. 3.8 Lateral strain–vertical strain curve for mortar

CHAPTER 4

CONCENTRICALLY AND ECCENTRICALLY LOADED CONCRETE BLOCK MASONRY PRISMS

4.1 INTRODUCTION

This chapter presents the results of an experimental and theoretical investigation carried out to study the behaviour and to determine the ultimate compressive strength, f'_m, of blockwork masonry prisms.

Thirty five full and half-block 4-course high prisms were tested consisting of eighteen prisms with concrete infill and seventeen without. The effect of the strain gradient caused by the eccentricity on f'_m was studied by adopting two different eccentricities, t/6 and t/3. All the prisms tested were modelled and analysed using a finite element analysis program.

Previous researchers [27][28][44][45] who tested eccentrically loaded brickwork and blockwork masonry prisms noted an increase in the compressive strength of masonry compared with prisms loaded axially. This increase in the compressive strength of masonry, f'_m, was attributed to the strain gradient.

4.2 EXPERIMENTAL PROGRAMME

4.2.1 Specimen Construction

A total of seventeen full and eighteen half, 4-course high blockwork masonry prisms were tested using one type of mortar and one type of concrete infill. The prisms were constructed by an experienced mason using 10 mm

horizontal mortar joints between the concrete blocks, and a high strength mortar mix, 1:¼:3 (cement:lime:sand) proportions. The prisms were cured under polythene sheeting to enable the mortar joints to gain in strength. After four days, nine full and nine half-block prisms were filled with medium strength concrete, proportions 1:3:2 (cement:sand:aggregate) and batched by volume to produce a high slump mix of 150 mm. The fill was laid in two layers, each of which was compacted using a 25 mm poker vibrator until full compaction was achieved. The prisms were then left to cure under polythene sheeting for fourteen days, after which the polythene was removed. The specimens were then cured for a further fourteen days under ambient temperatures in the laboratory prior to testing. Steel moulded cubes and cylinders were also cured in a water tank for twenty eight days, then tested in compression to determine the strength of both the mortar and concrete infill.

4.2.2 Strain Measurements

For each set of three specimens, two were tested without strain measurements. The third specimen was fitted with electrical strain gauges. For specimens tested under axial load, strains were obtained using two axis (vertical and horizontal) 10 mm electrical strain gauges mounted on two opposite sides at the mid-height mortar joint and at the centre of the two block faces. For specimens tested under eccentric loads, the strains were obtained using two axis (vertical and horizontal) 10 mm electrical strain gauges mounted at the compression side in positions similar to those described previously. Uni-axis (vertical) 20 mm electrical strain gauges were mounted at three equal distances across the specimen width and on the tension side at mid-height.

The gauge positions were first marked, cleaned, filled with concrete adhesive, then left for 24 hours. The surface was then cleaned and the gauges bonded and wired.

4.2.3 Capping

Prior to testing all the specimens were capped with a (1 - 2 mm) layer of dental plaster [28], prepared by mixing with water in plastic bags using an area slightly larger than the specimen's area to achieve the required workability. The same method of capping was used as explained in chapter 3 to determine the mechanical properties of the blockwork. The dental plaster layer fills out any surface irregularities providing a smooth level surface between the specimen and the steel plates.

A load of 10% of the ultimate load of the specimen was applied and the dental plaster left to set for a period of 10 -15 minutes.

4.2.4 Testing Procedure

Five full blocks, two unfilled and three filled prisms were tested under axial compression. The load was applied by two 2MN capacity jacks through a 150 mm thick steel bearing plate to ensure uniformity. The remaining thirty prisms were tested in an Avery Universal testing machine with a capacity of 1MN.

After positioning the specimen in the testing machine, the strain measuring devices were connected to a data logger. A builder's level was used to check the specimens vertically. In each set of three specimen, two were

tested to failure without measuring strains and one was tested using electrical strain gauges.

All the specimens were tested at a loading rates in compliance with BS 6073: Part 1: 1981 [36]. For prisms with strain gauges, initial readings were taken at zero load. The load was then applied at the required rate until a stress of 0.5 N/mm^2 was reached, when the first set of readings were taken. The next set of readings were taken at a load corresponding to approximately one third of the ultimate prism stress, to calculate the Modulus of Elasticity in accordance with BS 1881: Part 121: 1983 [38]. For the axially loaded half block prisms the load was transferred from the machine base through 50 mm steel plates and across the capped ends to the prisms. A spherical ball seating head was used at the machine top head to allow the loading plate to be slightly off level when necessary.

Twenty four prisms, twelve full and twelve half-block were tested with eccentricities of t/6 and t/3 using pin/pin end conditions. For each load situation three unfilled and three filled prisms were tested. The test setup for the eccentrically loaded prisms is shown in Fig. 4.1. The load is transferred from the machine base through a continuously supported roller and steel bar, 25 x 12.5 mm cross-sectional area, and distributing the load along the length of the prisms through a 50 mm steel plate which spreads the load across the capped ends of the prisms. The same arrangement was used in the machine upper head except that for some half-block prisms (two prisms) the upper roller was replaced by a pinned spherical seat machine head.

4.3 THEORETICAL PROGRAMME

4.3.1 Introduction

The analysis of concrete masonry prisms composed of different materials, several degrees of freedom, and complex geometry mathematically is complicated. To solve problems of this type therefore approximate numerical methods must be used.

A general purpose finite element analysis (FEA) package, LUSAS[46], was selected for this investigation. The processing was carried out using a graphical interactive system, MYSTRO, (the graphics part within the LUSAS package has a capability of dealing with 2- and 3-dimensional linear and non-linear material properties problems). MYSTRO has a special facility which selects the different materials of the prism. This has the advantage of enabling the study of the stress distribution in each selected material separately.

4.3.2 Three Dimensional Finite Element Model

A 3-dimensional finite element model was developed using HX8, an eight node solid element with 24 degrees of freedom, and PN6, a six node solid element with 18 degrees of freedom.

To keep the size of the mesh to a minimum, the tapering of the face shells and webs was ignored and an average shell thickness assumed (see Table 3.1, section 2). Full advantage was taken of symmetry to minimise the mesh size. Figure 4.2 shows the meshes used to simulate the axially loaded full and half-block prisms. Only one quarter of the prism was therefore considered in the analysis.

For eccentrically loaded full-block prisms, half of the prism was considered. The same mesh was used to analyse the eccentrically loaded half-block prisms. Figure 4.3 shows the meshes used to simulate eccentrically loaded full and half-block prisms.

To take into account the boundary conditions due to symmetry, nodal points which fall on the symmetry axes were assumed to be free to move vertically, and fixed against horizontal movement. The following additional assumptions were made to simplify the mesh:

(a) A rigid interface between the blocks and mortar as the frictional forces created by compression prevent slipping [27][39][47][48][53].

(b) The concrete infill shrinkage can be ignored and a perfect bond assumed between the blocks and the concrete infill.

A previous study [26] showed that applying the compressive stress directly to the prism gave unrealistic results compared with prisms with steel bearing plates in between. As in the experimental tests, 50 mm thick steel bearing plates were used in modelling the top and base of the specimen. For any prism tested in the steel rig, namely the axially loaded full-block prisms, the whole of the surface of the specimen was assumed to be restrained against translation and rotation in the X- and Z-directions, and free to translate and rotate in the Y-direction while the bottom surface of the plate was assumed to be restrained against translation and rotation in all global directions. For any prism tested in the Avery machine, where the load was applied from the specimen's base upward, the whole base was assumed to be restrained

against translation and rotation in the X- and Z-directions and free to translate and rotate in the Y-direction, while the whole surface of the top bearing plate was assumed to be restrained against translation and rotation in the three global directions. The axial load was applied by means of uniform pressure. The face load was assumed to be applied at the nodes, acting on all elements connected to that node in the case of axially loaded prisms, and by a number of concentrated loads acting along the row of nodes at eccentricities equal to t/6 and t/3 in the case of the eccentrically loaded prisms. The maximum level of stress applied to the prisms was taken as the average compressive strength of the three specimens tested in the experimental part of the investigation.

The blocks, the mortar and the concrete infill were modelled as an elasto-plastic implicit backward Euler von Mises yield surface model, and for the unfilled prisms, the concrete infill elements were omitted from the element topology section.

The non-linear analysis section of LUSAS requires the input of the mechanical properties of each component material of the prism. These were obtained experimentally and given in Table 3.8. The non-linear analysis section requires also the input of the stress-strain curve of each material. These curves were approximated by a series of straight lines. The stress-strain curves used for the block material and the concrete infill were obtained from the equations given by BS: 8110: Part 2 [37] for rigorous analysis of non-critical concrete sections (equations 3.1, 3.2 and 3.3). The material compressive strength and modulus of elasticity used in the equations are given in Table 3.8. The compressive stress-strain curve for

the mortar material was obtained by testing unfilled two block prisms constructed with a 10 mm mortar joint and is given in Fig. 3.7.

Since the top and base steel plates remain elastic up to the maximum loading applied, the two 50 mm thick plates were modelled as a linear material. Table 4.1 gives details of the material properties used to develop the 3-dimension finite element model.

4.4 DISCUSSION OF EXPERIMENTAL RESULTS

In this section the observed modes of failure for the unfilled and filled full and half-block prisms loaded under axial compression at eccentricities of t/6 and t/3 are discussed. The experimental results obtained from testing prisms with and without strain measurements are also considered.

4.4.1 Modes of Failure

4.4.1.1 Concentrically Loaded Prisms

The mode of failure for all the unfilled prisms was a result of longitudinal cracking propagated along the block side shells during the final stage of loading, with consequent crushing and shearing of the block mid-web.

The mode of failure observed for all the filled full-block prisms was a result of longitudinal splitting along the block shells causing separation of the block shells from the concrete infill. Crushing of the concrete infill near to a mortar joint was noted in some prisms.

The unfilled half-block prisms failed as a result of longitudinal block splitting along the specimen. Shell cracking was noted prior to overall shell splitting.

The half-block filled prisms failed as a result of the block shells splitting from the concrete infill. The concrete infill exhibited a pyramid type of crushing Figs 4.4, 4.5, 4.6 and 4.7 show the different failures for the prisms discussed in this section.

4.4.1.2 Eccentrically Loaded Prisms with an Eccentricity of t/6

The unfilled full-block prisms failed by splitting along the block end shells and separation of the block shells around the two corners of the compression side of the prism. Crushing and shearing of the mid-web of the block also occurred on the compression side of the specimen.

The mode of failure for the filled full-block prisms compressed under eccentric load of t/6 is shown in Fig. 4.8. Longitudinal splitting along the block end shells and separation of the shells was observed at the two corners of the compression side of the prism. Crushing of the concrete infill was also observed.

The unfilled half-block prisms failed as a result of local crushing at the mid-mortar joint on the compression side followed by longitudinal cracking then splitting at the final stages of loading (Fig. 4.9).

The eccentrically loaded filled half-block prisms failed as a result of crushing on the outer face of the mid mortar joint on the compression side of the specimen followed by sudden crushing of the mid-joint of the two blocks located above and below the joint. Figure 4.10 show typical mode of failure for filled half-block prism compressed at t/6.

4.4.1.3 Eccentrically Loaded Prisms with an Eccentricity of t/3

The mode of failure observed for the unfilled full-block prism was a result of cracking along the mid-mortar joint followed by face shell splitting on the compression side of the prism.

The failure of the filled full-block prism was a result of cracking of the mid and upper mortar joints. Crushing of the block shells, the mid-web and the concrete infill occurred on the compression side of the upper half of the prism (Fig. 4.11).

The modes of failure observed for the unfilled and filled half-block prisms shown in Figs 4.12 and 4.13 were a result of cracking along the mid-mortar joint and the upper mortar joint on the tension side respectively, followed by debonding of the mortar from the block prior to a compression failure on the opposite side of the prism.

4.4.2 Experimental Results

The stress-strain curves for unfilled and filled full-block 4-course high prisms compressed under axial load are given in Figs 4.14 and 4.15. The curves shown are compressive stress-strain and vertical stress-lateral strain curves for the block and the mortar. The curves exhibit a decrease in the block stiffness of the filled prism compared to the unfilled one. This decrease in stiffness is due to the presence of the concrete infill with its high Poisson's ratio[26][39][40][41][42][43][47][49][50][51][52][53][57], compared to that for blocks, which produces tensile stresses in the block shells. As a result of

these high tensile stresses, failure of the prism occurs prior to it attaining the block strength.

Figures 4.16 and 4.17 show the stress-strain curves for unfilled and filled half-block 4-course high prisms under axial load. The curves are similar to those obtained for unfilled and filled full-block prisms. The reduction in the prism aspect ratio, l/t, from 2.05 for full block to 1.00 for the half-block prisms influences the overall shape of the curves, and the prism's ultimate strength.

The stress-strain curves for both unfilled and filled full and half-block prisms show that the mortar joints yield at a higher strain than for the block material, also that the mortar joint in the unfilled prism was more plastic than in the filled ones.

The difference in stiffness between the mortar and block created tri-axial compression stress in the mortar and bi-axial lateral tension stresses in the concrete block with axial compression. This led to a pulling apart of the block by the mortar due to the bonded connection between them[49], causing disintegration of the face shell or splitting on the webs throughout starting at the bed joint.

Figures 4.18 and 4.19 show the load-strain curves for the unfilled and filled 4-course high full-block prisms, loaded with an eccentricity of t/6. The block stiffness is less for the filled prisms compared to the unfilled prisms. Also the mortar joint at the extreme compression fibres of the unfilled prism showed more plasticity.

The load-strain curves for unfilled and filled half-block 4-course high prisms with an eccentricity of t/6 are given in Figs 4.20 and 4.21. The curves show that the stiffness of the block material is less for the filled half-block prism than for the unfilled prism. The mortar joint at the extreme compression fibre of the unfilled prisms show more plasticity compared to the filled prisms.

Figures 4.22 and 4.23 show the load-strain curves for unfilled and filled 4-course high full-block prisms loaded with an eccentricity of t/3. These show that the stiffness of the filled prism block material is less than the stiffness of the unfilled prism.

Figures 4.24 and 4.25 show the load-strain curves for unfilled and filled half-block 4-course high prisms loaded with an eccentricity of t/3. These show that the yield strain was reached on the mortar joint of the extreme compression side of the unfilled half-block prism. An increase in stiffness occurred at about three-quarters of the prism's ultimate capacity. This was caused by the deformation of the mortar joint. The figures show a decrease in the block stiffness of the filled prism.

Figure 4.26 shows the load-moment interaction diagrams for the unfilled and filled full and half-block prisms. The curves were plotted with axial load strengths as ordinates and moment strengths as abscissa. From the figure it can be seen that the axial strength decreased slightly for load eccentricities between 0 and t/6 in the cases of unfilled and filled full-block and filled half-block prisms, and between 0 and t/3 in the case of unfilled half-block prisms. The axial load strength is significantly decreased when the load

eccentricities are taken between t/6 and t/3 in the cases of the unfilled and filled full-block and filled half-block prisms.

Tables 4.2 and 4.3 summarise the results for the unfilled and filled full and half-block prisms tested in this investigation. The Tables showed that when the prism aspect ratio, l/t, changed from 2.05 (full-block) to 1.0 (half-block) the compressive strength, f'_m,was enhanced. The Table also showed that in all the eccentrically loaded prisms, except the unfilled full-block prisms compressed under eccentricity of t/6, the average compressive strength was higher than that of the prism's component materials.

The ultimate extreme fibre stress for eccentrically loaded prisms were calculated using three different methods. The first method, suggested by Khalaf [39], is based on an idealised stress vs strain curve for a 10 mm confined mortar joint, and assumes that the stress distribution in the prism's compression zone consists of the triangular and rectangular areas shown in Fig. 4.27. It also assumes that the failure occurred when the mortar reached yield at 0.75 of the prism's compressive strength. Yielding was assumed to occur at a compressive strain of 0.0048. The maximum value of strain was assumed to be 0.0096.

The second method was similar to the first except that it considers crack formation in the calculation of the ultimate stress. The moments of the forces was taken about the compression side to calculate the depth of the neutral axis. The depth of the cracks on the tension side was therefore estimated and compared with the experimental results.

The third method was an approximate method based on the assumption that the distribution of the compressive stresses varies linearly from zero on the tension side to a maximum value on the compression side.

Compared to the concentrically loaded prisms, the ultimate extreme fibre stresses, calculated by the trapezoidal centre method for prisms loaded under an eccentric loading of t/6, increased by 51% and 45% respectively for the unfilled and filled full-block prisms, and by 62% and 50% respectively for the unfilled and filled half-block prisms. When calculated using the trapezoidal method, the extreme fibre stress increased by 51% and 24% respectively for the unfilled and filled full-block prisms, and by 39% and 29% respectively for the unfilled and filled half-block prisms. Using the linear method the extreme fibre stresses increased by 46% and 40% respectively for the unfilled and filled full-block prisms and by 56% and 45% respectively for the unfilled and filled half-block prisms.

Compared to the concentrically loaded prisms, the extreme fibre stresses calculated by the trapezoidal centre method for prisms loaded under an eccentric loading of t/3 increased by 78% and 59% respectively for the unfilled and filled full-block prisms, and by 154% and 84% respectively for the unfilled and block prisms. The extreme fibre stresses calculated using the trapezoidal method were 53% and 36% respectively greater for the unfilled and filled full-block prisms and by 118% and 57% for the unfilled and filled half-block prisms. The extreme fibre stresses calculated using the linear method were 72% and 53% respectively greater for the unfilled and filled full-block prisms and 145% and 55% for the unfilled half-block prisms.

The trapezoidal centre method estimated that 108 mm of the unfilled and filled full-block specimen thickness (190 mm) and 105 mm of the unfilled and filled half-block specimen thickness (190 mm) was in tension. These results agreed with the crack lengths observed during testing.

The results obtained from the linear method show discrepancies of 4% in both t/6 and t/3 eccentricities compared to values obtained from the trapezoidal centre method. This discrepancy increased to 14% when the trapezoidal method was used. Unlike the trapezoidal centre method, both the linear and the trapezoidal methods fail to estimate the depth of the cracks.

4.5 DISCUSSION OF THEORETICAL RESULTS

4.5.1 General

Colour contour plots were obtained using a non-linear 3-dimensional finite element analysis for deformation and stress for the ¼ prism model in the case of axially loaded prisms and the ½ prism model in the case of eccentrically loaded full-block prisms. A full prism model was used for the half-block eccentrically loaded prism.

To obtain a clear picture of how the stresses are distributed through the prism, an understanding of the contour plots of the prism's deformation in the X-, Y- and Z-direction is essential [26].

4.5.2 Analysis of Axially Loaded Prisms

The levels of stress applied to the unfilled full and half-block prisms were 12.0 N/mm^2 and 12.3 N/mm^2 respectively. The levels applied to the filled

full and half block prisms were 16.4 N/mm^2 and 19.5 N/mm^2, respectively. All the stresses quoted were based on the average compressive strength of three prisms (except the unfilled full-block prisms for which it was the average of two specimens).

4.5.2.1 Axially Loaded Unfilled Full-Block Prism

Contour plots of the prism deformation in the Y-, X- and Z-directions are shown in Figs 4.28, 4.29 and 4.30 respectively. The contour plot of the prism deformation in the Y-direction shows that the top surface shortens vertically with a maximum deformation of 0.98 mm relative to the prism bottom surface. The contour plot of the prism's horizontal deformation in the X-direction shows that the prism end shells tend to deform outward up to a maximum of 0.10 mm. The contour plot of the prism's horizontal deformation in the Z-direction shows that the prism side shells tend to deform outwards with a maximum deformation of 0.07 mm at the prism mid-height.

Stresses in the Block Material

Contour plots of the principal stresses in the block material are shown in Figs 4.31, 4.32 and 4.33. The distribution of the major principal stress (Fig. 4.31) shows high confinement stresses on the top and bottom corners of the prism with a maximum compressive stress of 25.4 N/mm^2 located at the bottom corners of the prism near the steel platen. The rest of the block shells are subjected to compressive stresses ranging from 17.7 N/mm^2 to 23.1 N/mm^2. The minor principal stresses 1 and 2 show a maximum tension stress of 1.9 N/mm^2. High tensile stresses occur around the mortar joint and in different locations in the blocks on the top and bottom.

Figure 4.34 shows the distribution of the maximum shear stress with the largest value of shear stress, 10.9 N/mm^2, located around the mortar joints on the block webs. Most of the prism is subjected to an almost uniform stress which decreased towards the prism's top and bottom ends.

Stresses in the Mortar

Contour plots of the principal stresses in the mortar material are shown in Figs 4.35, 4.36 and 4.37 respectively. The distribution of the major principal stresses shows high compressive stress in the mortar joints inner faces. High confinement stresses, with a maximum value of 21.7 N/mm^2, occurred in the two mortar joints at the top and bottom of the prism, where stresses tend to decrease towards the outside. The mid-joint stress distribution was uniform with a compressive stress of 20.2 N/mm^2.

The minor principal stresses 1 and 2 show that high confinement stresses are located at the inner faces of the mortar joints. The contour plot of the maximum shear stress (Fig. 4.38) shows uniformly distributed shear stresses, ranging only from 7.1 N/mm^2 to 8.1 N/mm^2.

4.5.2.2 Axially Loaded Filled Full-Block Prism

Prism deformations in the Y-, X- and Z-direction are shown in Figs 4.39, 4.40 and 4.41 respectively. The contour plot of the prism deformation in the Y-direction shows that the top surface shortens vertically with a maximum deformation of 0.83 mm relative to the prism's bottom surface. The contour plot of the prism's horizontal deformation in the X-direction shows that the prism end shells tend to deform outward with a maximum deformation of 0.09 mm. The contour plot of the prism's horizontal deformation in the Z-direction

shows that the prism side shells tend to deform outward with a maximum deformation of 0.06 mm at the prism mid-height. The difference in the horizontal deformation is attributed to the prism's aspect ratio (l/t = 2.05). Compared to the unfilled prism, the values of the maximum deformations in the Y-, X- and Z-directions for the filled prisms are 16%, 6% and 13% lower than for the unfilled prism. This indicated that the filled prisms are stiffer than the unfilled ones.

Stresses in the Block Material

Contour plots of the principal stresses in the block material are shown in Figs 4.42, 4.43 and 4.44. The distribution of the major principal stress (Fig. 4.42) gives a maximum compressive stress of 23.1 N/mm^2, which is 9% less than the maximum stress for the unfilled prism, and is located at the bottom corner of the block shells near the steel platen. The rest of the block shells are subjected to compressive stresses ranging from 16.1 N/mm^2 to 21.0 N/mm^2.

The minor principal stresses 1 and 2 produce a maximum tension stress of 1.8 N/mm^2 at the block's outer face. Localised tensile stresses were observed around the mortar joint at the corners of the prism at mid-height.

Figure 4.45 shows the distribution of the shear stresses in the block material. High shear stresses are induced with a maximum value of 10.3 N/mm^2 located at the block mid-web. The remainder of the block shells is subjected to a shear stress which ranges from 7.7 N/mm^2 at the top and the bottom parts of the prism to 10.1 N/mm^2.

Stresses in the Mortar

Contour plots of the principal stresses in the mortar material are shown in Figs 4.46, 4.47 and 4.48. The distribution of the major principal stress shows high compressive stresses at the outer faces of the mortar joints with a maximum value of 19.1 N/mm^2, which is 12% less than the maximum stress for the unfilled prism. These high stresses tend to decrease towards the inner faces of the mortar joints reaching a value of only 7.4 N/mm^2. This is therefore completely different from the unfilled full block prism where the compressive stresses are higher in the inner faces of the mortar joints.

The minor principal stresses 1 and 2 show that the mortar joints are subjected to confinement stresses by the block material with a maximum stress of 4.9 N/mm^2. This is different from the unfilled full block prism where the confinement stresses are higher on the outer face.

The distribution of the shear stresses at the mortar joints are shown in Fig. 4.49. High shear stresses are located at the outer face of the mortar joints with a maximum value of 7.1 N/mm^2, occurring at the mid-joint.

Stresses in the Concrete Infill

Contour plots of the principal stresses in the concrete infill are shown in Figs 4.50, 4.51 and 4.52 respectively. The distribution of the major principal stress (Fig. 4.50) shows that the highest values of compressive stress are located in small areas of the concrete at the level of the mortar joint with a maximum value of 23.3 N/mm^2. Large confinement stresses also occur in

larger areas around the mortar joint level. The remainder of the concrete is in compression with stresses ranging from 11.5 N/mm^2, to 19.7 N/mm^2.

Contour plots of the minor principal stresses show that a maximum tensile stress of 1.4 N/mm^2, occur at the mid-height of the two mid blocks. Confinement stresses with a maximum value of 6.4 N/mm^2, are located in small areas around the corners at the level of the mortar joints.

Figure 4.53 shows that high shear stresses are located at the corners around the mortar joint levels with a maximum value of 8.7 N/mm^2. These stresses tend to reduce away from those locations reaching minimum values close to the steel platens.

4.5.2.3 Axially Loaded Unfilled Half-Block Prisms

Contour plots of the prism deformation in the Y-, X- and Z-directions are given in Figs 4.54, 4.55 and 4.56 respectively. The contour plot of the prism deformation in the Y-direction shows that the prism's bottom surface shortens vertically with a maximum deformation of 1.04 mm relative to the prism's top surface. The contour plot of the prism's horizontal deformation in the X-direction shows that the prism end shells tend to deform outward with a maximum deformation of 0.10 mm. The contour plot of the prism's horizontal deformation in the Z-direction, shows that the prism side shells tend to deform outward with a maximum deformation of 0.10 mm. The plot also identifies a horizontal deformation difference of between 0.10 mm and +0.05 mm in the Z-direction in two opposite outer shells of the prism. This results in the separation of the two outer shells in areas with neutral values of deformation.

Stresses in the Block Material

Contour plots of the principal stresses in the block material are shown in Figs 4.57, 4.58 and 4.59. The distribution of the major principal stress (Fig. 4.57) shows that high compressive stresses are located near the steel platens, with a maximum value of 25.8 N/mm^2. The rest of the prism shells are under compression with stresses ranging from 18.4 N/mm^2, to 23.6 N/mm^2.

The plot of the minor principal stresses 1 and 2 shows that high tensile stresses occur around the mortar joints and block shells at the top and bottom of the blocks with a maximum value of 2.0 N/mm^2.

The contour plot of the maximum shear stress (Fig. 4.60) shows that high shear stresses occur in the top and bottom blocks with a maximum value of 11.4 N/mm^2. The remainder of the prism has a uniform stress distribution with values ranging between 8.6 N/mm^2 and 11.1 N/mm^2.

Stresses in the Mortar

Contour plots of the principal stresses in the mortar material are shown in Figs 4.61, 4.62 and 4.63. The distribution of major principal stress show that high compressive stresses occur in the inner faces of the mortar joint with a maximum value of 22.1 N/mm^2. This is completely different from the filled prisms where the compressive stresses are higher in the outer faces of the mortar joints.

The plot of the minor principal stresses 1 and 2 shows that the highest confinement stresses are located at the inner faces of the mortar joints.

The contour plot of the maximum shear stress (Fig. 4.64) shows uniformly distributed shear stresses ranging from 7.7 N/mm^2 to 8.2 N/mm^2.

4.5.2.4 Axially Loaded Filled Half-Block Prisms

Contour plots of the prism's deformation in the Y-, X- and Z-directions are given in Figs 4.65, 4.66 and 4.67 respectively. The contour plot of deformation in the Y-direction shows that the prism's bottom surface shortens vertically with a maximum deformation of 1.09 mm relative to the prism's top surface. The contour plot of the prism's horizontal deformation in the X-direction shows that the prism end shells tend to deform outward with a maximum deformation of 0.04 mm at the prism's mid-height. The contour plot of the prism's horizontal deformation in the Z-direction shows that the prism side shells tend to deform outward in a similar manner to the end shells in the X-direction with a maximum value of 0.05 mm. This difference in horizontal deformation is attributed to the prism aspect ratio (l/t = 1.00). Figure 4.67 also shows that the horizontal deformation difference varied between -0.04 mm and +0.05 mm in the Z-direction in two opposite outer shells of the prism. This causes separation of the two outer shells in areas of neutral values of deformation. Compared to the unfilled half-block prism, the values of maximum deformation in the Y-, X- and Z-directions of the filled half-block prism are 5%, 53% and 12% lower than for the unfilled one. This indicates that the filled prisms are stiffer than the unfilled ones.

Stresses in the Block Material

Contour plots of the principal stresses in the block material are shown in Figs 4.68, 4.69 and 4.70. The distribution of the major principal stress shows that the maximum compressive stress is 27.1 N/mm^2. This value is almost the same as for the unfilled half-block prism, and is located at the bottom corner of the block shells near the steel platen. The remainder of the block shells are in compression with stresses ranging from 19.4 N/mm^2 to 24.8 N/mm^2.

The major principal stresses 1 and 2 show that high tensile stresses occur at the block outer face, with a maximum value of 2.6 N/mm^2. This value of maximum tensile stress is 29% higher than for an unfilled prism, and is caused by tensile stresses in the concrete infill using the infill to push the block out. As a result of those high tensile stresses the filled half-block prisms have a tendency to split along the side shells. The shear stress distribution (Fig. 4.71) shows that the shear stresses are almost constant ranging from 9.3 N/mm^2 to 12.3 N/mm^2.

Stresses in the Mortar

Contour plots of the principal stresses in the mortar material are shown in Figs 4.72, 4.73 and 4.74. The distribution of the major principal stress indicates that high compressive stresses occur at the outer faces of the mortar joints with a maximum value of 23.2 N/mm^2, which is 5% higher than the maximum compressive stress for the unfilled prism. These stresses decrease towards the inner faces of the mortar joints, reaching a value of 9.2 N/mm^2.

The plot of the principal stresses 1 and 2 shows that the mortar joints are subjected to confinement stresses by the block with a maximum stress of 5.8 N/mm^2. This is different from the unfilled half-block prism where the confinement stresses are higher on the outer face.

The distribution of shear stresses at the mortar joint (Fig. 4.75) show that high shear stresses are located at the outer face of the mortar joints with a maximum value of 8.8 N/mm^2.

Stresses in the Concrete Infill

Contour plots of the principal stresses in the concrete infill are shown in Figs 4.76, 4.77 and 4.78. The distribution of the major principal stresses shows that high values of compressive stresses are located in small areas at the levels of the mortar joints with a maximum value of 27.4 N/mm^2. The remainder of the concrete is in compression with stresses ranging from 13.5 N/mm^2 to 23.3 N/mm^2.

Contour plots of the minor principal stresses 1 and 2 show that high tensile stresses occur at the mid-heights of the four blocks with a maximum value of 1.3 N/mm^2.

The contour plot of the shear stress (Fig. 4.79) shows that high shear stresses are located at the corners around the mortar joint levels with a maximum value of 10.2 N/mm^2. It also shows that shear stresses decrease away from these locations reaching a minimum value close to the steel platens.

4.5.3 Analysis of Eccentrically Loaded Prisms

The level of loading applied to the finite element was based on the average strength of three prisms obtained from the experimental part of this study.

4.5.3.1 Unfilled Full-Block Prism Compressed under an Eccentric Load at t/6

Contour plots of the prism's deformations in the Y-, X- and Z-directions are given in Figs 4.80, 4.81 and 4.82 respectively. The contour plot of the prism's deformation in the Y-direction shows that the prism's bottom surface shortened vertically with a maximum deformation of 1.05 mm located at the prism end shells on the compression side. The contour plot of the prism's horizontal deformation in the X-direction shows that the prism side shells deformed outward with a maximum deformation of 0.82 mm at the prism mid-height. The contour plot of the prism's horizontal deformation in the Z-direction shows that the prism corner on the compression side deformed outward with a maximum deformation of 0.08 mm at the prism mid-height.

Stresses in the Block Material

Contour plots of the principal stresses in the block material are given in Figs 4.83, 4.84 and 4.85. The major principal stress distribution shows that high confinement stresses occurred at the top and bottom corners near the steel platens, also around the web of the two mid-blocks on the compression side of the prism with a maximum value of 28.1 N/mm^2. This value is 17% higher than the maximum major principal stress for the concentrically loaded unfilled full block prism.

Contour plots of the minor principal stresses 1 and 2 show that most of the block shells were in tension with stresses of 0.8 N/mm^2 (MST1), and 1.2 N/mm^2 (MST2). Higher tensile stresses are found at the prism's side shell in areas near to the level of the mortar joints with tensile stresses of 3.9 N/mm^2 (MST2). This value is 34% higher than the allowable tensile stress for concrete predicted by using the following formula given by ACI 318M-83[38], which relates the concrete tensile strength to the cube compressive strength as follows:

$$f_{ct} = 0.58 \times (f_{cu})^{1/2} \qquad .....(4.1)$$

Figure 4.86 shows the distribution of the shear stresses with a maximum value of 12.4 N/mm^2 occurring on the compression side. This was noted during testing by the formation of cracks near to the mortar joints.

Stresses in the Mortar

Contour plots of the principal stresses in the mortar are shown in Figs 4.87, 4.88 and 4.89. The major principal stress distribution shows that high confinement stresses occurred on the compression side of the mortar joints with a maximum stress of 27.0 N/mm^2. These stresses are 24% higher than those for the axial loaded prism.

Contour plots of the minor principal stresses 1 and 2 show that the mortar joints are subjected to confinement stresses, with a maximum value of 8.7 N/mm^2 (MST1). Tensile stresses with maximum values of 0.3 N/mm^2 (MST1) and 0.9 N/mm^2 (MST2) were located at the extreme tension fibre. These values are less than the allowable stresses calculated from equation

4.1, which supports the assumption made earlier that the neutral axis depth increases on the tension side face of the t/6 eccentrically loaded prism.

The contour plot of the maximum shear stress in the mortar is shown in Fig. 4.90. This figure shows that high shear stresses are located on the compression side with a maximum value of 9.3 N/mm^2.

4.5.3.2 Filled Full Block Prisms Compressed under an Eccentric Load at t/6

Contour plots of the prism's deformation in the Y-, X- and Z-directions are given in Figs 4.91, 4.92 and 4.93 respectively. The contour plot of the prism's deformation in the Y-direction shows that the prism's upper surface shortened vertically, with a maximum deformation of 0.92 mm located at the prism's upper corner on the compression side. The contour plot of the prism's horizontal deformation in the X-direction show that the prism side shells deformed outward with a maximum deformation of 0.79 mm at the prism mid-height. The contour plot of the prism's horizontal deformation in the Z-direction shows that the prism's corners on the compression side deformed outward with a maximum deformation of 0.07 mm at the prism mid-height. Compared to the unfilled prism, the values of maximum deformation in the Y-, X- and Z-directions for the filled prism are 13%, 4% and 12% lower respectively.

Stresses in the Block Material

Contour plots of the principal stresses in the block material are shown in Figs 4.94, 4.95 and 4.96. The major principal stress distribution shows high confinement stresses located at the top and bottom corners on the

compression side of the prism with a maximum value of 25.9 N/mm^2. The major principal stresses are 12% higher than for the axial prism and 8% lower than for the unfilled full-block prism compressed under the same eccentricity.

Contour plots of minor principal stresses 1 and 2 show confinement stresses at the top and bottom corners on the compression side of the prism. The remainder of the block was under tensile stresses of 0.8 N/mm^2 (MST1) and 3.1 N/mm^2 in most of the prism outer shells (MST2). This value is 9% higher than the allowable tensile stress for the concrete, as given by equation 4.1.

The contour plot of the maximum shear stress in the block material is shown in Fig. 4.97. The figure shows that high shear stresses occurred in the blocks of the compression side, with a maximum value of 11.6 N/mm^2. This is 6% less than the unfilled full block prism compressed under the same eccentricity.

Stresses in the Mortar

Contour plots of the principal stresses in the mortar are shown in Figs 4.98, 4.99 and 4.100. The major principal stress distribution shows that high confinement stresses occurred on the compression side with a maximum stress of 25.9 N/mm^2. These stresses are 36% higher than those for the axially loaded prism. Compared to the unfilled prism compressed under the same eccentricity the stresses are 4% lower.

Contour plots of the minor principal stresses 1 and 2 show that the mortar joints are subjected to confinement stresses on the compression side with

maximum values of 7.5 N/mm^2 (MST1) and 7.4 N/mm^2 (MST2). The figures also indicate high tensile stresses distributed on the tension side of the prism with maximum values of 1.0 N/mm^2 (MST1) and 3.0 N/mm^2 (MST2) located at the extreme tension fibre.

Figure 4.101 shows high shear stresses distributed on the compression side of the mortar joints with a maximum value of 9.3 N/mm^2. However, these high stresses reduced towards the tension side.

Stresses in the Concrete Infill

Contour plots of the principal stresses in the concrete infill are shown in Figs 4.102, 4.103 and 4.104. The contour plot of the major principal stresses show that a compressive stress of 24.9 N/mm^2 which is 9% higher than those for the axially loaded prism occurred at small areas at the level of the mortar joints. The remainder of the concrete infill was subjected to compressive stresses, ranging from 2.9 N/mm^2 to 16.3 N/mm^2, which were 7% higher than those for the axially loaded prism.

The plot of the principal stress 1 showed compressive stresses with a maximum value of 7.7 N/mm^2, located in small areas at the level of the mortar joints. Most of the concrete infill is under a compressive stress of 0.3 N/mm^2.

The contour plot of the maximum shear stresses (Fig. 4.105) showed that high shear stresses occurred on the compression side at the level of the mortar joints with a maximum value of 9.3 N/mm^2. The remainder of the

concrete infill was subjected to shear stresses ranging from 1.9 N/mm^2 to 8.6 N/mm^2.

4.5.3.3 Unfilled Half-Block Prism Compressed under Eccentric Load at t/6

The prism's deformations in the Y-, X- and Z-directions are shown in Figs 4.106, 4.107 and 4.108 respectively. The contour plot of the deformation in the Y-direction indicates that the prism bottom surface shortened vertically with a maximum deformation of 1.23 mm on the prism end shells on the compression side. The contour plot of the horizontal deformation in the X-direction showed that the prism side shells deformed outward with a maximum deformation of 0.95 mm at the prism's mid-height. The contour plot of the horizontal deformation in the Z-direction shows a variation of between -0.04 mm and +0.07 mm for the two opposite outer shells of the prism. This causes separation of the two outer shells in areas of neutral values of deformation.

Stresses in the Block Material

Contour plots of the principal stresses in the blocks are shown in Figs 4.109, 4.110 and 4.111. The major principal stress distribution shows that high confinement stresses occurred at the top and bottom corners on the compression side with a maximum value of 31.1 N/mm^2 which is 20% higher than that for the axially loaded prism.

Contour plots of the minor principal stresses 1 and 2 show that confinement stresses occurred at the top and bottom corners on the compression side of the prism. Figure 4.111 shows that most of the block shells are in tension

with stresses ranging from 0.4 N/mm^2 to 3.3 N/mm^2. This value is higher than the allowable tensile stress given by equation 4.1.

Figure 4.112 shows the distribution of shear stresses in the block shells. High shear stresses occurred on the compression side with a maximum value of 13.9 N/mm^2.

Stresses in the Mortar

Contour plots of the principal stresses in the mortar are shown in Figs 4.113, 4.114 and 4.115. The distribution of the major principal stress shows high confinement stresses on the compression side outer face with a maximum value of 30.0 N/mm^2, which is 36% higher than that for the axially loaded prism.

The plot of the minor principal stresses 1 and 2 shows that the mortar is subjected to confinement stresses over most of its area, with a maximum value of 10.2 N/mm^2 (MST1). The figures show maximum values for the tensile stresses of 0.4 N/mm^2. (MST1) and 1.2 N/mm^2. (MST2). These values are lower than the maximum allowable stresses calculated from equation 4.1. This supports the assumption made earlier that the neutral axis depth increases on the tension side face of the t/6 eccentrically loaded prism.

Figures 4.116 shows that high shear stresses occurred in the mortar joint outer faces on the compression side with a maximum value of 10.0 N/mm^2.

4.5.3.4 Filled Half-Block Prism Compressed Under Eccentric Load at t/6

The prism deformations in the Y-,X-, and Z-directions are given in Figs 4.117, 4.118 and 4.119 respectively. The contour plot of deformation in the Y-direction shows that the prism bottom surface shortened vertically with a maximum deformation of 1.29 mm at the prism end shells on the compression side. The contour plot of the horizontal deformation in the X-direction shows that the prism side shells deformed outward with a maximum deformation of 1.15 mm at the prism's mid-height. The contour plot of the horizontal deformation in the Z-direction shows variations of between -0.06 mm and +0.06 mm for the two opposite outer shells of the prism. This causes separation of the two outer shells in areas of neutral values of deformation.

Stresses in the Block Material

Contour plots of the principal stresses in the block material are shown in Figs 4.120, 4.121 and 4.122. The major principal stress distribution shows that high confinement stresses occurred on the compression side of the prism, with a maximum value of 33.1 N/mm^2. This value is 22% higher than for the axially loaded prism.

The contour plot of the minor principal stress 1 shows the presence of confinement stresses, with a maximum value of 11.3 N/mm^2 in small areas located at the top and bottom corners of the prism on the compression side. The remainder of the block shells are under a tensile stress of 0.9 N/mm^2.

The contour plot of the minor principal stress 2 shows that most of the compressive stresses are located in small areas around the top and bottom corners on the compression side of the prism.

Most of the block shells are subjected to a tensile stress of 4.1 N/mm^2. This value is 41% higher than the allowable tensile stress given by equation 4.1.

Figure 4.123 shows the distribution of high shear stresses in the block material, with a maximum value of 14.7 N/mm^2.

Stresses in the Mortar

Contour plots of the principal stresses in the mortar material are given in Figs 4.124, 4.125 and 4.126. The distribution of the major principal stress shows that high confinement stresses occurred on the compression side outer face with a maximum value of 31.4 N/mm^2. This value is 35% higher than for the axially loaded prism and 4% higher than for the unfilled half-block prism compressed under the same eccentricity.

Contour plots of the minor principal stresses 1 and 2 show that confinement stresses exist over most of the mortar area, with a maximum value of 10.9 N/mm^2 (MST1). The contour plot of the minor principal stress 2 indicate the presence of high tensile stresses with a maximum value of 4.8 N/mm^2. This value is higher than the allowable stress calculated from equation 4.1, and supports the assumption made earlier that crack formation takes place on the tension side (the trapezoidal centre method).

The contour plot of maximum shear stress (Fig. 4.127) shows that the maximum value of shear stress, 10.3 N/mm^2, was located at the outer faces of the mortar joints on the prism compression side. These stresses decreased towards the tension side of the prism.

Stresses in the Concrete Infill

Contour plots of the principal stresses in the concrete infill are shown in Figs 4.128, 4.129 and 4.130. The contour plot of the major principal stress show that high values of compressive stress were located in small areas at the level of the mortar joints with a maximum value of 30.4 N/mm^2. This value is 11% higher than for the axially loaded prism and 22% higher than for the filled full block prism compressed under the same eccentricity.

The contour plot of maximum shear stress (Fig. 4.131) shows that the highest value of shear stress was located in an area around the mortar joints on the compression side. This stress reduced towards the tension side.

4.5.3.5 Unfilled Full Block Prism Compressed Under Eccentric Load at t/3

Contour plots of the prism's deformation in the Y-, X- and Z-directions are given in Appendix A, Figs A.1, A.2 and A.3 respectively. The contour plot of the prism's deformation in the Y-direction shows that the prism's bottom surface shortened vertically with a maximum deformation of 0.79 mm on the compression side. The contour plot of the prism's horizontal deformation in the X-direction shows that the prism deformed outward with a maximum deformation of 0.80 mm at the prism mid-height. The contour plot of the prism's horizontal deformation in the Z-direction shows that the prism

deformed outward with a maximum deformation of 0.05 mm at the prism's bottom corner on the compression side.

Stresses in the Block Material

Contour plots of the principal stresses in the block material are given in Figs A.4, A.5 and A.6. The major principal stress distribution shows the presence of high confinement stresses at the top and bottom corners on the compression side.

The minor principal stress 2 shows that high tensile stresses occurred on the prism's tension side. This was reflected during testing by the formation of a gap between the blocks and the mortar joints.

Figure A.7 shows the distribution of the maximum shear stresses, with a maximum shear value of 9.8 N/mm^2 located on the compression side of the prism's block shells.

Stresses in the Mortar

Contour plots of the principal stresses in the mortar are shown in Figs A.8, A.9 and A.10. The major principal stress distribution shows that high confinement stresses existed over most of the mortar joints with a maximum value of 22.2 N/mm^2. These stresses decreased in the opposite direction and changed to tensile stresses on the prism tension side, with a maximum value of 2.2 N/mm^2.

The contour plot of the minor principal stress 2 show that high tensile stresses occurred on the tension side. These high tensile stresses were reflected during testing by the mortar debonding from the blocks.

Figure A.11 shows the distribution of shear stresses on the mortar material, also that a maximum value of 8.2 N/mm^2 was located at the outer faces of the mortar joints on the compression side.

4.5.3.6 Filled Full Block Prism Compressed under Eccentric Load at t/3

Contour plots of the prism's deformation in the Y-, X- and Z-directions are given in Figs A.12, A.13 and A.14. The contour plot of the prism's deformation in the Y-direction shows that the prism's bottom surface shortened vertically with a maximum deformation of 0.70 mm on the compression side bottom corner. The contour plot of the prism's horizontal deformation in the X-direction shows that the prism deformed outward with a maximum deformation of 0.73 mm at the prism's mid-height. The contour plot of the prism's horizontal deformation in the Z-direction shows that the prism deformed outward with a maximum deformation of 0.04 mm at the corners on the compression side.

Stresses in the Block Material

Contour plots of the principal stresses in he block material are given in Figs A.15, A.16 and A.17. The major principal stress distribution shows that high confinement stresses were located at the top and bottom corners on the stiff steel platen and the concrete blocks.

The mortar debonding from the blocks during testing and the formation of a gap between the two materials resulted from high tensile stresses as shown in Fig. A.17. The figure also shows a 67% increase in the tensile stresses on the tension side resulting from increasing the eccentricity from t/6 to t/3. Compared to the unfilled full block prism compressed under an eccentricity of t/3 the tensile stresses show an increase of 38%.

The contour plot for the maximum shear stresses is given in Fig. A.18 which shows that high shear stresses occurred at the shell's outer faces on the compression side.

Stresses in the Mortar

Contour plots of the principal stresses in the mortar are shown in Figs A.19, A.20 and A.21. The distribution of the major principal stress shows that high confinement stresses existed on the outer faces of the mortar joints.

The distribution of the minor principal stress 2 (Fig. A.21) shows that high tensile stresses occurred on the prism tension side. This was due to the mortar cap increasing an observed during testing. The figure also shows that an increase of 184% in the tensile stress was achieved by increasing the eccentricity from t/6 to t/3, and an increase of 18% compared to the unfilled full block prism compressed under the same eccentricity.

The contour plot of the maximum shear distribution is given in Fig. A.22 which shows that high values of shear stress were located at the outer faces of the mortar joints on the compression side.

Stresses in the Concrete Infill

Contour plots of the principal stresses in the concrete infill are given in Figs A.23, A.24 and A.25. The plot of the major principal stress shows that high compressive stresses were located in small areas at the levels of the mortar joints on the compression side.

The contour plot of the minor principal stress 2 indicated the presence of high tensile stresses. This shows that an increase of 94% in the tensile stress on the tension side is produced by increasing the eccentricity from t/6 to t/3.

The contour plot of the maximum shear stress is given in Fig. A.26 which shows that the highest values of shear stress were located in small areas at the level of the mortar joints.

4.5.3.7 Unfilled Half-Block Prisms Compressed under an Eccentric Load at t/3

The prism's deformations in the Y-, X- and Z-directions are given in Figs A.27, A.28 and A.29 respectively. The contour plot of the deformation in the Y-direction shows that the prism's bottom surface shortened vertically with a maximum deformation of 1.41 mm on the prism end shells on the compression side. The contour plot of the horizontal deformation in the X-direction shows that the prism side shells deformed outward with a maximum deformation of 1.29 mm at the prism's mid-height. The contour plot of the horizontal deformation in the Z-direction showed variations between -0.05 mm to +0.07 mm in the two opposite outer shells of the prism. This causes separation of the two outer shells from the rest of the prism in areas of

neutral values of deformation. These results show that increasing the eccentricity from t/6 to t/3 increased the maximum deformation by 15% and 36% in the Y- and X-directions respectively.

Stresses in the Block Material

Contour plots of the principal stresses in the block material are given in Figs A.30, A.31 and A.32. The major principal stress distribution shows that high confinement stresses were located at the top and bottom corners on the compression side. These high stresses are caused by differences in material properties of the stiff steel platen and the concrete blocks.

The contour plot of the minor principal stress 2 is shown in Fig. A.32 which shows that increasing the eccentricity from t/6 to t/3 increased the tensile stresses by 86%. The high level of tension was reflected during testing by the mortar debonding from the blocks and the formation of a gap between the two materials.

The contour plot of the maximum shear distribution is given in Fig. A.33 which shows that high shear stresses were distributed on the compression side block shells.

Stresses in the Mortar Material

Contour plots of the principal stresses in the mortar material are shown in Figs A.34, A.35 and A.36. The distribution of the major principal stress shows that high confinement stresses existed on the compression side of the mortar joints.

The distribution of the minor principal stress 2 shows the presence of high tensile stresses. This high level of tension was reflected during testing by the mortar debonding from the blocks.

The colour contour plot of the maximum shear stress, given in Fig. A.37, shows that high shear stresses were located on the outer faces of the compression side mortar joints.

4.5.3.8 Filled Half-Block Compressed under an Eccentric Load at t/3

Contour plots of the prism's deformations in the Y-, X- and Z-directions are given in Figs A.38, A.39 and A.40 respectively. The contour plot of the deformation in the Y-direction shows that the prism bottom surface shortened vertically, with a maximum deformation of 1.11 mm on the prism's end shells on the compression side. The contour plot of the horizontal deformation in the X-direction shows that the prism's side shells deformed outward with a maximum deformation of 1.07 mm at the prism's mid-height. The contour plot of the horizontal deformation in the Z-direction shows variations of -0.04, and +0.04 mm for the two opposite outer shells on the prism's compression side. Compared to an unfilled half-block prism compressed under the same eccentricity, the maximum deformation values in the Y- and X-directions are 22% and 17% less, respectively.

Stresses in the Block Material

Contour plots of the principal stresses in the block material are given in Figs A.41, A.42 and A.43. The major principal stress distribution shows that high confinement stresses were located at the top and bottom corners on the

compression side as a result of differences in the material properties of the stiff steel platen and the concrete blocks.

The contour plot of the minor principal stress 2 is given in Fig. A.43 which shows that increasing the eccentricity from t/6 to t/3 increased the tensile stresses by 86%. This high level of tension was reflected during testing by the mortar debonding from the surrounding blocks on the tension side and the formation of a gap between the two materials. The maximum value of tensile stress shows an increase of 18% compared with those for the unfilled half-block prisms compressed under the same eccentricity.

The contour plot of the maximum shear stress distribution is given by A.44 and shows that high shear stresses occurred at the outer shells on the compression side.

Stresses in the Mortar Material

Contour plots of the principal stresses in the mortar material are given in Figs A.45, A.46 and A.47. The distribution of the major principal stress shows that high confinement stresses occurred on the compression side outer faces of the mortar joint, also high tensile stresses on the tension side.

The distribution of the minor principal stress 2 shows that increasing the eccentricity from t/6 to t/3 increased the tensile stresses by 199%. This high level of tension was reflected during testing by the mortar debonding itself from the blocks.

The colour contour plot of the maximum shear stress is given in Fig. A.48. This figure shows that high shear stresses were located on the outer faces of the compression side mortar joints.

Stresses in the Concrete Infill

Contour plots of the principal stresses in the concrete infill are given in Figs A.49, A.50 and A.51. The major principal stress shows that high compressive stresses were located in small areas at the level of the mortar joints.

The contour plot of the minor principal stress 2 shows the existence of tensile stresses. The results show that increasing the eccentricity from t/6 to t/3 increased the tensile stresses by 98%.

The contour plot of the maximum shear stress is given by Fig. A.52 which shows that the highest values of shear stresses were located in small areas at the level of the mortar joints.

4.6 A BRIEF DISCUSSION ON THE EFFECT OF THE ECCENTRICITY ON ENHANCING THE COMPRESSIVE STRENGTH, f'_m, OF BLOCKWORK PRISMS

The mortar joints of the concentrically loaded full and half-block prisms showed higher confinement stresses at the outer and inner sides of the unfilled and filled prisms respectively.

In the case of eccentrically loaded prisms, the high confinement stresses were only created on the compression side. These stresses reduced

gradually towards the tension side leaving the webs under lower confinement stresses than the extreme compression face. The greater the eccentricity the greater the reduction of the confinement stresses.

The difference in stiffness between the mortar and block created a tri-axial compression stress field in the mortar and bi-axial lateral tension stresses in the concrete block with axial compression. This led to a pulling apart of the block causing a splitting cracks on the face shells and the webs starting at the bed joint. This behaviour was similar for eccentrically loaded prisms except that the high lateral tensile stresses in the blocks, caused by a high confinement stress in the mortar, took place at the compression side of the prism. Compared to the extreme compression side of the prism, the lateral tensile stresses in the webs were small. This explains the increase in the ultimate extreme fibre stress which occurred under eccentric loading; the greater the eccentricity the greater the increase in the ultimate extreme fibre stress. Figure 4.132 shows the state of stresses at the mortar and block interface near failure.

4.7 CONCLUSIONS

(1) The compressive strength, f'_m, increased by 19% and 18% for unfilled and filled concentrically loaded prisms when the prism's aspect ratio, l/t, changed from 2.05 (full block) to 1.0 (half-block) respectively.

(2) The ultimate compressive strength, f'_m, for unfilled full and half-block prisms is higher than the ultimate compressive strength for filled full and half-block prisms. The presence of the concrete infill induced splitting of the block shells before reaching ultimate strength. This

was due to lateral expansion and the high value of Poisson's ratio of the concrete infill compared to that of the block.

(3) The effect of the strain gradient on enhancing the ultimate extreme fibre stress of eccentrically loaded blockwork masonry is significant. Compared to concentrically loaded prisms, the ultimate extreme fibre stress for prisms loaded under an eccentric loading of t/6 increased by 51% and 45% for unfilled and filled full-block prisms respectively and by 62% and 50% for unfilled and filled half-block prisms respectively. The ultimate extreme fibre stress for prisms loaded under an eccentric loading of t/3 increased by 78% and 58% for unfilled and filled full block prisms respectively, and by 153% and 83% for unfilled and filled half-block prisms respectively.

The explanation of the increase in the ultimate extreme fibres stress which occurs under eccentric loading is as follows: The greater the eccentricity, the greater the increase in ultimate extreme fibre stress is related to the high lateral tensile stresses in the blocks, caused by a high confinement stress in the mortar taking place on the compression side of the eccentrically loaded prisms, where the lateral tensile stresses in the block webs are small. This is different to the case of concentrically loaded prisms where the mortar is under high confinement stresses causing high lateral tensile stresses in the block face shells as well as the webs.

(4) The trapezoidal centre method, based on the stress-strain relationship for a 10 mm mortar joint [39] was more accurate than the trapezoidal and linear methods to calculate the ultimate extreme fibre

stress for eccentrically loaded prisms. The depth of the neutral axis can also be estimated using this method.

(5) The results obtained from the finite element analysis supported the prism's behaviour during the experimental part of this study and gave information on the prism's deformation and stress distribution which are impossible to observe experimentally.

(6) To obtain more accurate results for eccentrically loaded prisms, especially those with eccentricities higher than t/6, a three-dimensional finite element crack formation model should be simulated.

Table 4.1 The material properties used in developing the non-linear three-dimensional finite element model

Material	Model	Secant Modulus of Elasticity (N/mm^2)	Poisson's Ratio (%)	Initial Uniaxial Yield Stress (N/mm^2)	No. of Straight Line approximations to the hardening curve	The slope of the (i)th section of the uniaxial yield stress against effective plastic strain curve	The limit on effective plastic strain up to which the (i)th section of the hardening curve is valid
Concrete Block	Implicit backward Euler von Mises yield surface model	26340*	0.19	13.17	2	S_1=21050 S_2=1567	L_1=0.0005 L_2=0.0010
Concrete Infill	Implicit backward Euler von Mises yield surface model	14100*	0.24	12.12	2	S_1=11497 S_2=2514	L_1=0.00084 L_2=0.00115
Mortar	Implicit backward Euler von Mises yield surface model	4054	0.25	15.91	3	S_1=3540 S_2=1658 S_3=1417	L_1=0.0025 L_2=0.0046 L_3=0.0058

*Secant modulus of elasticity at 2/3 f_{max} where f_{max} is the peak value of the idealised stress-strain curve given by equations 3.1 to 3.3.

Table 4.2 Compressive strength of 4-course high full block prisms

Specimen Description	Average Ultimate Load (kN)	Number of Tests	Average Ultimate Stress f'_m (N/mm^2)	Method+ used in calculating f'_m	Area* used	Compressive Strength (N/mm^2)	
						Infill	Mortar
Prisms under Axial Load							
Filled	1214	3	16.38		Gross	22.5	27.20
Unfilled	892	2	21.39		Net	-	27.20
Prisms under Eccentric Load t/6							
Filled	850	3	20.39	1	Gross	22.5	27.20
			23.79	2			
			22.94	3			
Unfilled	650	3	27.71	1	Net	-	27.20
			32.32	2			
			31.17	3			
Prisms under Eccentric Load t/3							
Filled	465	3	22.31	1	Gross	22.5	27.20
			26.03	2			
			25.10	3			
Unfilled	383	3	32.65	1	Net	-	27.20
			38.09	2			
			36.73	3			

*Gross Area 74100 mm^2

Net Area 41700 mm^2

+Methods of calculating f'_m
1. Trapezoidal Method
2. Trapezoidal Centre Method
3. Linear Method

Table 4.3 Compressive strength of 4-course high half-block prisms

Specimen Description	Average Ultimate Load (kN)	Number of Tests	Average Ultimate Stress f'_m (N/mm^2)	Method+ used in calculating f'_m	Area* used	Compressive Strength (N/mm^2)	
						Infill	Mortar
Prisms under Axial Load							
Filled	703	3	19.47		Gross	24.5	28.30
Unfilled	443	3	22.26		Net	-	28.30
Prisms under Eccentric Load t/6							
Filled	509	3	25.06	1	Gross	24.5	28.30
			29.24	2			
			28.19	3			
Unfilled	346	3	30.91	1	Net	-	28.30
			36.06	2			
			34.77	3			
Prisms under Eccentric Load t/3							
Filled	311	3	30.63	1	Gross	24.5	28.30
			35.74	2			
			34.45	3			
Unfilled	271	3	48.42	1	Net	-	28.30
			56.48	2			
			54.47	3			

*Gross Area 36100 mm^2

Net Area 19900 mm^2

+Methods of calculating f'_m
1. Trapezoidal Method
2. Trapezoidal Centre Method
3. Linear Method

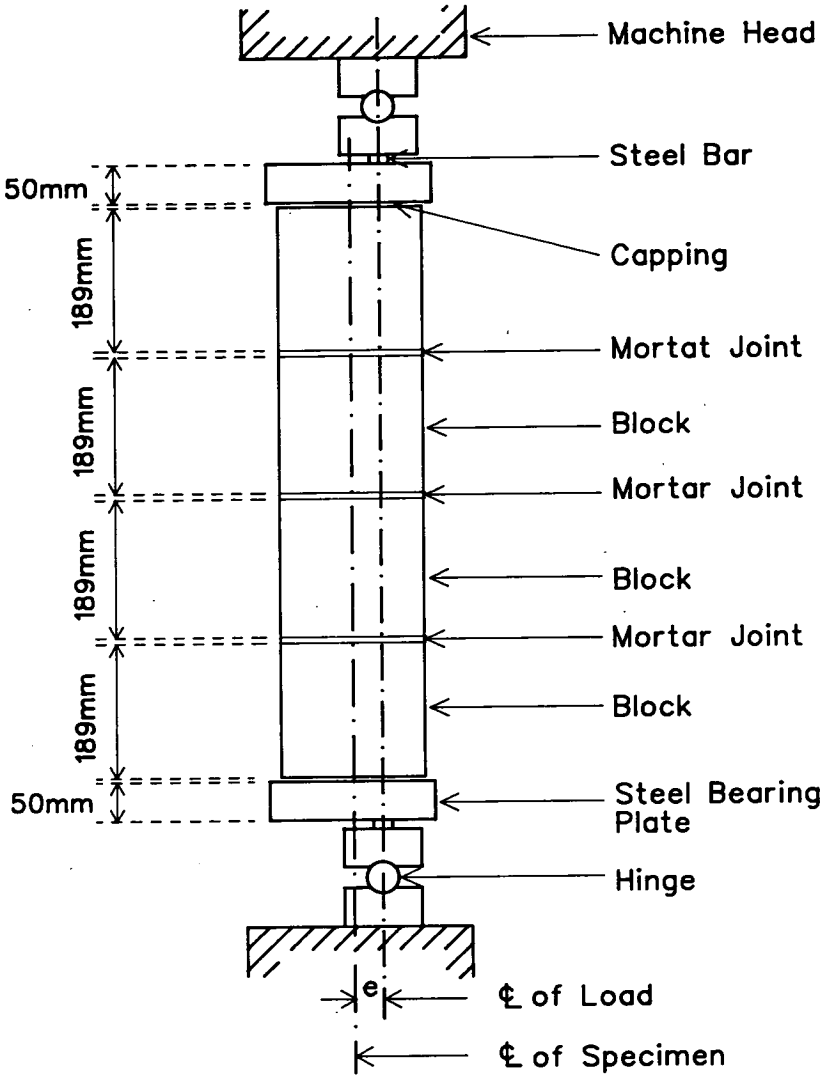
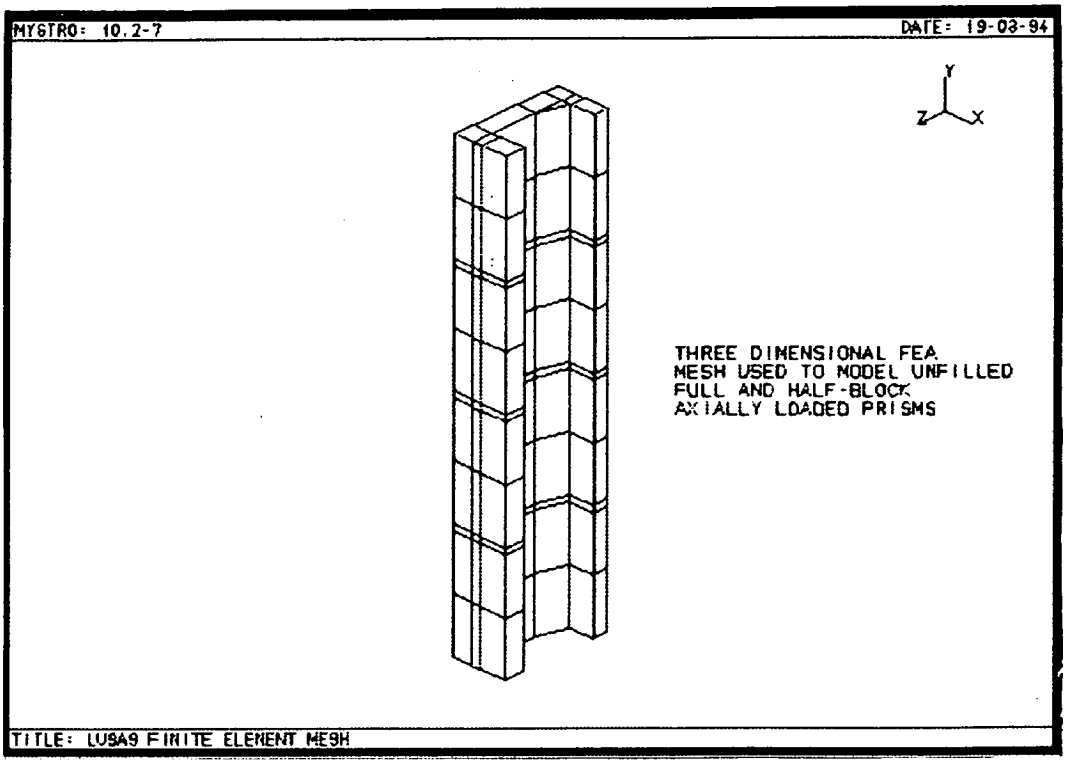
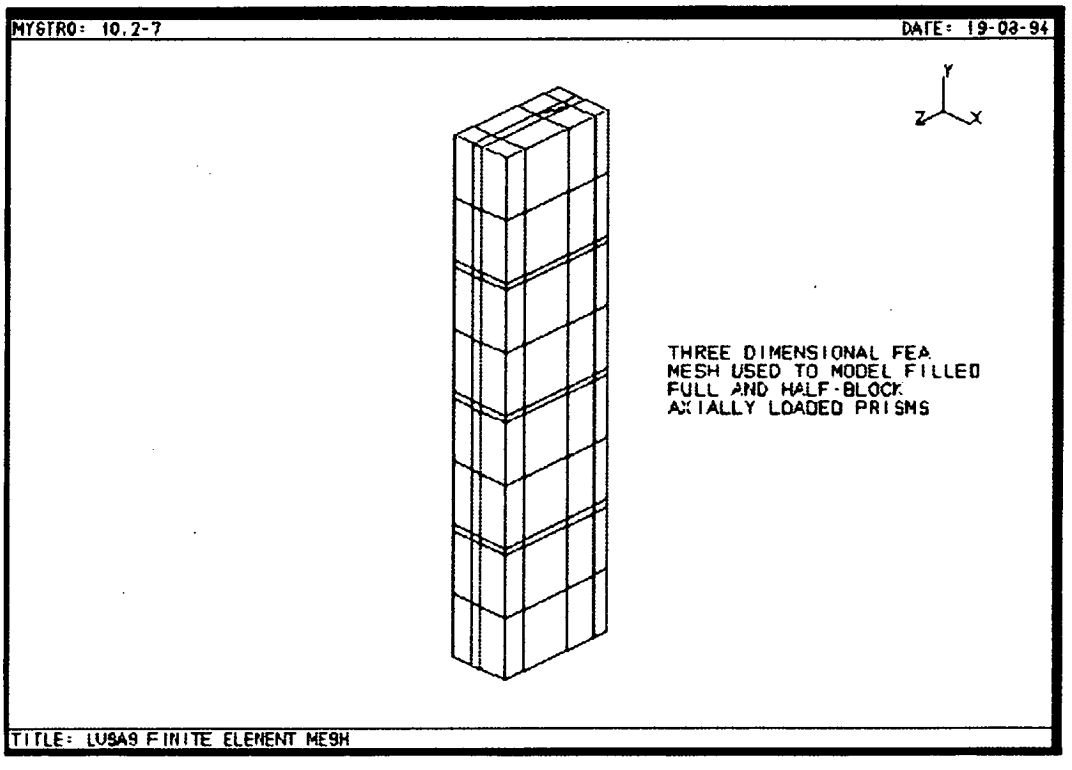


Fig. 4.1 Test setup for eccentrically loaded prisms.

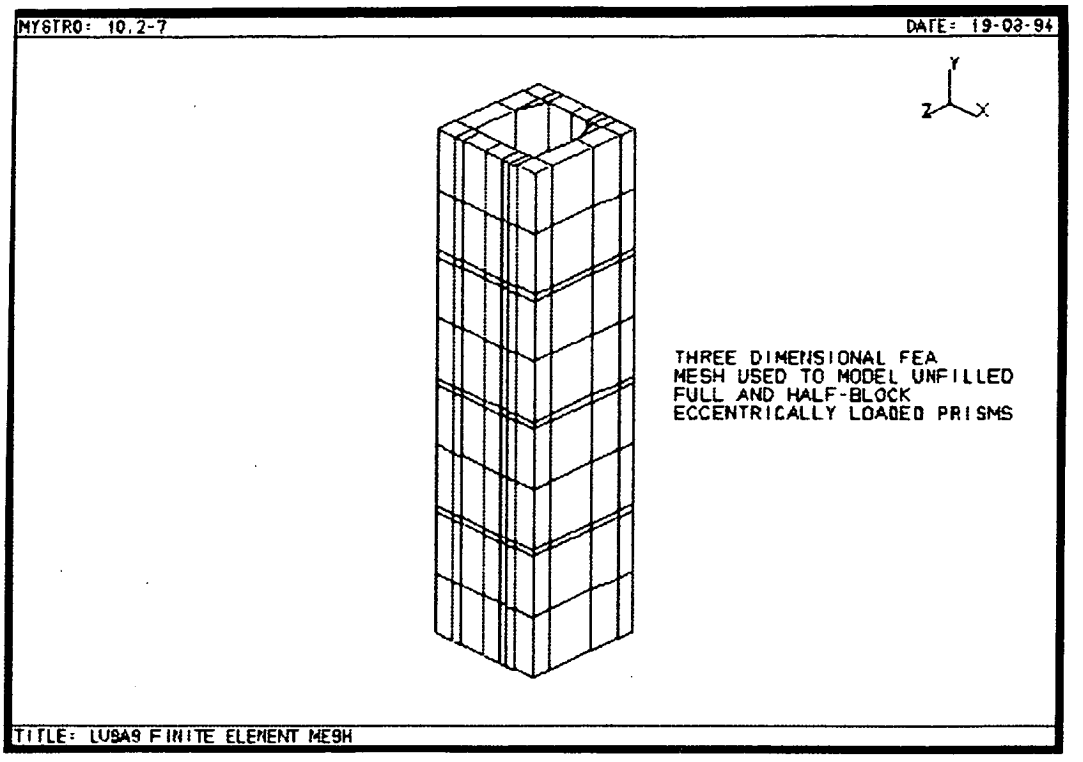


(a) Unfilled

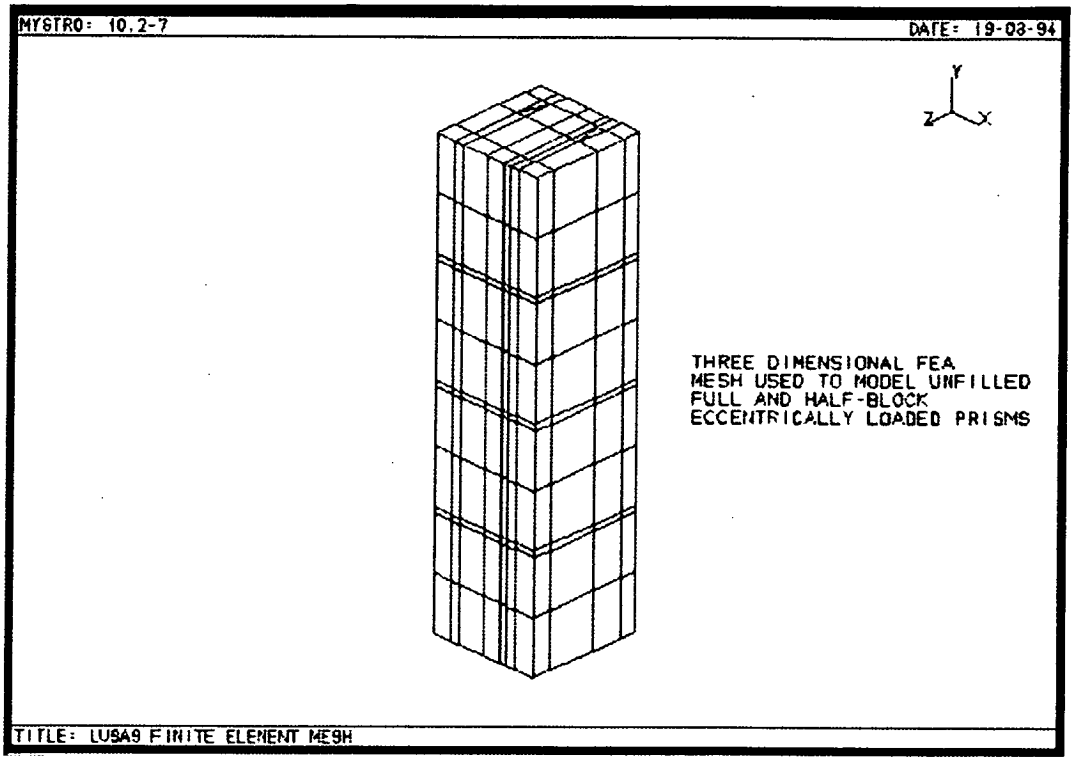


(b) Filled

Fig. 4.2 Typical FEA meshes used to model the concentrically loaded prisms



(a) Unfilled



(b) Filled

Fig. 4.3 Typical FEA meshes used to model the eccentrically loaded prisms

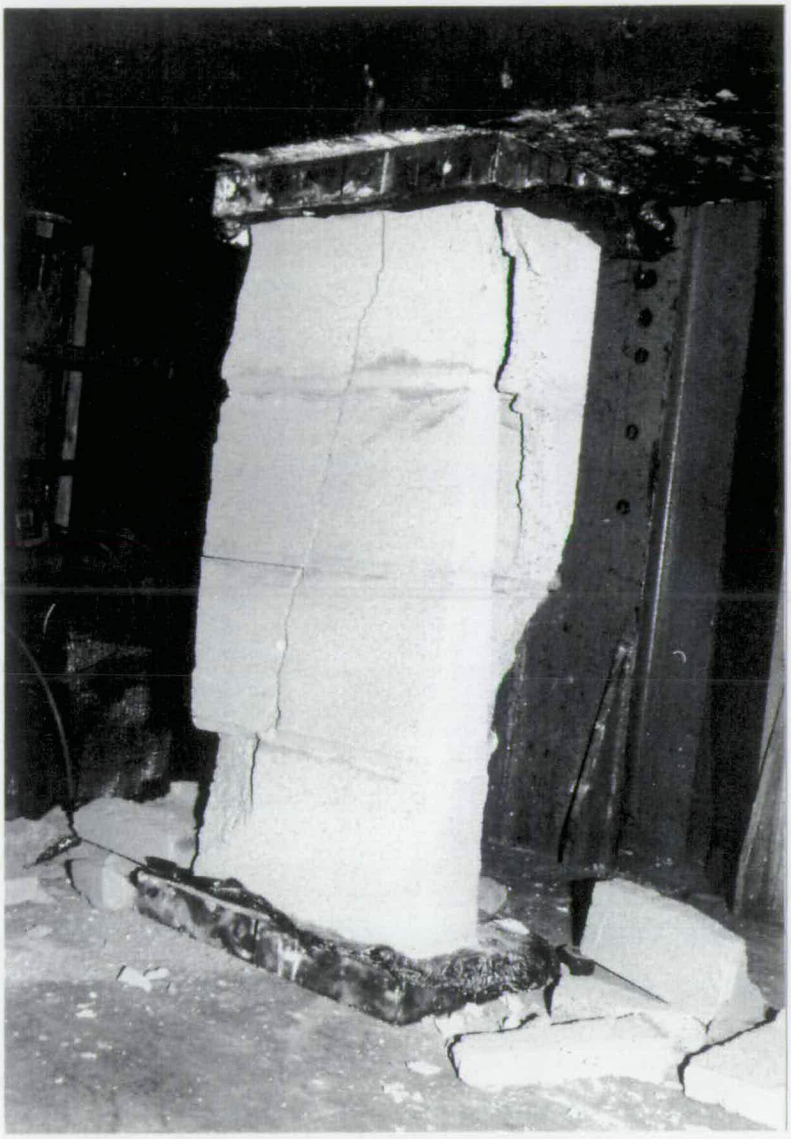


Fig. 4.4 Typical mode of failure for concentrically loaded unfilled full-block prism



Fig. 4.5 Typical mode of failure for concentrically loaded filled full-block prism



Fig. 4.6 Typical mode of failure for concentrically loaded unfilled half-block prism



Fig. 4.7 Typical mode of failure for concentrically loaded filled half-block prism

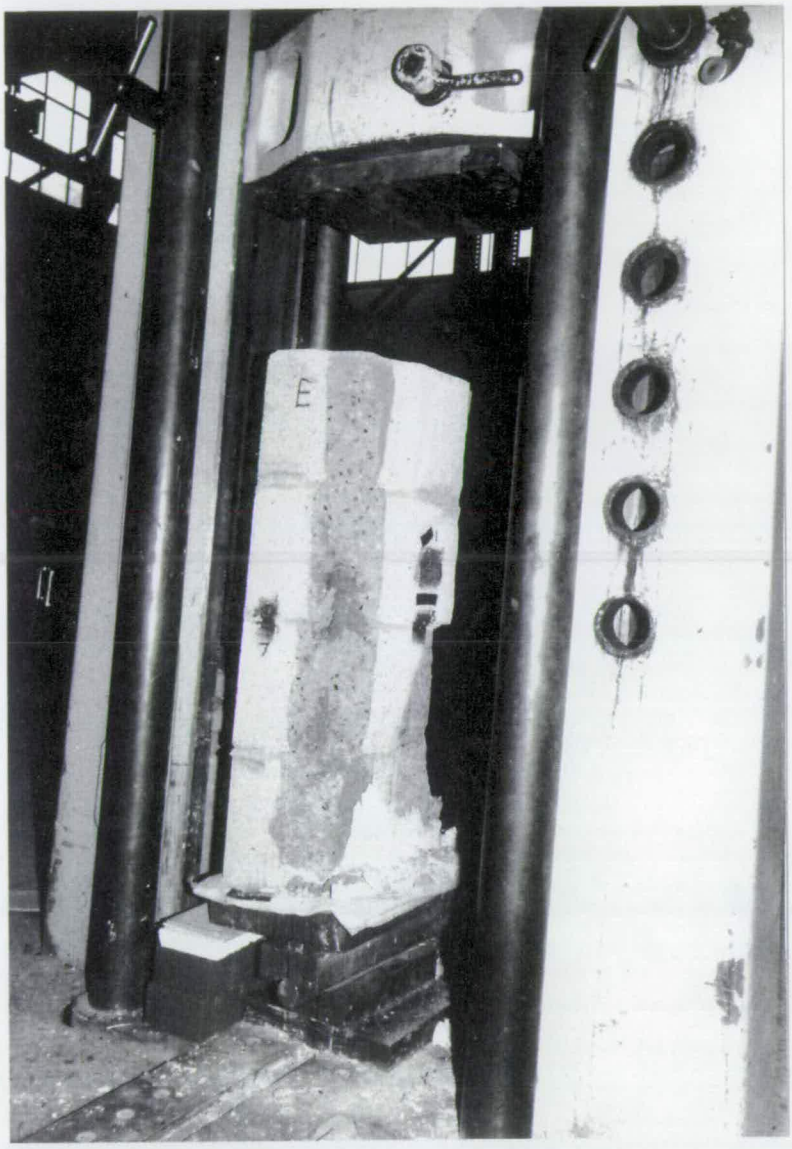


Fig. 4.8 Typical mode of failure for eccentrically loaded filled full-block prism compressed at t/6

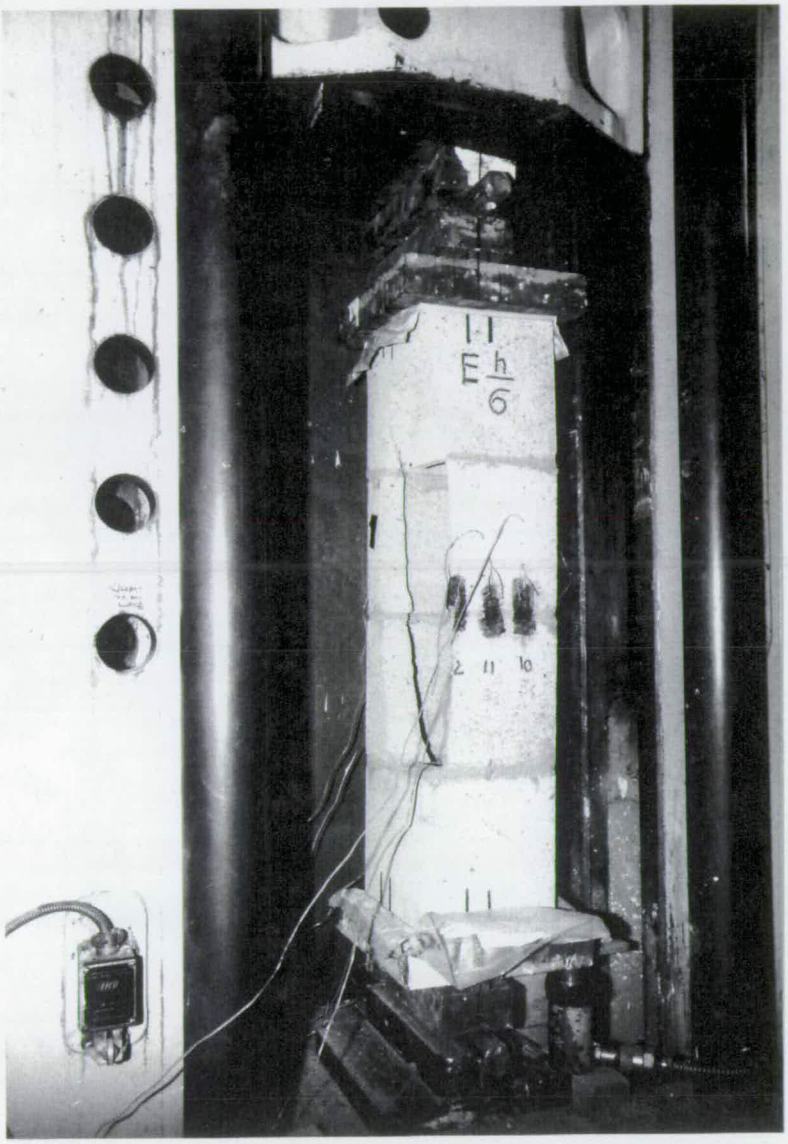


Fig. 4.9 Typical mode of failure for eccentrically loaded unfilled half-block prism compressed at t/6

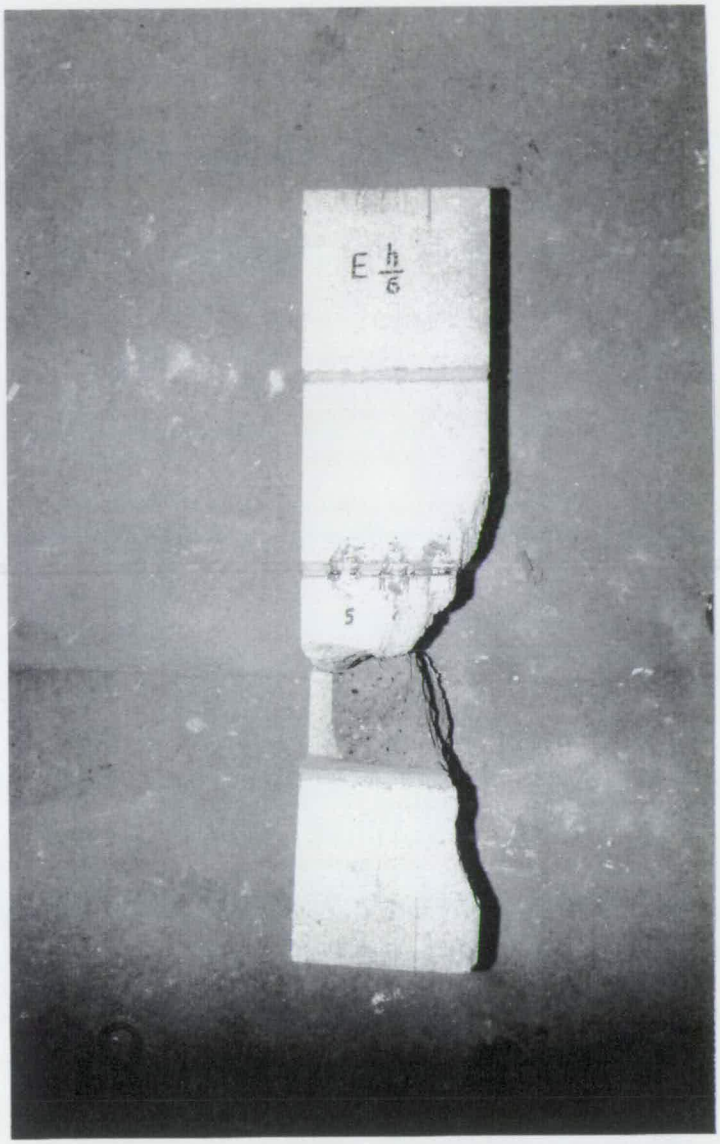


Fig. 4.10 Typical mode of failure for eccentrically loaded filled half-block prism compressed at t/6

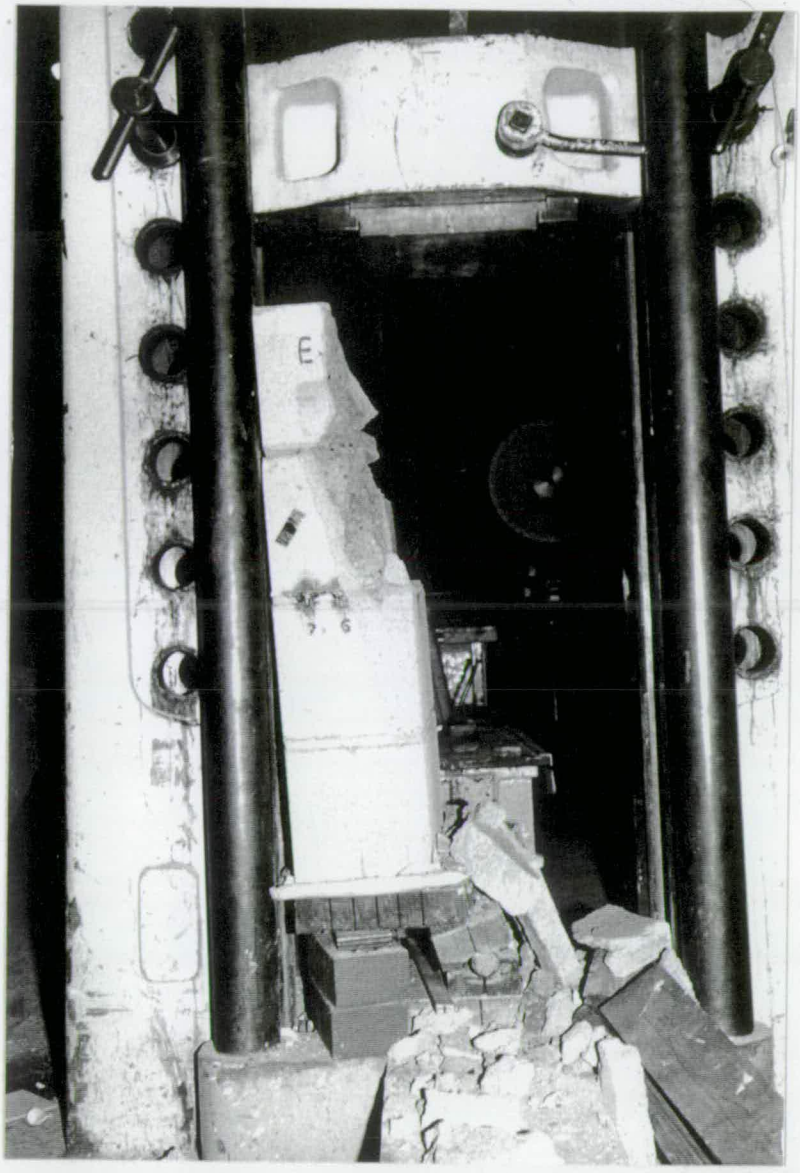


Fig. 4.11 Typical mode of failure for eccentrically loaded filled full-block prism compressed at t/3

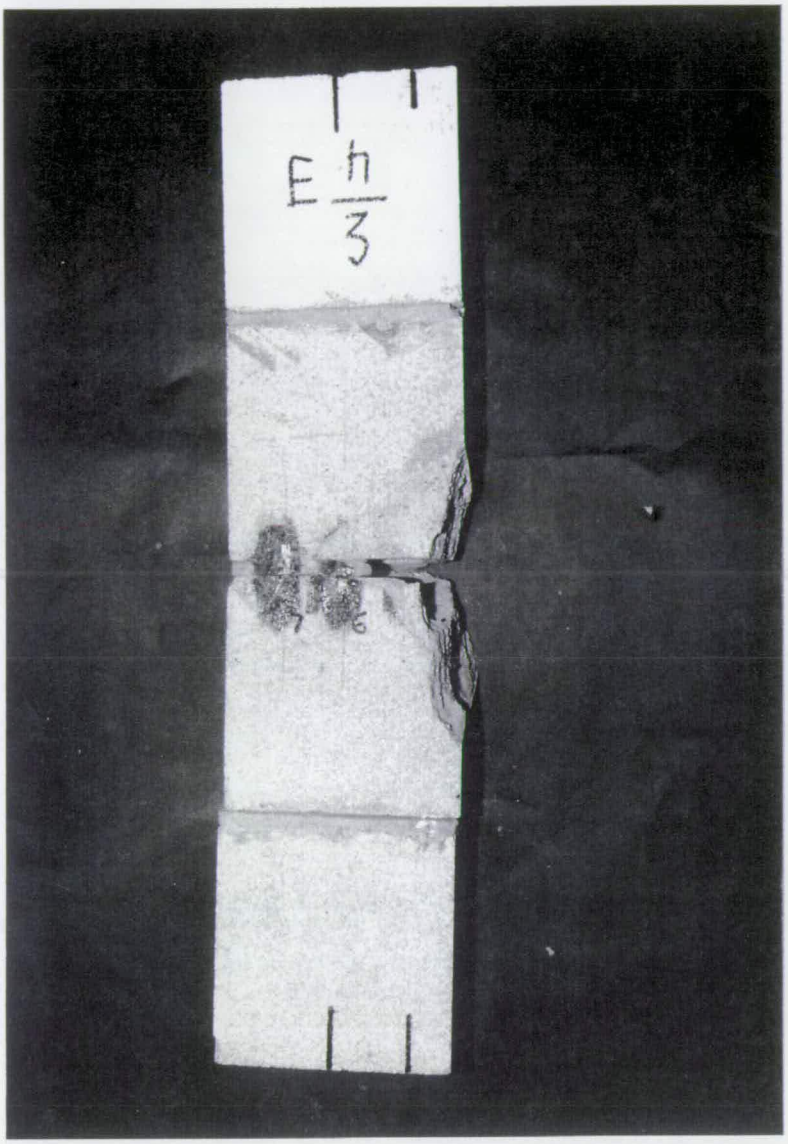


Fig. 4.12 Typical mode of failure for eccentrically loaded unfilled half-block prism compressed at t/3

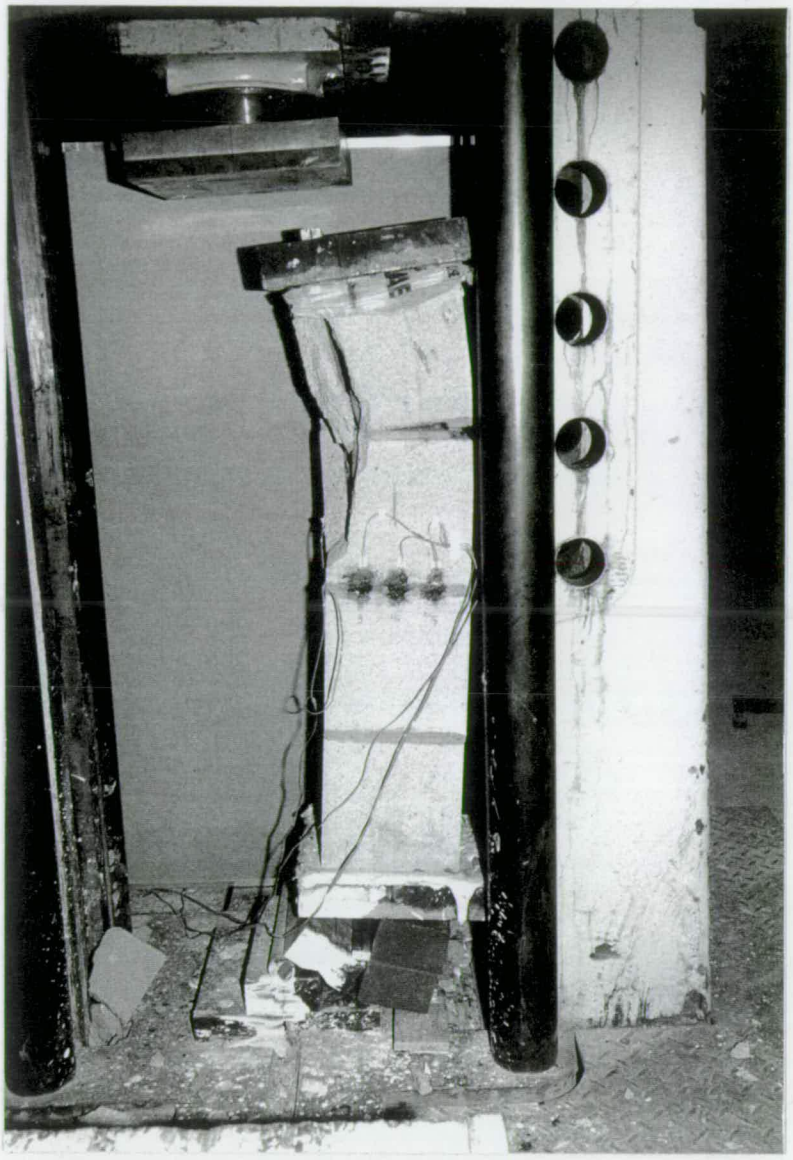


Fig. 4.13 Typical mode of failure for eccentrically loaded filled half-block prism compressed at t/3

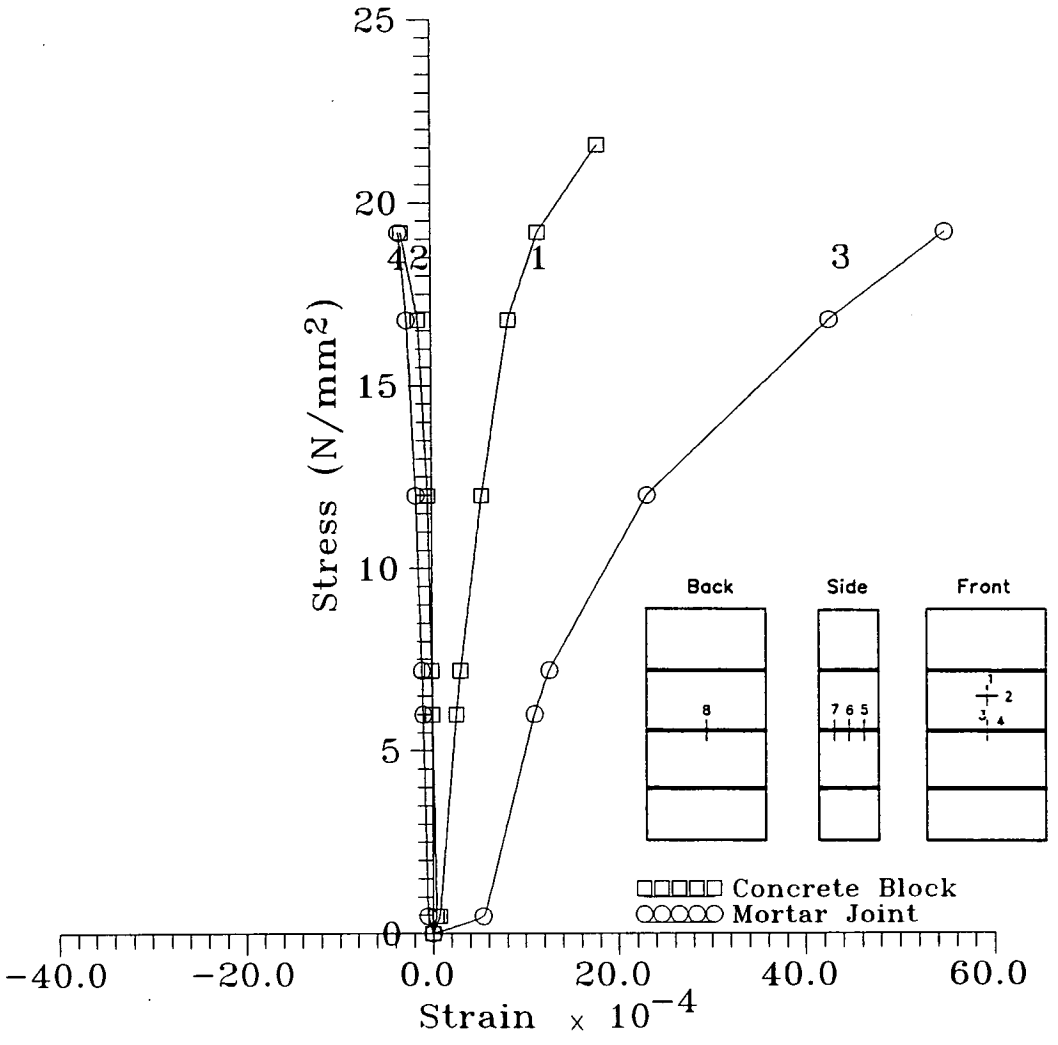


Fig. 4.14 Stress–strain curves for unfilled full–block axially loaded prism

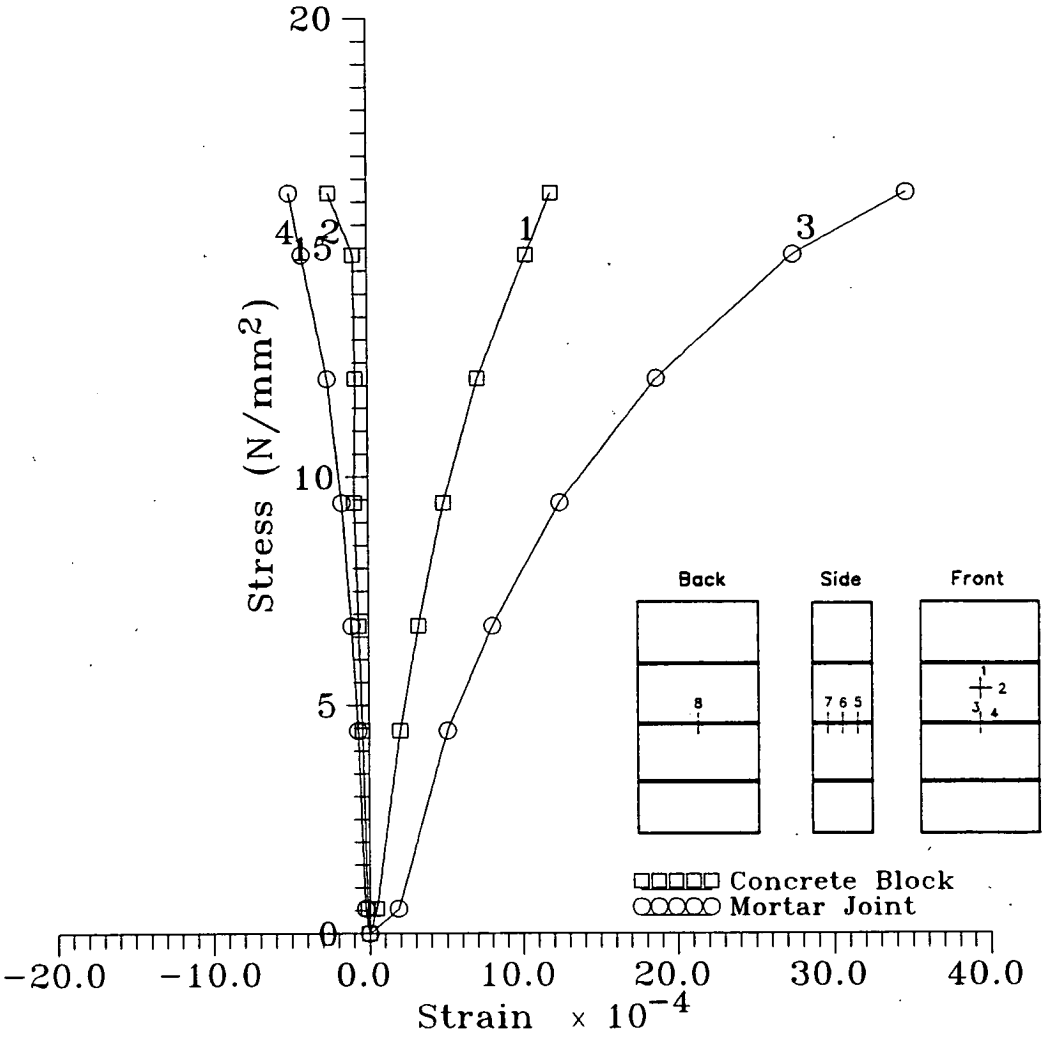


Fig. 4.15 Stress–strain curves for filled full–block axially loaded prism

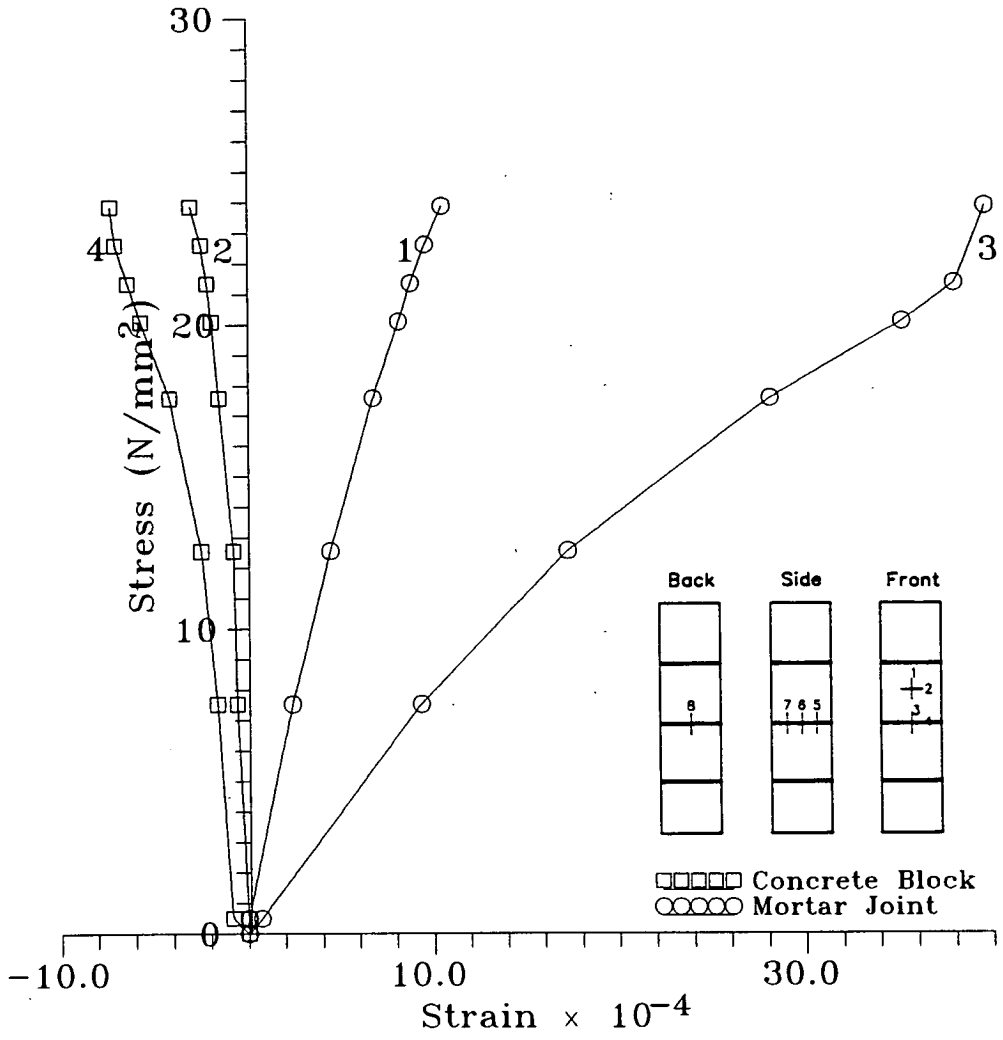


Fig. 4.16 Stress–strain curves for unfilled half–block axially loaded prism

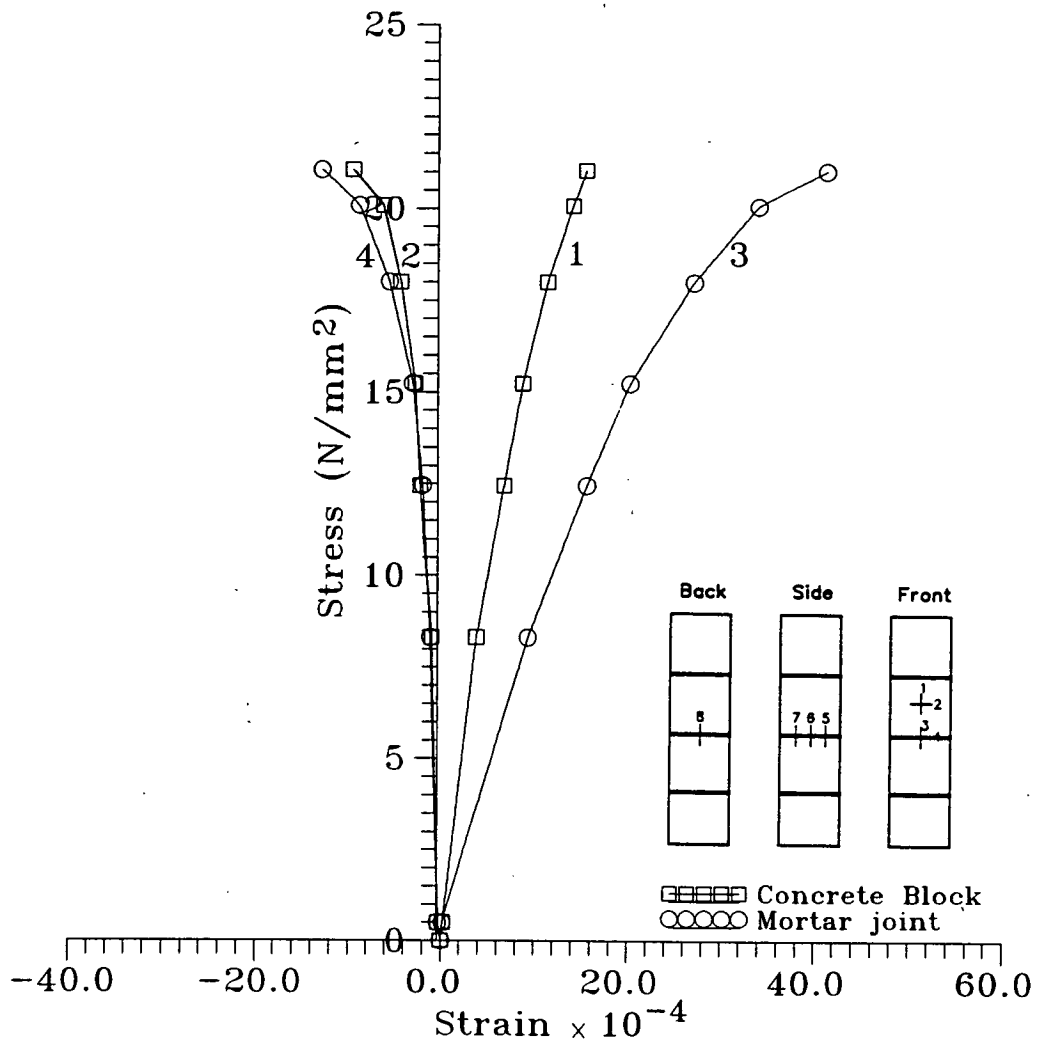


Fig. 4.17 Stress–strain curves for filled half-block axially loaded prism

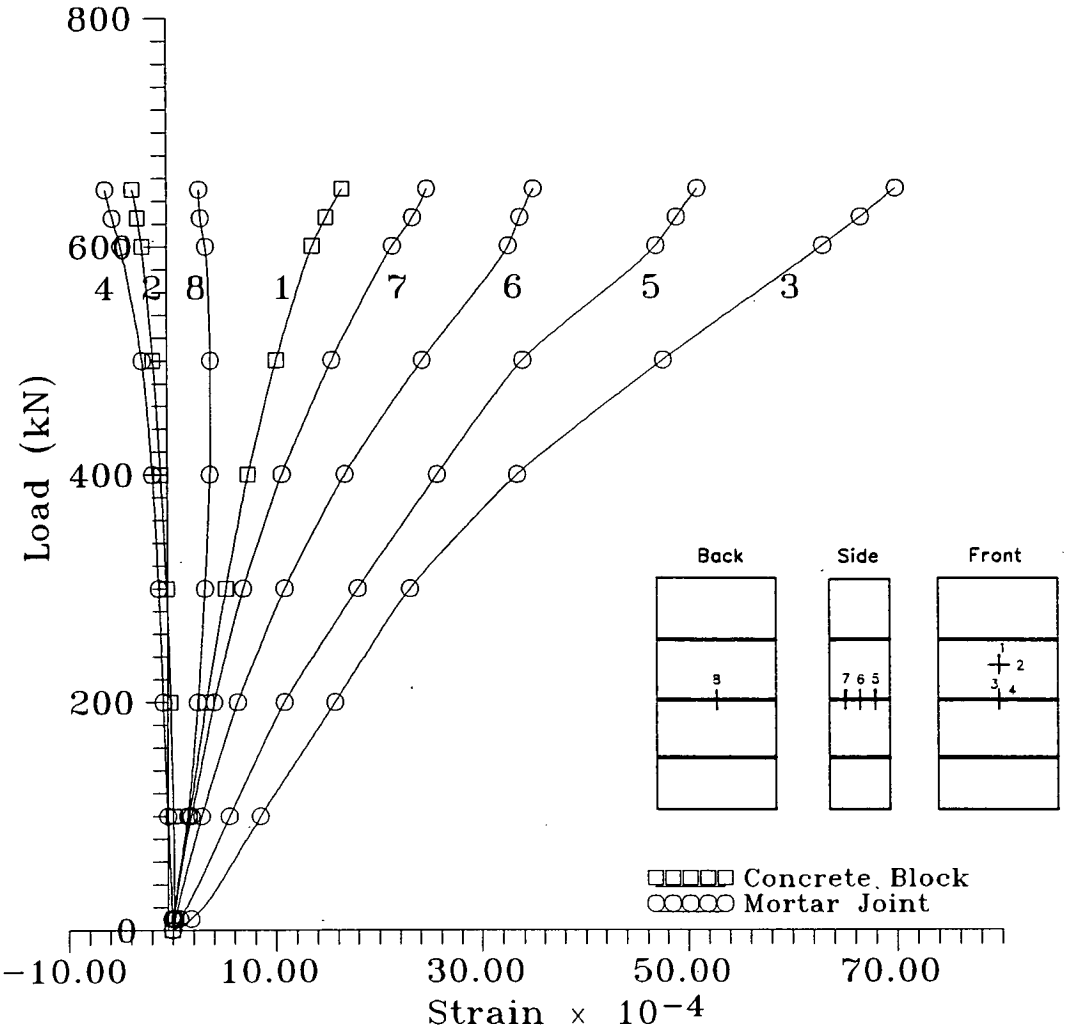


Fig. 4.18 Load–strain curves for unfilled full–block prism compressed under eccentric load at e = t/6

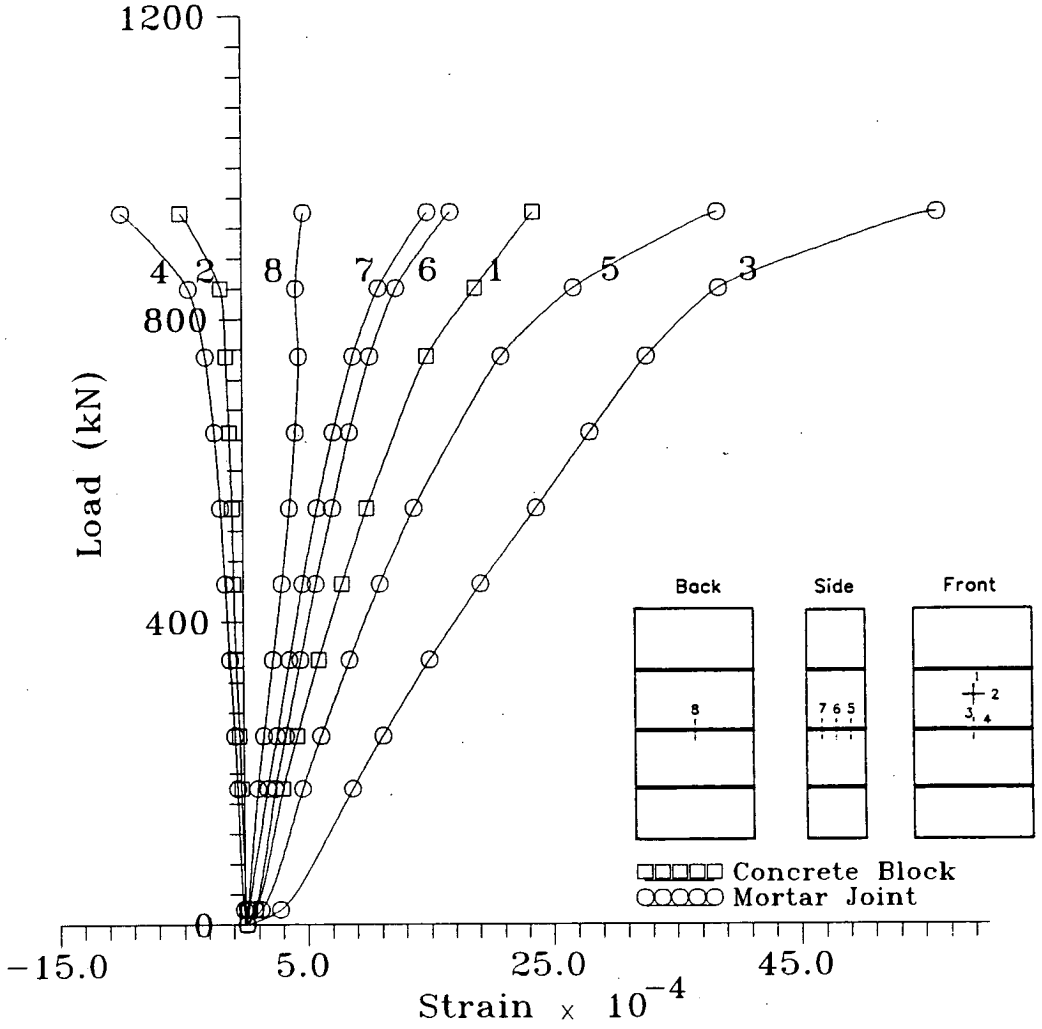


Fig. 4.19 Load–strain curves for filled full–block prism compressed under eccentric load at e = t/6

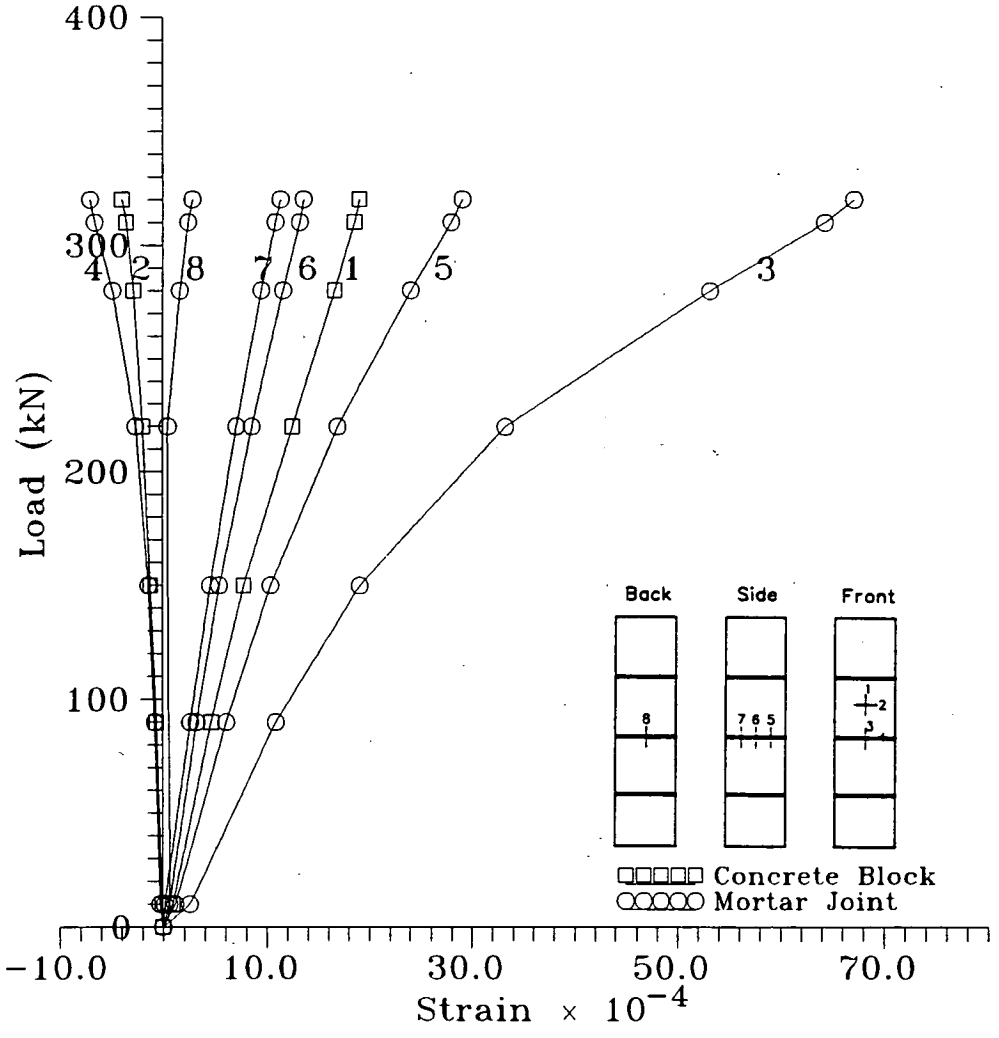


Fig. 4.20 Load–strain curves for unfilled half-block prism compressed under eccentric load at e = t/6

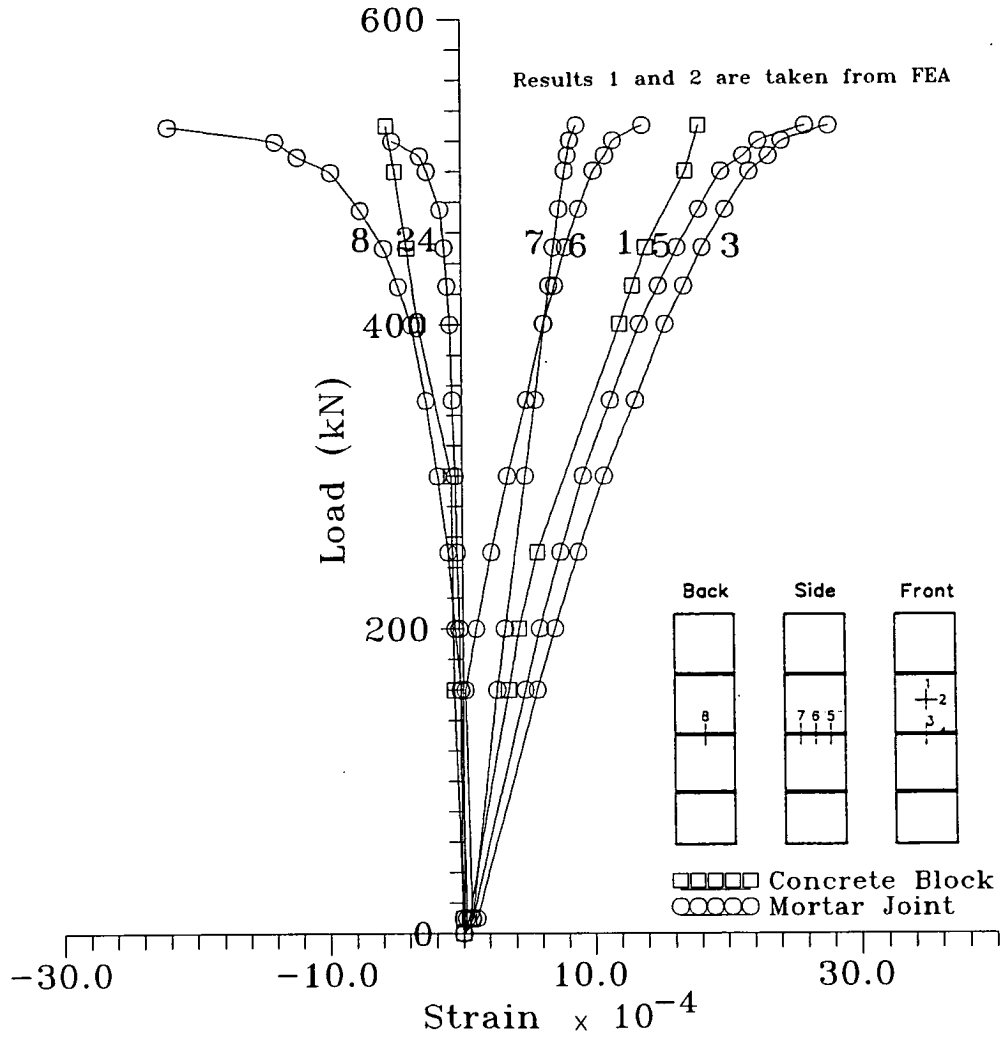


Fig. 4.21 Load–strain curves for filled half–block prism compressed under eccentric load at e = t/6

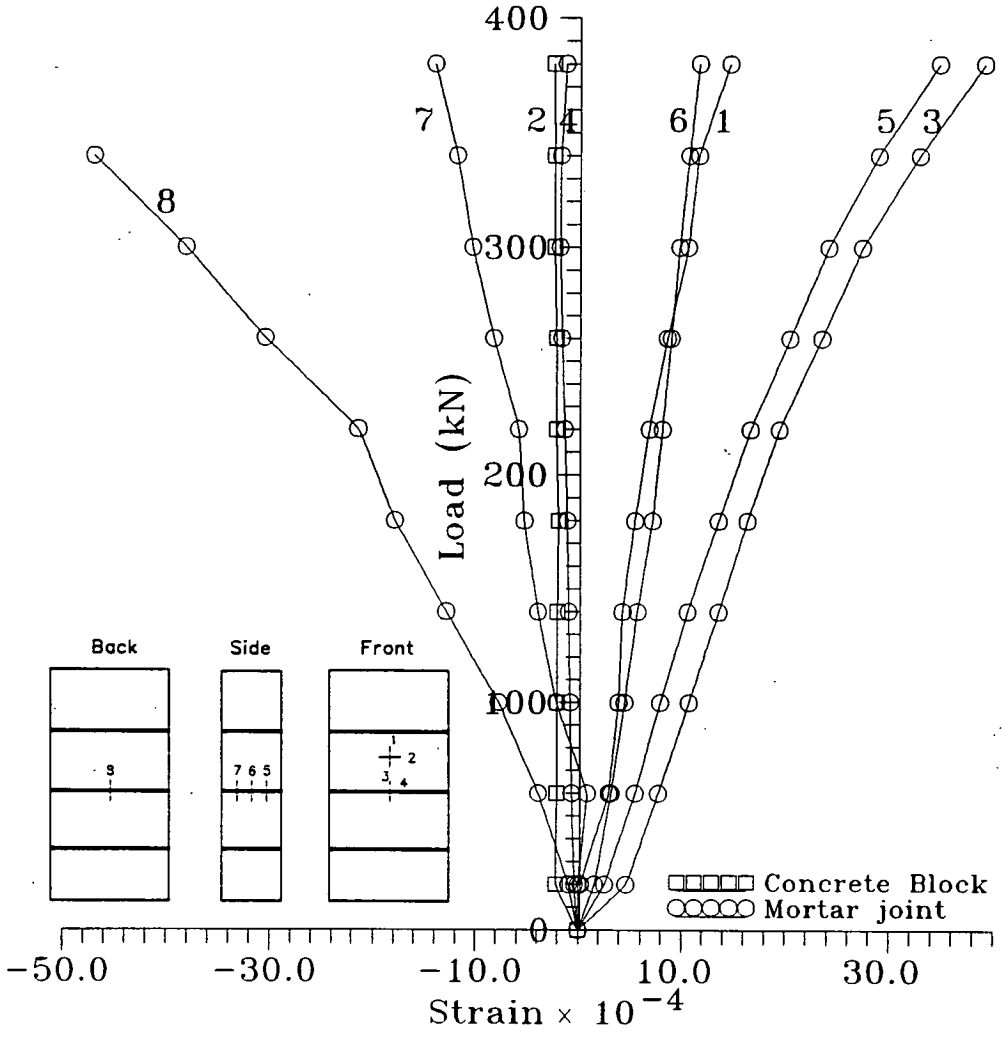


Fig. 4.22 Load–strain curves for unfilled full–block prism compressed under eccentric Load at e = t/3

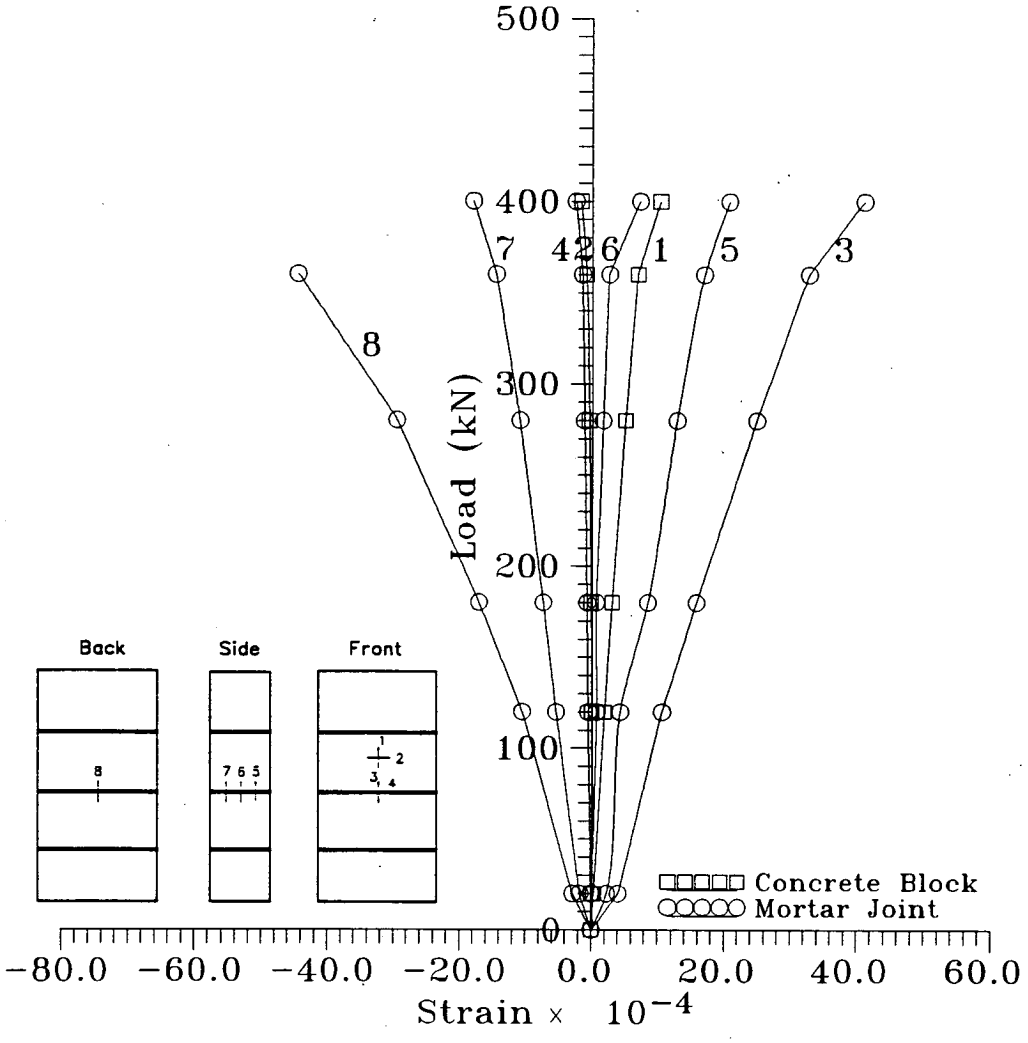


Fig. 4.23 Load–strain curves for filled full–block prism compressed under eccentric load at e = t/3

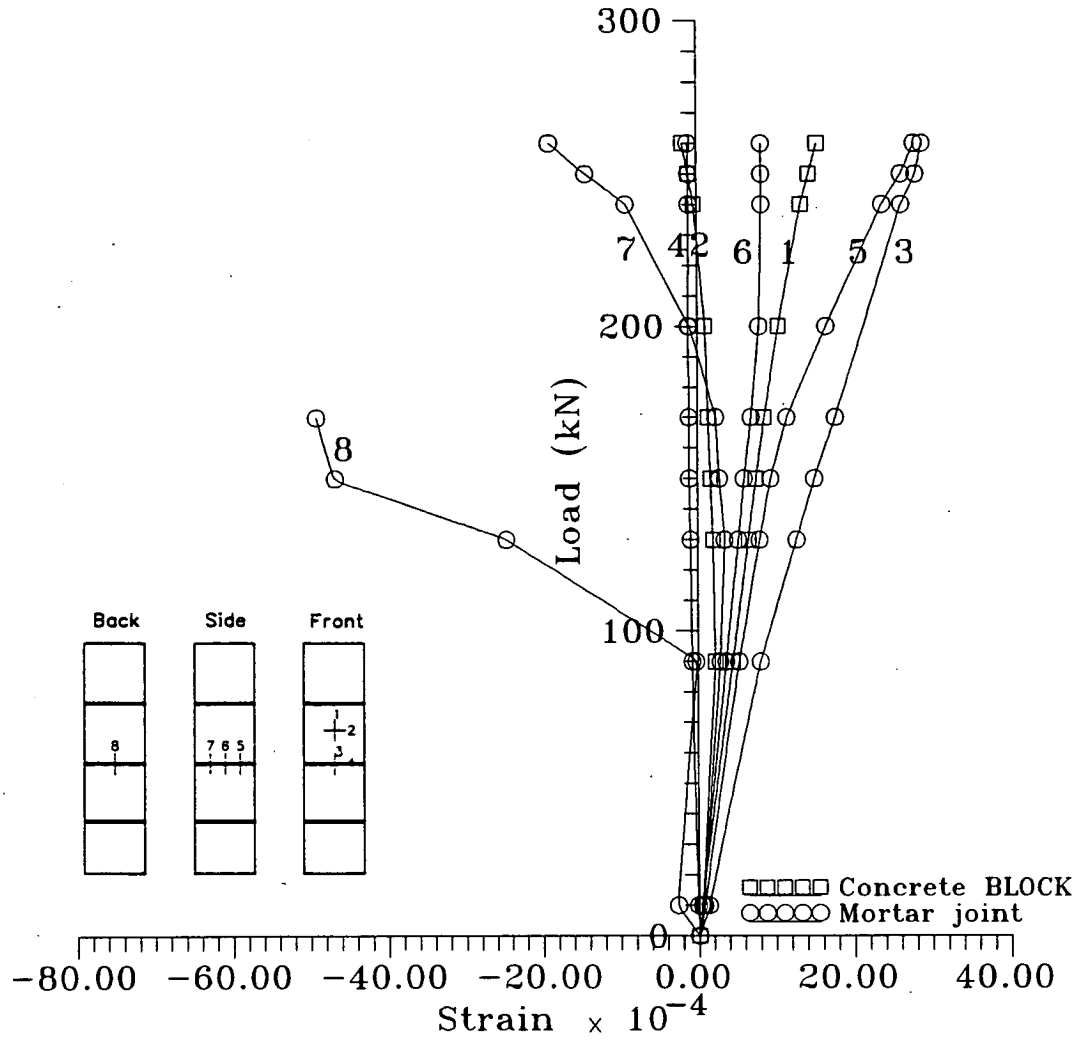


Fig. 4.24 Load–strain curves for unfilled half–block prism compressed under eccentric load at e = t/3

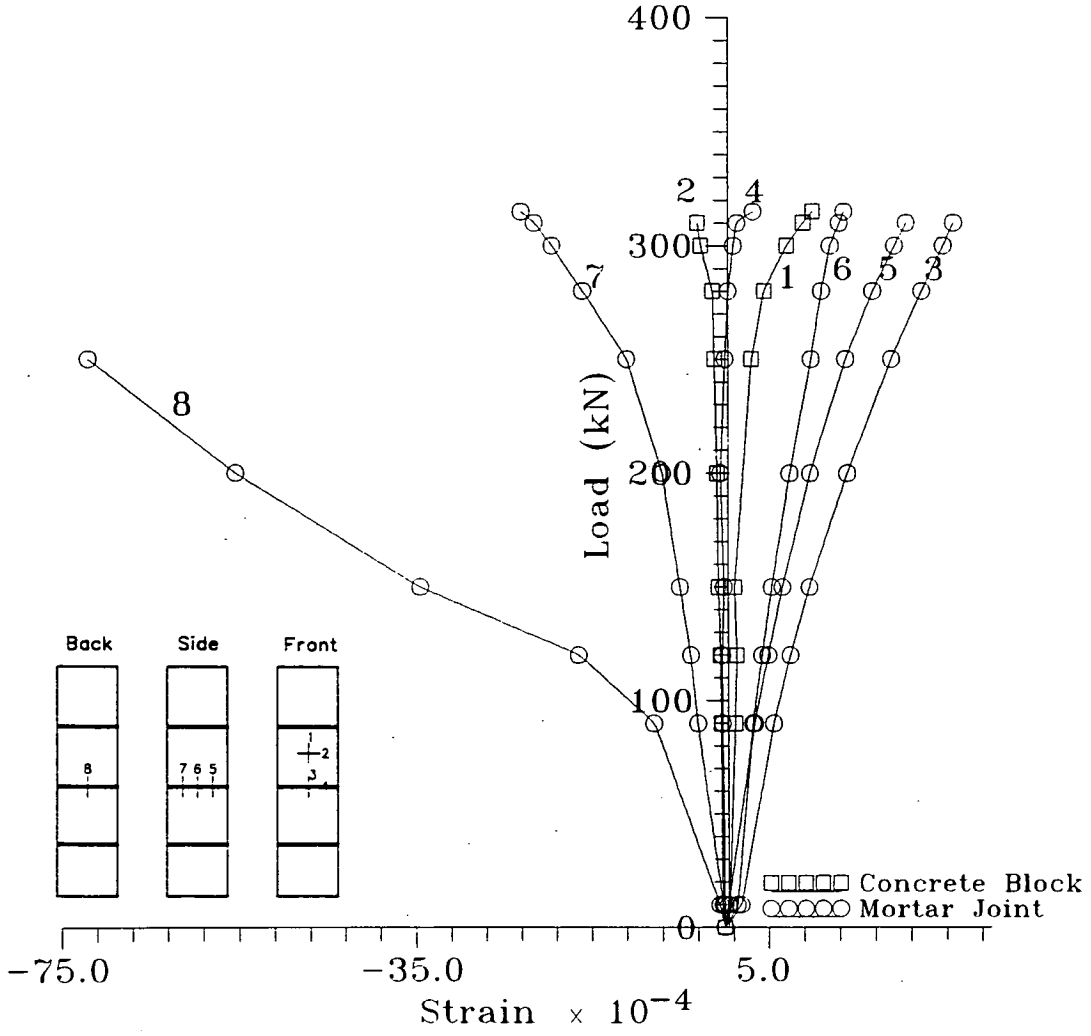


Fig. 4.25 Load-strain curves for filled half-block prism compressed under eccentric load at e = t/3

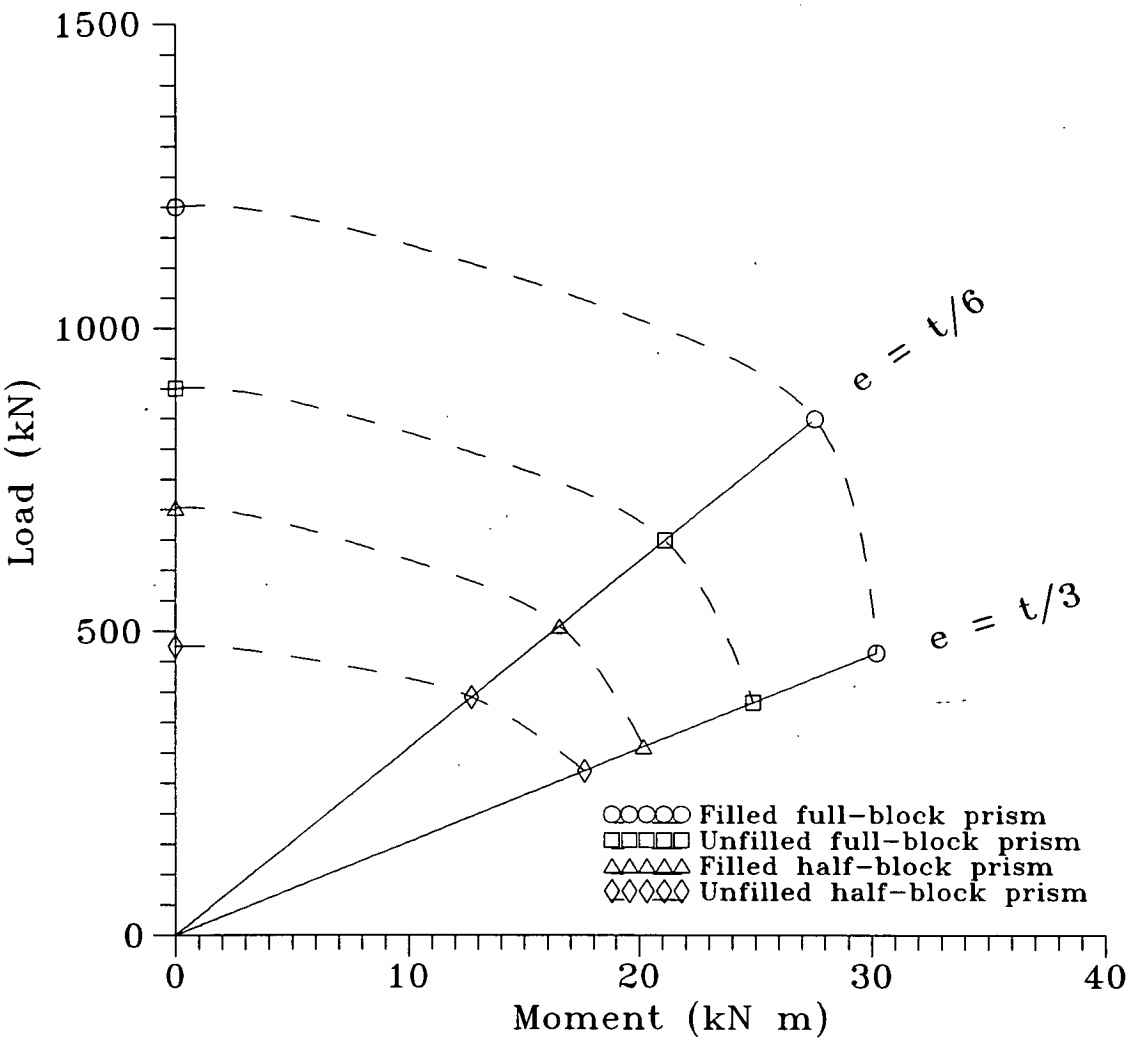


Fig. 4.26 Load–moment interaction diagrams for blockwork masonry prisms

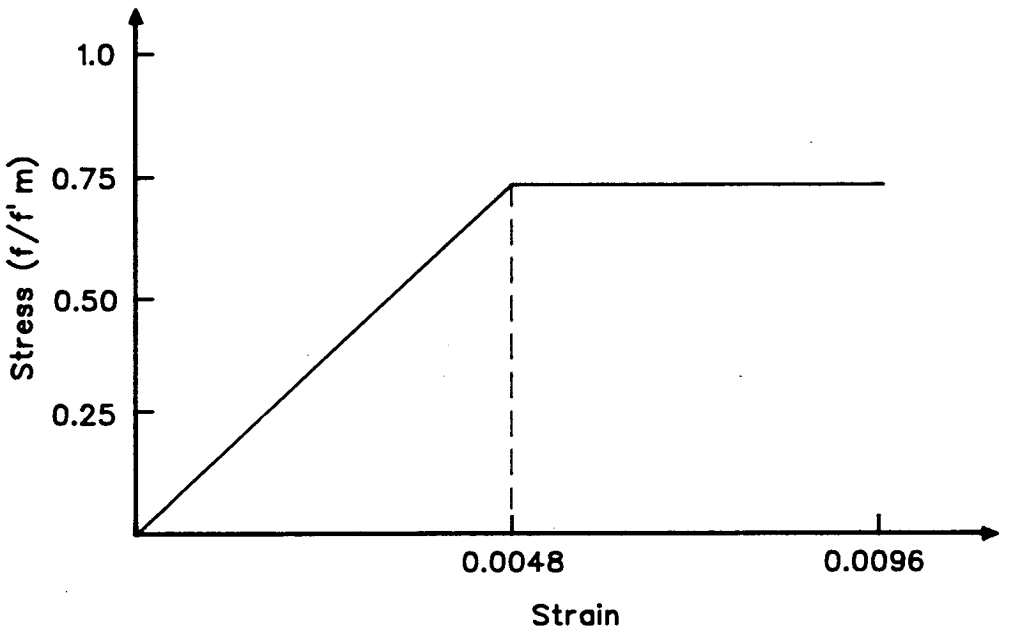


Fig. 4.27 Idealised Stress–Strain relationship for confined 10 mm mortar joint (based on a suggestion by Khalaf [39])

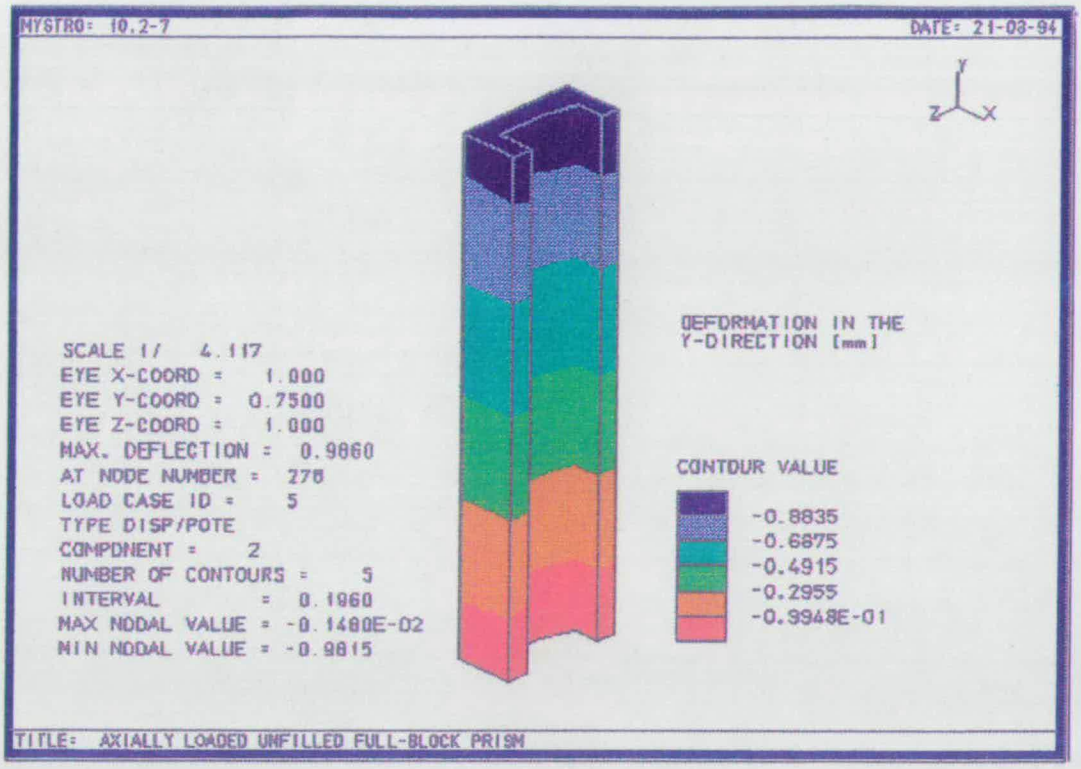


Fig. 4.28 Deformation of axially loaded unfilled full-block prism, in the Y-direction

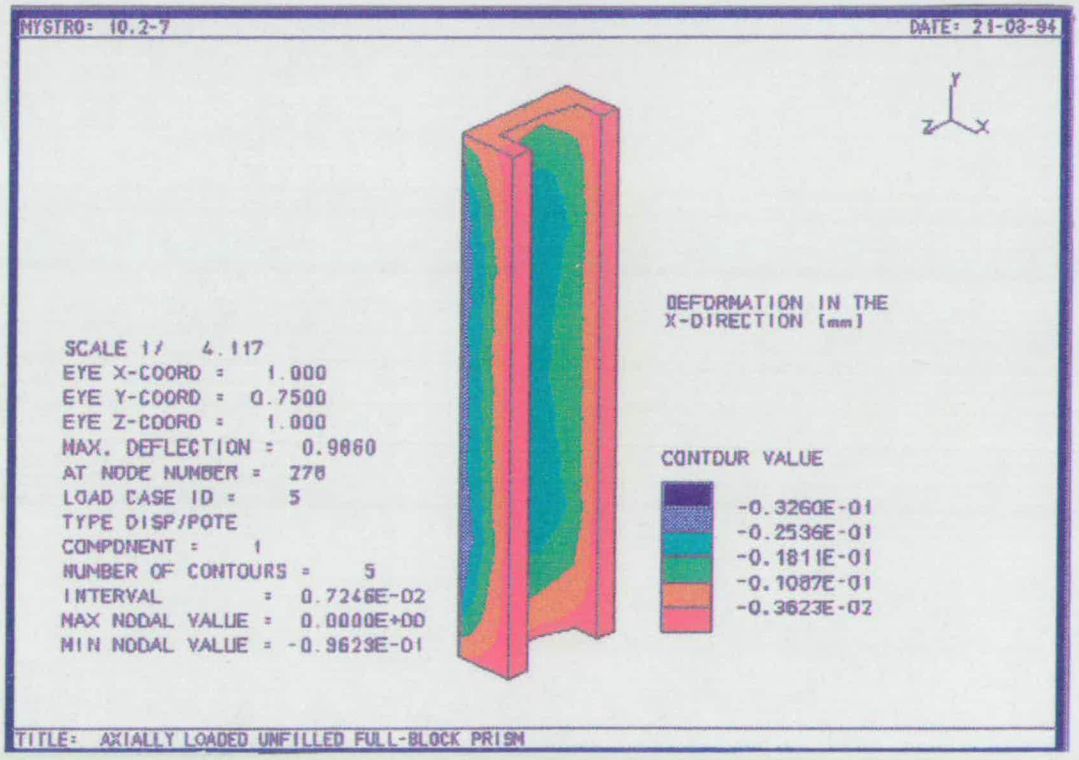


Fig. 4.29 Deformation of axially loaded unfilled full-block prism, in the X-direction

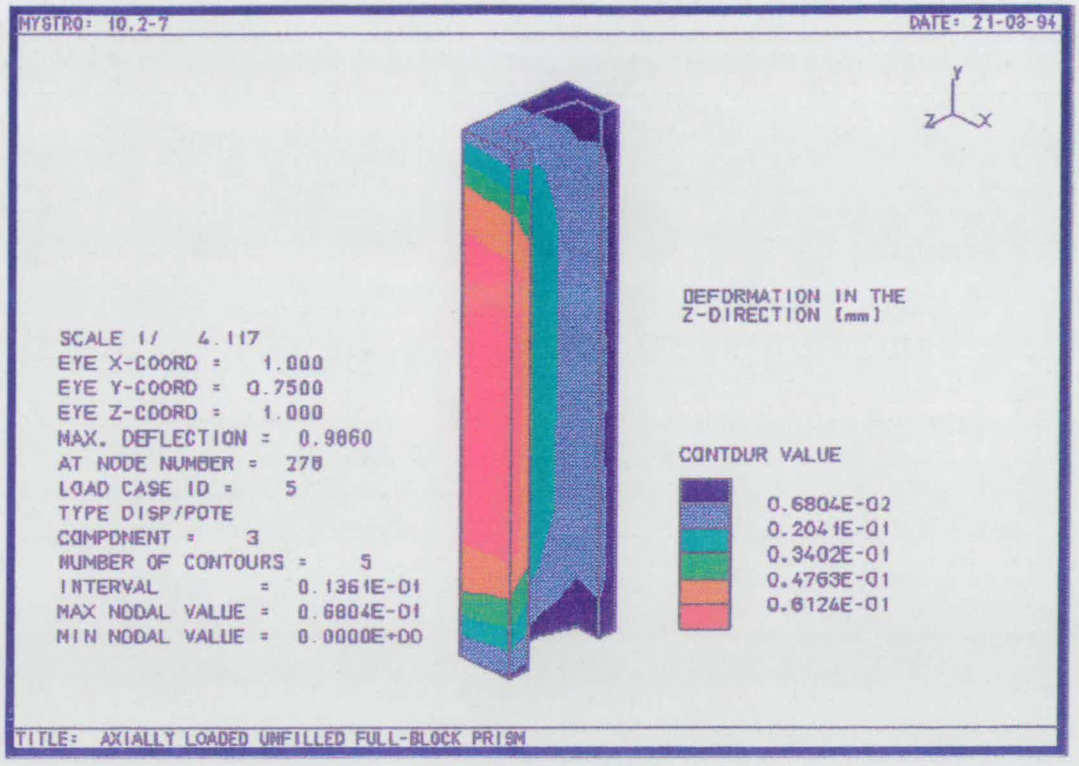


Fig. 4.30 Deformation of axially loaded unfilled full-block prism, in the Z-direction

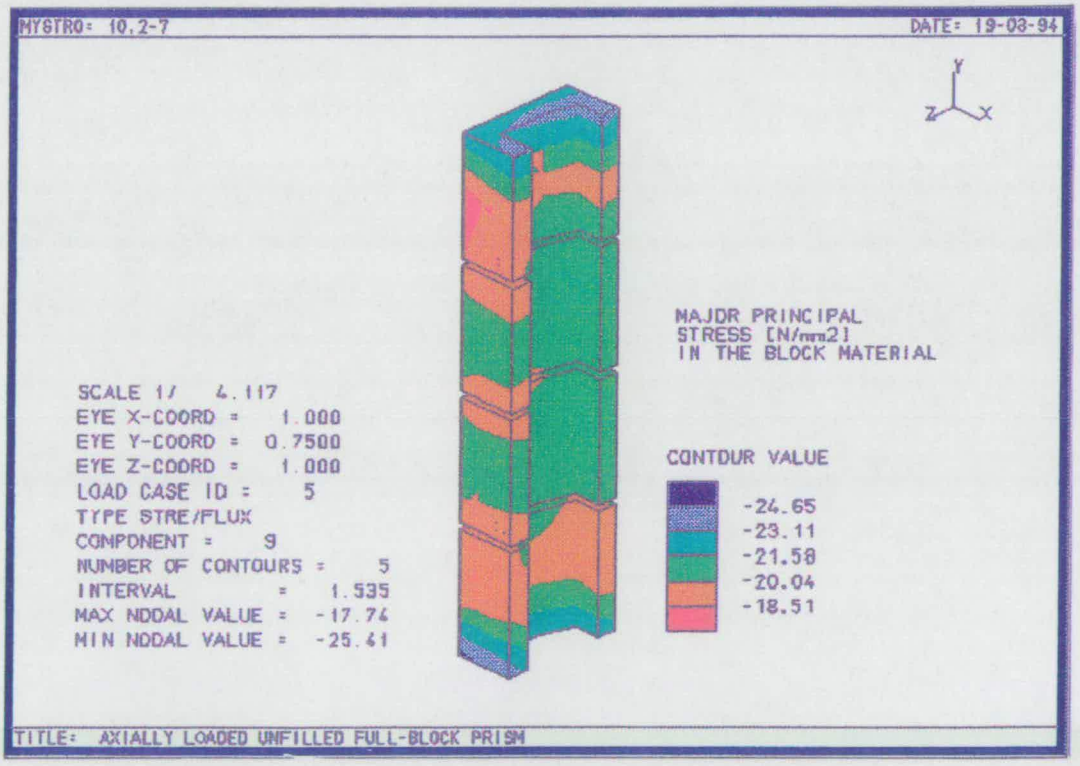


Fig. 4.31 Major principal stress in the block material, for an axially loaded unfilled full-block prism

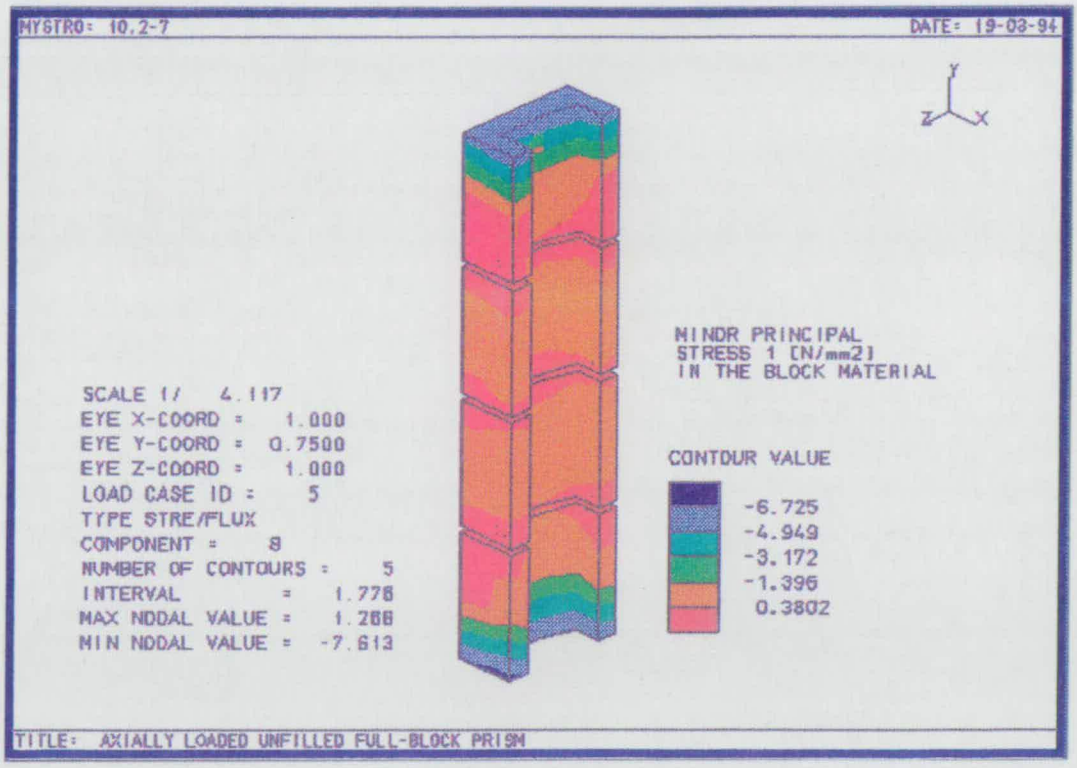


Fig. 4.32 Minor principal stress 1 in the block material for an axially loaded unfilled full-block prism

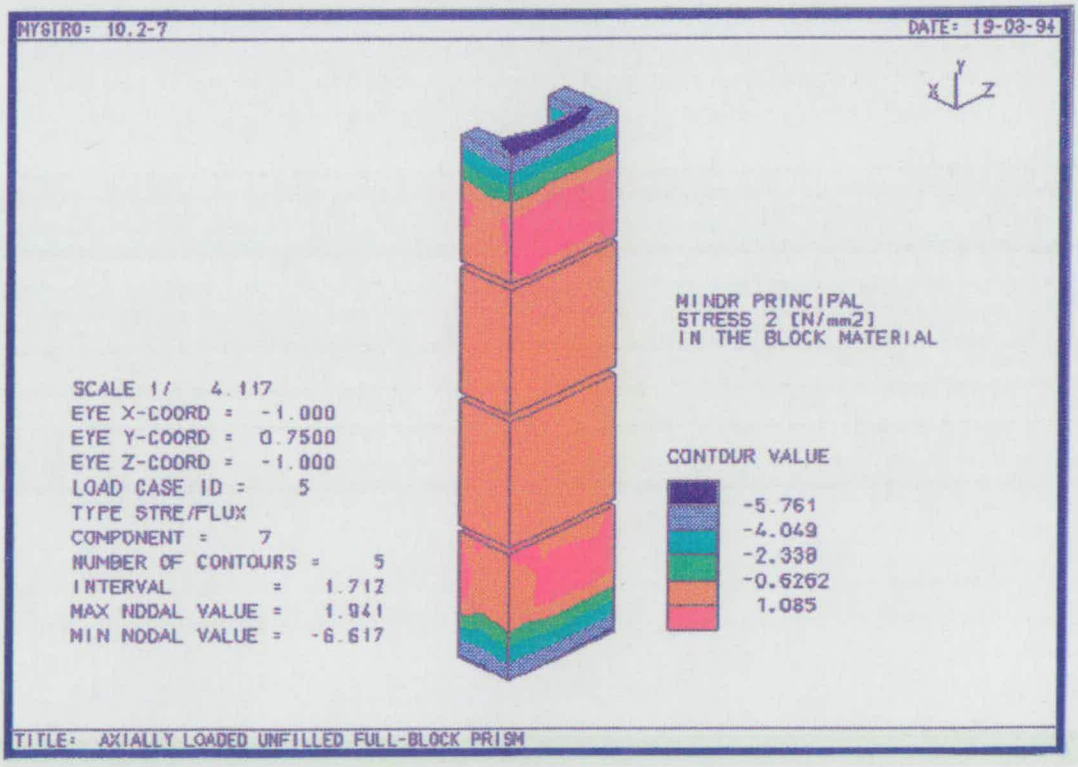


Fig. 4.33 Minor principal stress 2 in the block material for an axially loaded unfilled full-block prism

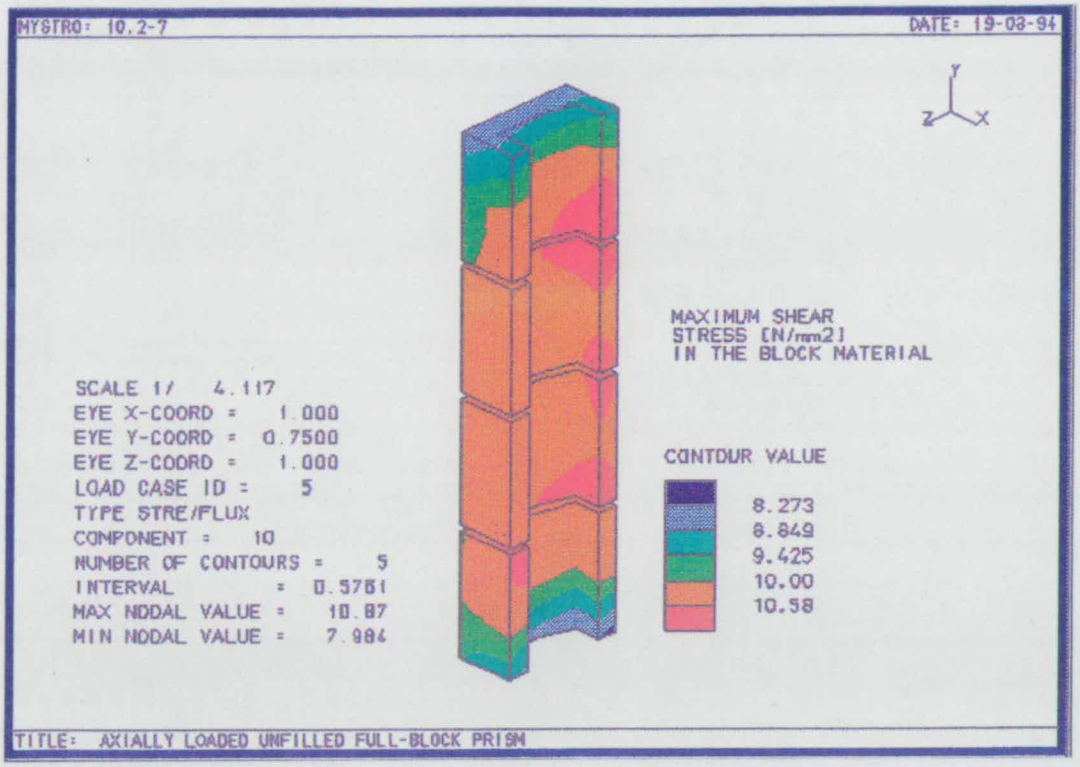


Fig. 4.34 Shear stress in the block material for an axially loaded unfilled full-block prism

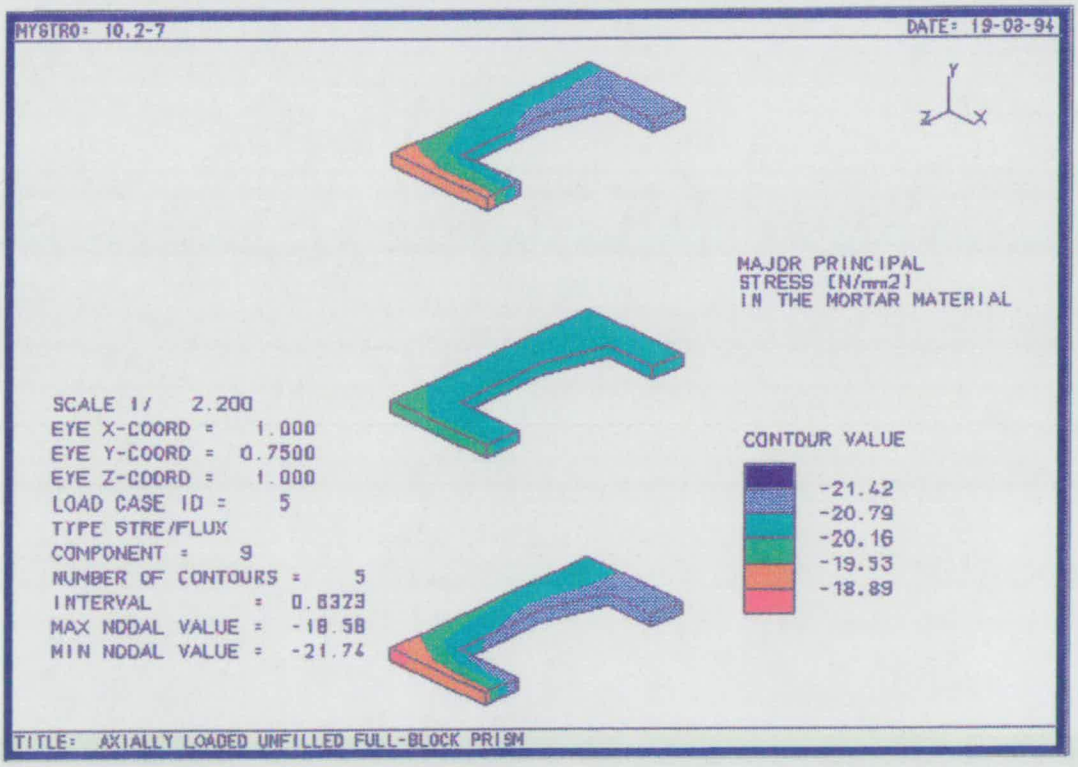


Fig. 4.35 Major principal stress in the mortar material for an axially loaded unfilled full-block prism

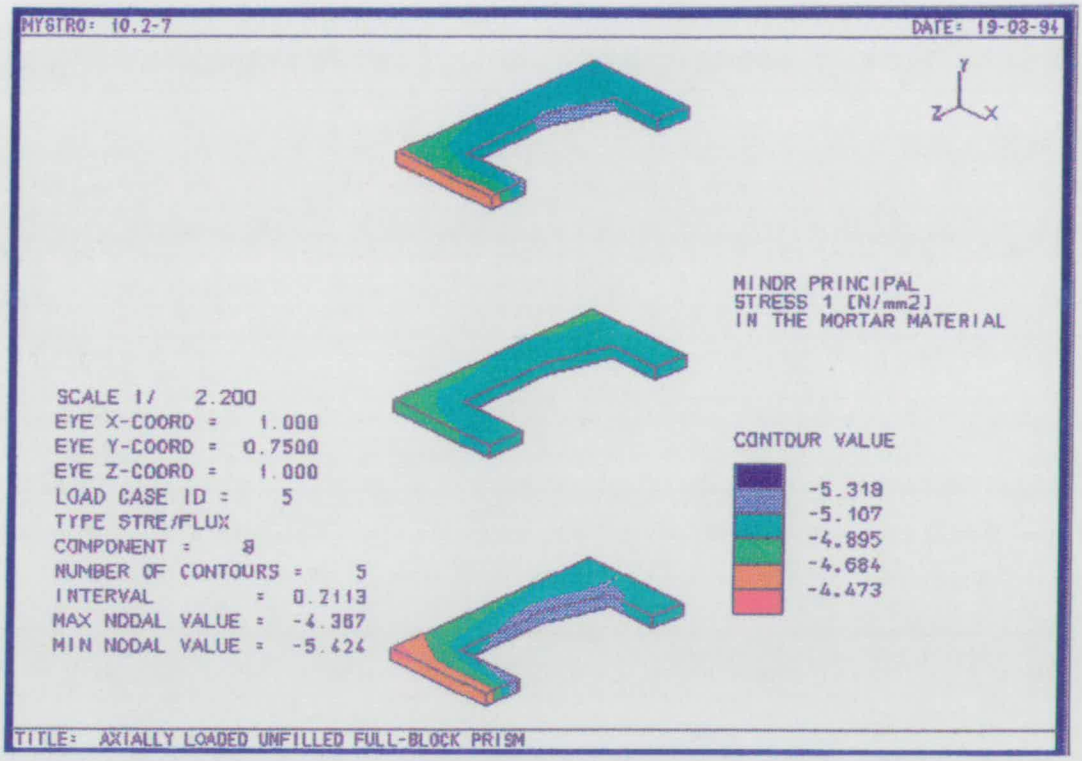


Fig. 4.36 Minor principal stress 1 in the mortar material for an axially loaded unfilled full-block prism

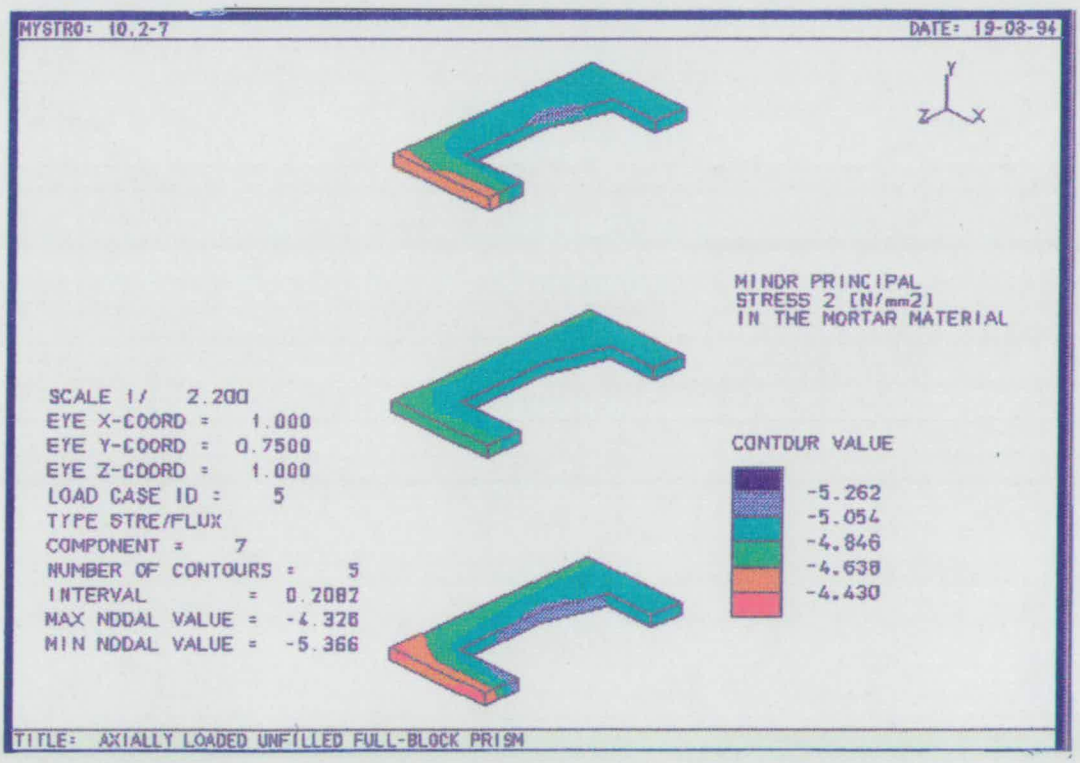


Fig. 4.37 Minor principal stress 2 in the mortar material for an axially loaded unfilled full-block prism

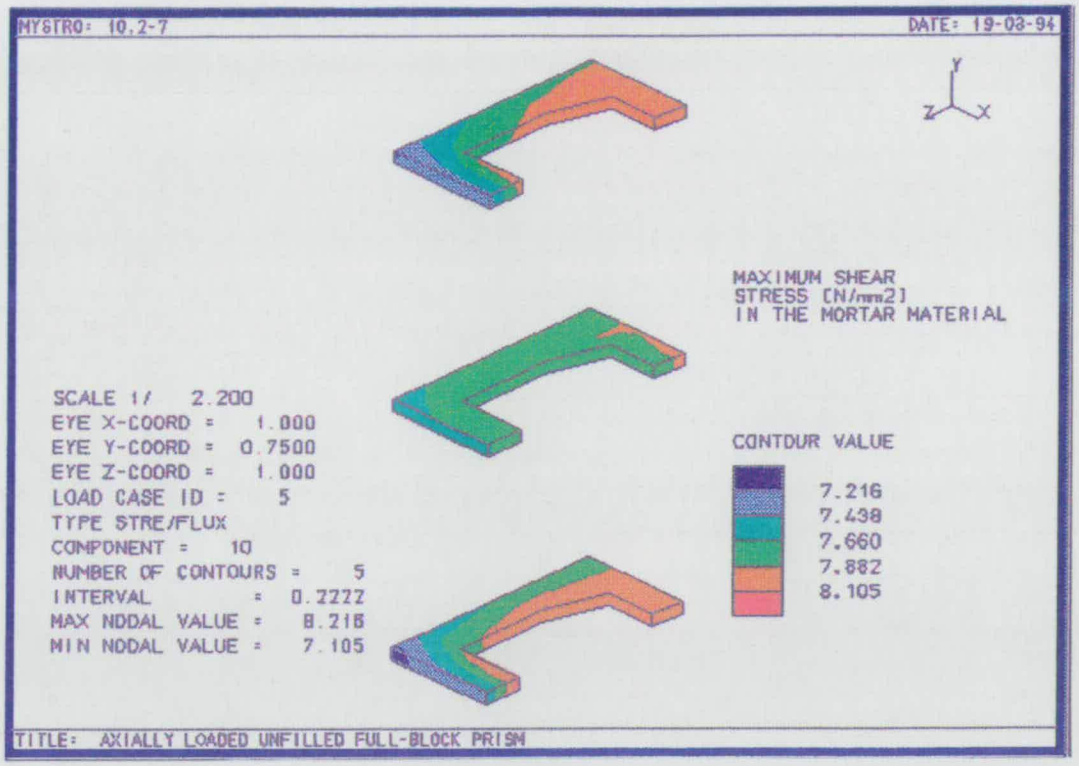


Fig. 4.38 Shear stress in the mortar material for an axially loaded unfilled full-block prism

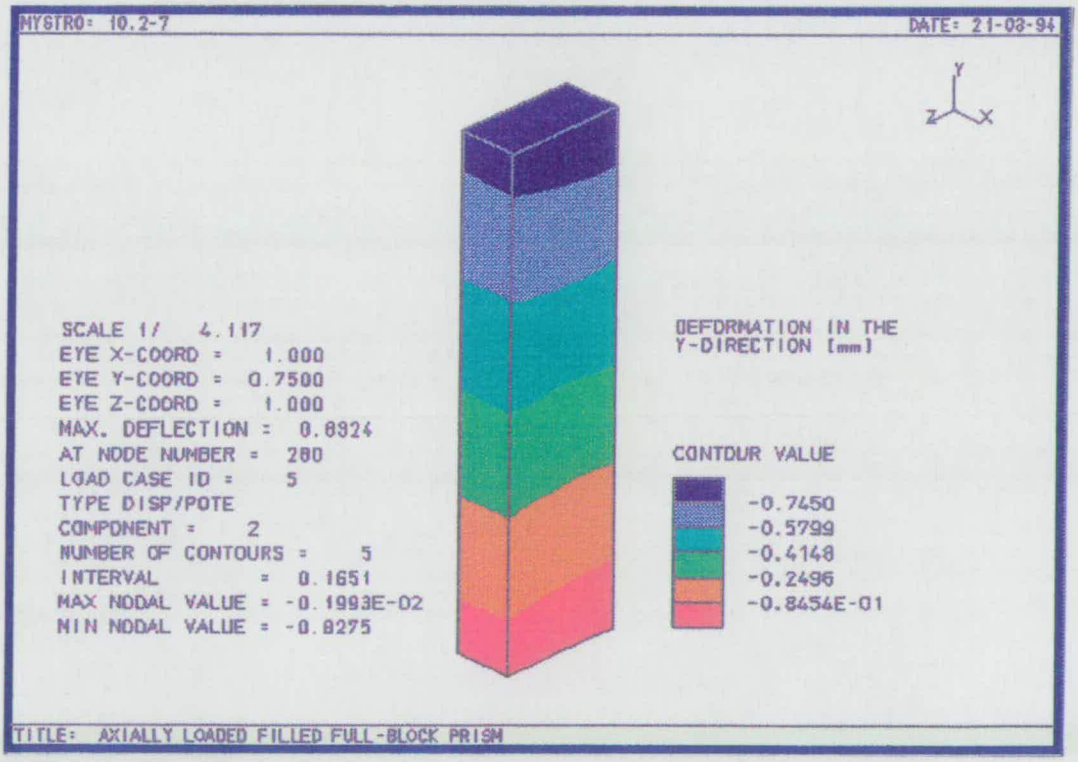


Fig. 4.39 Deformation of axially loaded filled full-block prism, in the Y-direction

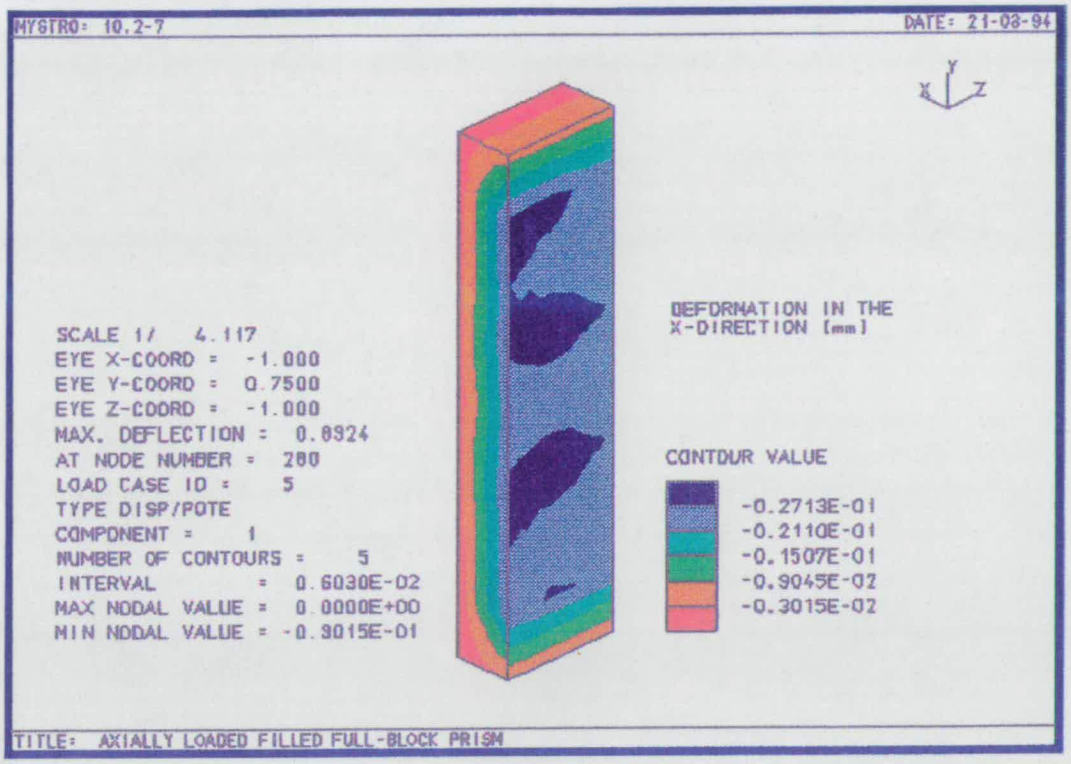


Fig. 4.40 Deformation of axially loaded filled full-block prism, in the X-direction

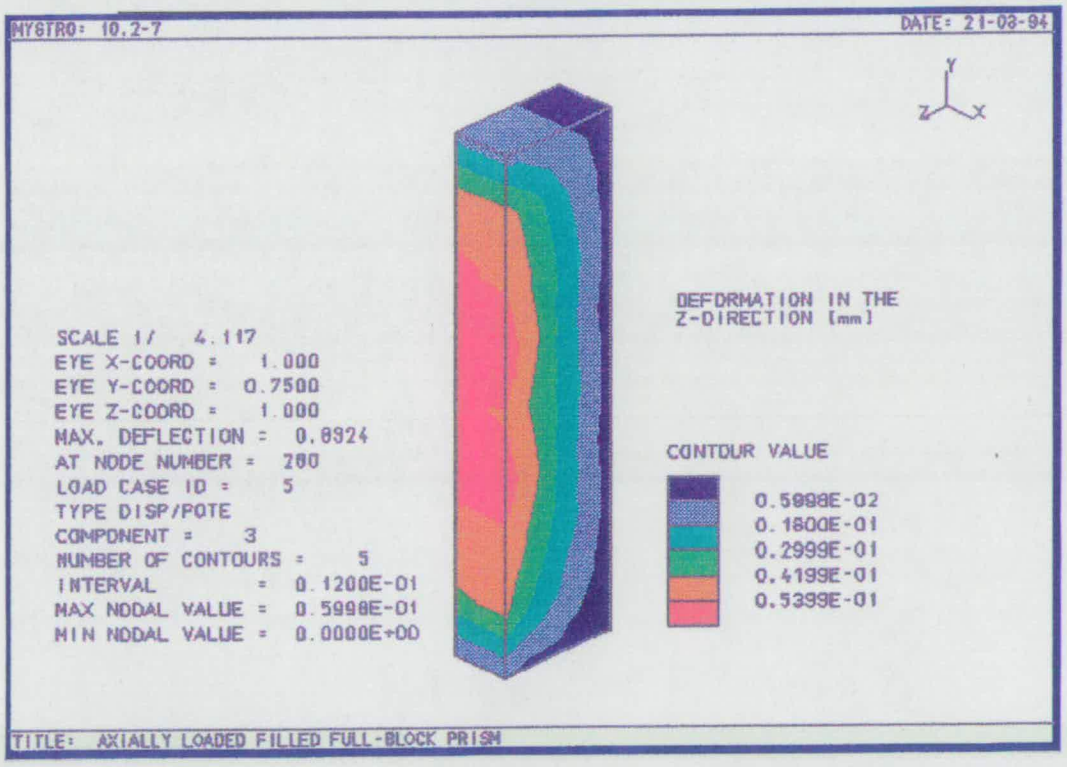


Fig. 4.41 Deformation of axially loaded filled full-block prism, in the Z-direction

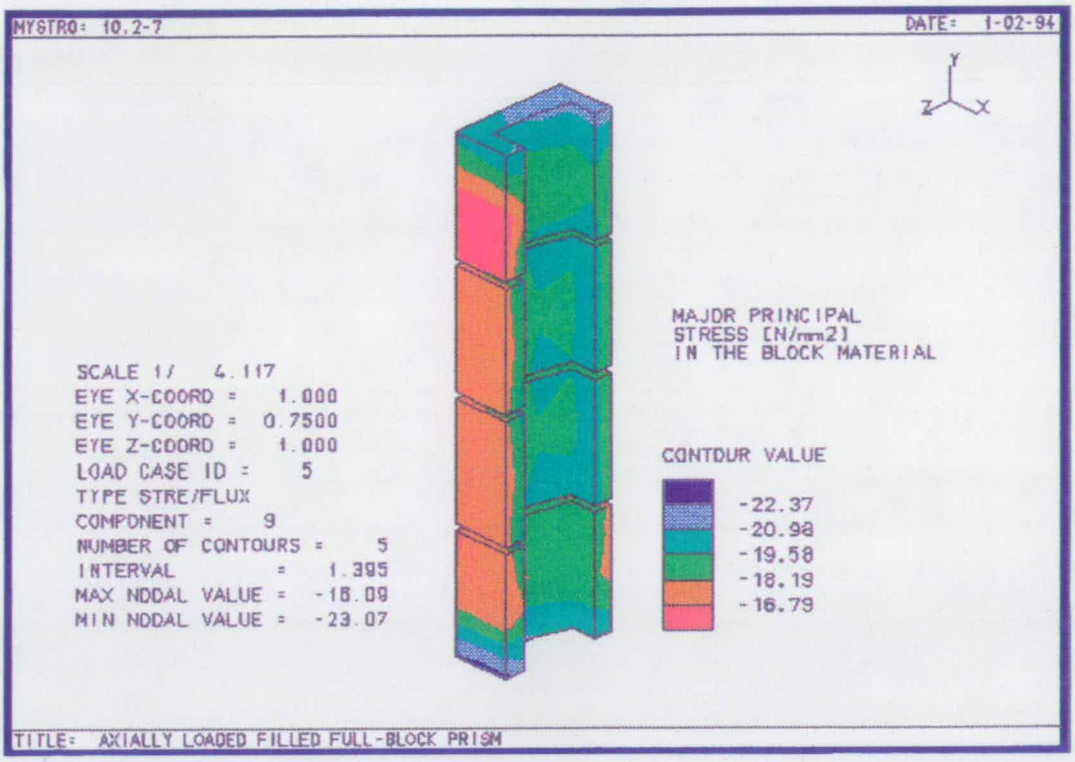


Fig. 4.42 Major principal stress in the block material for an axially loaded filled full-block prism

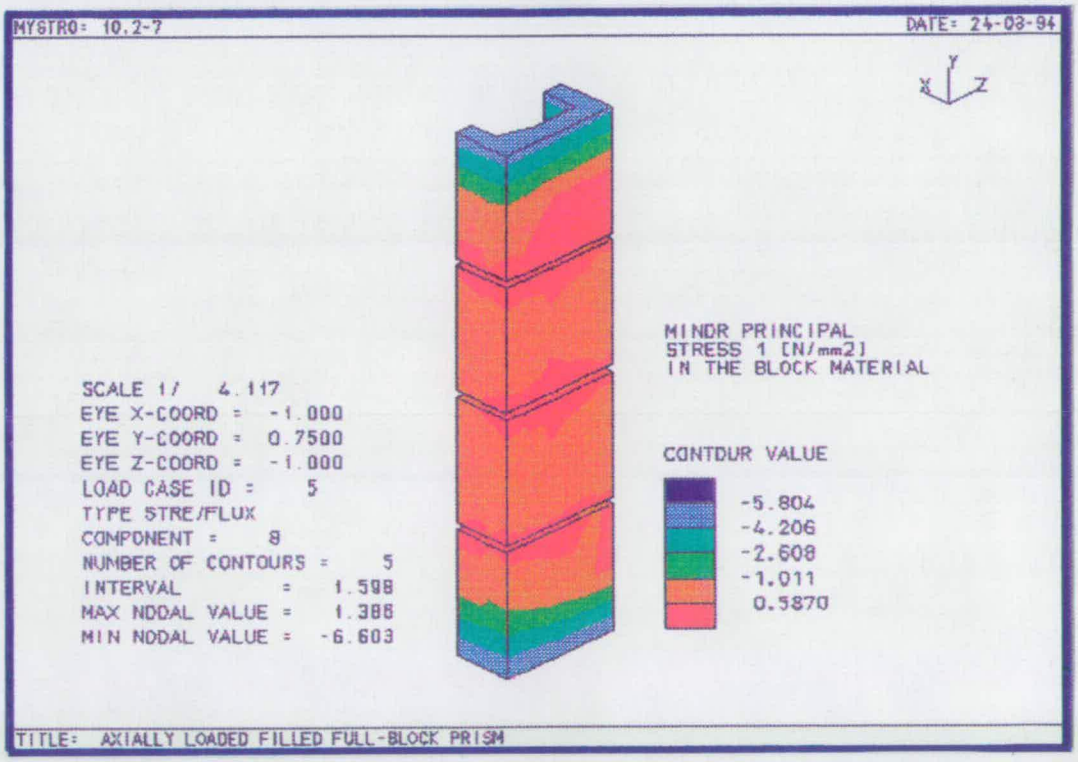


Fig. 4.43 Minor principal stress 1 in the block material for an axially loaded filled full-block prism

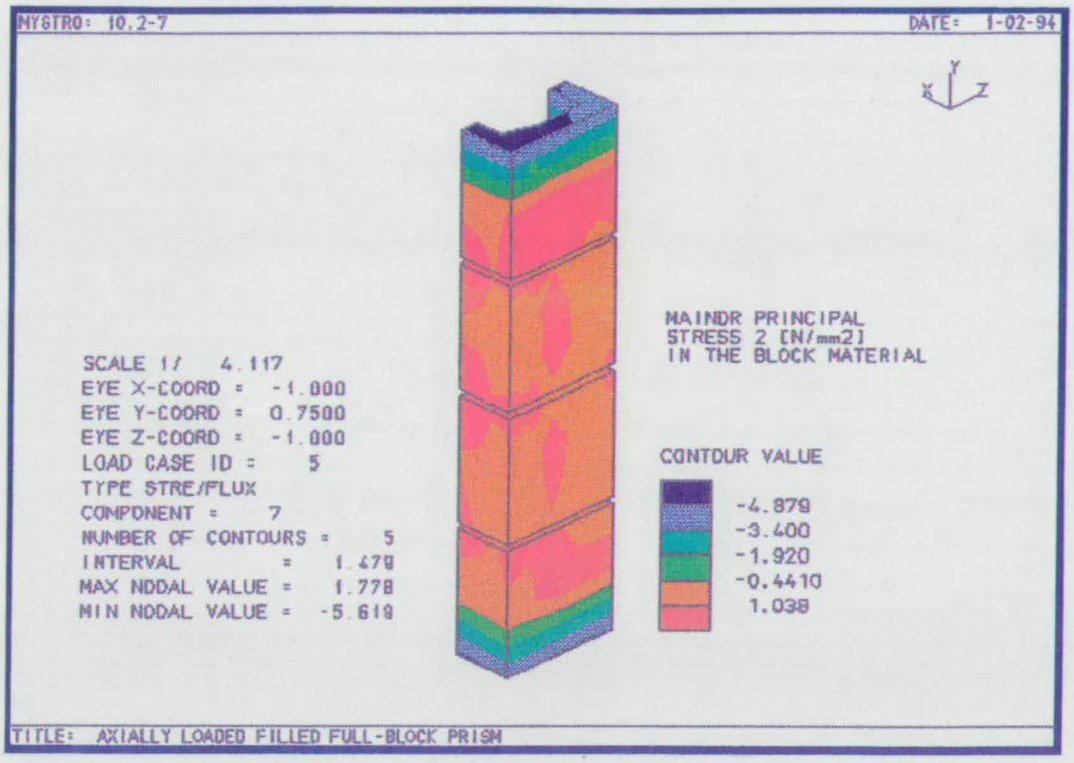


Fig. 4.44 Minor principal stress 2 in the block material for an axially loaded filled full-block prism

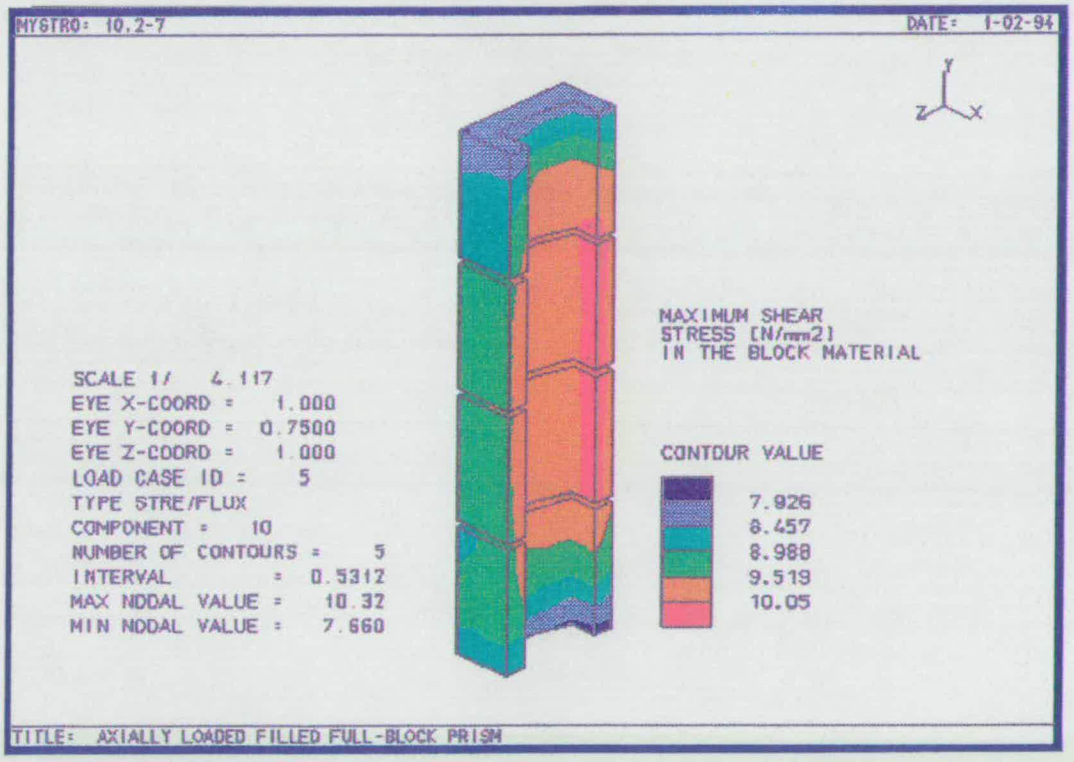


Fig. 4.45 Shear stress in the block material for an axially loaded filled full-block prism

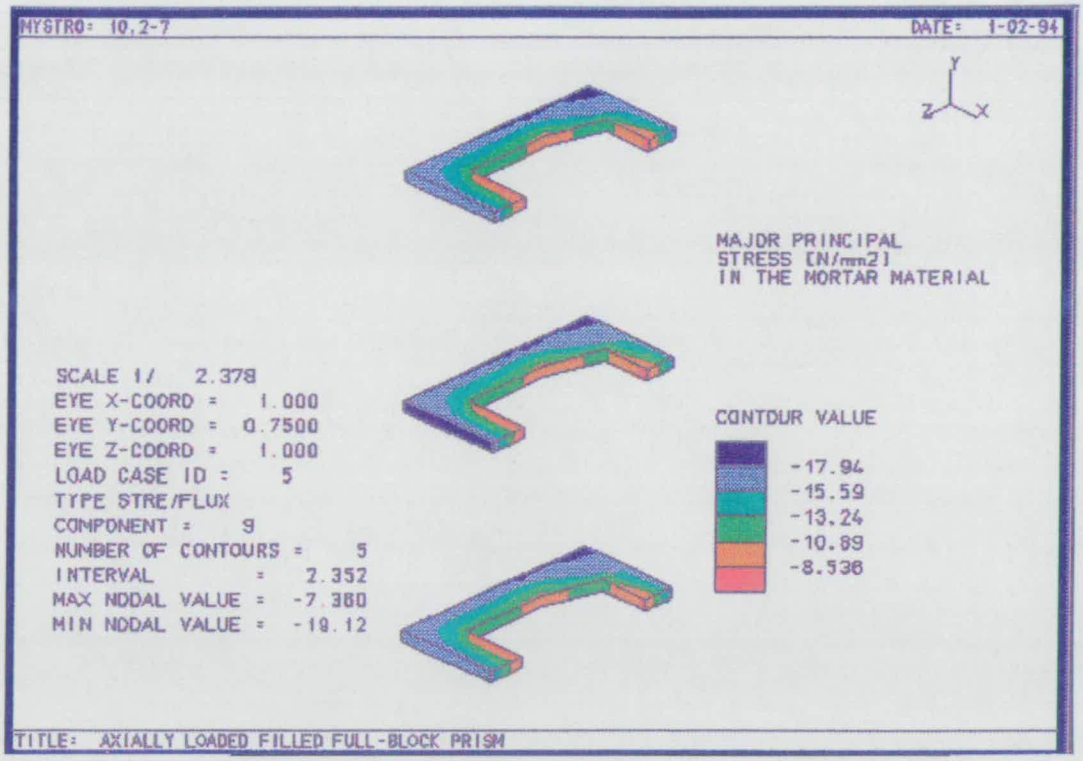


Fig. 4.46 Major principal stress in the mortar material for an axially loaded filled full-block prism

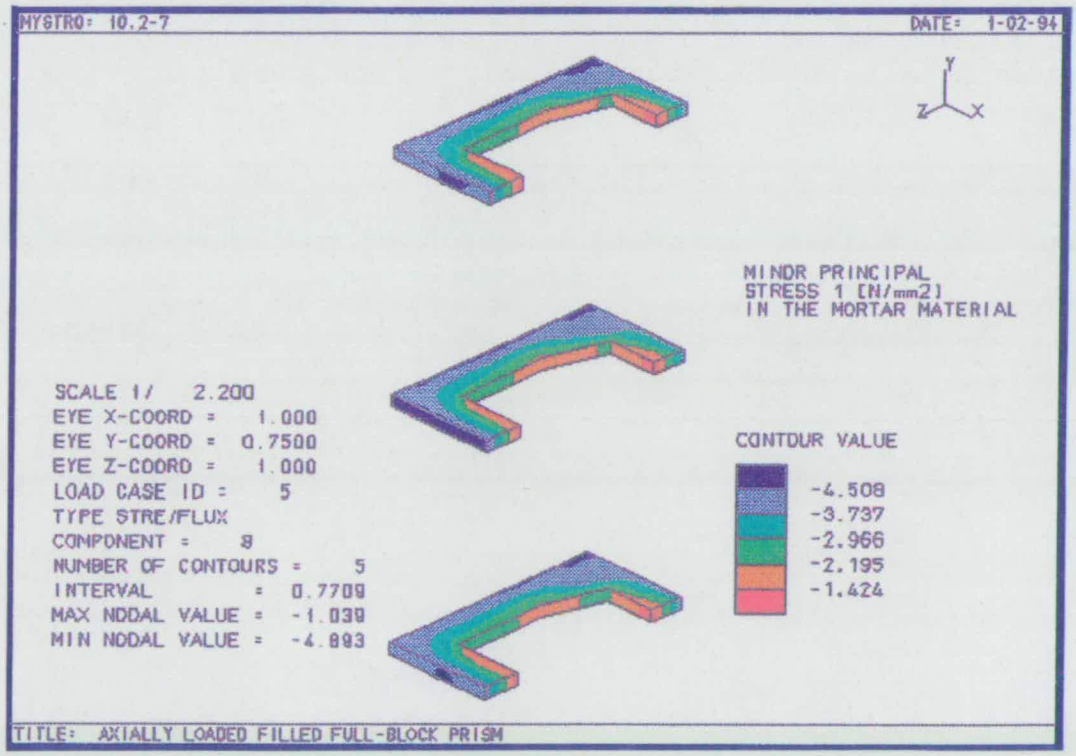


Fig. 4.47 Minor principal stress 1 in the mortar material for an axially loaded filled full-block prism

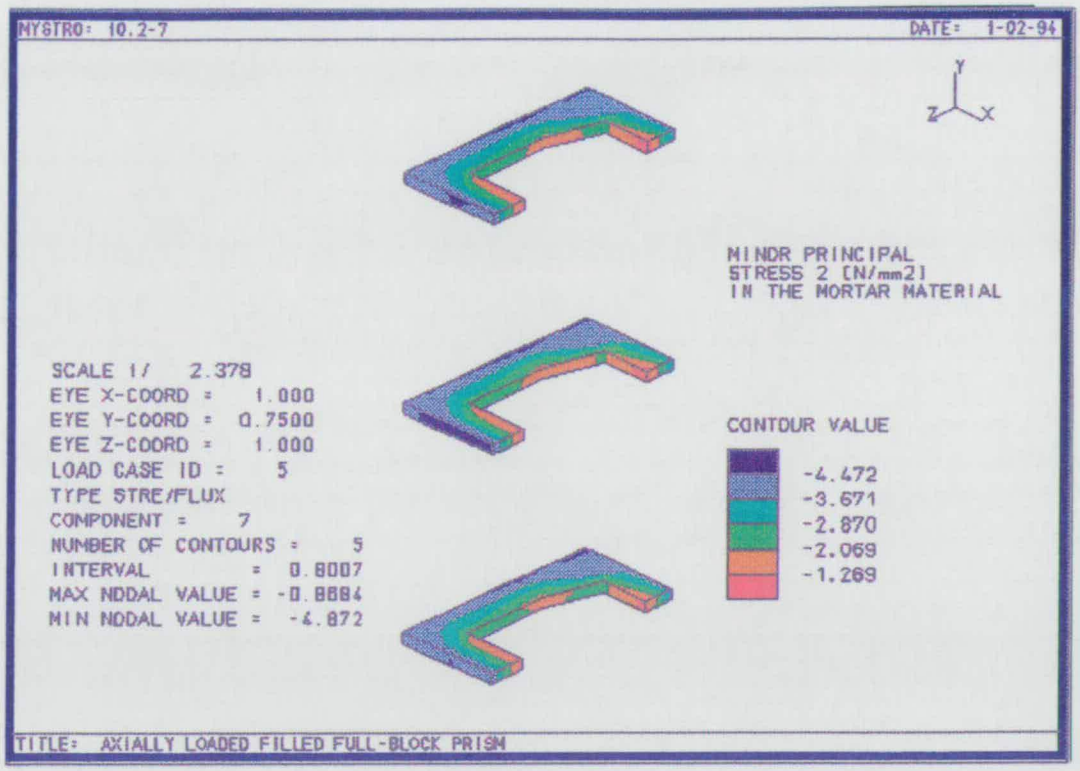


Fig. 4.48 Minor principal stress 2 in the mortar material for an axially loaded filled full-block prism

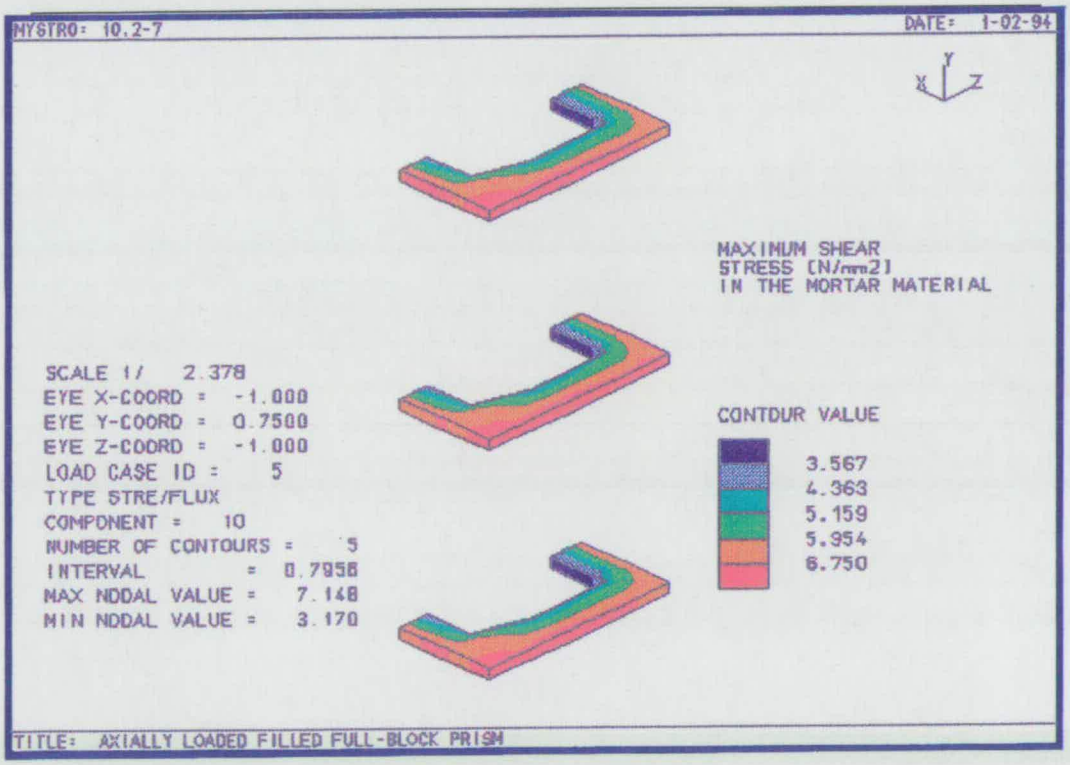


Fig. 4.49 Shear stress in the mortar material for an axially loaded filled full-block prism

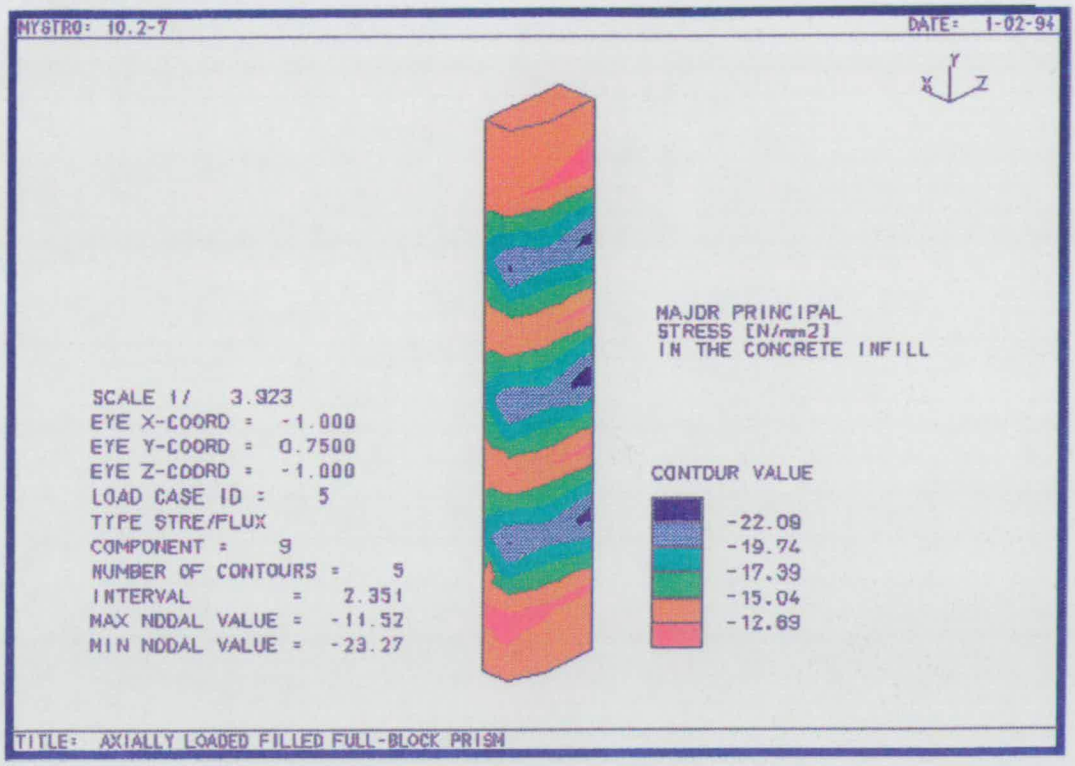


Fig. 4.50 Major principal stress in the concrete infill for an axially loaded filled full-block prism

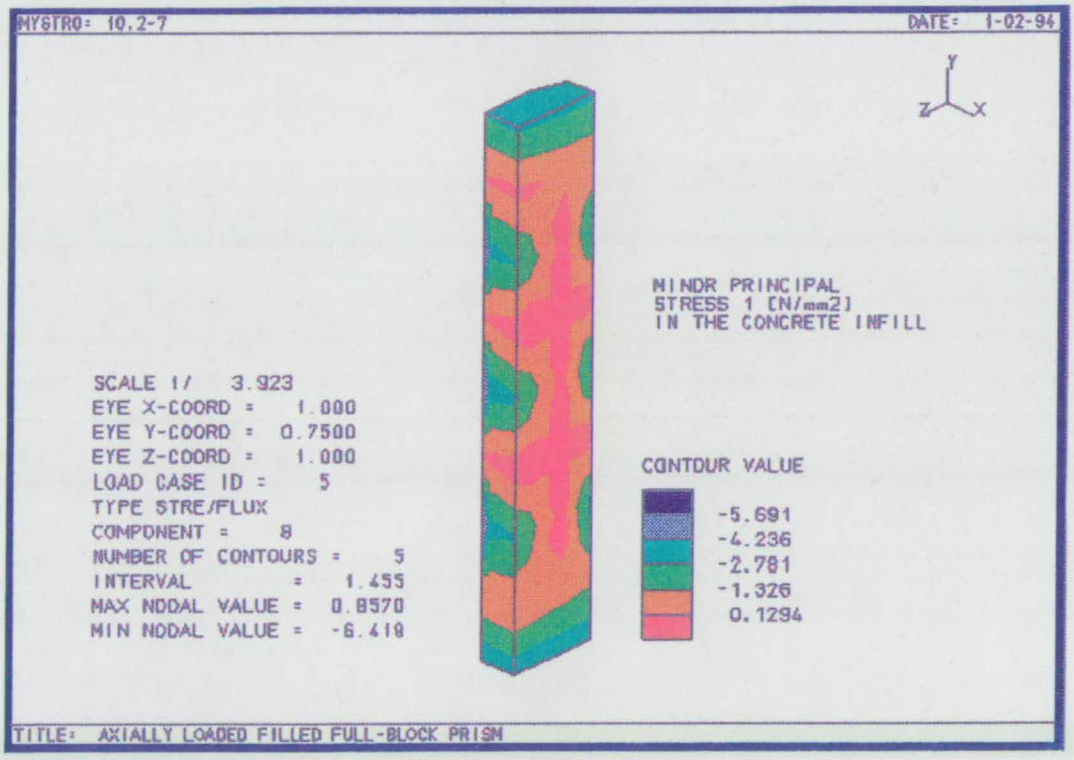


Fig. 4.51 Minor principal stress 1 in the concrete infill for an axially loaded filled full-block prism

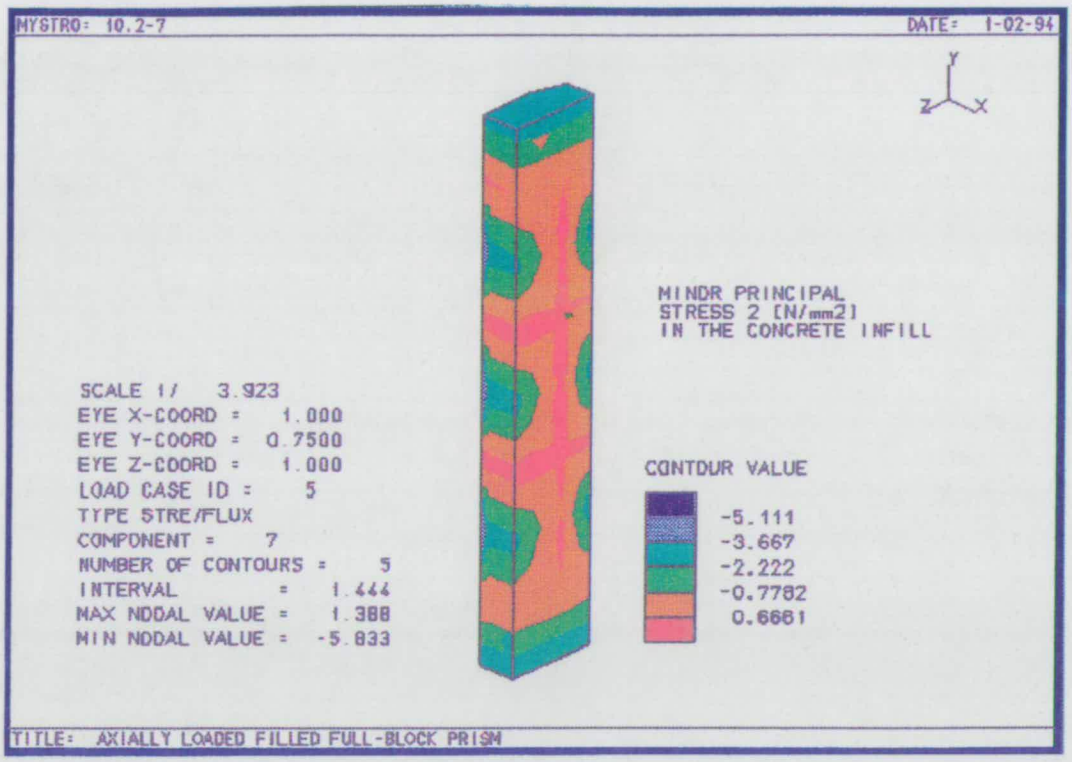


Fig. 4.52 Minor principal stress 2 in the concrete infill for an axially loaded filled full-block prism

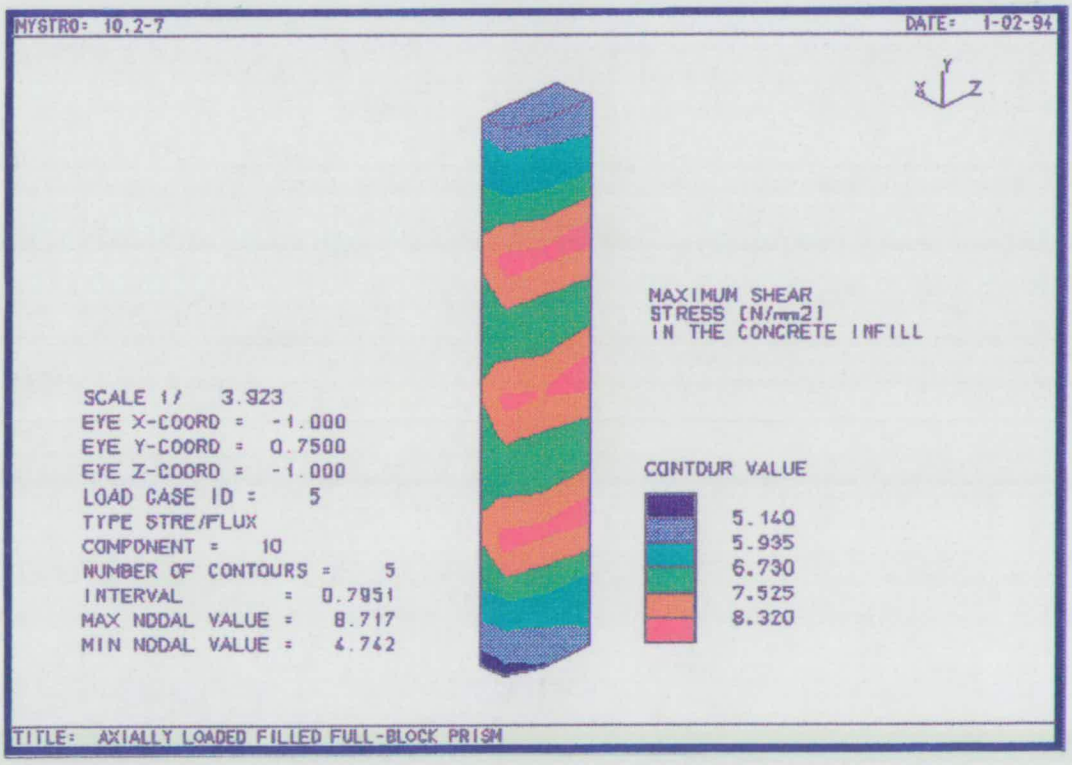


Fig. 4.53 Shear stress in the concrete infill for an axially loaded filled full-block prism

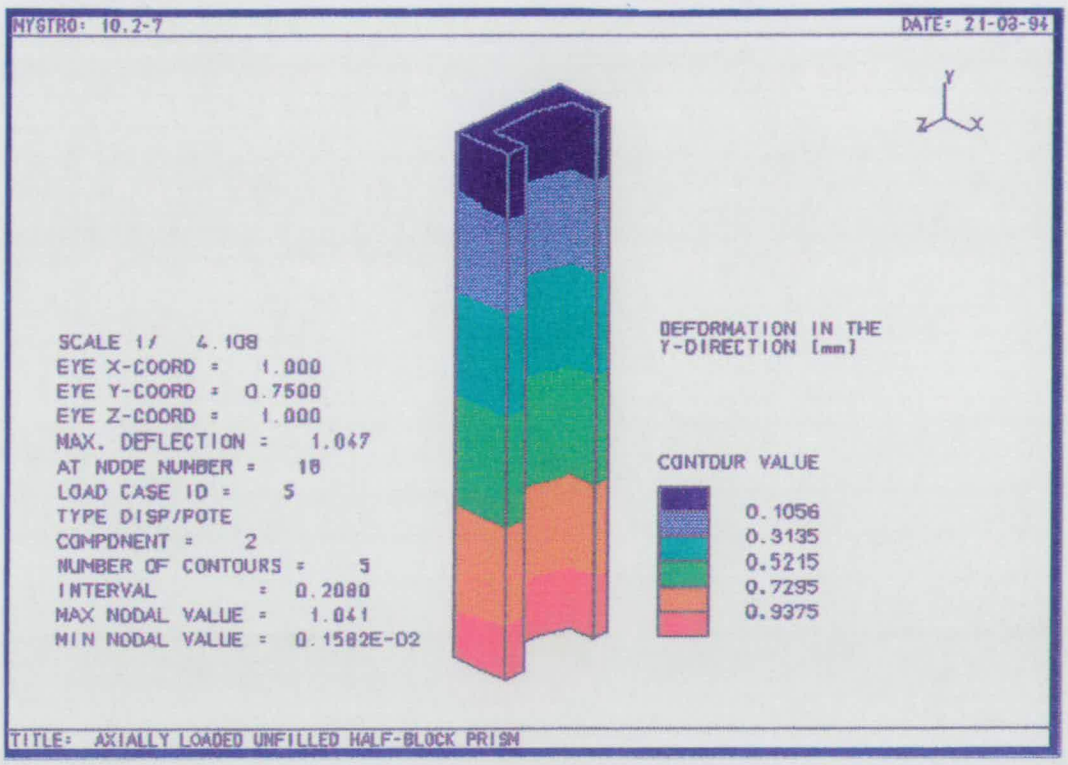


Fig. 4.54 Deformation of axially loaded unfilled half-block prism, in the Y-direction

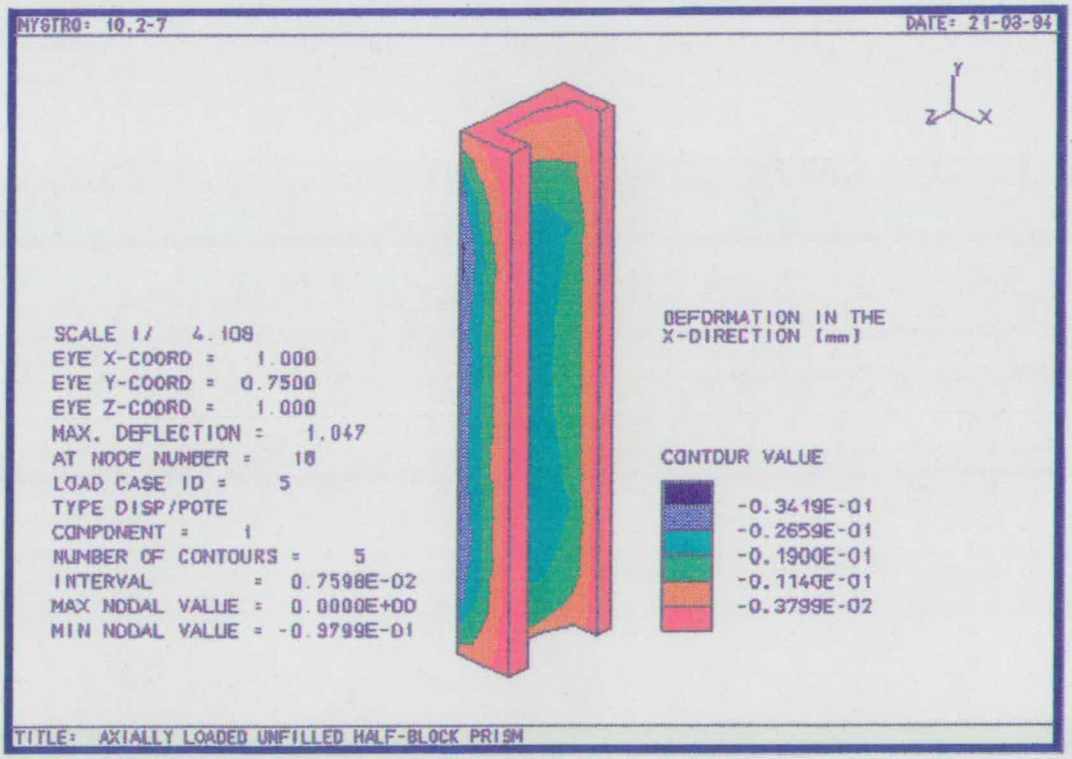


Fig. 4.55 Deformation of axially loaded unfilled half-block prism, in the X-direction

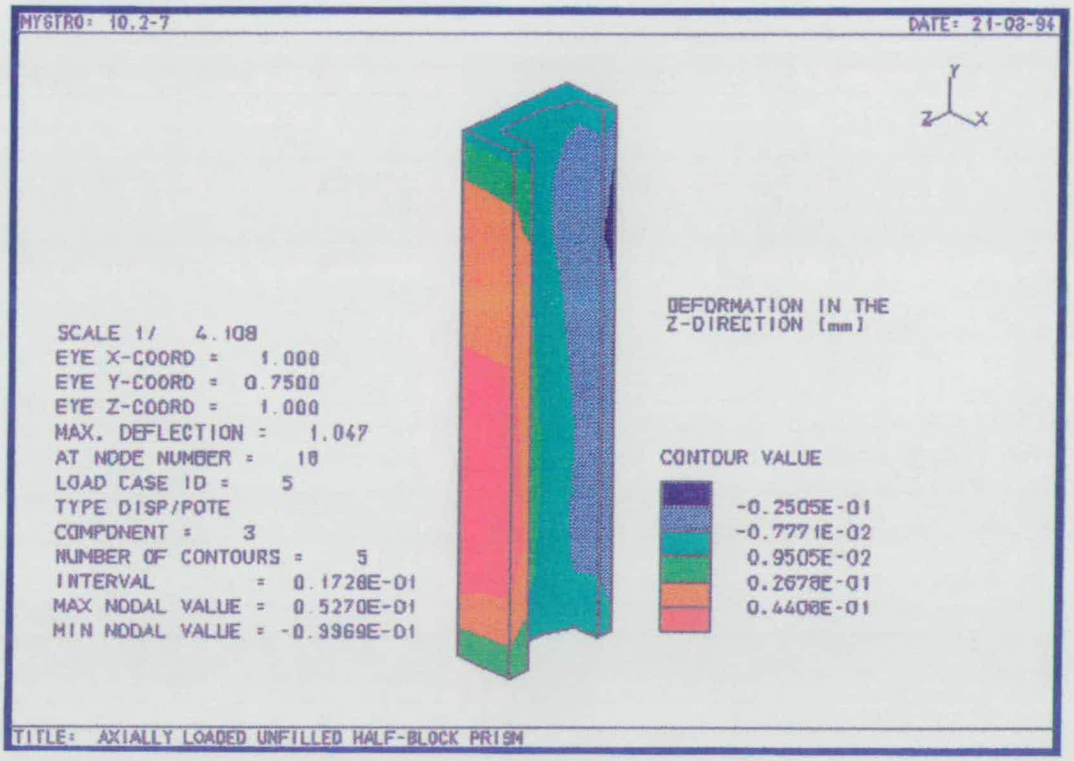


Fig. 4.56 Deformation of axially loaded unfilled half-block prism, in the Z-direction

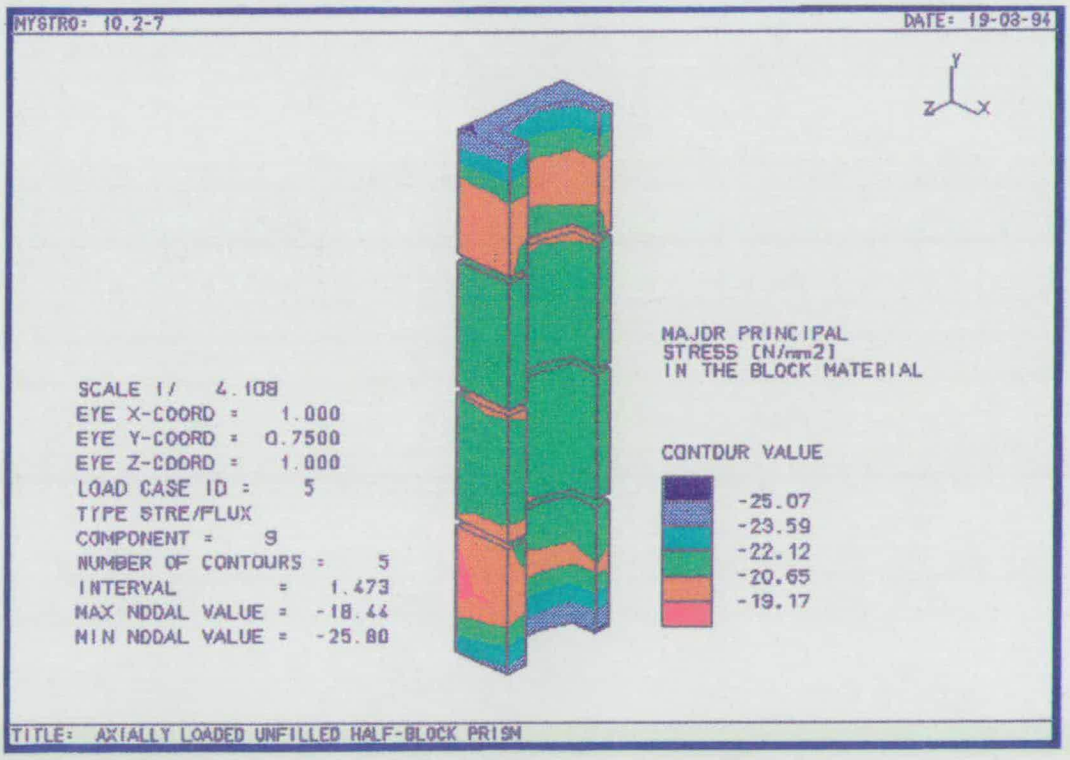


Fig. 4.57 Major principal stress in the block material for an axially loaded unfilled half-block prism

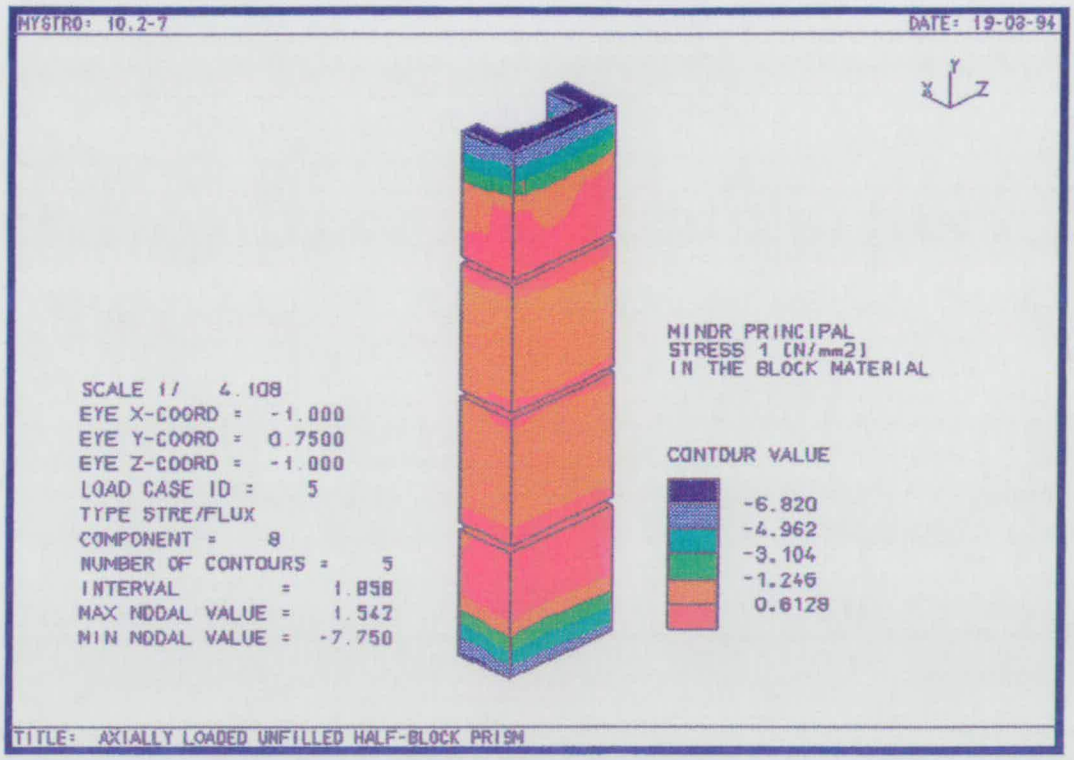


Fig. 4.58 Minor principal stress 1 in the block material for an axially loaded unfilled half-block prism

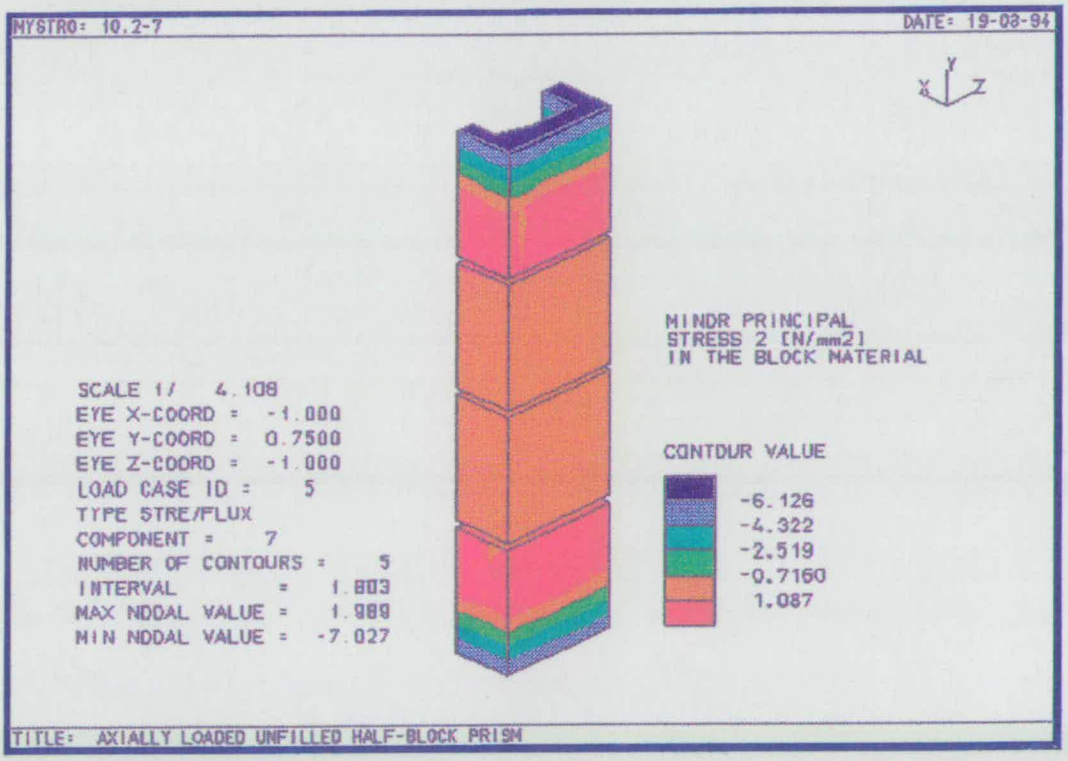


Fig. 4.59 Minor principal stress 2 in the block material for an axially loaded unfilled half-block prism

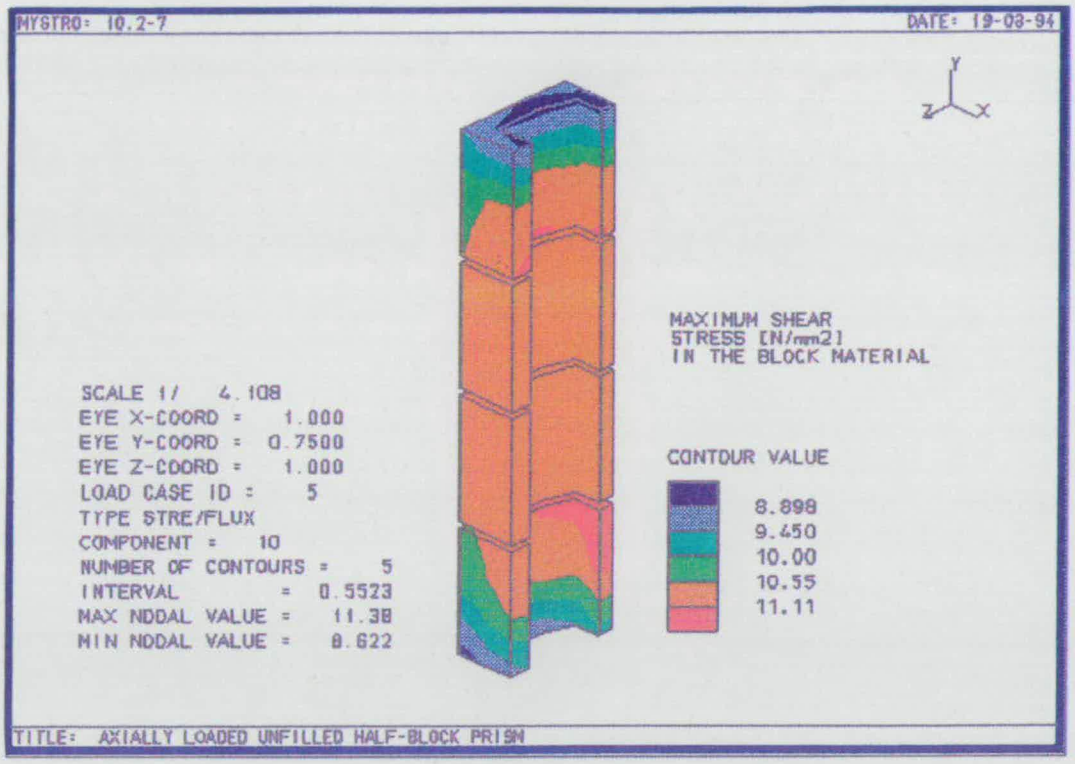


Fig. 4.60 Shear stress in the block material for an axially loaded unfilled half-block prism

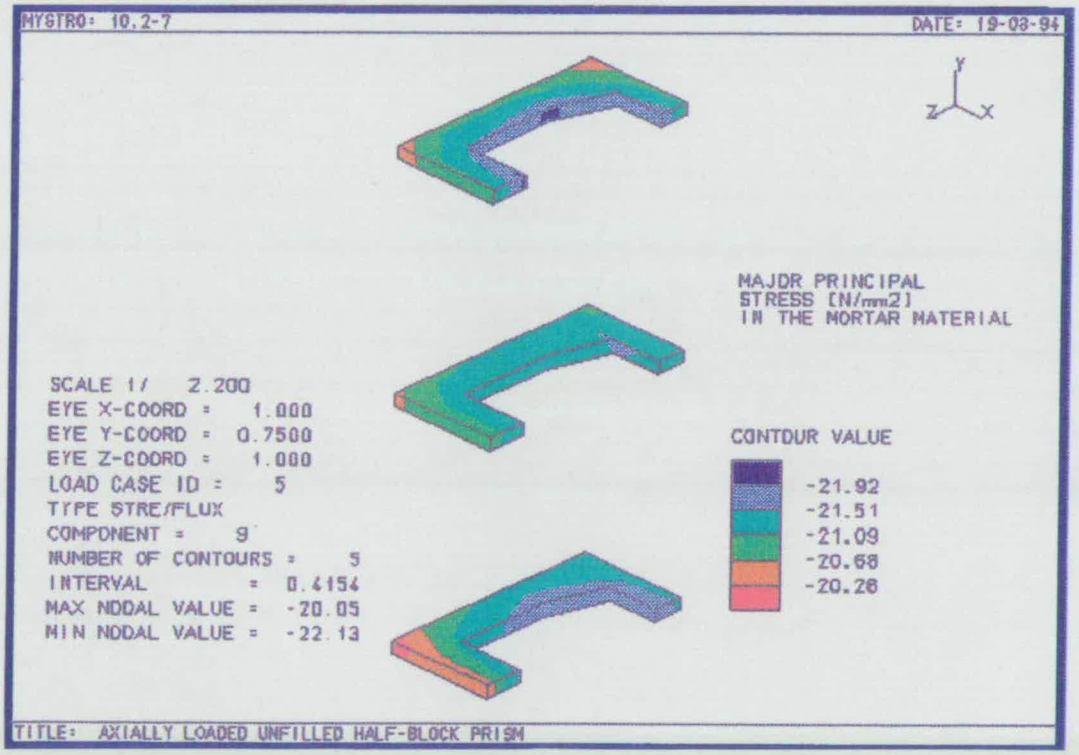


Fig. 4.61 Major principal stress in the mortar material for an axially loaded unfilled half-block prism

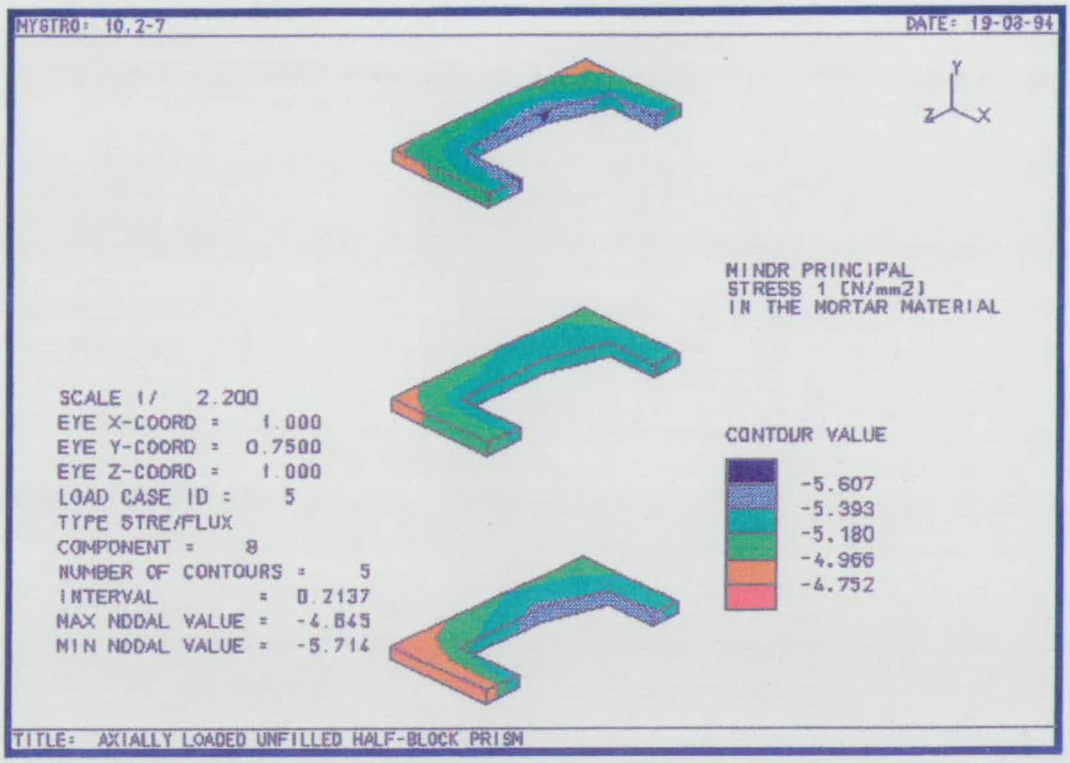


Fig. 4.62 Minor principal stress 1 in the mortar material for an axially loaded unfilled half-block prism

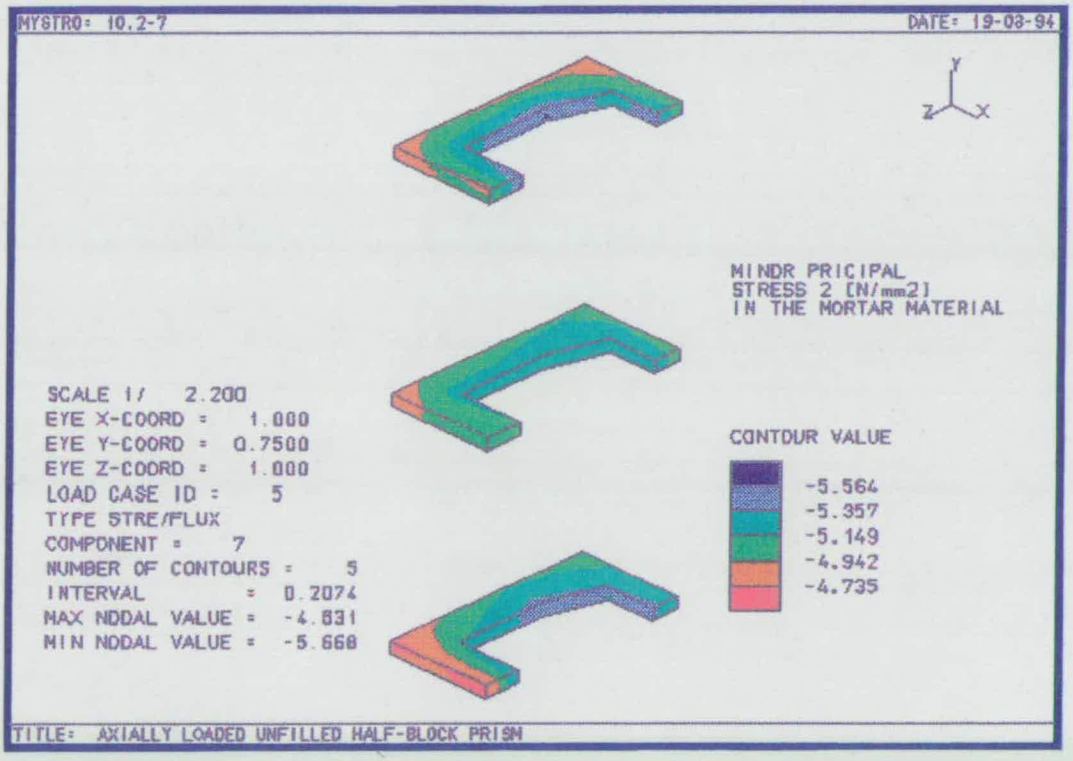


Fig. 4.63 Minor principal stress 2 in the mortar material for an axially loaded unfilled half-block prism

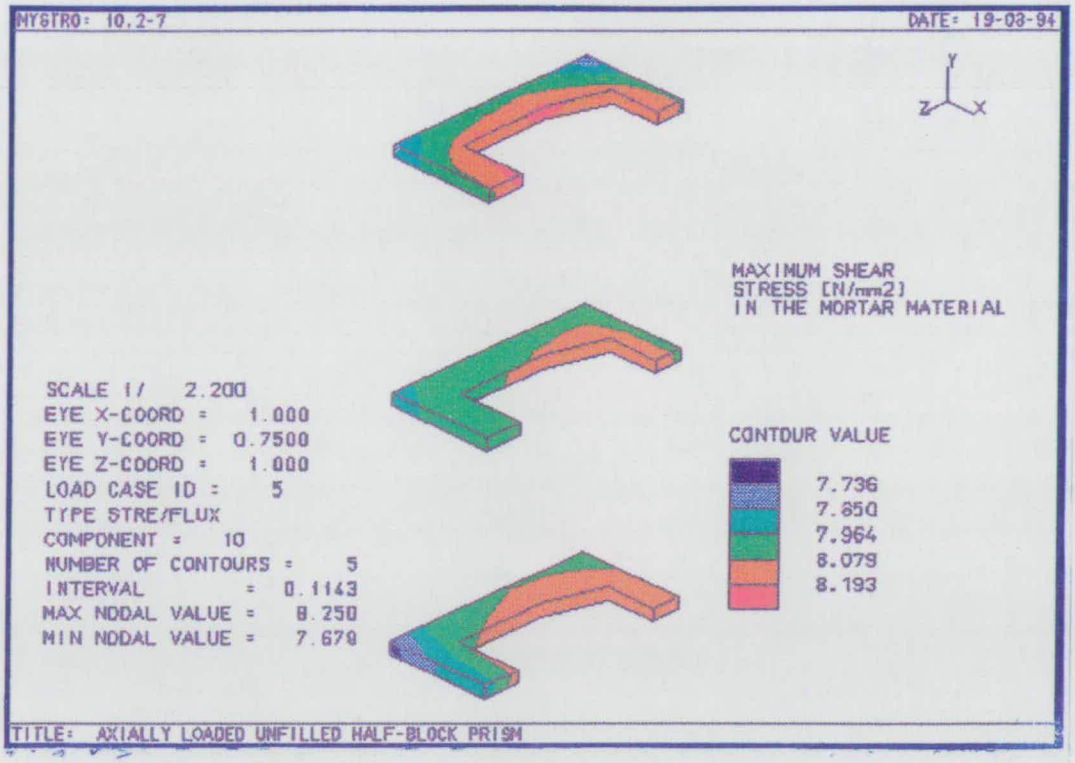


Fig. 4.64 Shear stress in the mortar material for an axially loaded unfilled half-block prism

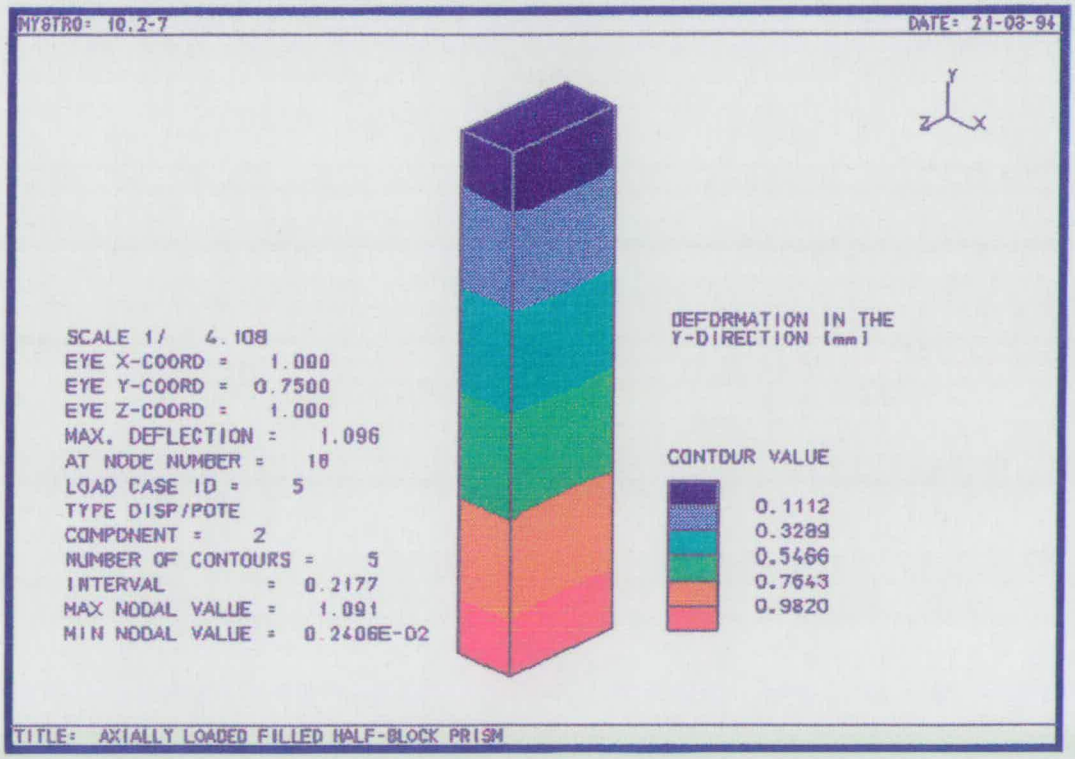


Fig. 4.65 Deformation of axially loaded filled half-block prism, in the Y-direction

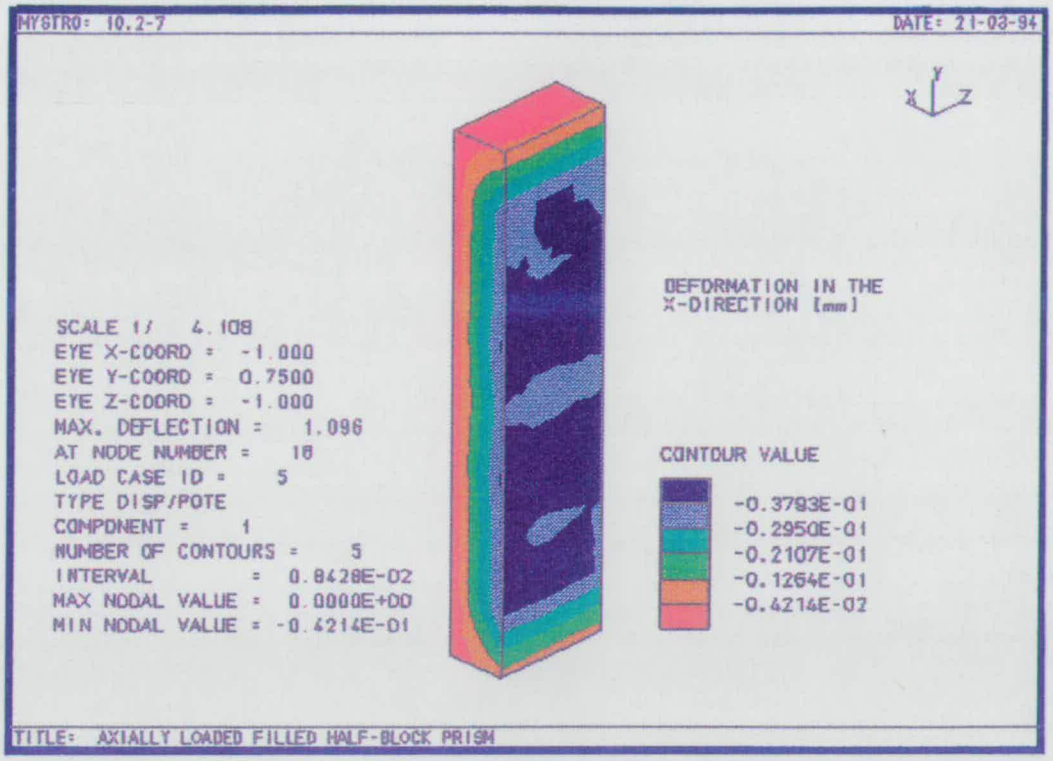


Fig. 4.66 Deformation of axially loaded filled half-block prism, in the X-direction

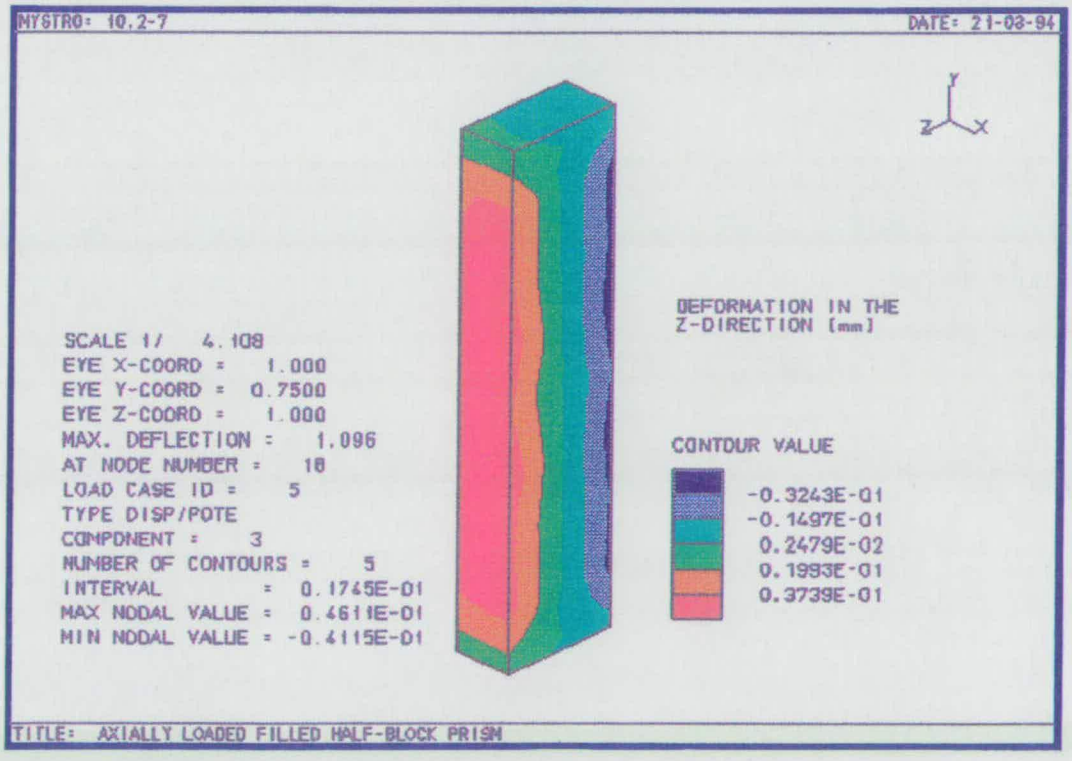


Fig. 4.67 Deformation of axially loaded filled half-block prism, in the Z-direction

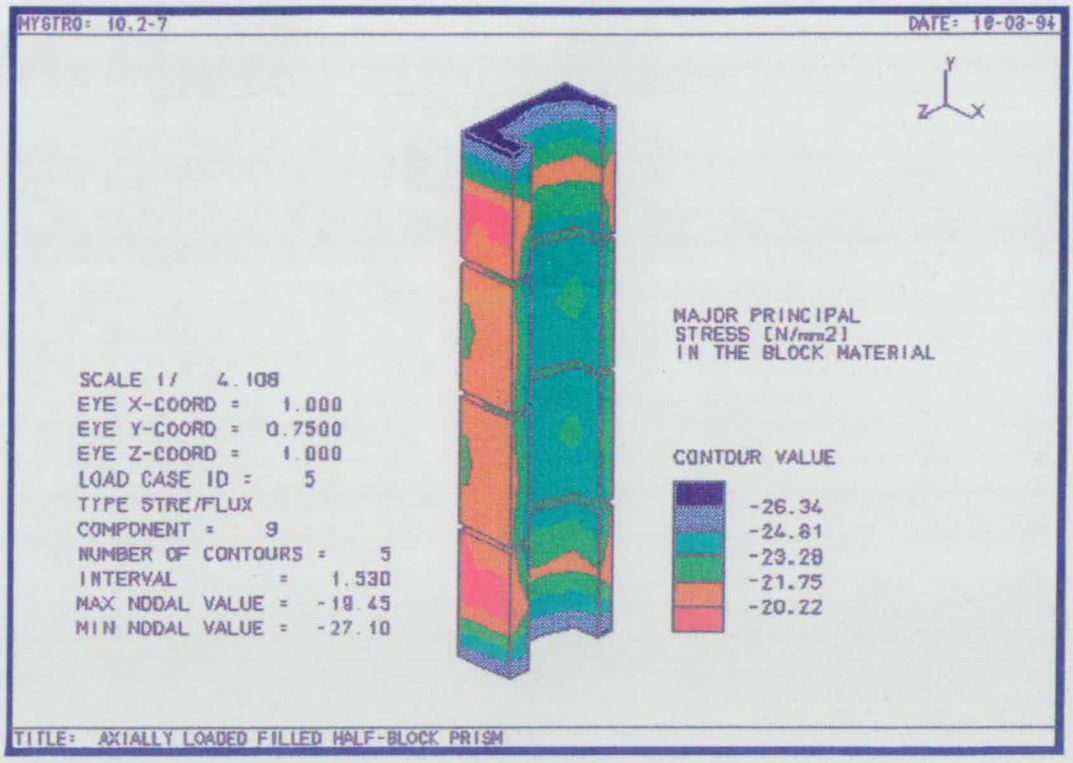


Fig. 4.68 Major principal stress in the block material for an for an axially loaded filled half-block prism

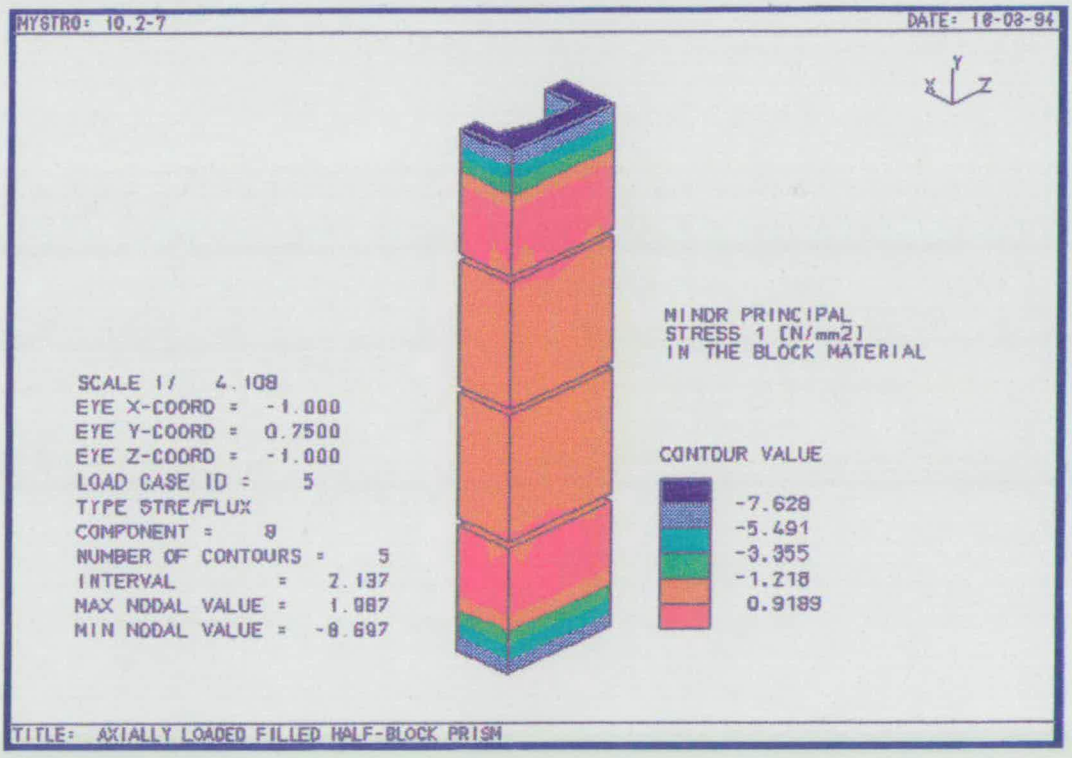


Fig. 4.69 Minor principal stress 1 in the block material for an axially loaded filled half-block prism

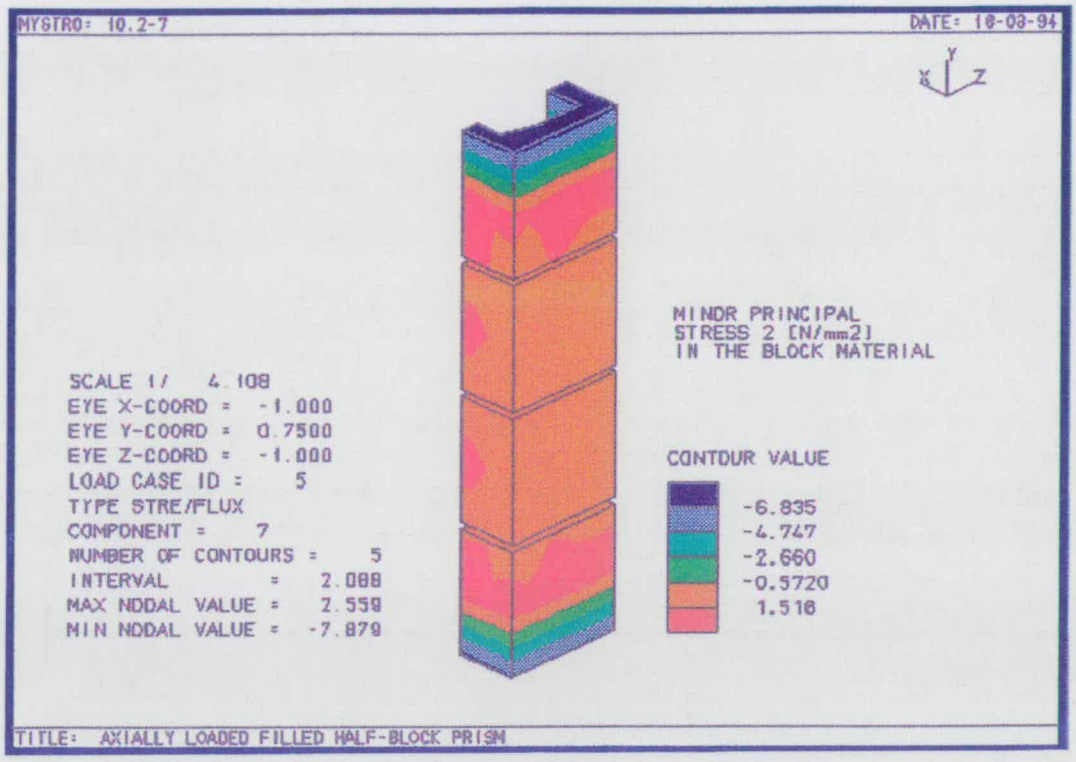


Fig. 4.70 Minor principal stress 2 in the block material for an axially loaded filled half-block prism

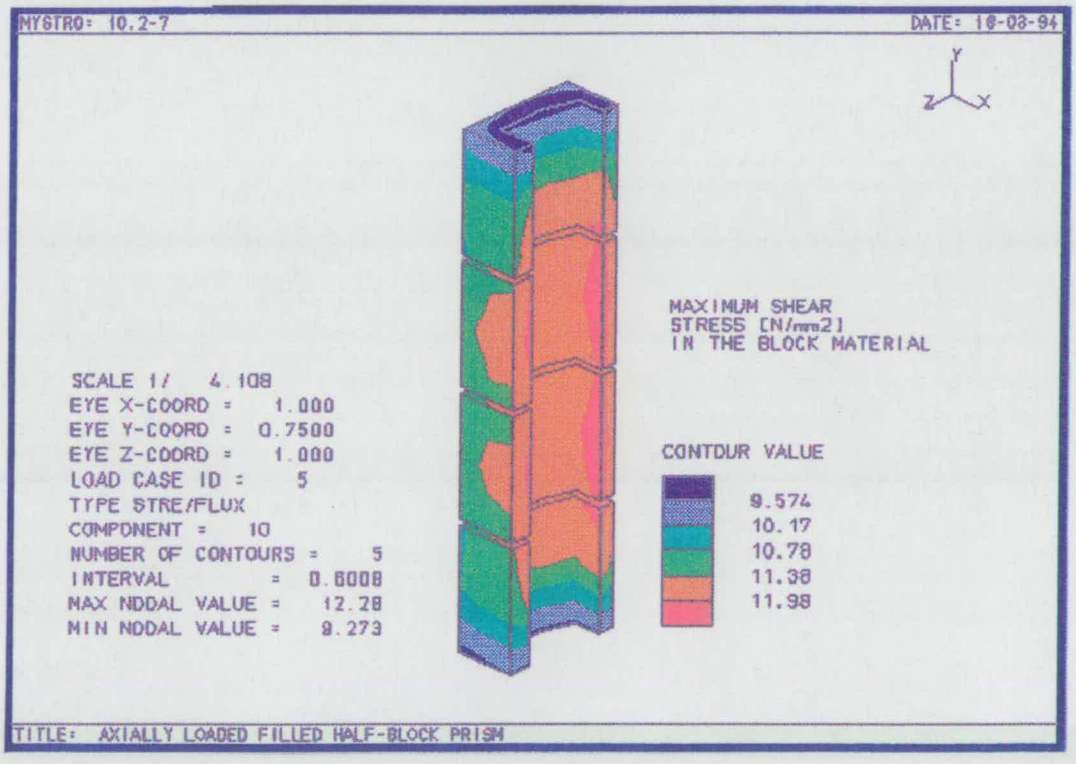


Fig. 4.71 Shear stress in the block material for an axially loaded filled half-block prism

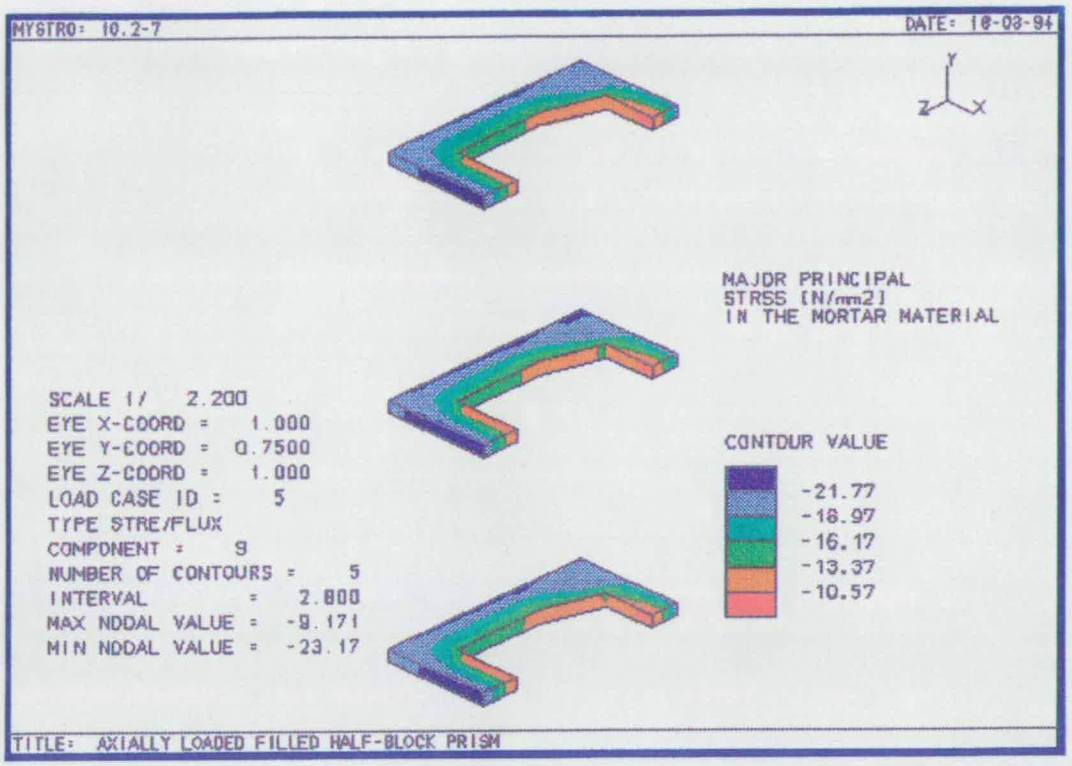


Fig. 4.72 Major principal stress in the mortar material for an axially loaded filled half-block prism

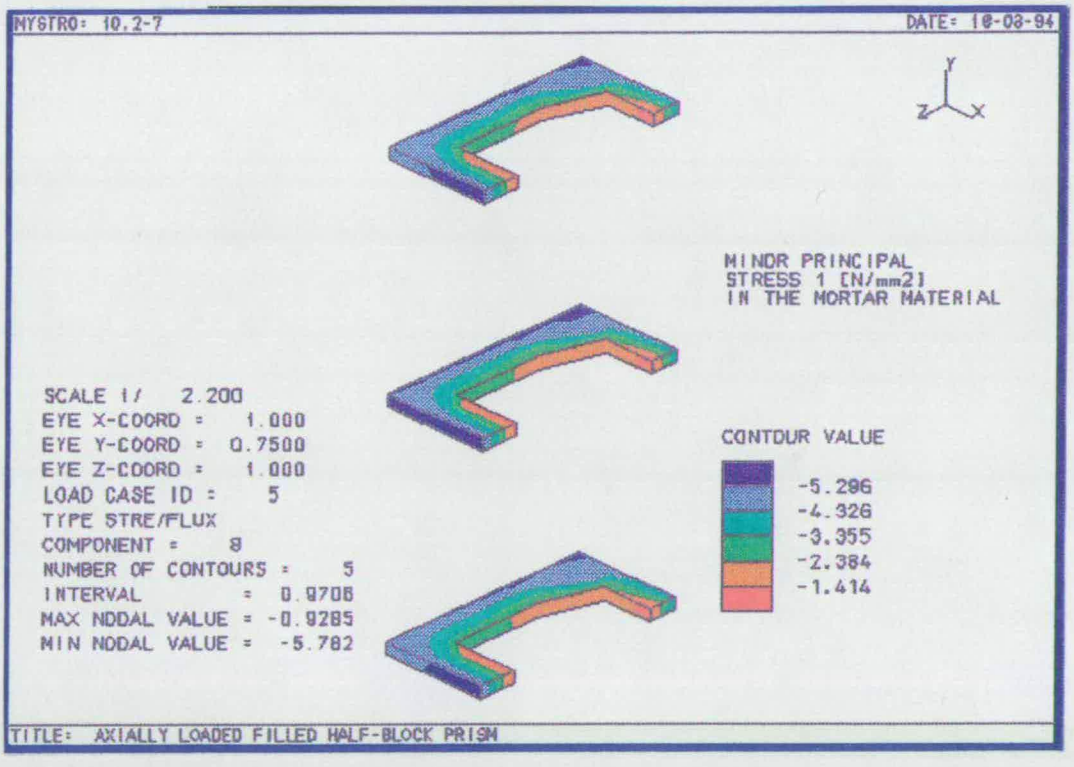


Fig. 4.73 Minor principal stress 1 in the mortar material for an axially loaded filled half-block prism

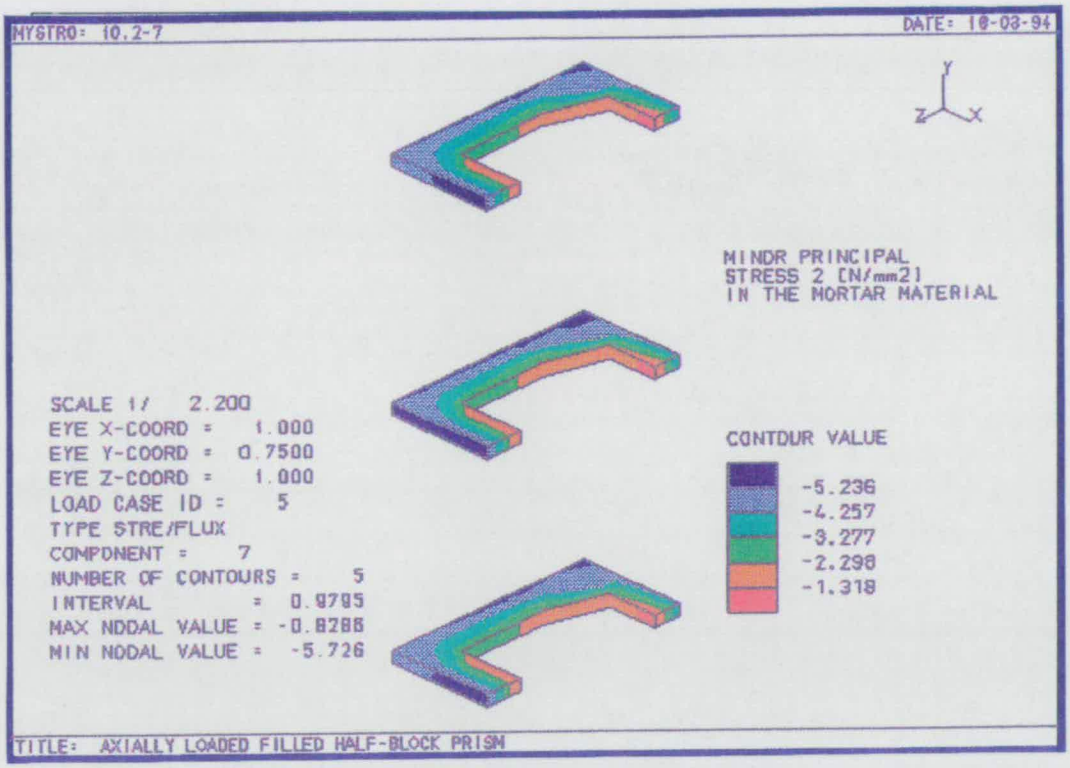


Fig. 4.74 Minor principal stress 2 in the mortar material for an axially loaded filled half-block prism

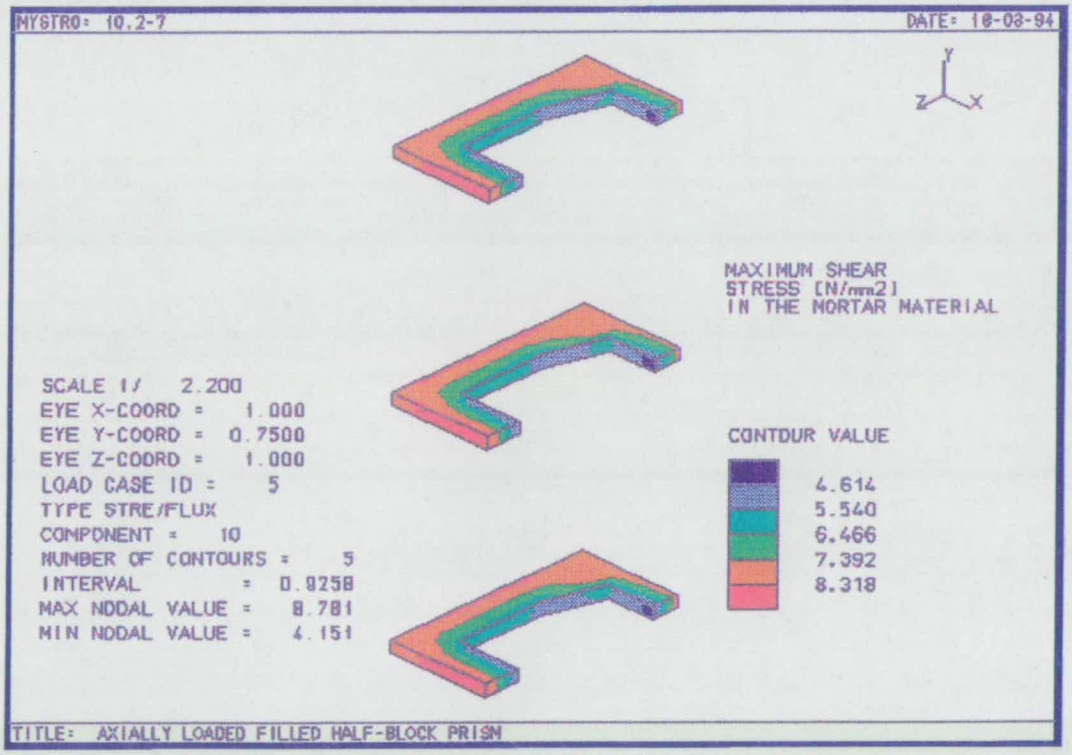


Fig. 4.75 Shear stress in the mortar material for an axially loaded filled half-block prism

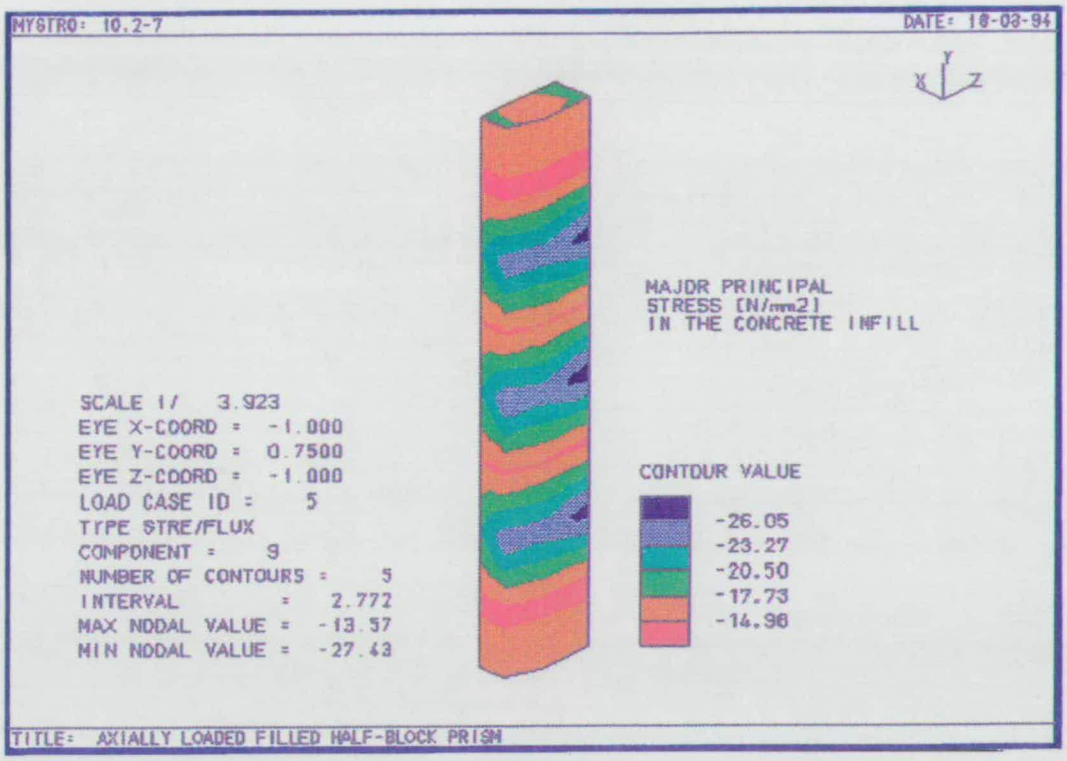


Fig. 4.76 Major principal stress in the concrete infill for an axially loaded filled half-block prism

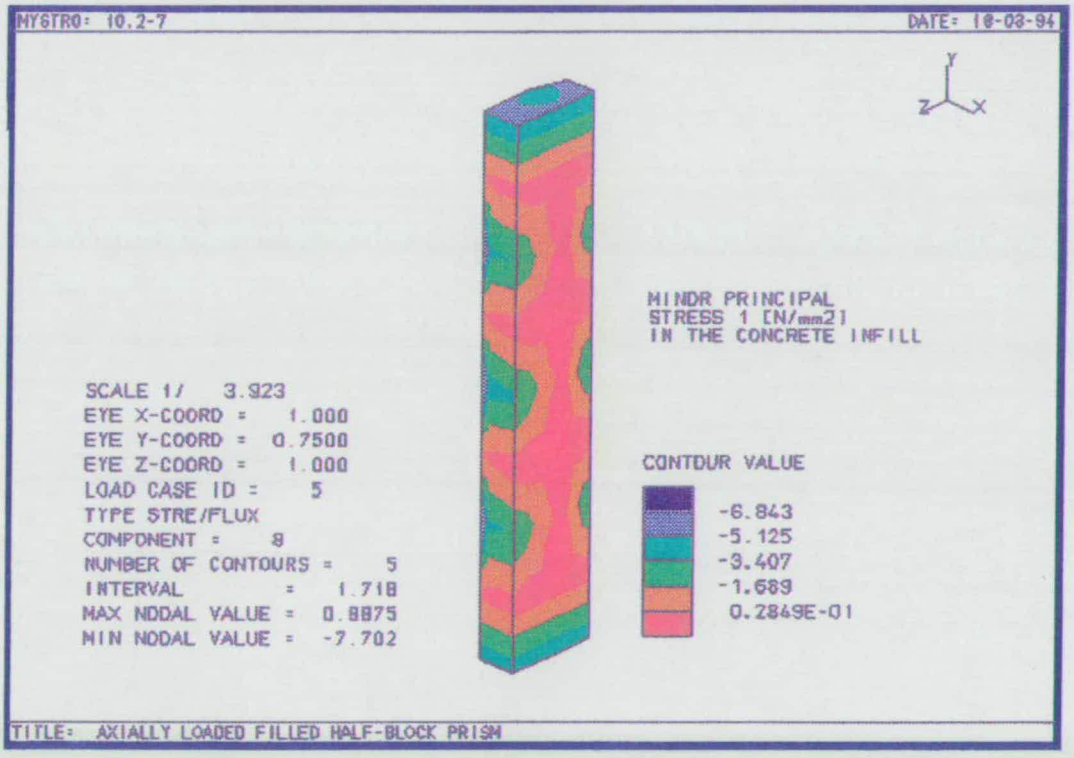


Fig. 4.77 Minor principal stress 1 in the concrete infill for an axially loaded filled half-block prism

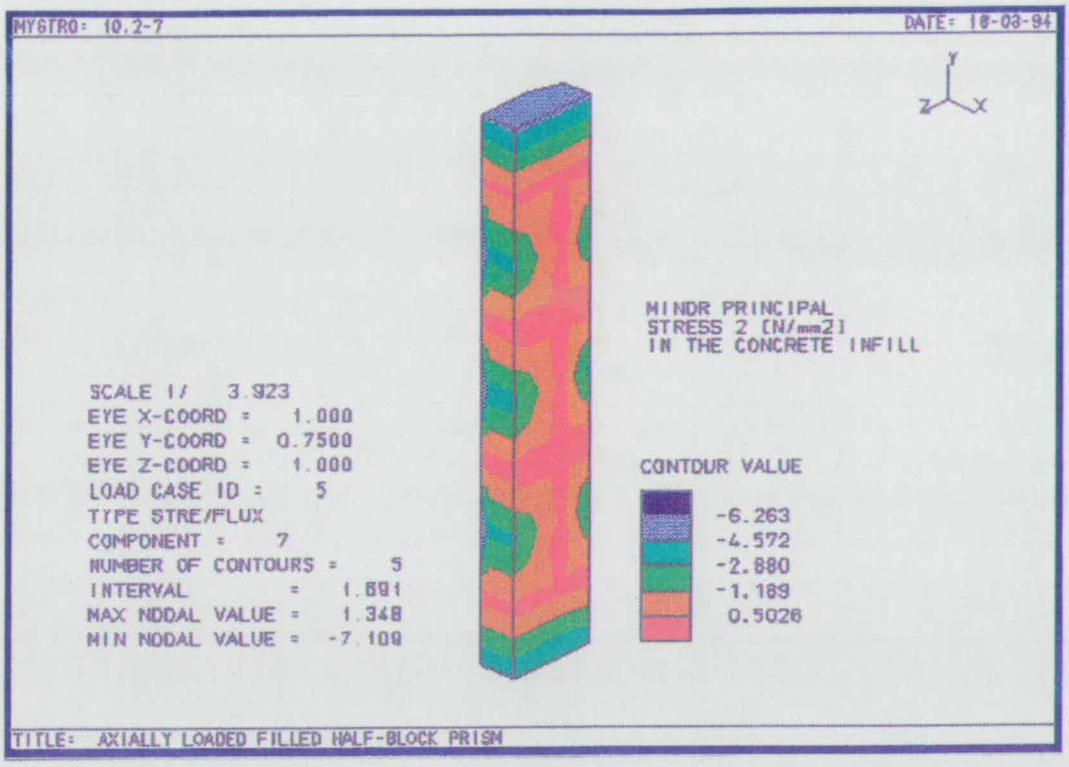


Fig. 4.78 Minor principal stress 2 in the concrete infill for an axially loaded filled half-block prism

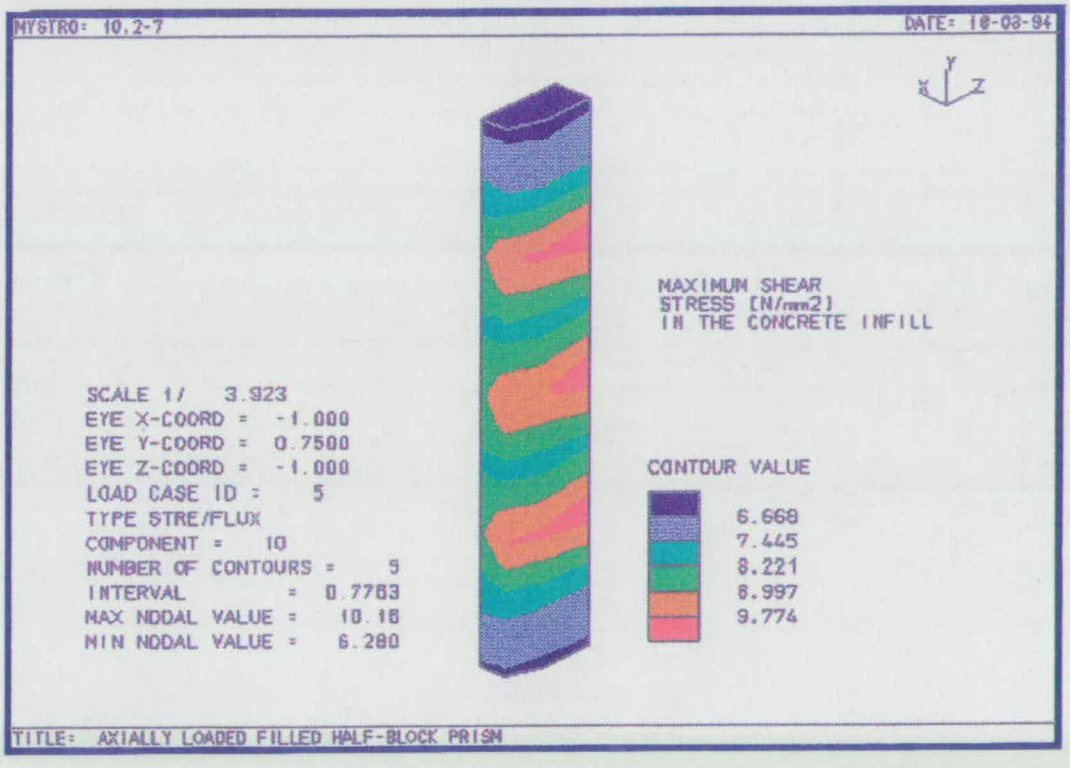


Fig. 4.79 Shear stress in the concrete infill for an axially loaded filled half-block prism

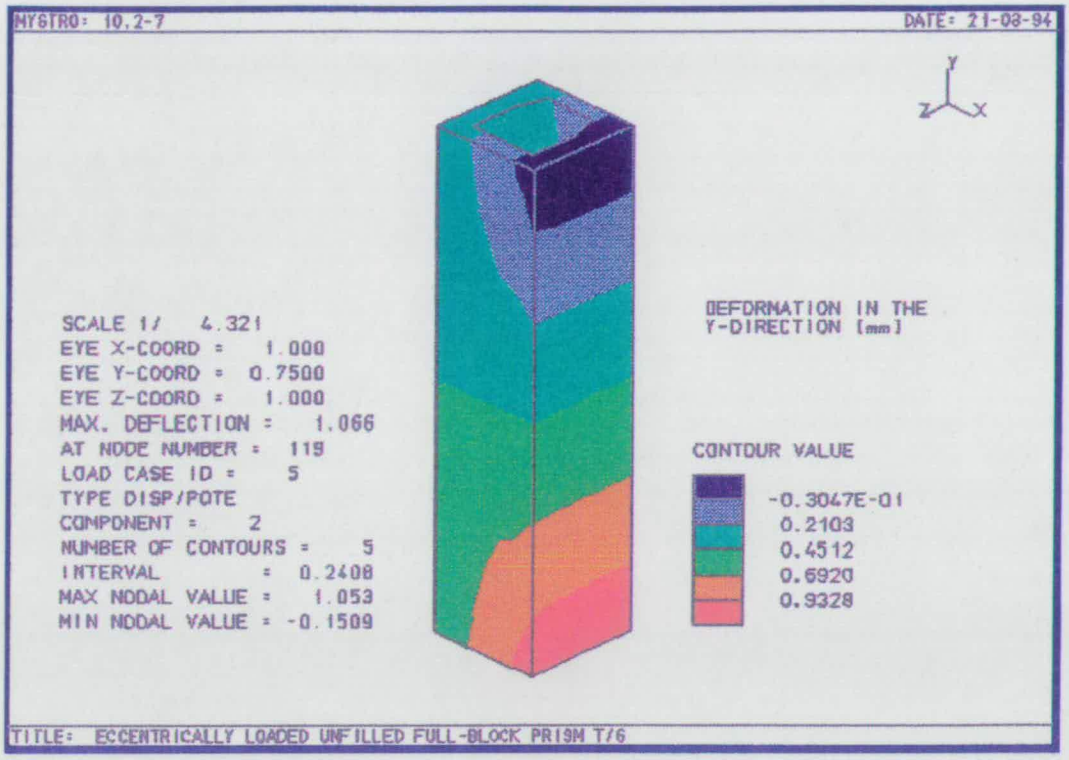


Fig. 4.80 Deformation in the Y-direction of unfilled full-block prism compressed under eccentric load for e = t/6

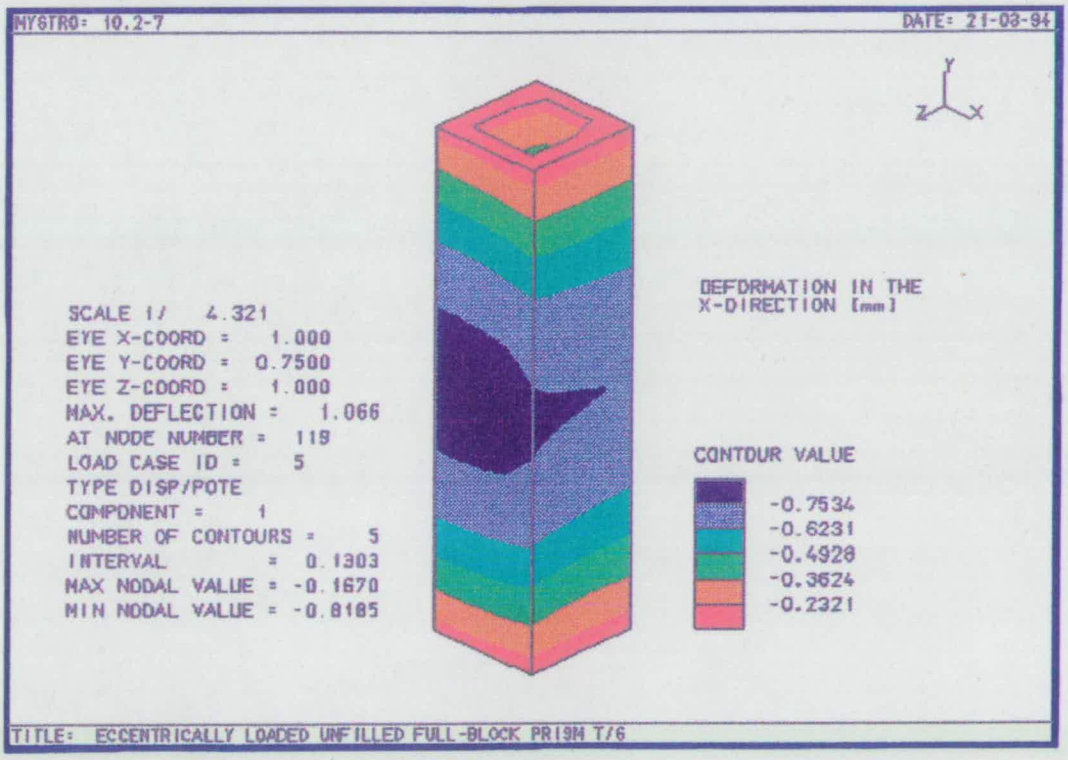


Fig. 4.81 Deformation in the X-direction of unfilled full-block prism compressed under eccentric load for e = t/6

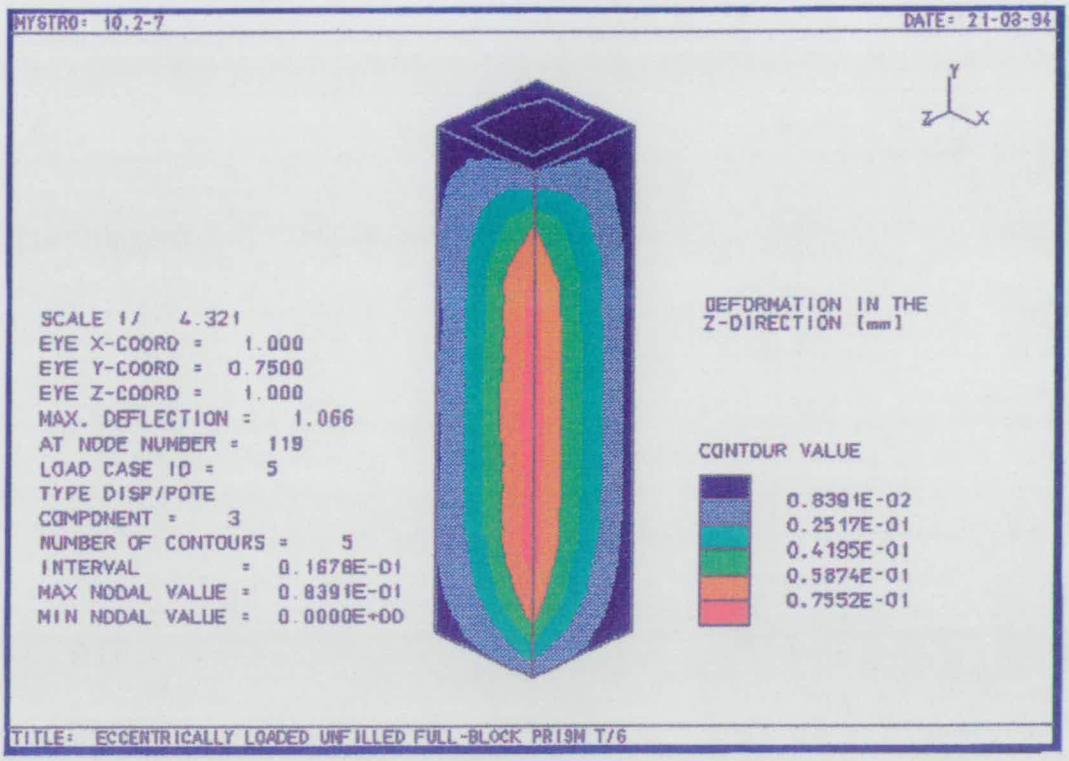


Fig. 4.82 Deformation in the Z-direction of unfilled full-block prism compressed under eccentric load for e = t/6

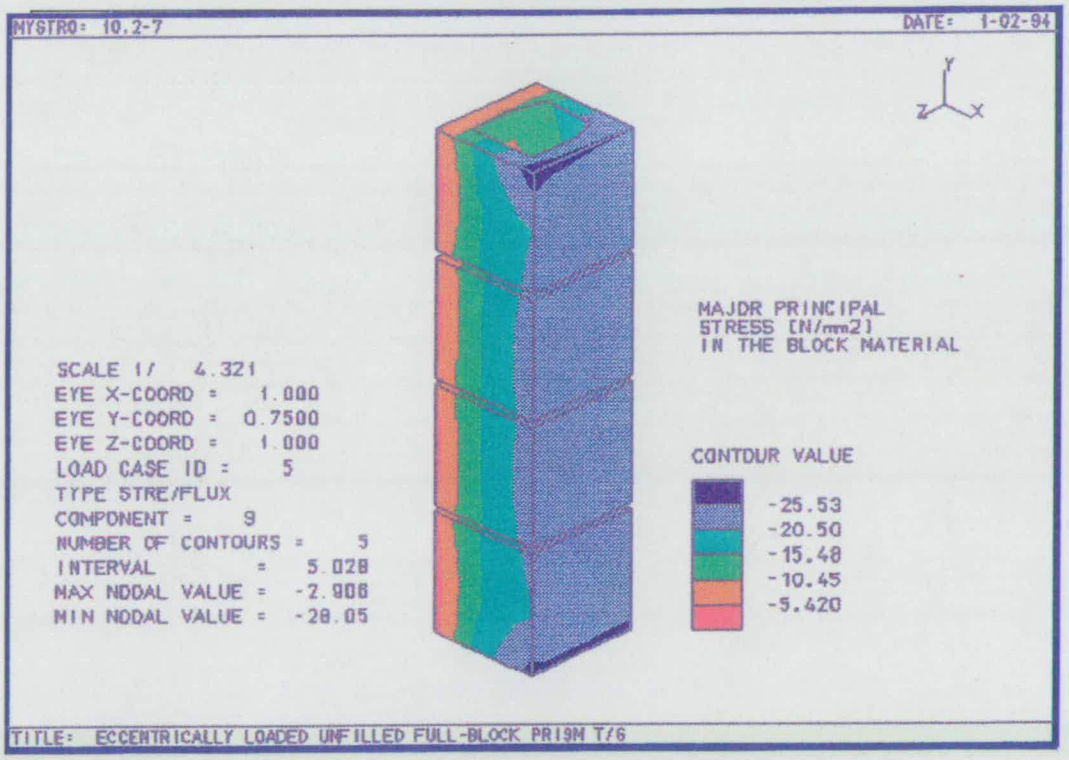


Fig. 4.83 Major principal stress in the block material of unfilled full-block prism compressed under eccentric load for e =t/6

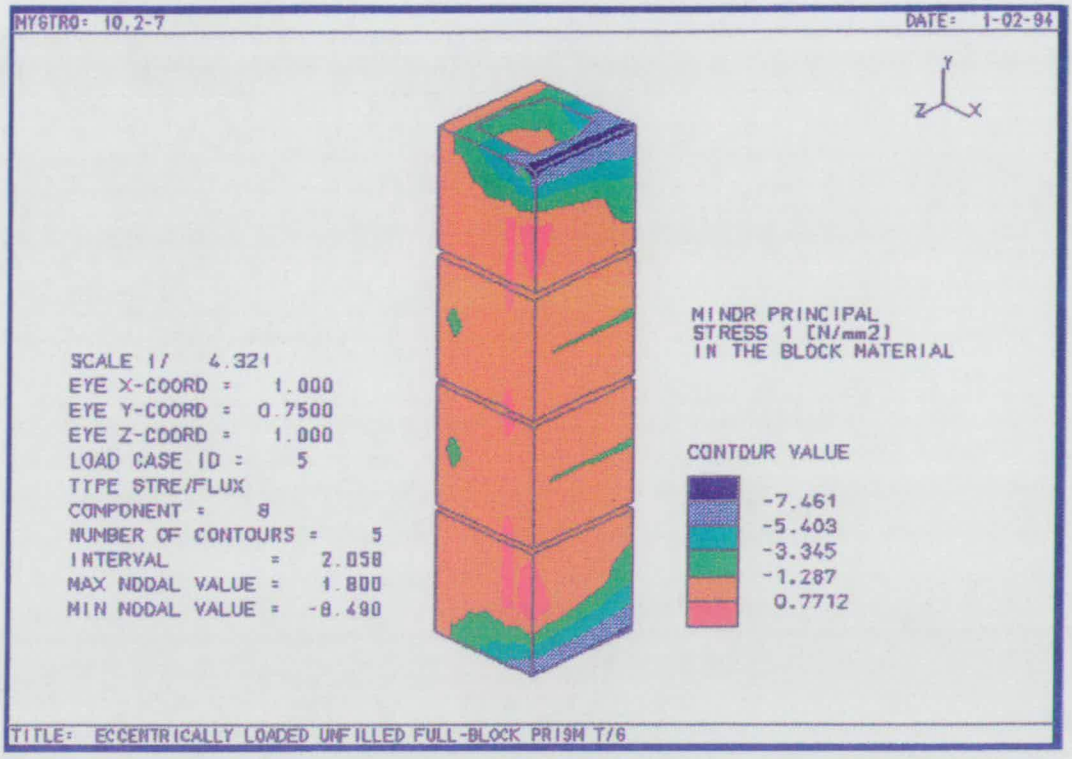


Fig. 4.84 Minor principal stress 1 in the block material of unfilled full-block prism compressed under eccentric load for e = t/6

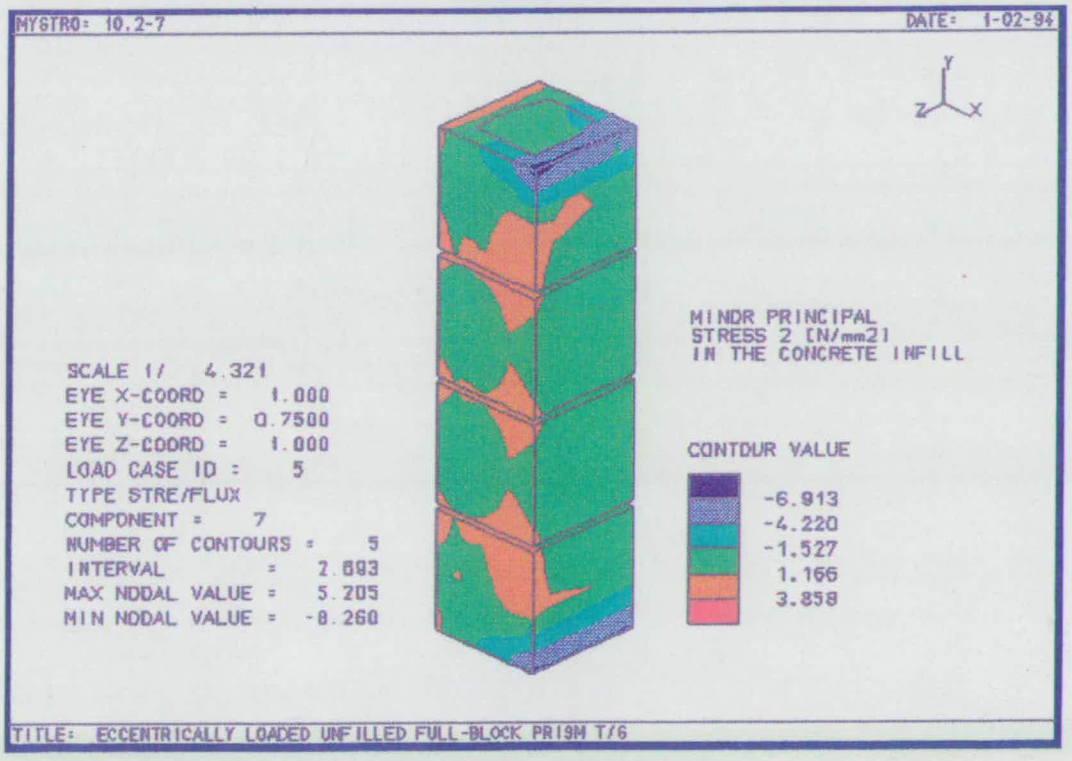


Fig. 4.85 Minor principal stress 2 in the block material of unfilled full-block prism compressed under eccentric load for e = t/6

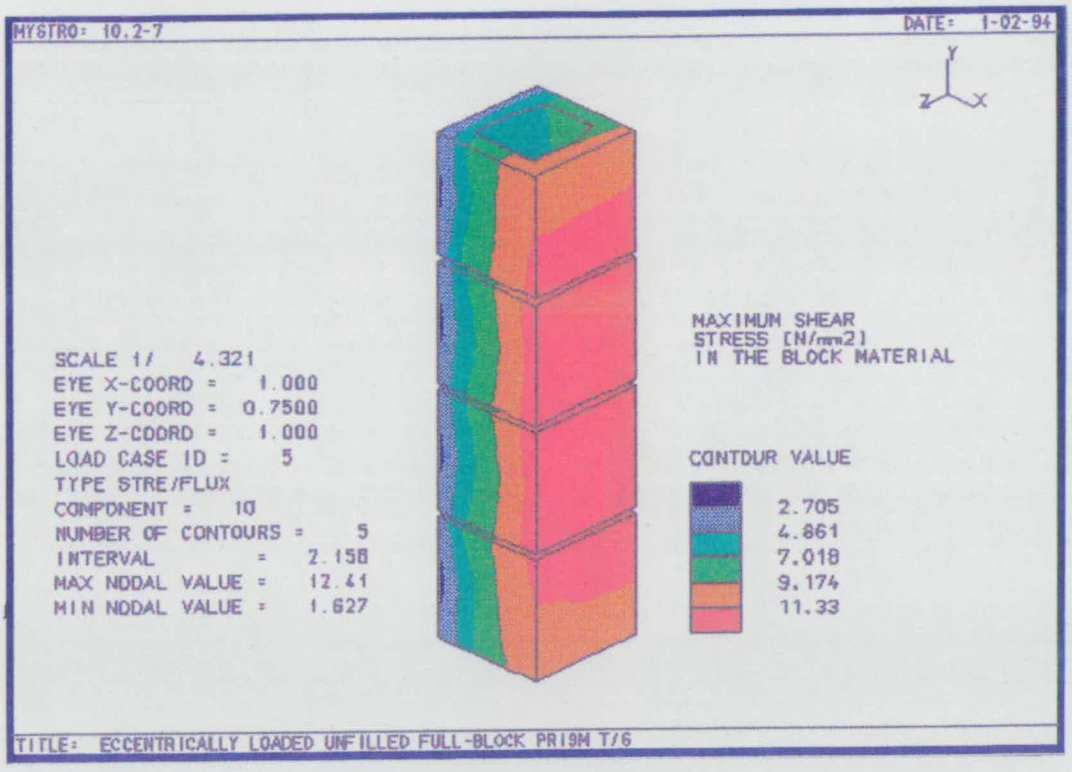


Fig. 4.86 Shear stress in the block material of unfilled full-block prism compressed under eccentric load for e = t/6

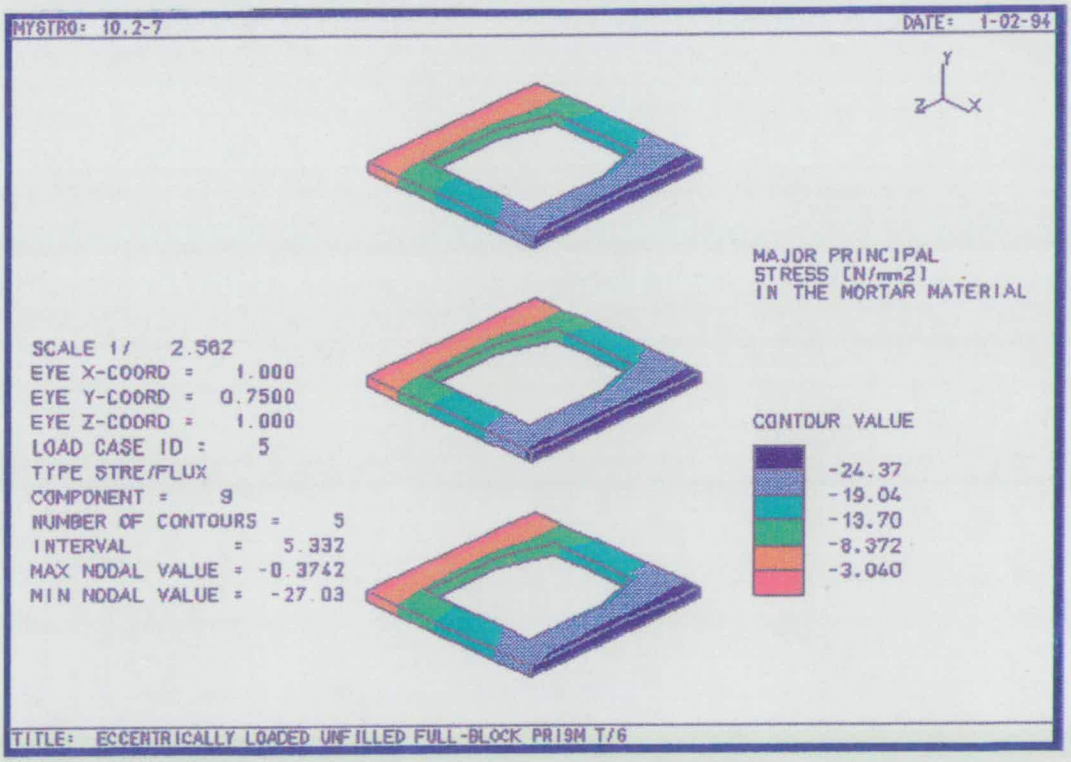


Fig. 4.87 Major principal stress in the mortar material of unfilled full-block prism compressed under eccentric load for e = t/6

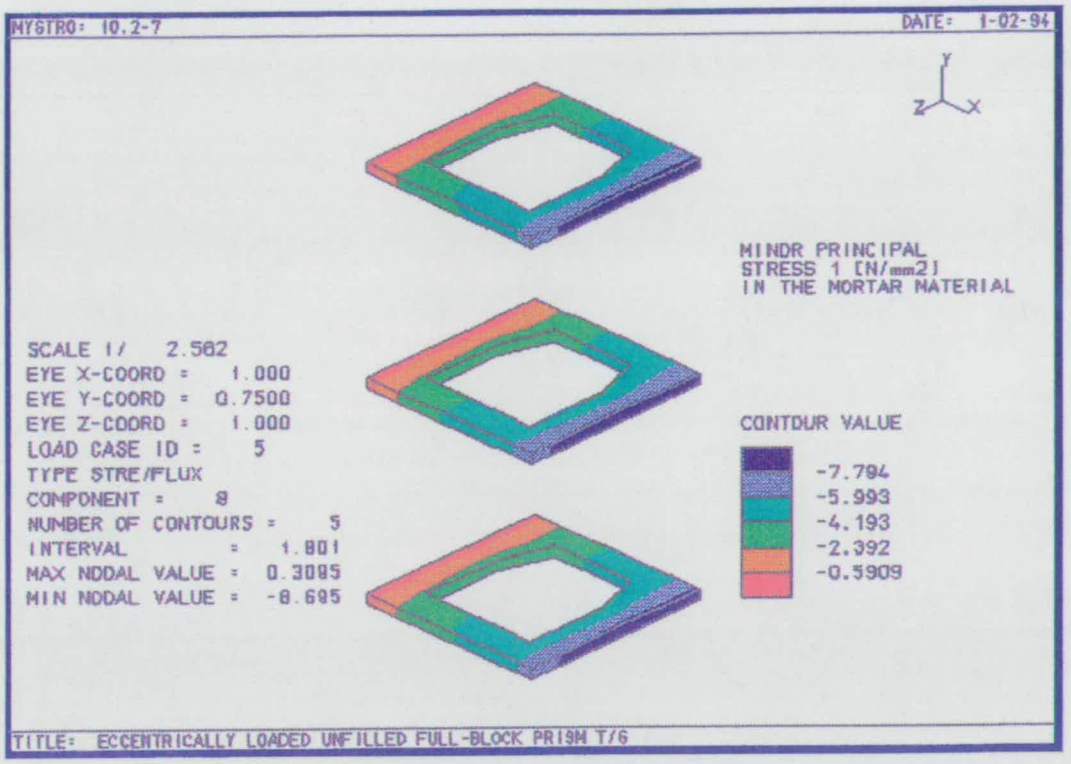


Fig. 4.88 Minor principal stress 1 in the block material of unfilled full-block prism compressed under eccentric load for e = t/6

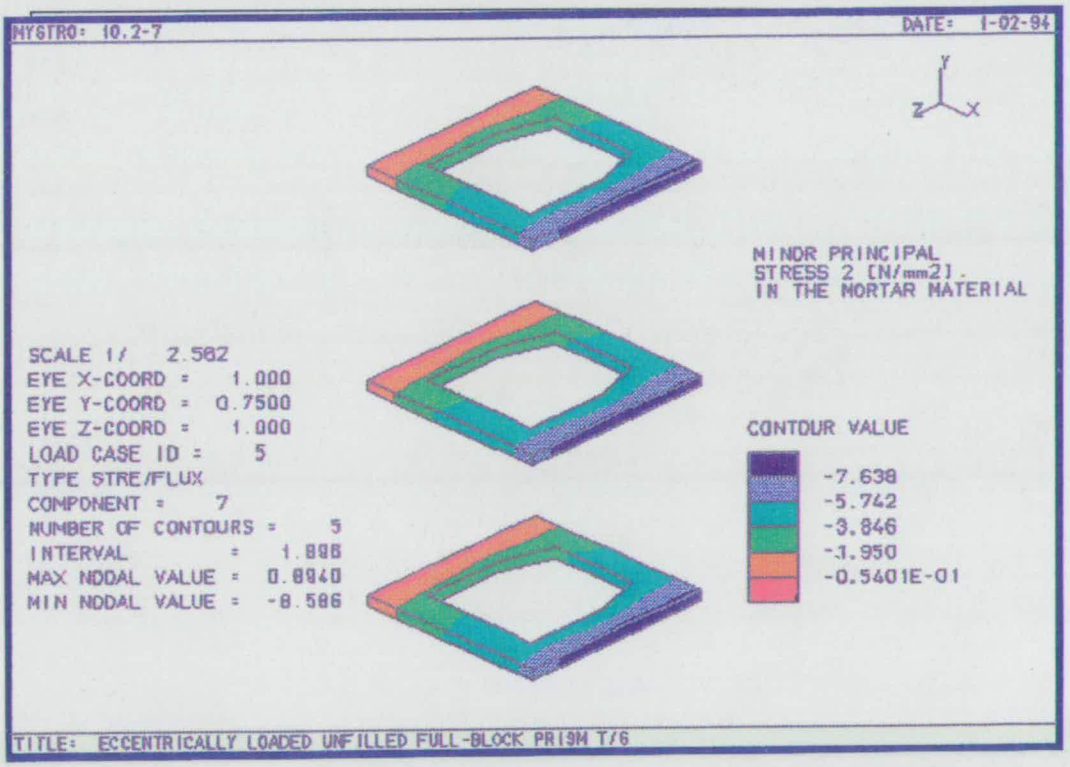


Fig. 4.89 Minor principal stress 2 in the block material of unfilled full-block prism compressed under eccentric load for e = t/6

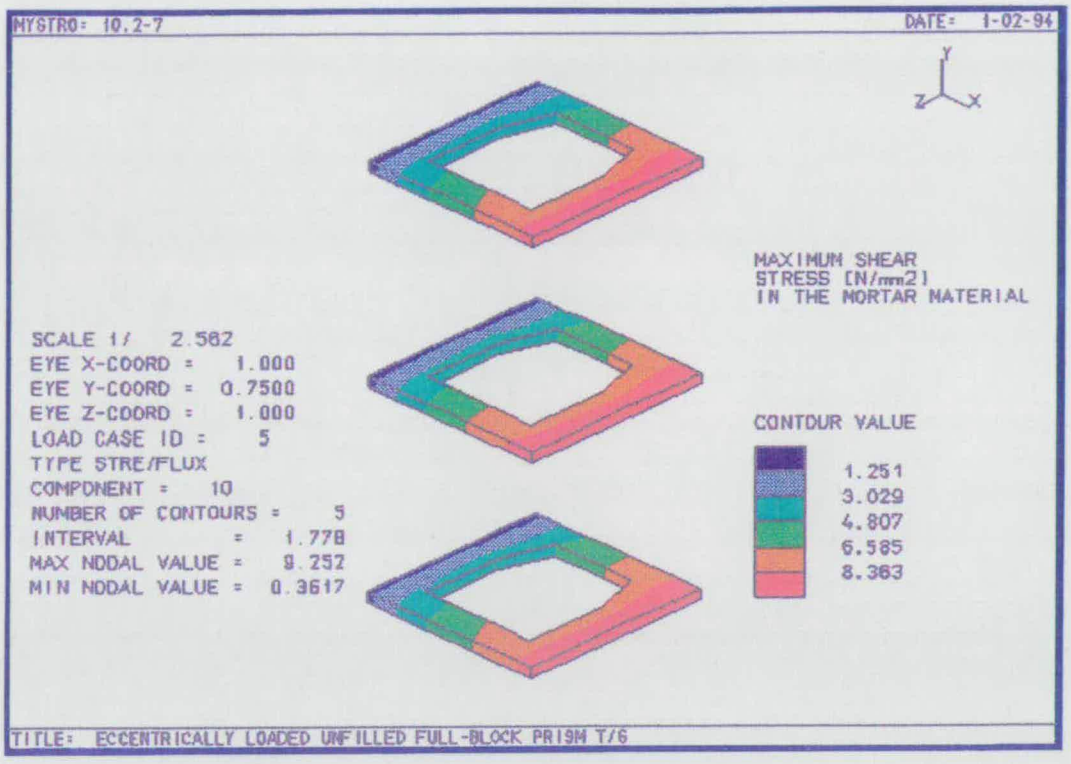


Fig. 4.90 Shear stress in the block material of unfilled full-block prism compressed under eccentric load for e = t/6

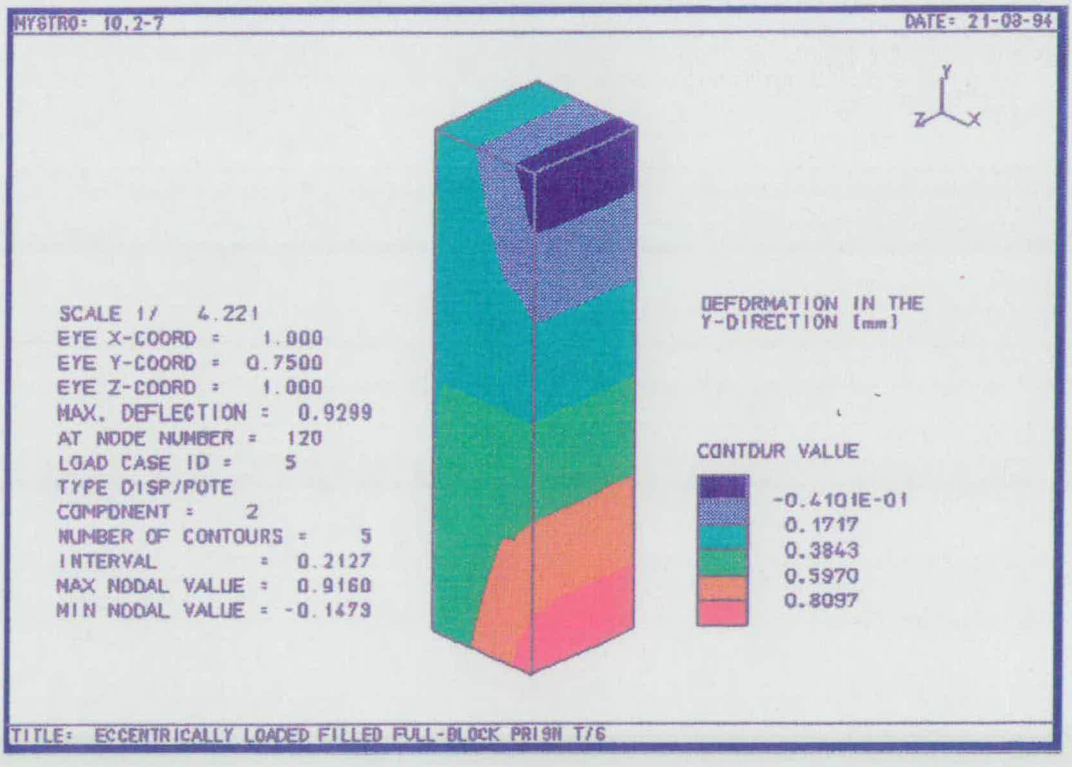


Fig. 4.91 Deformation in the Y-direction of filled full-block prism compressed under eccentric load for e = t/6

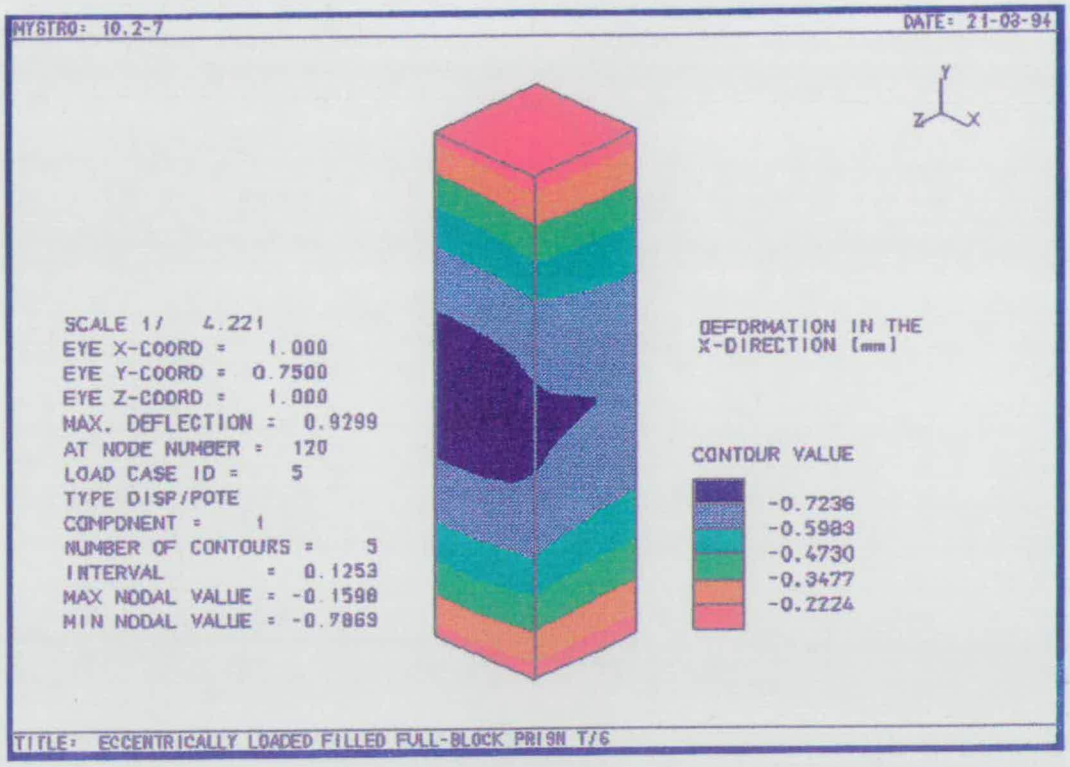


Fig. 4.92 Deformation in the X-direction of filled full-block prism compressed under eccentric load for e = t/6

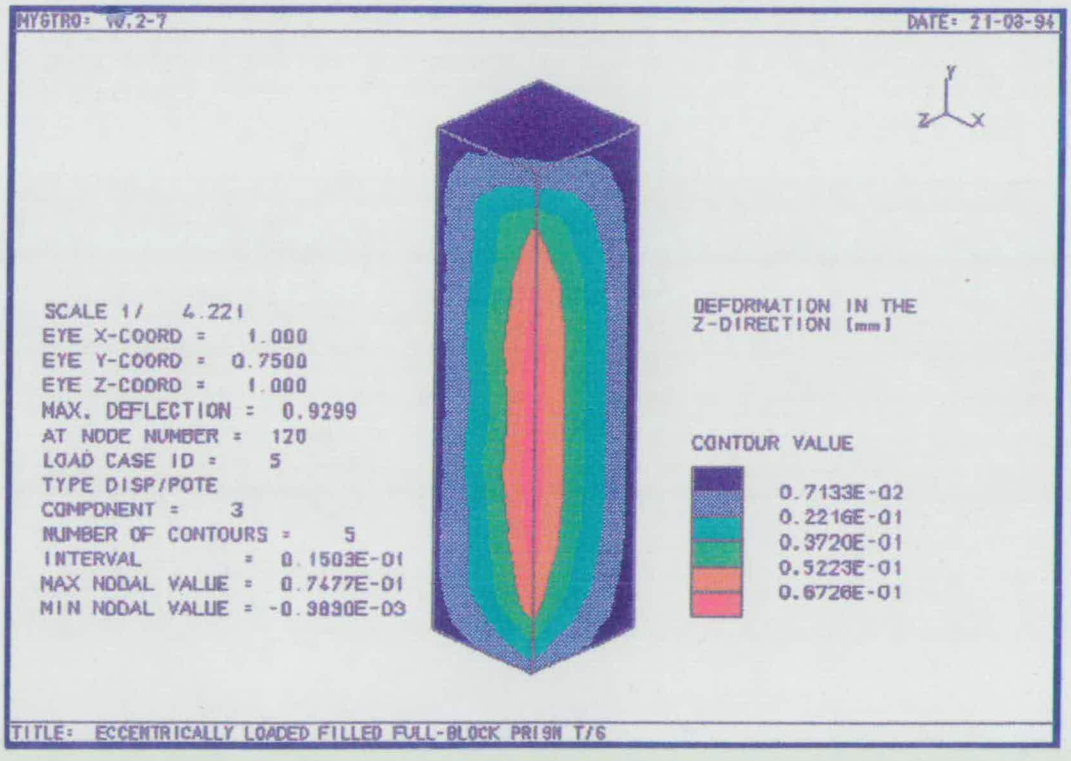


Fig. 4.93 Deformation in the Z-direction of filled full-block prism compressed under eccentric load for e = t/6

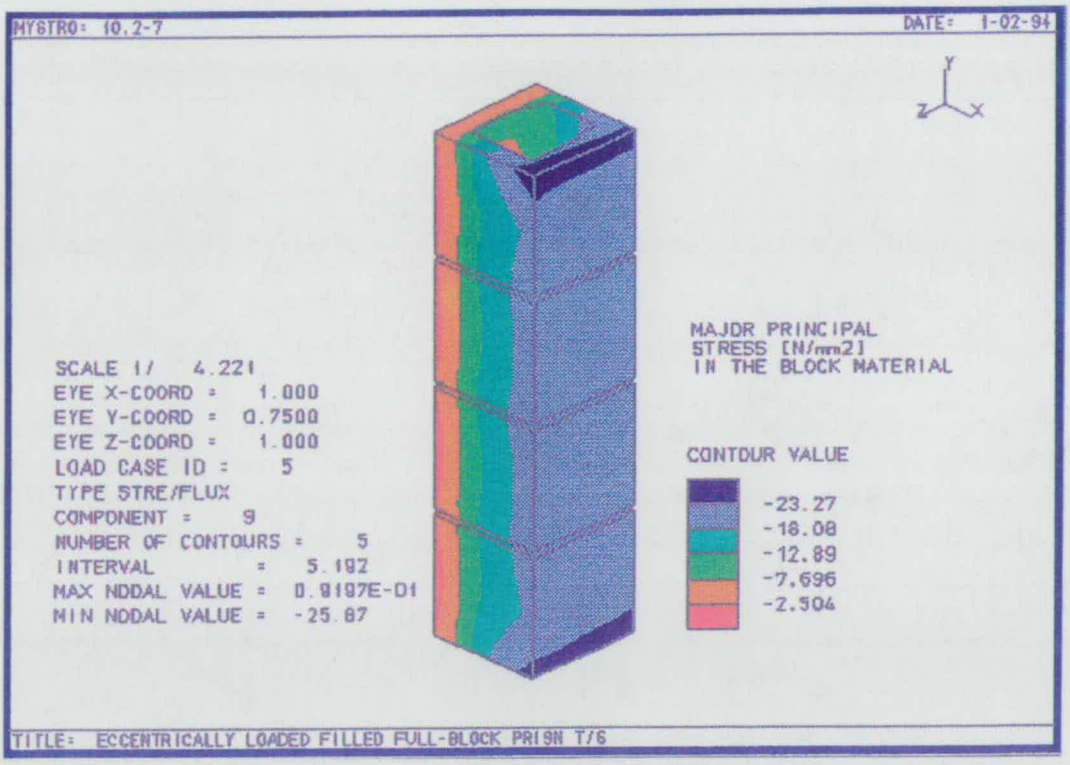


Fig. 4.94 Major principal stress in the block material of filled full-block prism compressed under eccentric load for e = t/6

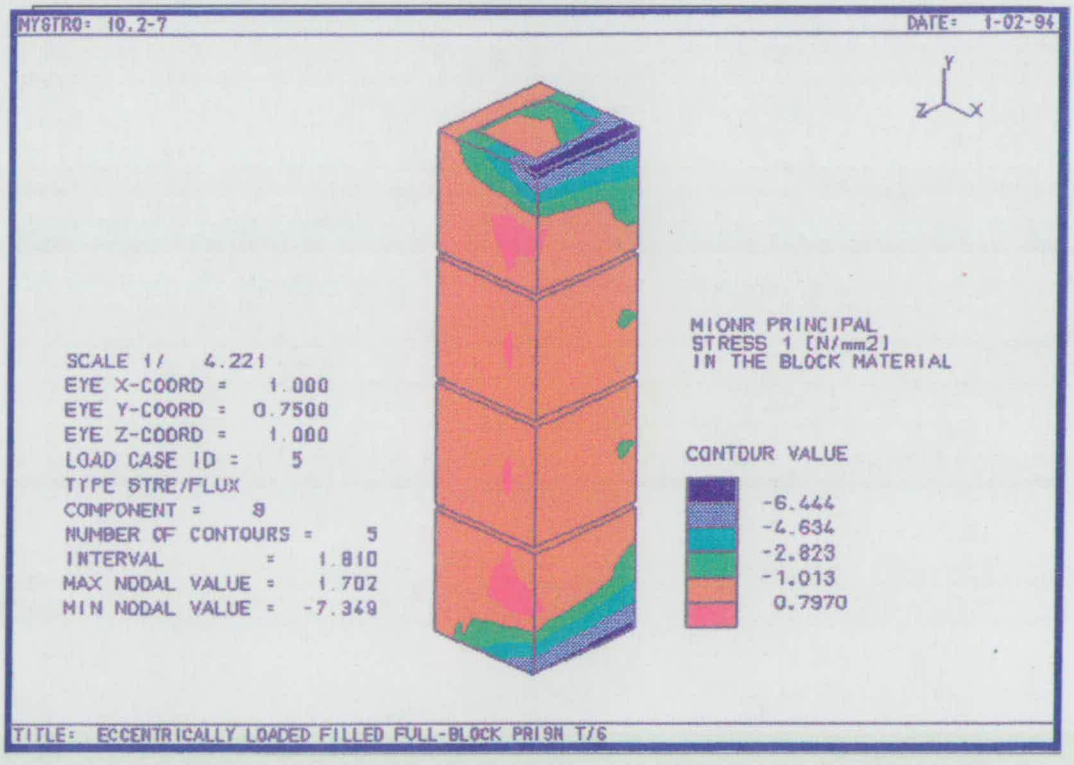


Fig. 4.95 Minor principal stress 1 in the block material of filled full-block prism compressed under eccentric load for e = t/6

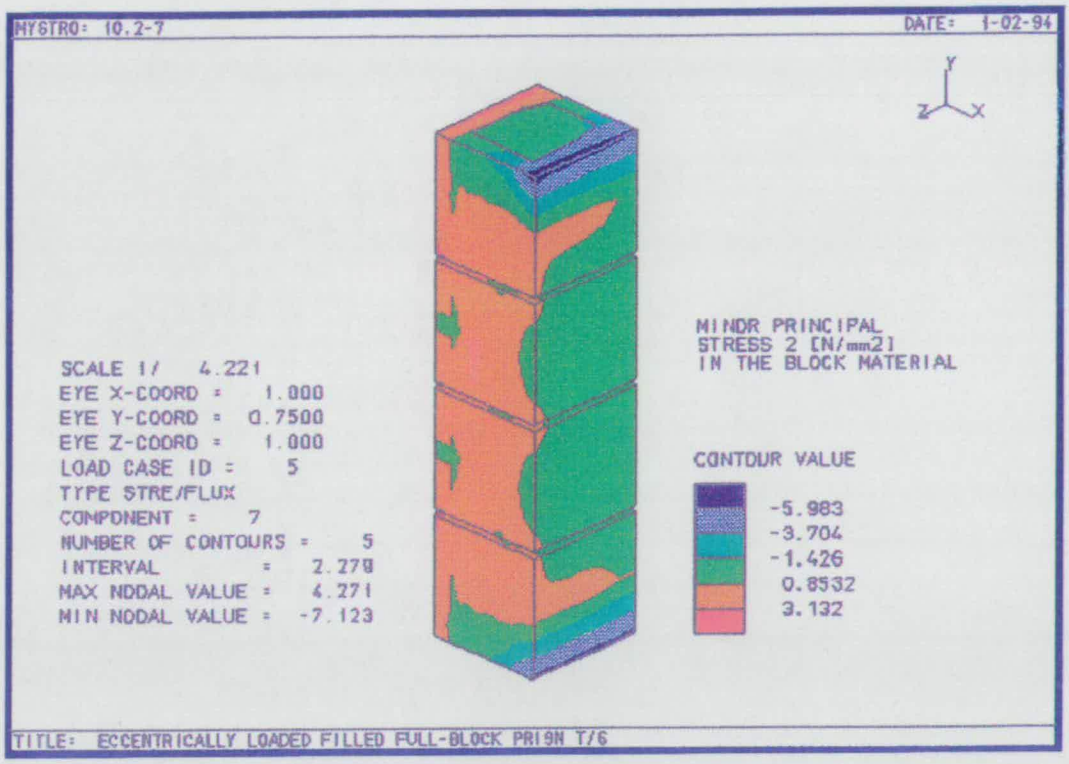


Fig. 4.96 Minor principal stress 2 in the block material of filled full-block prism compressed under eccentric load for e = t/6

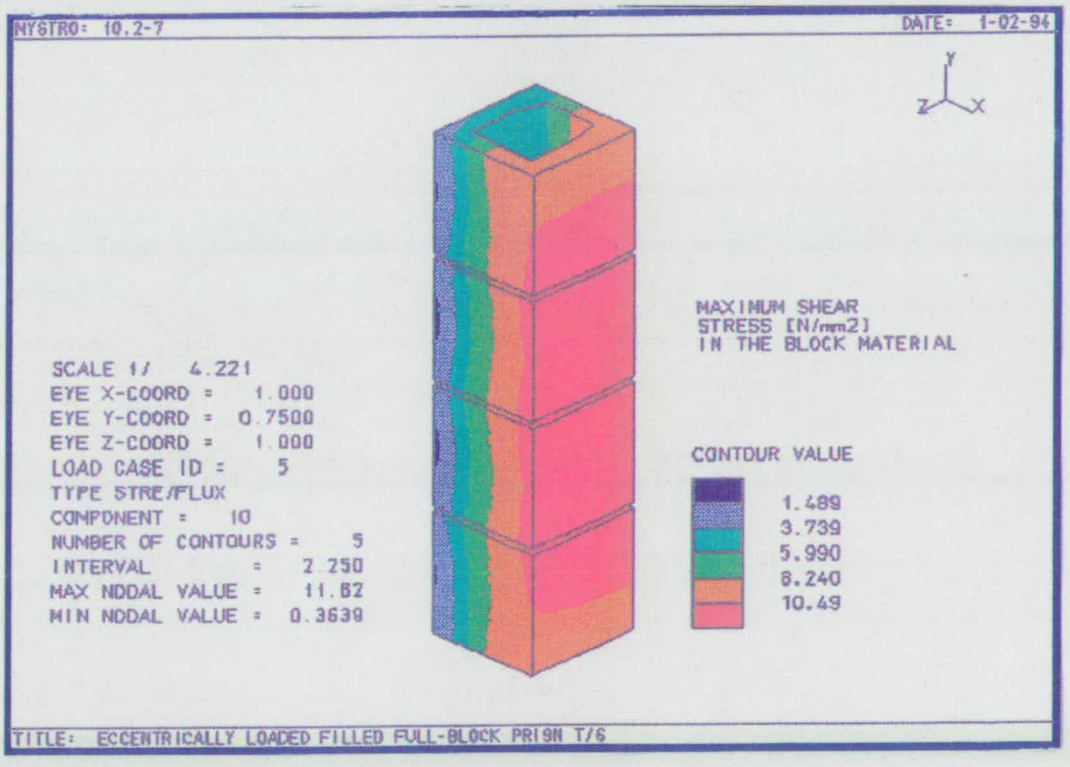


Fig. 4.97 Shear stress in the block material of filled full-block prism compressed under eccentric load for e = t/6

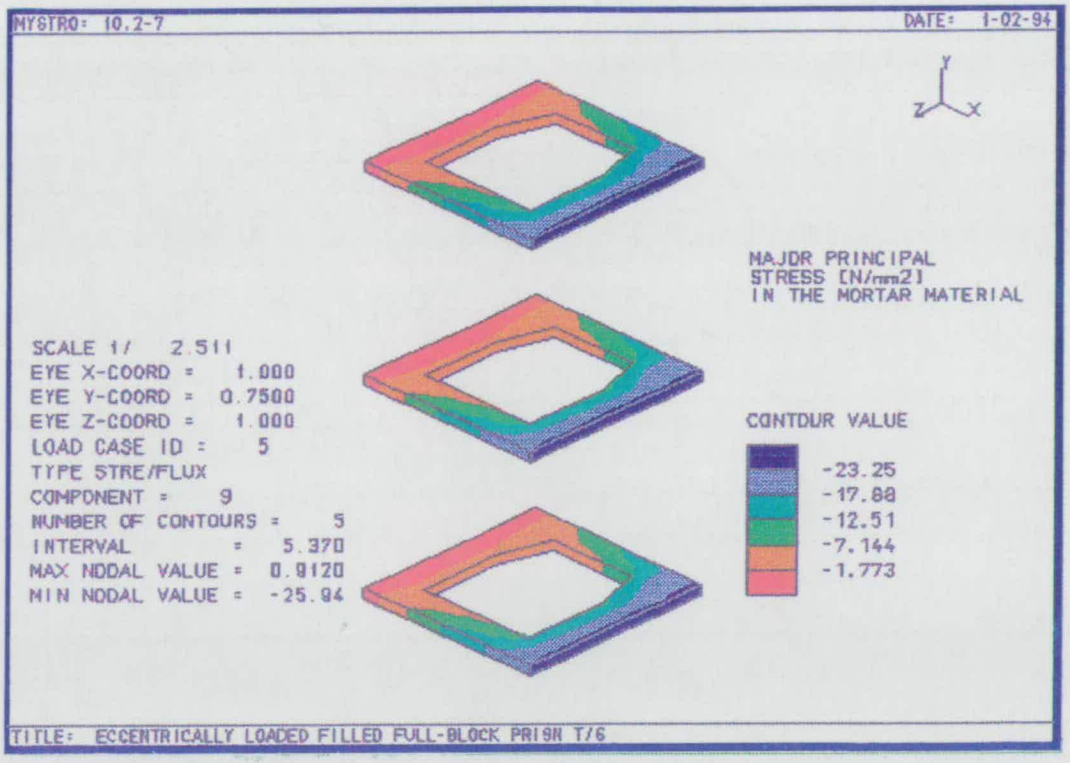


Fig. 4.98 Major principal stress in the mortar material of filled full-block prism compressed under eccentric load for e = t/6

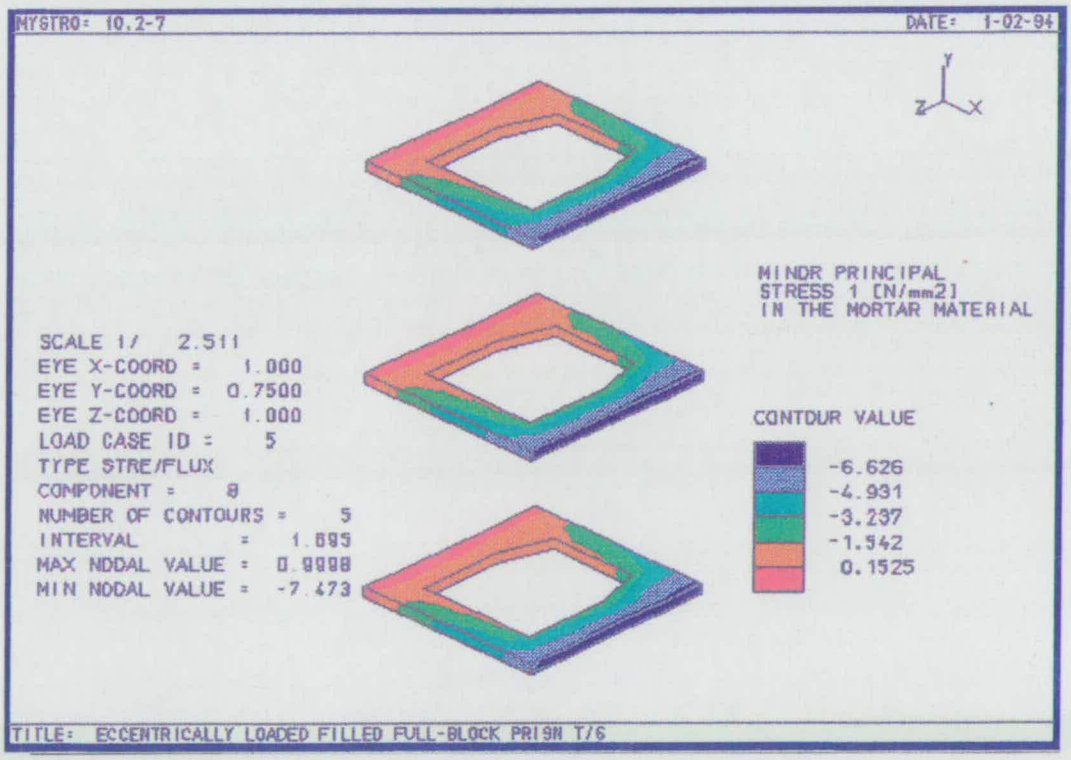


Fig. 4.99 Minor principal stress 1 in the mortar material of filled full-block prism compressed under eccentric load for e = t/6

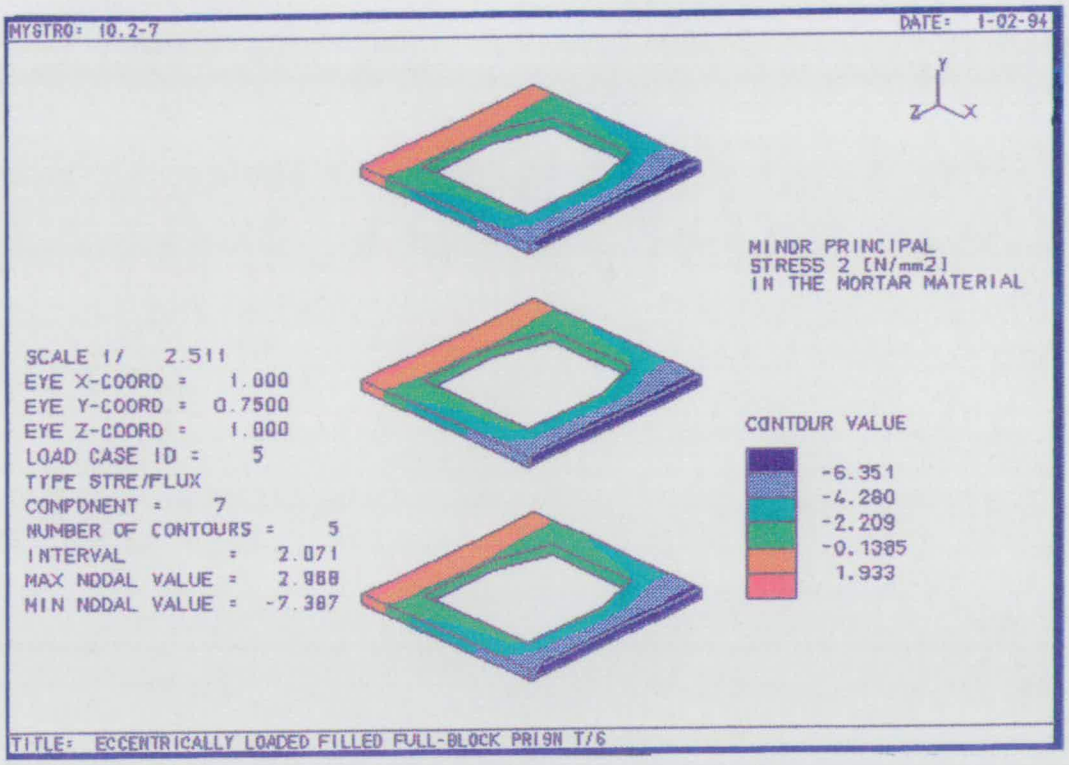


Fig. 4.100 Minor principal stress 2 in the mortar material of filled full-block compressed under eccentric load for e = t/6

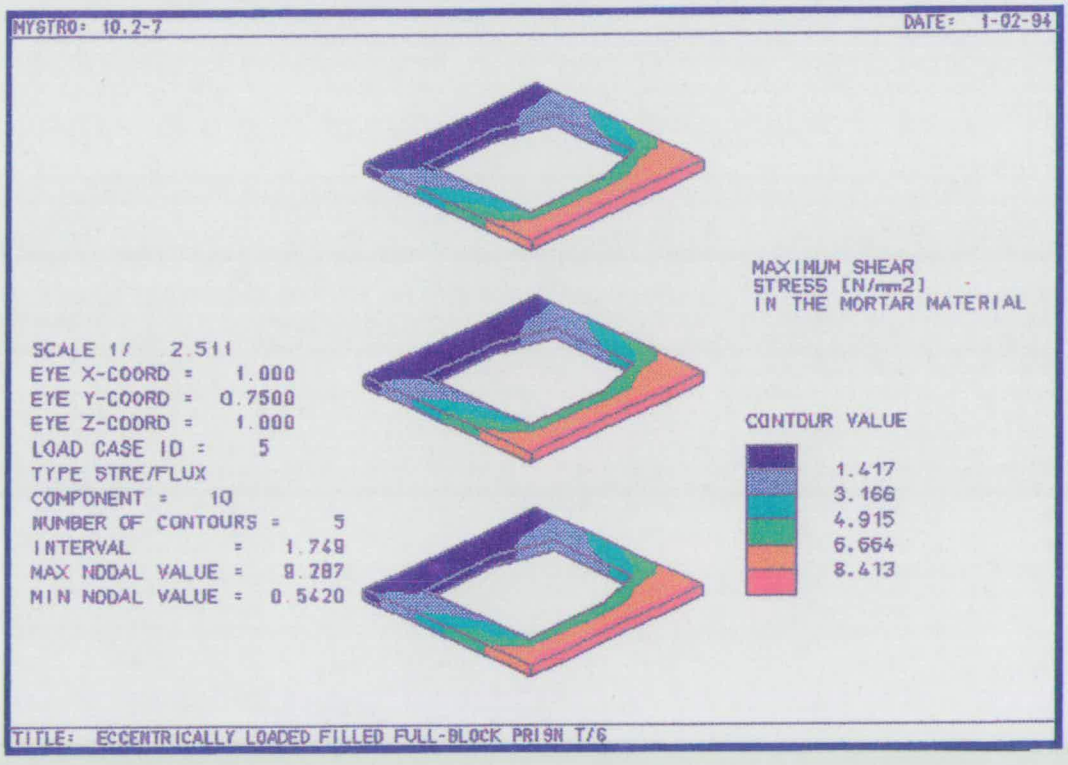


Fig. 4.101 Shear stress in the mortar material of filled full-block prism compressed under eccentric load for e = t/6

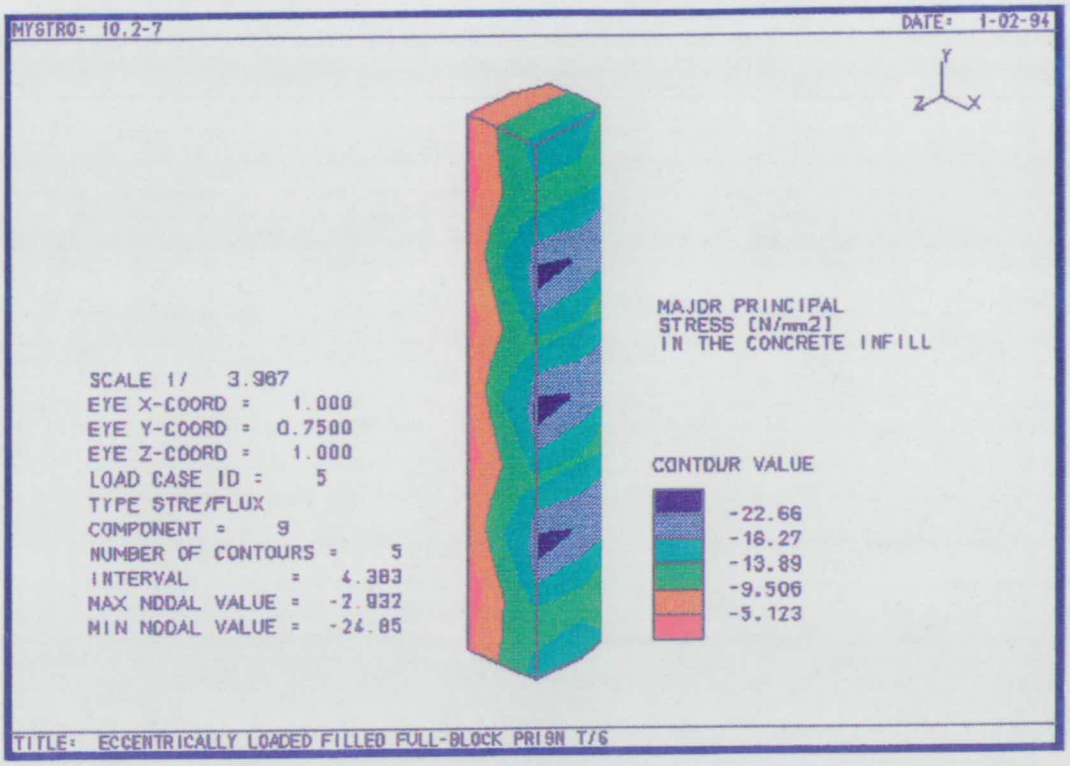


Fig. 4.102 Major principal stress in the concrete infill of full-block prism compressed under eccentric load for e = t/6

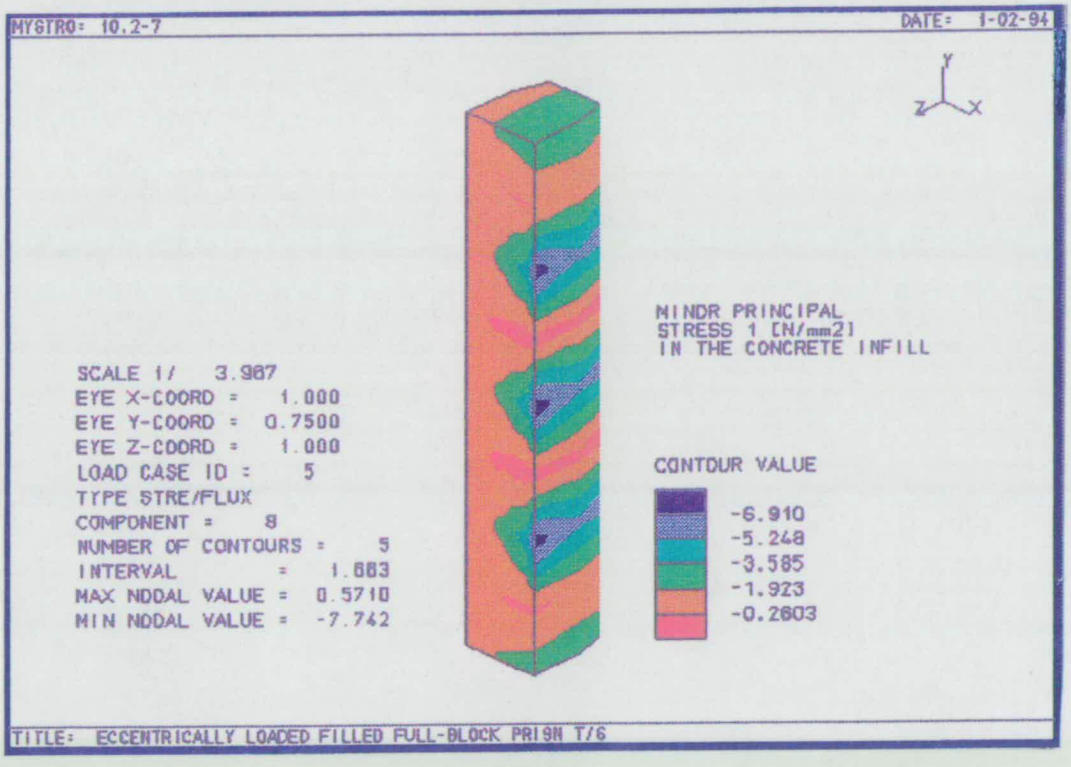


Fig. 4.103 Minor principal stress 1 in the concrete infill of filled full-block prism compressed under eccentric load for e = t/6

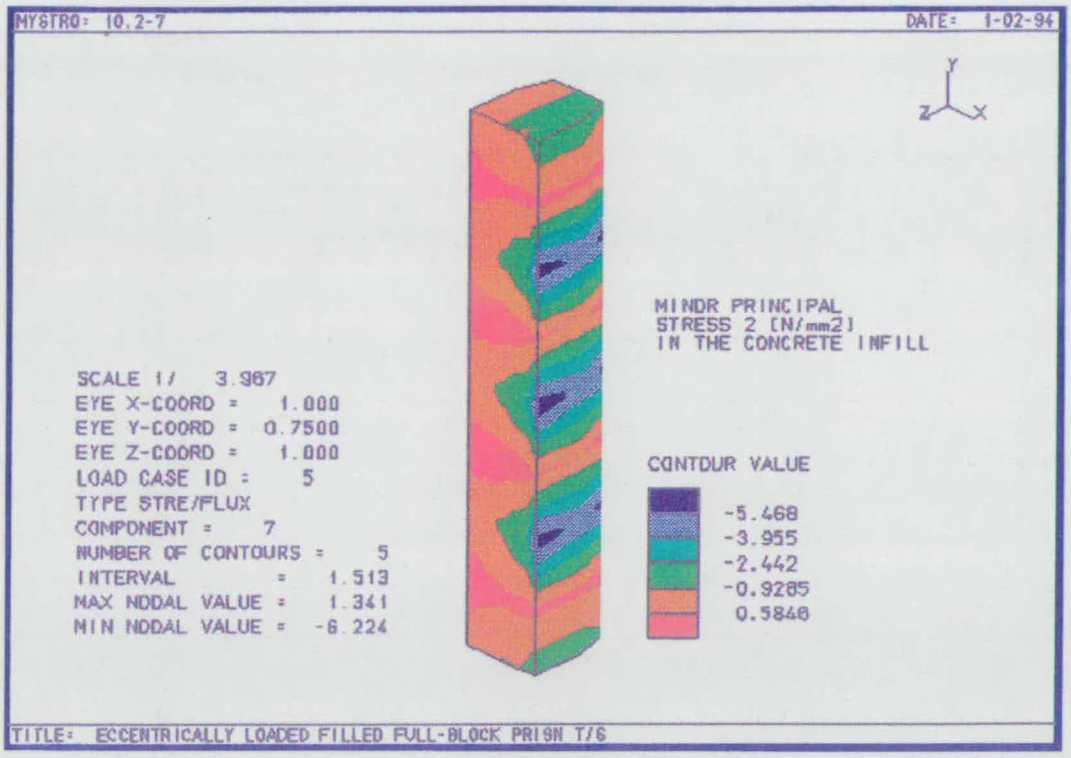


Fig. 4.104 Minor principal stress 2 in the concrete infill of full-block prism compressed under eccentric load for e = t/6

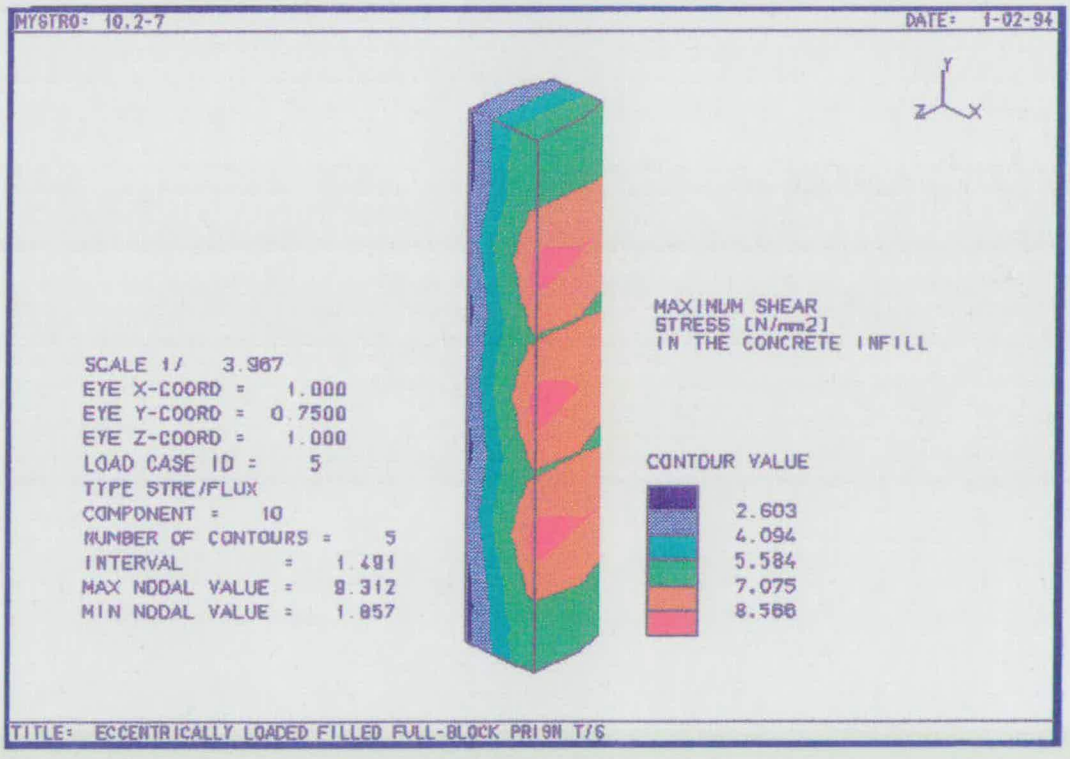


Fig. 4.105 Shear stress in the concrete infill of filled full-block prism compressed under eccentric load for e = t/6

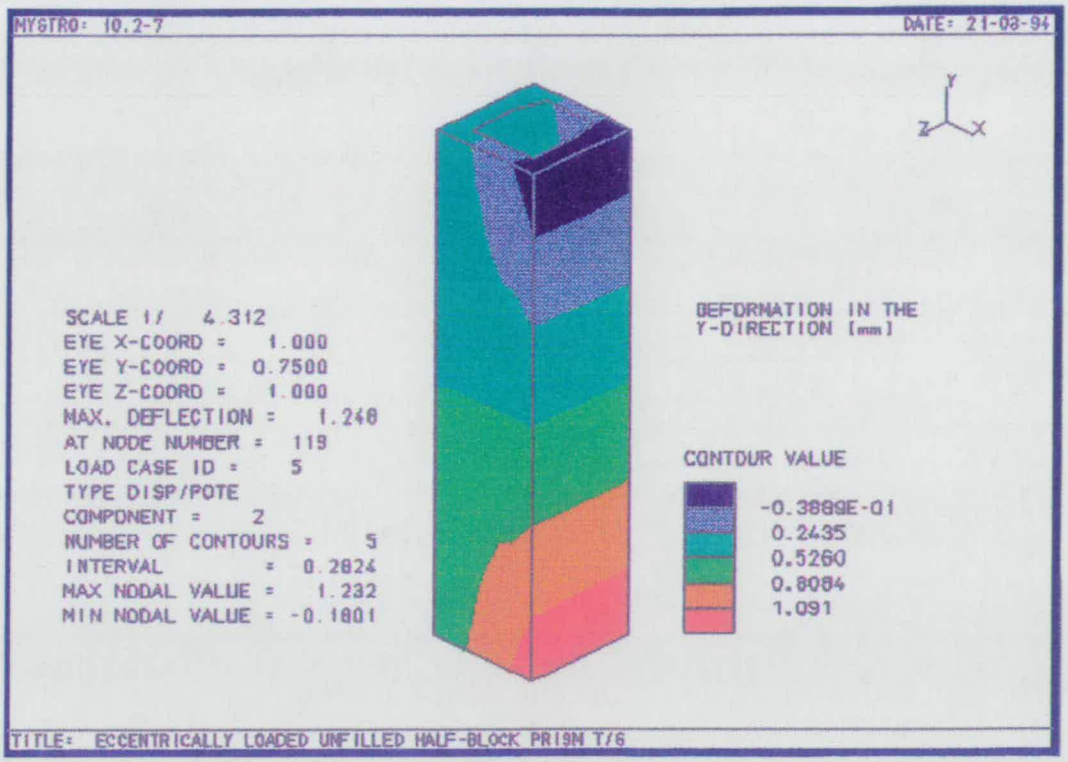


Fig. 4.106 Deformation in the Y-direction of unfilled half-block prism compressed under eccentric load for e = t/6

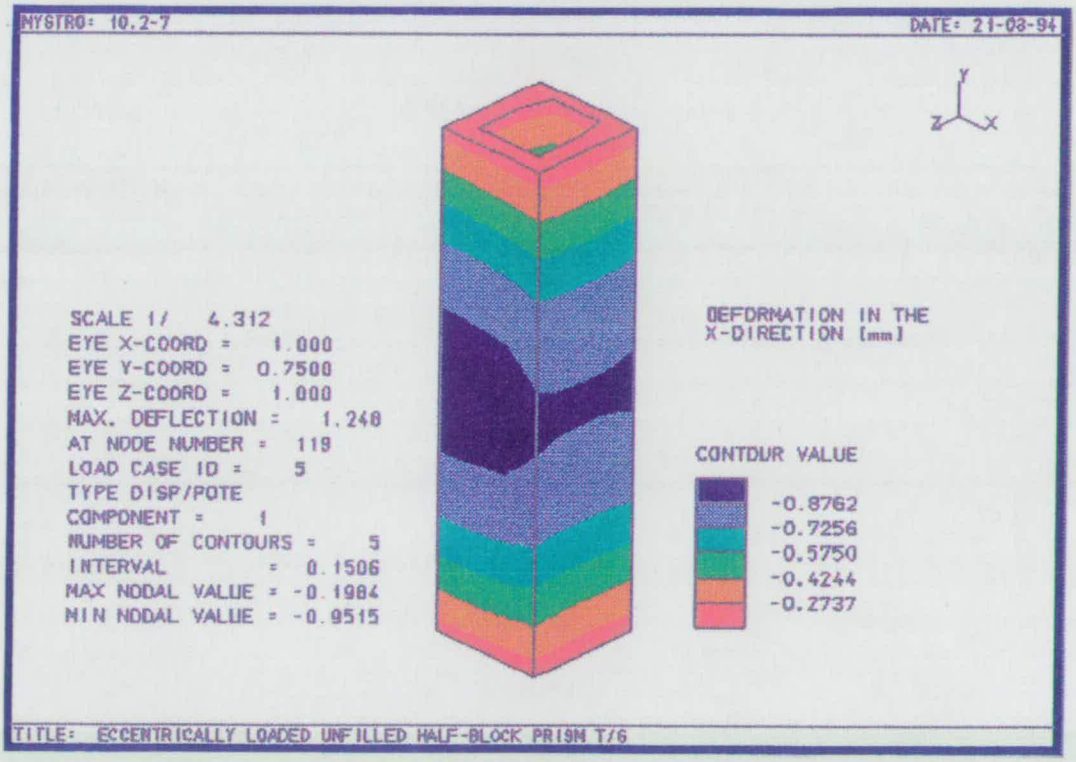


Fig. 4.107 Deformation in the X-direction of unfilled half-block prism compressed under eccentric load for e = t/6

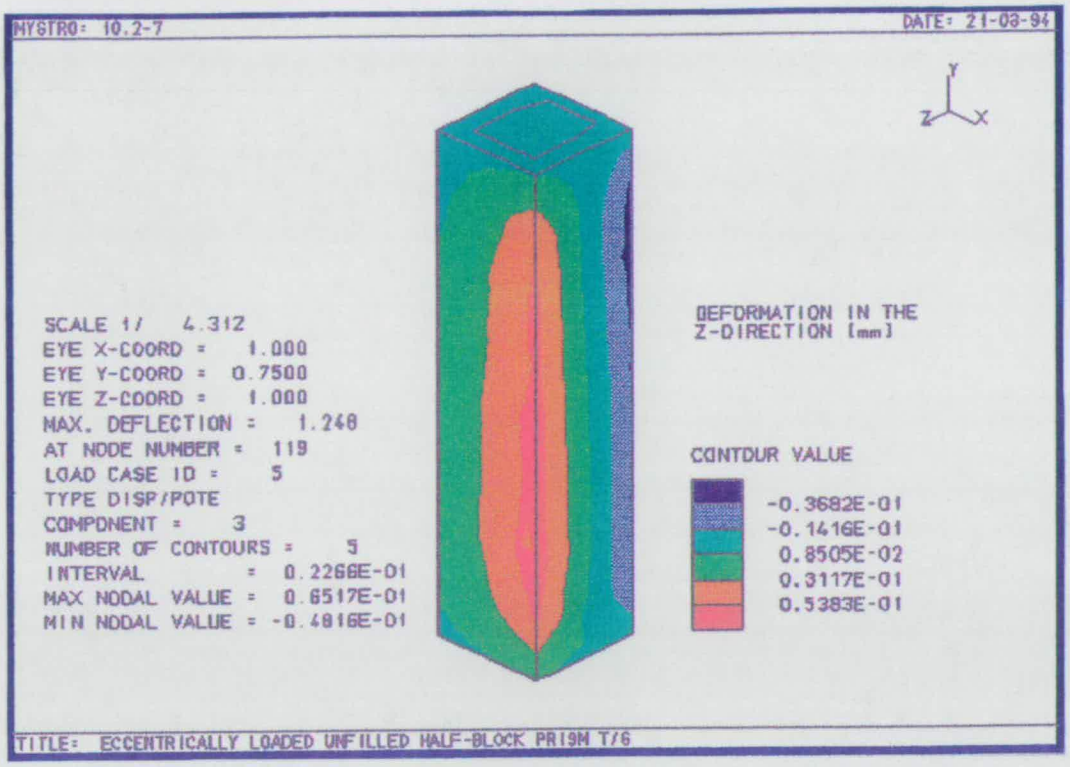


Fig. 4.108 Deformation in the Z-direction of unfilled half-block prism compressed under eccentric load for e = t/6

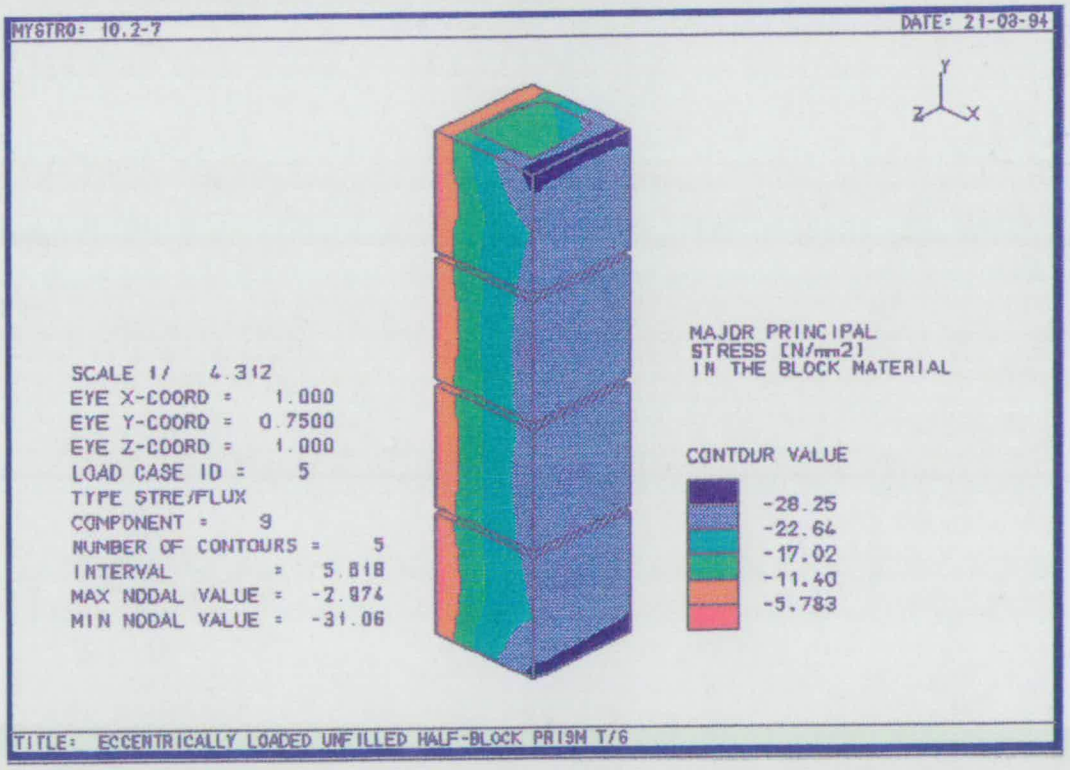


Fig. 4.109 Major principal stress in the block material of unfilled half-block prism compressed under eccentric load for e = t/6

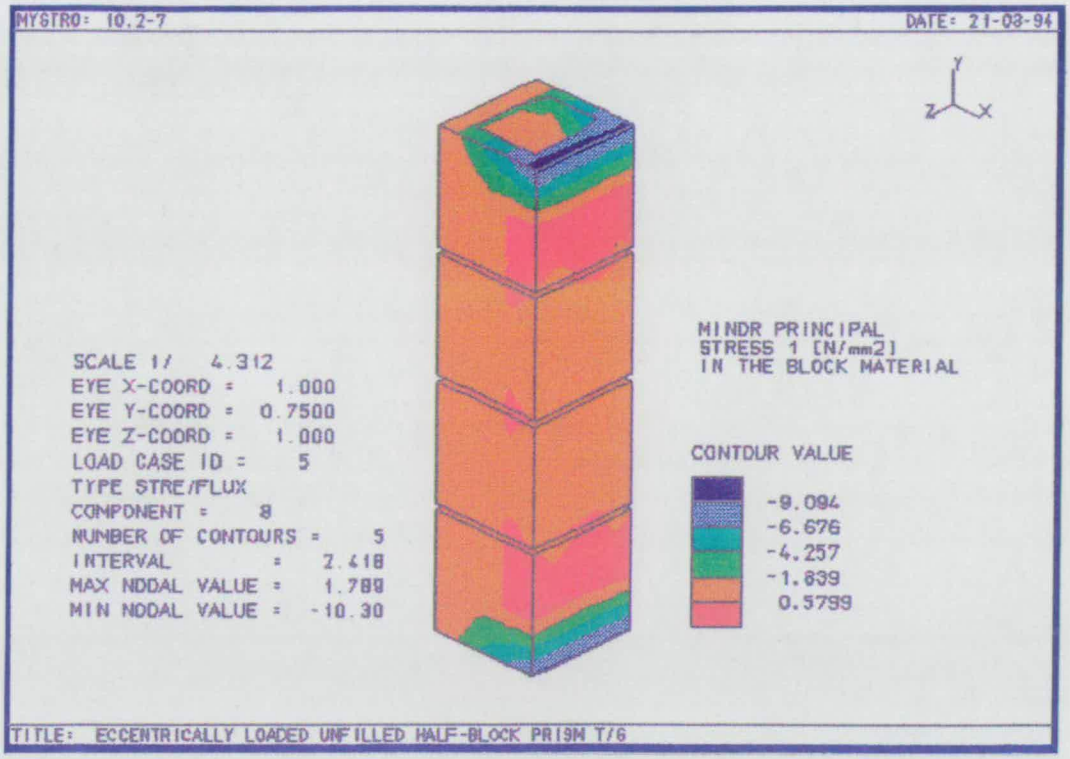


Fig. 4.110 Minor principal stress 1 in the block material of unfilled half-block prism compressed under eccentric load for e = t/6

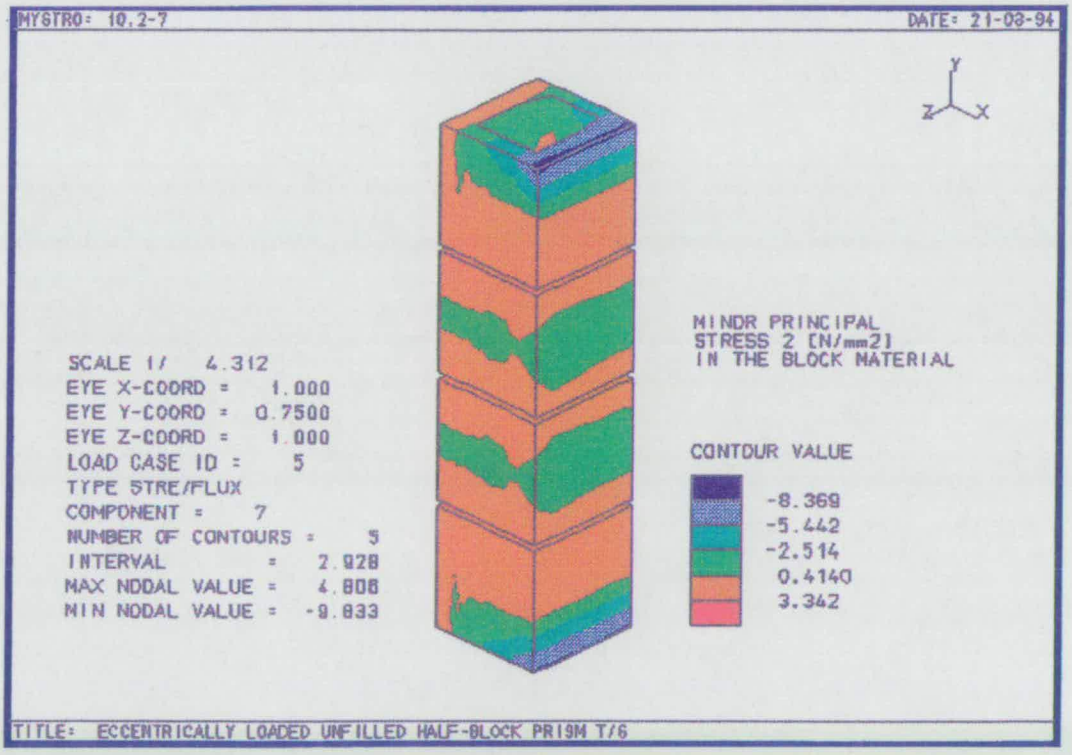


Fig. 4.111 Minor principal stress 2 in the block material of unfilled half-block prism compressed under eccentric load for e = t/6

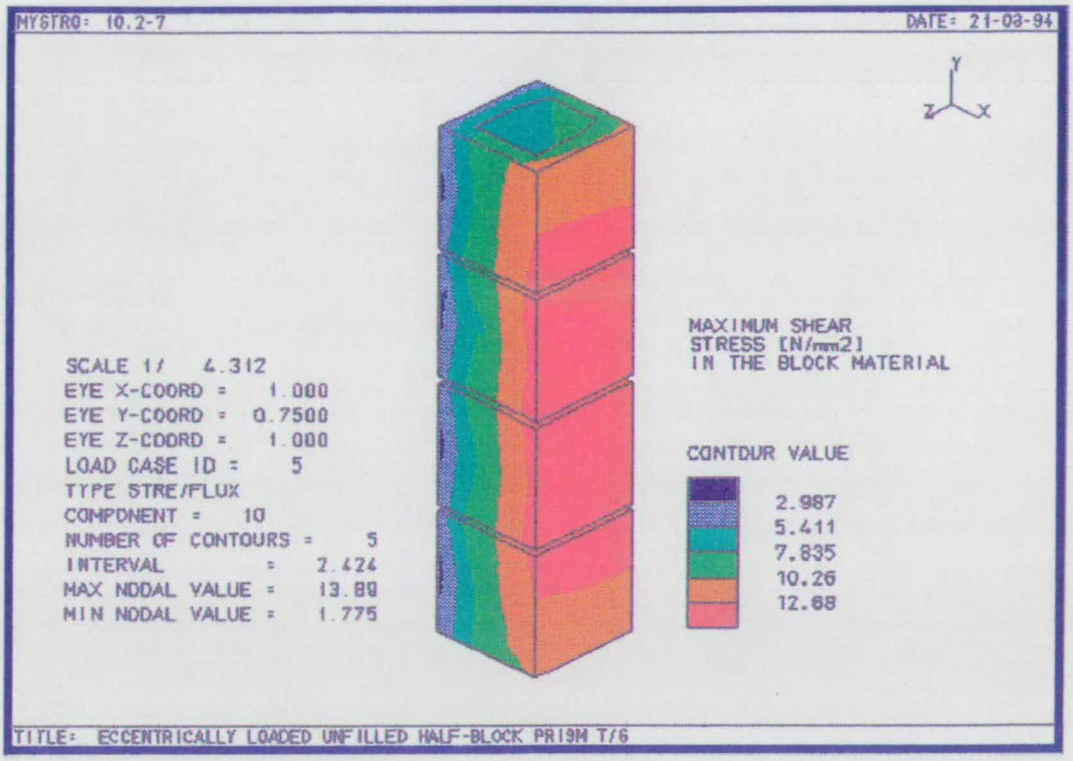


Fig. 4.112 Shear stress in the block material of unfilled half-block prism compressed under eccentric load for e = t/6

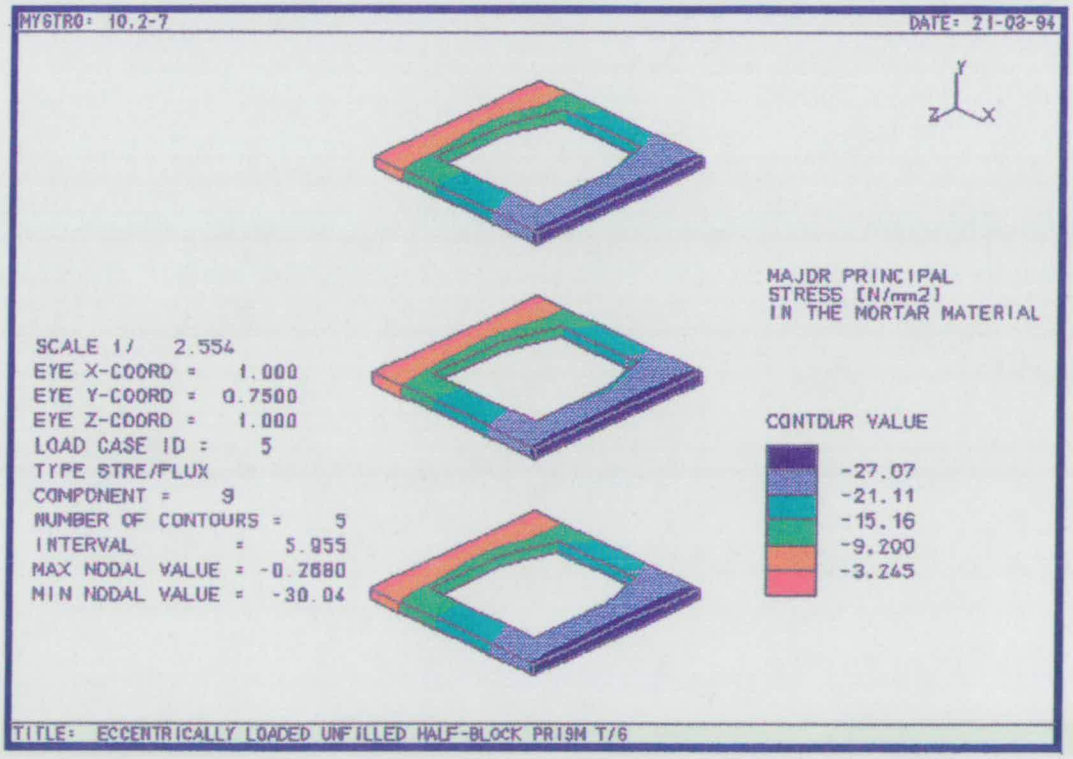


Fig. 4.113 Major principal stress in the mortar material of unfilled half-block prism compressed under eccentric load for e = t/6

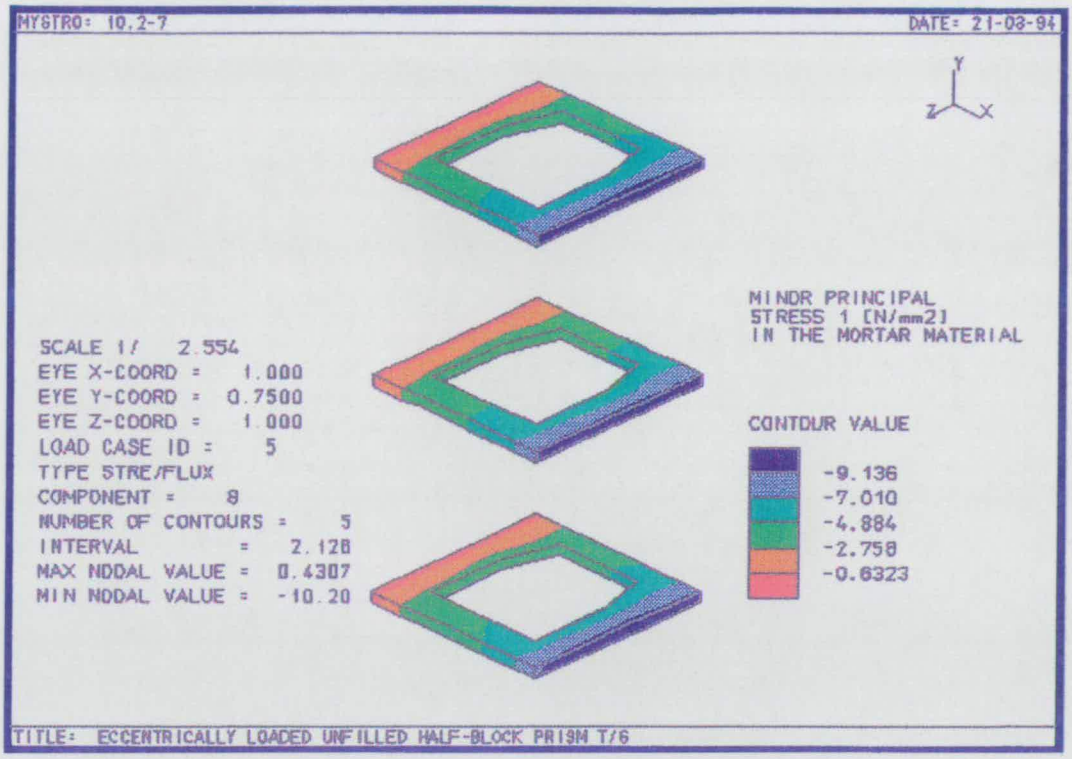


Fig. 4.114 Minor principal stress 1 in the mortar material of unfilled half-block prism compressed under eccentric load for e = t/6

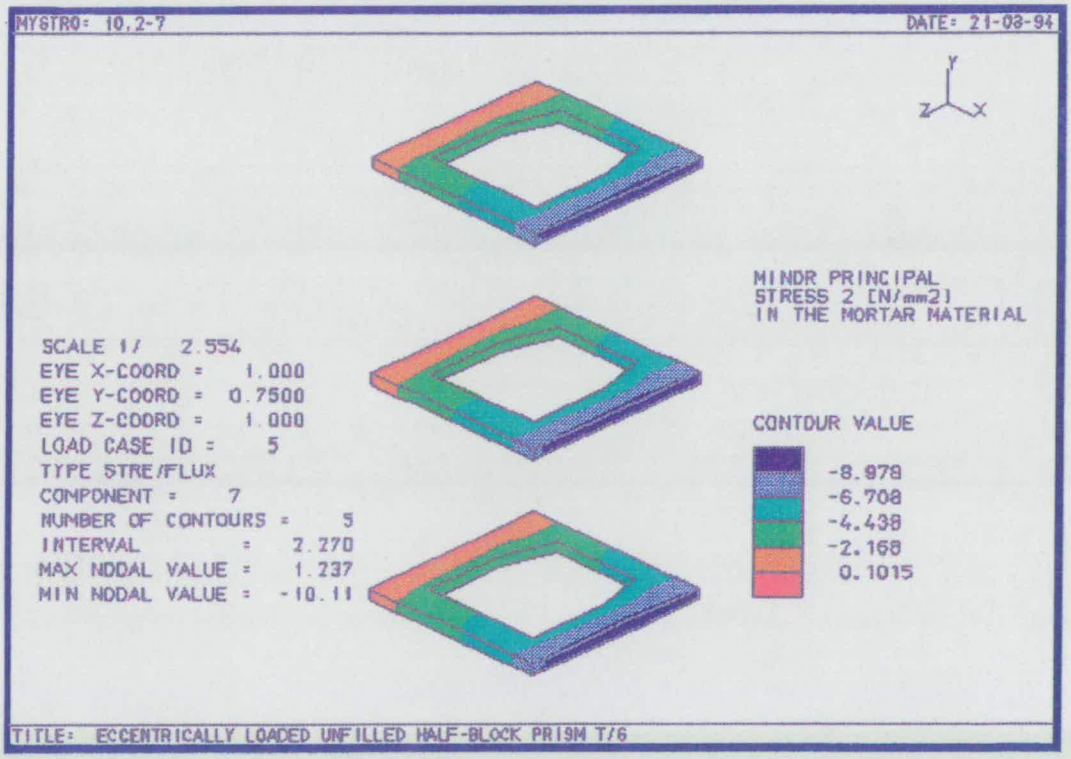


Fig. 4.115 Minor principal stress 2 in the mortar material of unfilled half-block prism compressed under eccentric load for e = t/6

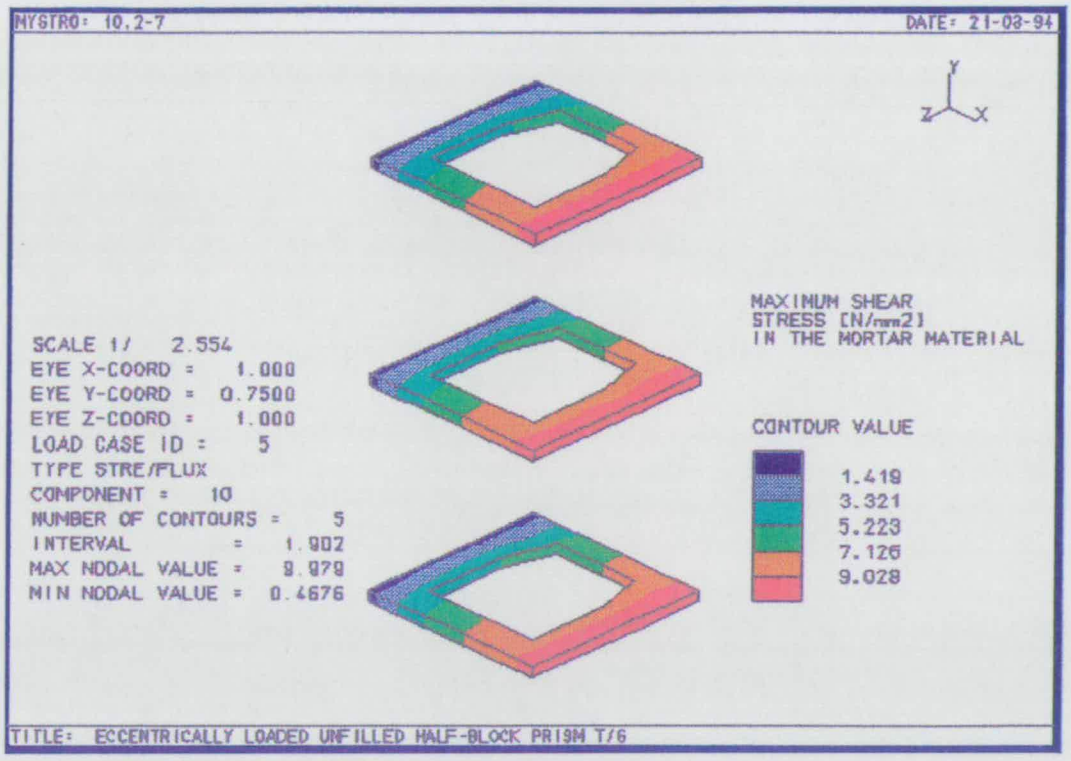


Fig. 4.116 Shear stress in the mortar material of unfilled half-block prism compressed under eccentric load for e = t/6

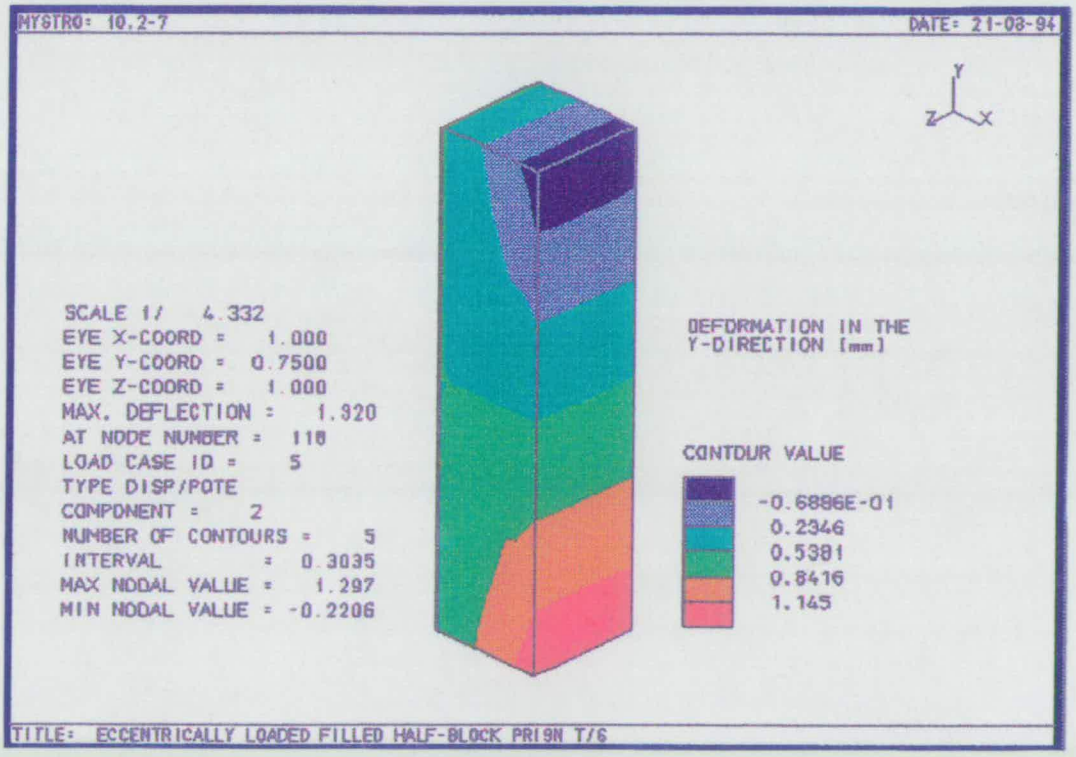


Fig. 4.117 Deformation in the Y-direction of filled half-block prism compressed under eccentric load for e = t/6

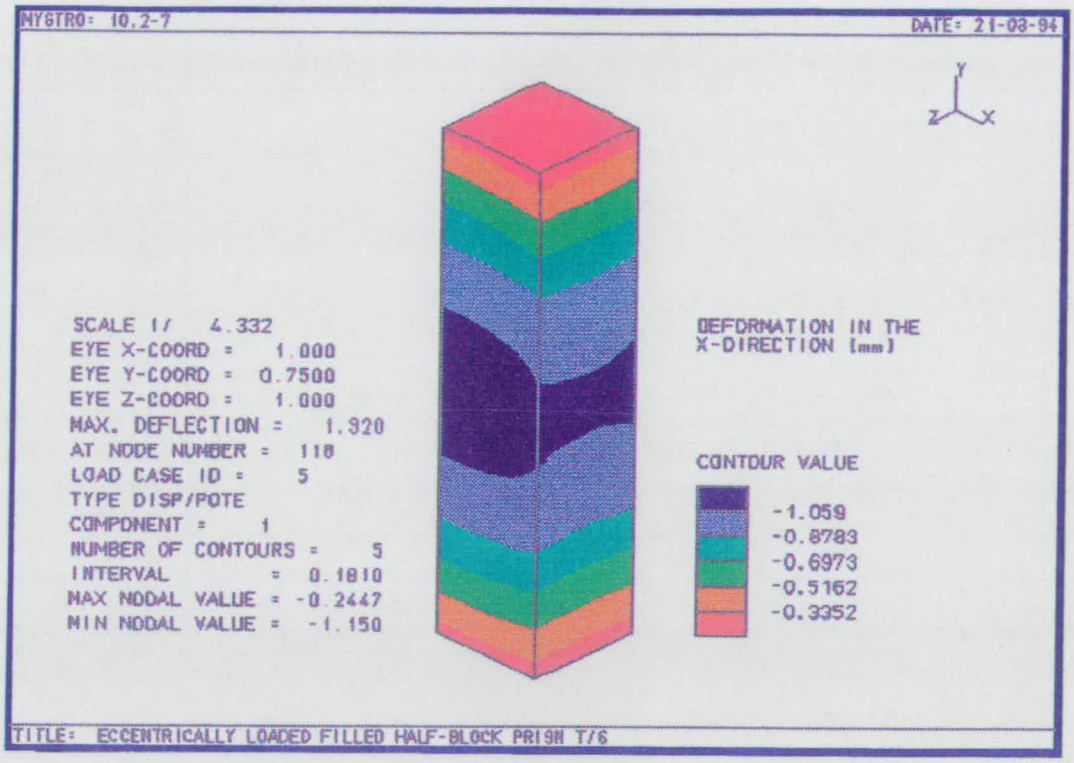


Fig. 4.118 Deformation in the X-direction of filled half-block prism compressed under eccentric load for e = t/6

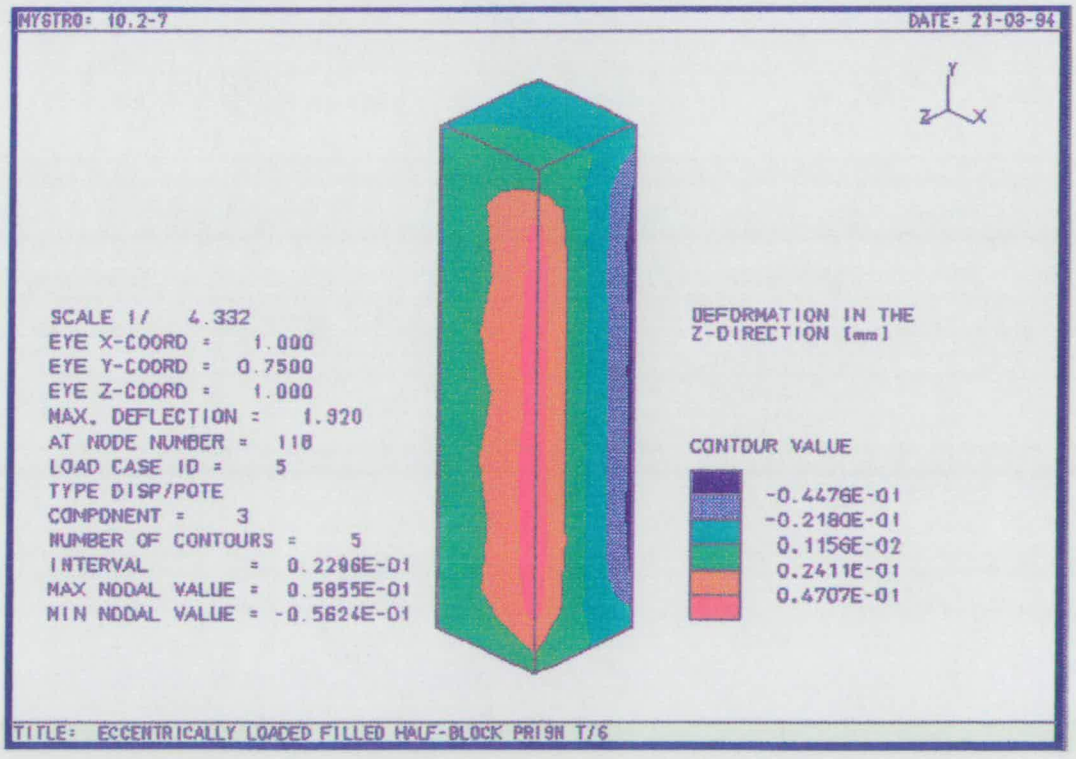


Fig. 4.119 Deformation in the Z-direction of filled half-block prism compressed under eccentric load for e = t/6

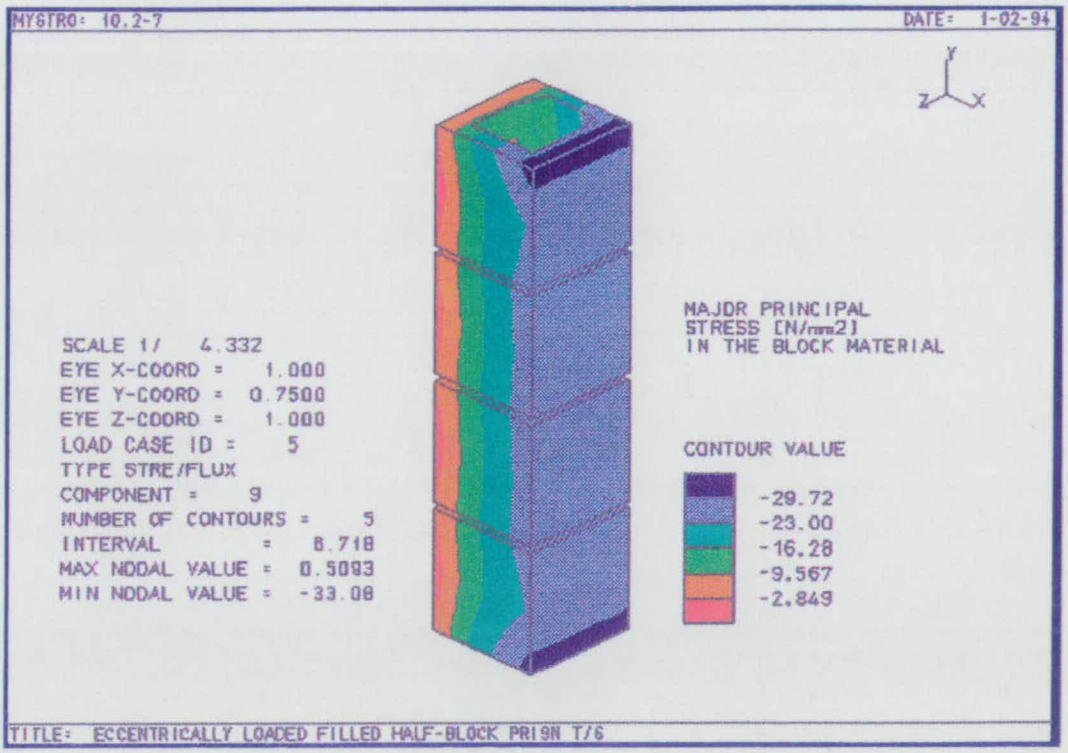


Fig. 4.120 Major principal stress in the block material of filled half-blockprism compressed under eccentric load for e = t/6

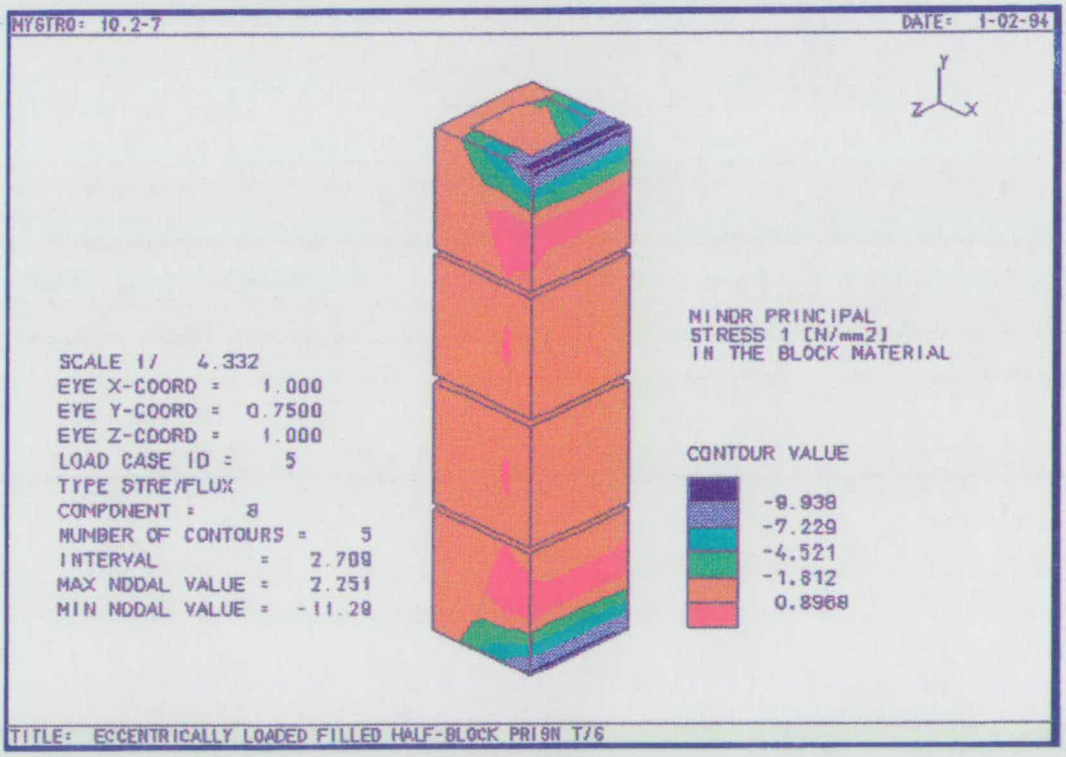


Fig. 4.121 Minor principal stress 1 in the block material of filled half-block prism compressed under eccentric load for e = t/6

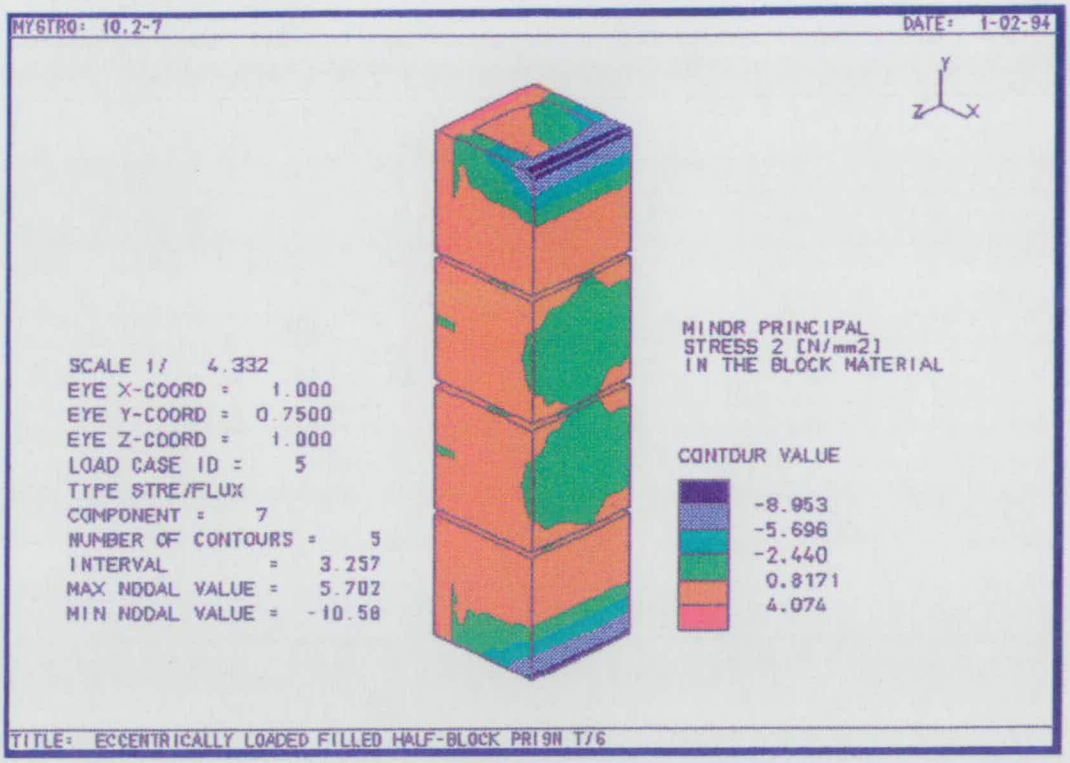


Fig. 4.122 Minor principal stress 2 in the block material of filled half-block prism compressed under eccentric load for e = t/6

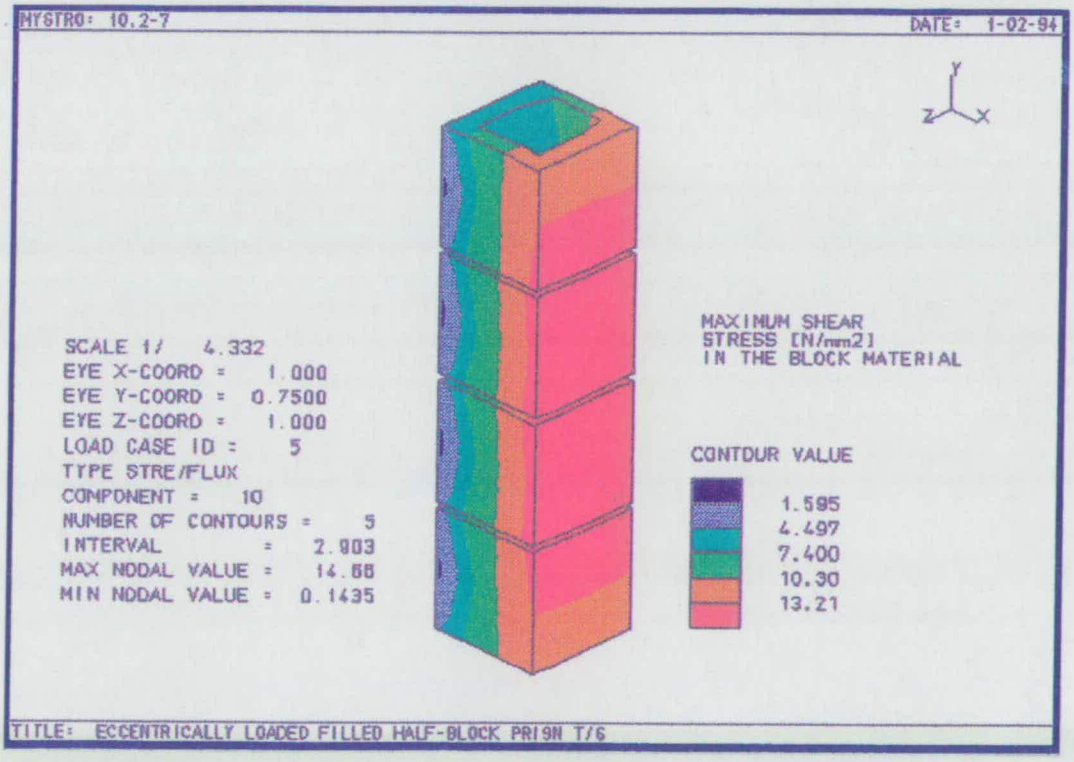


Fig. 4.123 Shear stress in the block material of filled half-block prism compressed under eccentric load for e = t/6

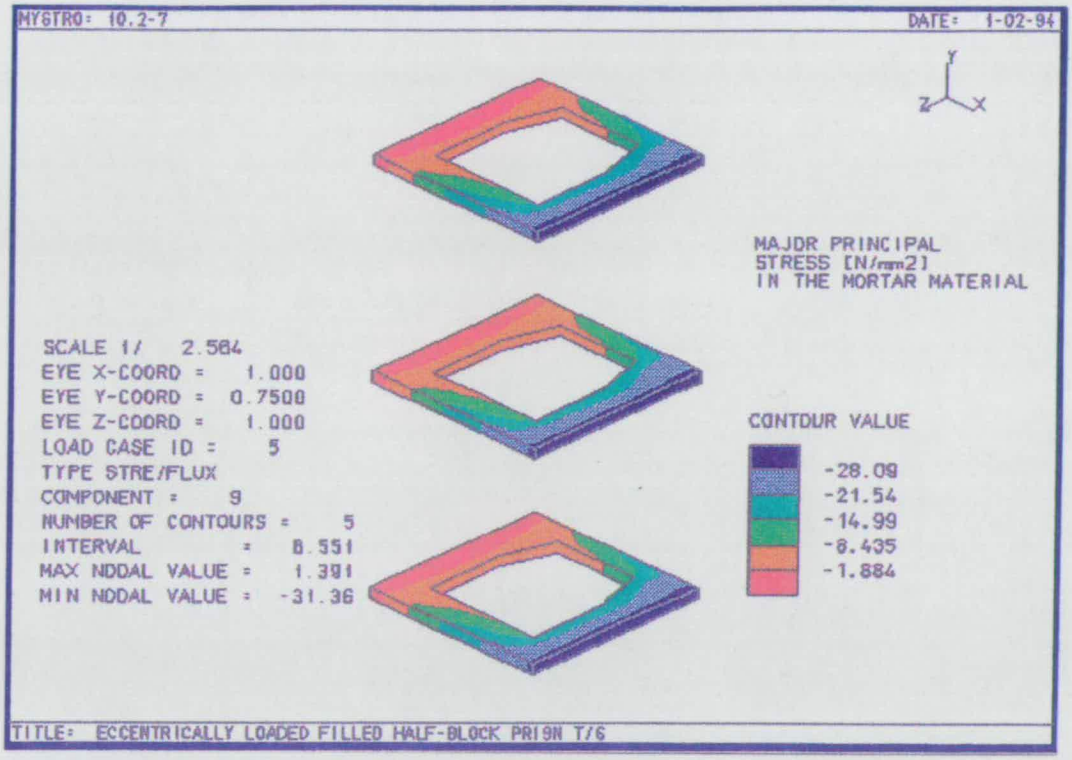


Fig. 4.124 Major principal stress in the mortar material of filled half-block compressed under eccentric load for e = t/6

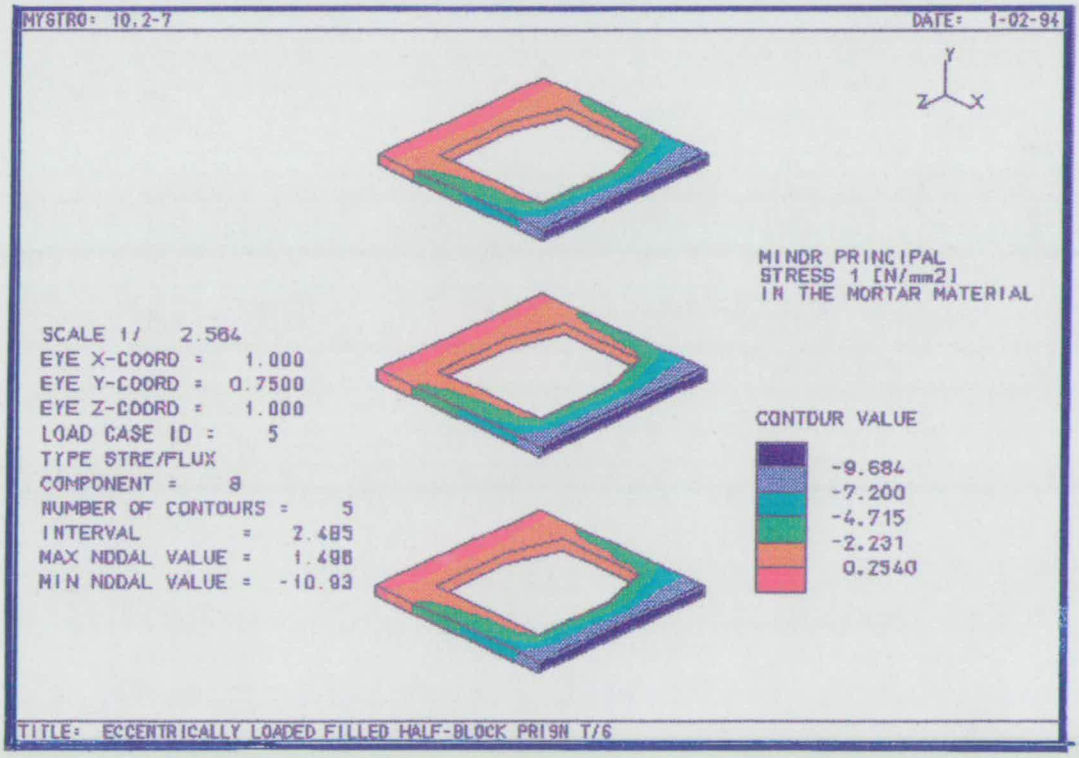


Fig. 4.125 Minor principal stress 1 in the mortar material of filled half-block prism compressed under eccentric load for e = t/6

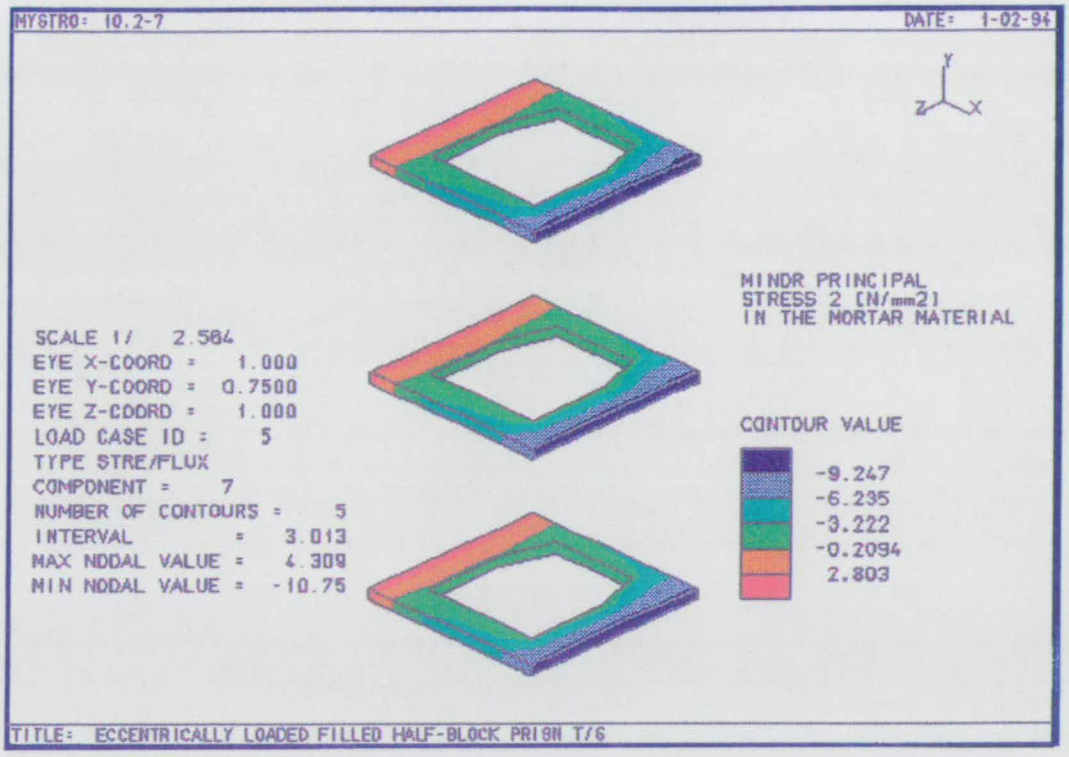


Fig. 4.126 Minor principal stress 2 in the mortar material of filled half-block prism compressed under eccentric load for e = t/6

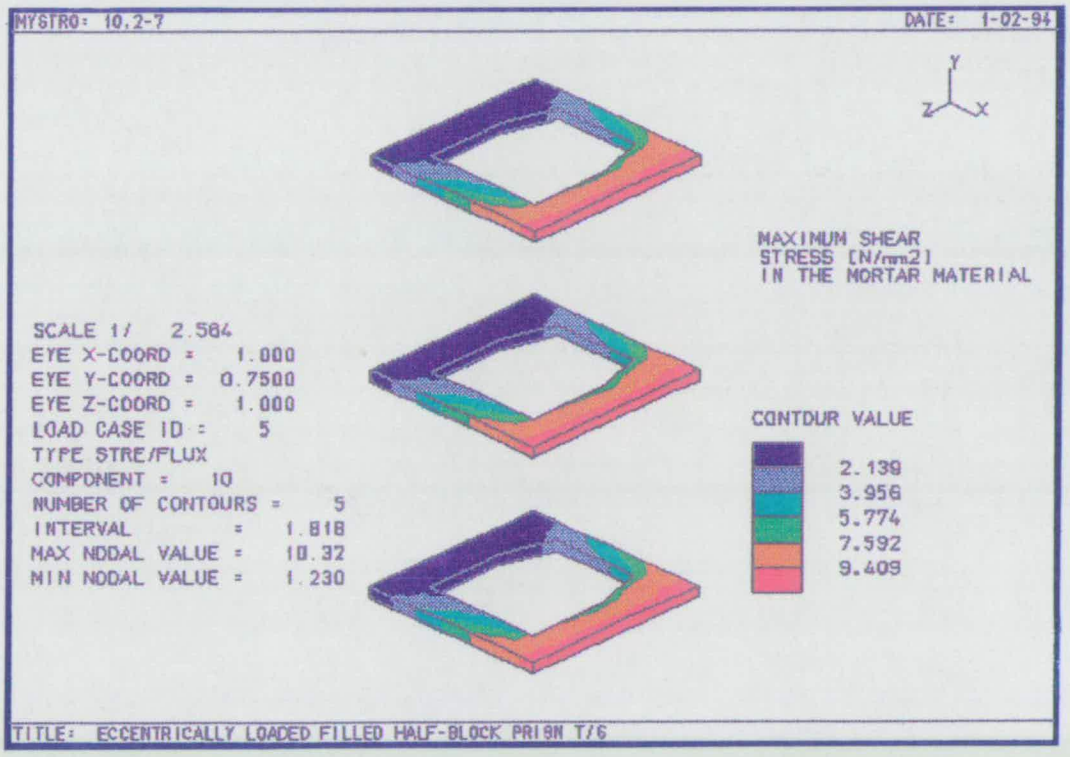


Fig. 4.127 Shear stress in the mortar material of filled half-block prism compressed under eccentric load for e = t/6

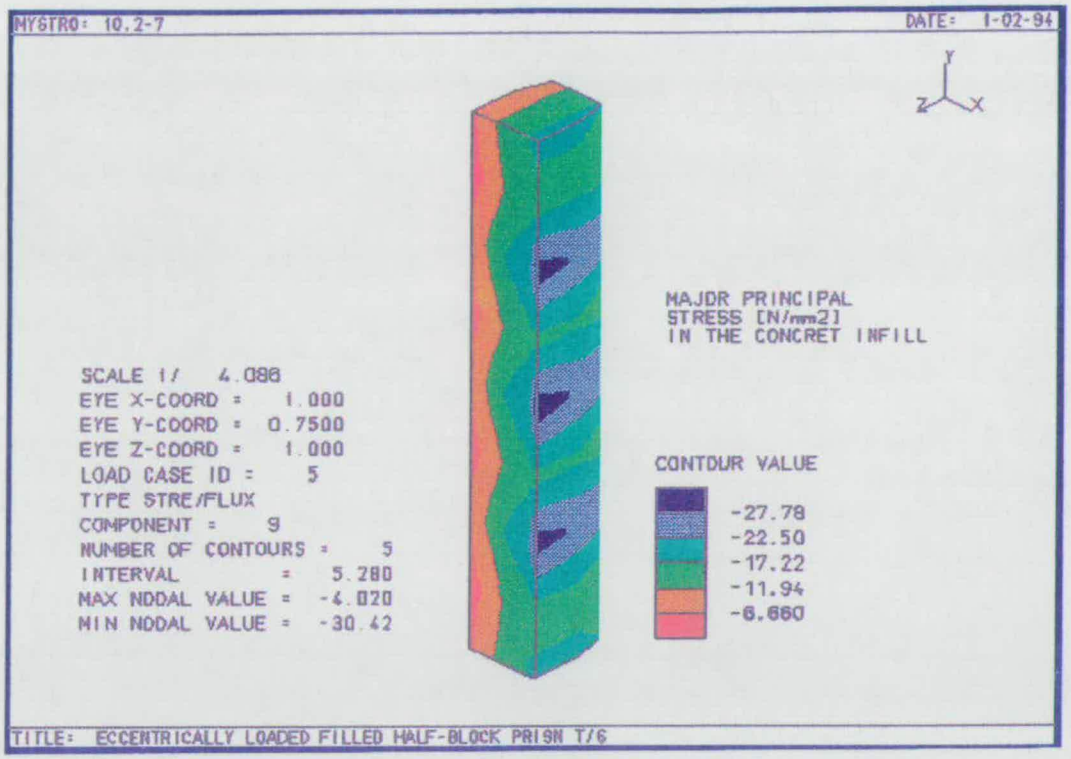


Fig. 4.128 Major principal stress in the concrete infill of filled half-block prism compressed under eccentric load for e = t/6

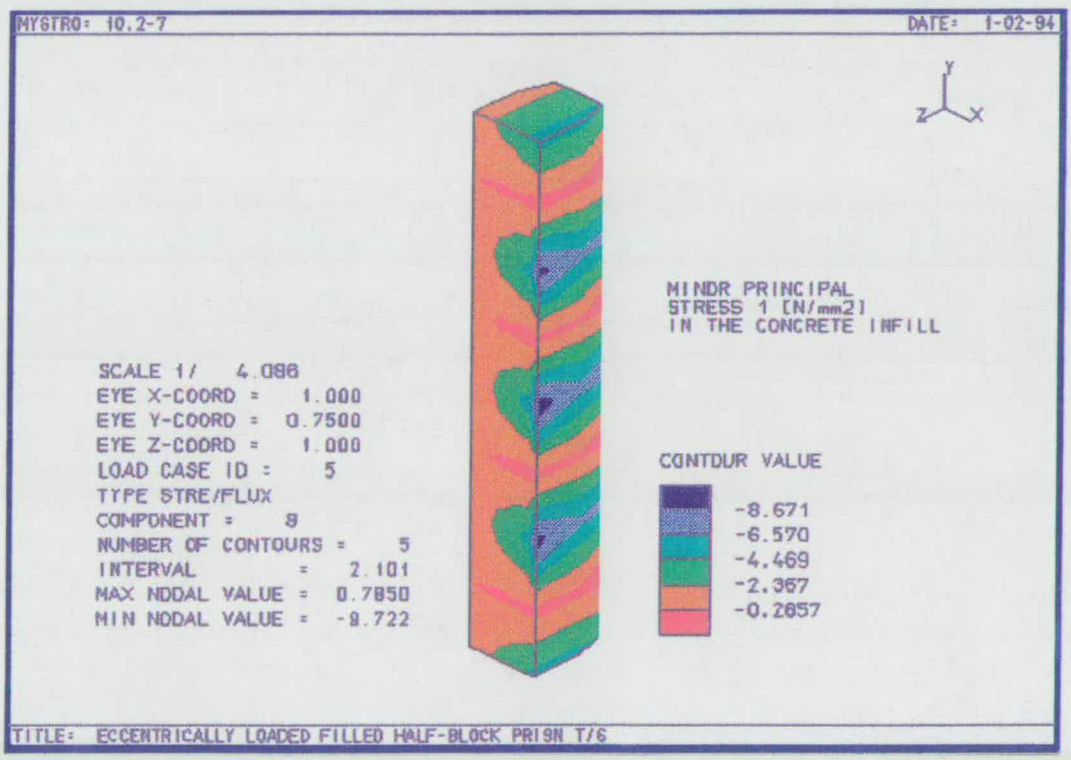


Fig. 4.129 Minor principal stress 1 in the concrete infill of filled half block prism compressed under eccentric load for e = t/6

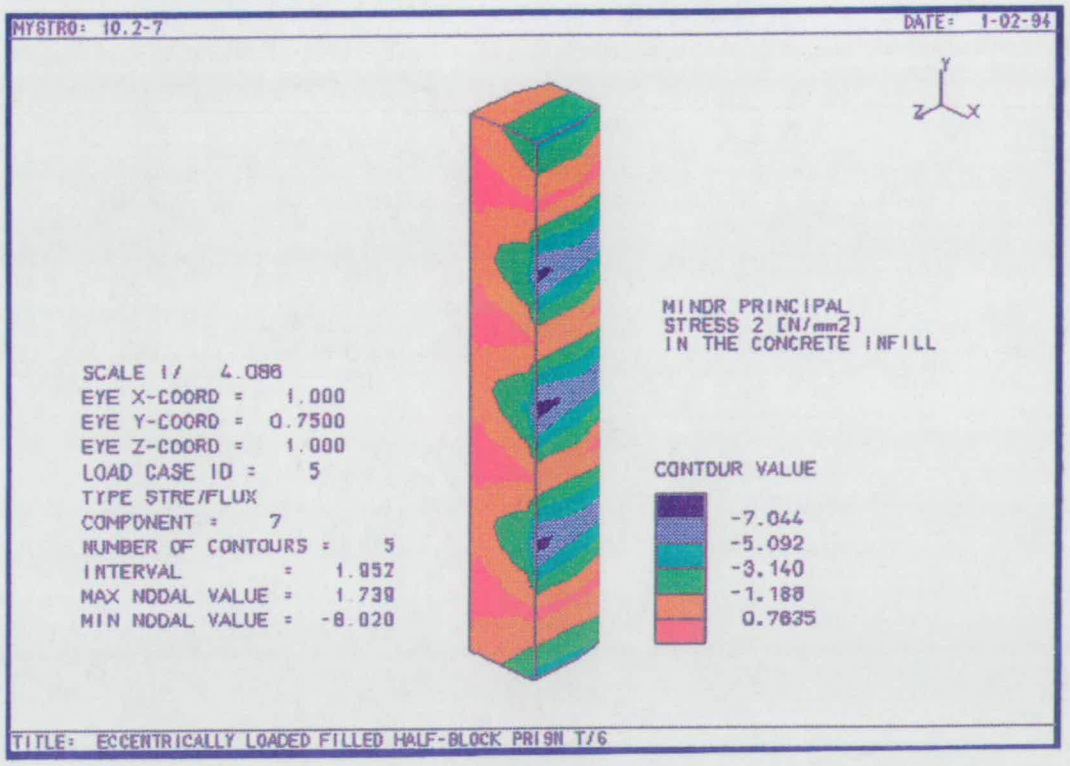


Fig. 4.130 Minor principal stress 2 in the concrete infill of filled half-block prism compressed under eccentric load for t/6

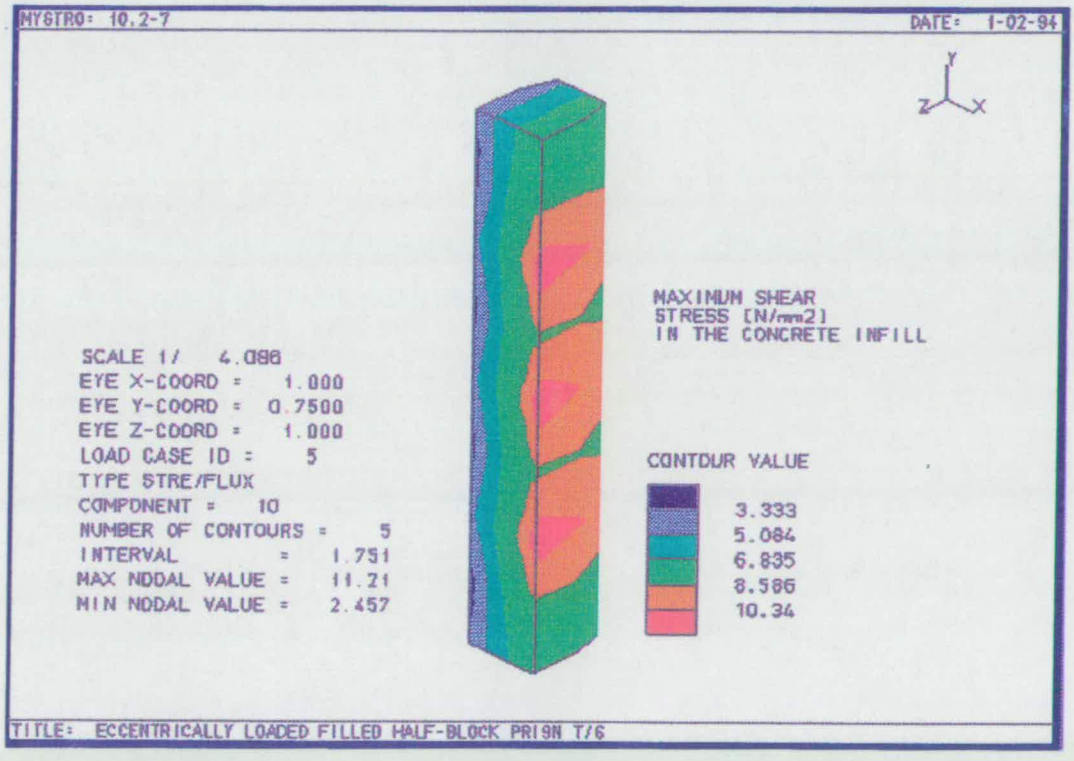


Fig. 4.131 Shear stress in the concrete infill of filled half-block prism compressed under eccentric load for e = t/6

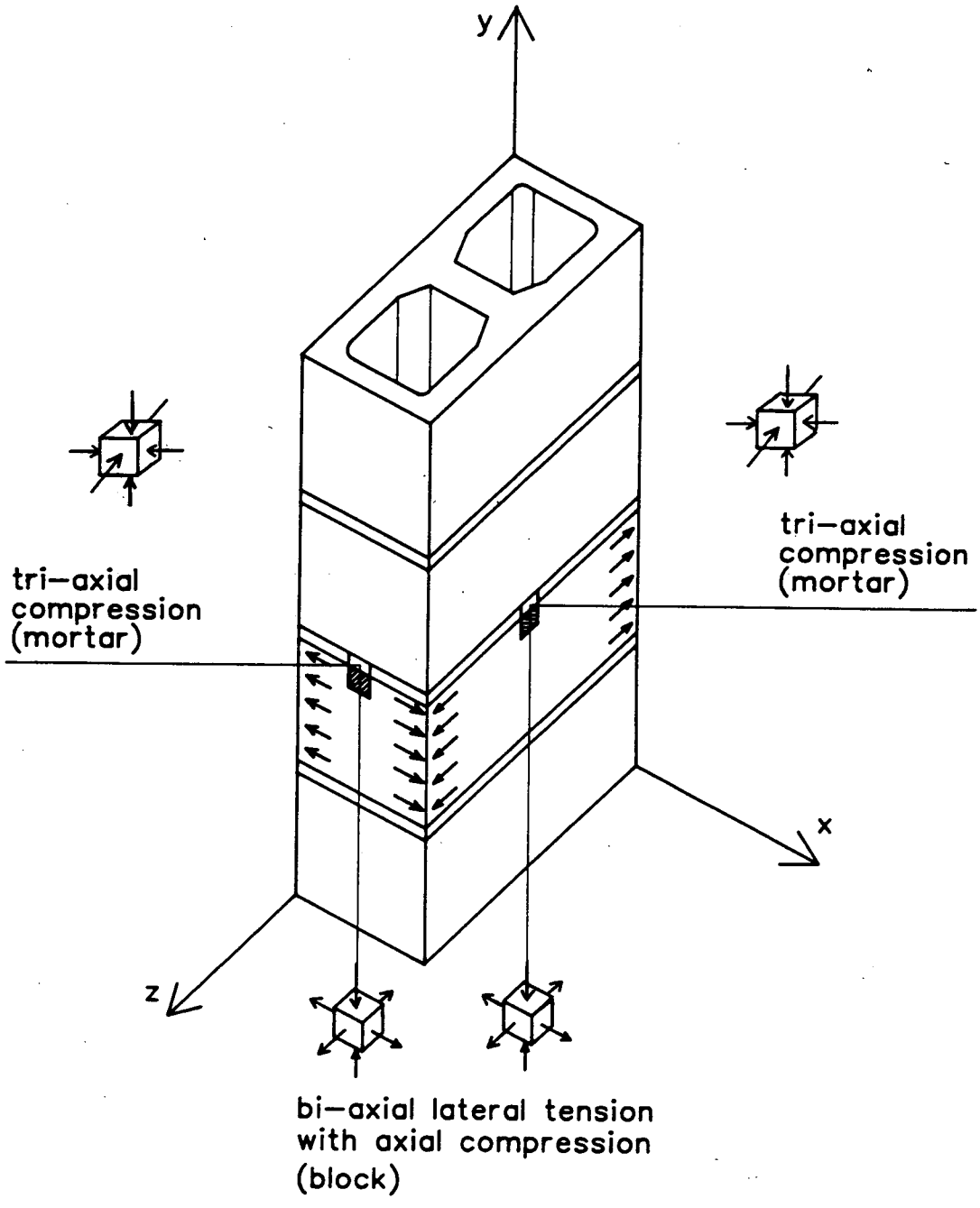


Fig. 4.132 State of stresses at the mortar and block interface near failure

CHAPTER 5

CONCENTRICALLY AND ECCENTRICALLY LOADED REINFORCED BLOCKWORK MASONRY COLUMNS

EXPERIMENTAL AND THEORETICAL PROGRAMME

5.1 INTRODUCTION

Reinforced blockwork masonry columns are good examples of structural elements that support compressive loads. They can be used as compression or stiffening elements when combined with other bearing elements such as masonry walls, or with non-bearing masonry walls where they serve as stiffening elements providing lateral support.

For the purpose of this study it was decided to use one type of concrete infill. All the columns were built with a 1:¼:3 (cement: sand : aggregate) concrete mix to produce a high strength mortar and a medium strength of concrete infill.

No lateral ties were placed at the mortar joints. Previous studies[22] have found that placing lateral ties at the mortar joints creates a high

concentration of tensile stresses around the ties causing a reduction in the column ultimate strength.

The only type of lateral tie used in this study was hot rolled deformed high yield 8 mm ϕ steel bars, supplied by the fabricator and shaped in dimensions according to BS 4466: 1981[29]. This diameter was selected on the observations and recommendations of Khalaf[26].

This chapter is divided into three major sections. The first deals with the experimental investigations which includes test preparation, construction details and testing methods concerned with the determination of the strength of and a study of the behaviour of concentrically and eccentrically loaded blockwork masonry columns. The second section presents a theoretical investigation using a three and two-dimensional non-linear finite element analysis method. The third section presents, axial load-moment interaction curves for full and half-block masonry columns with different percentages of vertical reinforcement based on the same methods as those used for reinforced concrete.

5.2 EXPERIMENTAL STUDY

5.2.1 Programme Variables

The major variables investigated in this study were the percentage of vertical reinforcement, and the eccentricity of the applied load. The columns were divided into main groups according to their cross-sectional areas viz., full-block (390 x 190 mm) and half-block (190 x 190 mm). For each full block

and half block column two percentages of longitudinal reinforcement, 0.43%, 1.70% and 0.56%, 3.40% respectively, based on the column's gross cross-sectional area were used.

For the full-block columns, longitudinal steel percentages of 0.43% and 1.70% were achieved by using four 10 mm ϕ and four 20 mm ϕ bars respectively. For the half-block columns, longitudinal steel percentages of 0.56% and 3.40% was obtained using four 8 mm ϕ and four 20 mm ϕ bars respectively.

Twelve full and twelve half-block columns were tested in this study to establish axial load-moment interaction diagrams for different eccentricities and different percentages of longitudinal reinforcement.

The twelve full-block columns consisted of three groups, each of four columns. The first group comprises columns reinforced with 20 mm ϕ bars, the second group contained columns reinforced with 10 mm ϕ bars, and the third group were columns with no steel reinforcement. The half-block columns had the same group divisions except that the second group was reinforced with 8 mm bars instead of 10 mm ϕ bars.

Four types of loading were applied. Axial and small eccentric loads of t/6 were used to provide data for the construction of interaction diagrams in the region of $e < e_b$. Two other load cases were applied with eccentricities > t/6 to achieve the states of a balanced condition and a tension failure.

5.2.2 Geometry of Columns

All the columns tested in this investigation were eight-courses high with a height to smallest plan dimension ratio of 8.36. The cross sections for which the study is based are given in Figs 5.1 and 5.2. Pinned ended columns were chosen throughout, as this kind of support condition provides a simple method of representing the problem mathematically.

Columns to be tested axially or under an eccentricity of t/6 were provided with two reinforced concrete caps, one at each end, to prevent local failure. The cap dimensions were equivalent to a single full-block and single half-block for the full and half-block columns respectively. The remaining columns, tested under large eccentricities exceeding t/6, were provided with two corbels. Each corbel had a width of one block and a height of a two-block prism with a 10 mm joint thickness. These dimensions were chosen to maintain an equal height for all the specimens.

5.2.3 Test Procedure and Equipment

Axially and t/6 eccentrically loaded full-block columns were tested in a steel rig. The load was applied by two jacks with a total capacity of 2MN ,then transferred by a steel bearing plate having a thickness of 150 mm. The other columns, namely the twelve half-block and six full-block columns were tested in an Avery machine with a maximum capacity of 1MN.

Measurements of forces, strains and deflections were recorded throughout the loading stages. A data logger was used to record strains and displacements continuously up to failure. When failure was imminent, the transducers were removed to eliminate the risk of damaging the instruments. Figures 5.3 and 5.4 show the column instrumentation.

Prior to testing, all the specimens were capped with a thin layer, 1 - 2 mm of dental plaster prepared by mixing with water in plastic bags, as explained in chapters 3 and 4. The reason for using a thin dental plaster layer is to provide a smooth, level surface between the specimen and the steel plates. The load was applied at a rate in accordance with BS 6073: Part 1 : 1981[36]. The loading pattern was applied in accordance with BS 1881: Part 121: 1981[38] to determine the static modulus of elasticity.

Auxiliary reinforcement was provided by two tied 100 x 100 mm steel angles in the case of the columns with caps, and by 75 x 38 mm steel channels in the case of columns provided with corbels. These were attached to the columns caps and corbels to provide additional confinement.

5.2.4 Building Test Specimens

Wooden moulds with inner dimensions equal to these of the full and half-blocks were prepared. The longitudinal bars were cut 40 mm shorter than the column height. The four vertical bars were welded with four lateral splices at one end to maintain a regular spacing between the bars and to keep the longitudinal bars perpendicular. The bars were then placed inside

the mould over 20 mm spacers to keep a constant provision of concrete cover.

After checking the verticality of the longitudinal bars, the mould was filled with concrete having mix proportions similar to that for the concrete infill. The concrete was then compacted and trowelled. After three days, construction of the column continued by building six-courses. The lower blocks were provided with 80 x 80 mm holes, cut in two opposite sides of the block in the case of full-block columns and one side of the half-block columns. These holes were cut with a diamond saw. Any blocks with flaws, such as large chips or cracks, were rejected.

The reinforced full-block columns were provided with 20 mm wide by 20 mm deep grooves. These were cut with a diamond saw to accommodate the lateral ties which were placed in every course during the column construction.

Columns prepared for axial loading were fitted with steel brackets 25 mm wide by 6 mm thick, positioned on the second and fifth mortar joints to mount two electrical displacement transducers (LVDT's) on the front and back sides of the columns.

Six courses of block were built with 10 mm mortar joints and kept under polythene sheeting for four days to allow the mortar joints to gain in strength. The top ends of the longitudinal bars were then welded with splices to form

lateral ties similar to those on the opposite side of the longitudinal bars. A wooden mould was fixed on top of the upper block. The column was then filled with a high slump (150 mm) mix batched by volume with 1:3:2 (cement:sand:aggregate) proportions. The concrete was cast in two layers. Each layer was compacted using a 25 mm poker vibrator. The top surface of the concrete was then trowelled level and kept under polythene sheeting for four days. Steel moulded cubes and cylinders were taken from each mortar and concrete mix, cured in a water tank at laboratory temperature, then tested after 28 days in compression to determine the compressive strength of the mortar and the concrete.

The same method was adopted to build the columns with no steel reinforcement. The longitudinal reinforcement was replaced by four dowels having a length of 360 mm and a diameter of 20 mm, to develop a sufficient bond between the caps and the rest of the column.

For those columns built with corbels, wooden moulds were prepared with inner dimensions similar to those shown in Figs 5.1 and 5.2 for full and half-block columns respectively. The height of the corbel section was chosen to be equal to a two-course high prism. This dimension gives a total height equivalent to the axially and t/6 loaded columns, when four-courses of blocks are built in between. The section was designed to resist the worst loading case. A high strength concrete mix, with 1:2:2 (cement:sand:aggregate) was chosen to fill the corbels.

In the lower corbels, the two main reinforcement bars were welded to two longitudinal bars in the column to form a right-angled shape for the steel reinforcement. The welding was carried out by a professional welder using the arc welding method. Three samples of welded joints similar to those used for the corbels were tested in tension to evaluate their strength. All three samples failed in areas away from the joints. No evidence of cracking or weakening of the steel were observed close to the welded joints.

Two equal lateral splices were welded between the two angles to maintain a regular spacing between the bars and ensure that the longitudinal bars were perpendicular. The two compression steel bars and the remainder of the lower corbel reinforcement were assembled using tack welding. The cage was then placed inside the mould using 20 mm spacers to maintain constant concrete cover. After checking that the longitudinal bars were vertical, the mould was filled with concrete, then compacted and trowelled. After three days, construction of the column was resumed by building four-courses with 10 mm mortar joints. The column was kept under polythene sheeting for four days. The lower blocks were provided with 80 x 80 mm holes similar to those used for the axially and t/6 eccentrically loaded columns to remove mortar or welding filler droppings. The upper corbel main reinforcement was then welded and the remaining reinforcement assembled by tack welding. A wooden mould with inner dimensions equal to those used for the lower corbel was placed on top. The cleaning holes on the lower blocks were closed using plywood pieces after removing any residue from inside. The blocks were filled with a high slump (150 mm) concrete mix, batched by

volume with 1:3:2 (cement:sand:aggregate) proportions. The concrete was cast in two layers, each compacted using a 25 mm poker vibrator. The upper corbel was then filled, compacted and trowelled level. The column was kept under polythene sheeting for four days. Steel moulded cubes and cylinders were taken from each mortar and concrete mix, cured in a water tank at laboratory temperature, then tested in compression after 28 days to determine the compressive strength of the mortar and the concrete.

The same method was adopted to build columns with no steel reinforcement. The longitudinal reinforcement was replaced by five dowels (three in the tension side) having length of 560 mm, and diameter, 20 mm. Additional pieces of steel of the same diameter and of length, 40 mm, were welded perpendicular to the dowels inside the column to form an additional bond surface. Figures 5.1 and 5.2 show typical cross-sections for the concentrically and eccentrically loaded full and half-block masonry columns.

5.2.5 Measurement of Strains and Deflections

The strains on the vertical bars and the lateral ties were measured by 5 mm post-yield electrical strain gauges utilising a special plastic carrier base capable of withstanding extremely large elongations without cracking and reading large strains very accurately. The gauges were fixed at the mid-height level of each vertical bar and at the lateral tie located at the middle of the column. The gauge positions were marked and cleaned. The gauges were then bonded with CN (Cyanoacrylate) adhesive, wired, protected by a water proof coating and finally covered by rubber tape. For the eccentrically

loaded columns, five 90 mm electrical strain gauges were mounted at the mid-height of the column at intermediate positions on the front and back faces. Three gauges were also mounted at the same level on one of the column side faces equal distant from the compression and tension faces. For the axially loaded columns, four 110 mm electrical strain gauges were mounted on two opposite sides of the column at mid-height. The positions of the strain gauges were first marked then filled with concrete adhesive to fill the coarse-grained surface. After 24 hours, the surface was cleaned and the gauges then bonded and wired.

The strains on the compression and tension faces of the column were measured using LVDT's spanning four courses high and centred at the column mid-height. Special pin supports were manufactured and fixed using strong adhesive. These pins provide rotational freedom for the LVDT's in the direction of the column bending.

The load-strain curves for the unreinforced full and half-block columns with eccentricities > t/6 were obtained from measurements using demec gauges instead of electrical strain gauges, since early debonding of the mortar joints creates strains above the limits of the electrical gauges. Demec points were also used on the tension face of the reinforced columns where e > t/6 to cope with the larger strain measurements.

For the eccentrically loaded columns, lateral deflections were measured at every second course on the column tension side using LVDT's fixed on an independent support.

5.3 THEORETICAL ANALYSIS

5.3.1 Introduction

The complicated behaviour of reinforced blockwork masonry columns, consisting of four different materials, several degrees of freedom and complex geometry, make it extremely difficult to perform an analysis by using a classical approach. As a result, approximate numerical methods are used to solve problems of this type. Two and three dimensional non-linear finite element analyses were conducted using LUSAS[46], a general purpose FEA package. The processing was carried out using MYSTRO the graphical interactive system within the LUSAS package as described in chapter 4.

5.3.2 Three Dimensional Non-linear Finite Element Model

A three dimensional finite element model was developed using the solid element used for prisms in chapter 4. Figures 5.5 and 5.6 show the mesh used to simulate axially loaded and t/6 eccentrically loaded full and half-block columns respectively. Only 1/2 of the column was considered in the analysis to keep the mesh size to a minimum. Other assumptions adopted in generating the mesh are similar to those used to generate the three dimensional models of the prisms considered in chapter 4. The material

properties used in the non-linear FEA material data section are similar to those used for prisms and given in Table 4.1. The material properties used for the steel reinforcement are given in Table 5.1.

5.3.3 Two Dimensional Non-linear Finite Element Model

A two-dimensional finite element model was developed using a biaxial non-linear concrete model. This model was used with an eight noded plain stress element QPM8, which can consider a non-linear stress-strain relationship in compression as well as in tension with the ability to consider cracks and transverse shear through the cracked sections. Figures 5.7 and 5.8 show the mesh used to simulate the full and half-block columns with t/6 eccentricities.

Columns with large eccentricities were modelled using four and three noded plain stress elements QPM4 and TPM3. Figures 5.9 and 5.10 show the mesh used to simulate the full and half-block columns with large eccentricities. The material properties used in the non-linear finite element section are given in Tables 5.1 and 5.2.

5.4 Applying N/M Interaction Curves to Blockwork Columns Using Different Stress Blocks

A theoretical study was conducted enabling one to compare N/M interaction curves adopted by a similar method to those used for reinforced concrete with the N/M blockwork interaction curves obtained experimentally. The comparison was based on the ultimate strength capacity of the column cross sections under different load cases.

The following assumptions are made when analysing the column cross-sections to determine the ultimate moment of resistance:

i) Plane sections remain plane after bending.

ii) The tensile strength of masonry is ignored.

iii) No slip occurs between steel, concrete infill and blockwork.

iv) Masonry elements form a homogeneous material.

v) The column cross-section is rectangular with a symmetrical arrangement of steel reinforcement.

The compressive strength of masonry is obtained by testing three prisms after 28 days using mortar and concrete mixes similar to those used in the columns.

Figure 5.11 shows the four cases of loading which may arise when a normal force is applied to a short blockwork column. The locations of the applied load are similar to those for the columns tested in the experimental part of this study. These cases are as follows:

1) The case of pure compression where $e = 0$ and $M = 0$.

2) The case of a compression failure where $e = t/6$ and $N_u > N_b$

3) Balanced failure

4) The case of a tension failure where $e > e_b$ and $N_u < N_b$

The ultimate axial load capacity of a column section in pure compression, assuming a symmetrical arrangement of vertical reinforcement, is given by

$$N_u = \frac{f'_m A_m + f_y A_s}{1000} \quad \text{.....(5.1)}$$

where

N_u = The ultimate axial load capacity of the column, kN

f'_m = The compressive strength of masonry, N/mm^2

A_m = Gross area of the column cross section, mm^2

f_y = Yield stress of longitudinal reinforcement, N/mm^2

A_s = Area of reinforcement steel, mm^2

If the whole of the masonry section is in compression and the load is applied at a small eccentricity,(< t/6), the above equation becomes:

$$N_u = \frac{f'_m A_m + A_{s1} f_y + A_{s2} f_{s2}}{1000} \quad \text{.....(5.2)}$$

If $A_{s1} = A_{s2} = \frac{A_s}{2}$

$$N_u = \frac{f'_m A_m + \frac{A_s}{2}(f_y + f_{s2})}{1000} \quad \text{.....(5.3)}$$

where

A_{s1} = Area of reinforcement in the more highly compressed face of the column section, mm^2

A_{s2} = Area of reinforcement near the less compressed face of the column section, mm^2

f_{s2} = Stress in the reinforcement A_{s2}, N/mm^2. This can be calculated from the following equation

$$f_{s2} = \varepsilon_{s2} \times E_s \quad \text{.....(5.4)}$$

where

E_s = Modulus of elasticity for steel obtained from Table 3.5, kN/mm^2

ε_{s2} = Compressive strain in column reinforcement A_{s2}

To apply the ultimate limit state theory to flexural members a non-linear stress block is used. The variation of stresses along the section is reflected by the stress strain relationship of the material. The stress-strain curve is assumed to be represented by a parabolic curve characterised by the following three factors: k_1, which is used to express the average compressive stress for the rectangular stress block, k_2 which is involved in the distance of the centroid of the parabolic stress block from the compression face and k_3 which is used to express the compressive strength in the outermost compression fibre of the section. Most of the current codes for reinforced concrete and masonry have adopted an equivalent rectangular stress block of area equal to the area of the parabolic stress block. The rectangular block is based on the characteristic compressive stress at maximum strain. Figures 5.12 and 5.13 show typical BS 8110 stress-strain relationships for concrete and reinforcement respectively. Figure 5.14 shows the simplified design stress block method for ultimate limit state recommended by BS 8110.

The rectangular stress block could be determined by taking the reduced strain at maximum stress, as adopted by BS 5628 :Part 2 [10]. Figure 5.1 shows the two methods which simplify the active stress-strain parabolic area

of brickwork masonry [19] where the constant k_1 is dependent on the ratio $\varepsilon_u/\varepsilon_m$ and given as follows:

$$k_1 = (\varepsilon_u/\varepsilon_m) - \frac{(\varepsilon_u/\varepsilon_m)^2}{3} \qquad .....(5.5)$$

Table 5.3 gives the values of constants k_1, k_2 and k_3 for different values of $\varepsilon_u/\varepsilon_m$. The derivation of the equations to find the above three constants are given in Appendix B.

The ultimate moment capacity of the section, calculated by taking moments about the mid-section, is given by the following equation:

$$M_u = \frac{k_1 f'_m b x \frac{(t-k x)}{2} + A_{s1} f_{s1} \left(\frac{t}{2} - d_1\right) + A_{s2} f_{s2} \left(d + \frac{t}{2}\right)}{1000} \qquad .....(5.6)$$

If $A_{s1} = A_{s2} = \frac{A_s}{2}$ and $d_1 = d_2$

$$M_u = \frac{k_1 f'_m b x \frac{(t-k x)}{2} + \frac{A_s}{2} - \left(\frac{t}{2} - d_1\right)(f_{s1} + f_{s2})}{1000} \qquad .....(5.7)$$

where

M_u = The ultimate moment of resistance of the section, kN mm

k_1 = Masonry stress block factor

k = Neutral axis depth factor

f'_m = The compressive strength of masonry, N/mm^2

b = The width of the column section, mm

x = The neutral axis depth measured from the extreme compression fibre, mm

t = The depth of the column section, mm

A_s = Area of reinforcement steel, mm^2

A_{s1} = Area of reinforcement in the more highly compressed face of the column section, mm^2

A_{s2} = Area of reinforcement near the less compressed face of the column section, mm^2

d_1 = Depth to centroid of reinforcement A_{s1}, mm

d_2 = Depth to centroid of reinforcement A_{s2}, mm

f_{s1} = Stress in reinforcement A_{s1}, N/mm^2

f_{s2} = Stress in reinforcement A_{s2}, N/mm^2

If the whole of the concrete section is in compression the equation becomes:

$$M_u = A_{s1} f_{s1} \left(\frac{t}{2} - d_1\right) - A_{s2} f_{s2} \left(d - \frac{t}{2}\right) \quad \text{.....(5.8)}$$

If $A_{s1} = A_{s2} = \frac{A_s}{2}$ and $d_1 = d_2$

$$M_u = \frac{A_s}{2} \left[f_{s1}\left(\frac{t}{2} - d_1\right) - f_{s2}\left(d - \frac{t}{2}\right)\right] \quad \text{.....(5.9)}$$

Where f_{s2} is calculated from equation (5.4).

The column is considered to be at the ultimate limit state of collapse when the masonry strain at the extreme compression fibre reaches a specified value taken as 0.0035.

Figures 5.16 and 5.17 show the interaction diagrams for full and half-block blockwork masonry column cross-sections calculated by the same method as used for reinforced concrete columns, where the compressive strength for masonry, f'_m, is obtained from the average of testing three 4-course half and full-block prisms (reported in chapter 4) after 28 days. The mortar and concrete mix proportions used in constructing the prisms were similar to those used in the columns. Values of f_y, the yield strength of the reinforcement were obtained experimentally and are given in Table 3.5.

Table 5.1 The material properties for steel reinforcement used in developing the non-linear three and two-dimensional finite element models

Material	Model	Modulus of Elasticity (N/mm^2)	Poisson's Ratio (%)	Initial Uniaxial Yield Stress (N/mm^2)	No. of Straight Line approximations to the hardening curve	The slope of the (i)th section of the uniaxial yield stress against effective plastic strain curve	The limit on effective plastic strain up to which the (i)th section of the hardening curve is valid
Steel	Explicit (forward Euler) von Mises yield surface model	196000 (T20) 204000 (T10) 204000 (T8)	0.30	534(T20) 520(T10) 527(T8)	1	S_1=0.0001	0.01

Table 5.2 The material properties used in developing the two-dimensional finite element model

Material	Model	Secant Modulus of Elasticity (N/mm^2)	Poisson's Ratio (%)	Compressive Strength (N/mm^2)	Shear Retention Factor	Tensile Strength (N/mm^2)	Strain at Peak Compressive Strength
Concrete Block	Biaxial non-linear concrete model	26340*	0.19	24.69	1.0	1.64	0.0015
Concrete Infill	Biaxial non-linear concrete model	14100*	0.24	22.75	1.0	1.52	0.0022
Concrete (Corbels)	Biaxial non-linear concrete model	20000	0.20	30.00	1.0	2.20	0.0027
Mortar	Biaxial non-linear concrete model	4054	0.25	21.76	1.0	1.45	0.0098

*Secant modulus of elasticity at 2/3 f_{max} where f_{max} is the peak value of the idealised stress-strain curve given by equations 3.1 to 3.3.

Table 5.3 Values of the parabolic stress block factors for different $\frac{\varepsilon_u}{\varepsilon_m}$

$\frac{\varepsilon_u}{\varepsilon_m}$	1.0	1.50	1.75
k_1	0.667	0.750	0.729
k_2	0.375	0.417	0.450
k_3	1.00	0.750	0.438

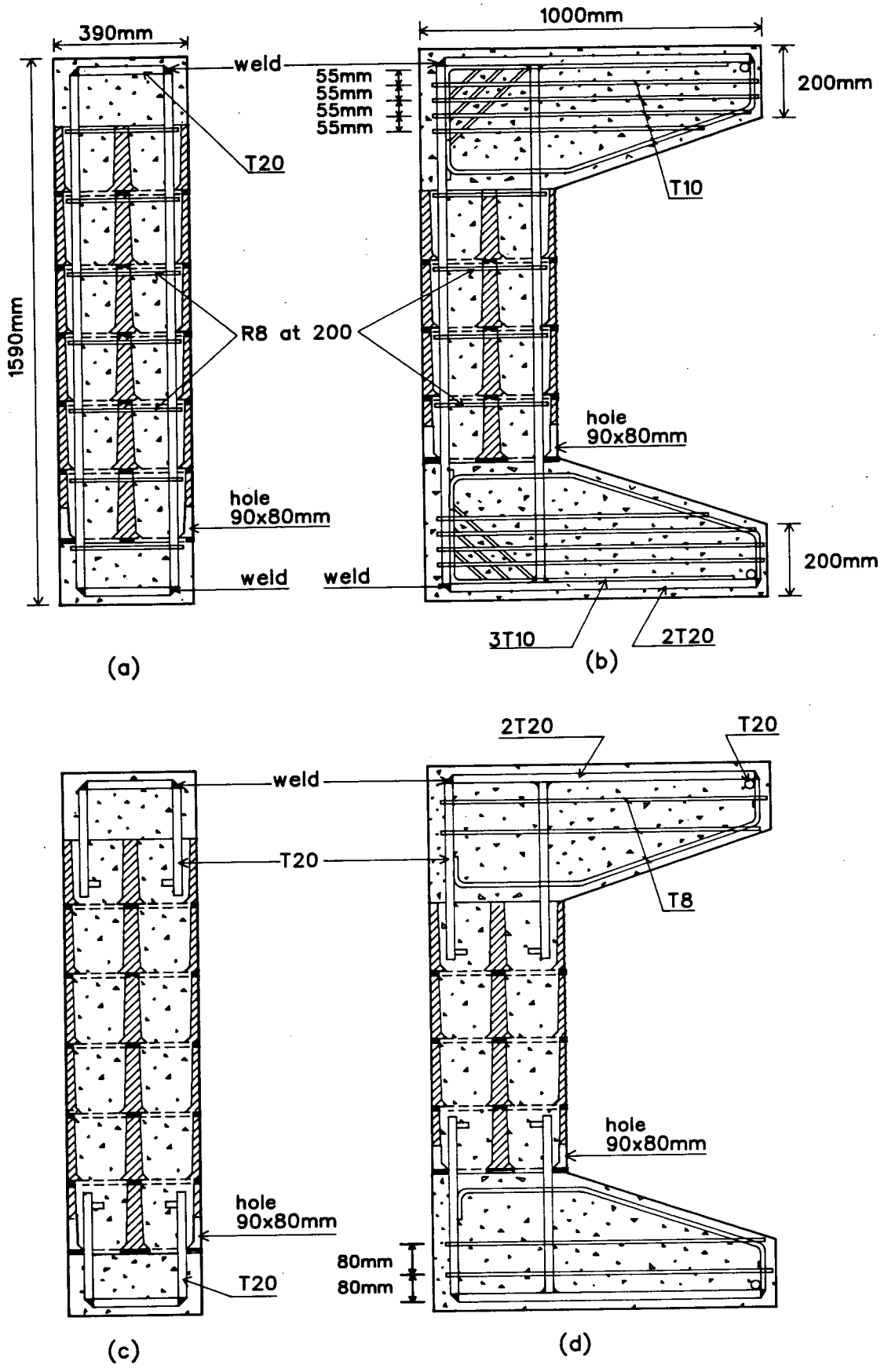


Fig. 5.1 Typical cross-sections of full-block masonry columns

(a) reinforced, concentrically and eccentrically loaded ($e < t/6$)
(b) reinforced, loaded with large eccentricity ($e > t/6$)
(c) unreinforced, concentrically and eccentrically loaded ($e < t/6$)
(d) unreinforced, loaded with large eccentricity ($e > t/6$)

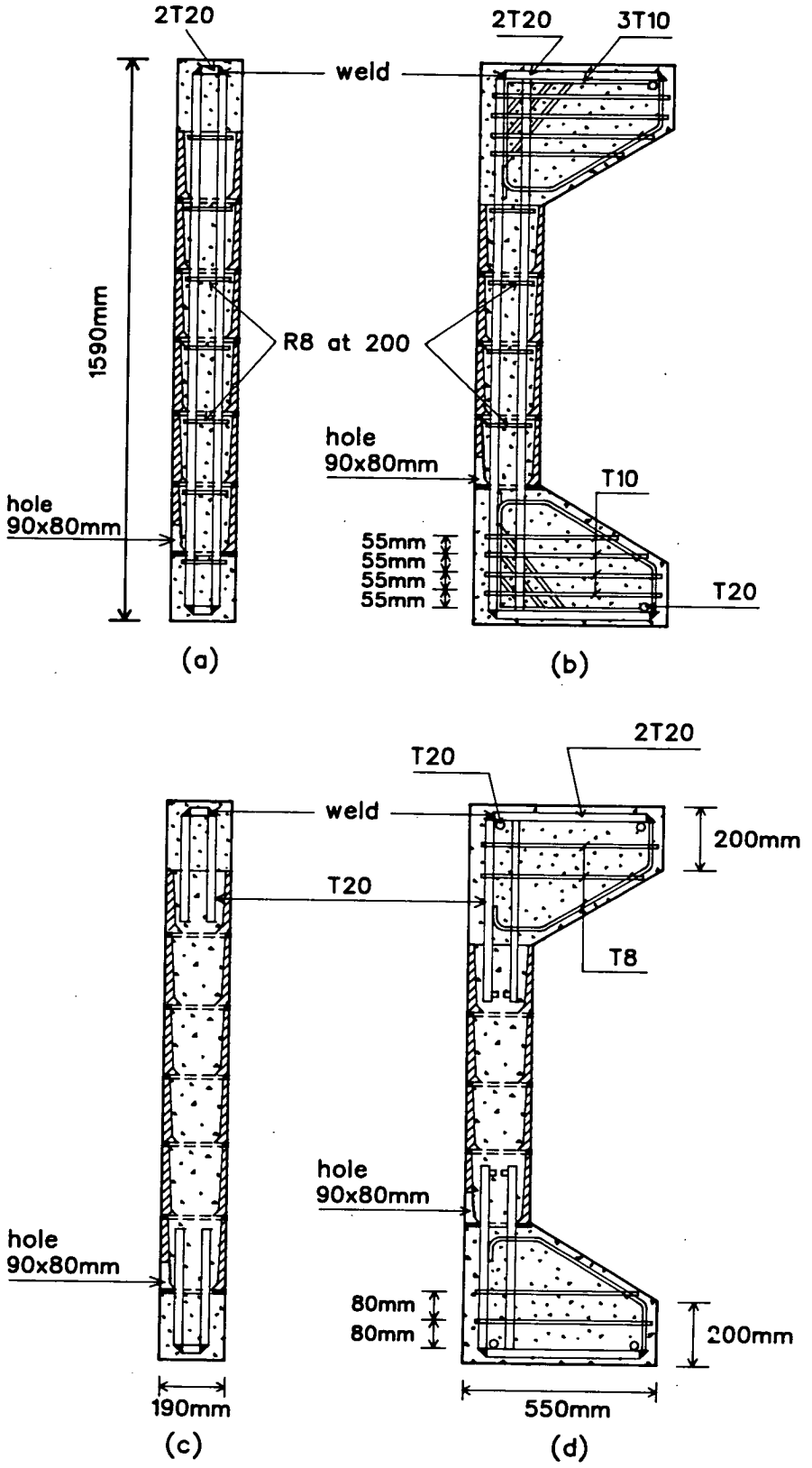


Fig. 5.2 Typical cross-sections of half-block masonry columns

(a) reinforced, concentrically and eccentrically loaded ($e < t/6$)
(b) reinforced, loaded with large eccentricity ($e > t/6$)
(c) unreinforced, concentrically and eccentrically loaded ($e < t/6$)
(d) unreinforced, loaded with large eccentricity ($e > t/6$)

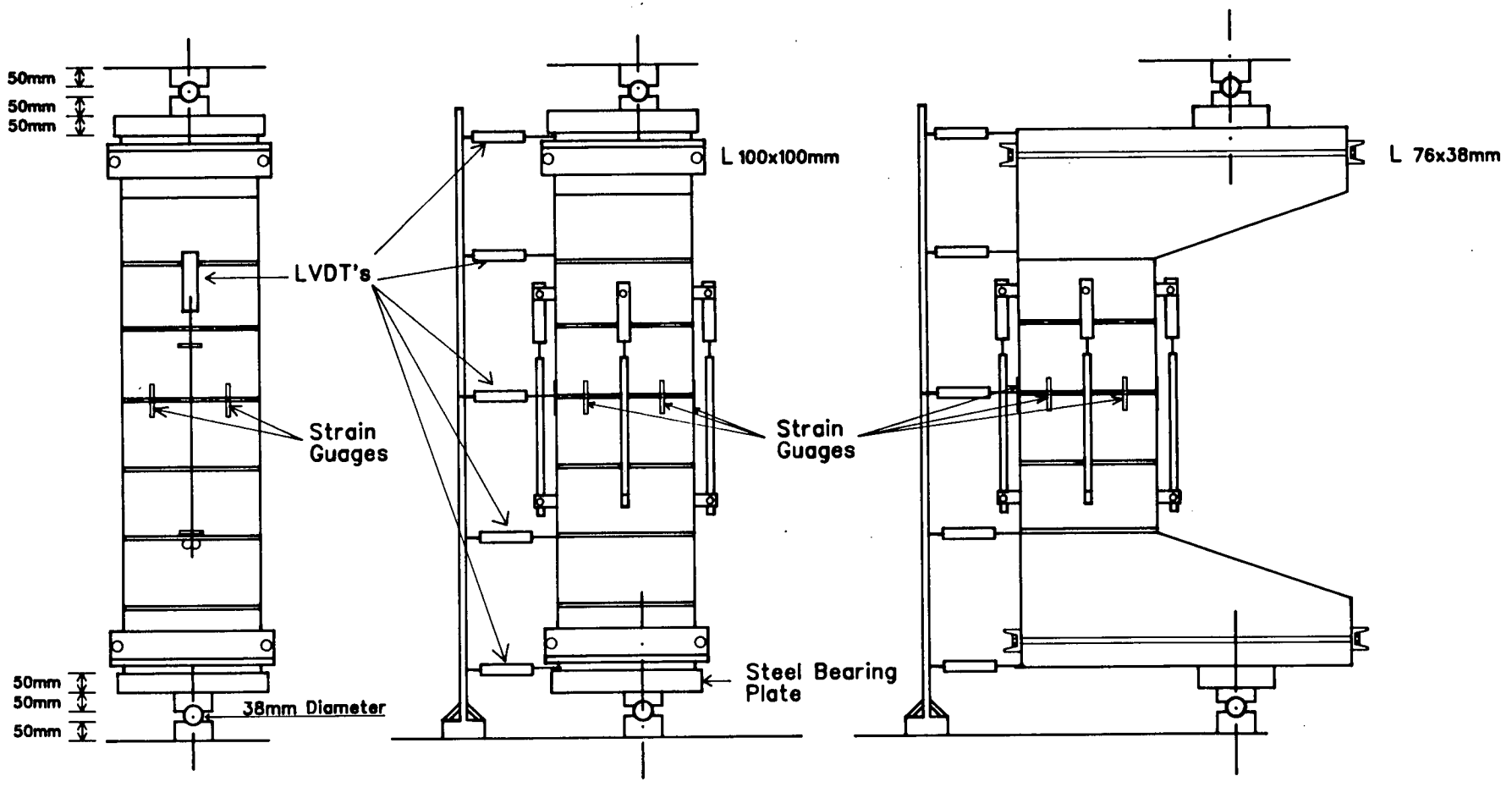


Fig. 5.3 Test setup for the concentrically and eccentrically loaded full-block masonry columns

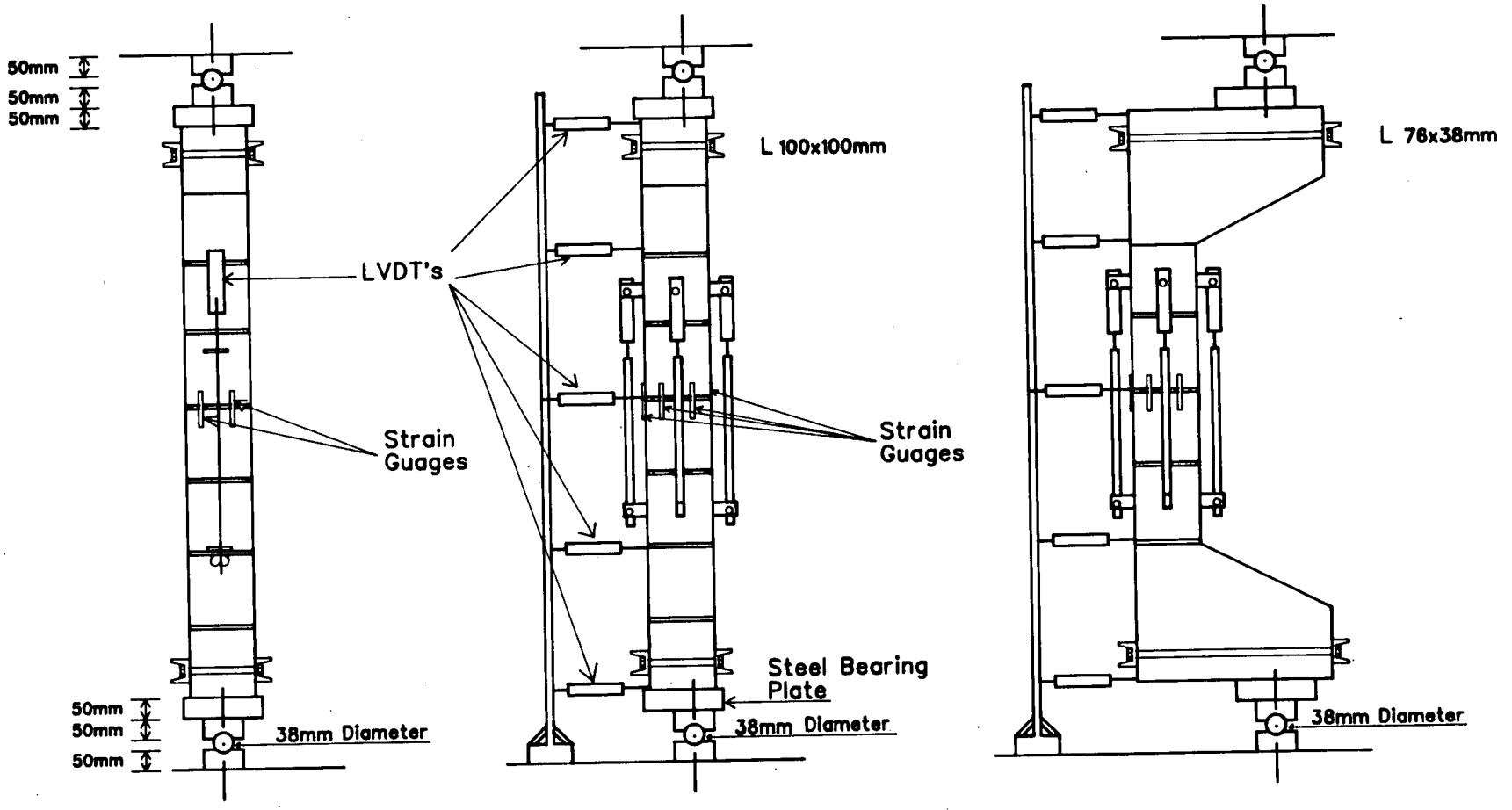


Fig. 5.4 Test setup for the concentrically and eccentrically loaded half-block masonry columns

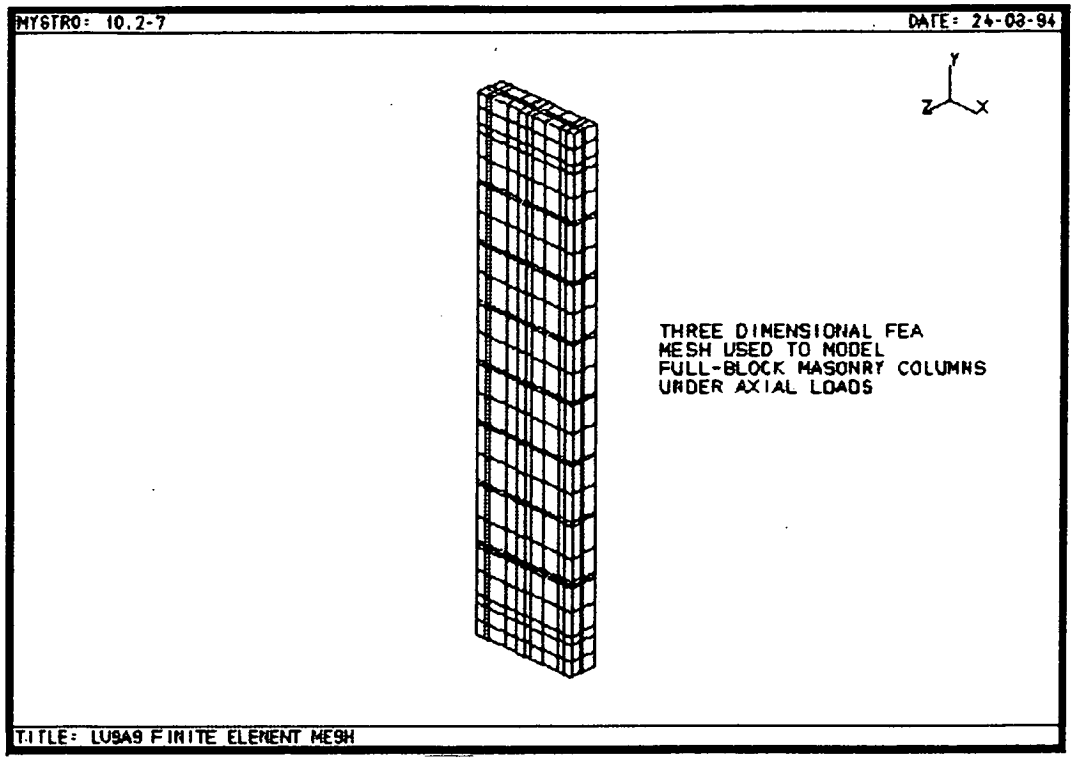


Fig. 5.5 Typical FEA mesh used to model full-block masonry columns under axial loads.

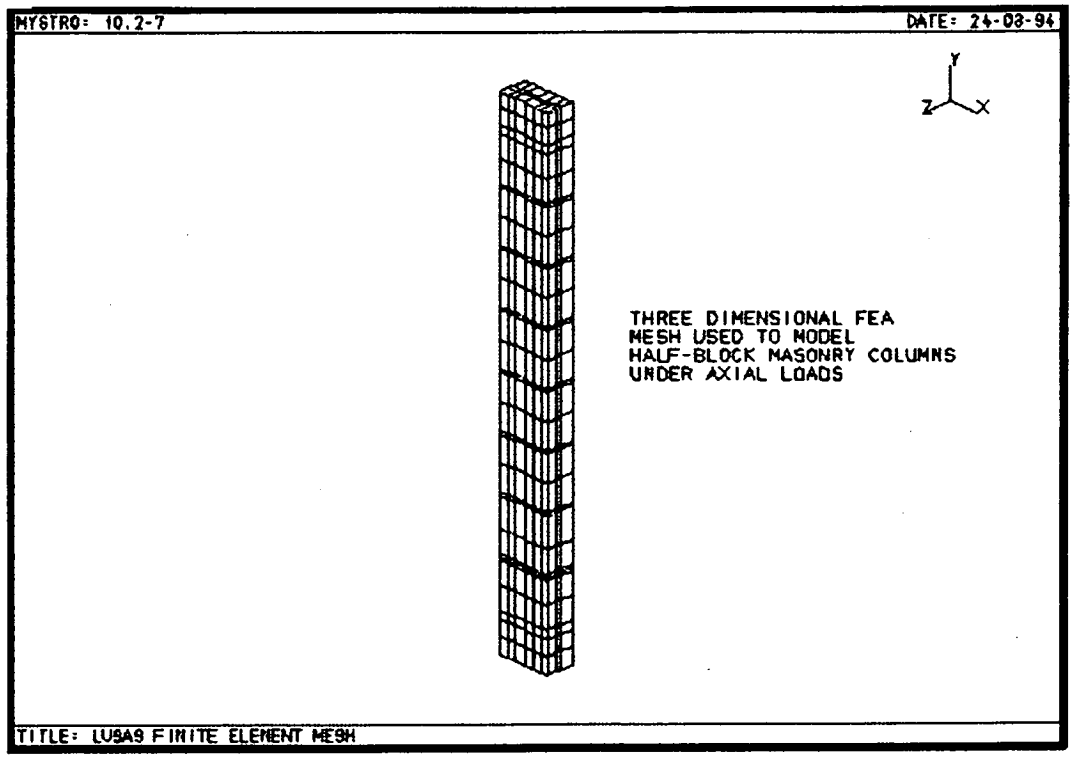


Fig. 5.6 Typical FEA mesh used to model half-block masonry columns under axial loads.

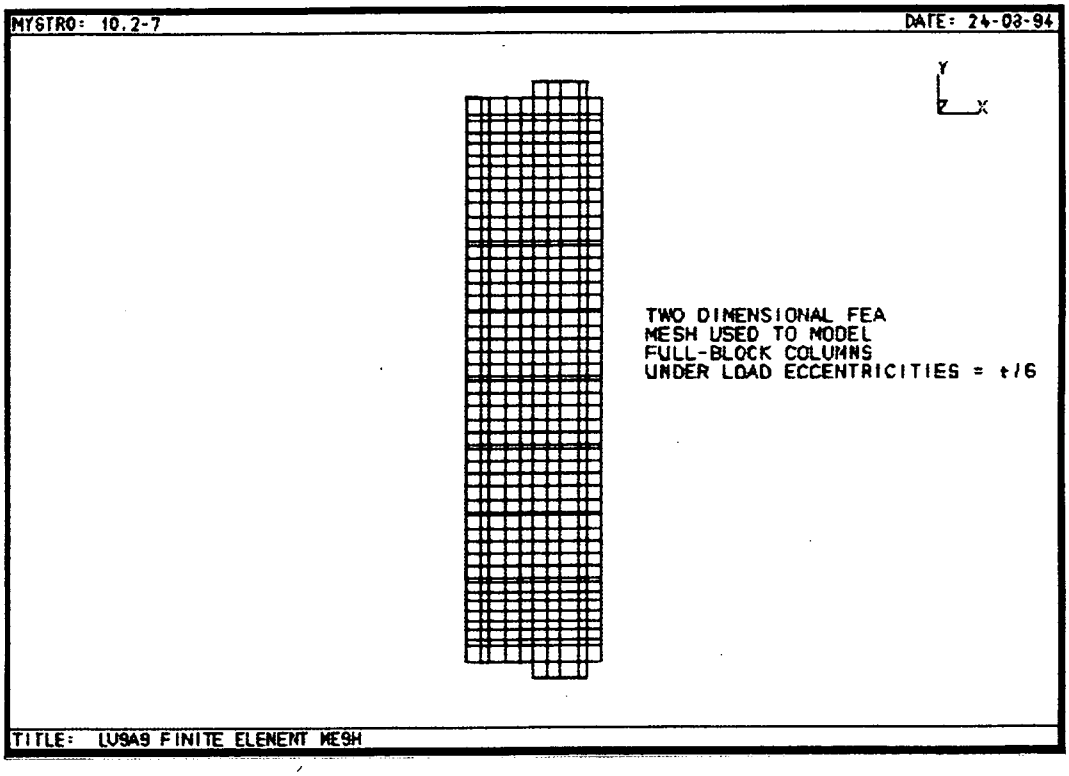


Fig. 5.7 Typical FEA mesh used to model full-block masonry columns under load eccentricities = t/6

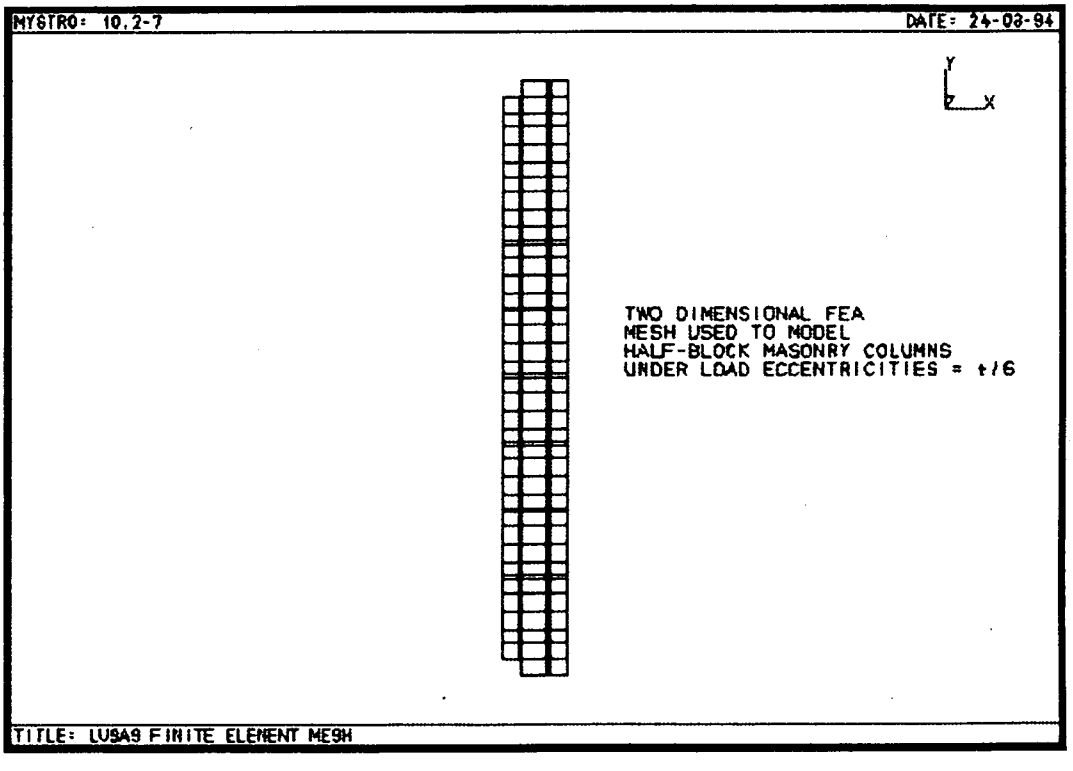


Fig. 5.8 Typical FEA mesh used to model half-block masonry columns under load eccentricities = t/6

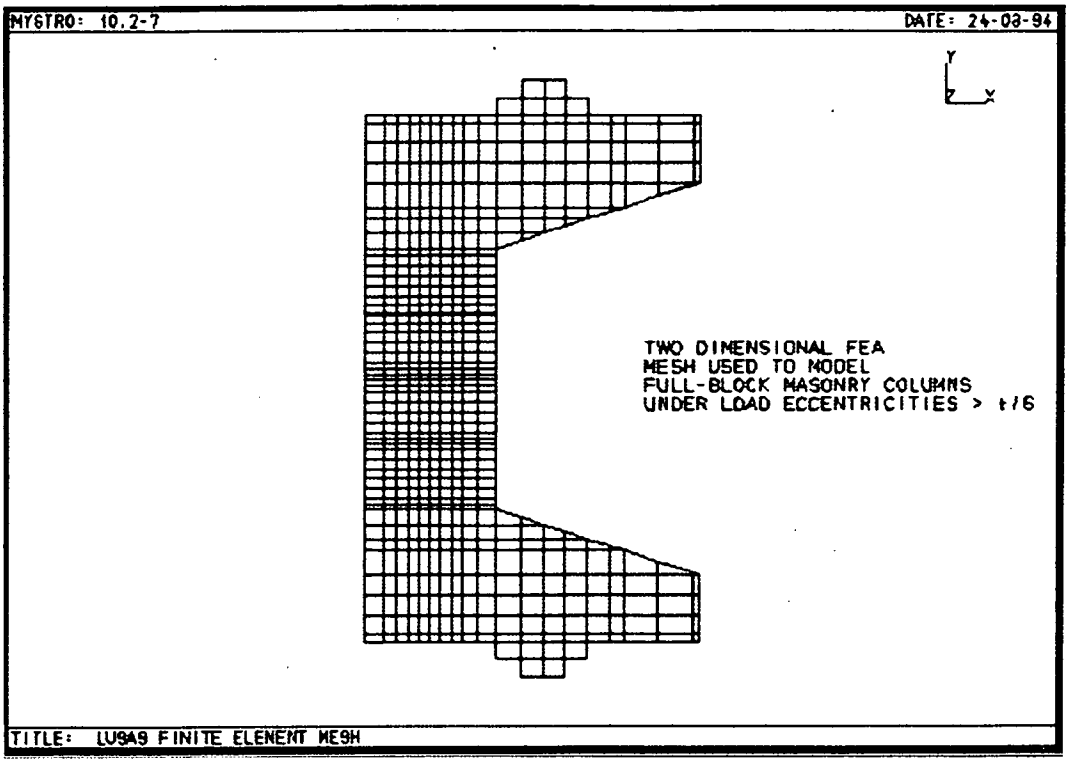


Fig. 5.9 Typical FEA mesh used to model full-block masonry columns under load eccentricities > t/6

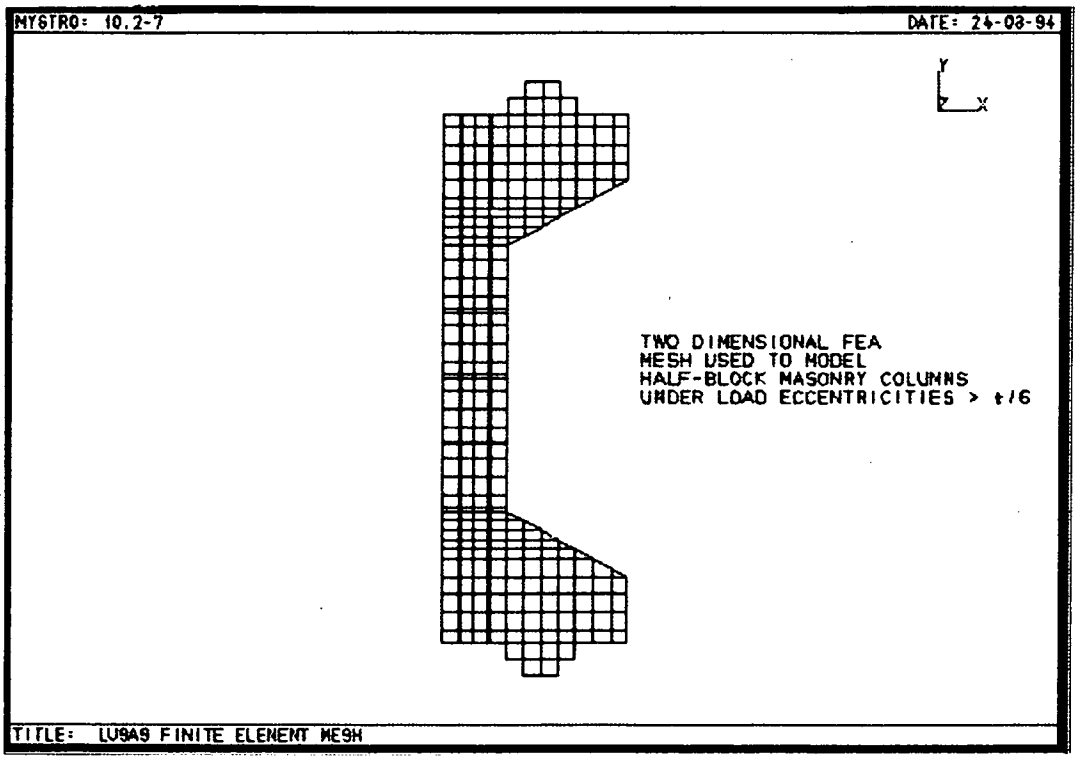
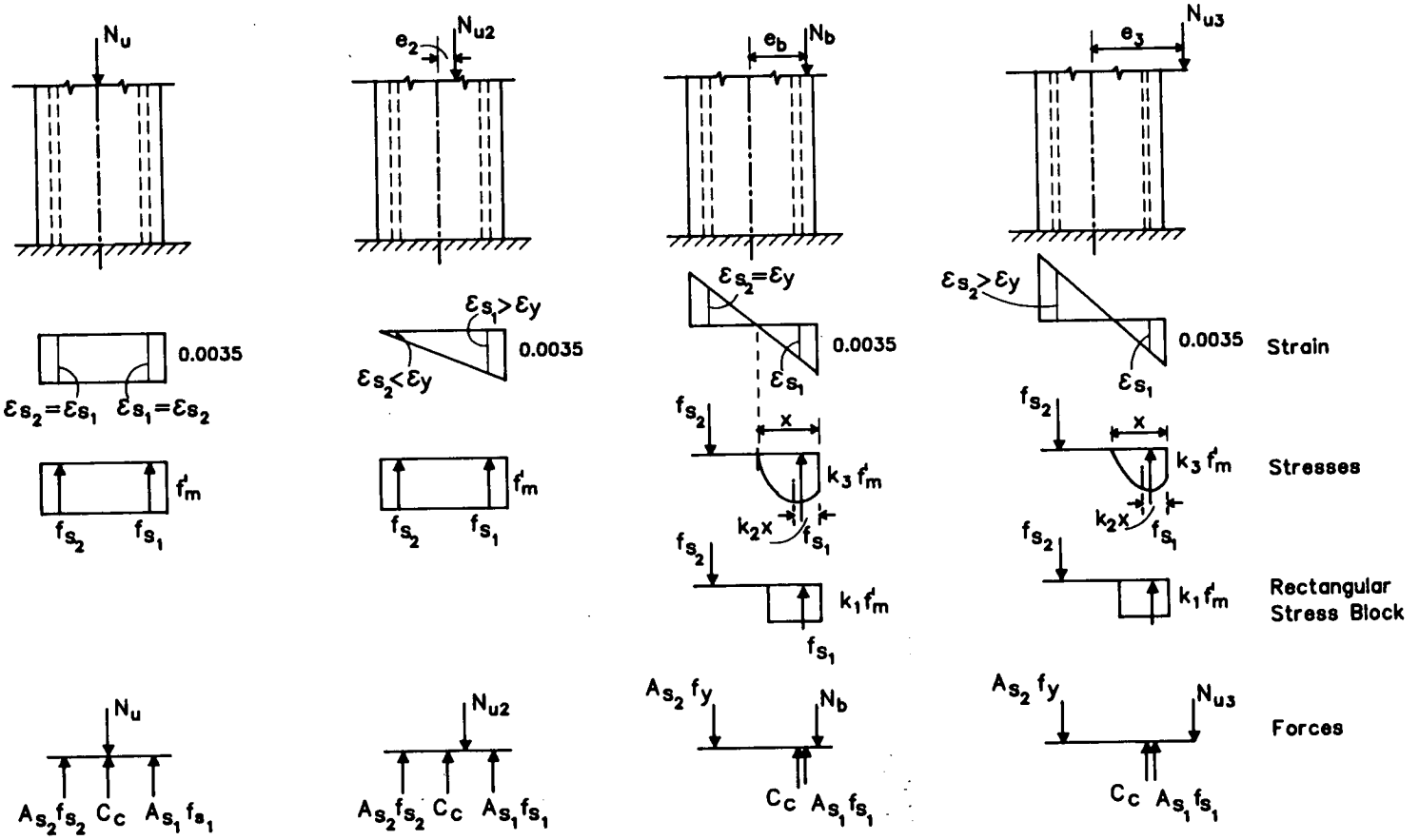


Fig. 5.10 Typical FEA mesh used to model half-block masonry columns under load eccentricities > t/6



(a) Case 1 – Pure Compression
$e = o$, $M_u = o$

(b) Case 2 – Compression failure
$e = t/6$, $N_u > N_b$

(c) Case 3 – Balanced Condition

(d) Case 4 – Tension Failure
$e > e_b$, $N_u < N_b$

Fig. 5.11 Conditions at failure for reinforced blockwork masonry colums under different cases of loading

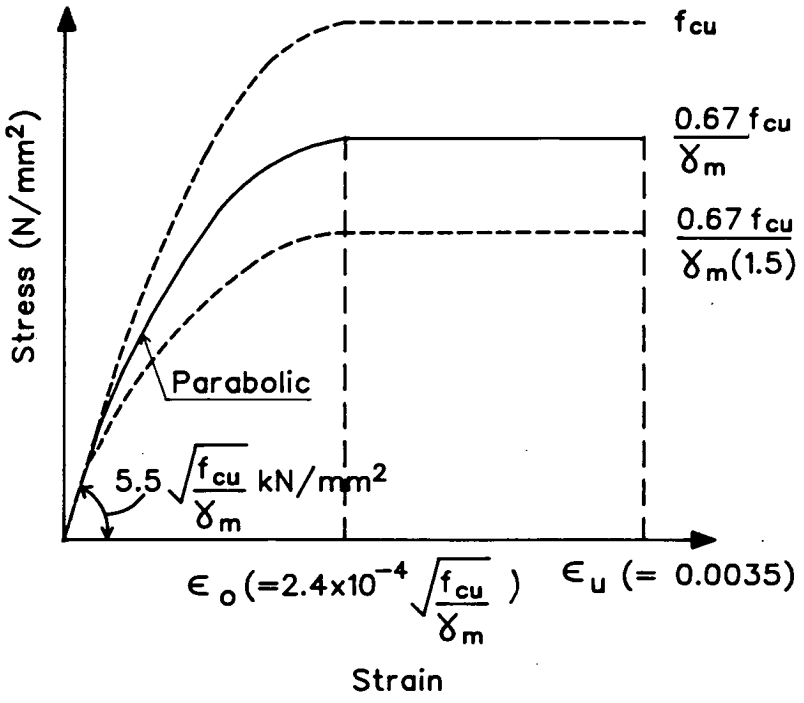


Fig. 5.12 Stress–strain relationship for concrete (BS 8110[37])

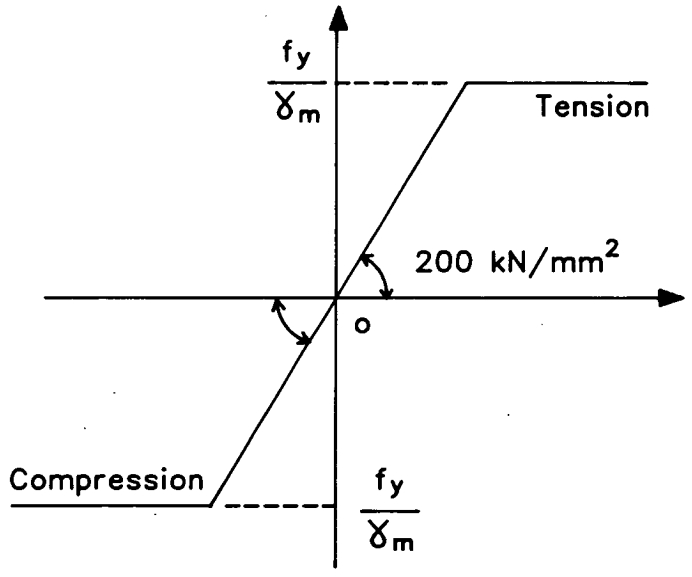


Fig. 5.13 Short term design stress–strain curve for reinforcement (BS 8110[37])

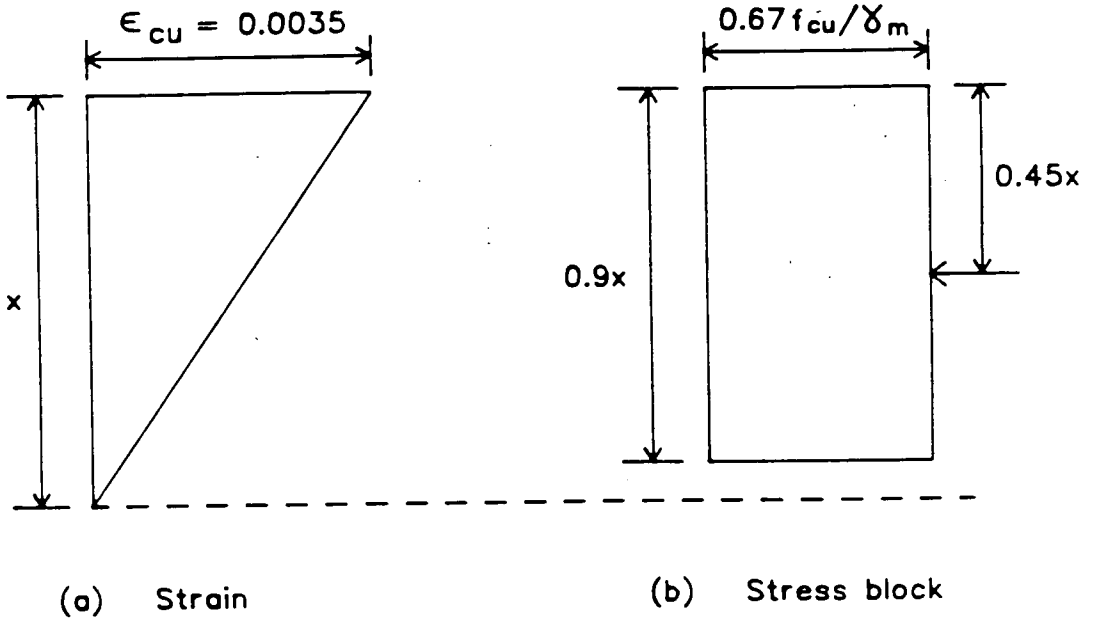


Fig. 5.14 Simplified stress block for concrete at ultimate limit state (BS 8110[37])

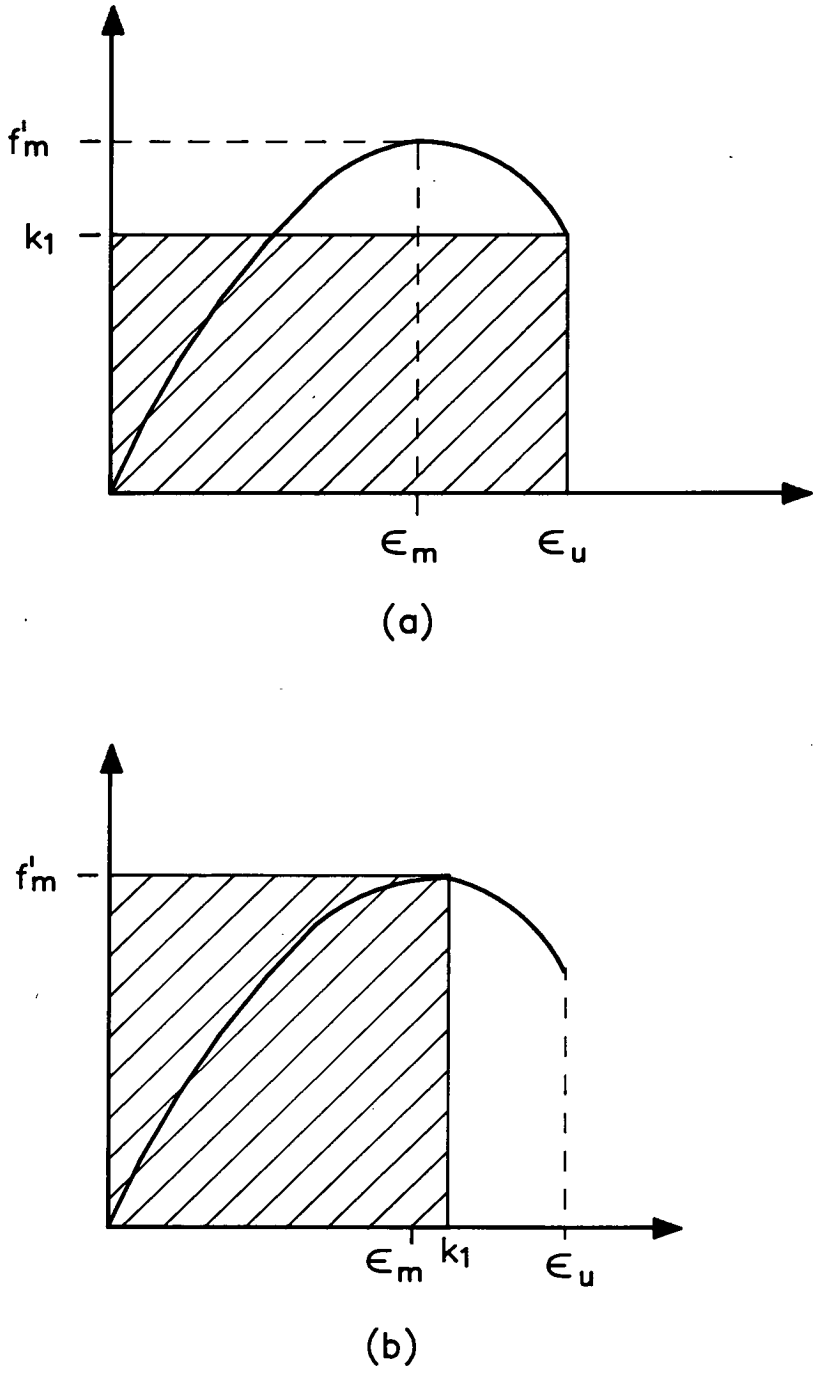


Fig. 5.15 Methods used to simplify the active stress–strain parabolic area for brickwork masonry.

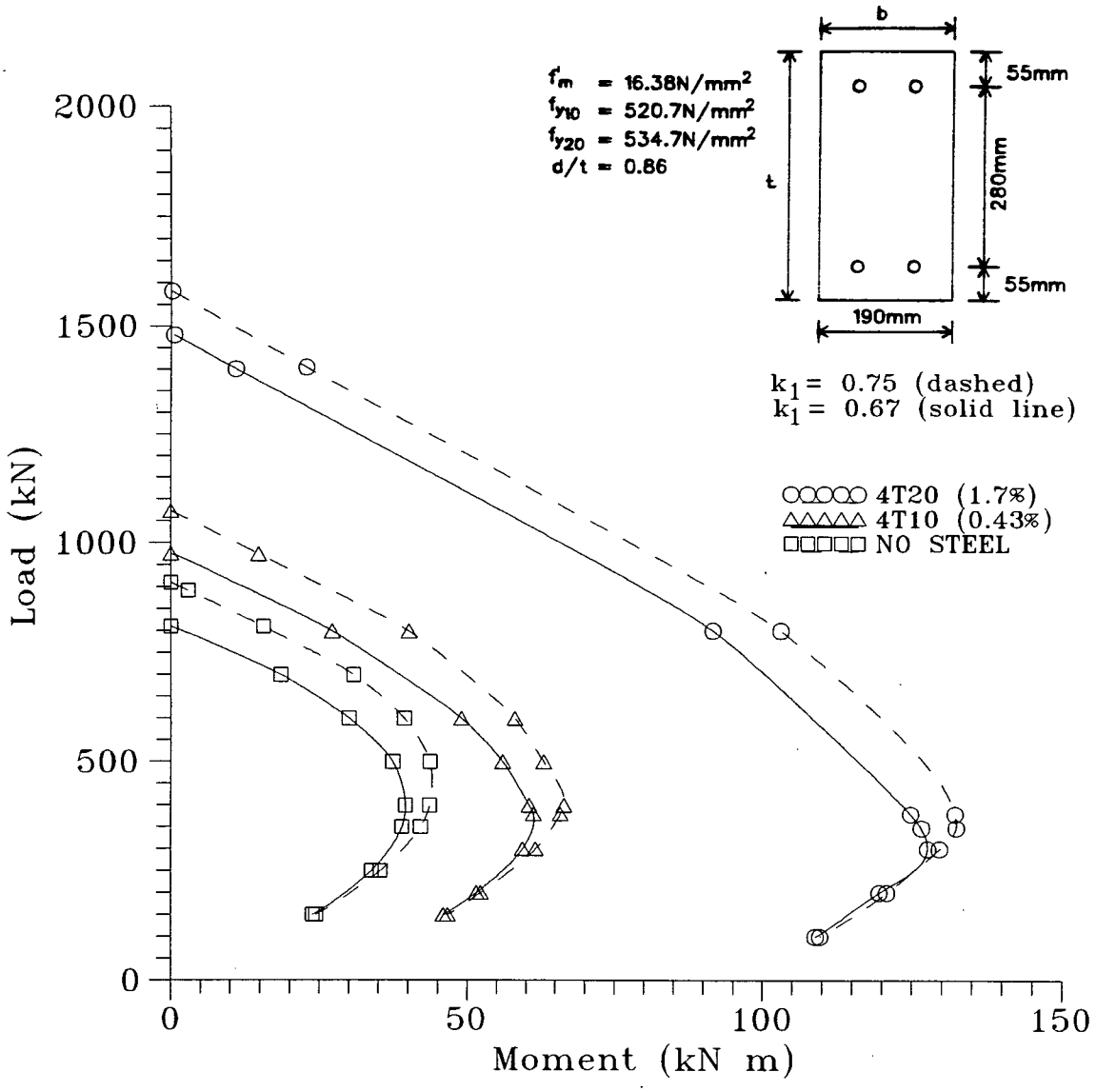


Fig. 5.16 Load–moment interaction diagrams for full–block masonry columns

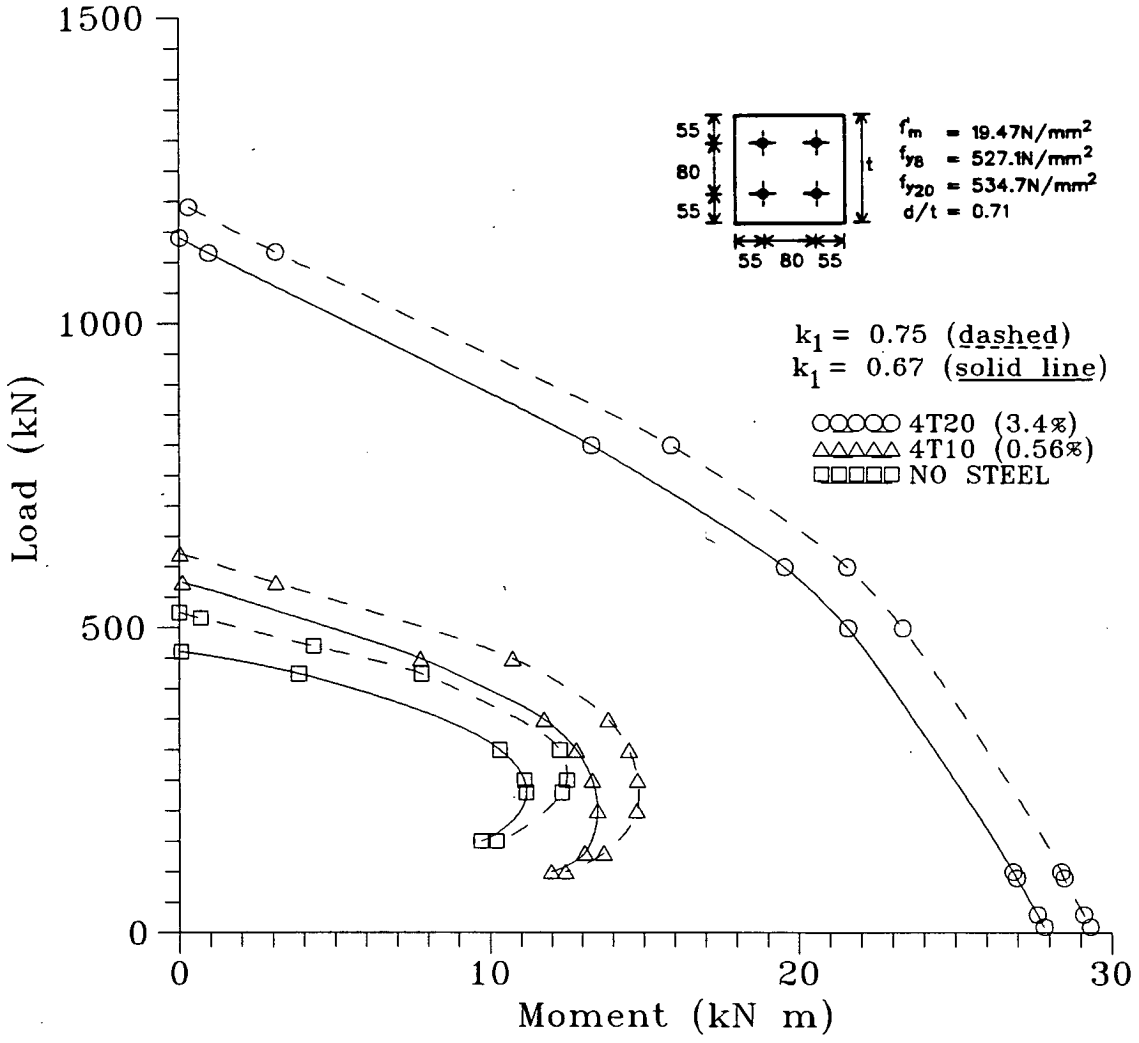


Fig. 5.17 Load–moment interaction diagrams for half–block masonry columns

CHAPTER 6

COMPARISON OF EXPERIMENTAL AND THEORETICAL RESULTS

6.1 INTRODUCTION

This chapter presents the results of an experimental and analytical investigation carried out on twenty four blockwork masonry columns to study their capacity and behaviour for different load eccentricities and percentages of the vertical reinforcement. A three dimensional non-linear finite element model was used to simulate axially loaded columns. A two dimensional non-linear finite element analysis plain stress concrete model was used for columns tested with eccentricities equal or larger than t/6. This model gave good results for analyses where cracking and crushing of the concrete section are considered.

In this chapter a design method is suggested to predict the ultimate strength of reinforced masonry blockwork columns under axial and eccentric loads.

6.2 AXIALLY LOADED BLOCKWORK COLUMNS

6.2.1 Modes of Failure

6.2.1.1 Unreinforced Columns

The unreinforced full-block columns failed by crushing of the concrete core at the mid-height of the column and splitting of the block shells over the full column height.

The half-block column failed by vertical splitting of the block shells. Crushing of the concrete around one of the mortar joints was also observed.

In both the full and half-block unreinforced columns, the failure was sudden, and an explosive type of failure was observed.

Figures 6.1 and 6.2 show typical modes of failure for the full and half-block columns respectively.

6.2.1.2 Reinforced Columns

The mode of failure for both the full and half-block columns, reinforced with 10 and 8 mm ϕ vertical bars and 8 mm ϕ lateral ties, was by localised block shell crushing, concrete crushing and buckling of the vertical bars. Failure occurred in the lower courses of the column while the rest of the column remained intact. The full-block columns, reinforced with 20 mm ϕ vertical bars and 8 mm ϕ lateral ties, failed by crushing of the upper cap and at the edges of the block located below the cap. The inside core and the rest of the column remained intact. Cracks were observed at different locations on the side shells just prior to failure. The half-block columns, reinforced with 20 mm ϕ vertical bars and 8 mm ϕ lateral ties, failed by localised block shell crushing at the upper third of the column. Buckling of the two vertical bars was observed between the lateral ties. The concrete core and the rest of the column remained intact.

6.2.3 Modulus of Elasticity of Blockwork Masonry Columns

The short term static modulus of elasticity for blockwork masonry columns was calculated from the average masonry strains measured by two electrical

displacement transducers (LVDT's) mounted on steel brackets on two opposite sides of the column and by electrical strain gauges attached to the vertical reinforcement at the column mid-height for the reinforced columns. Four 100 mm electrical strain gauges were attached to the block faces at the column mid-height to compare the results with those obtained by measuring the change of length over the 4-courses of the blockwork masonry columns.

The load was applied at the specified rate up to a stress of 0.5 N/mm^2 when the first strain readings were recorded using a data logger. The load was then applied up to one-third of the ultimate load. This was known approximately from the tests on the 4-course prisms described in chapter 4 where the loads were recorded then released to a stress of 0.5 N/mm^2. Readings were then recorded at specific load states until failure.

The stress-strain curves obtained for the full and half-block masonry columns are given in Figs 6.3 and 6.4. The figures show that the axial stiffness increases significantly with an increase in percentage of vertical reinforcement.

The difference between the strains on the vertical bars and those on the outer block face were small. This indicates a uniform strain distribution across the column cross-section. Also there was no indication of any slippage between the vertical bars, core and block shells. Figures 6.5 and 6.6 show comparisons between the average masonry strains, measured by the 110 mm electrical strain gauges attached to the column at mid-height and the LVDT's measuring the change of length over the 4-course high blockwork for full and half-block unreinforced columns respectively. Figures

6.7, 6.8, 6.9 and 6.10 show comparisons between the average strains in the vertical reinforcement and the LVDT's strains for the reinforced blockwork columns.

A review of previous works was considered in an attempt to find an expression for the modulus of elasticity of blockwork masonry.

Sahlin [55] in 1971 derived the following theoretical equation in which he related the modulus of elasticity to both the block modulus of elasticity and the mortar modulus of elasticity as follows:

$$E_m = \frac{1}{\frac{1-\delta}{E_j} + \frac{\delta}{E_b}} \quad \text{... ..(6.1)}$$

where

E_m = Elastic modulus of masonry, N/mm^2

E_j = Elastic modulus of the mortar, N/mm^2

E_b = Elastic modulus of block unit, N/mm^2

and

$$\delta = \frac{h_b}{h_b + h_j} \quad \text{..... (6.2)}$$

where

h_b = Block height, mm

h_j = Mortar joint thickness, mm

Hatzinikolas, Longworth and Warwaruk [48], 1978, recommended the following relationship, based on tests carried out on unfilled masonry walls:

$$E_m = 750\, f'_m \quad \text{..... (6.3)}$$

Feeg et al [22], 1979, suggested the following relationship based on an experimental study of reinforced blockwork columns:

$$E_m = 800\, f'_m \quad \text{..... (6.4)}$$

Some Codes of Practice relate the modulus for masonry to f_k or f'_m as follows:

i) The British Code of Practice (BS 5628: Part 2: 1985) [10] recommends the following formula for concrete, clay and calcium silicate masonry.

$$E_m = 900\, f_k \text{ N/mm}^2 \quad \text{.... .(6.5)}$$

ii) The Canadian Standard (CSA-S304-1978) [8] recommends the following formula for unfilled masonry:

$$E_m = 1000\, f'_m < 20685 \text{ N/mm}^2 \quad \text{.... .(6.6)}$$

iii) The American Building Code for Masonry Structures (ACI 531R-79)[9] recommends the following:

$$E_m = 1000\, f'_m < 17225 \text{ N/mm}^2 \quad \text{... ..(6.7)}$$

Sturgeon et al [24], in 1980, suggested that the gross area elastic modulus of composite materials, such as masonry with a grout core containing vertical reinforcement and block shell can be expressed as:

$$E_m = \frac{k\,E_c\,(A_c - A_s) + E_{Shell} \times A_{Shell} + E_s\,A_s}{A_g} \quad \ldots\ldots (6.8)$$

where

E_m = Modulus of elasticity of blockwork masonry, N/mm^2

E_c = Modulus of elasticity of concrete infill, N/mm^2

A_c = Core area, mm^2

E_s = Modulus of elasticity of vertical reinforcement, N/mm^2

A_s = Vertical reinforcement area, mm^2

E_{Shell} = Modulus of elasticity of block shells, N/mm^2

A_{Shell} = Block shell area, mm^2

A_g = Gross cross-sectional area of column perpendicular to the applied load, mm^2

k = Conversion factor taken as 0.8

Sturgeon et al noted that the elastic modulus, measured by standard cured concrete control cylinders, is not an adequate representation of the core and overestimates the experimental modulus of elasticity for prisms and columns. A conversion factor, k, taken as 0.8, has been calculated. Figures 6.11 and 6.12 show the comparison between the experimental results and the predicted modulus of elasticity for full and half-block columns using equation 6.8 as suggested by Sturgeon et al. The figures show that the theoretical and experimental results are in good agreement.

Khalaf [26] in 1991, suggested that the short term static modulus of elasticity of unfilled blockwork masonry could be determined from the theoretical expression derived by Sahlin as:

$$E_m = \frac{1}{\frac{(1-\delta)}{\alpha E_{mrs}} + \frac{\delta}{E_{bs}}} \qquad .....(6.9)$$

where

$$\alpha = \frac{E_{js}}{E_{mrs}} = 0.45 \text{ (for 10mm mortar joint)}$$

The short term static modulus of elasticity of filled blockwork masonry can be determined as:

$$E_m = \frac{1}{\frac{(1-\delta)}{\alpha E_{mrs}} + \frac{\delta}{E_{bs}}} + E_{cs} \qquad .....(6.10)$$

where

Γ = 0.25 (the contribution of concrete infill to the modulus of elasticity of masonry).

E_{cs} = The secant modulus of elasticity of the concrete derived from testing three cube prisms as described in chapter 3.

Based on the results of the present study and on the above theoretical expression for filled blockwork masonry suggested by Khalaf, the short term static modulus of elasticity of reinforced blockwork columns can be determined by adding the contribution of steel reinforcement to the columns stiffness as follows:

$$E_m = \frac{1}{\frac{(1-\delta)}{\alpha E_{mrs}} + \frac{\delta}{E_{bs}}} + \Gamma E_{cs} + \frac{E_s \times A_s}{A_g} \qquad .....(6.11)$$

where

E_s = Modulus of Elasticity of vertical reinforcement, N/mm^2

A_s = Vertical reinforcement area, mm^2

A_g = Area gross, mm^2

Figures 6.13 and 6.14 show a comparison between the experimental and predicted modulus of elasticity using equation 6.11 for full and half-block masonry columns respectively. The theoretical results obtained from the above formula were in good agreement with the experimental results.

6.2.4 Column Strength

Table 6.1 shows the failure loads of the unreinforced and reinforced concentrically loaded full and half-block columns. The compressive strength of the full-block column, reinforced with vertical reinforcement of 0.56% and 8 mm ϕ lateral ties was 4% greater than the compressive strength of the unreinforced column. The column reinforced with 1.7% vertical reinforcement and 8 mm ϕ lateral ties was 15% greater than the unreinforced column.

The compressive strength of the half-block column reinforced with 0.42% vertical reinforcement and 8 mm ϕ lateral ties was 9% greater than the unreinforced column, while the column reinforced with 3.4% vertical reinforcement and 8 mm ϕ lateral ties was 23% greater than the unreinforced half-block column.

The experimental results for concentrically loaded columns show that the column ultimate strength is increased when the percentage of vertical

reinforcement was increased. This is similar to the behaviour of the reinforced concrete.

6.2.5 Strain Measurements

Table 6.1 gives the average strain measurements recorded on the column outer face using 110 mm electrical strain gauges, the strains in the vertical bars at mid-height and the strains calculated from the changes in length over 4-courses of the column height. In most columns minor variations exist between the three strain readings. Table 6.1 also shows that the average compressive strains recorded on the vertical bars at failure are approximately 44% and 50% of the yield strains given in Table 3.5 for the full and half-block columns respectively. Strain measurements recorded on the lateral ties are also given in Table 6.1. A maximum reading of 0.000287 was recorded on the half-block column reinforced with 20 mm vertical bars and of 0.00018 on the full-block column reinforced with 20 mm vertical bars.

Table 6.2 gives the results obtained by calculating the ultimate capacity of blockwork columns from the following equation used to determine the ultimate capacity of reinforced concrete columns as:

$$N_u = f_c(A_g - A_s) + f_y \times A_s$$

The contribution of the vertical bars was based on a percentage of the yield point strength.

Table 6.2 also gives the values for ultimate load estimated from BS 5628: Part 2 [10] formula. These values are 45% lower than the experimental

values for the unreinforced full-block columns and by 46% and 51% for the full-block columns reinforced with 10 mm ϕ and 20 mm ϕ vertical bars and 8 mm ϕ lateral ties respectively.

The ultimate load estimated for the half-block unreinforced columns is 57% lower than the experimental results and 59% and 64% lower for half-block columns reinforced with 20 and 8 mm ϕ vertical bars and 8 mm ϕ lateral ties respectively.

In previous works carried at on blockwork masonry columns reinforced with lateral ties [22][24][26][59] it was found that the contribution of the lateral ties to the ultimate strength of the columns was small. Within this investigation the maximum strains measured on ties located at the column mid-heights were found to be 7% and 11% lower than the yield strains for 8 mm ϕ bars obtained experimentally and given in Table 3.6 for the full and half-block columns respectively.

Figures 6.15, 6.16, 6.17 and 6.18 show the load-strain relationships for reinforced full and half-block columns. The average strain readings at the mid-height of the vertical reinforcement of the concentrically loaded columns is compared with strain readings obtained from the finite element analysis. Excellent agreement was obtained between the experimental and FEA results.

6.3 ECCENTRICALLY LOADED BLOCKWORK COLUMNS WITH AN ECCENTRICITY OF t/6

6.3.1 Modes of Failure

6.3.1.1 Unreinforced Columns

The unreinforced full and half-block columns failed by crushing and splitting of the block shells on the compression face. Figure 6.19 shows a typical failure for an unreinforced full-block column compressed with an eccentricity of t/6. For both the full and half-block columns the failure was sudden and an explosive type of failure was observed.

6.3.1.2 Reinforced Columns

The reinforced full block columns failed by explosive removal of the block shell on the compression face in the lower half of the column. Buckling of two vertical bars between two lateral ties was observed on the compression side of the full-block column reinforced with 10 mm ϕ vertical bars and 8 mm ϕ lateral ties. Vertical cracks were observed in the area where crushing took place shortly before failure of the column. Figure 6.20 shows a typical mode of failure for a full-block column reinforced with 20 mm ϕ vertical bars and 8 mmϕ lateral ties.

The mode of failure observed for the half-block reinforced columns was a compression failure, with crushing of the block shells on the compression face and buckling of the two vertical bars between two lateral ties while the rest of the column remained intact.

Figures 6.21 and 6.22 show typical modes of failure for the columns reinforced with 4T8 mm ϕ and 4T20 mm ϕ vertical bars and 8 mm ϕ lateral

ties respectively. Both columns were compressed under an eccentricity of t/6.

6.3.2 Ultimate Strain

The ultimate strains recorded on the columns are given in Table 6.3. Unlike the concentrically loaded columns, large failure strains developed on the compression face. The average failure strains recorded on the compression face of the columns was 0.00167 in the case of the full-block columns and 0.00227 in the case of half-block columns. These values are less than the mean experimental value of 0.0035 recommended by BS 8110: 1985 [37] for concrete.

6.3.3 Strain Distribution

Typical strain distributions across the masonry blockwork column cross-sections are given as a function of load in Figs 6.23. 6.24 and 6.25 for unreinforced and reinforced full-block columns. Figures 6.26, 6.27 and 6.28 show typical strain distributions for unreinforced and reinforced half-block columns.

The strains recorded by the 90 mm electrical strain gauges mounted on the masonry surface show good agreement with the strains measured by the LVDT's.

No slippage was found between the block shells and the reinforcement steel. Two additional 90 mm electrical strain gauges were mounted on the masonry surface in two locations adjacent to the vertical bars at the column mid-height. The strains measured on the vertical bars are in excellent

agreement with the strain measured on the outer face. This indicated that the vertical bars, the concrete core and the block shells all act as one unit throughout the various stages of loading.

6.3.4 Load-Deflection Relationship (e = t/6)

The load and deflection readings for the full and the half-block columns are shown in Figs, 6.29, 6.30, 6.31, 6.32, 6.33 and 6.34 in which deflection readings are given over four equal sections of the column height. The applied load was measured by a load cell and the deflections by five LVDT's fixed on an independent stand. Both devices were connected to a data logger which recorded the load-deflection relationship up to failure.

The experimental results are in good agreement with the finite element analysis results for the column mid-height sections. Figures 6.35, 6.36, 6.37, 6.38, 6.39 and 6.40 show the comparison between experimental and finite element results for full and half-block columns subjected to an eccentric load of t/6.

6.4 BLOCKWORK COLUMNS LOADED WITH AN e > t/6 ECCENTRICITY

6.4.1 Modes of Failure

The unreinforced and reinforced full and half-block columns loaded with eccentricities greater than t/6 failed by cracking along the mortar joints on the tension side. The cracking occurred prior to crushing of the concrete blocks on the compression side at the column mid-height sections. Figures 6.41, 6.42, 6.43, 6.46, 6.47 and 6.48 show the modes of failure of the full-block columns. Figures 6.44, 6.45, 6.49, 6.50 and 6.51 show the modes of

failure of the half-block columns. All the reinforced full and half-block columns, except one half-block column reinforced with 20 mm ϕ vertical bars and 8 mm ϕ lateral ties, failed in tension failure. Cracking first started along the mortar joints, followed by yielding of the tension steel, after which crushing occurred on the compression side of the column. One half-block column failed in compression. Crushing first occurred on the compression face. The average strain on the tension reinforcement was 0.0025. The yield strain for 20 mm ϕ bars obtained experimentally and given in Table 3.5 was 0.0028.

6.4.2 Strain Distribution

Typical strain distributions across the reinforced blockwork columns are given in Figs 6.52 to 6.63 for the full and half-block columns. The strains shown in the figures were obtained at the mid-height level on the tension face, compression face and at the middle of the side face, using LVDT's gauges 550 mm in length (see Figs 5.3 and 5.4). The vertical steel strains were measured by post-yield electrical strain gauges.

6.4.3 Column lateral deflections for e > t/6

The load and deflection readings for the full and the half-block columns are shown in Figs 6.64 to 6.75. Figures 6.76 to 6.87 show comparisons between the moment-deflection curves obtained experimentally and by finite element analysis. Only the mid-height deflections are given in the figures. The load was applied in small increments up to failure. The deflections were measured by displacement transducers (LVDT's) fixed on a steel stand as shown in Figs 5.3 and 5.4. The relationship was found to be linear up to cracking. The deflection increased more rapidly during the inelastic stage,

and in the final stage small increases in load produced large increases in deflection. This behaviour was more apparent in the unreinforced columns.

6.4.4 Column cracking loads

In blockwork masonry, as in reinforced concrete structures, cracking is a major problem and can result from bending stresses, volumetric change, shrinkage and fatigue load.

Blockwork is very weak in tension, hence members under flexural loads crack when the load is increased. It is important that these cracks are kept under control to protect the reinforcement against corrosion. If cracks are not kept within specific widths, penetration of corrosive elements occurs reducing the cross-sectional area of the reinforcement, and increasing the stresses in the main reinforcement. The permissible cracking width specified by BS 8110: Part 2[37] is 0.3 mm, whereas BS 5628: Part 2 cl 22.7 and 23.5 [10] lays more emphasis on careful detailing to inhibit cracking without specifying any limiting crack size.

Unlike concrete structures, cracks in blockwork masonry occur first at the block-mortar interface. The interface bond strength is much lower than that of the strength of mortar or block.

Experimental results for the load-cracking width relationship are given in Tables 6.6 to 6.17. The crack width was measured by using demec points fixed at three locations on three mortar joint levels on the tension side of the column. An average of three readings was recorded on each level at each load stage.

6.5 LOAD-MOMENT INTERACTION DIAGRAMS

6.5.1 Introduction

This section presents a comparison between the load/moment interaction curves obtained experimentally and those obtained by applying the theoretical method used for reinforced concrete to the ultimate strength capacity of blockwork masonry columns.

6.5.2 Experimental Results and Comparison with Theoretical Load/Moment Curves

Figures 6.88 and 6.89 show the load/moment interaction curves for full and half-block masonry unreinforced and reinforced columns. 0.43% and 1.70% vertical reinforcement were adopted in this study for the full-block columns and 0.56% and 3.4% for the half-block columns. The experimental ultimate load capacity of reinforced masonry columns was found to be lower where a compression failure governed.

Previous experimental studies were carried out by Sturgeon et al [24] on concentrically and eccentrically loaded reinforced blockwork masonry short columns of 400 x 400 mm cross-sectional . The mean ultimate strain on the vertical bars at the mid-height of 37 concentrically loaded columns built from different concrete mixes and reinforced with different percentages and grades of vertical bars was 0.00142. The ultimate strain on the mid-height compression face of the eccentrically loaded column was 0.0020.

In an experimental study conducted by Khalaf [26] on axially loaded reinforced blockwork masonry short columns, 390 x 190 mm and 190 x 190 mm cross-sectional areas, the failure strain on the vertical reinforcement was found to be half the yield strain of the steel.

In this study the average ultimate strains on the vertical steel bars located at the column mid-height in the case of concentrically loaded columns were 0.00133 and 0.00143 for the full and half-block columns respectively. The average ultimate strain on the compression face of the columns compressed under eccentricities of t/6 were 0.0017 and 0.0023 for full and half block columns respectively.

The average ultimate strain values recorded for columns compressed under eccentricities > t/6 (case of E_1) were 0.00296 and 0.00284 for the full and half-block columns. These values were the average failure strains for six columns five of which failed in the tension zone where $e_t > e_b$.

Based on the experimental results, the contribution of the steel reinforcement to the strength of the concentrically loaded columns was determined by the value of ultimate strain reached when the column collapsed. Therefore the ultimate strength equation 5.1 for reinforced masonry blockwork columns was assumed as follows:

$$N_u = [f'_m A_m + k_s f_y \times A_s]/1000 \qquad .....(6.13)$$

where

k_s =0.44 (full-block columns), 0.50 (half-block columns)

Masonry columns were considered to be at an ultimate limit state of collapse when the masonry strain reached a specified value, ε_m. This value varied for full-block sections from 0.00133, in the case of pure compression, to 0.0017 and 0.0023 on the more highly compressed face for a small eccentricity of t/6 for full and half-block columns respectively. For sections where $t/6 < e < e_b$, the ultimate strain on the more highly compressed face was assumed to be 0.0029. The ultimate strain on the highly compressed face could be taken as 0.0033 in the case of a tension failure.

Applying the ultimate strain values at collapse, as given in Tables 6.1, 6.3, 6.4, 6.5 to the most highly compressed fibre assuming the strain diagram shown in Fig. 5.11c, the strain in the compression steel and tension steel could be calculated from:

$$\varepsilon_{s1} = \varepsilon_m (x - d_1)/x \qquad .....(6.14)$$

$$\varepsilon_{s2} = \varepsilon_m (d - x)/x \qquad .....(6.15)$$

The stresses in both the compression and tension steel could be calculated from:

$$f_s = \varepsilon_s \times E_s \qquad .....(6.16)$$

To calculate the ultimate axial load capacity for eccentricities < t/6, equations 5.2 or 5.3 could be used where f_{s2} is the stress in the reinforcement located near the less compressed face. The ultimate moment capacity of the masonry section could be calculated from equations 5.8 or 5.9 for eccentricities < t/6 and equations 5.6 or 5.7 for eccentricities > t/6.

A computer program was written to calculate the ultimate moment capacity of reinforced blockwork masonry short columns with rectangular sections and symmetrical arrangement of vertical steel. The program input parameters were:

1) column section depth, t (390 mm for full-block columns, 190 mm for half-block columns).
2) compressive strength of masonry, f'_m
3) yield stress of the vertical reinforcement, f_y
4) depth to centroid of steel A_{s1} and A_{s2}, d_1 (where $d_1 = d_2$)
5) bar diameter, D
6) rectangular stress block factor, k_1
7) neutral axis depth factor, k
8) failure strain factors, k_s, k_m, for the more highly compressed face of the masonry column. These values are given in Figs 6.90 and 6.91 for full and half-block columns respectively
9) axial load at column section, N

The program calculates the column's ultimate moment of resistance corresponding to specific ultimate axial loads. The results are in good agreement with those obtained from the experimental load/moment strength curves.

6.6 GENERAL DISCUSSION

Tables 6.18 and 6.19 summarise the stress results of the three dimensional non-linear FEA for concentrically loaded full and half-block columns respectively. The analysis was conducted on columns with and without cut-

out holes in the lower blocks (two in the case of full-block columns). The tensile stress of block material for columns with openings and columns provided with lateral ties at the level of the soffit of an opening are given in order to compare with columns without openings. The results of the minor principal stress 2 show that 90 x 90 mm openings created tensile stresses which were 36%, 32%, 1%, 53%, 38% and 39% higher than the columns without openings for FCA (No Steel), FCA (10 mm), FCA(20 mm), HCA (No Steel), HCA (8 mm) and HCA(20 mm) columns respectively. They show also that 156 x 120 mm (height x width) openings created tensile stresses which were 84%, 80%, 37%, 113%, 92% and 89% higher than the columns without openings for FCA (No Steel), FCA (10 mm), FCA (20 mm), HCA (No Steel), HCA (8 mm) and HCA (20 mm) columns respectively. The results show that the lateral ties reduced the tensile stress on blocks in the Z-direction (for columns with 90 x 90 mm openings) by 13%, 14%, 14%, 12%, 21% and 20% for columns FCA (No Steel), FCA (10 mm), FCA (20 mm), HCA (No Steel), HCA(8 mm) and HCA (20 mm) respectively. This led to a conclusion that the bigger the size of the openings the higher the tensile stresses on areas at the top of the opening. Placing 8 mm ϕ lateral ties on the level of the openings was found to be beneficial in reducing the harmful tensile stresses created at the centre of the block by the beam action.

Another FEA study was carried out on axially loaded full and half-block columns (with 90 x 90 mm openings) using different material properties for the concrete in the caps and openings. Columns were provided with concrete caps and openings having higher modulus of elasticity than the concrete infill. The results show that when E_{cs} changed from 14100 N/mm^2 (secant modulus of elasticity for concrete infill reported in chapter 3) to

17225 N/mm^2 (secant modulus of elasticity at 2/3 f_{max} where f_{max} is the peak value of idealised stress-strain curve given by equations 3.1 to 3.3 for concrete with f_c = 27 N/mm^2) the maximum value of the minor principal stress 2 in the block material for columns provided with caps and openings having higher concrete mix was reduced by 24%, 23%, 23%, 24%, 21% and 21% for FCA (No steel), FCA (10 mm), FCA (20 mm), HCA (No Steel), HCA (8 mm) and HCA (20 mm) columns respectively. This leads to the conclusion that higher strength concrete mixes diminish the tensile stresses. Therefore concrete strengths lower than that of the concrete infill are not recommended.

Applying the trapezoidal centre method which is described in chapter 4 and used to predict f'_m based on the idealised stress-strain curve [39] for confined 10 mm mortar joint to the full and half-block columns compressed under e = t/6, the position of the neutral axis was calculated by taking moments of forces about the extreme compression face.

The trapezoidal centre method estimated average cracks of 55.7 mm and 57.1 mm for the full and half-block unreinforced columns respectively. These results show the validity of the method in estimating the ultimate extreme fibre stresses as well as the estimation of the neutral axis depth.

When applied to the unreinforced columns with eccentricities larger than t/6 the trapezoidal centre method estimated that 90% to 92% of the specimen's thickness were cracked for both full and half-block columns.

The effect of the strain gradient in enhancing the ultimate extreme fibre stress of eccentrically loaded full and half-block columns was found to be significant. The ultimate strength for the axially loaded columns and the ultimate extreme fibre stresses for columns compressed under e = t/6 are given in table 6.20.

The results show an increase of 51%, 45% and 41% in f'_m (using the trapezoidal centre method) for unreinforced and reinforced full-block columns (10 mm and 20 mm ϕ vertical bars) respectively. They show also an increase of 66%, 61% and 75% for unreinforced and reinforced half-block columns (8 mm and 20 mm ϕ vertical bars).

6.7 CONCLUSIONS

(1) Columns provided with reinforced caps at both ends were found to be good in preventing the crushing from occurring in areas near the machine platens.

(2) Buckling of longitudinal bars throughout the length of two lateral ties was the dominant mode of failure for all the axially loaded reinforced blockwork columns.

(3) A new formula is suggested based on the test results to predict the short term static modulus of elasticity for reinforced blockwork columns (equation 6.11).

(4) The effect of strain gradient in enhancing the ultimate extreme fibre of full and half-block columns is significant. Compared to the concentrically loaded columns, the ultimate extreme fibre stresses for unreinforced columns compressed under e = t/6 increased by 51%, 44% and 40% (using the trapezoidal centre method) for

unreinforced and reinforced full-block columns (10 mm and 20 mm ϕ vertical bars) respectively. It is also increased by 66%, 61% and 74% for unreinforced and reinforced half-block columns (8 mm and 20 mm ϕ vertical bars).

(5) The trapezoidal centre method based on the stress-strain relationship for a 10 mm mortar joint was found to be good at predicting the depth of neutral axis of the eccentrically loaded blockwork columns.

(6) The results obtained from the finite element analysis (FEA) compared well with the experimental behaviour of the columns.

(7) From the results of a FEA survey carried on blockwork columns with cut-outs or openings in the lower block it was found that such openings create a concentration of high tensile stresses on the soffit. The bigger the dimensions of the opening the higher the tensile stress created. Columns provided with lateral ties at the level of the upper side of the rectangular opening were found to be beneficial in reducing the harmful tensile stresses.

(9) From the results of a FEA survey carried on blockwork columns with different strength of concrete in the caps and openings, it was found that the stronger the concrete in the caps and openings the lower the tensile stresses which occurred on blocks adjacent to the caps and openings.

(10) A new method of predicting the ultimate load capacity of blockwork masonry columns using the assumptions employed in describing the behaviour of reinforced concrete columns, founded on ultimate limit state principles, is presented. The method is based on the failure strains of the columns tested in the experimental part of this study.

Table 6.1 Test results for concentrically loaded blockwork masonry columns

Column Type	Vertical+ Reinforcement No. mm ϕ	A_s/A_c (%)	Failure Load (kN)	% of Failure Load at which the Last Strain Reading was Taken (%)	Ultimate Strain				ε_m Average of Steel and LVDT (mm/mm)	Load** taken by Steel (kN)	Load taken by Masonry (kN)
					ε_t Ties (mm/mm)	ε_b* Blockwork (mm/mm)	ε_s Vertical Steel (mm/mm)	ε_{ml} LVDT's (mm/mm)			
					Full-Block Columns						
FCA (No Steel)	-	-	1302	100	-	0.00141	-	0.00158	-	-	1302
FCA (10 mm)	4T10	0.43	1355	100	0.00016	0.00155	0.00122	0.00126	0.00124	79.5	1275.5
FCA (20 mm)	4T20	1.70	1501	100	0.00018	-	0.00114	0.00122	0.00118	290.6	1210.4
					Half-Block Columns						
HCA (No Steel)	-	-	810	98.7	-	0.00125	-	0.00161	-	-	810
HCA (8 mm)	4T8	0.56	884	90.5	0.00016	0.0014	0.00134	0.00147	0.0014	57.4	826.6
HCA (20 mm)	4T20	3.40	1000	100	0.00028	0.00133	0.00128	0.00129	0.00128	289.7	710.3

Note: For those columns in which strain measurements terminated prior to failure, strains at failure are obtained by extrapolation of the load-strain curve to the measured failure load level.

+No. of bars Type (mm ϕ).

*Measured by 110 mm electrical strain gauges.

**Calculated from $\varepsilon_m \times E_s \times A_{s,}$ for E_s and A_s values (See Table 3.5).

Table 6.2 Ultimate axial load of brickwork masonry columns

Column Type	Vertical[+] Reinforcement No. mm ϕ	As/Ag (%)	N_u Experimental (kN)	N_u* BS 5628 (kN)	N_u** Theoretical (kN)
		Full-Block Columns			
FCA (No Steel)	-	-	1302	722.53	1214
FCA (10 mm)	4T10	0.42	1355	738.04	1282
FCA (20 mm)	4T20	1.70	1501	738.04	1489
		Half-Block Columns			
HCA (No Steel)	-	-	810	352	703
HCA (8 mm)	4T8	0.57	884	359.55	752
HCA (20 mm)	4T20	3.48	1000	359.55	1014

[+]No. of bars Type (mm ϕ)

*BS 5628[(10)], N_u = $[\beta A_g f_k]/1000$, Part1 cl 32.2.2

where β = 0.98 (unreinforced columns), Part1 Table 7

f_k = 9.96 N/mm^2 (from Table 3.1)

NB It could be deduced from Part2 cl 23.2.1 that β = 1.00 for reinforced columns

**From N_u = $f'_m (A_g - A_s) + k_s f_y \times A_s$

where k_s = 0.44 (full-block columns), 0.50 (half-block columns)

f'_m = 16.38 N/mm^2 (full-block), 19.47 N/mm^2 (half-block)

Table 6.3 Test results for eccentrically loaded columns with an eccentricity of t/6

Column Type	Vertical* Reinforcemet No. mm ϕ	A_S/A_C (%)	Failure Load N_u (kN)	% of Failure load at which LVDT's removed (%)	Failure Moment (kN m)	Mid-height Deflection at Failure Δ (mm)	Failure Moment + $N_u.\Delta$ (kN m)	Compression Failure Strain (mm/mm)
				Full-Block Columns				
$FCE_{t/6}$ (No Steel)	-	-	950	84.2**	61.75	2.09	63.73	0.002071
$FCE_{t/6}$ (10 mm)	4T10	0.43	960	97.3	62.40	1.61	63.94	0.001596
$FCE_{t/6}$ (20 mm)	4T20	1.70	1010	96.7**	65.65	1.69	67.34	0.001352
				Half-Block Columns				
$HCE_{t/6}$ (No Steel)	-	-	650	100	20.58	3.41	22.79	0.002196
$HCE_{t/6}$ (8 mm)	4T8	0.56	680	88	21.53	4.98	24.92	0.002369
$HCE_{t/6}$ (20 mm)	4T20	3.40	950	95**	30.08	3.93	33.81	0.002242

Note: For those columns having their LVDT's removed prior to failure, strains and deflections at failure are obtained by extrapolation of load-strain and load-deflection curves to the measured failure load level.

*No. of bars type (mm ϕ).

**Deflection measurements ceased.

Table 6.4 Test results for eccentrically loaded columns (the case of E_1 eccentricity)

Column Type	Vertical* Reinforcemet No. mm ϕ	Failure Load N_U (kN)	Load eccentricity e (mm)	% of Failure load at which LVDT's removed (%)	Failure Moment (kN m)	Mid-height Deflection at Failure Δ (mm)	Failure Moment + $N_U.\Delta$ (kN m)	Maximum Strain$^+$ on Compression side at Failure (mm/mm)
				Full-Block Columns				
FCE_1 (No Steel)	-	65	312	100	20.28	12.54	21.09	0.00283**
FCE_1 (10 mm)	4T10	140	338	100	47.32	7.76	48.40	0.002697
FCE_1 (20 mm)	4T20	250	536	100	134.00	7.06	135.76	0.003356
				Half-Block Columns				
HCE_1 (No Steel)	-	57.8	155	69.2	8.96	12.52	9.68	0.002597
HCE_1 (8 mm)	4T8	68	200	95.5	13.6	9.03	14.21	0.002474
HCE_1 (20 mm)	4T20	98	297	92	29.1	10.94	30.17	0.003438

Note: For those columns having their LVDT's removed prior to failure, strains and deflections at failure are obtained by extrapolation of load-strain and load-deflection curves to the measured failure load level.

*No. of bars type (mm ϕ)

**Taken by 90 mm electrical strain gauges

$^+$All columns except column HCE_1(20 mm) failed by tension failure.

Table 6.5 Test results for eccentrically loaded columns (the case of E_2 eccentricity)

Column Type	Vertical* Reinforcemet No. mm ϕ	Failure Load N_u (kN)	Load Eccentriciy e (mm)	% of Failure load at which LVDT's removed (%)	Failure Moment (kN m)	Mid-height Deflection at Failure Δ (mm)	Failure Moment + $N_u.\Delta$ (kN m)	Maximum Strain on Compression side at Failure (mm/mm)
				Full-Block Columns				
FCE_2 (No Steel)	-	23	575	97.8	13.225	6.79	13.38	0.00330
FCE_2(10 mm)	4T10	60	575	100	34.50	11.19	35.17	0.002688
FCE_2 (20 mm)	4T20	230	580	100	133.40	7.27	135.07	0.002814
				Half-Block Columns				
HCE_2 (No Steel)	-	15	355	83.33	5.32	7.56	5.43	0.0035
HCE_2 (8 mm)	4T8	52	355	100	18.46	11.18	19.04	0.0037
HCE_2 (20 mm)	4T20	80	400	87.5	28.4	14.14	29.53	0.0038

Note: For those columns having their LVDT's removed prior to failure, strains and deflections at failure are obtained by extrapolation of load-strain and load-deflection curves to the measured failure load level.

*No. of bars type (mm ϕ).

Table 6.6 Load-crack width experimental results for the FCE_1 (No Steel) column

Load (kN)	Eccentricity (mm)	Moment (kN m)	Crack Width (mm)		
			Level 1	Level 2*	Level 3
15	312	4.68	0.06	0.03	0.54
25	312	7.80	0.07	0.05	0.55
35	312	10.92	0.08	0.06	0.44
40	312	12.48	9.96	0.06	0.44

*The column mid-height mortar joint level. Levels 3 and 1 are the levels of the mortar joints located above and below the mid-height joint respectively.

Table 6.7 Load-crack width experimental results for the FCE_1 (10 mm) column

Load (kN)	Eccentricity (mm)	Moment (kN m)	Crack Width (mm)		
			Level 1	Level 2	Level 3
30	338	10.14	0.05	0.14	0.05
50	338	16.90	0.08	0.20	0.07
80	338	27.04	0.19	0.37	0.27
100	338	33.80	0.37	0.48	0.37
130	338	43.94	0.96	0.82	0.54

Table 6.8 Load-crack width experimental results for the FCE_1 (20 mm) column

Load (kN)	Eccentricity (mm)	Moment (kN m)	Crack Width (mm)		
			Level 1	Level 2	Level 3
20	536	10.72	0.04	0.07	0.06
60	536	32.16	0.16	0.21	0.24
100	536	53.60	0.18	0.18	0.32
160	536	85.76	0.26	0.38	0.48
200	536	107.20	0.42	0.64	0.52
240	536	128.64	0.57	0.84	0.60

Table 6.9 Load-crack width experimental results for the HCE_1 (No Steel) column

Load (kN)	Eccentricity (mm)	Moment (kN m)	Crack Width (mm)		
			Level 1	Level 2*	Level 3
15	155	2.32	0.02	0.03	0.15
25	155	3.87	0.11	0.05	0.16
30	155	4.65	0.04	2.64	0.15
40	155	6.20	0.08	3.53	0.20

*The column mid-height mortar joint level. Levels 3 and 1 are the levels of the mortar joints located above and below the mid-height joint respectively.

Table 6.10 Load-crack width experimental results for the HCE_1 (8 mm) column

Load (kN)	Eccentricity (mm)	Moment (kN m)	Crack Width (mm)		
			Level 1	Level 2	Level 3
20	200	4.00	0.16	0.26	0.26
30	200	6.00	0.22	0.30	0.28
40	200	8.00	0.47	0.54	0.26
50	200	10.00	1.14	0.99	0.31

Table 6.11 Load-crack width experimental results for the HCE_1 (20 mm) column

Load (kN)	Eccentricity (mm)	Moment (kN m)	Crack Width (mm)		
			Level 1	Level 2	Level 3
20	297	5.94	0.13	0.12	0.01
50	297	14.85	0.31	0.54	0.42
70	297	20.79	0.49	0.57	0.60
90	297	26.73	0.62	0.76	0.66

Table 6.12 Load-crack width experimental results for the FCE_2 (No Steel) column

Load (kN)	Eccentricity (mm)	Moment (kN m)	Crack Width (mm)		
			Level 1	Level 2*	Level 3
7	575	4.02	0.06	0.11	0.38
12	575	6.90	0.04	0.12	0.08
18	575	10.35	0.12	0.18	0.19
20	575	11.50	0.13	2.53	0.21

*The column mid-height mortar joint level. Levels 3 and 1 are the levels of the mortar joints located above and below the mid-height joint respectively.

Table 6.13 Load-crack width experimental results for the FCE_2 (10 mm) column

Load (kN)	Eccentricity (mm)	Moment (kN m)	Crack Width (mm)		
			Level 1	Level 2	Level 3
10	575	5.75	-	0.07	-
20	575	11.50	-	0.18	-
30	575	17.25	-	0.29	-
40	575	23.00	-	0.48	-
55	575	31.62	-	0.60	-

Table 6.14 Load-crack width experimental results for the FCE_2 (20 mm) column

Load (kN)	Eccentricity (mm)	Moment (kN m)	Crack Width (mm)		
			Level 1	Level 2	Level 3
20	580	11.60	0.21	0.1	0.15
60	580	34.80	0.37	0.49	0.32
100	580	58.00	0.49	0.37	0.40
140	580	81.20	0.55	0.57	0.57
180	580	104.40	0.71	0.07	0.72
220	580	127.60	0.79	0.88	0.82

Table 6.15 Load-crack width experimental results for the HCE_2 (No Steel) column

Load (kN)	Eccentricity (mm)	Moment (kN m)	Crack Width (mm)		
			Level 1	Level 2*	Level 3
5	355	1.77	0.04	0.05	0.08
7.5	355	2.66	0.05	0.13	0.11
10	355	3.55	-	0.16	-

*The column mid-height mortar joint level. Levels 3 and 1 are the levels of the mortar joints located above and below the mid-height joint respectively.

Table 6.16 Load-crack width experimental results for the HCE_2 (8 mm) column

Load (kN)	Eccentricity (mm)	Moment (kN m)	Crack Width (mm)		
			Level 1	Level 2	Level 3
10	355	3.55	0.15	0.28	0.20
22.5	355	7.98	0.39	0.63	0.37
25	355	8.87	1.12	0.90	0.45
32.5	355	11.53	1.12	1.84	0.98
45	355	15.97	1.24	2.19	1.48

Table 6.17 Load-crack width experimental results for the HCE_2 (20 mm) column

Load (kN)	Eccentricity (mm)	Moment (kN m)	Crack Width (mm)		
			Level 1	Level 2	Level 3
15	400	6.00	0.07	0.17	0.05
40	400	16.00	0.29	0.41	0.32
60	400	24.00	0.45	0.64	0.65
70	400	28.00	0..50	0.63	0.62

Table 6.18 Stress results of the FEA study for concentrically loaded full-block masonry columns

Column Type	Direct Stress in the Y-direction (N/mm^2)	Direct Stress in the X-direction (N/mm^2)	Direct Stress in the Z-direction (N/mm^2)	Shear Stress (N/mm^2)	Minor Principal Stress 1 (N/mm^2)	Minor Principal Stress 2 (N/mm^2)	Major Principal Stress (N/mm^2)
	Block Material						
FCA (No Steel)*	-17.64 -21.83	+3.23 -1.41	+2.87 -0.94	+11.42 +9.71	+2.87 -1.41	+3.23 -0.24	-17.65 -21.83
FCA (No Steel) with Two 90 x 90 mm Openings**	-16.73 -22.56 (-17.91) (-21.89)	+3.22 -1.46 (+2.49) (-1.48)	+4.32 -1.47 (+3.29) (-1.15)	+12.48 +9.71 (+11.57) (+9.70)	+2.90 -1.48 (+1.66) (-1.49)	+4.40 -0.94 (+3.35) (-0.68)	-16.84 -23.58 (-17.94) (-22.52)
FCA (No Steel) with Two 156 x 120 mm Openings	-13.95 -22.56	+4.31 -2.11	+5.85 -1.44	+11.47 +9.12	+4.30 -2.09	+5.95 -1.34	-14.04 -22.59
FCA (No Steel) with 8 mm ϕ Lateral Tie Placed at the Level of the Soffit of an Opening	-16.75 -22.94	+3.11 -1.89	+3.77 -1.18	+12.50 +9.71	+2.88 -2.44	+3.88 -1.12	-16.83 -23.95
FCA (10 mm)*	-17.25 -21.73	+3.15 -1.50	+2.89 -1.14	+11.28 +9.55	+2.86 -1.50	+3.15 -0.39	-17.26 -22.66
FCA (10 mm) with Two 90 x 90 mm Openings**	-16.47 -22.08 (-17.57) (-21.51)	+3.12 -1.56 (+2.51) (-1.56)	+4.10 -1.75 (+3.17) (-1.48)	+11.98 +9.55 (+11.27) (+9.39)	+2.86 -1.76 (+1.63) (-1.57)	+4.17 -1.01 (+3.21) (-0.80)	-16.58 -22.81 (-17.60) (-22.30)
FCA (10 mm) with Two 156 x 120 mm Openings	-13.73 -22.71	+4.14 -2.21	+5.58 -1.63	+11.48 +8.88	+4.14 -2.19	+5.68 -1.62	-13.63 -22.74
FCA (10 mm) with 8 mm ϕ Lateral Tie Placed at the Level of the Soffit of an Opening	-16.51 -22.75	+3.01 -2.40	+3.54 -1.50	+11.99 +9.51	+2.86 -3.10	+3.63 -1.15	-16.59 -23.19
FCA (20 mm)*	-16.61 -20.84	+3.76 -1.43	+3.15 -1.22	+11.06 +9. 13	+3.16 -1.54	+3.76 -0.42	-16.61 -21.46

Table 6.18 continued

FCA (20 mm) with Two 90 x 90 mm Openings**	-15.83 -20.96 (-16.26) (-20.49)	+3.74 -1.43 (+2.80) (-1.85)	+3.73 -1.61 (+2.89) (-1.76)	+11.21 +9.16 (+10.72) (+8.61)	+3.16 +1.62 (+1.44) (-1.93)	+3.79 -0.86 (+2.93) (-1.14)	-15.95 -21.55 (-16.31) (-20.89)
FCA (20 mm) with Two 156 x 120 mm Openings	-13.26 -21.45	+3.74 -2.03	+5.07 -1.53	+10.88 +8.49	+3.75 -2.01	+5.16 -1.48	-13.36 -21.48
FCA (20 mm) with 8 mm ϕ Lateral Tie Placed at the Level of the Sofitt of an Opening	-15.89 -21.66	+3.62 -2.09	+3.22 -1.38	+11.25 +9.12	+3.16 -2.73	+3.62 -1.09	-15.98 -21.93
				Mortar Material			
FCA (No Steel)*	-8.22 -20.47	-0.35 -5.14	-0.36 -5.11	+8.07 +3.70	-0.37 -5.16	-0.27 -5.06	-8.26 -20.48
FCA (10 mm)*	-6.22 -21.08	+0.76 -5.53	+1.25 -5.35	+8.39 +3.05	+0.24 -5.58	+1.94 -5.31	-6.39 -21.12
FCA (20 mm)*	-4.68 -20.23	+0.70 -5.37	+1.00 -5.22	+7.83 +2.49	+0.20 -5.43	+1.62 -5.17	-4.80 -20.27
				Concrete Infill			
FCA (No Steel)*	-12.36 -37.54	+2.02 -13.34	+1.86 -12.51	+12.64 +6.68	+1.92 -13.52	+2.08 -12.30	-12.53 -37.58
FCA (10 mm)*	-11.87 -34.74	+2.62 -10.46	+1.92 -10.69	+13.17 +6.55	+1.79 -11.55	+2.96 -8.55	-12.06 -34.78
FCA (20 mm)*	-11.56 -33.17	+2.17 -10.07	+1.96 -10.81	+12.09 +6.36	+1.98 -11.72	-2.59 -9.01	-11.80 -33.20

*Column without opening.

**Values in brackets are for columns provided with caps and openings having higher concrete mix than the concrete infill. The concrete was modelled as an elasto plastic implicit backward Euler von Mises yield surface model and the material properties were assumed as follows:
Secant modulus of elasticity = 17255 N/mm^2, Poisson's ratio = 0.24, the initial uniaxial yield stress = 14.4 N/mm^2, number of straight line approximations to the hardening curve, slope of the uniaxial yield stress against effective plastic strain curve = 15844 and 2866 and the limit on effect plastic strain up to which the hardening curve was valid = 0.00066 and 0.00136.

Table 6.19 Stress results of the FEA study for concentrically loaded half-block masonry columns

Column Type	Direct Stress in the Y-direction (N/mm^2)	Direct Stress in the X-direction (N/mm^2)	Direct Stress in the Z-direction (N/mm^2)	Shear Stress (N/mm^2)	Minor Principal Stress 1 (N/mm^2)	Minor Principal Stress 2 (N/mm^2)	Major Principal Stress (N/mm^2)
	Block Material						
HCA (No Steel)*	-23.41 -27.83	+4.12 -0.80	+3.22 -0.98	+14.64 +12.83	+2.76 -1.06	+4.12 -0.41	-23.55 -28.17
HCA (No Steel) with 90 x 90 mm Opening**	-21.31 -29.74 (-22.88) (-28.29)	+4.12 -1.78 (+2.55) (-1.38)	+6.17 -1.90 (+4.71) (-1.44)	+16.83 +12.71 (+15.32) (+12.66)	+3.58 -1.90 (+2.49) (-1.48)	+6.30 -1.57 (+4.81) (-1.16)	-21.44 -31.00 (-22.93) (-29.36)
HCA (No Steel) with 156 x 120 mm Opening	-17.68 -30.02	+6.62 -3.08	+8.63 -2.24	+16.15 +12.01	+6.55 -2.92	+8.80 -2.14	-17.78 -31.00
HCA (No Steel) with 8 mm ϕ Lateral Tie Placed at the Level of the Opening Soffit	-21.30 -29.70	+4.12 -2.49	+5.46 -2.36	+16.77 +12.61	+3.55 -3.17	+5.82 -1.78	-21.43 -30.88
HCA (8 mm)*	-22.61 -28.80	+3.87 -3.24	+3.91 -1.80	+14.88 +12.76	+2.85 -3.24	+4.53 -1.43	-23.19 -29.20
HCA (8 mm) with 90 x 90 mm Opening**	-21.02 -29.33 (-22.63) (-28.60)	+3.92 -3.28 (+2.71) (-3.24)	+6.15 -2.37 (+4.85) (-1.99)	+16.48 +12.55 (+15.33) (+12.61)	+3.62 -3.24 (+2.67) (-3.25)	+6.27 -1.73 (+4.94) (-1.40)	-21.17 -30.60 (-22.69) (-29.36)
HCA (8 mm) with 156 x 120 mm Opening	-17.30 -29.96	+6.68 -4.19	+8.52 -2.43	+15.76 +11.75	+6.61 -4.22	+8.72 -2.44	-17.41 -30.55
HCA (8mm) with 8 mm ϕ Lateral Tie Placed at the Level of the Opening Soffit	-20.01 -29.65	+3.91 -3.28	+4.86 -2.03	+16.28 -11.77	+3.68 -3.28	+5.07 -1.79	-21.06 -30.81
HCA (20 mm)*	-19.19 -23.87	+2.86 -2.35	+3.38 -1.26	+12.17 +10.62	+2.38 -2.35	+3.48 -0.84	-19.52 -24.01

Table 6.19 continued

HCA (20 mm) with 90 x 90 mm Opening**	-17.51 -24.14 (-18.38) (-23.51)	+2.86 -2.35 (+1.92) (-2.48)	+4.76 -1.78 (+3.75) (-1.86)	+13.63 +10.42 (+12.55) (+10.28)	+2.81 -2.35 (+1.91) (-2.48)	+4.85 -1.14 (+3.82) (-1.33)	-17.64 -25.29 (-18.43) (-23.99)
HCA (20 mm) with 156 x 120 mm Opening	-14.40 -24.22	+5.11 -2.91	+6.43 -1.78	+12.82 +9.63	+5.07 -2.90	+6.59 -1.73	-14.51 -24.79
HCA (20 mm) with 8 mm ϕ Lateral Tie Placed at the Level of the Opening Soffit	-16.76 -24.48	+2.98 -2.37	+3.83 -1.65	+13.52 +10.03	+2.87 -2.35	+3.98 -1.23	-17.87 -25.55
	Mortar Material						
HCA (No Steel)*	-12.06 -27.15	+1.53 -8.20	+3.09 -8.42	+10.46 +6.11	+0.87 -8.26	+4.30 -7.80	-12.61 -27.70
HCA (8 mm)*	-9.76 -27.76	+1.89 -8.41	+3.32 -8.24	+10.36 +4.95	+1.30 -8.46	+4.31 -8.19	-9.87 -27.78
HCA (20 mm)*	-5.22 -23.58	+1.01 -6.02	+1.81 -5.87	+9.11 +2.98	+0.64 -6.07	+2.62 -5.82	-5.66 -23.61
	Concrete Infill						
HCA (No Steel)*	-14.79 -44.38	+2.80 -14.54	+2.62 -13.51	+17.79 +8.35	+2.81 -14.54	+3.14 -10.89	-15.10 -44.43
HCA (8 mm)*	-14.14 -43.82	+4.37 -15.06	+2.69 -13.25	+17.22 +8.40	+2.60 -15.06	+4.66 -11.23	-14.34 -43.87
HCA (20 mm)*	-12.50 -36.89	+3.25 -12.29	+2.12 -11.79	+13.65 +7.16	+1.99 -12.56	+3.47 -9.88	-12.60 -36.98

*Column without opening.

**Values in brackets are for columns provided with caps and openings having higher concrete mix than the concrete infill. The concrete was modelled as an elasto plastic implicit backward Euler von Mises yield surface model and the material properties were assumed as follows:
Secant modulus of elasticity = 17225 N/mm^2, Poisson's ratio = 0.24, the initial uniaxial yield stress = 14.4 N/mm^2, number of straight line approximations to the hardening curve, slope of the uniaxial yield stress against effective plastic strain curve = 15844 and 2866 and the limit on effect plastic strain up to which the hardening curve was valid = 0.00066 and 0.00136.

Table 6.20 Compressive strength of concentrically and t/6 eccentrically loaded full and half-block masonry columns

Column Type	Load* Taken by Masonry (kN)	Masonry Ultimate Stress f'_m (N/mm^2)	Method+ used in calculating f'_m	Compressive Strength (N/mm^2)	
				Infill	Mortar
FCA (No Steel)	1302	17.57		22.75	27.20
FCA (10 mm)	1275.5	17.29		22.75	27.20
FCA(20 mm)	1210.4	16.62		22.75	27.20
$FCE_{t/6}$ (No Steel)	950	22.79	1	22.75	27.20
		26.59	2		
		25.64	3		
$FCE_{t/6}$ (10 mm)	960	21.81	1	22.75	27.20
		25.44	2		
		24.53	3		
$FCE_{t/6}$ (20 mm)	1010	20.03	1	22.75	27.20
		23.38	2		
		22.55	3		
HCA (No Steel)	810	22.44		22.75	27.20
HCA (8 mm)	826.6	23.03			
HCA (20 mm)	710.3	20.39			
$HCE_{t/6}$ (No Steel)	650	32.01	1	22.75	27.20
		37.34	2		
		36.01	3		
$HCE_{t/6}$ (8 mm)	643.3	31.86	1	22.75	27.20
		37.16	2		
		35.84	3		
$HCE_{t/6}$ (20 mm)	599.14	30.56	1	22.75	27.20
		35.66	2		
		34.39	3		

*For reinforced columns, load taken by masonry is obtained by applying equation 5.3 with the contribution of the steel ($\varepsilon_m \times E_s \times A_s$) removed from the overall load taken by a column.

+Methods used in calculating f'_m:

1. Trapezoidal method
2. Trapezoidal centre method
3. Linear method



Fig. 6.1 Typical mode of failure for an unreinforced full-block masonry column compressed under axial load

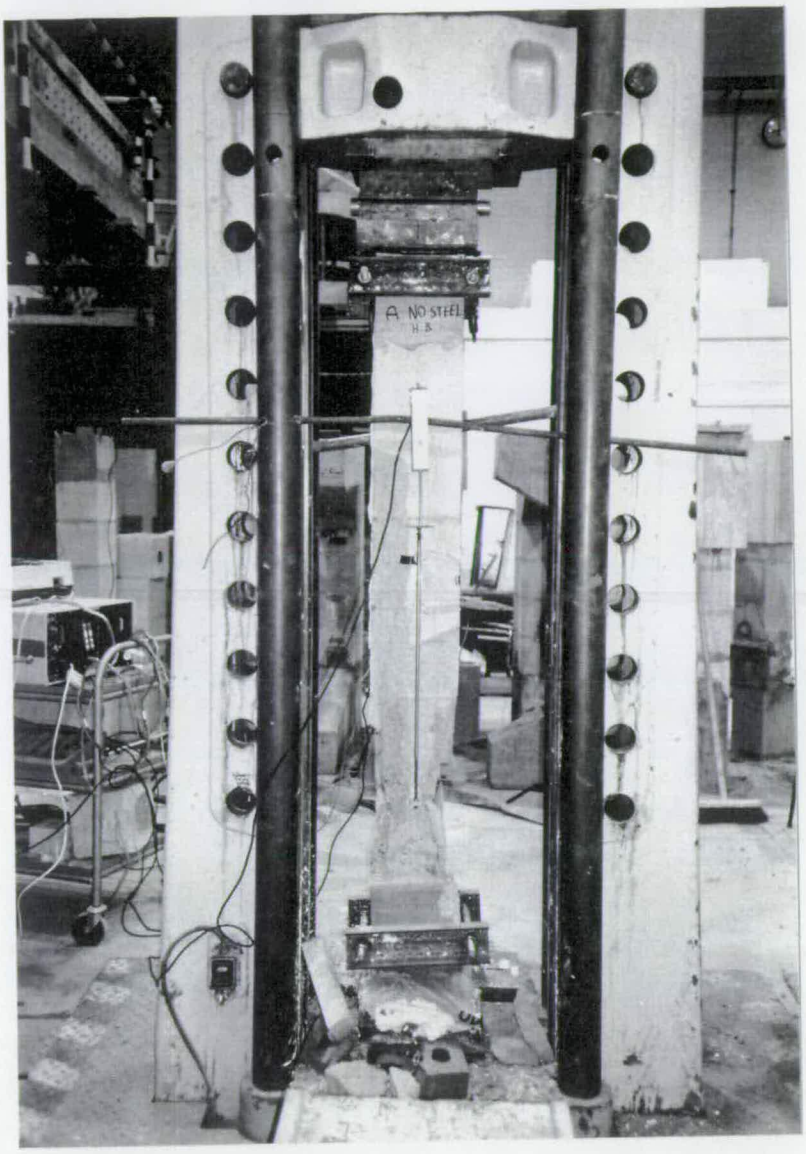


Fig. 6.2 **Typical mode of failure for an unreinforced half-block masonry column compressed under axial load.**

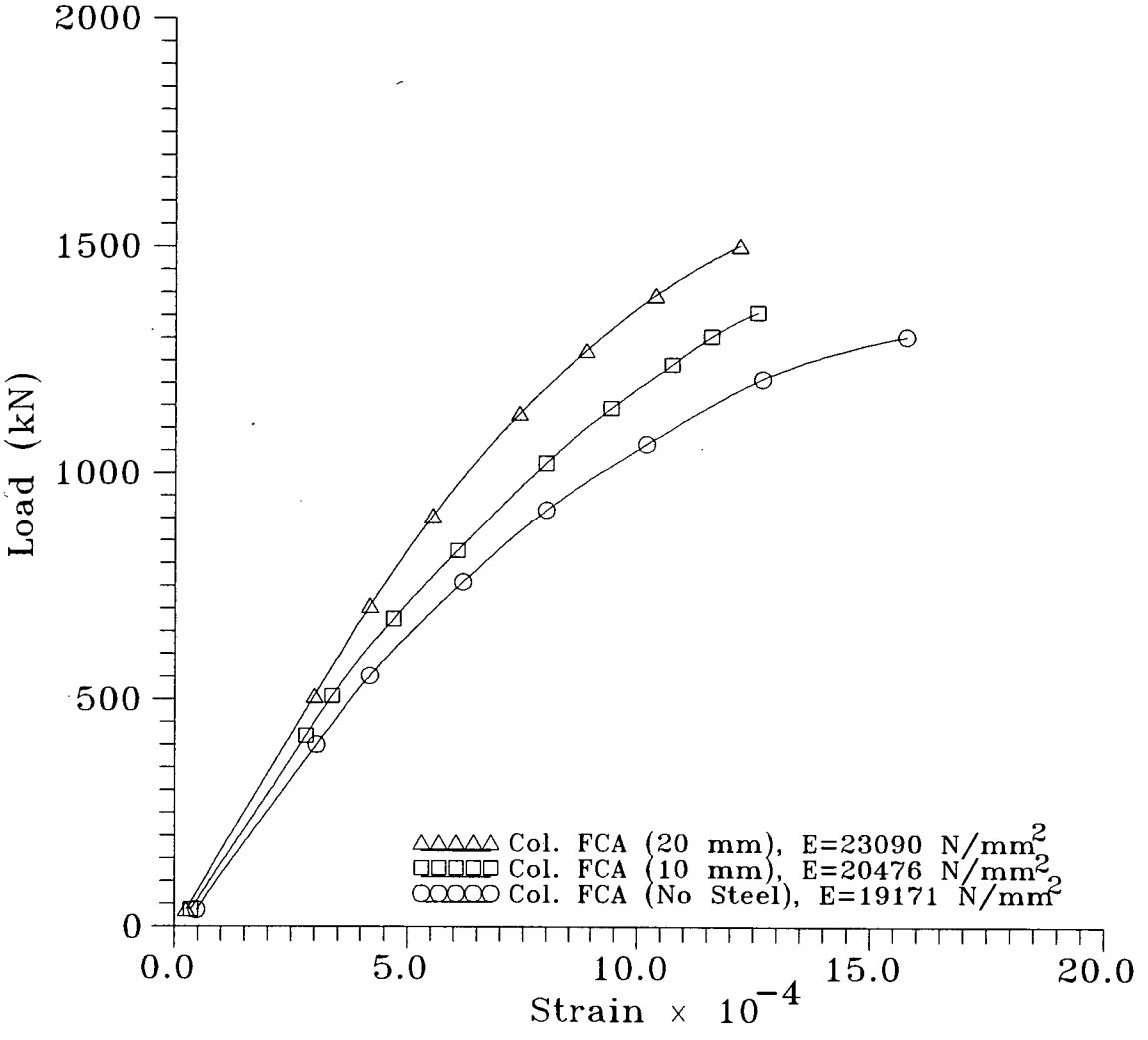


Fig. 6.3 Full-block columns elastic modulus

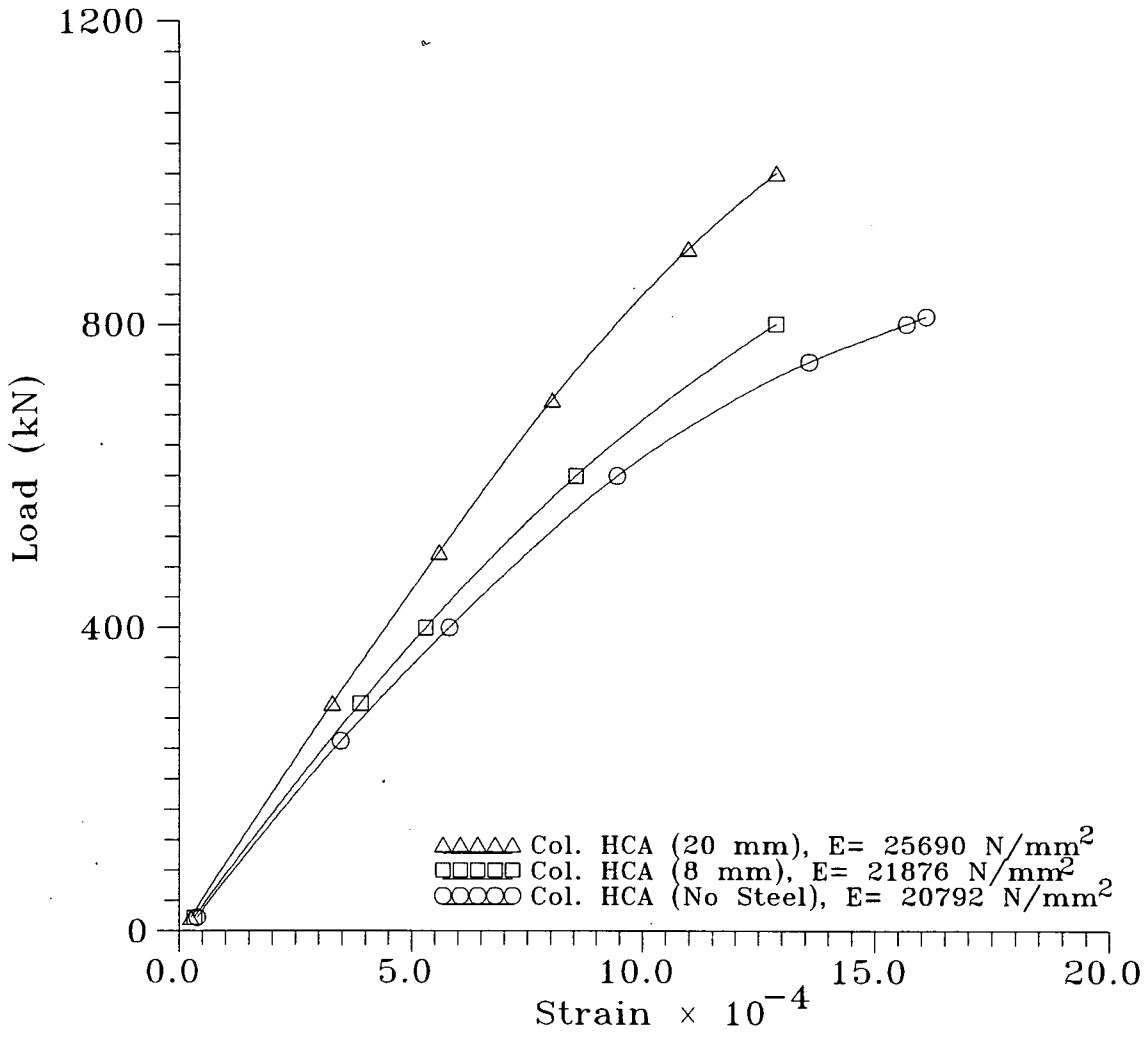


Fig. 6.4 Half-block columns elastic modulus

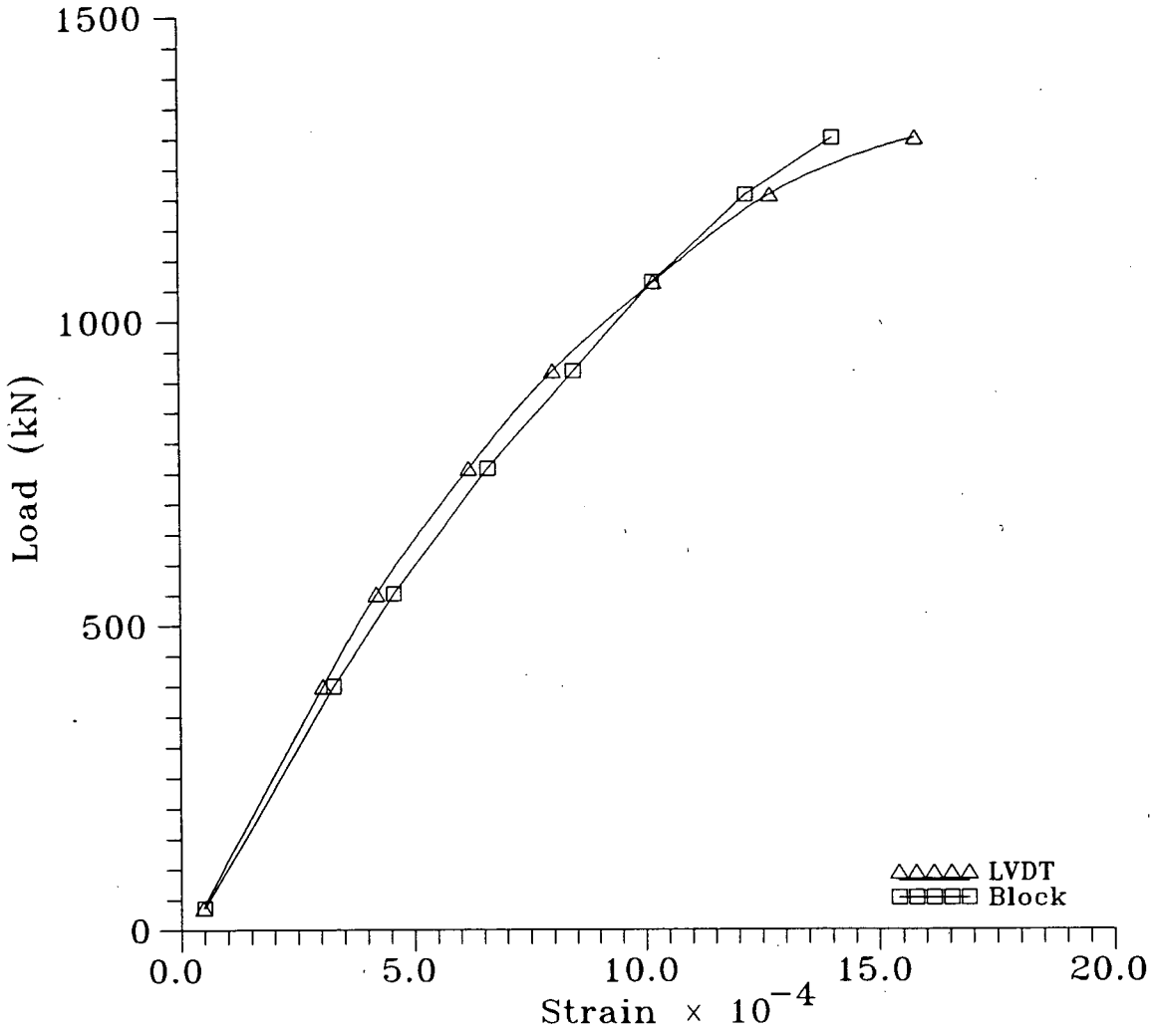


Fig. 6.5 Average masonry strains measured by electrical strain gauges and LVDT strains for the FCA (No Steel)* column

* The mnemonics used to identify specimens are explained in Appendix C

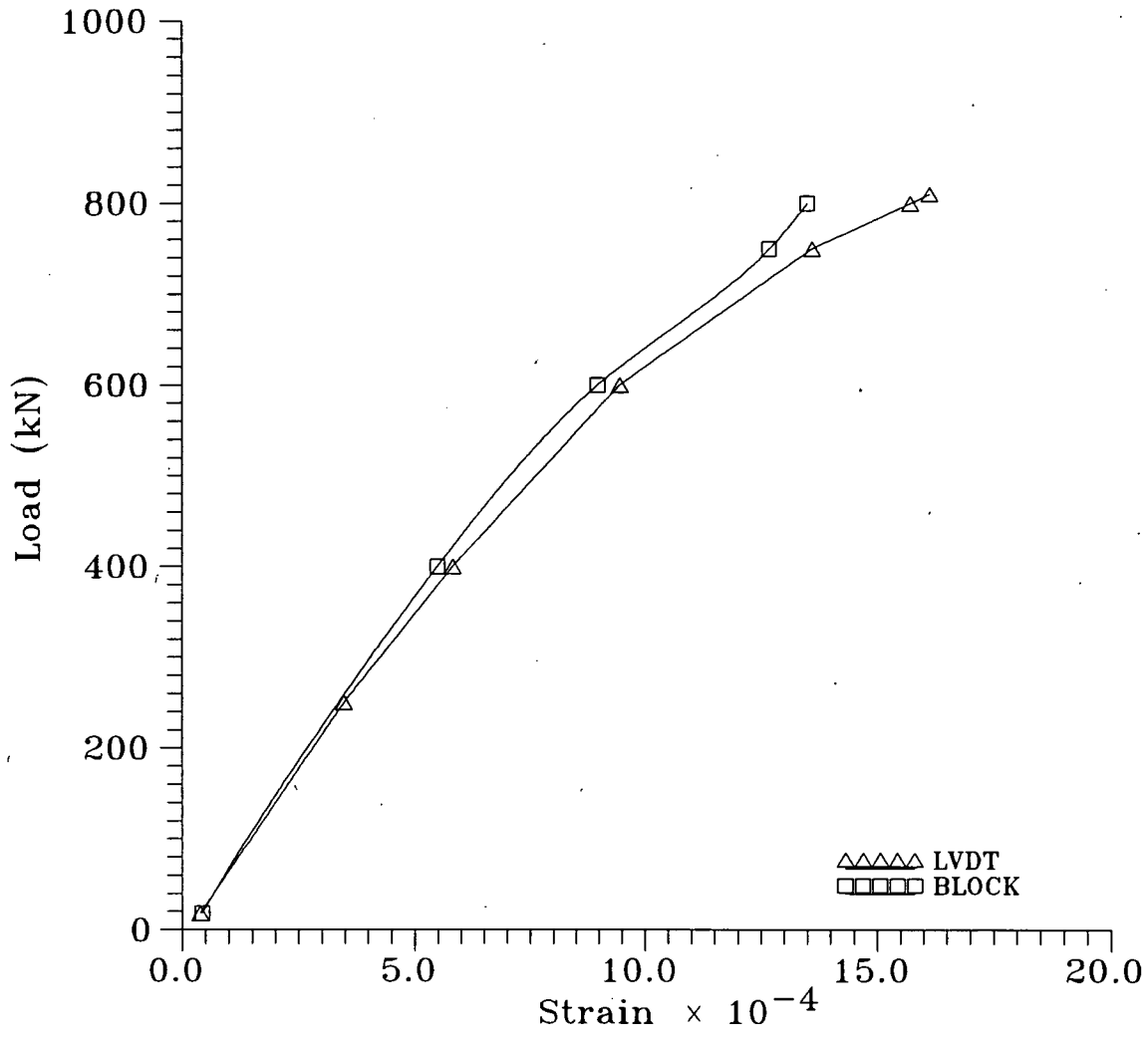


Fig. 6.6 Average masonry strains measured by electrical strain gauges and LVDT strains for the HCA (No Steel) column

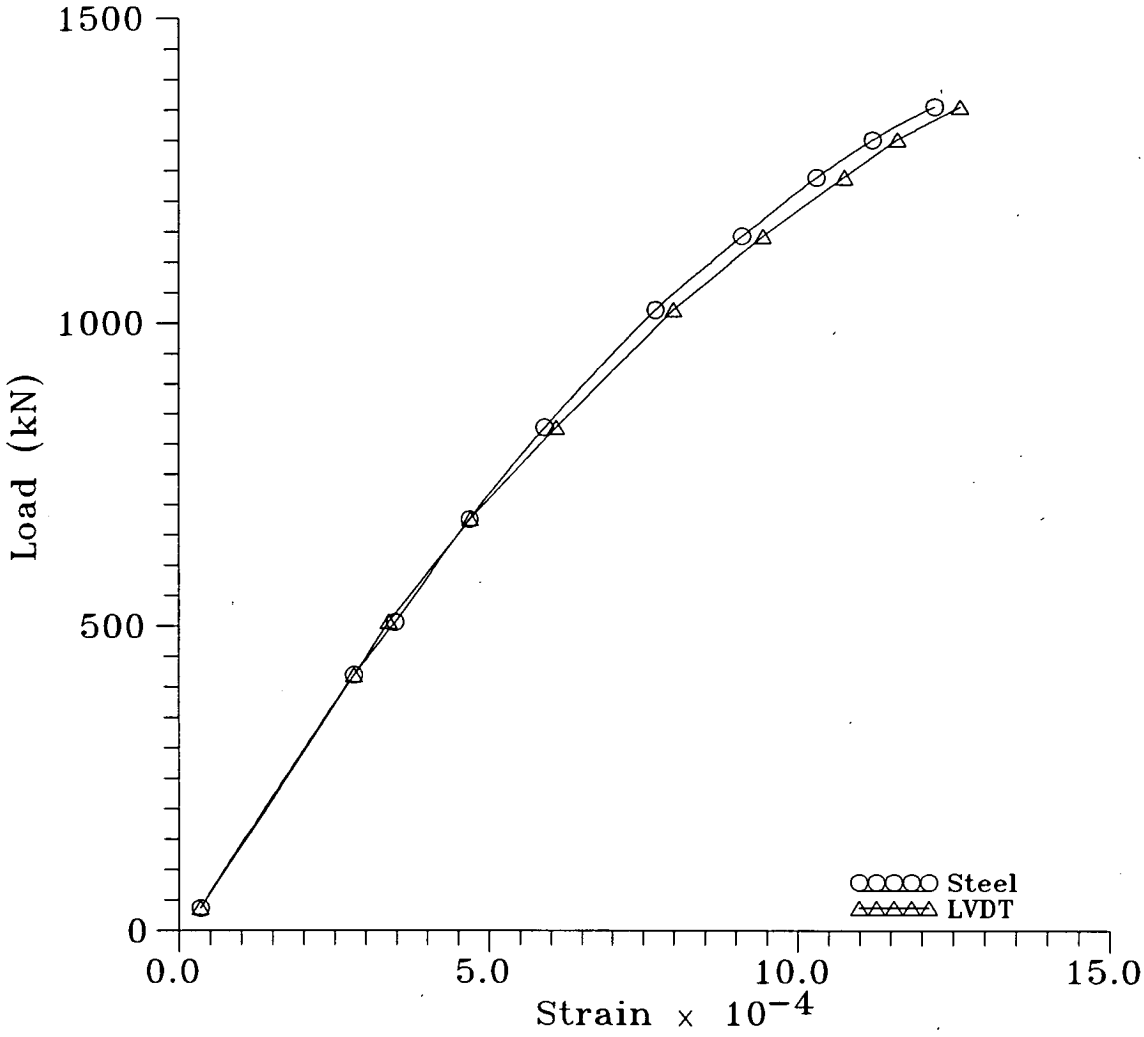


Fig. 6.7 Average vertical reinforcement strains and LVDT strains for the FCA (10 mm) column

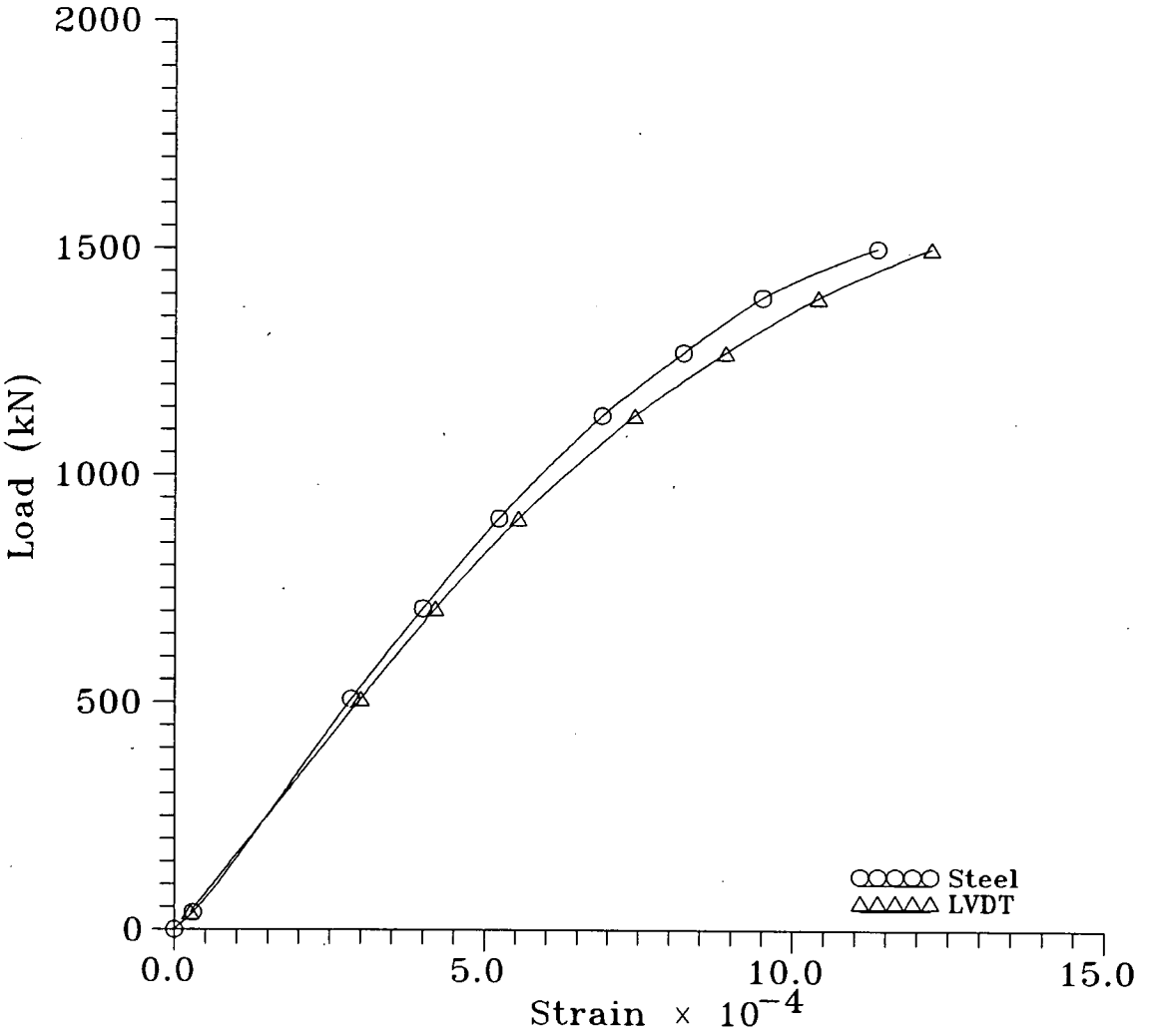


Fig. 6.8 Average vertical reinforcement strains and LVDT strains for the FCA (20 mm) column

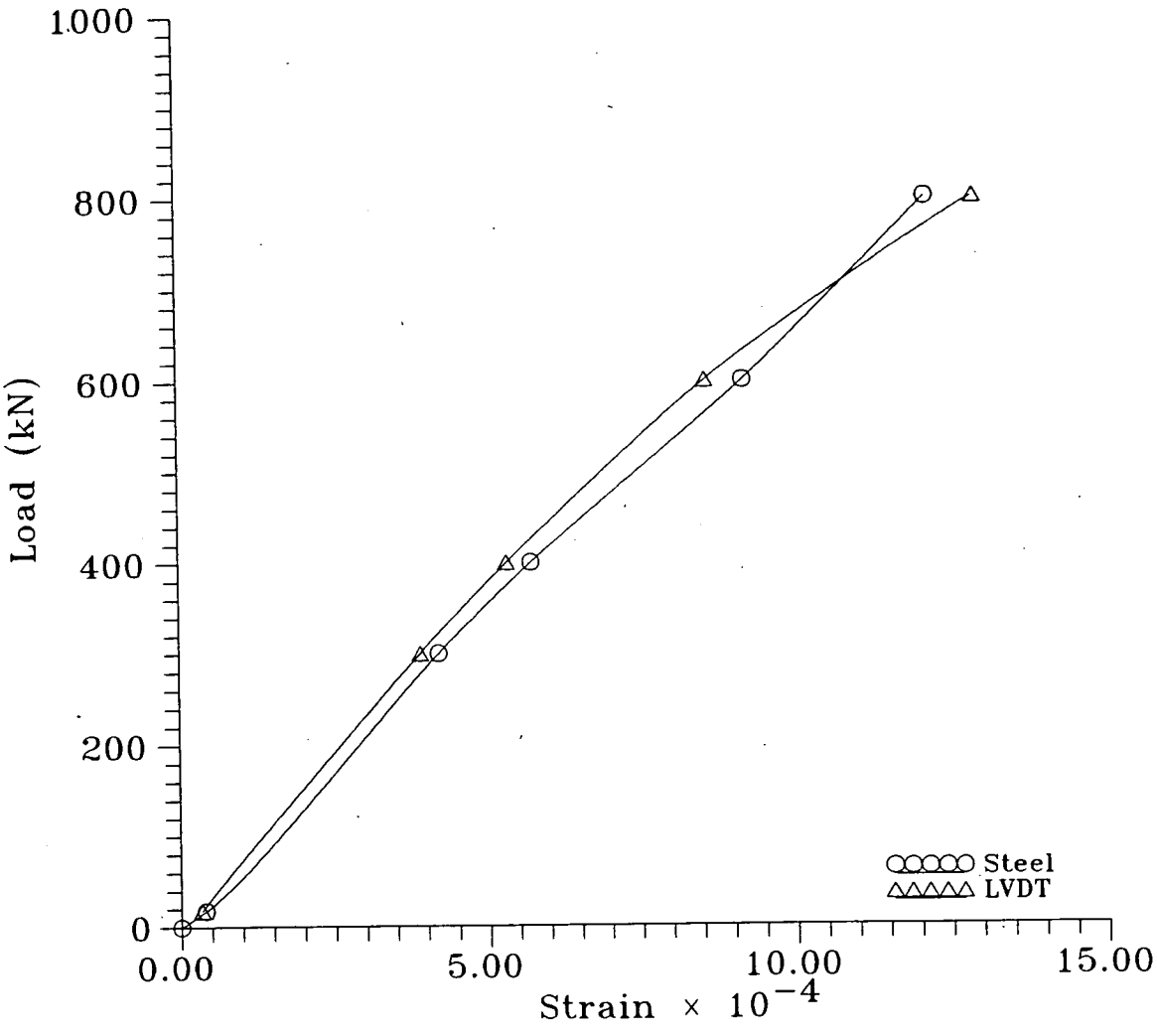


Fig. 6.9 Average vertical reinforcement strains and LVDT strains for the HCA (8 mm) column

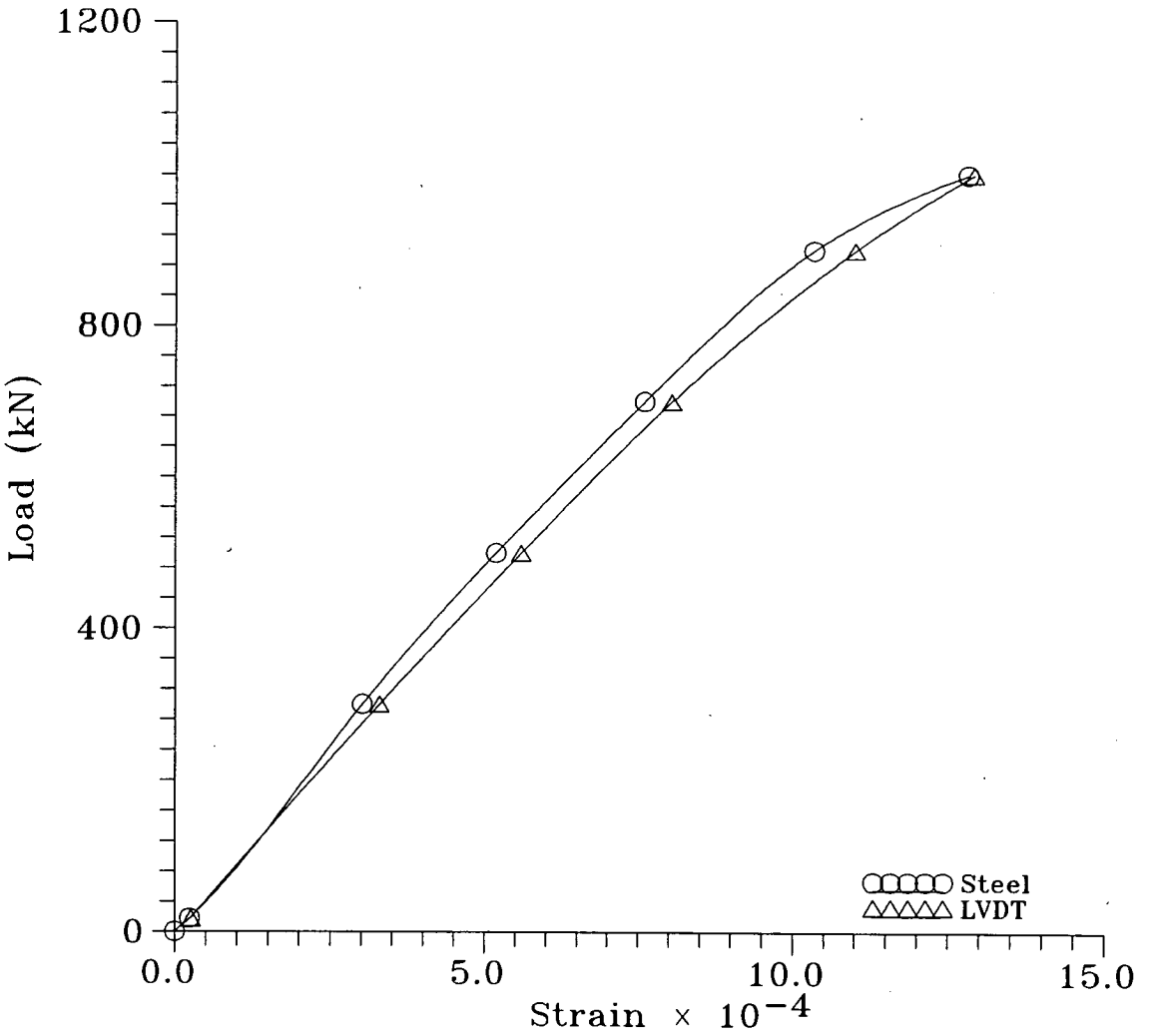


Fig. 6.10 Average vertical reinforcement strains and LVDT strains for the HCA (20 mm) column

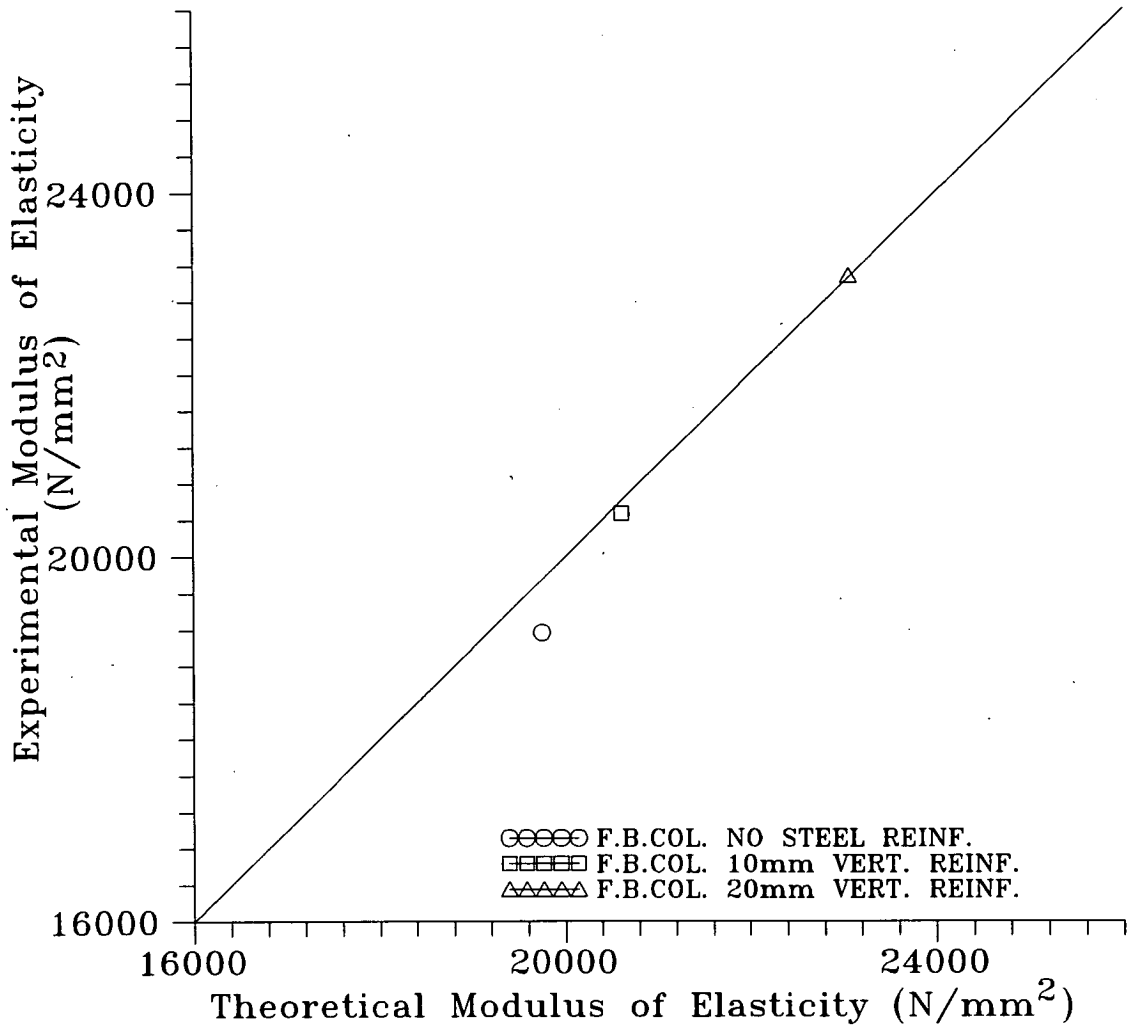


Fig. 6.11 Experimental and predicted modulus of elasticity for full-block masonry columns using equation 6.8 (24)

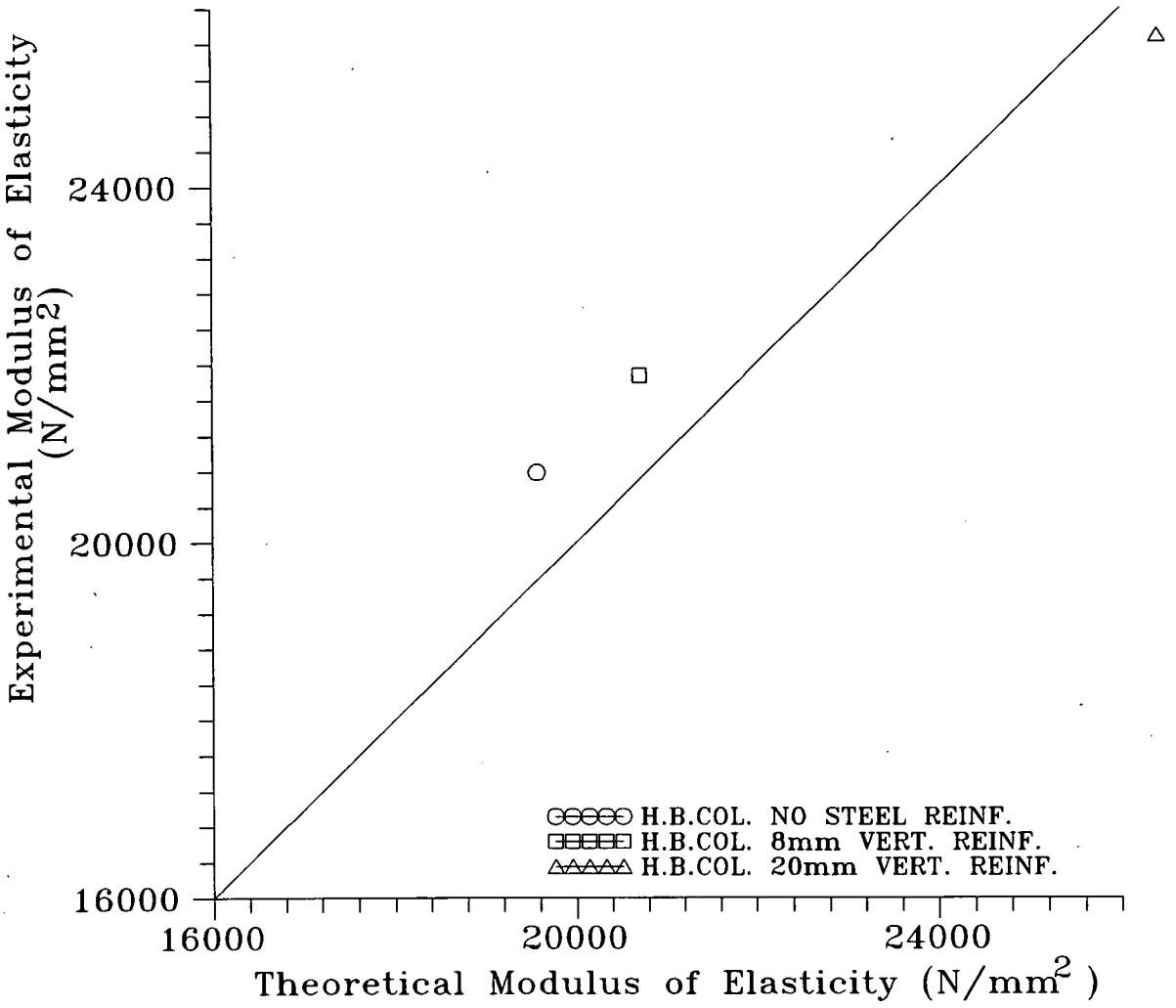


Fig. 6.12 Experimental and predicted modulus of elasticity for half-block masonry columns using equation 6.8(24)

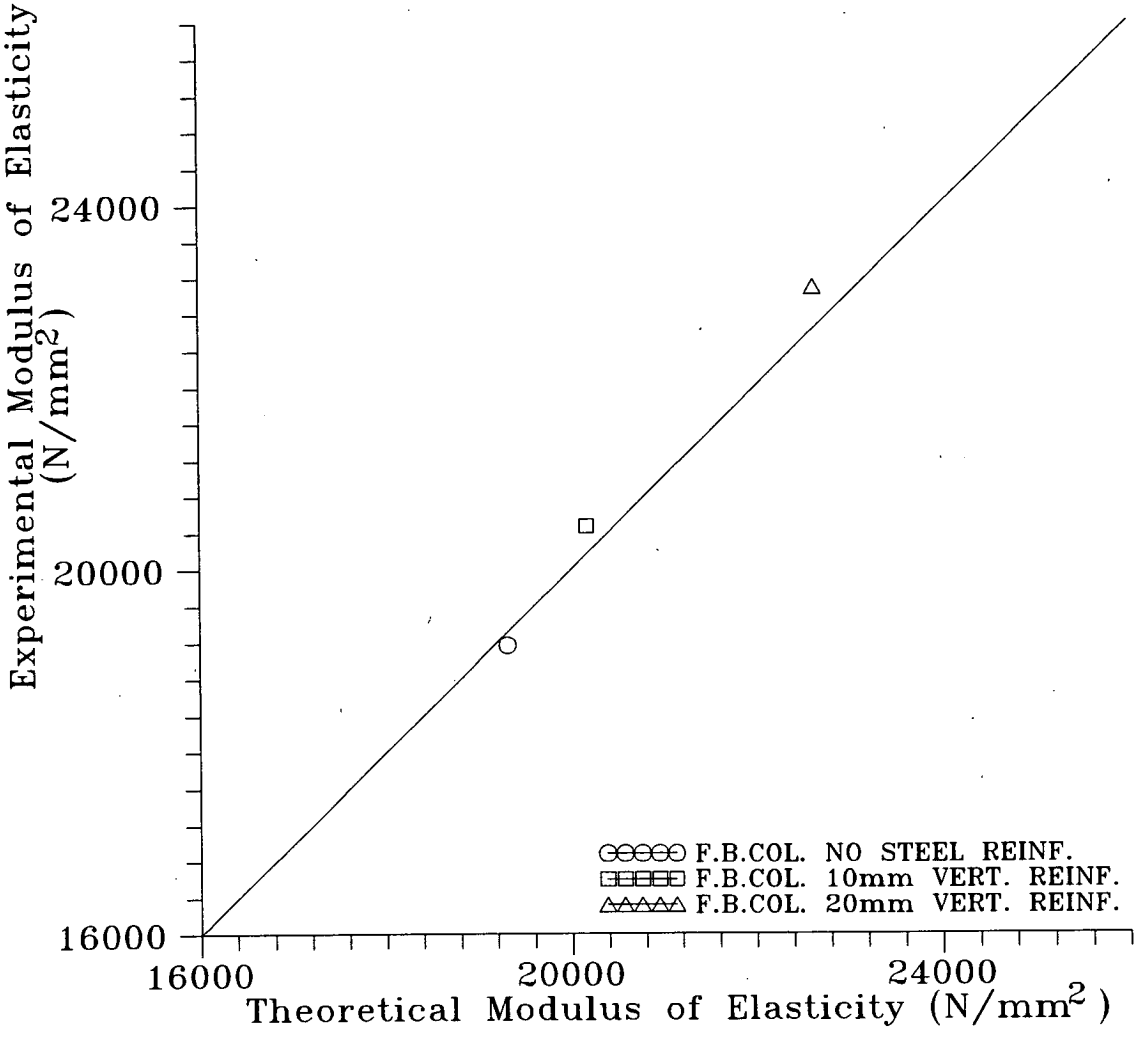


Fig. 6.13 Experimental and predicted modulus of elasticity for full-block columns

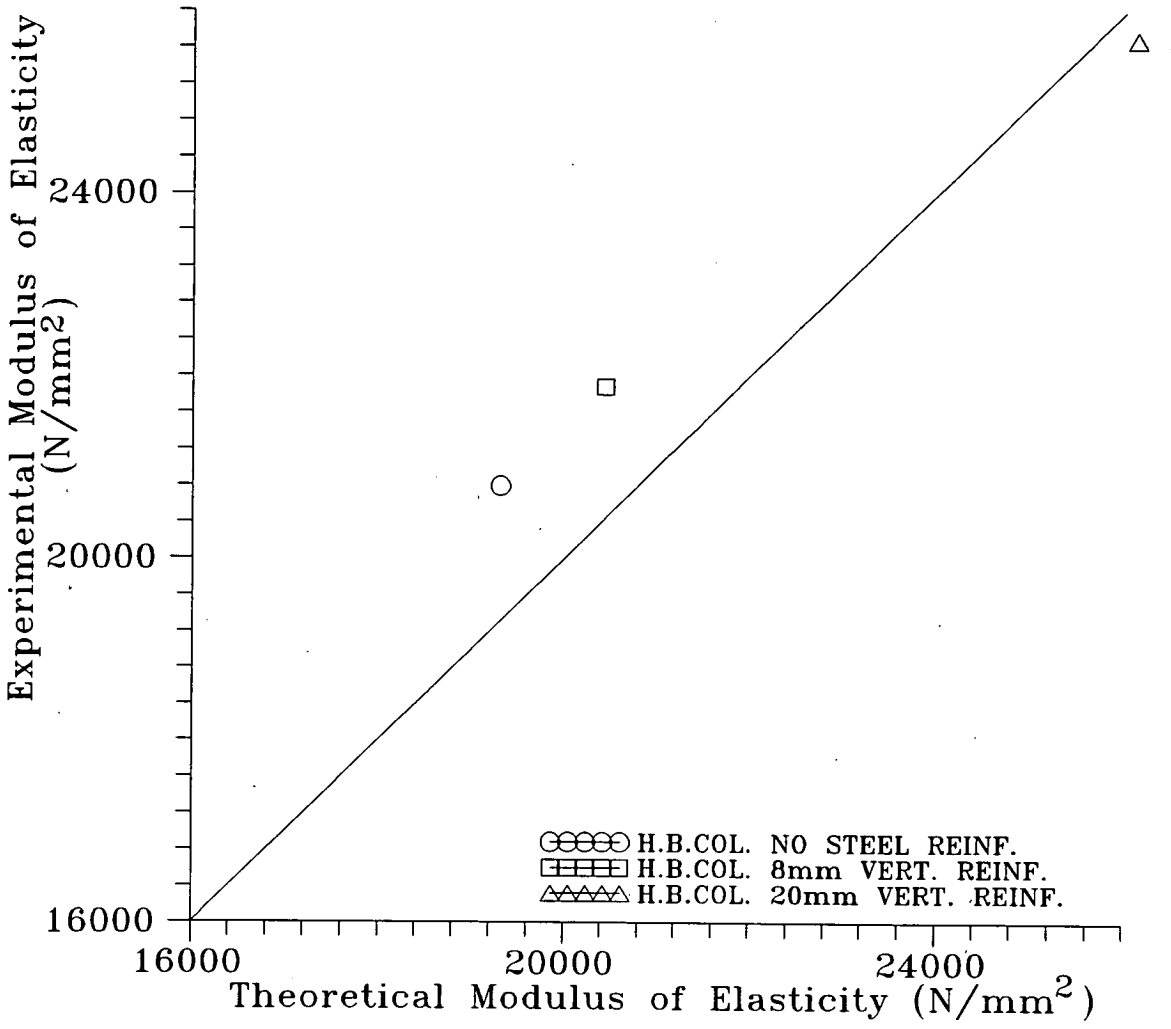


Fig. 6.14 Experimental and predicted modulus of elasticity for half-block columns

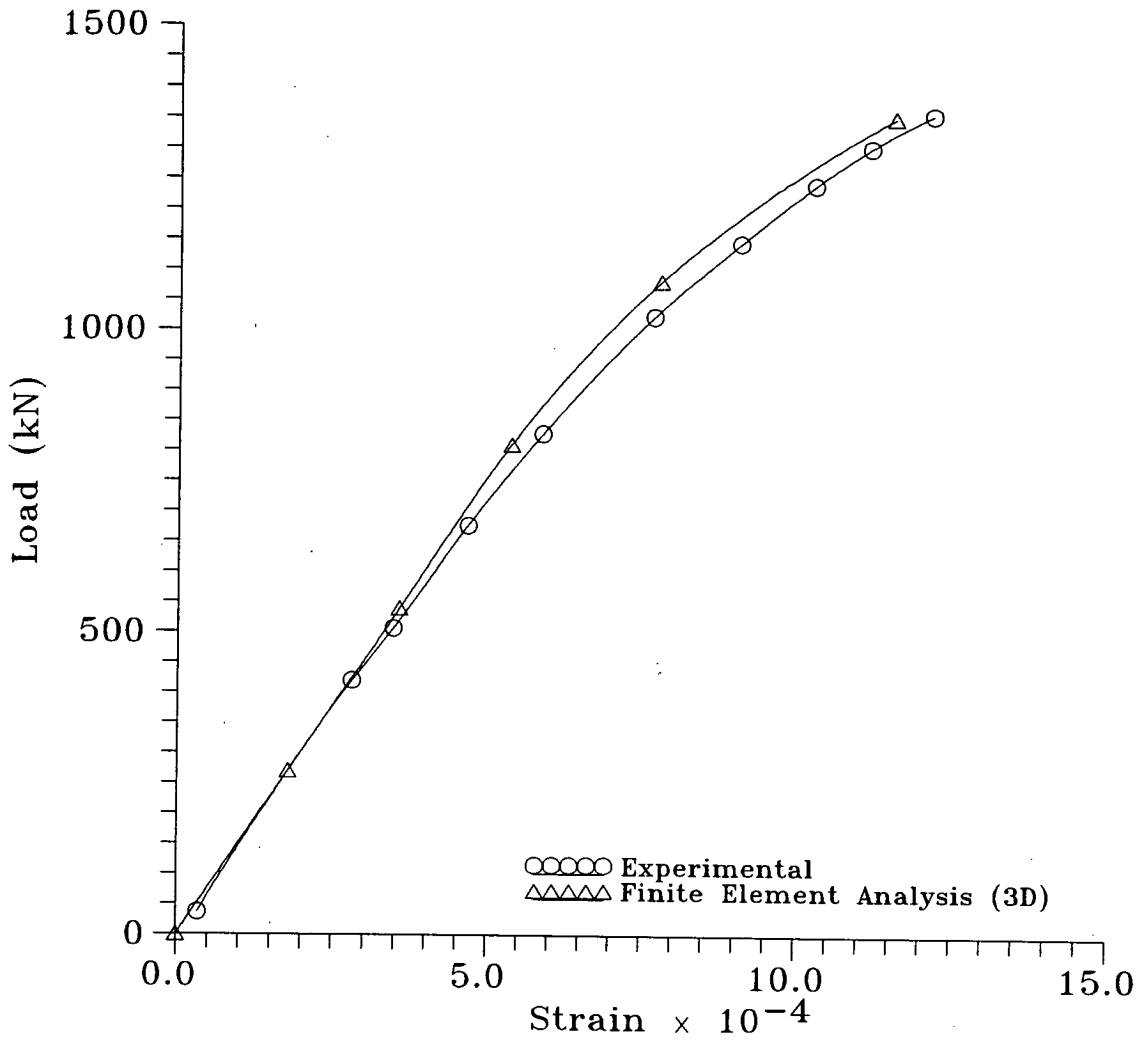


Fig. 6.15 Theoretical and experimental results for the FCA (10 mm) column

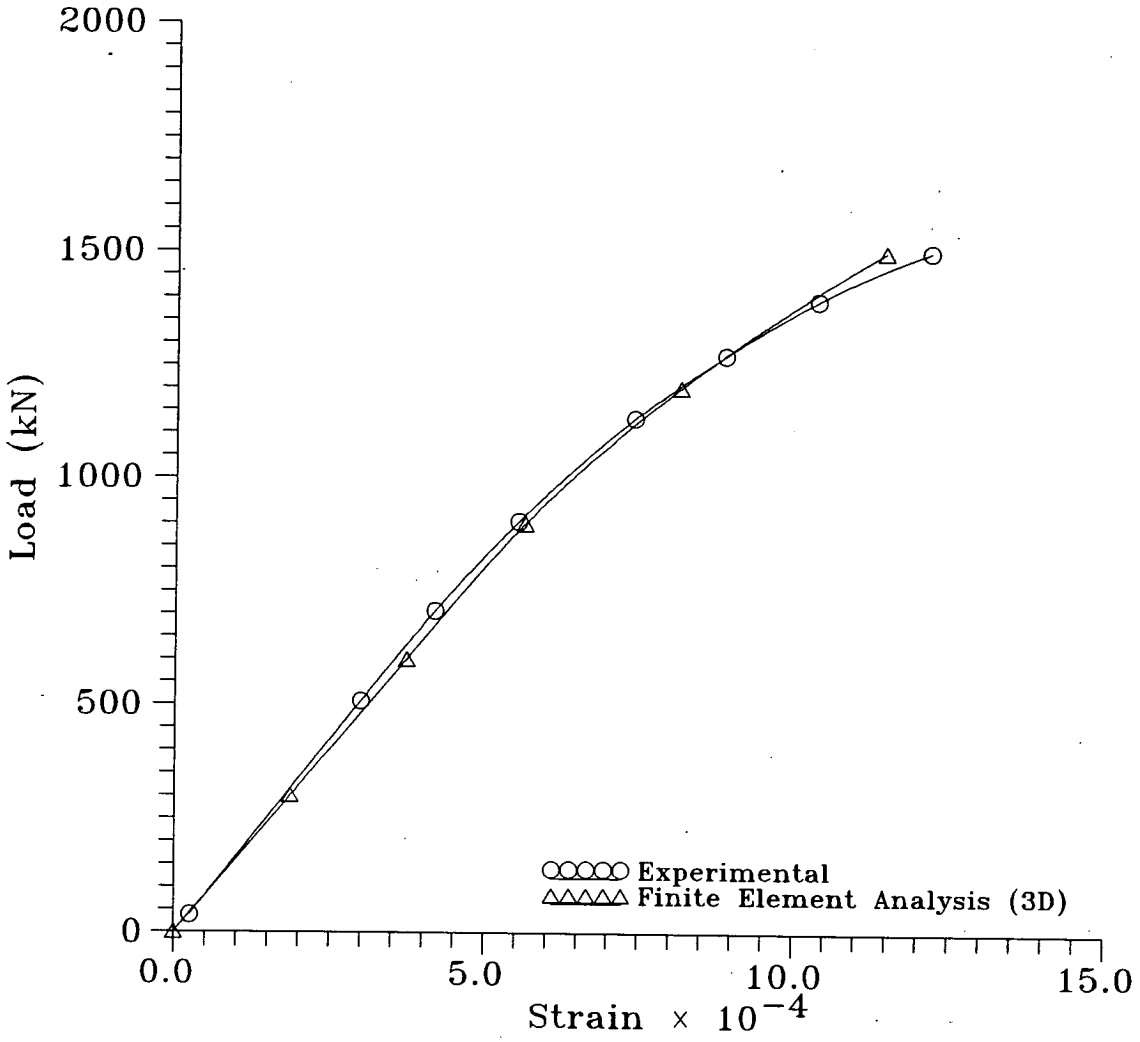


Fig. 6.16 Theoretical and experimental results for the FCA (20 mm) column

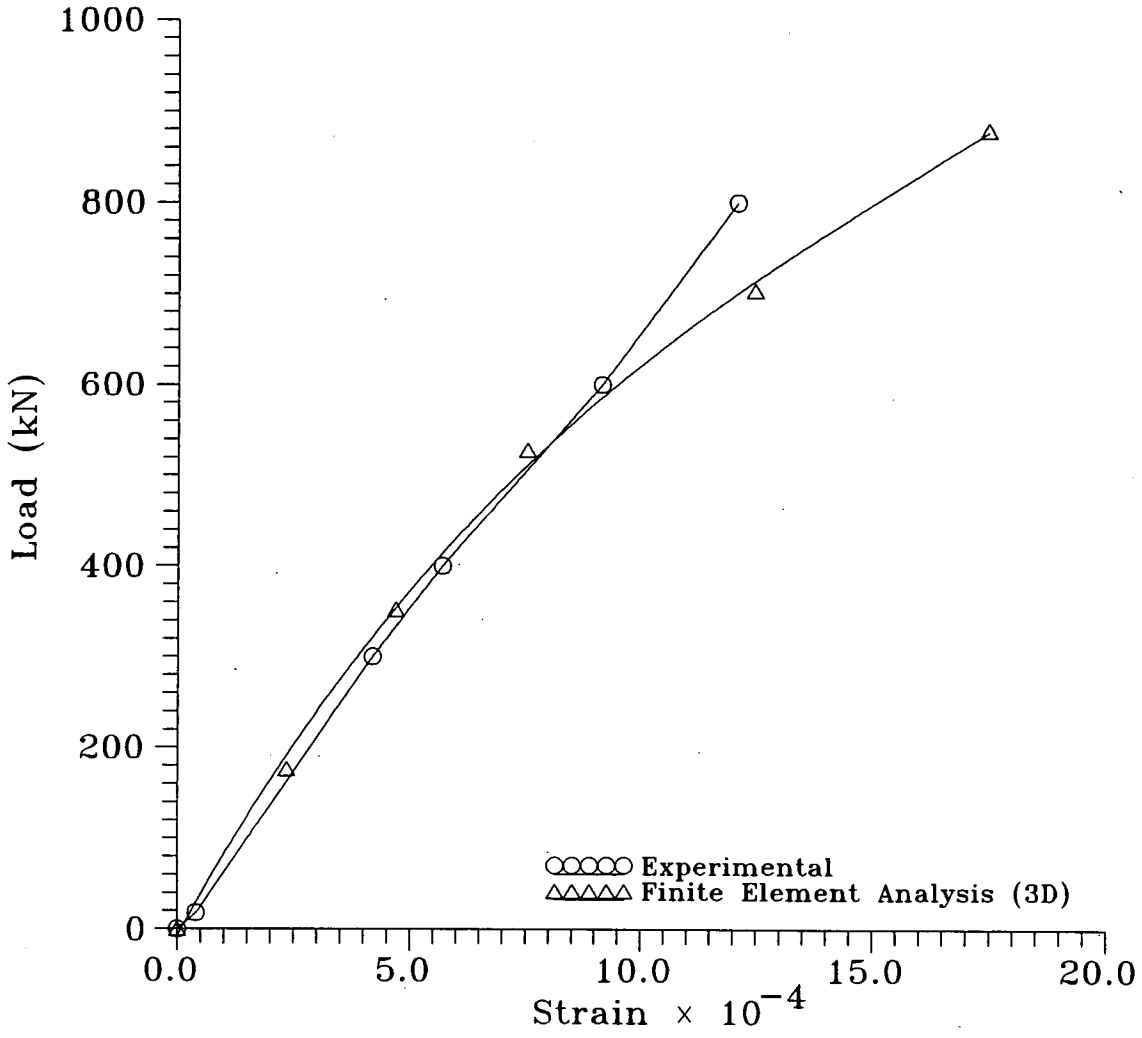


Fig. 6.17 Theoretical and experimental results for the HCA (8 mm) column

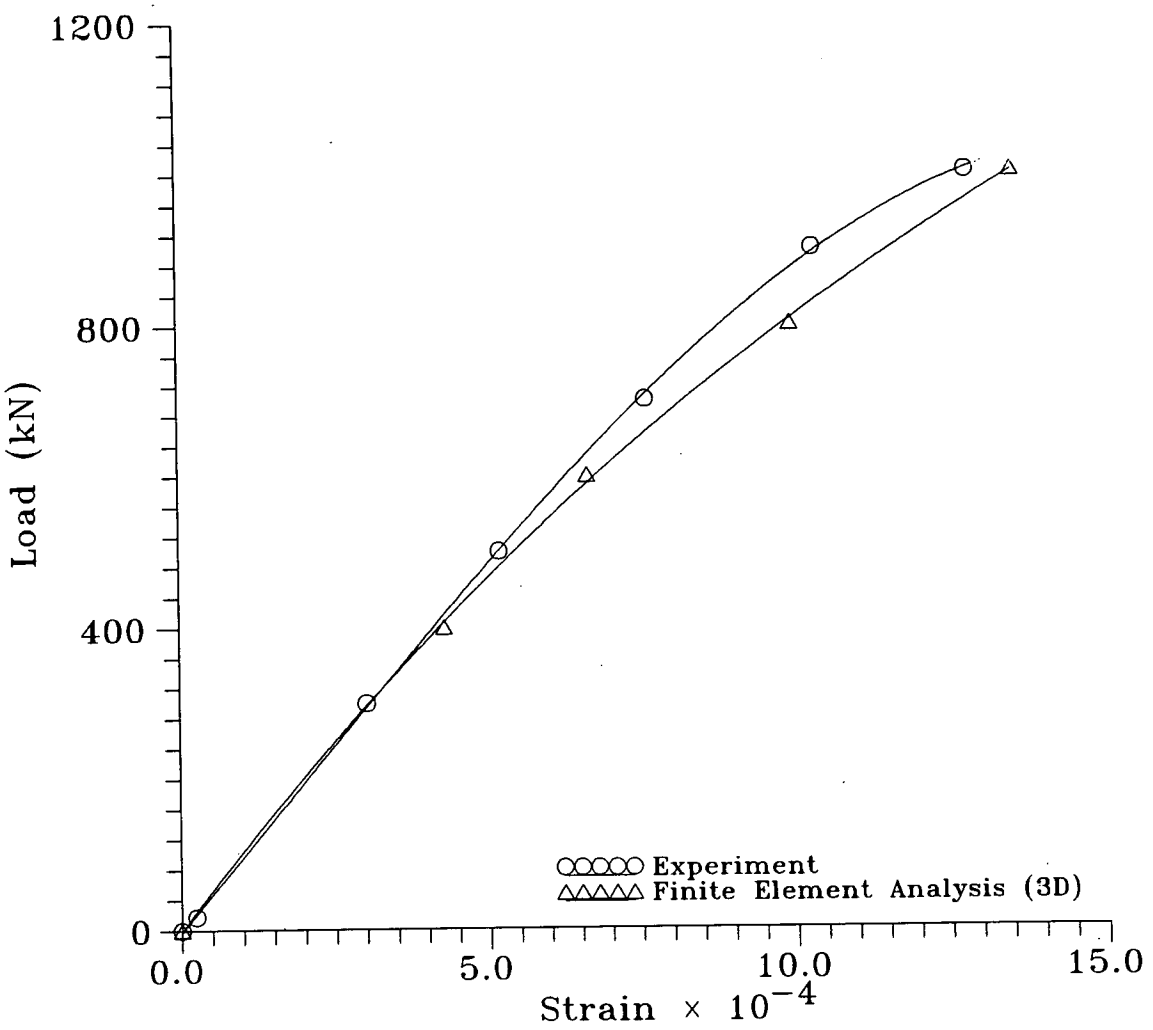


Fig. 6.18 Theoretical and experimental results for the HCA (20 mm) column

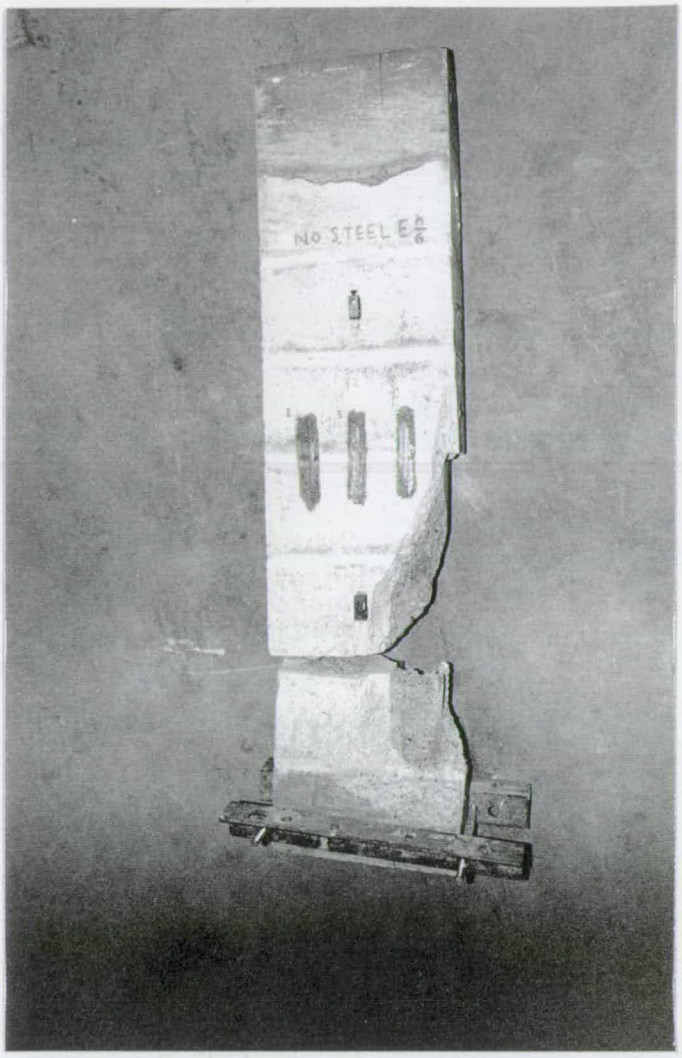


Fig. 6.19 **Typical mode of failure for an unreinforced full-block masonry column compressed with an eccentricity of t/6**

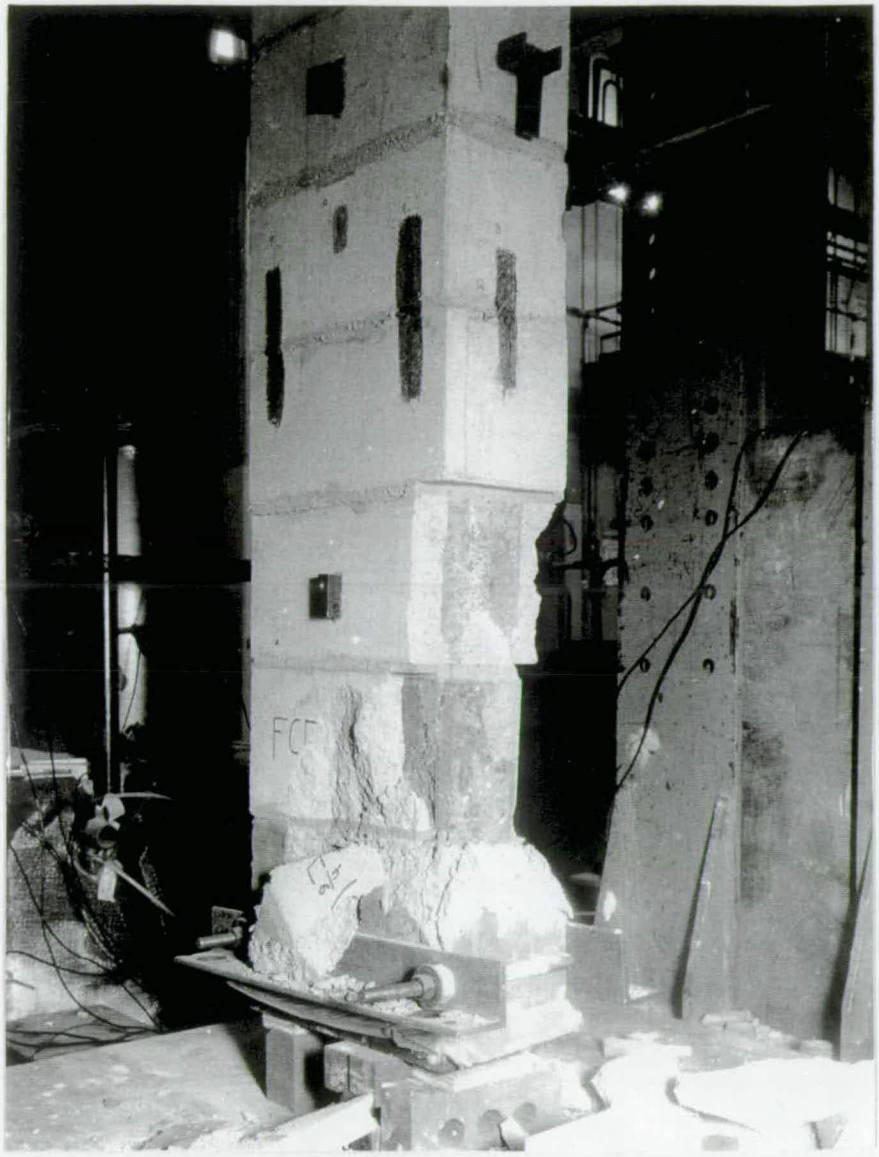


Fig. 6.20 Mode of failure for the $FCE_{t/6}$ (20 mm) column

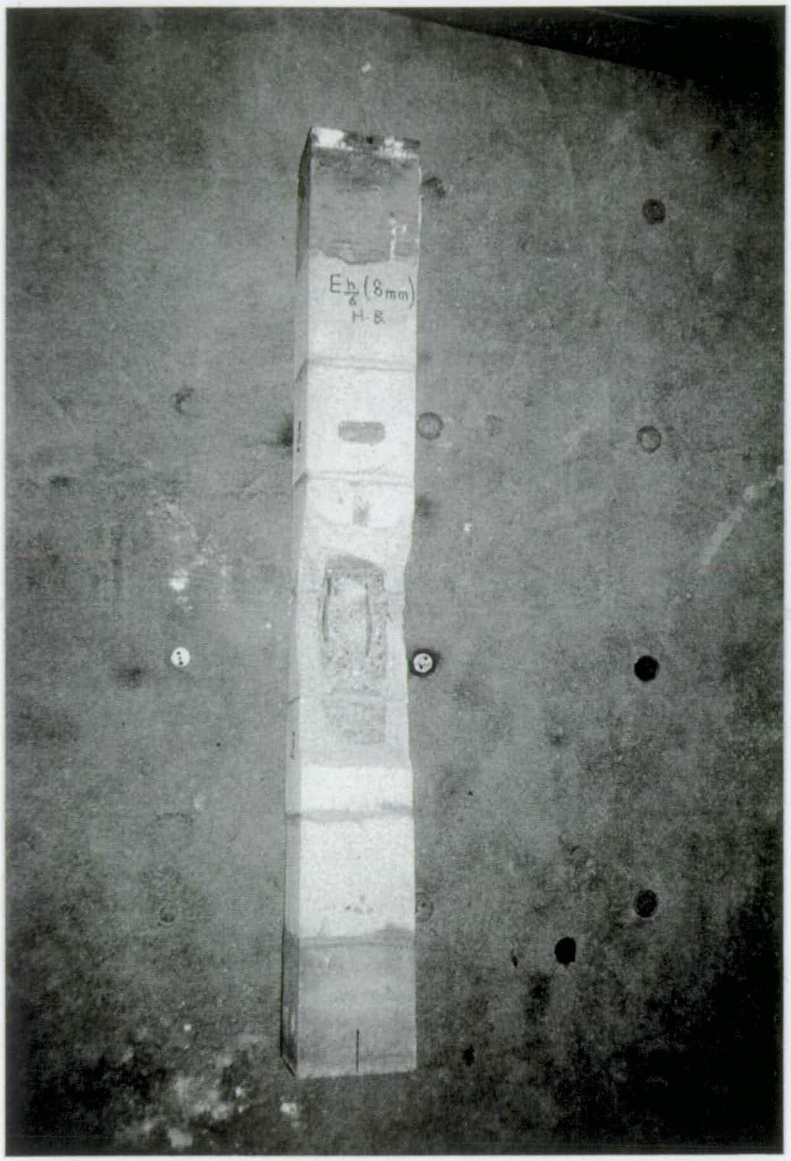


Fig. 6.21 Mode of failure for the $HCE_{t/6}$ (8 mm) column

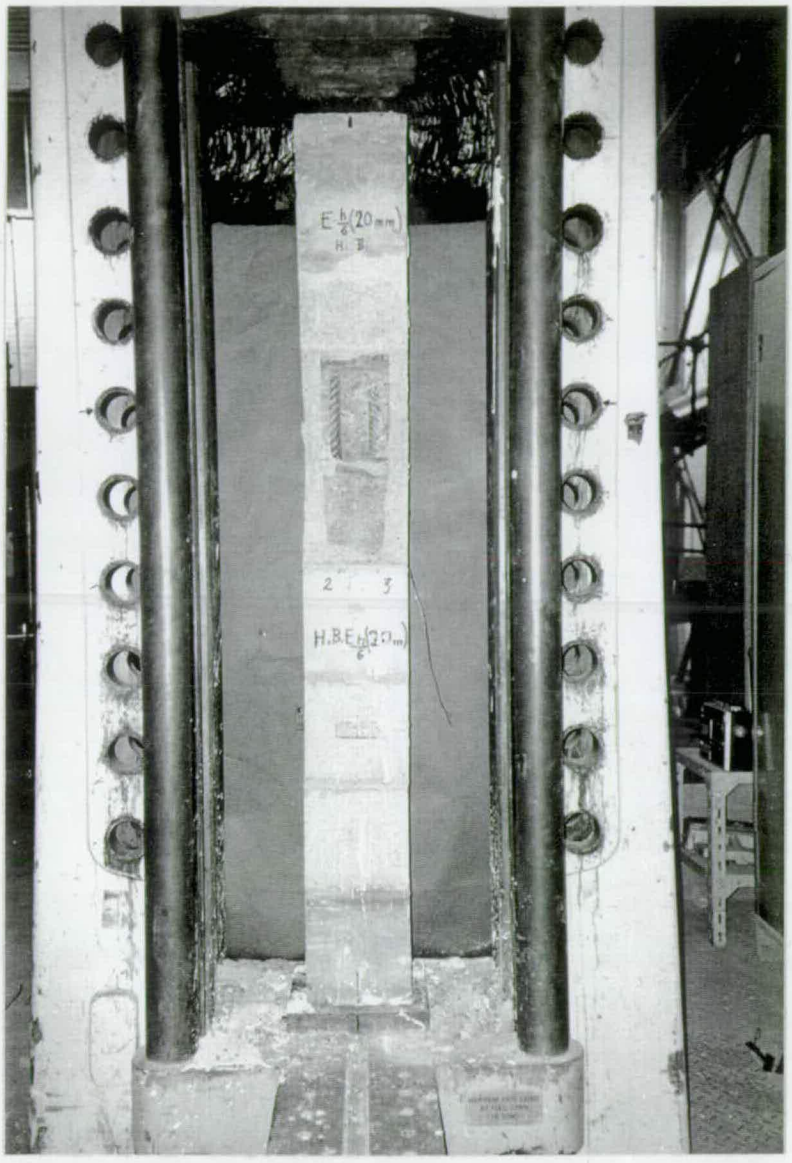


Fig. 6.22 Mode of failure for the $HCE_{t/6}$ (20 mm) column

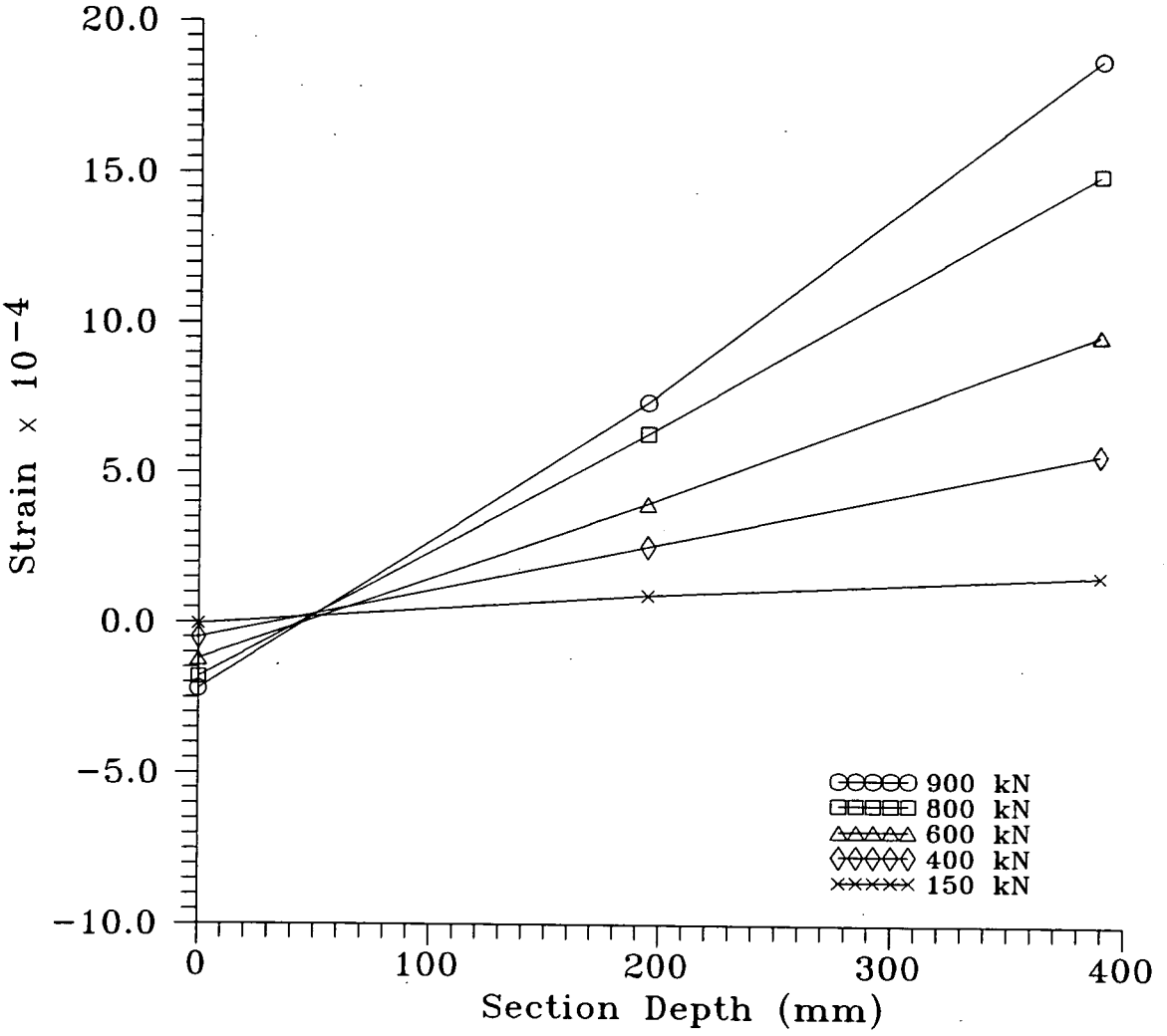


Fig. 6.23 Strain distribution for the $FCE_{t/6}$ (No Steel) column

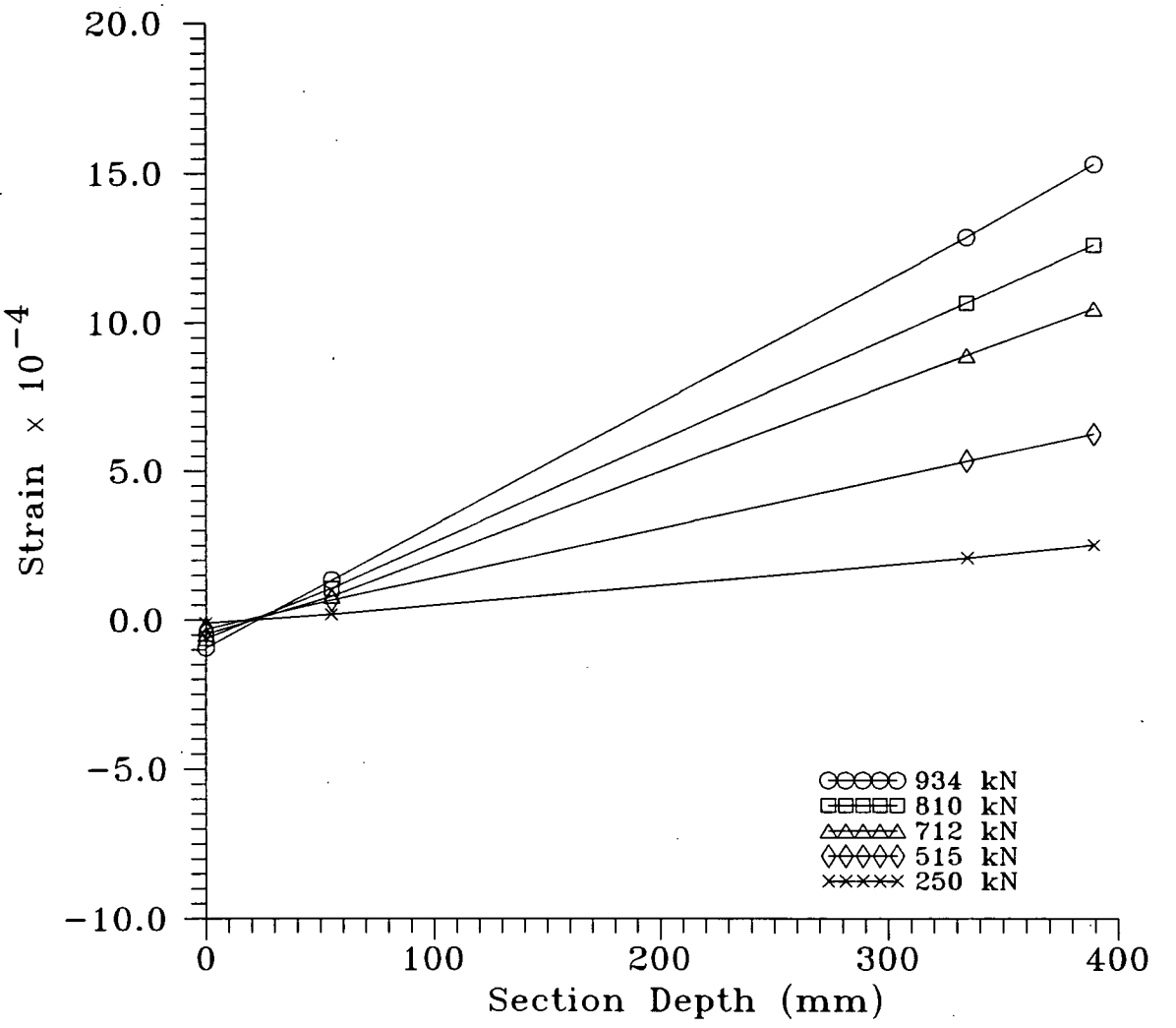


Fig. 6.24 Strain distribution across the $FCE_{t/6}$ (10 mm) column cross-section

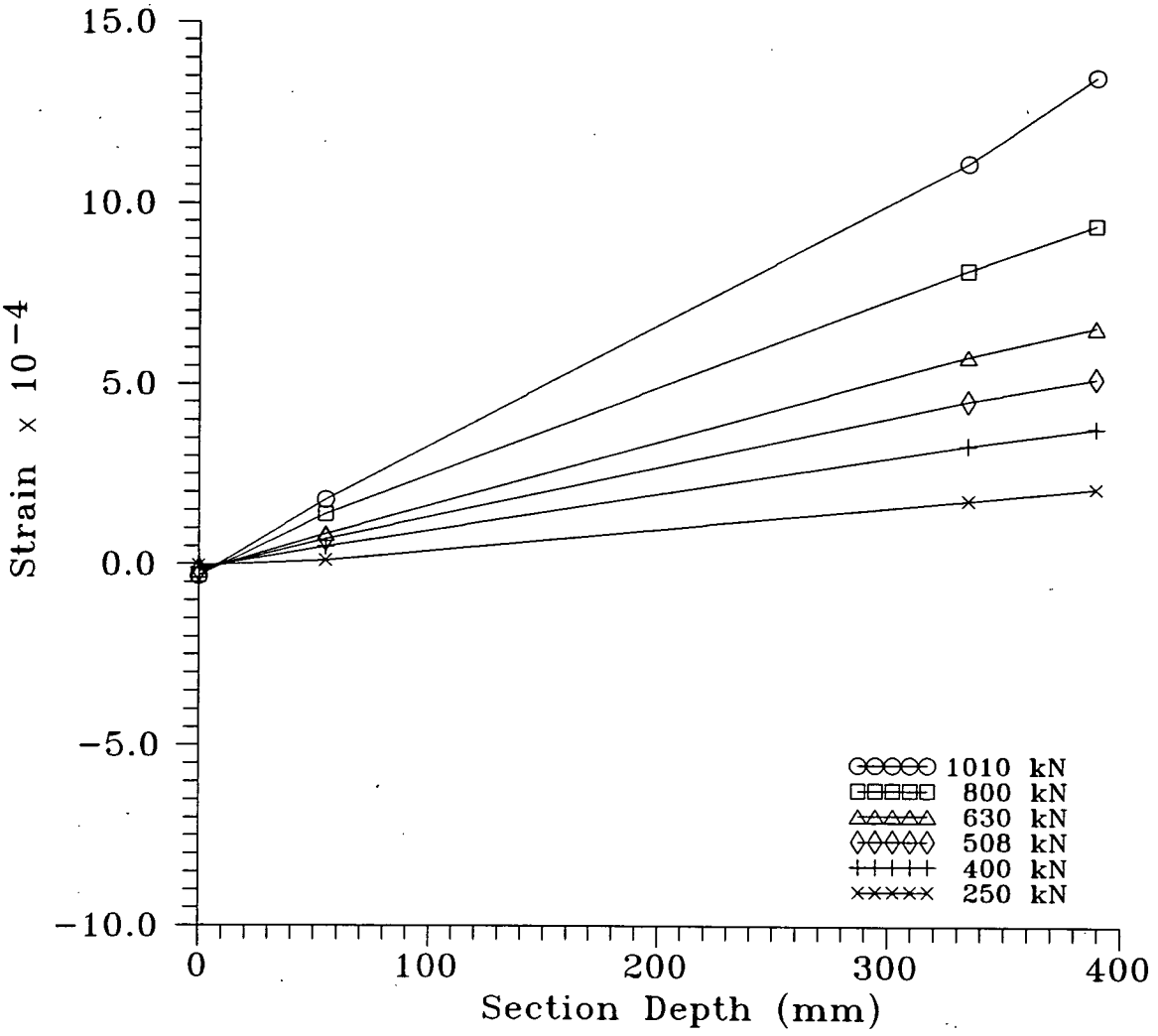


Fig. 6.25 Strain distribution across the $FCE_{t/6}$ (20 mm) column cross-section

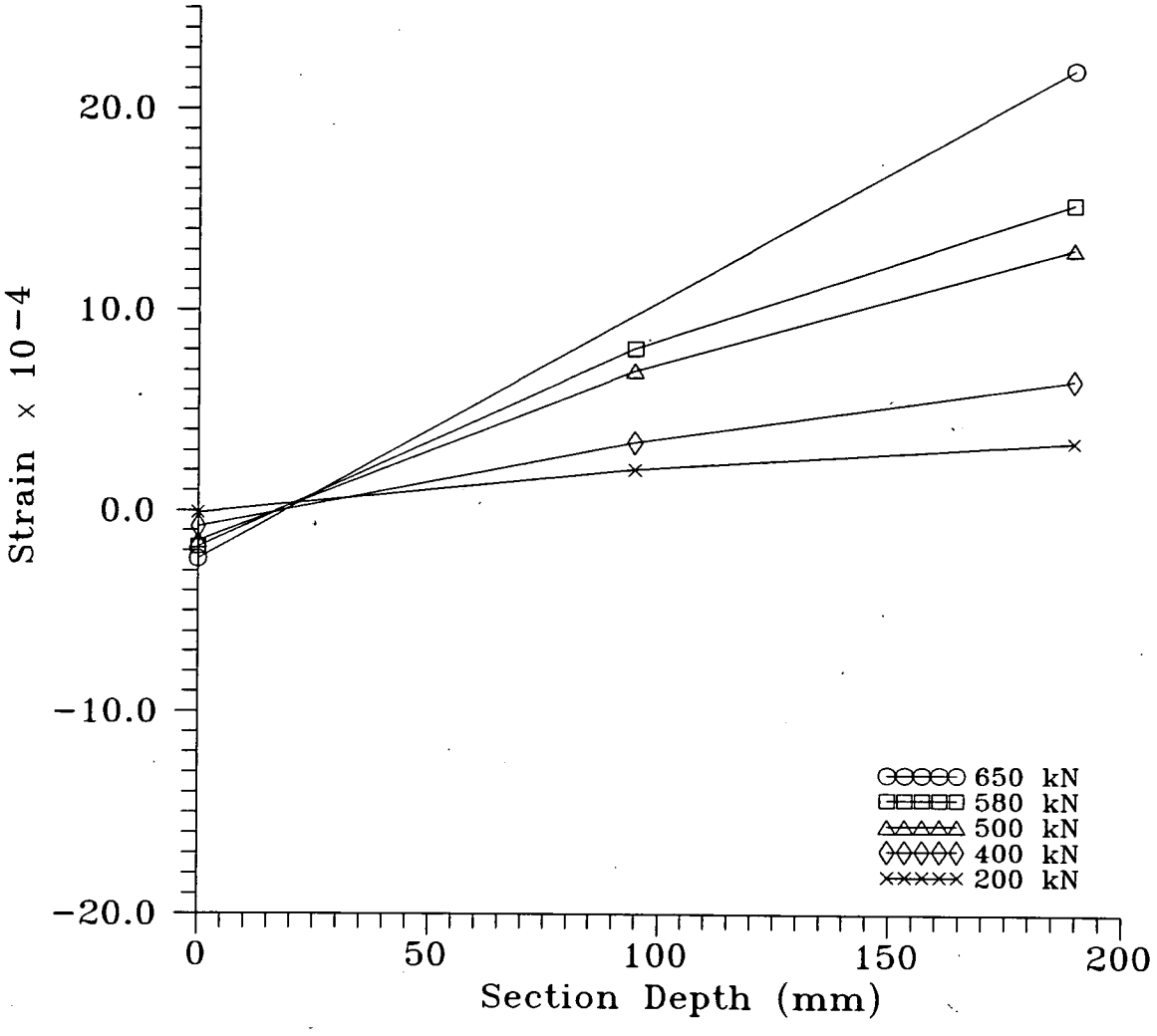


Fig. 6.26 Strain distribution for the $HCE_{t/6}$ (No Steel) column

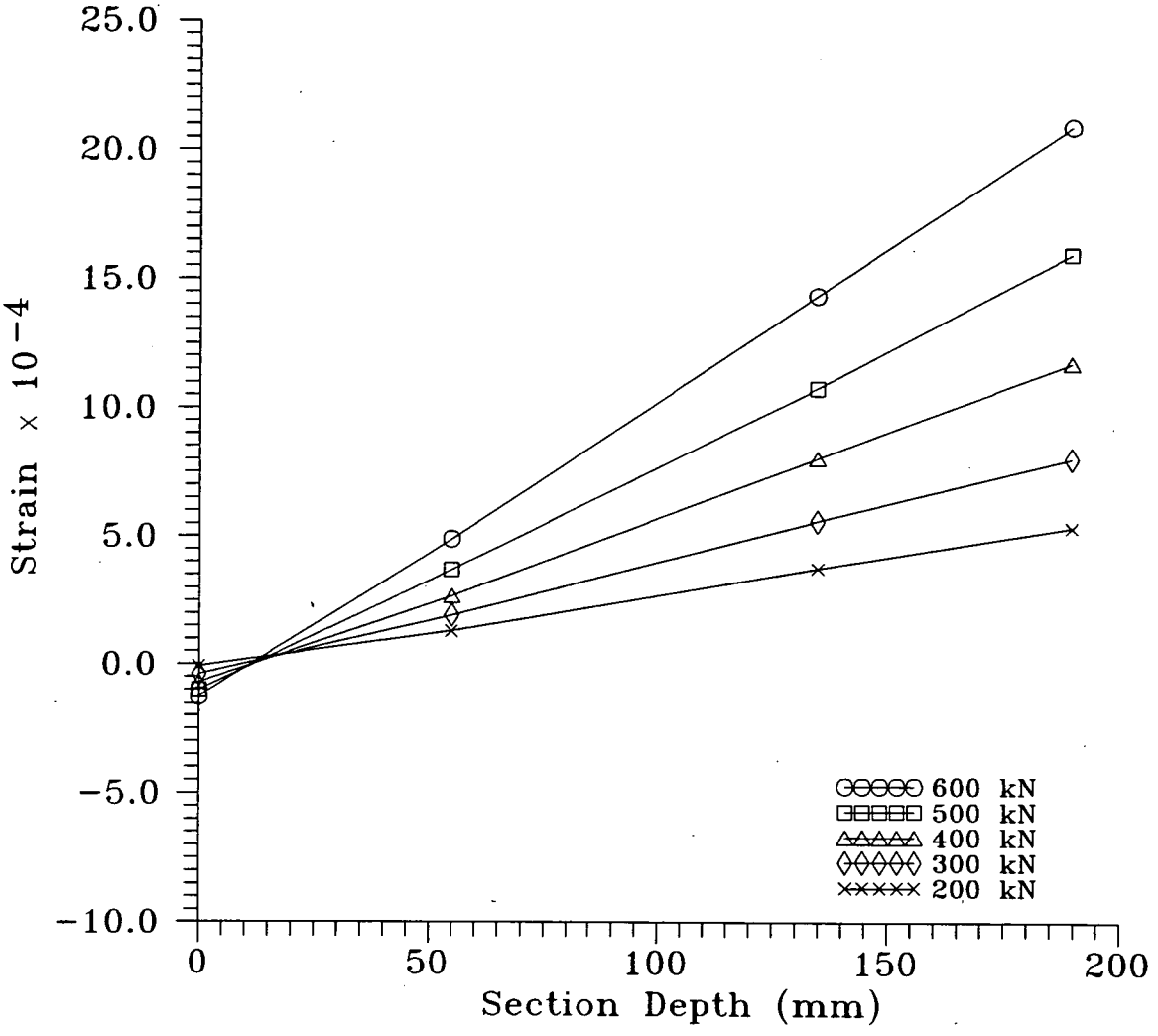


Fig. 6.27 Strain distribution across the $HCE_{t/6}$ (8 mm) column cross-section

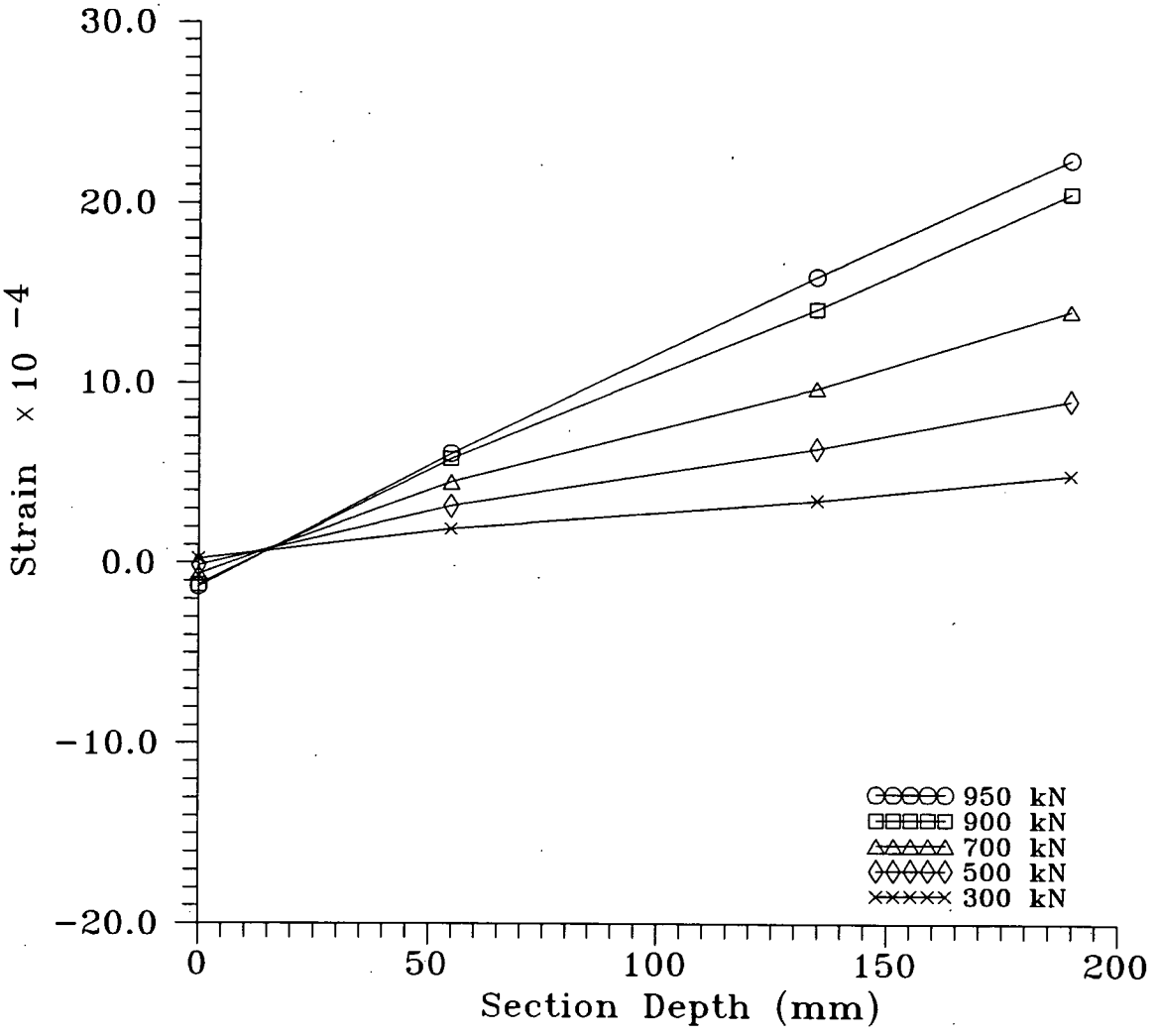


Fig. 6.28 Strain distribution across the $HCE_{t/6}$ (20 mm) column cross-section

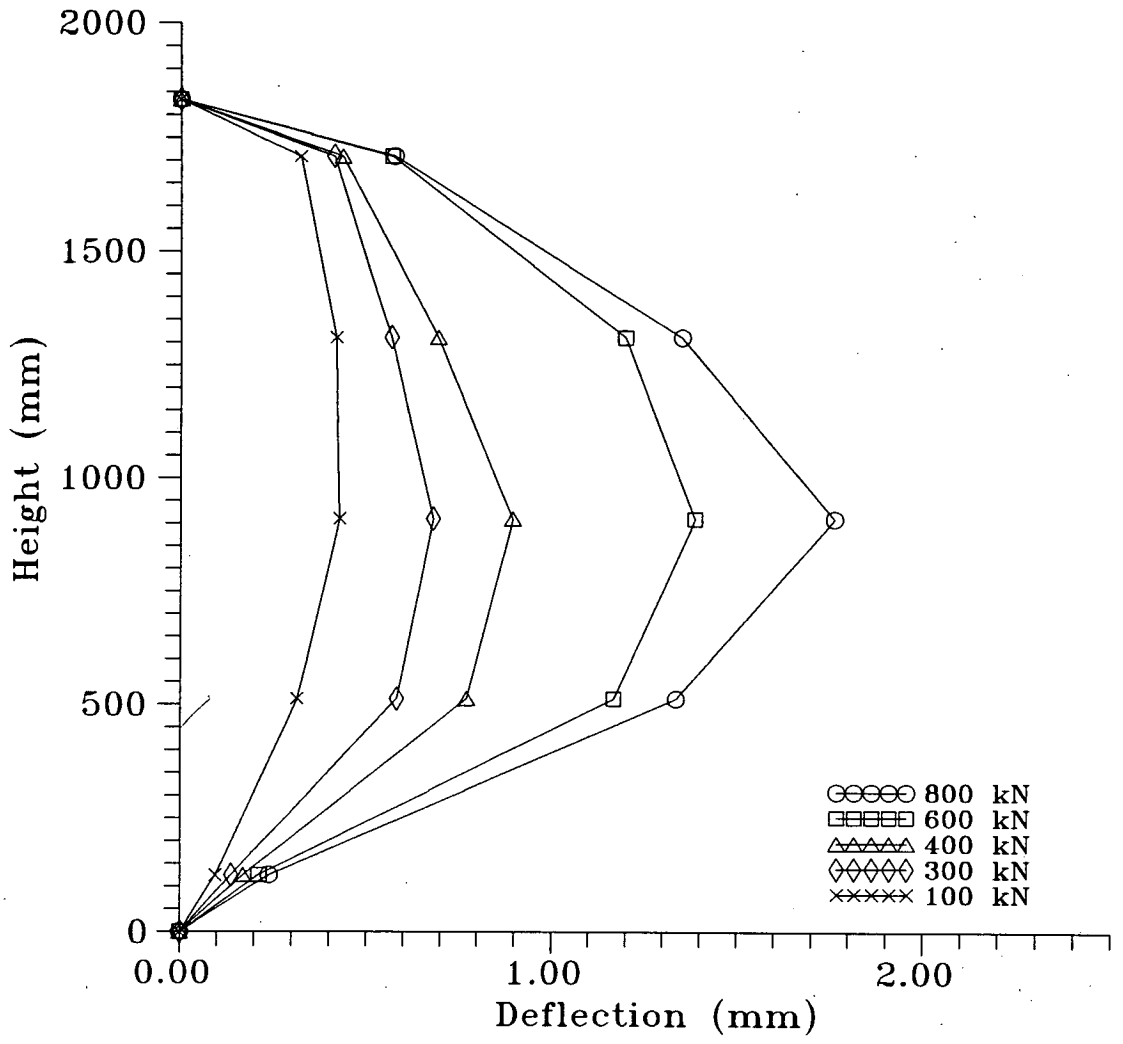


Fig. 6.29 Load deflection relationship for the $FCE_{t/6}$ (No Steel) column

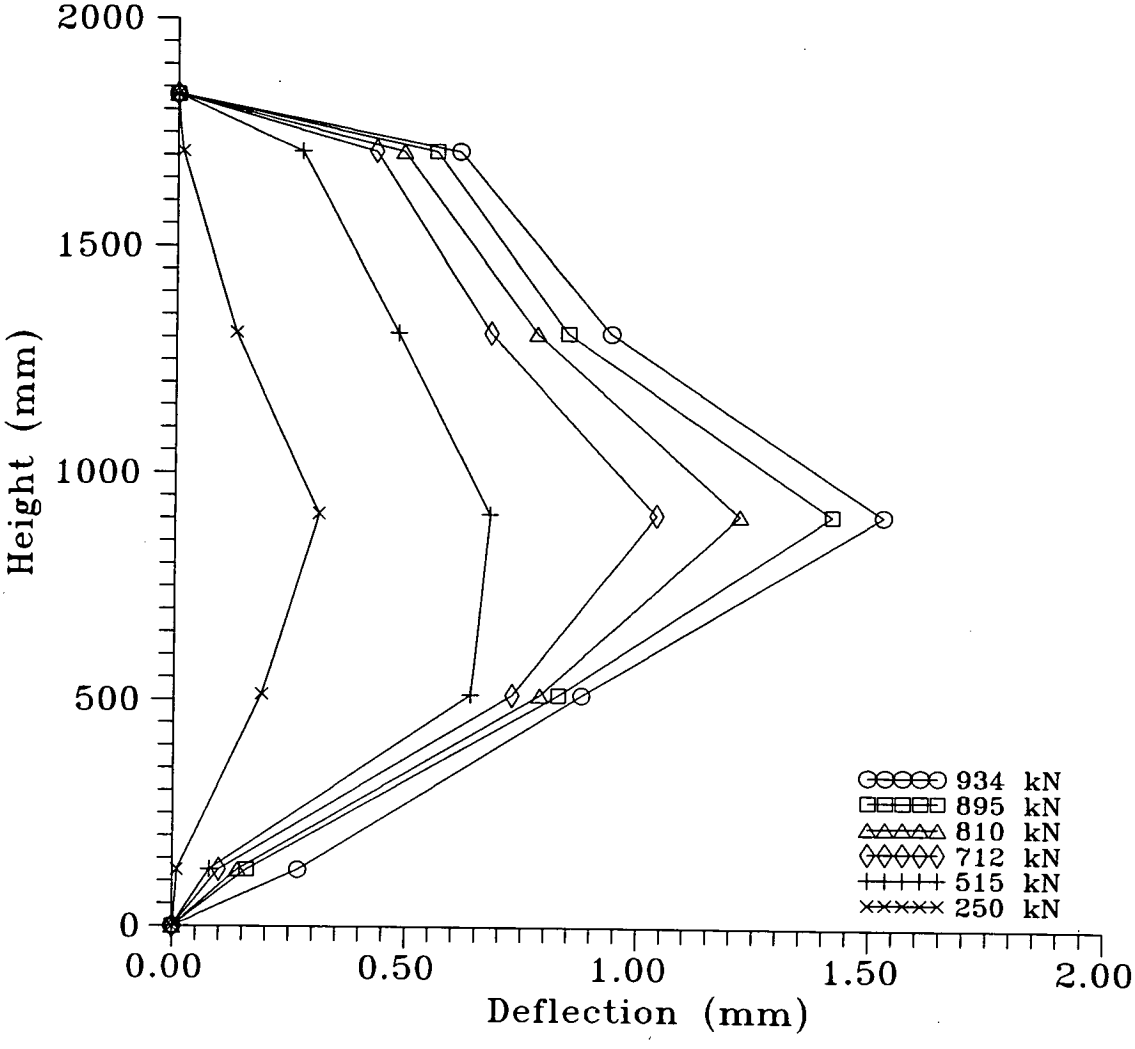


Fig. 6.30 Load-deflection relationship for the $FCE_{t/6}$ (10 mm) column

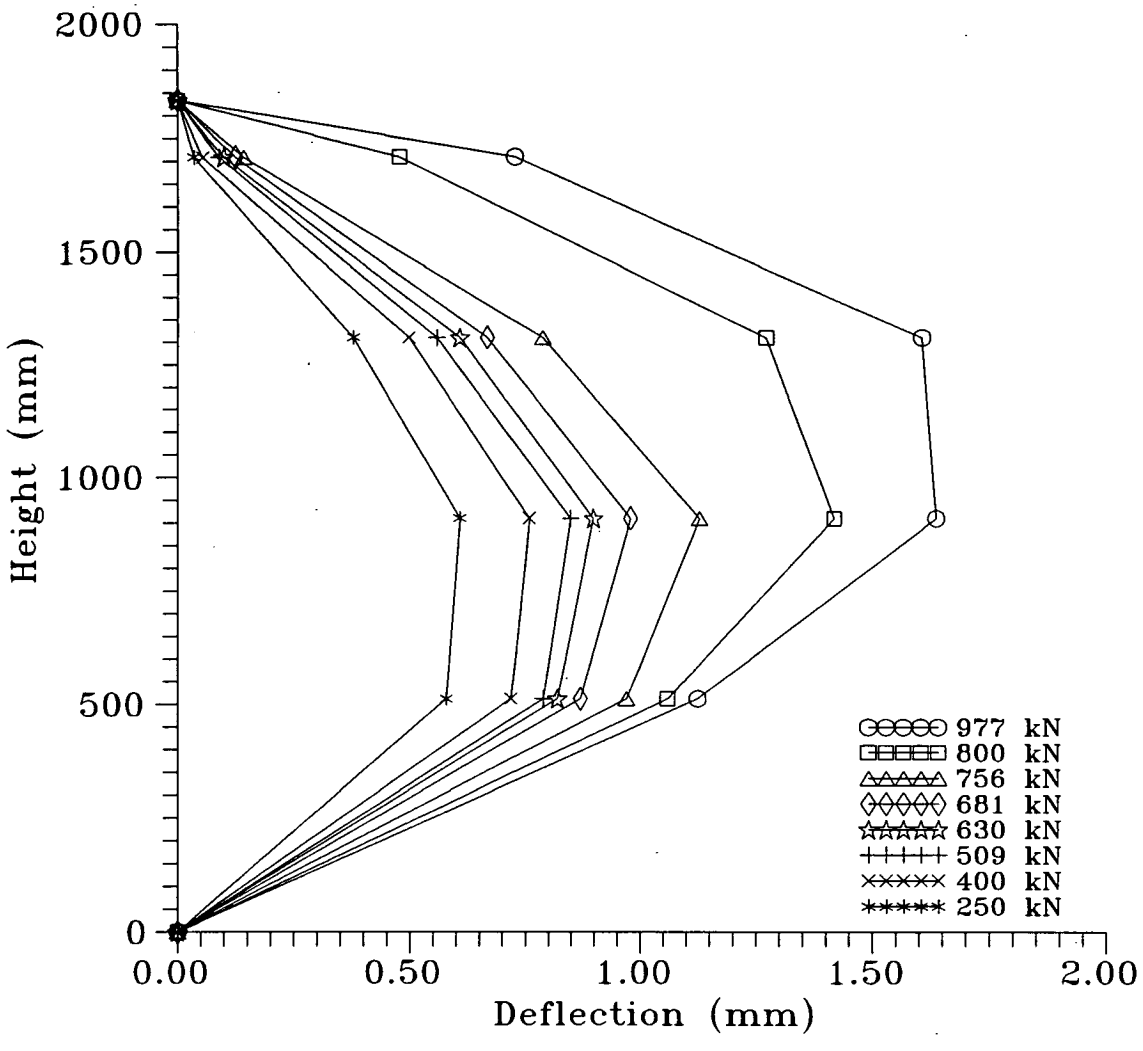


Fig. 6.31 Load–deflection relationship for the $FCE_{t/6}$ (20 mm) column

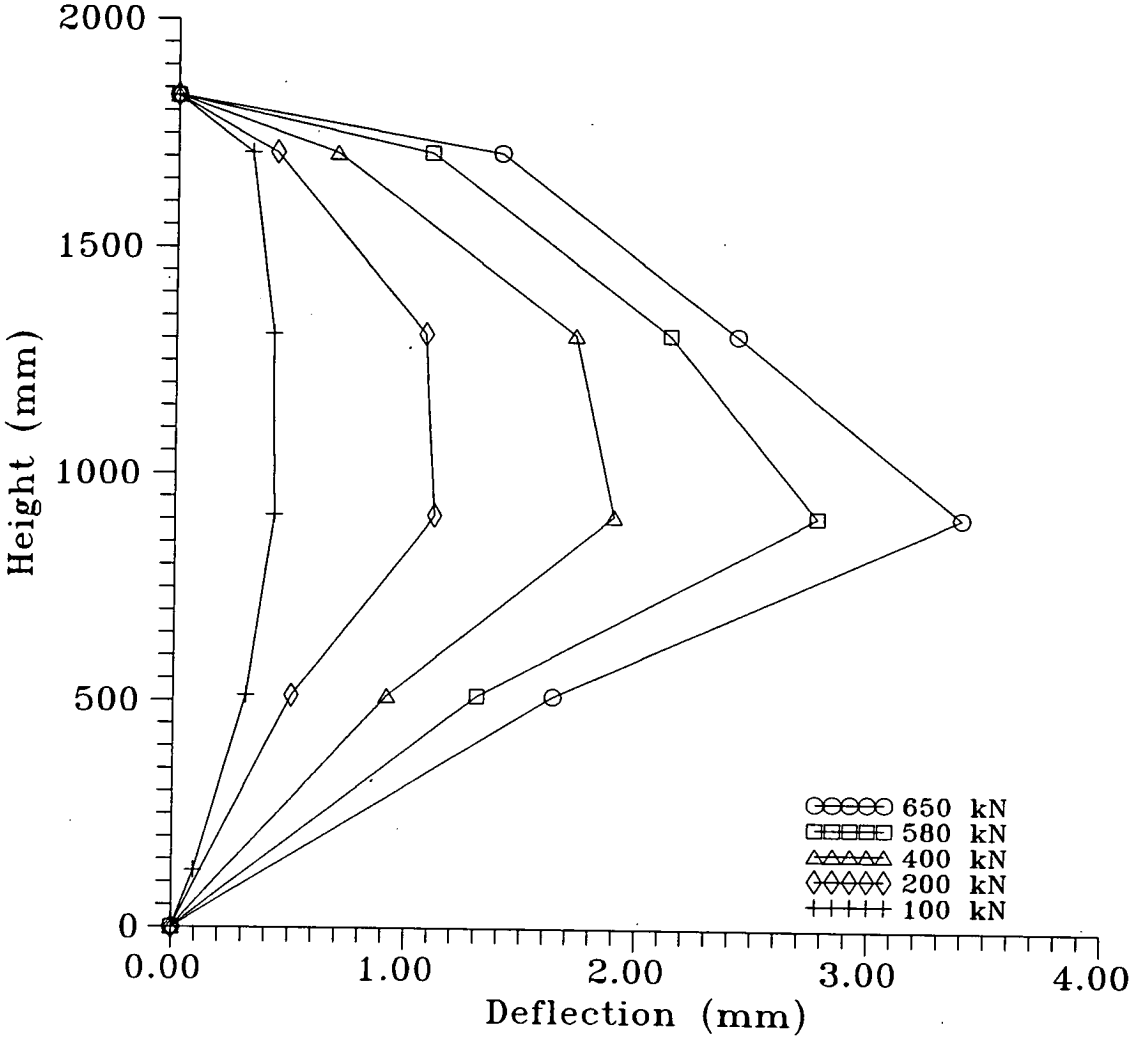


Fig. 6.32 Load–deflection relationship for the $HCE_{t/6}$ (No Steel) column

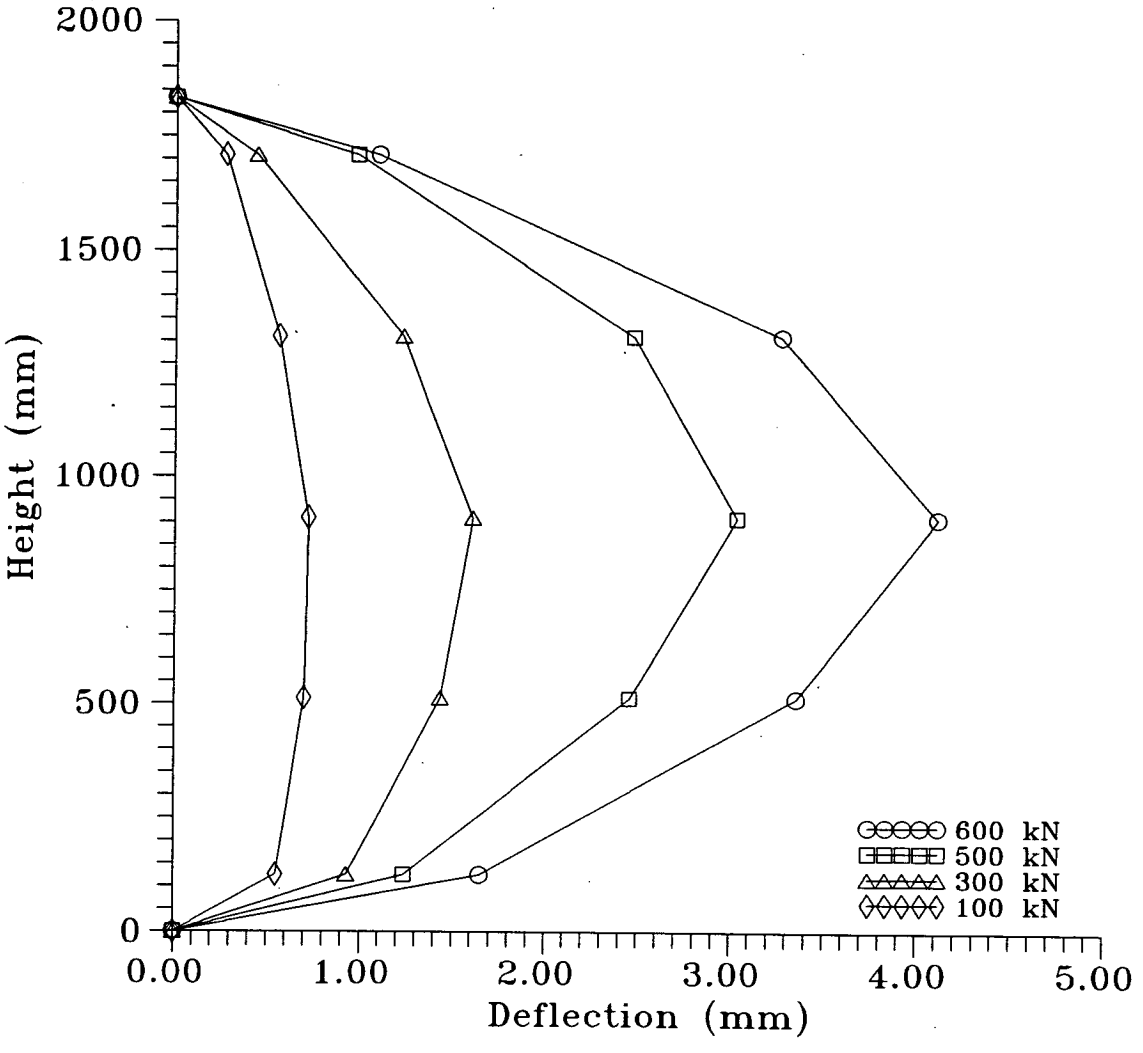


Fig. 6.33 Load–deflection relationship for the $HCE_{t/6}$ (8 mm) column

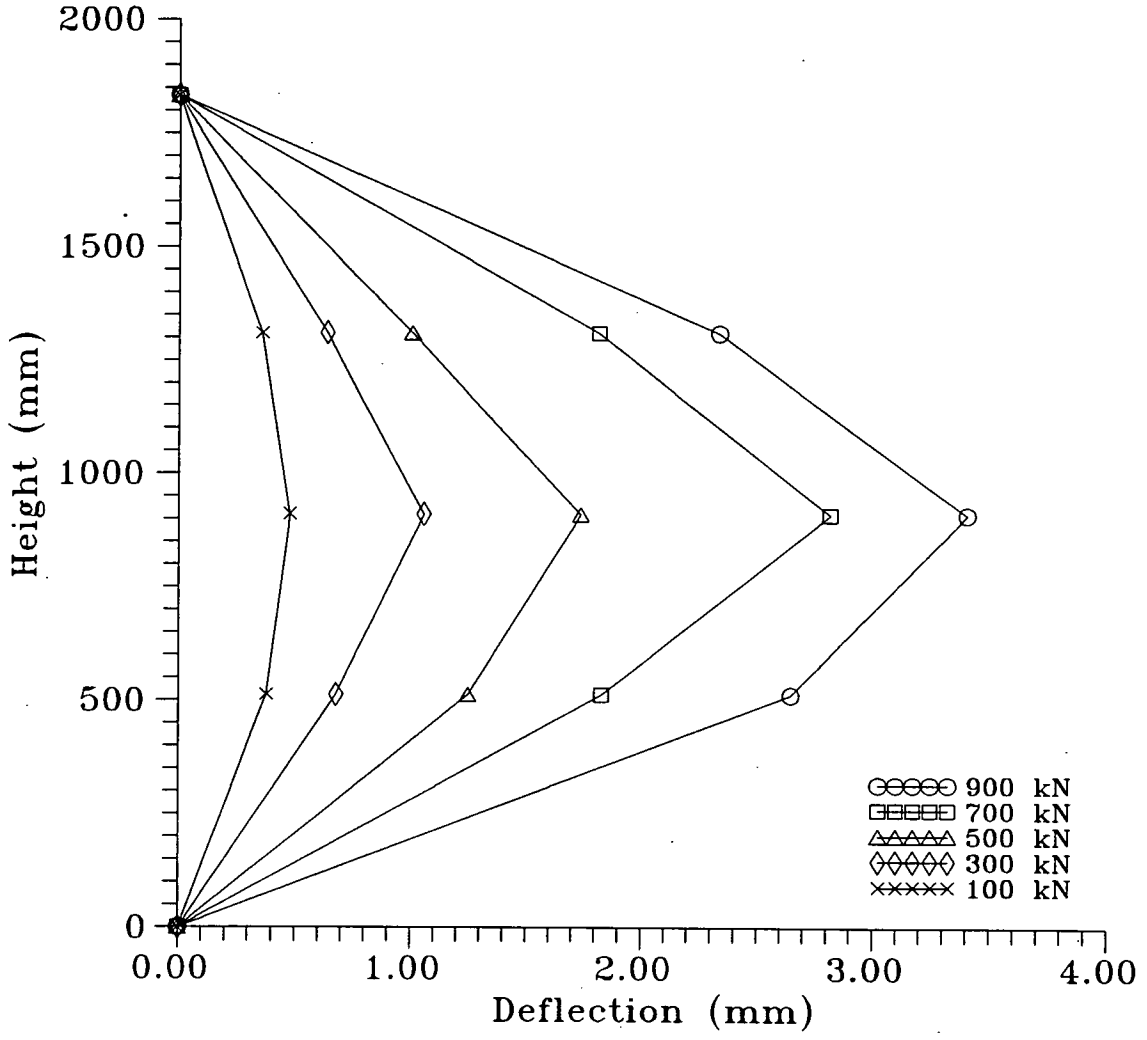


Fig. 6.34 Load–deflection relationship for the $HCE_{t/6}$ (20 mm)column

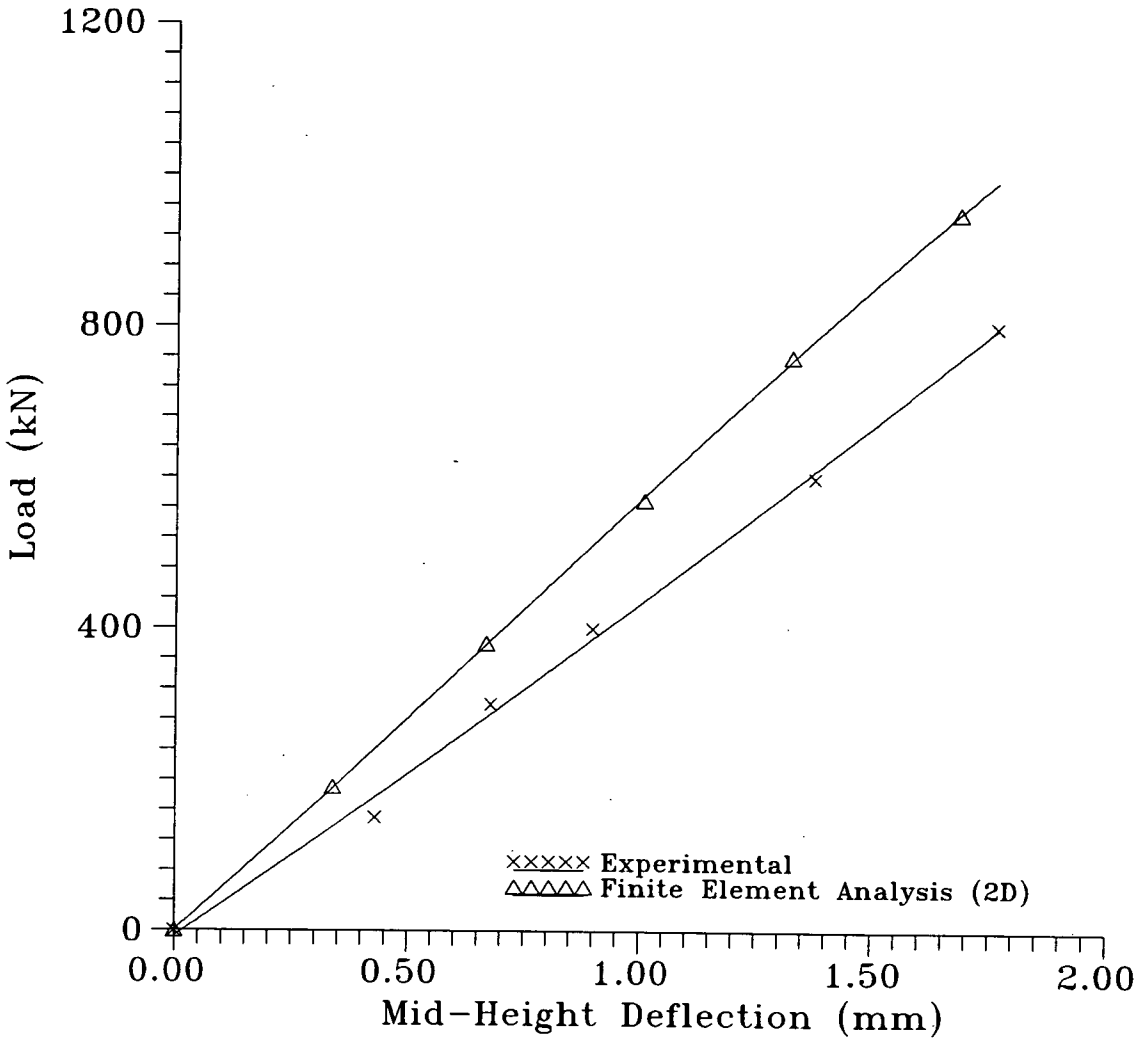


Fig. 6.35 Theoretical and experimental results for deflections at mid-height of column $FCE_{t/6}$ (No Steel)

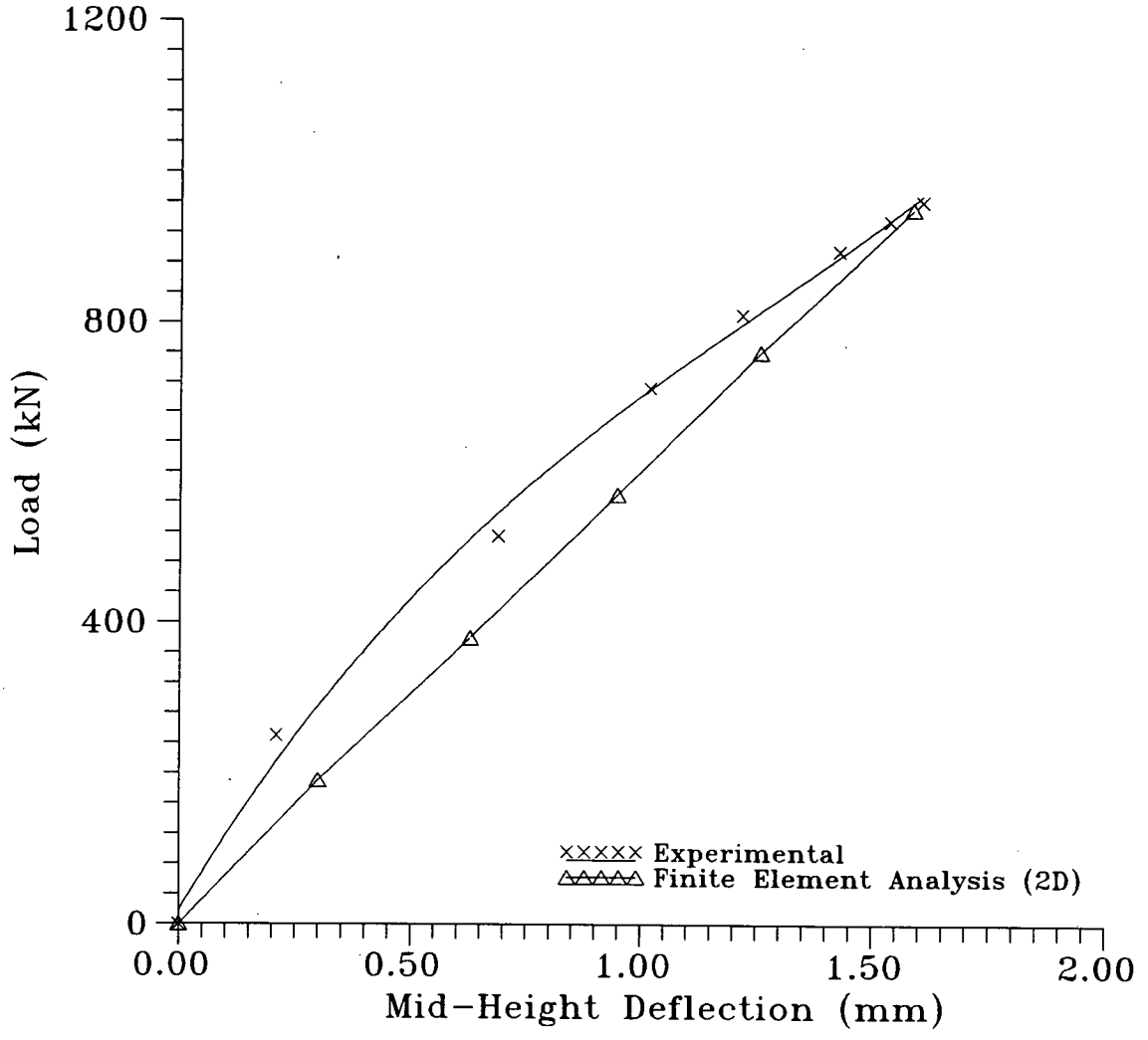


Fig. 6.36 Theoretical and experimental results for deflections at mid-height of column $FCE_{t/6}$ (10 mm)

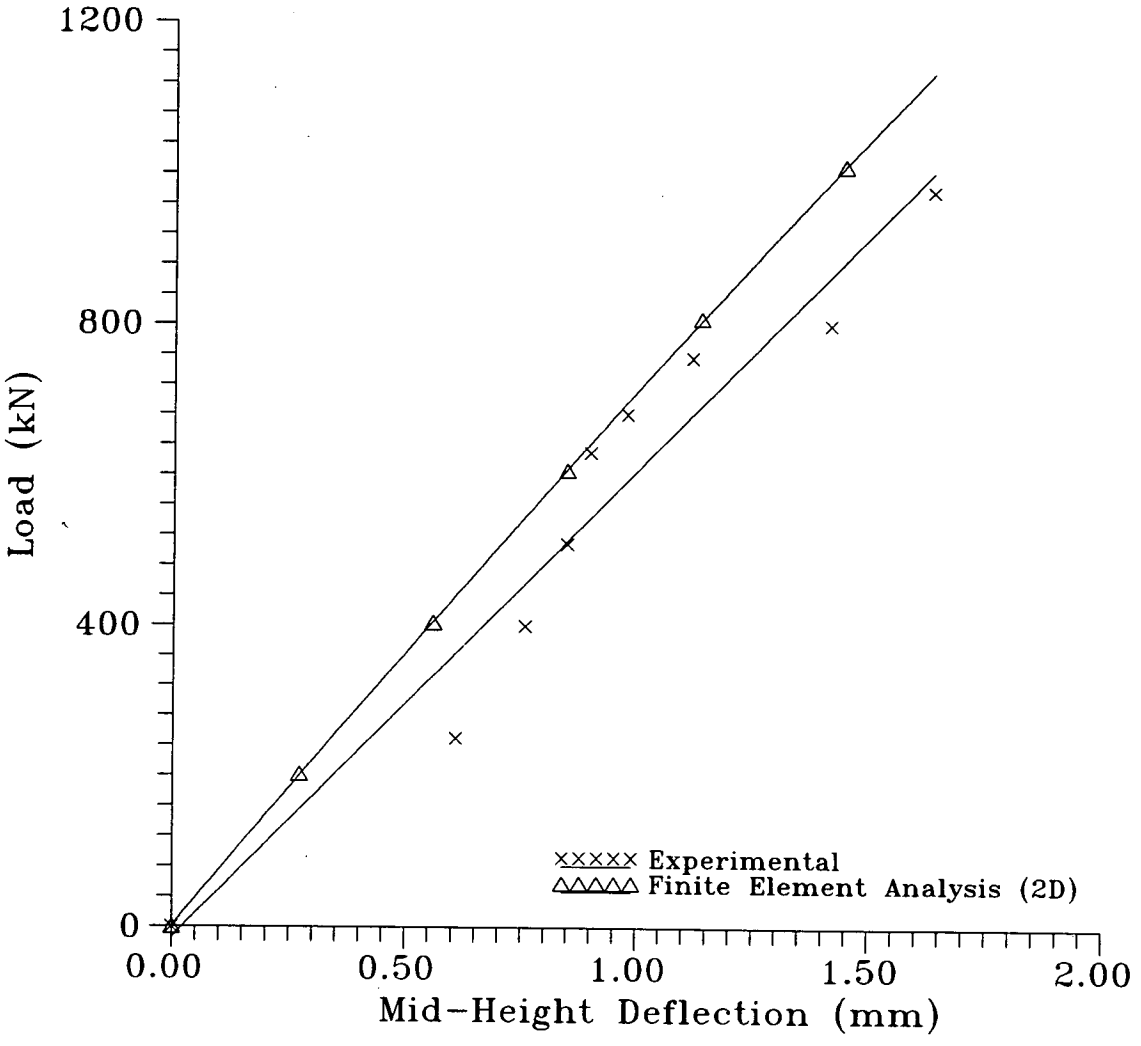


Fig. 6.37 Theoretical and experimental results for deflections at mid-height of column $FCE_{t/6}$ (20 mm)

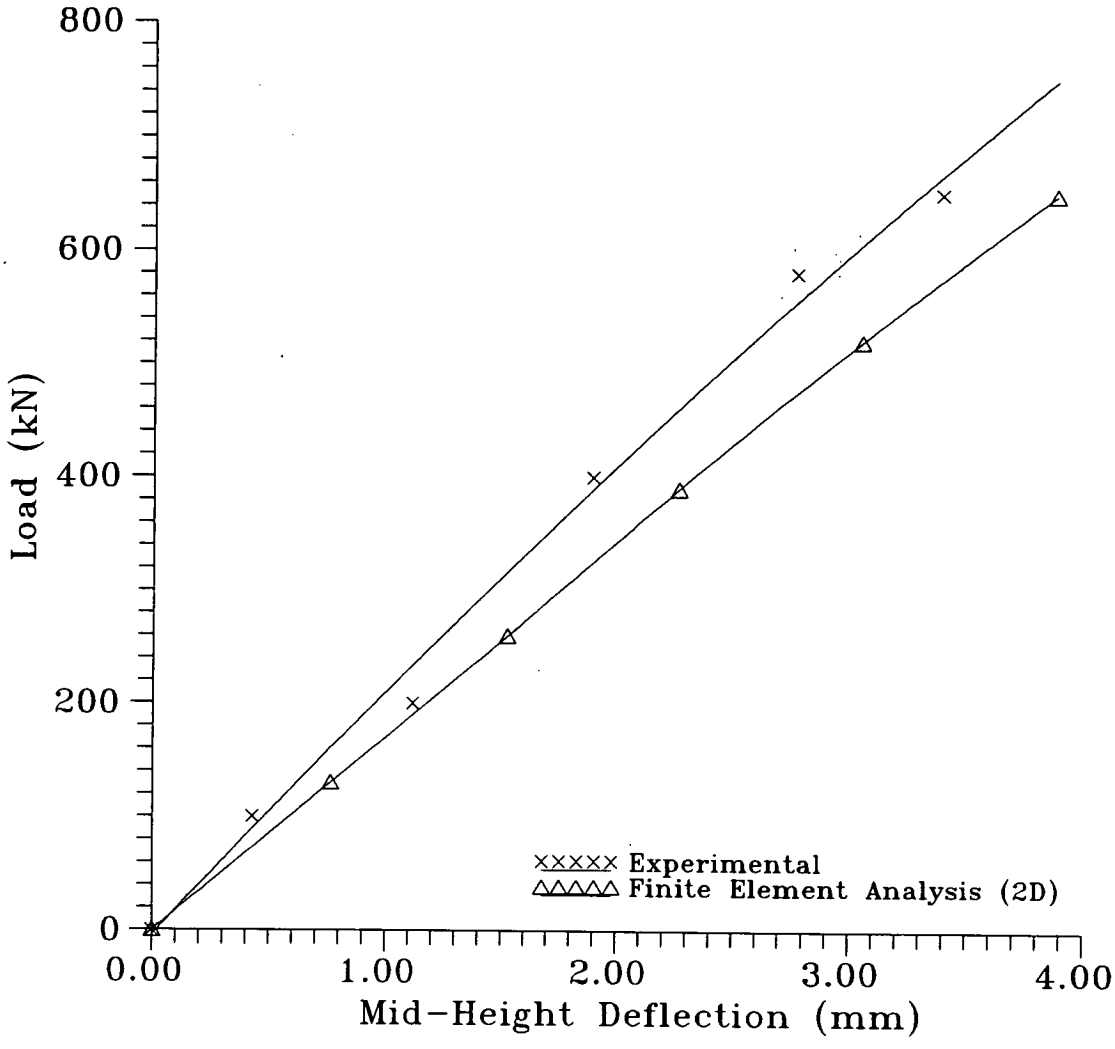


Fig. 6.38 Theoretical and experimental results for deflections at mid-height of column $HCE_{t/6}$ (No Steel)

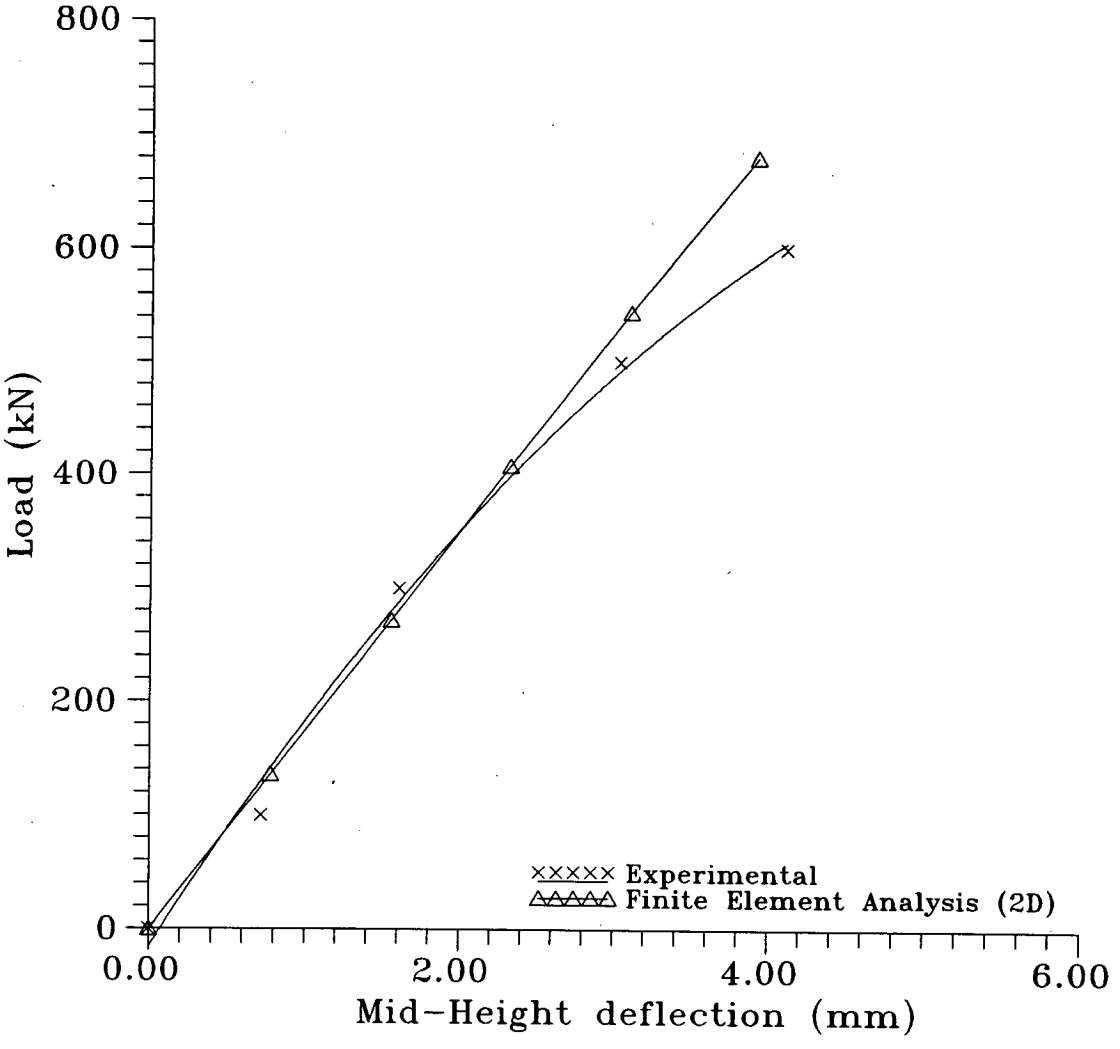


Fig. 6.39 Theoretical and experimental results for deflections at mid-height of column $HCE_{t/6}$ (8 mm)

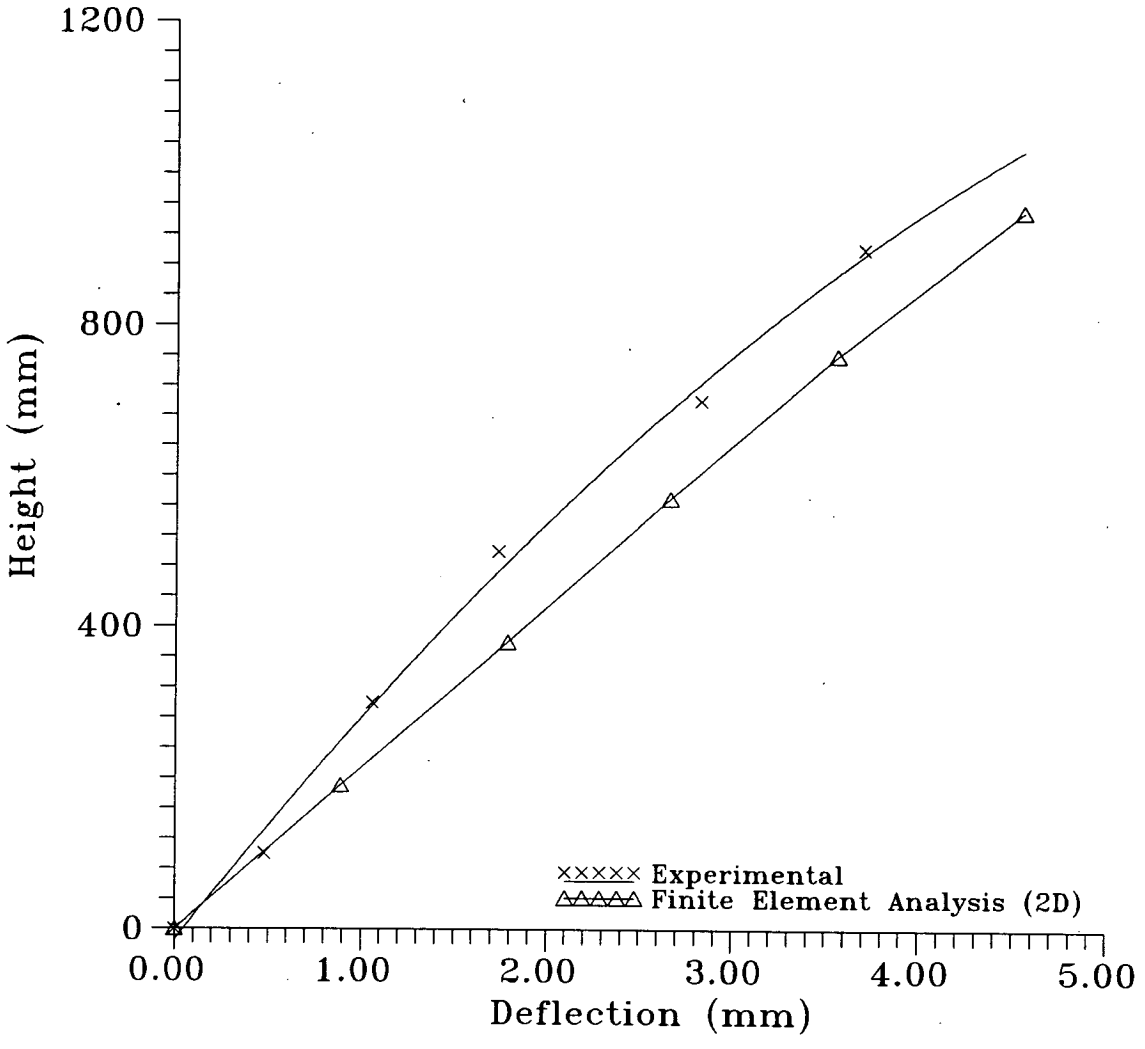


Fig. 6.40 Theoretical and experimental results for deflections at mid-height of column $HCE_{t/6}$ (20 mm)



Fig. 6.41 Mode of failure for the FCE_1 (No Steel) column

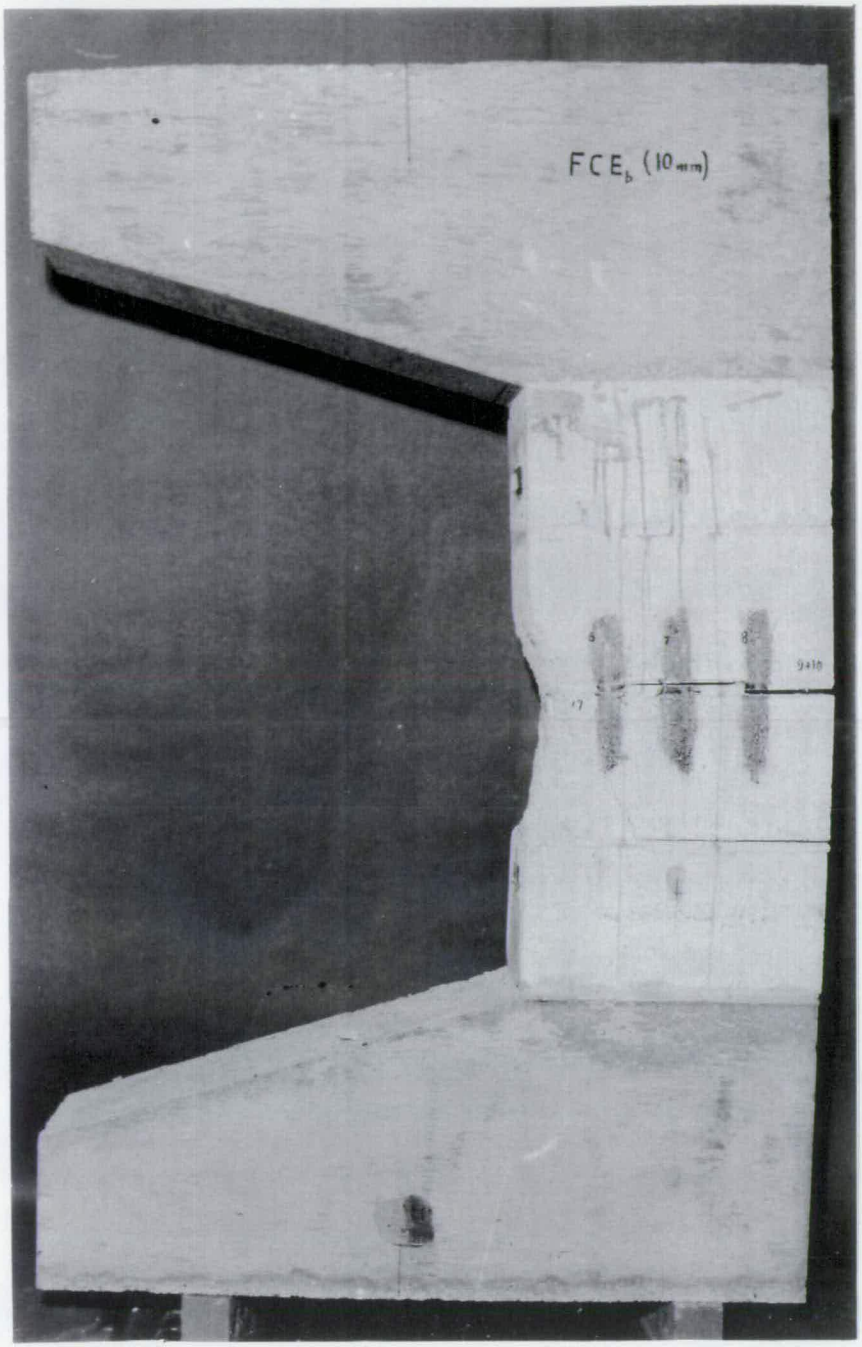


Fig. 6.42 Mode of failure for the FCE_1 (No Steel) column

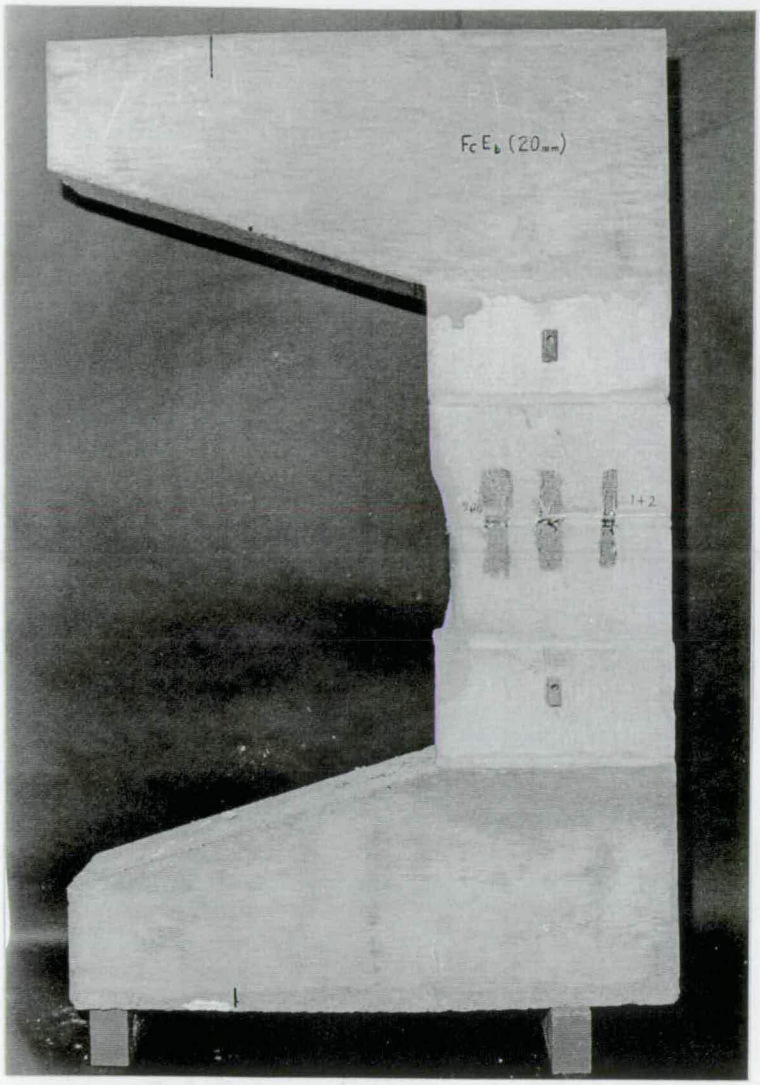


Fig. 6.43 Mode of failure for the FCE_1 (20 mm) column

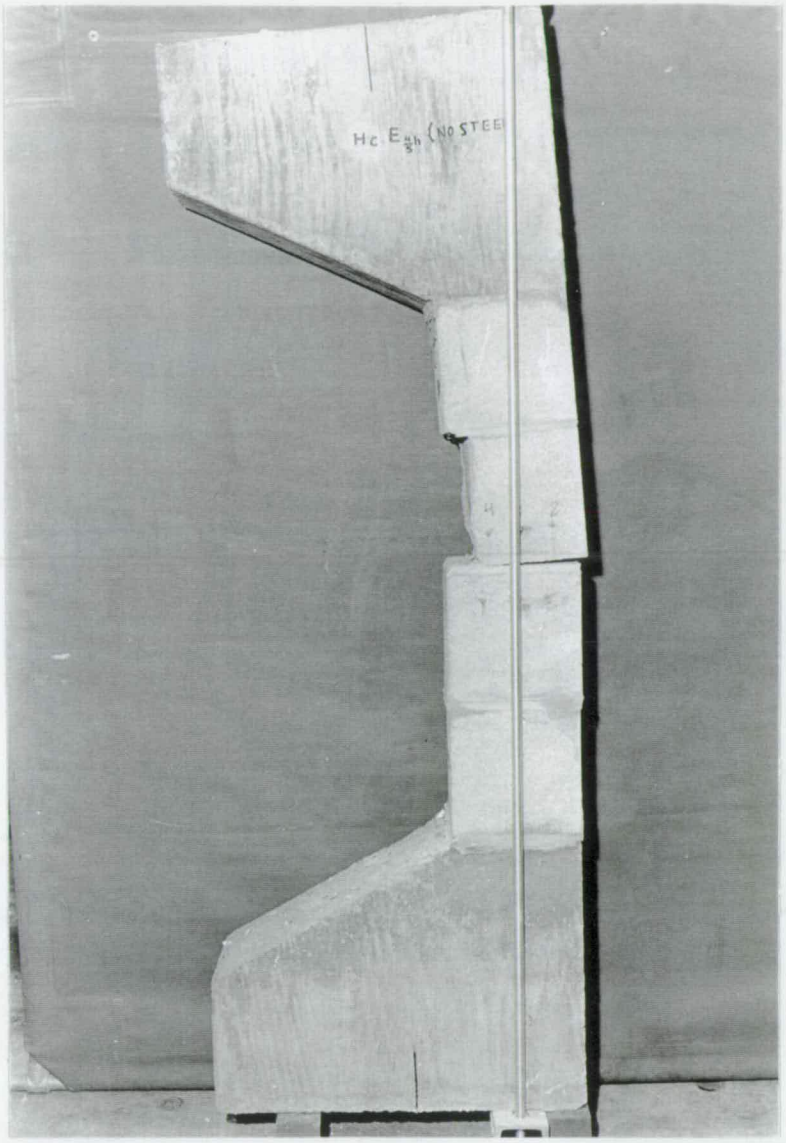


Fig. 6.44 Mode of failure for the HCE_1 (No Steel) column

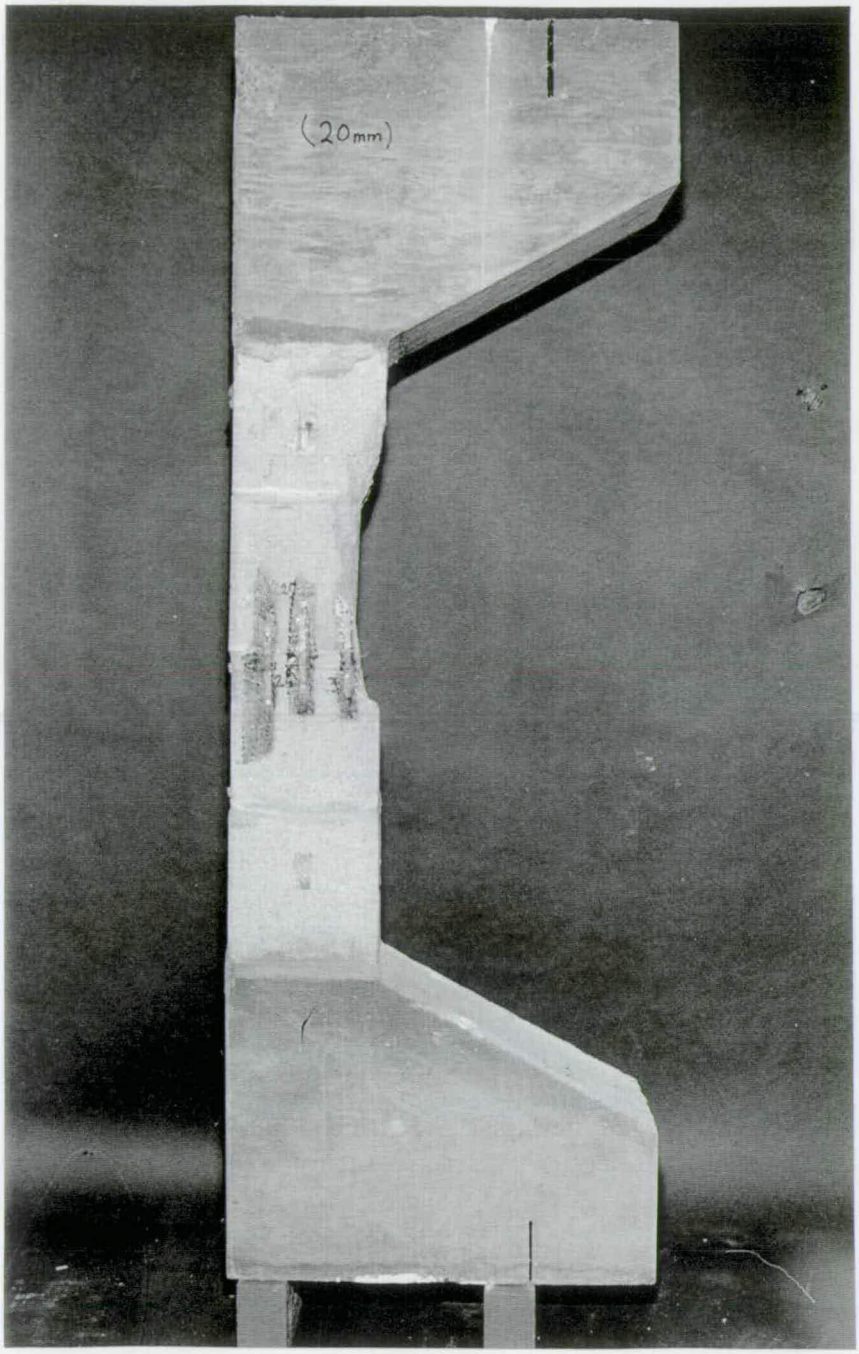


Fig. 6.45 Mode of failure for the HCE_1 (20 mm) column



Fig. 6.46 Mode of failure for the FCE_2 (No Steel) column

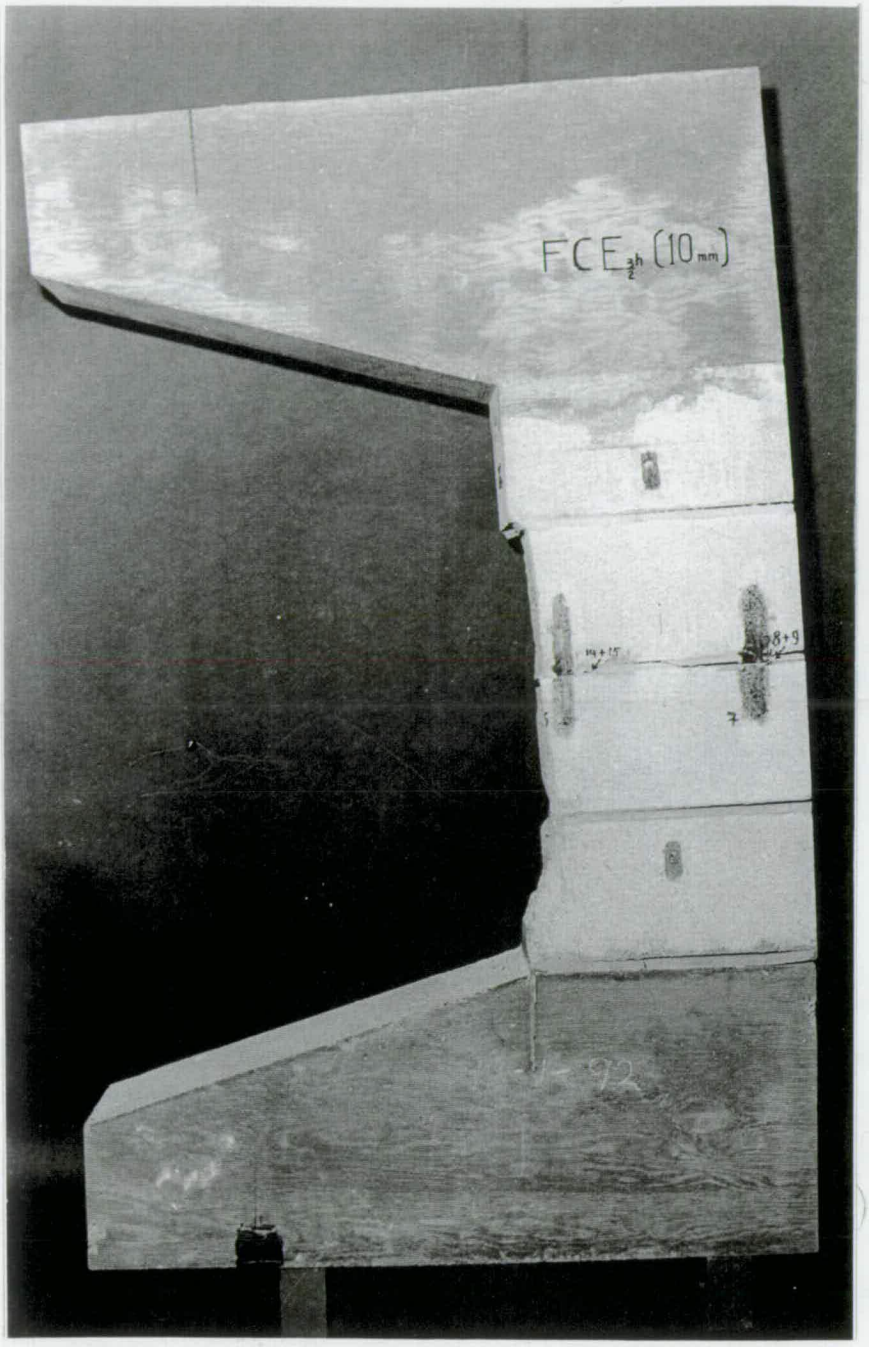


Fig. 6.47 Mode of failure for the FCE_2 (10 mm) column

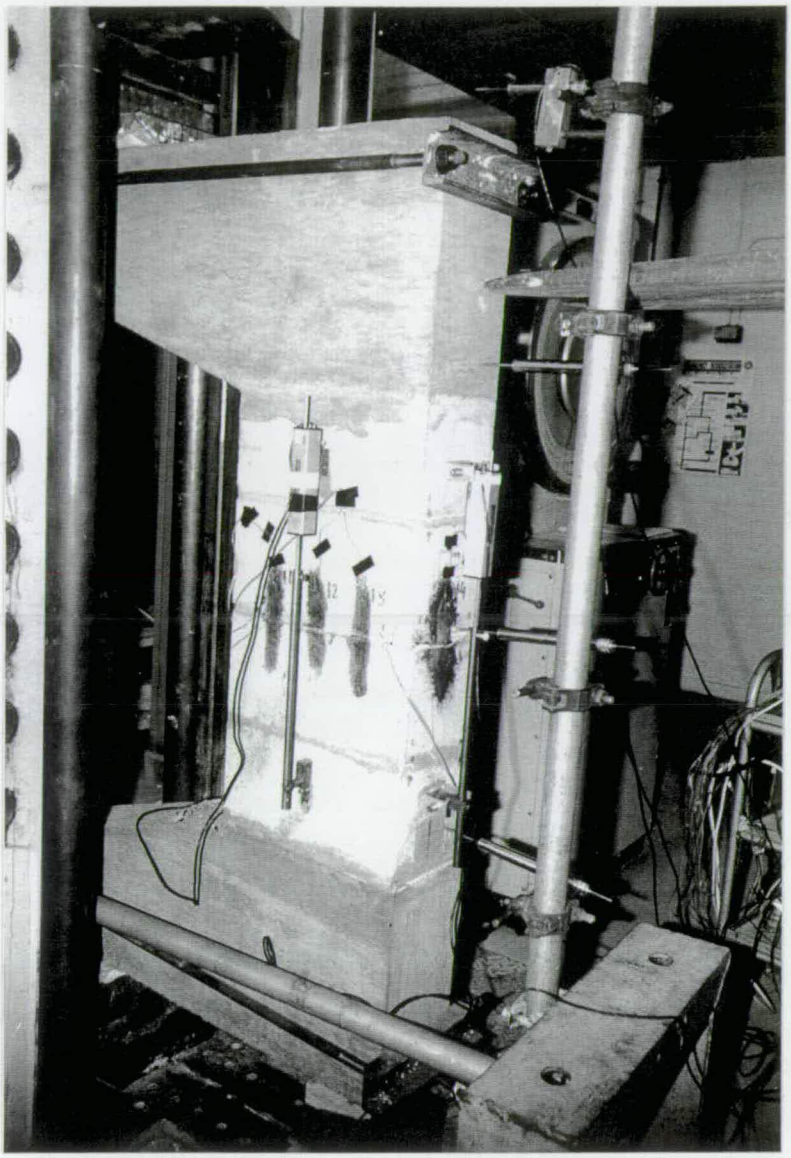


Fig. 6.48 Mode of failure for the FCE_2 (20 mm) column

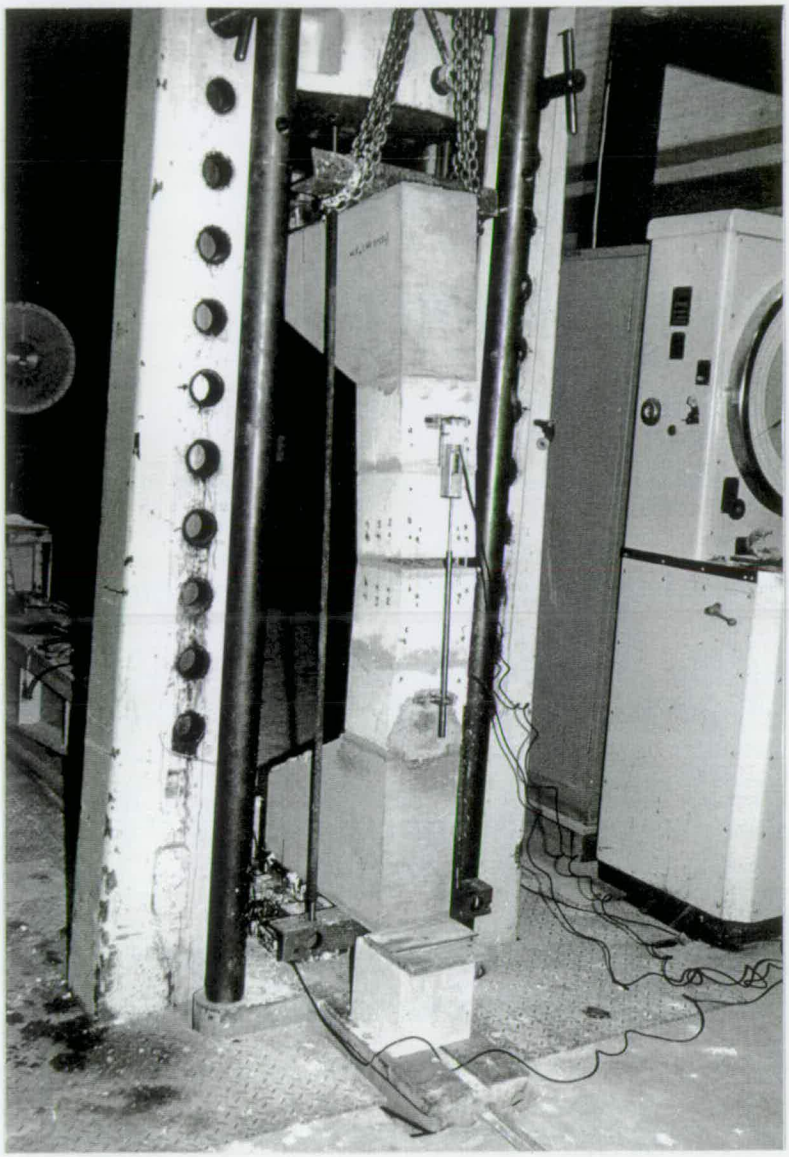


Fig. 6.49 Mode of failure for the HCE_2 (No Steel) column

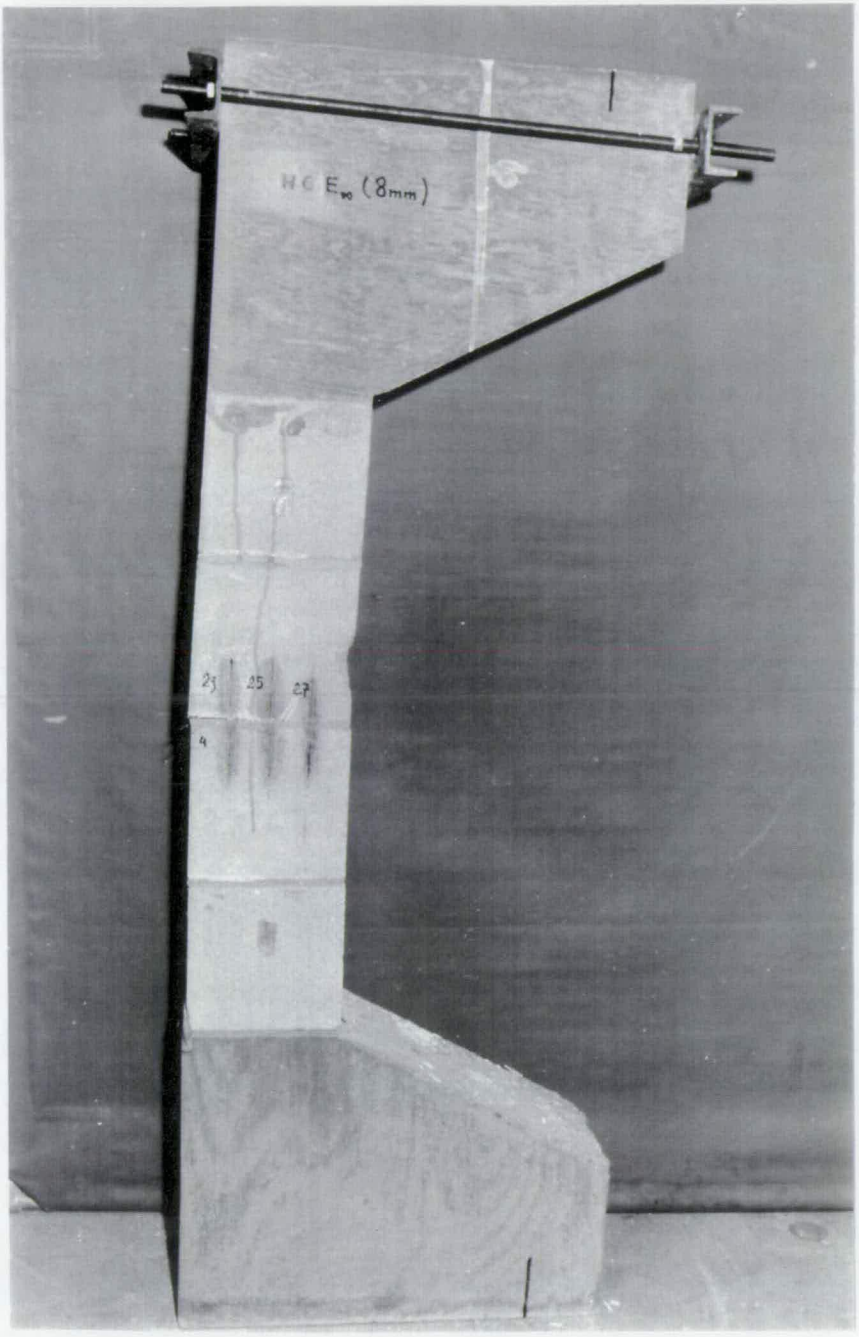


Fig. 6.50 Mode of failure for the HCE_2 (8 mm) column

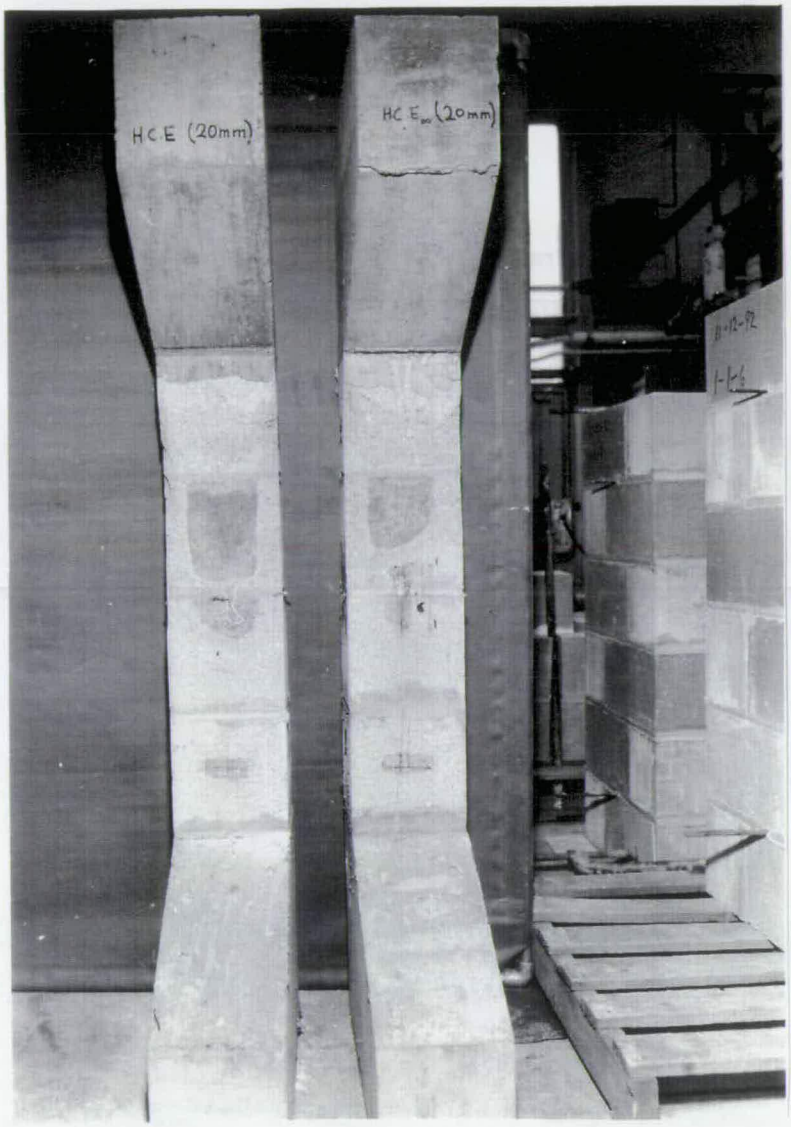


Fig. 6.51 Mode of failure for the HCE_2 (20 mm) column (right)

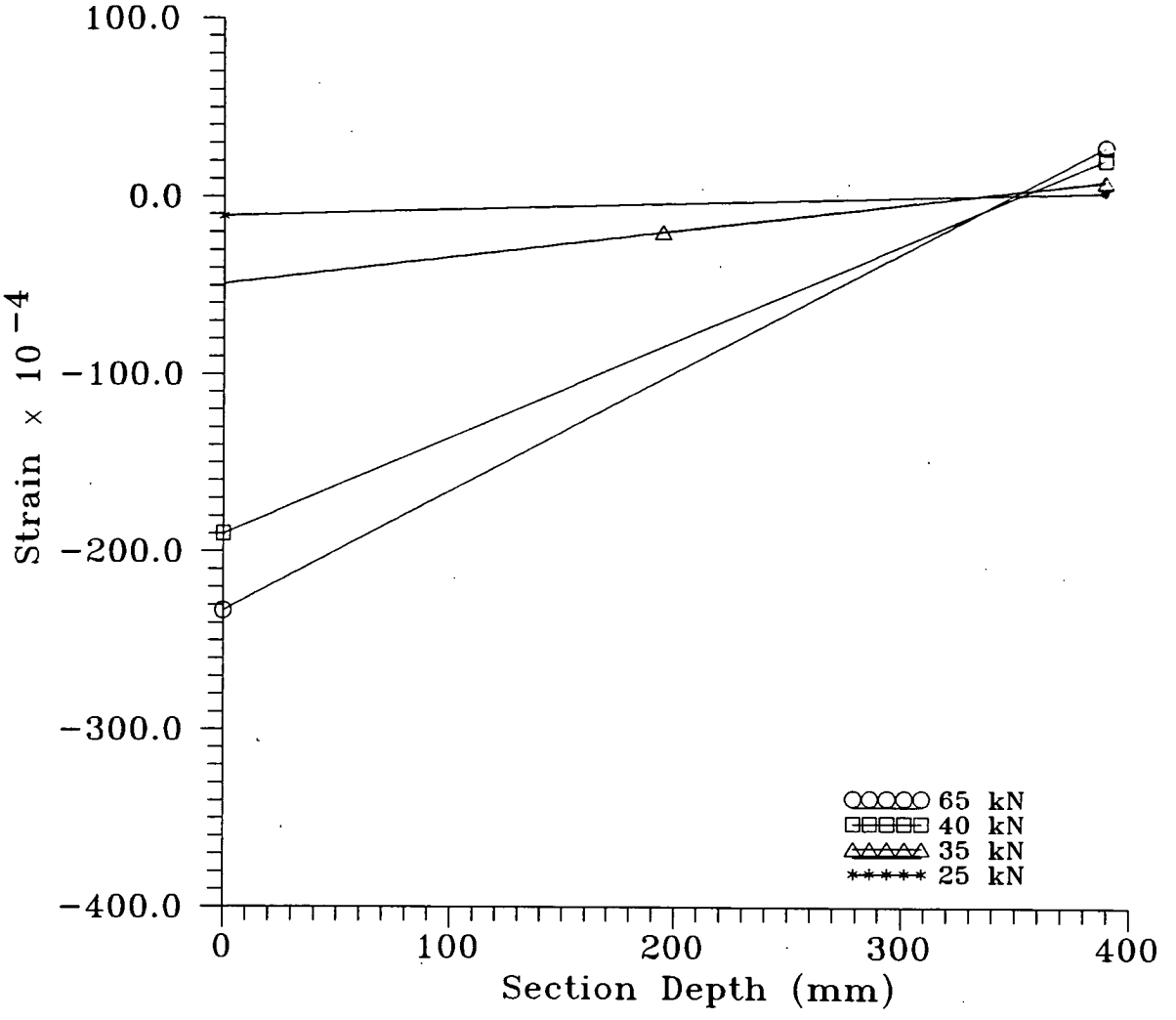


Fig. 6.52 Strain distribution for the FCE_1 (No Steel) column

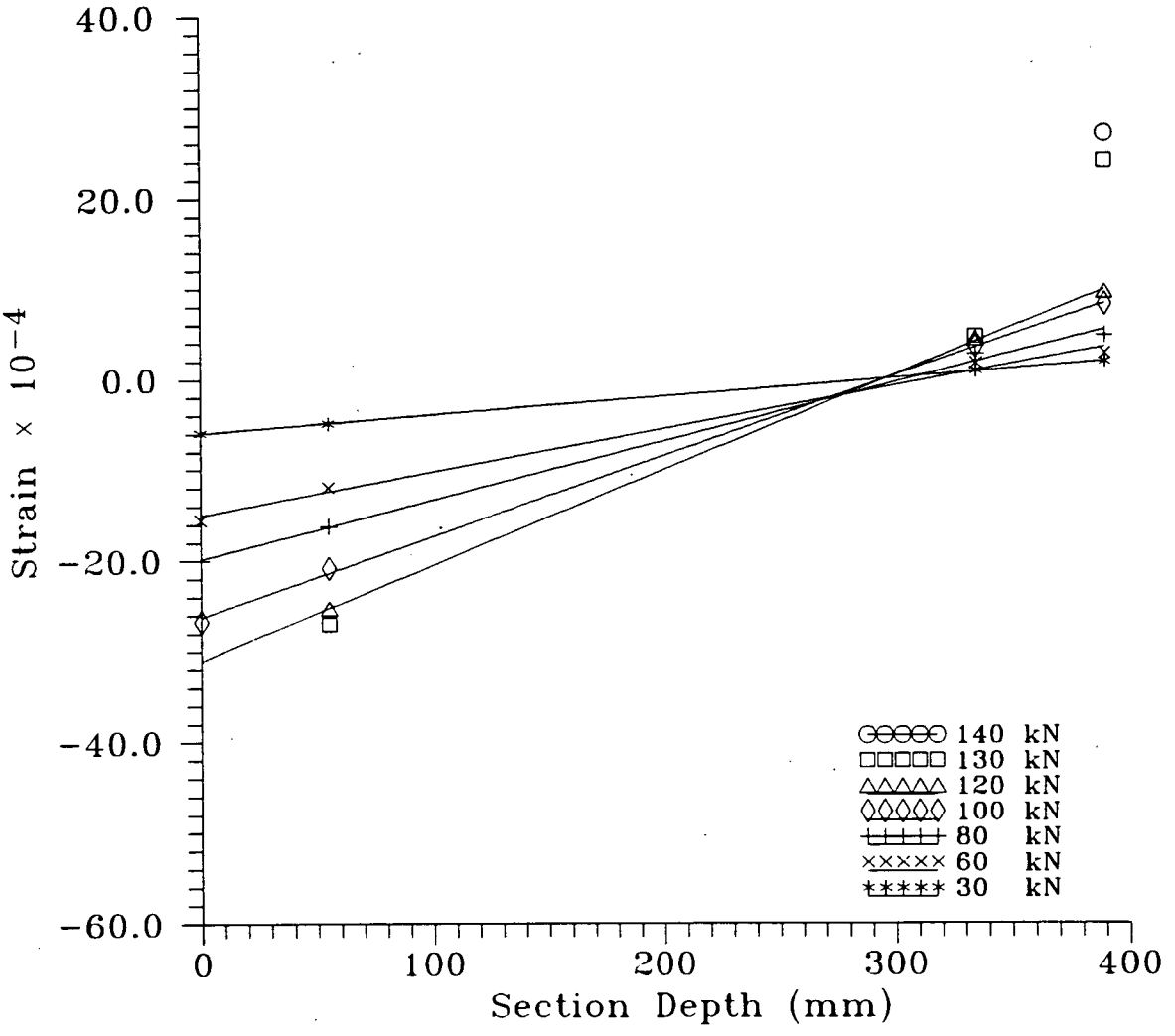


Fig. 6.53 Strain distribution across the FCE_1 (10 mm) column cross-section

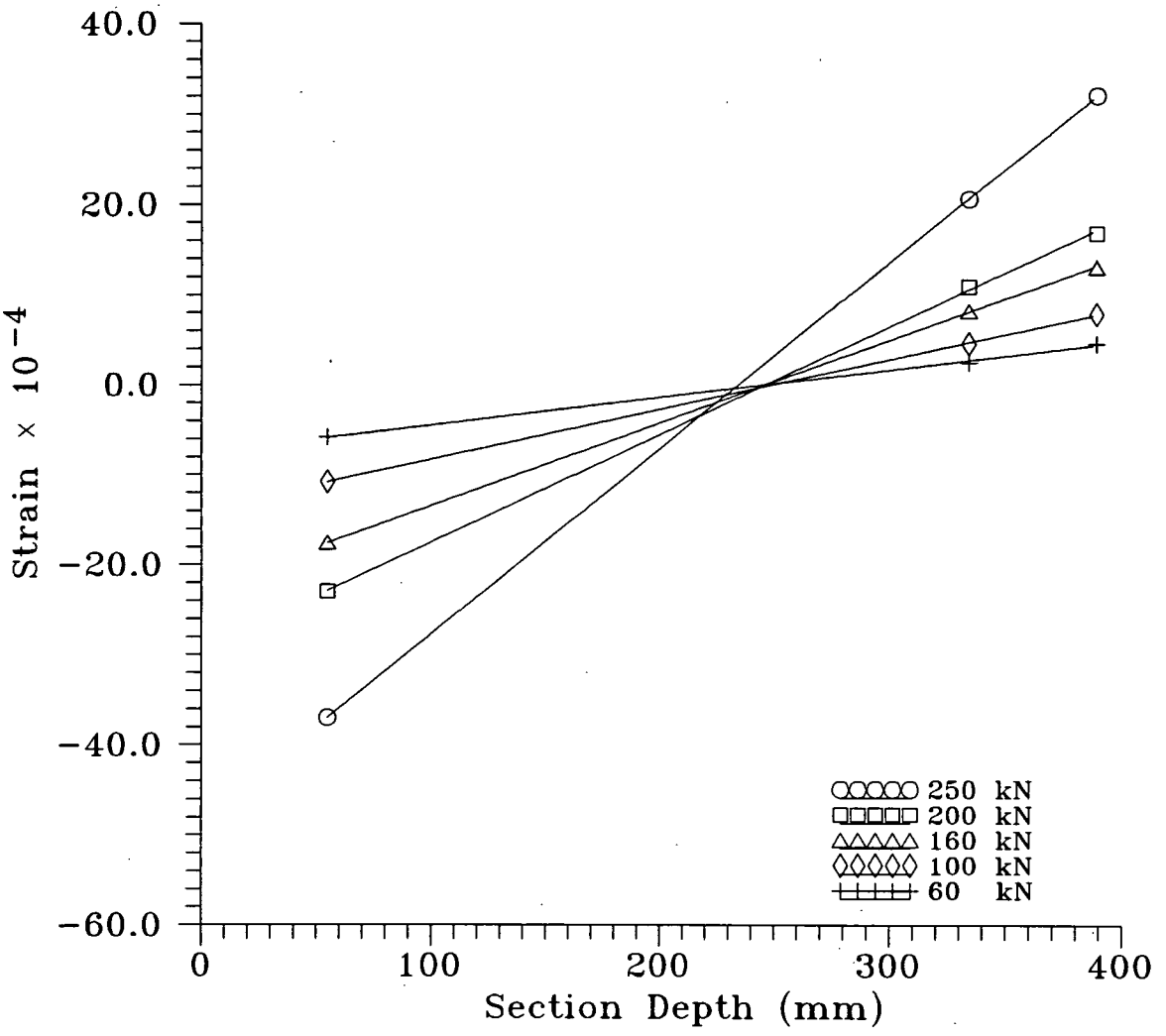


Fig. 6.54 Strain distribution across the FCE_1 (20 mm) column cross-section

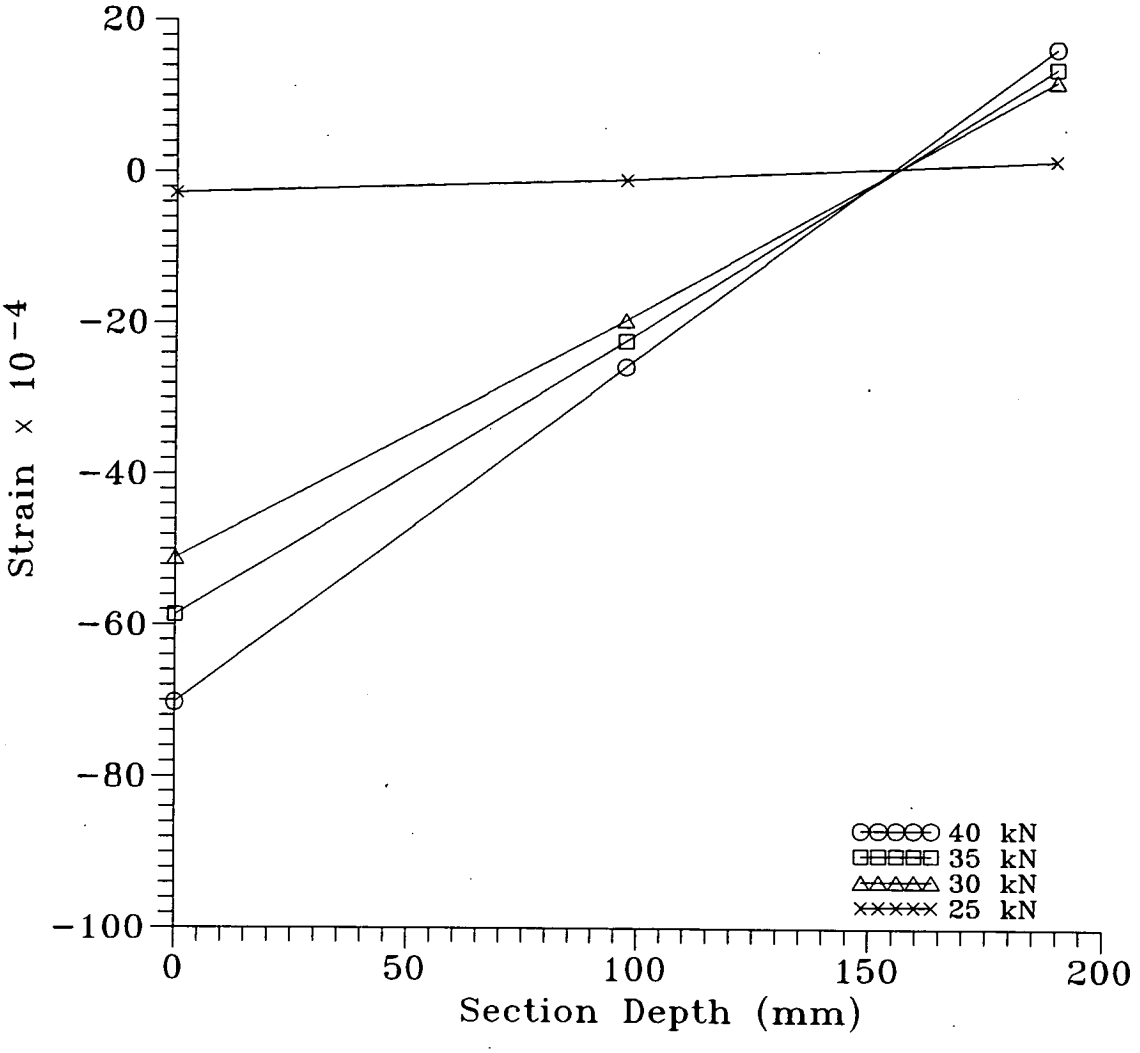


Fig. 6.55 Strain distribution for the HCE_1 (No Steel) column

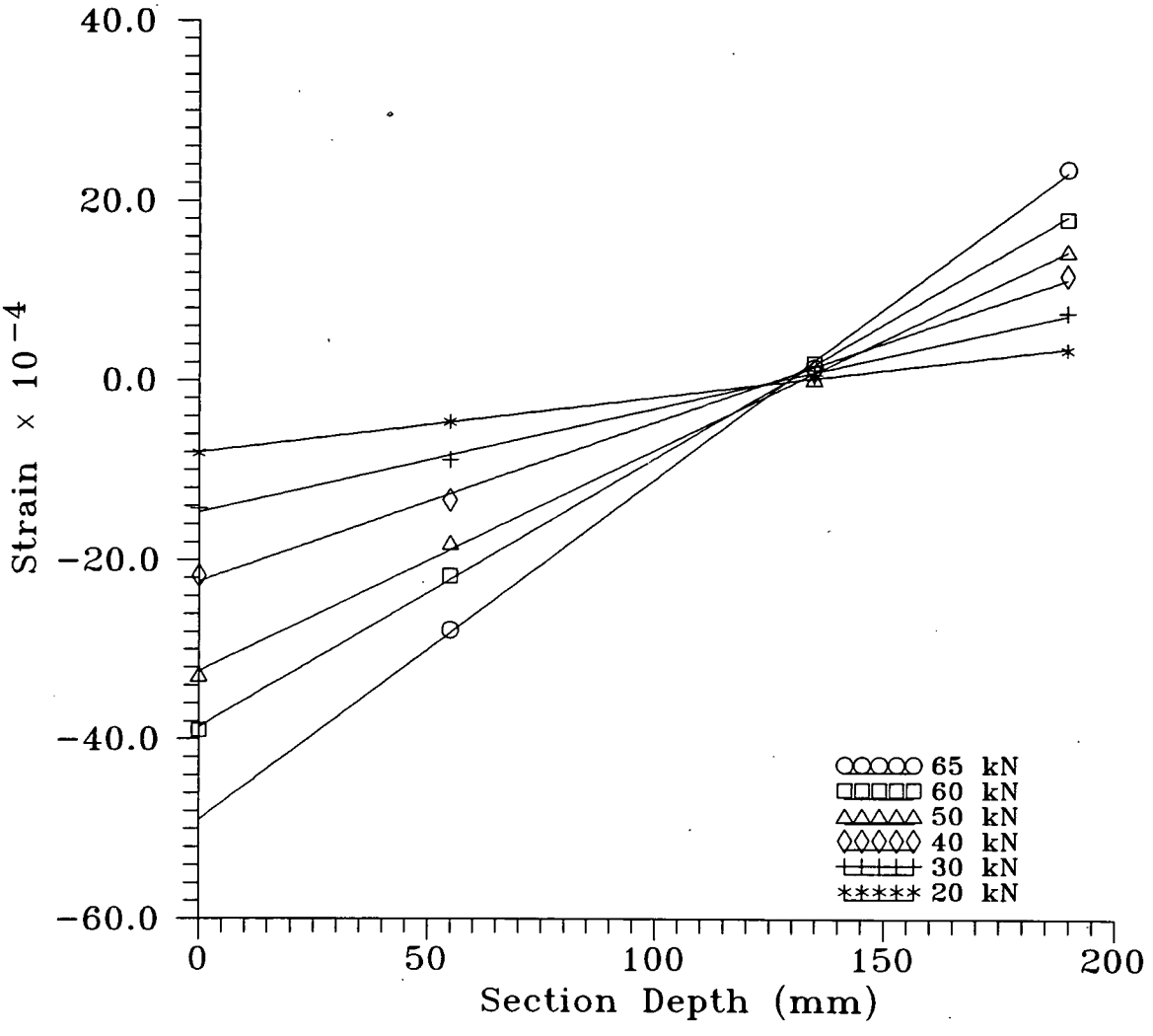


Fig. 6.56 Strain distribution across the HCE_1 (8 mm) column cross-section

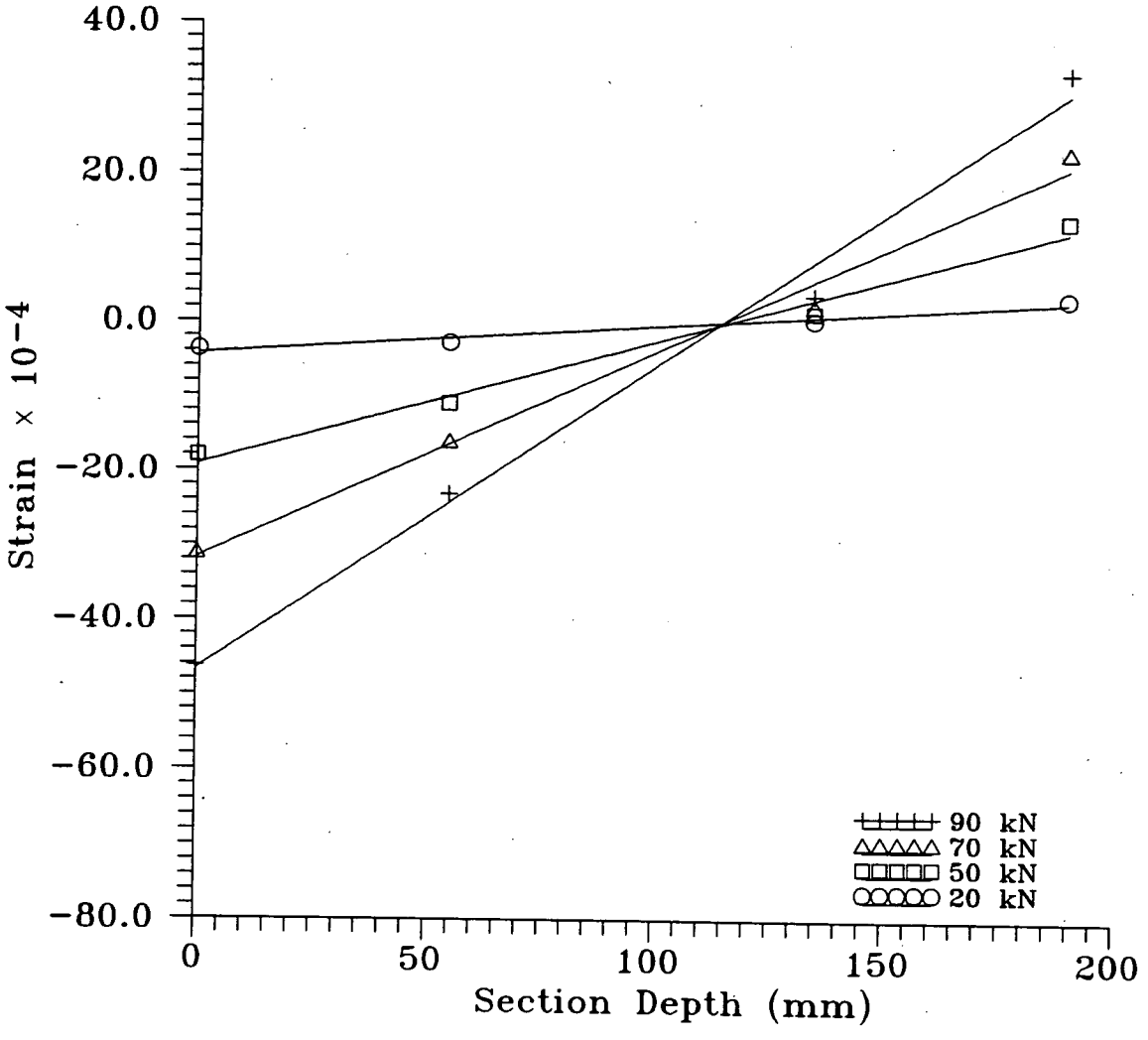


Fig. 6.57 Strain distribution across the HCE_1 (20 mm) column cross-section

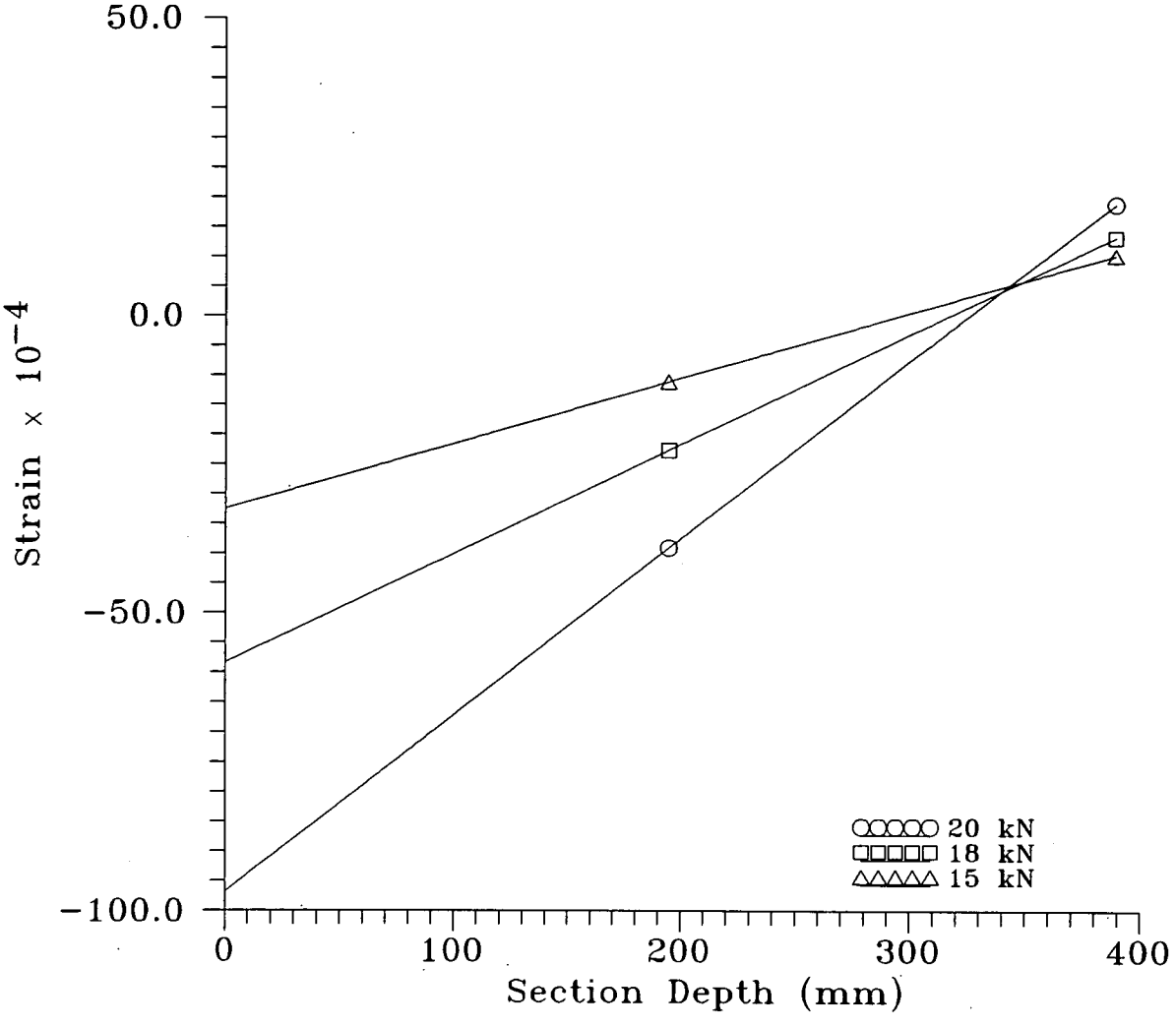


Fig. 6.58 Strain distribution for the FCE_2 (No Steel) column

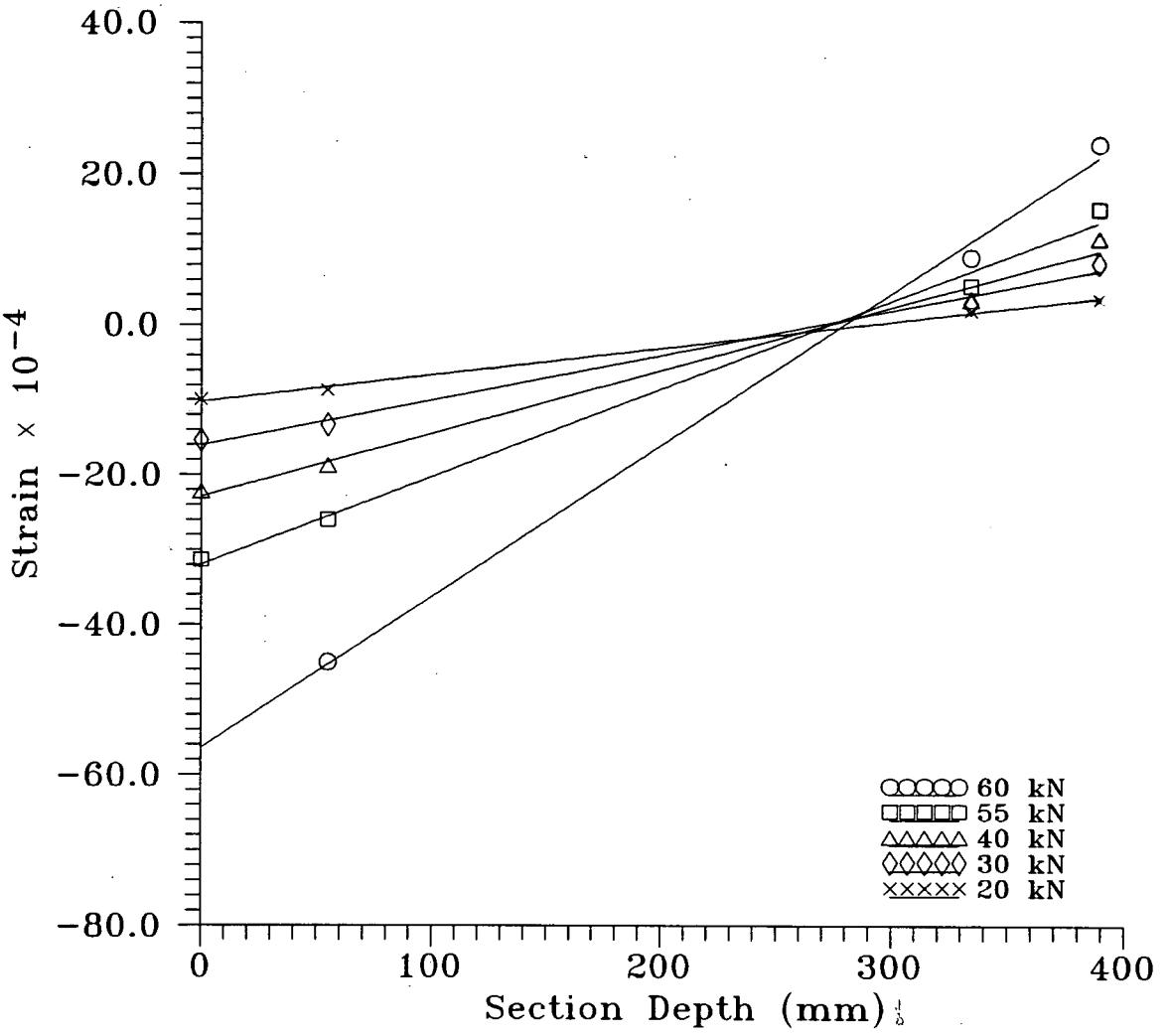


Fig. 6.59 Strain distribution across the FCE_2 (10 mm) column cross-section

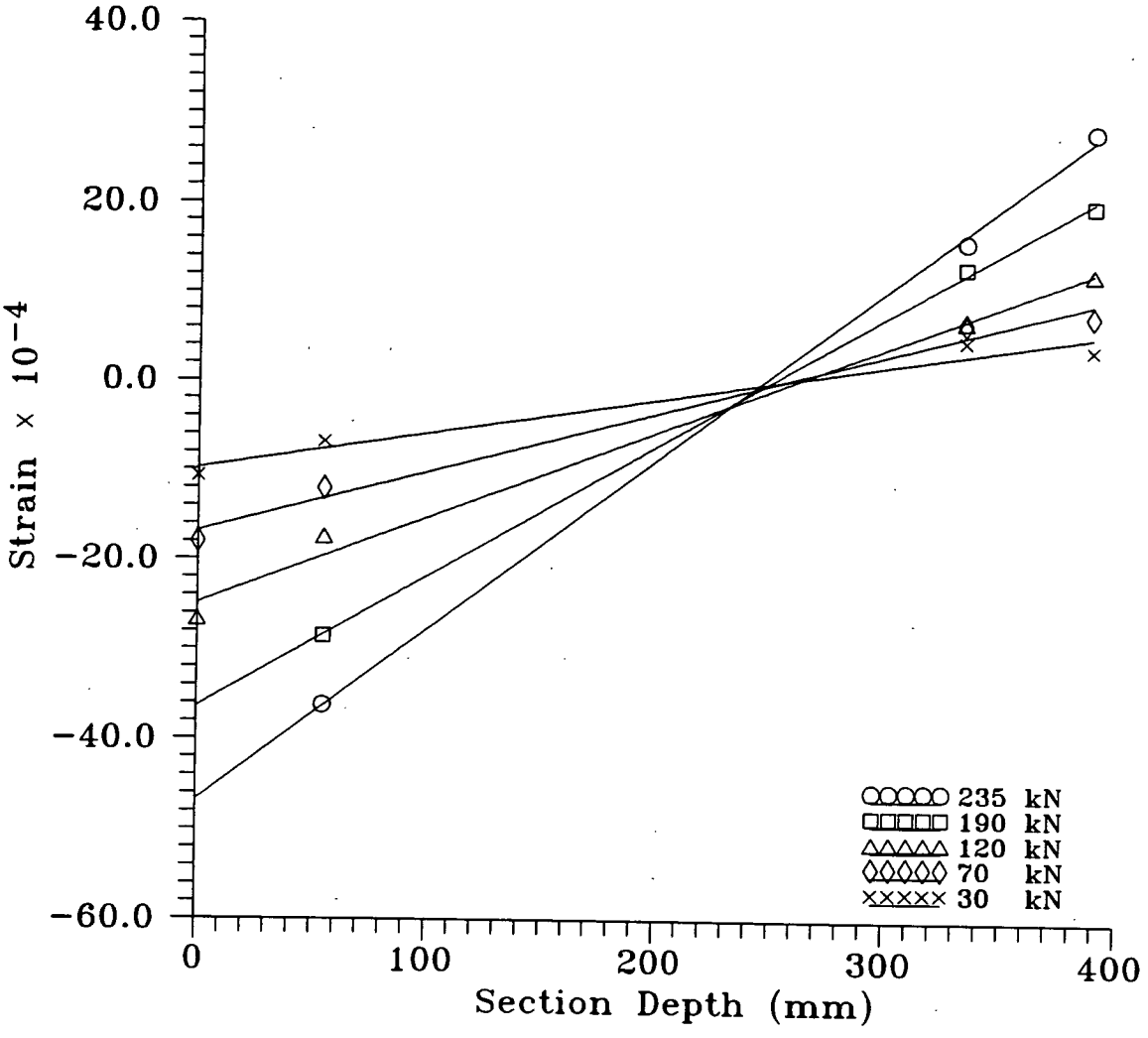


Fig. 6.60 Strain distribution across the FCE_2 (20 mm) column cross-section

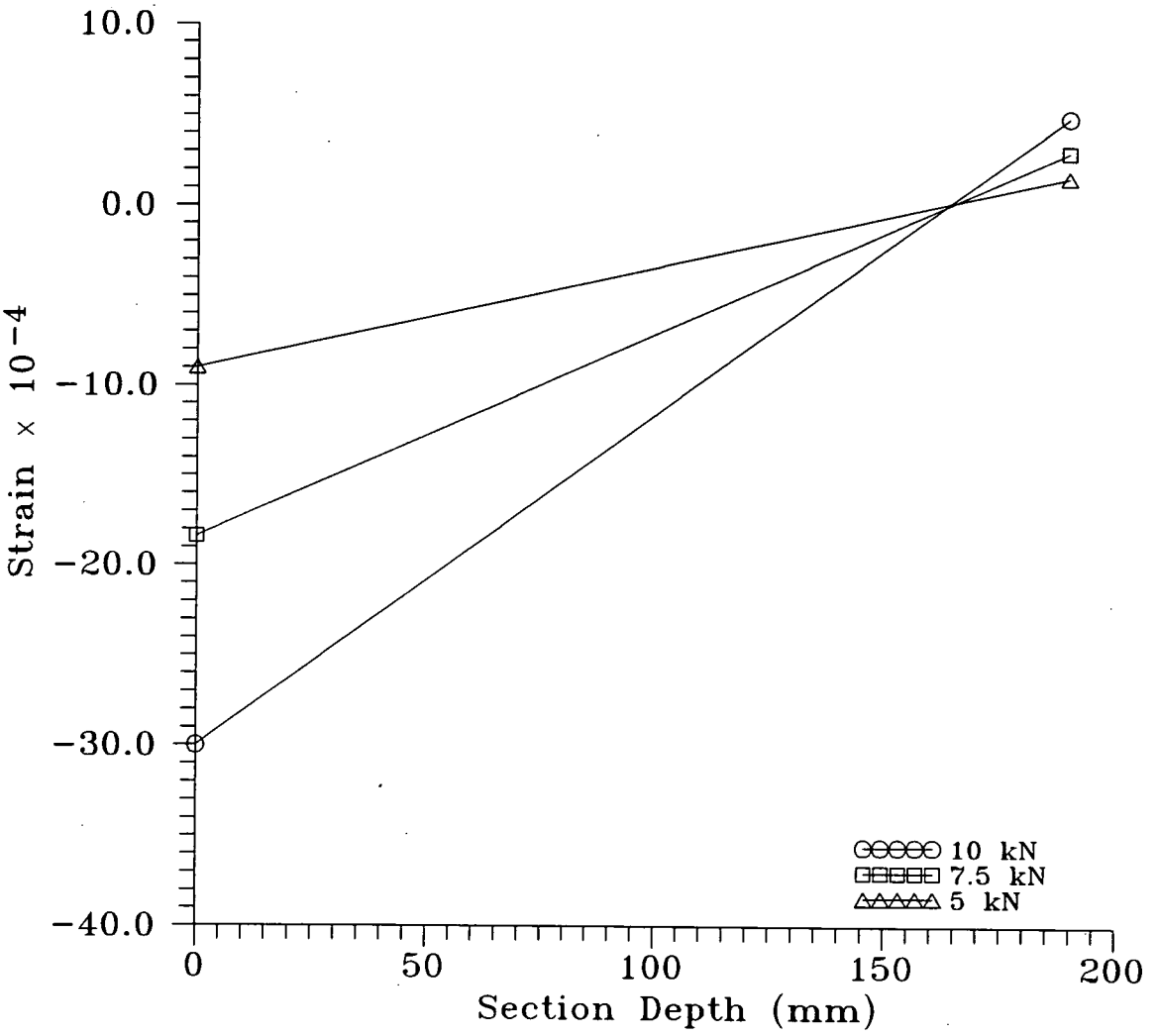


Fig. 6.61 Strain distribution for the HCE_2 (No Steel) column

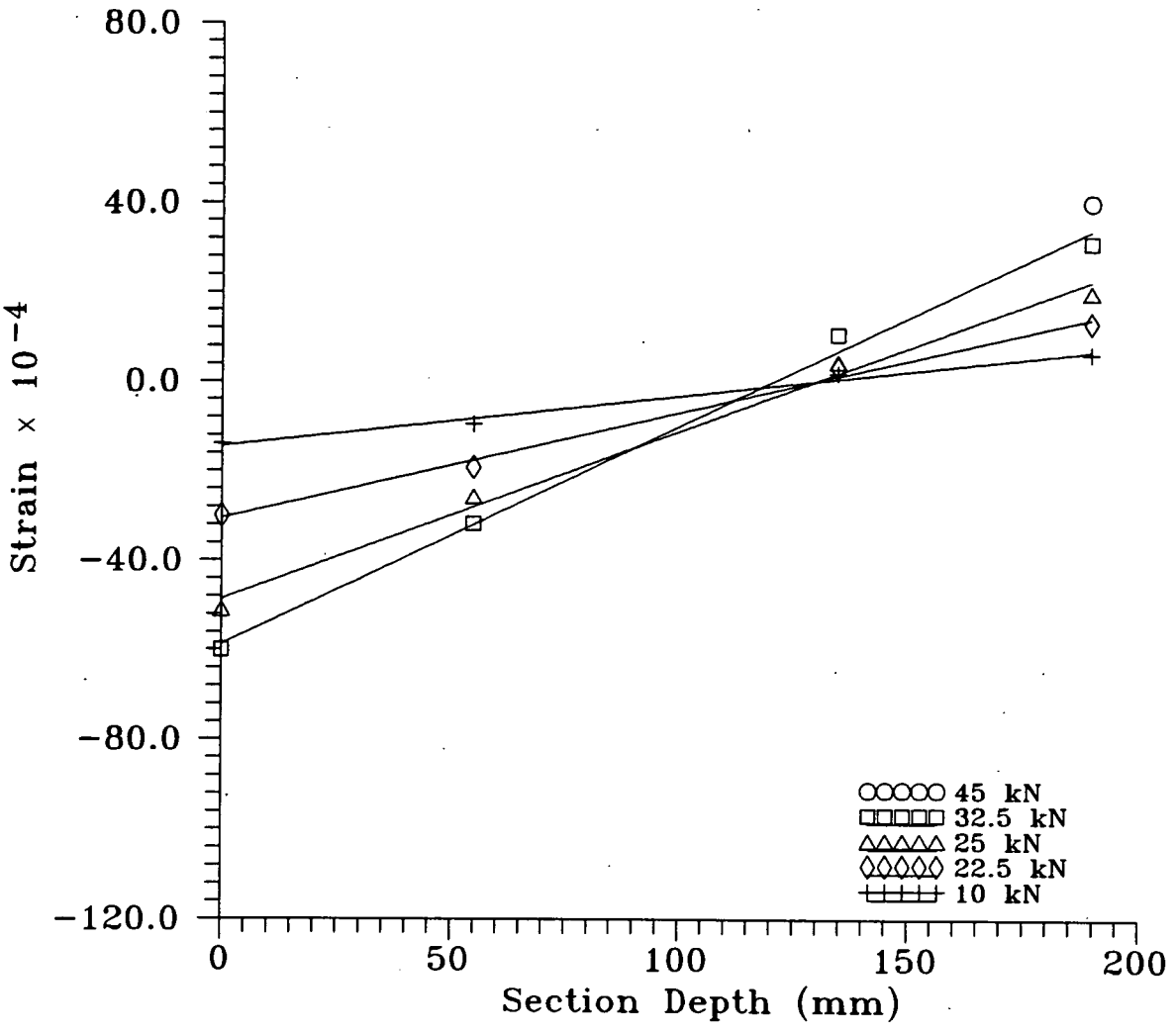


Fig. 6.62 Strain distribution across the HCE_2 (8 mm) column cross-section

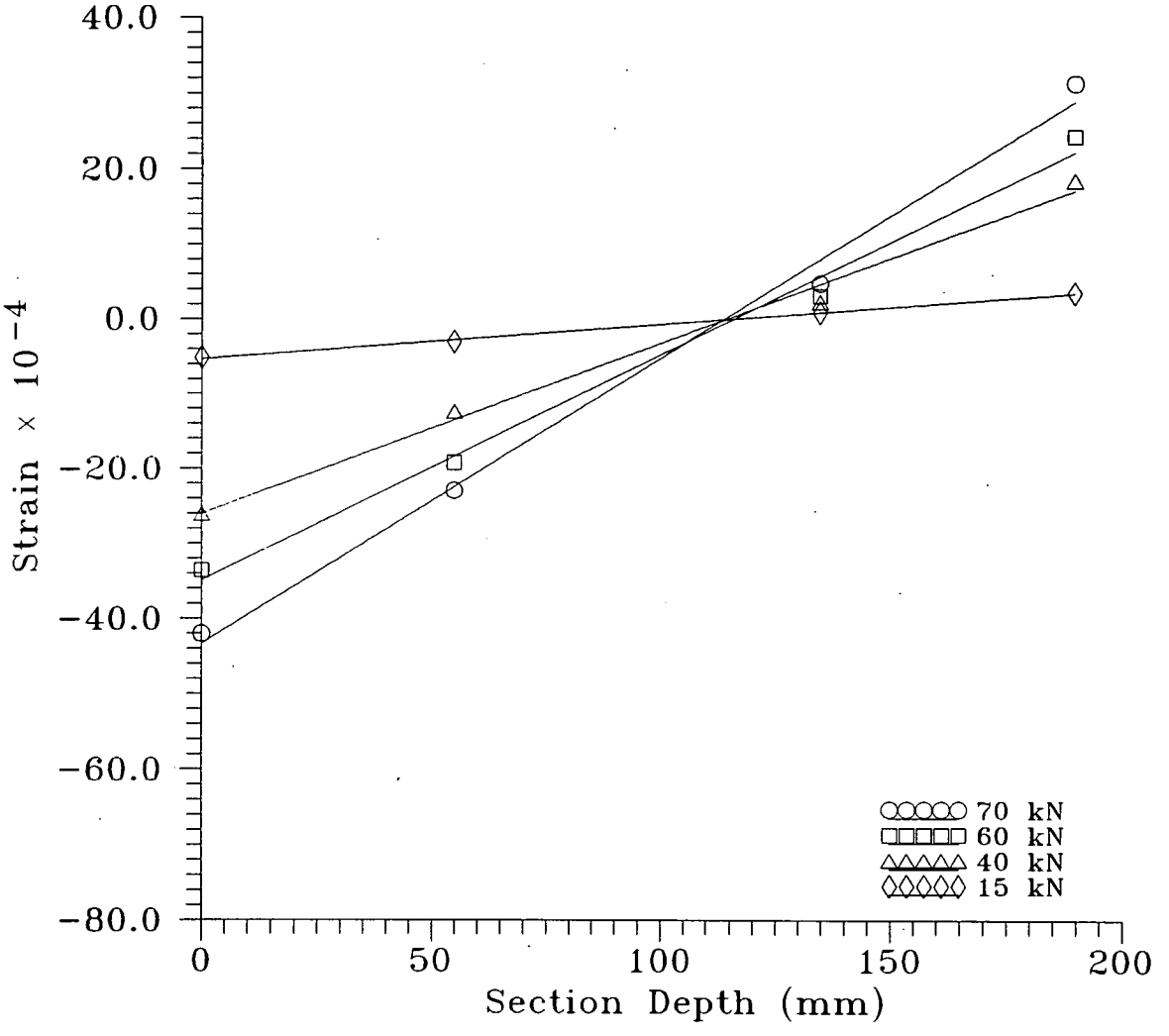


Fig. 6.63 Strain distribution across the HCE_2 (20 mm) column cross-section

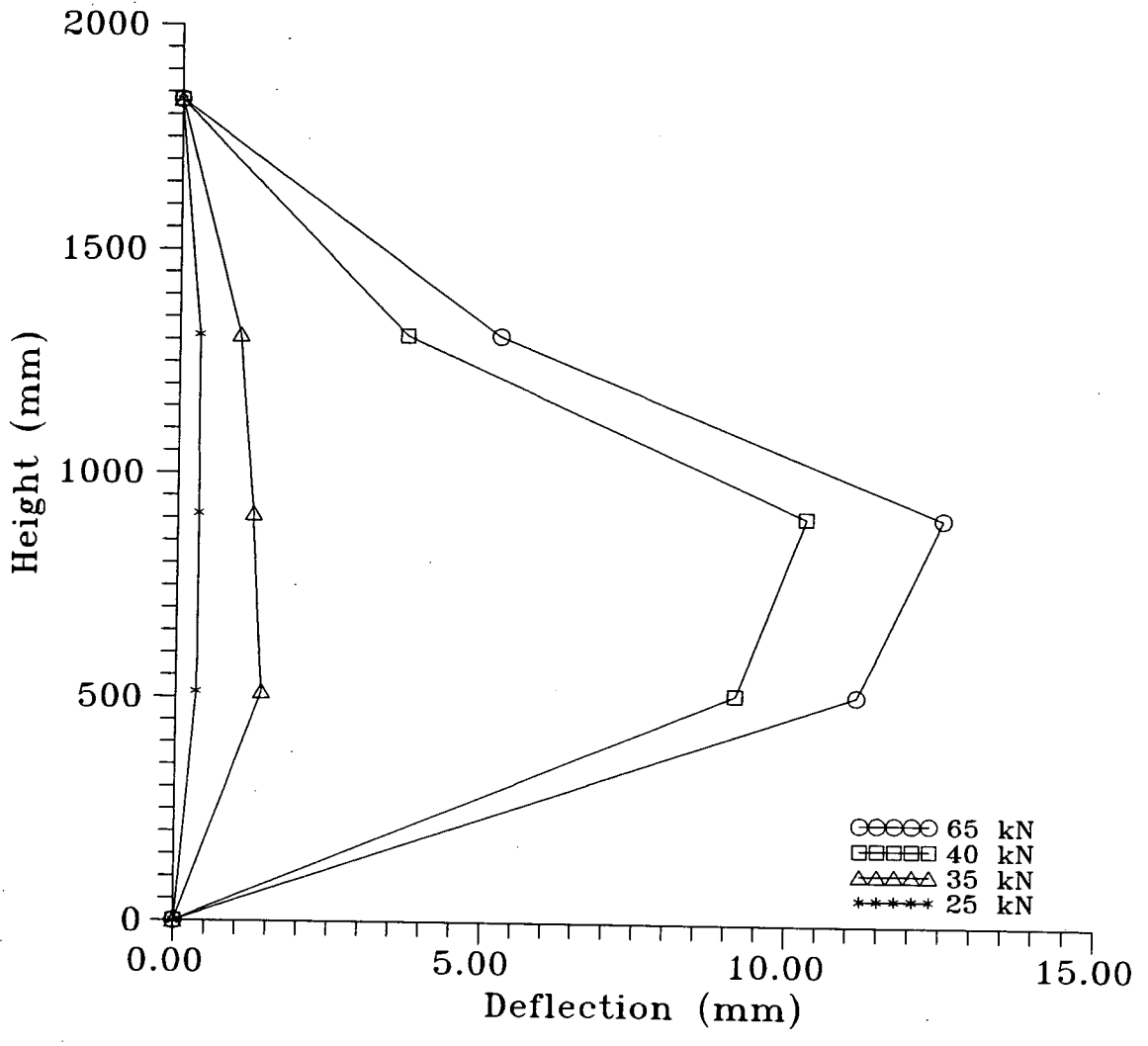


Fig. 6.64 Load–deflection relationship for the FCE_1 (No Steel) column

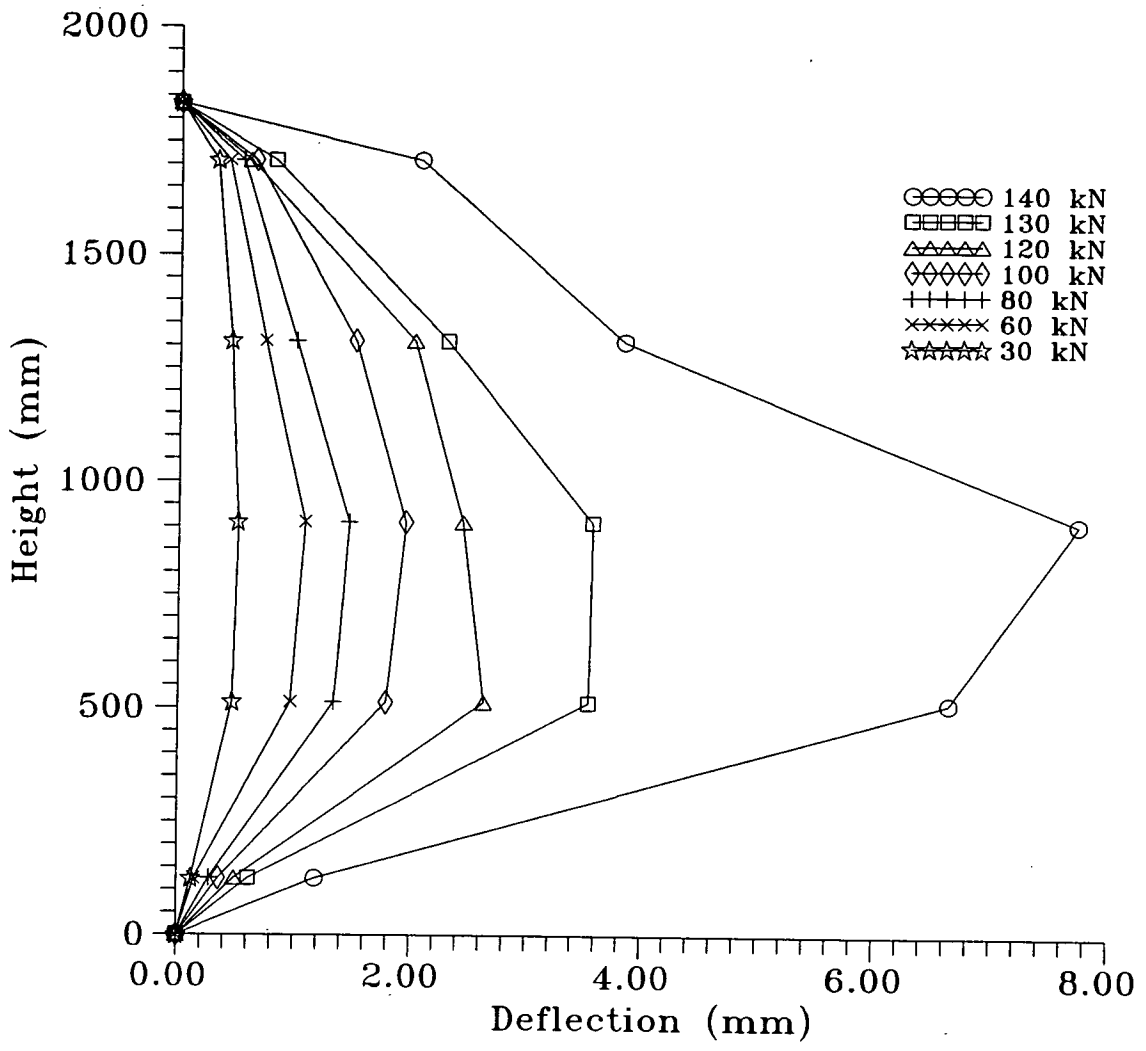


Fig. 6.65 Load–deflection relationship for the FCE_1 (10 mm) column

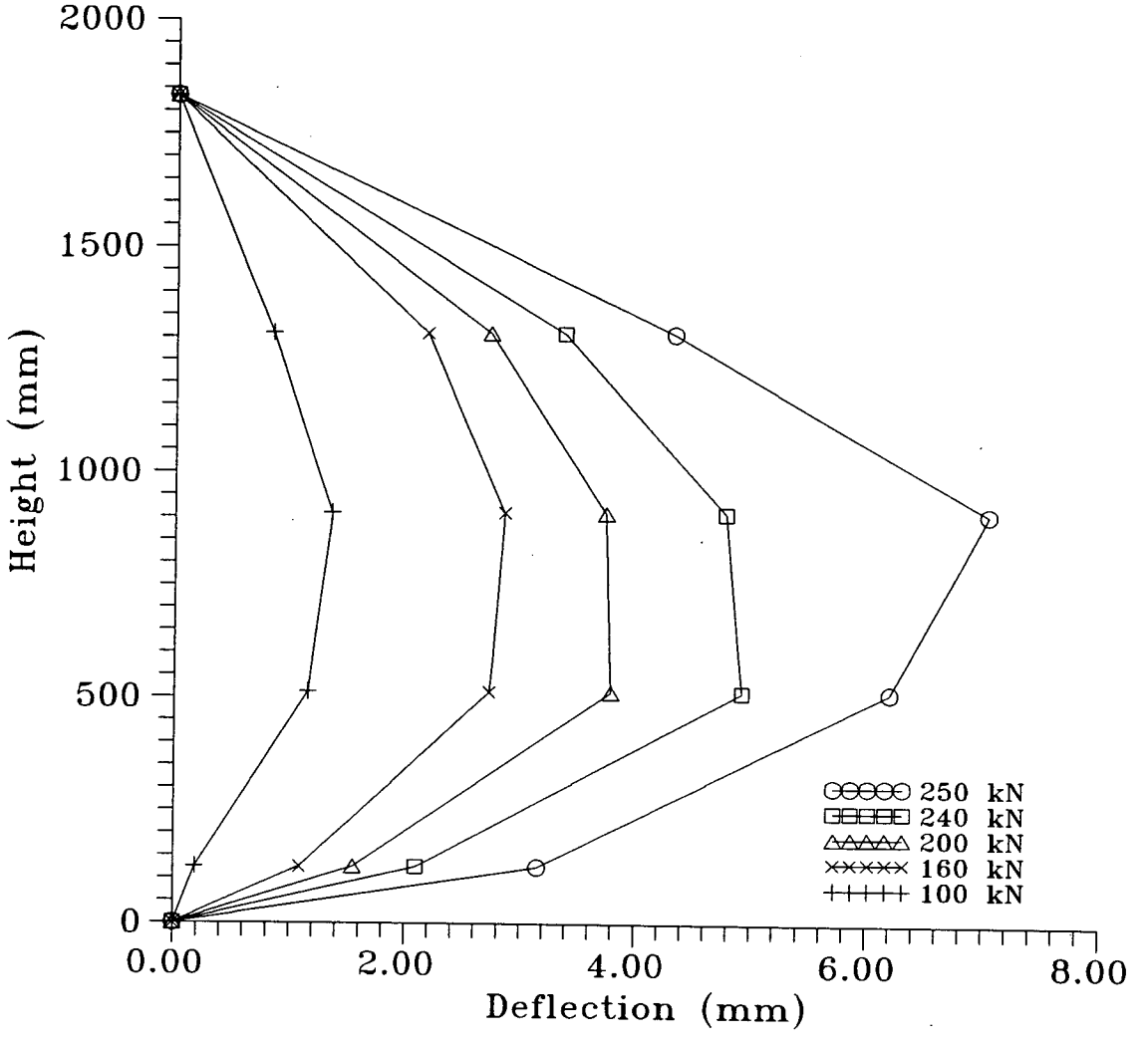


Fig. 6.66 Load–deflection relationship for the FCE_1 (20 mm) column

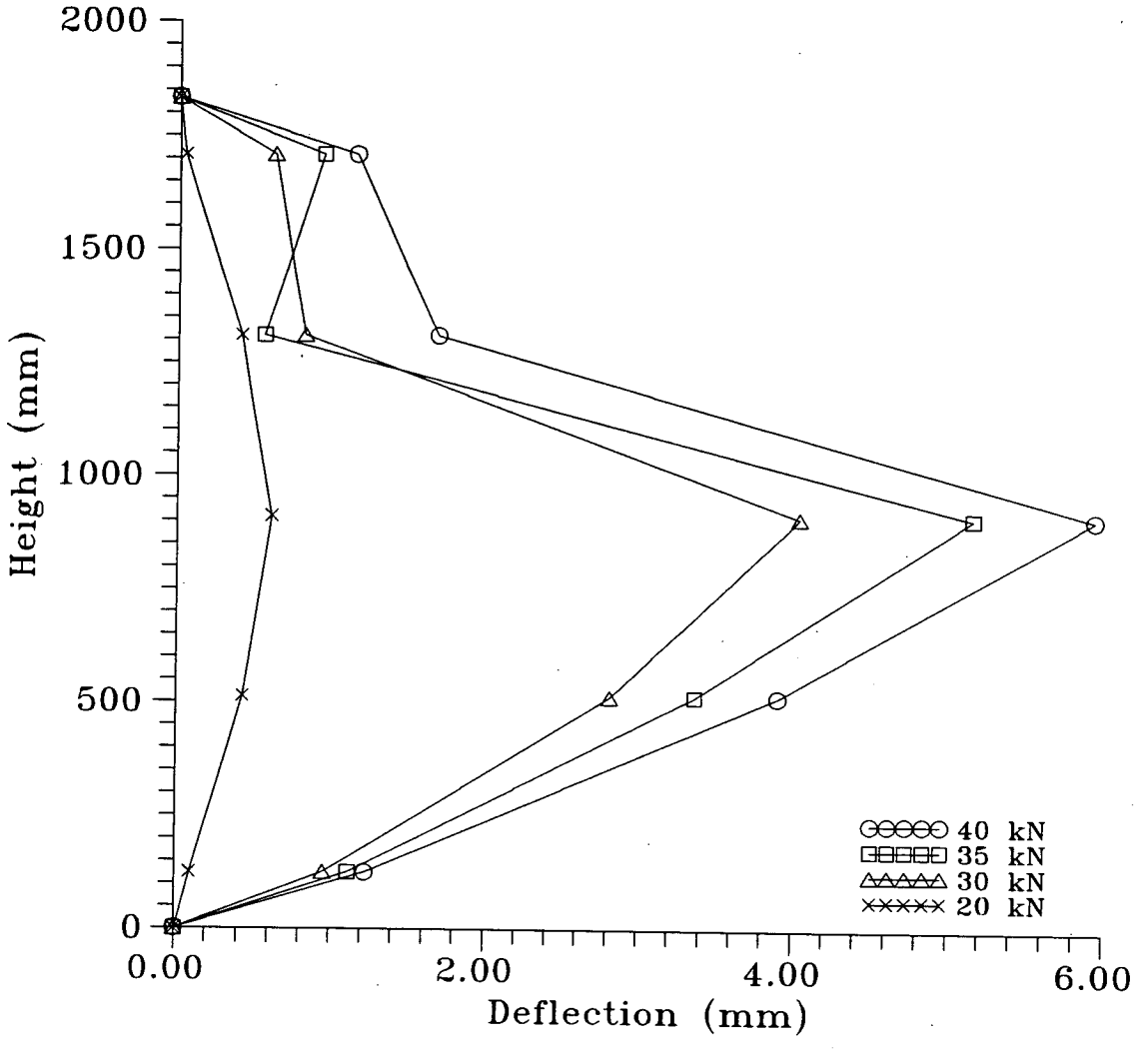


Fig. 6.67 Load–deflection relationship for the HCE_1 (No Steel) column

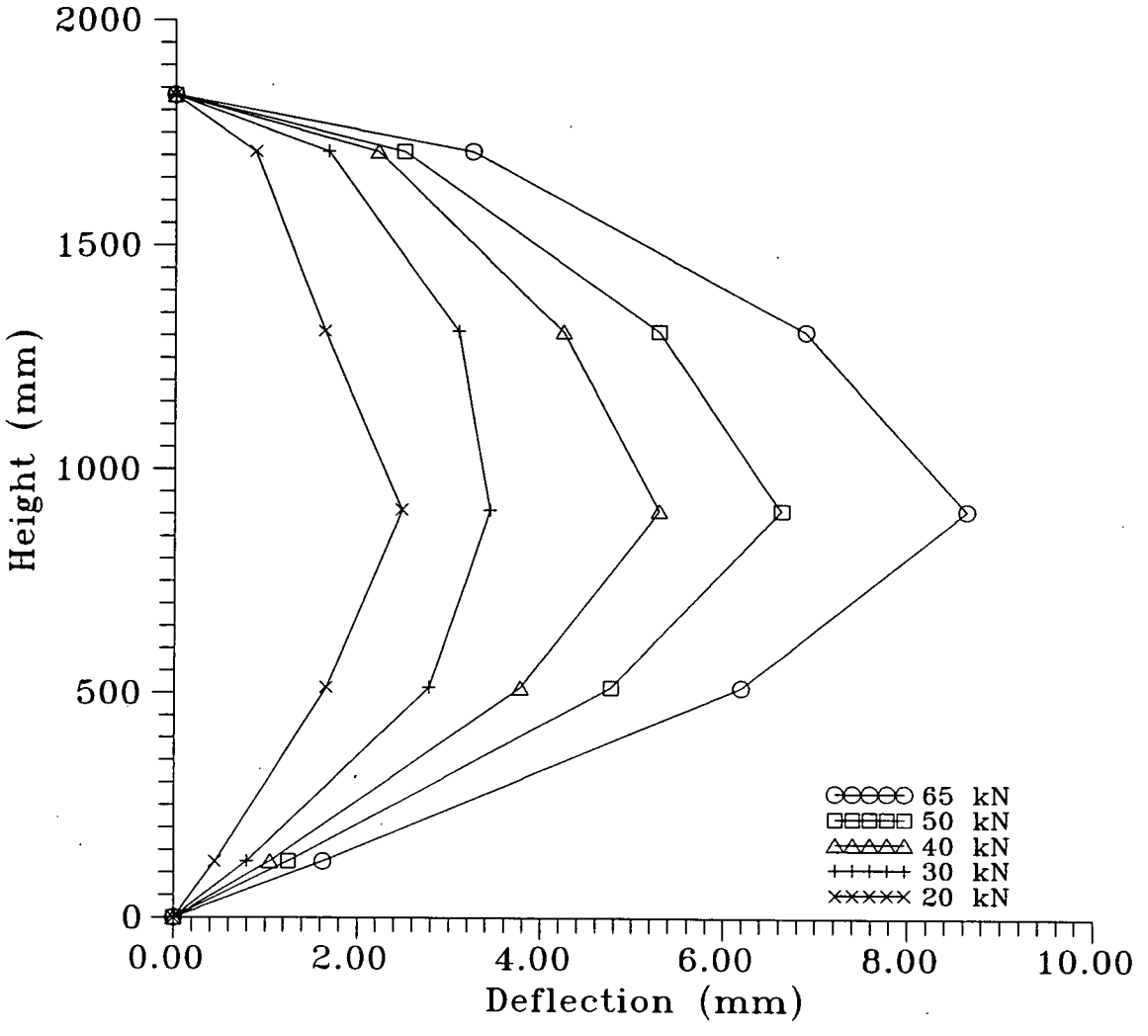


Fig. 6.68 Load–deflection relationship for the HCE_1 (8 mm) column

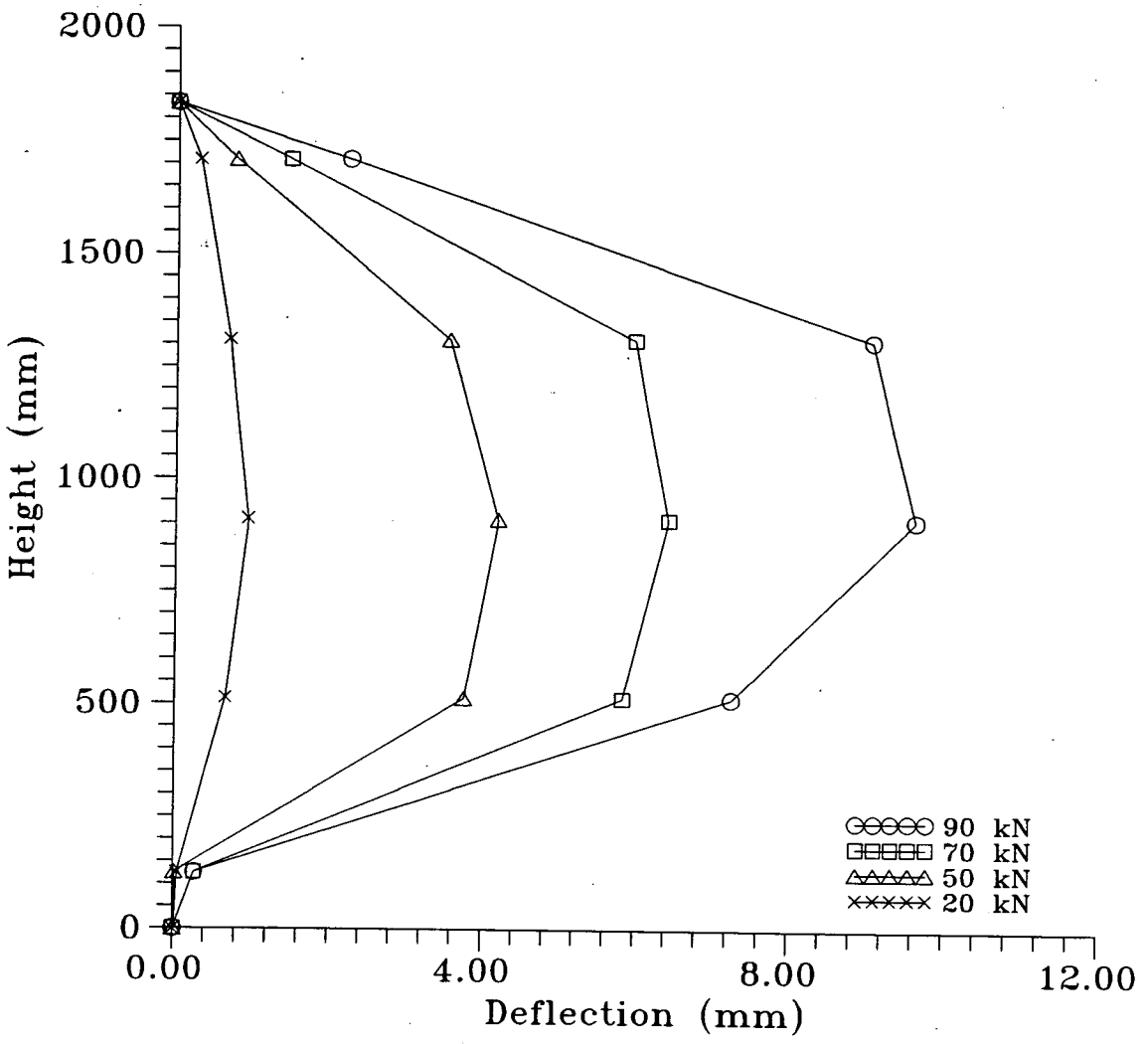


Fig. 6.69 Load deflection relationship for the HCE_1 (20 mm)

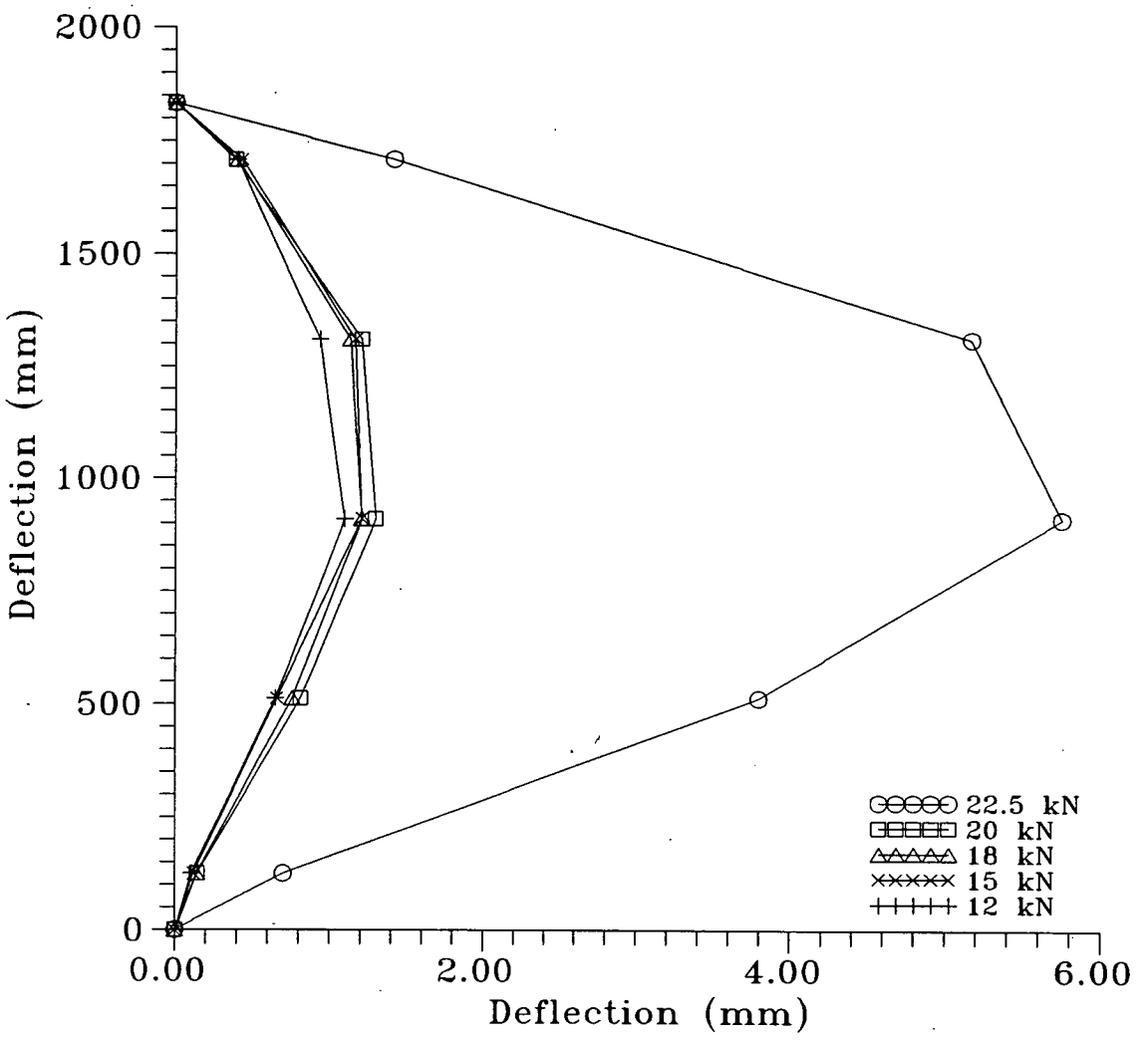


Fig. 6.70 Load–deflection relationship for the FCE_2 (No Steel) column

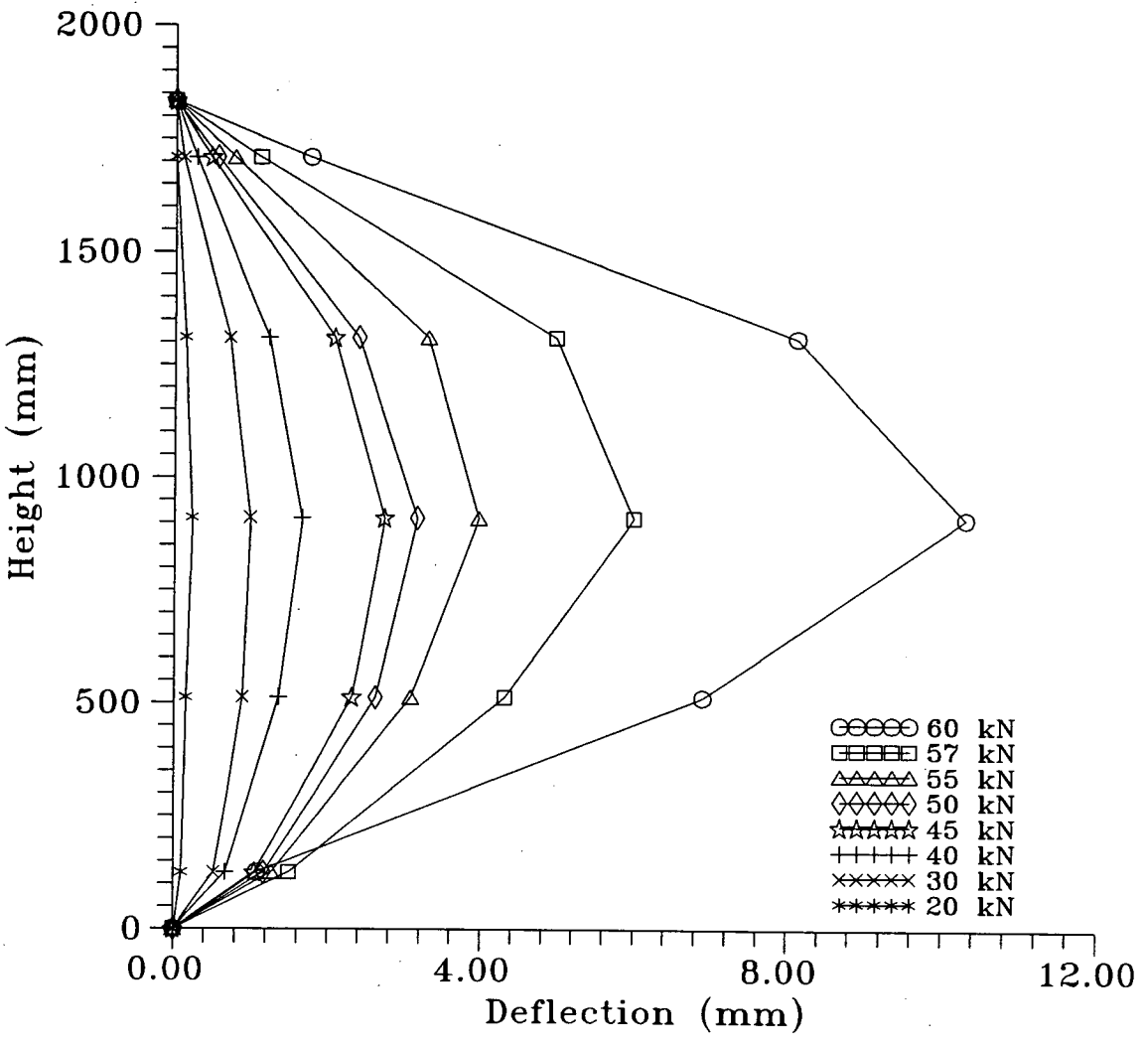


Fig. 6.71 Load-deflection relationship for the FCE_2 (10 mm) column

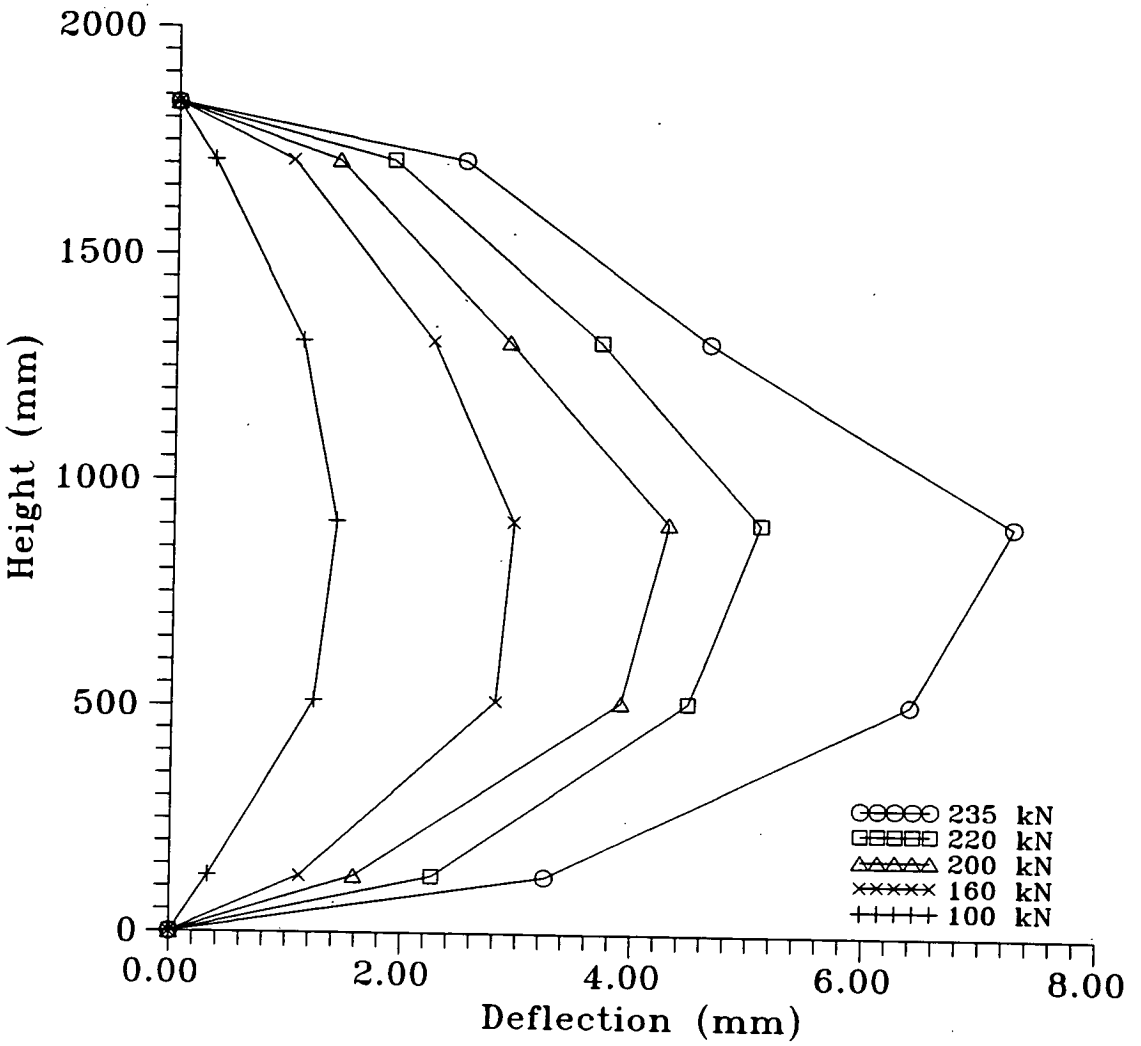


Fig. 6.72 Load–deflection relationship for the FCE_2 (20 mm) column

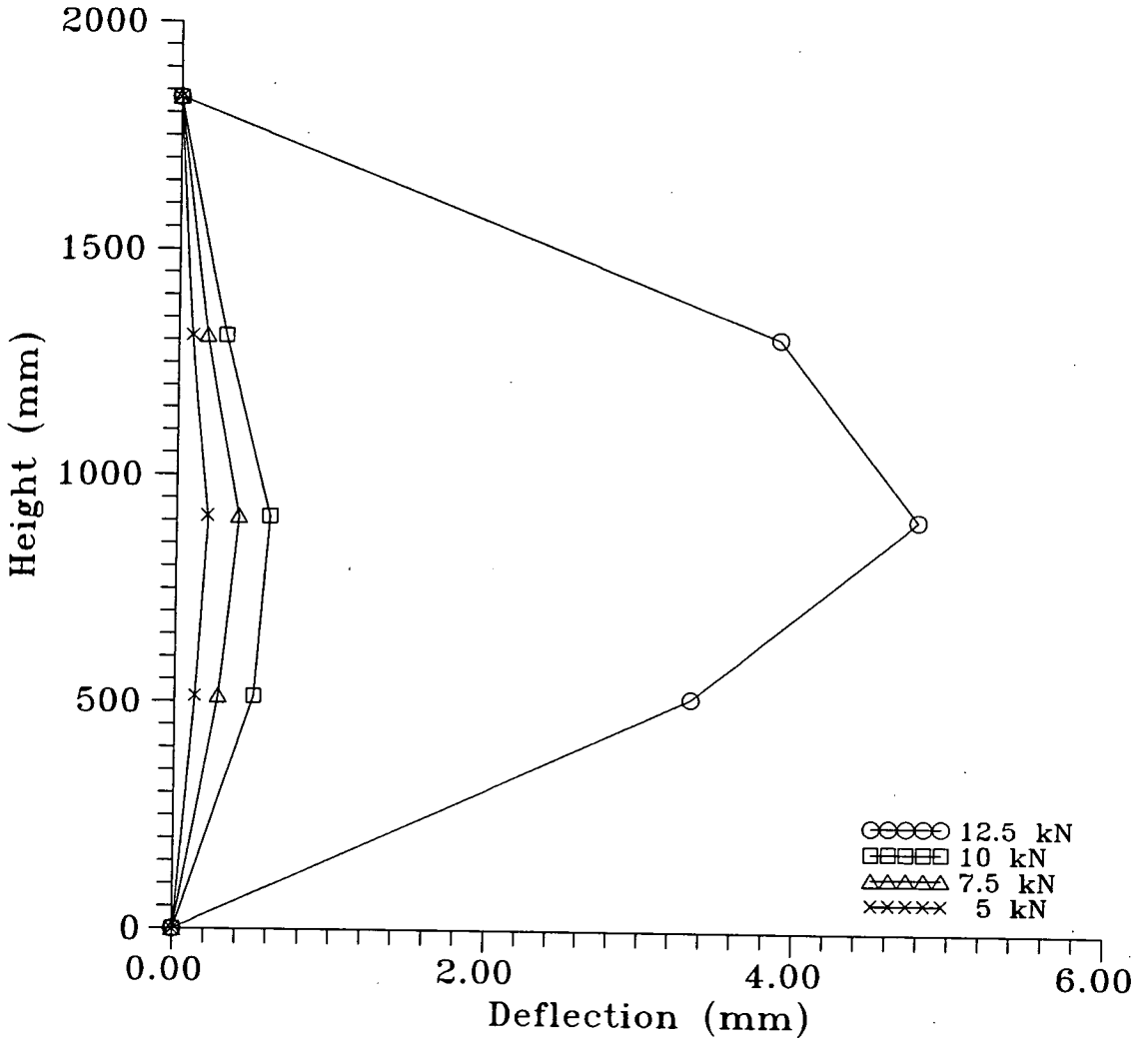


Fig. 6.73 Load–deflection relationship for the HCE_2 (No Steel) column

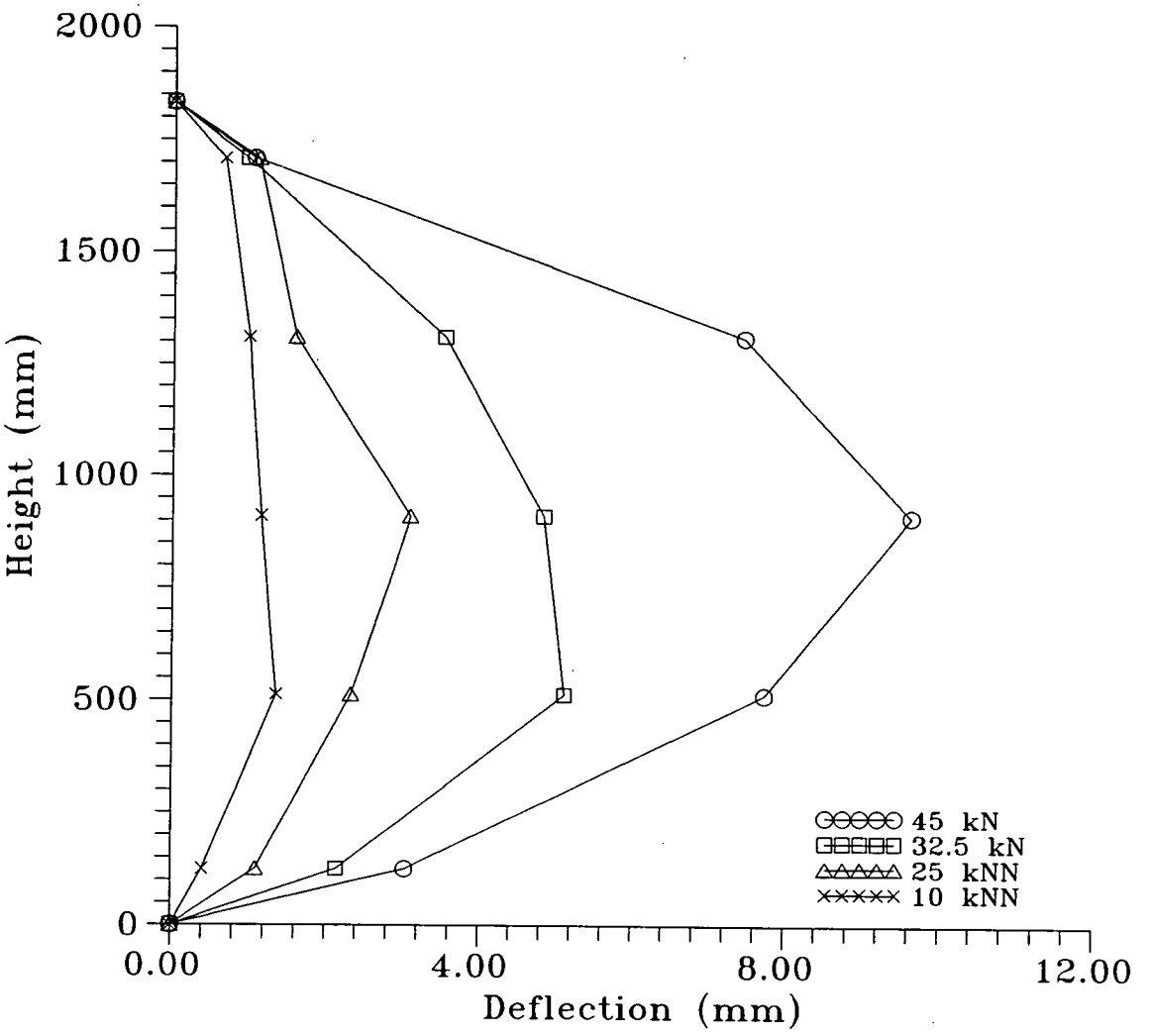


Fig. 6.74 Load–deflection relationship for the HCE_2 (8 mm) column

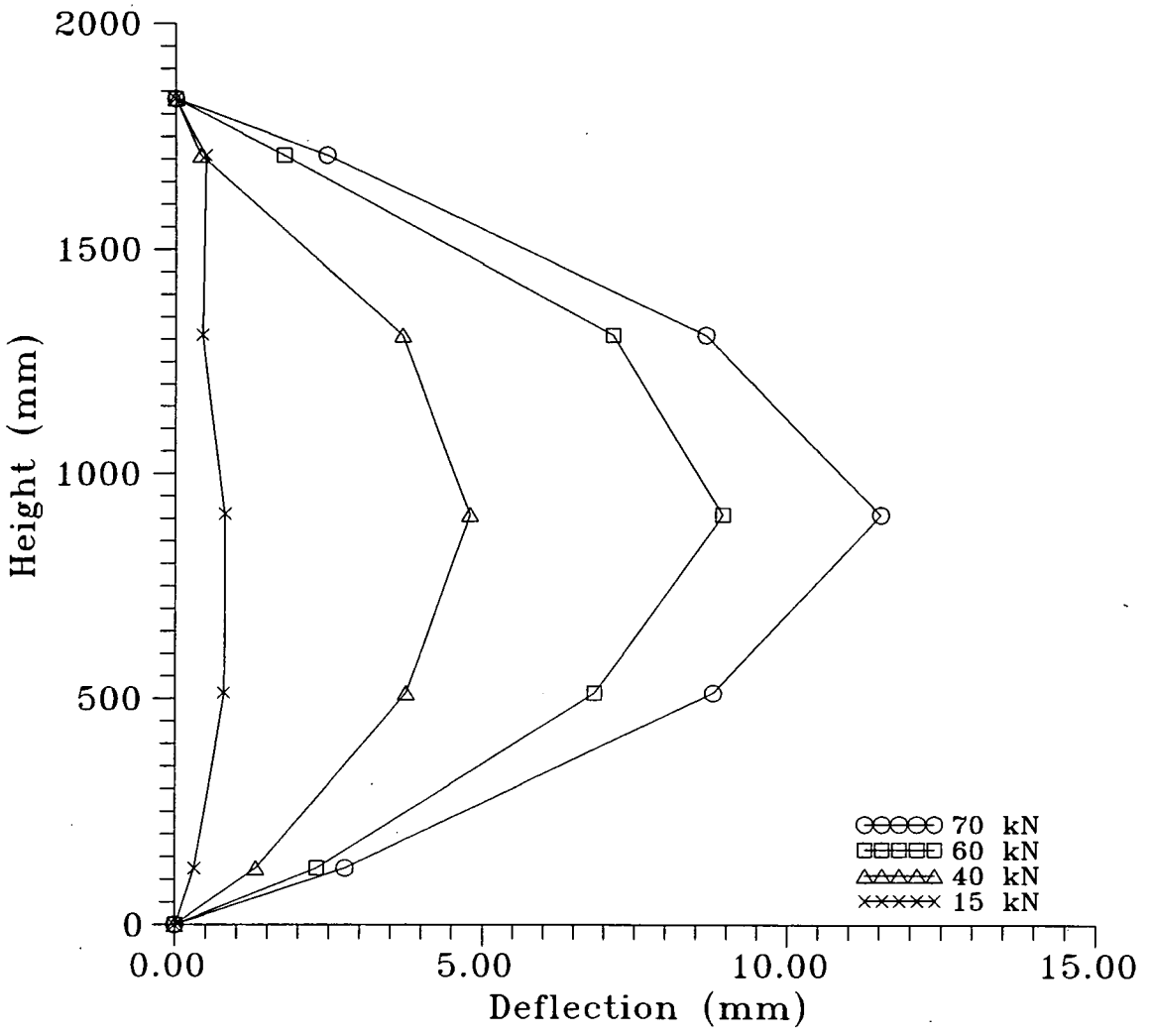


Fig. 6.75 Load–deflection relationship for the HCE_2 (20 mm)

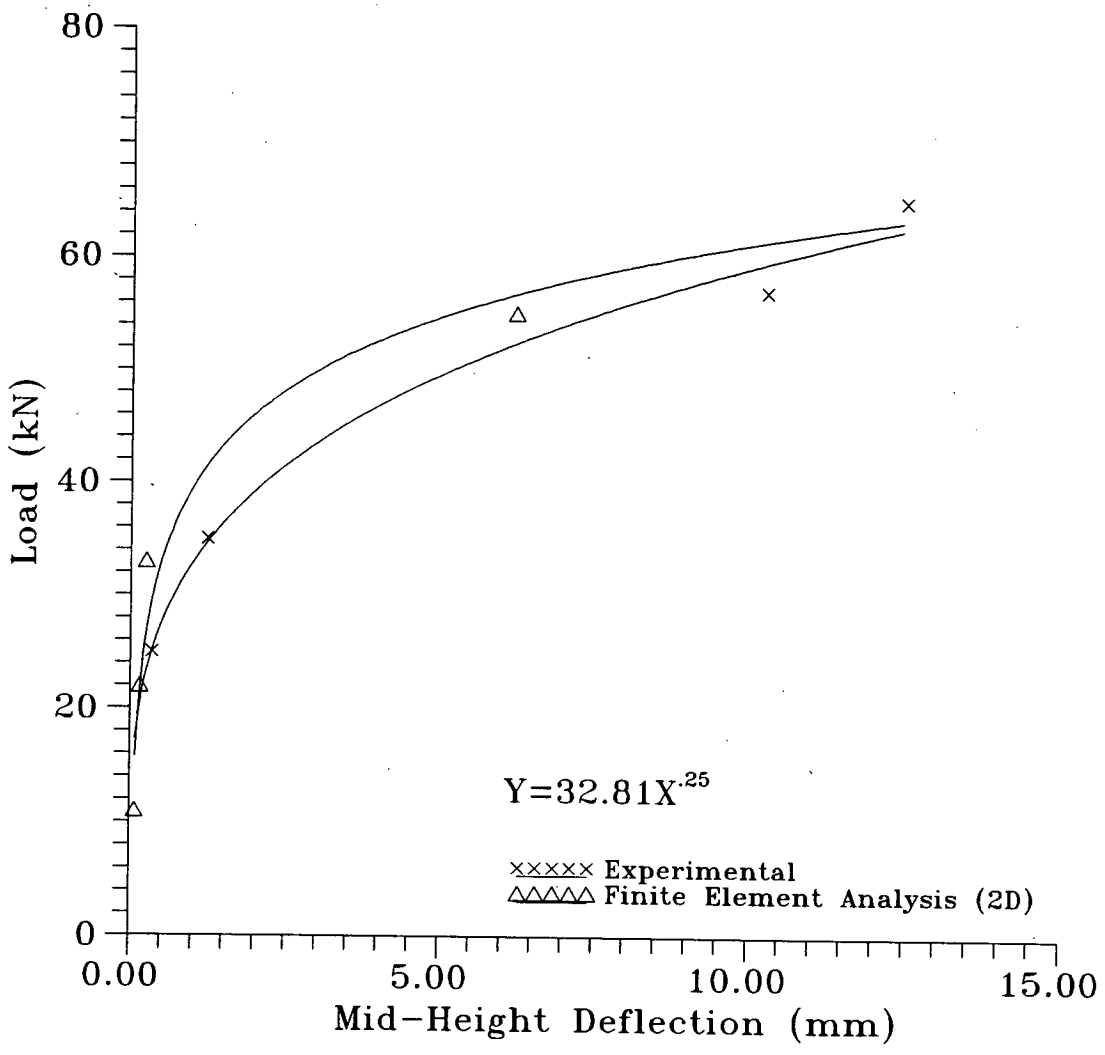


Fig. 6.76 Theoretical and experimental result for deflections at mid-height of column FCE_1 (No Steel)

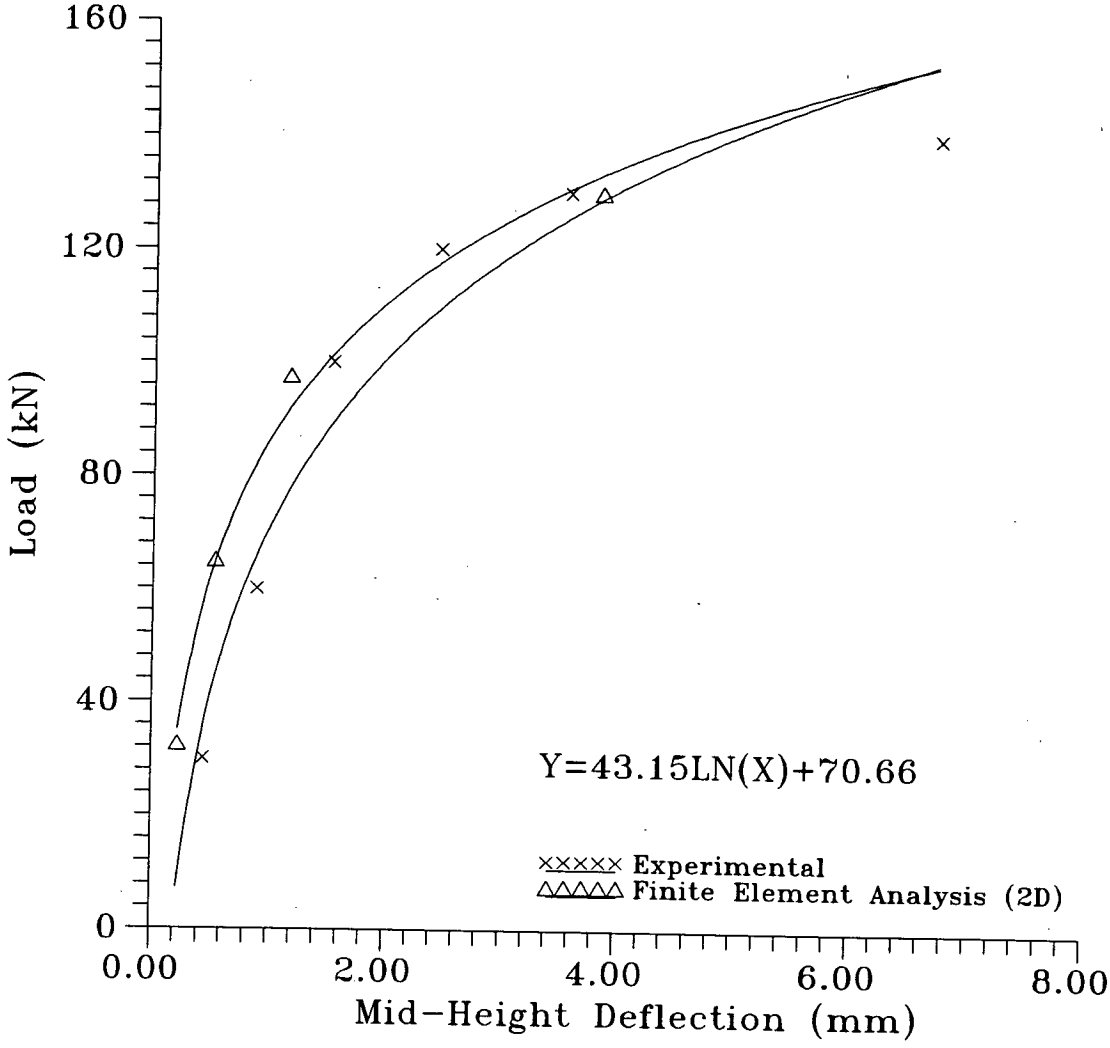


Fig. 6.77 Theoretical and experimental results for deflections at mid-height of column FCE_1 (10 mm)

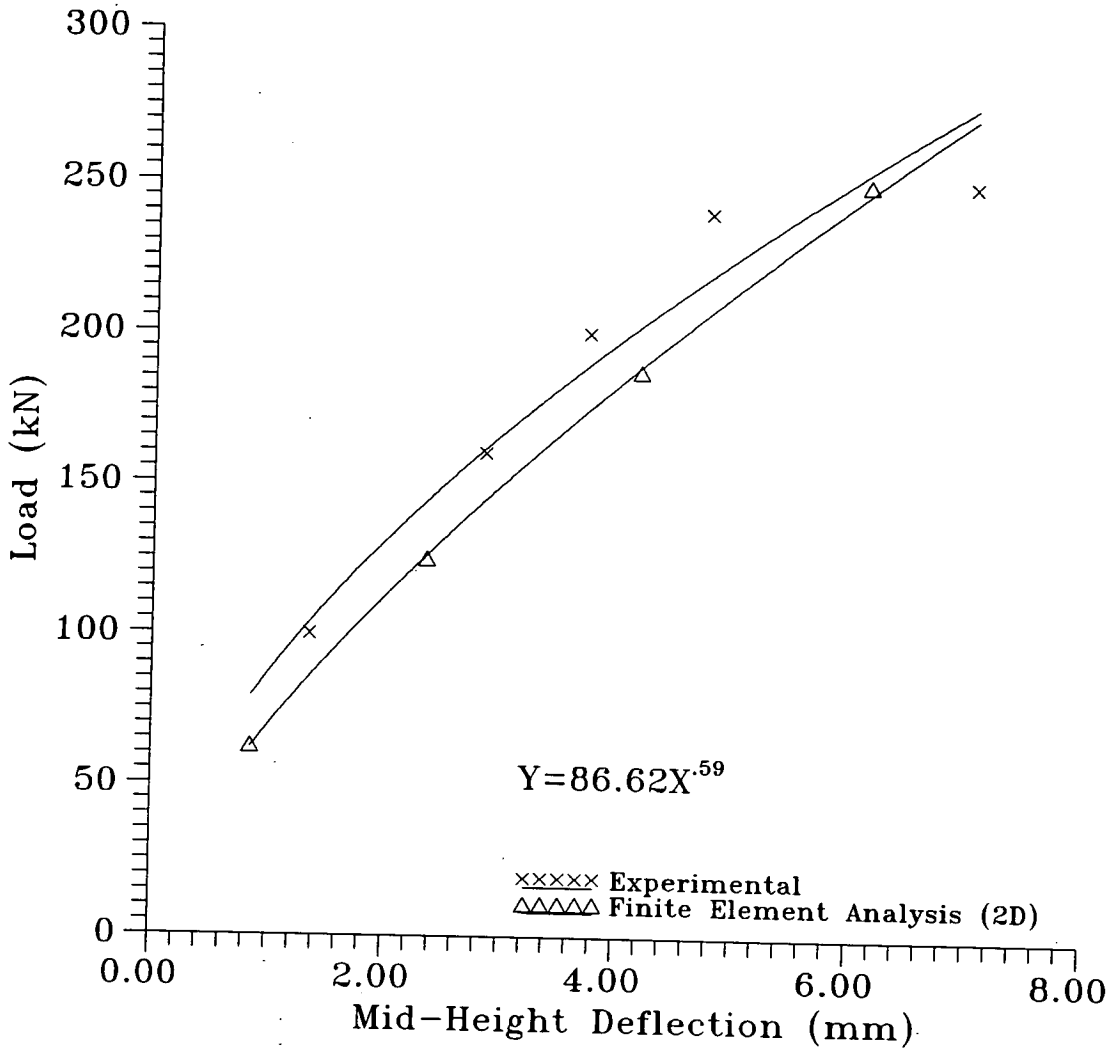


Fig. 6.78 Theoretical and experimental results for deflections at mid-height of column FCE_1 (20 mm)

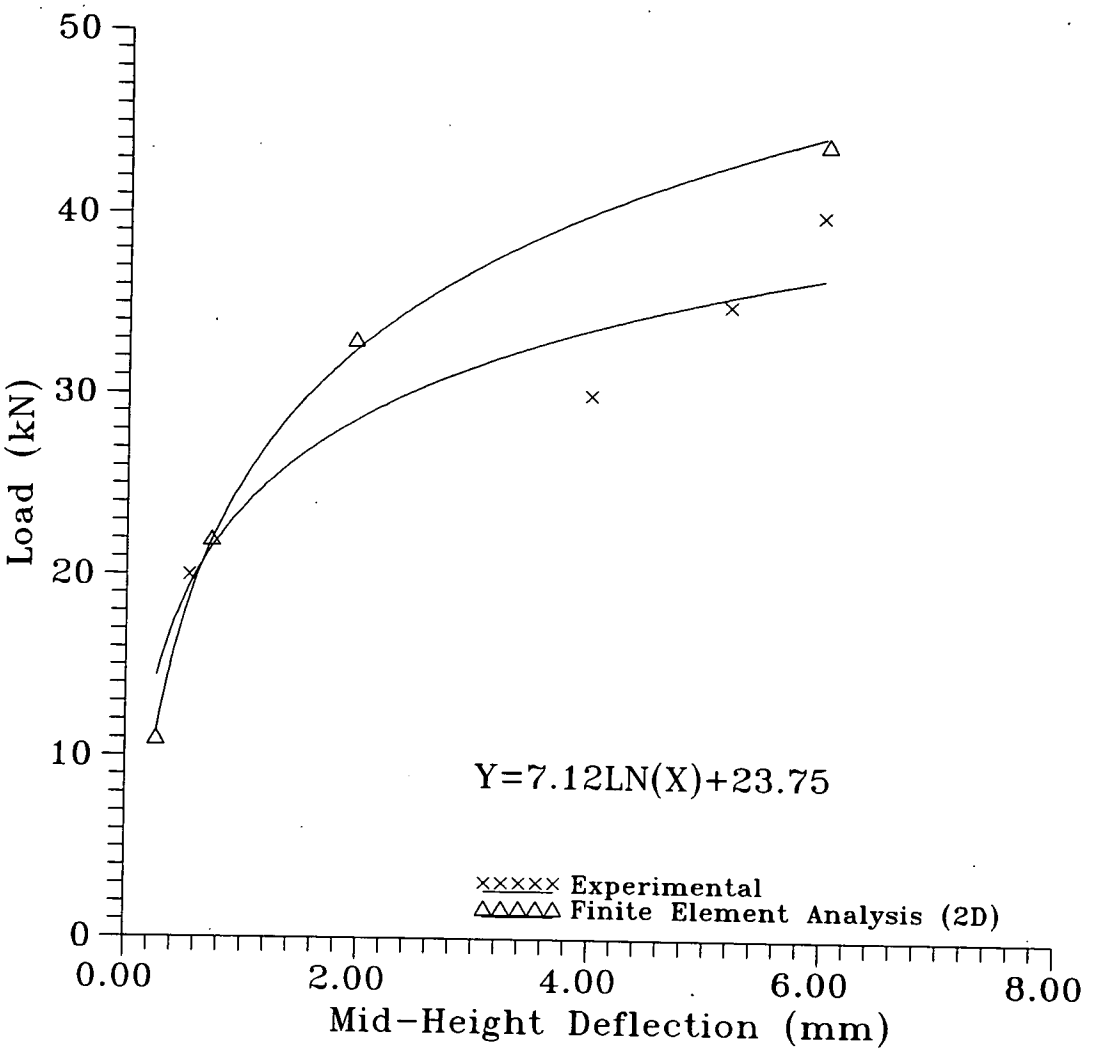


Fig. 6.79 Theoretical and experimental result for deflections at mid-height of column HCE_1 (No Steel)

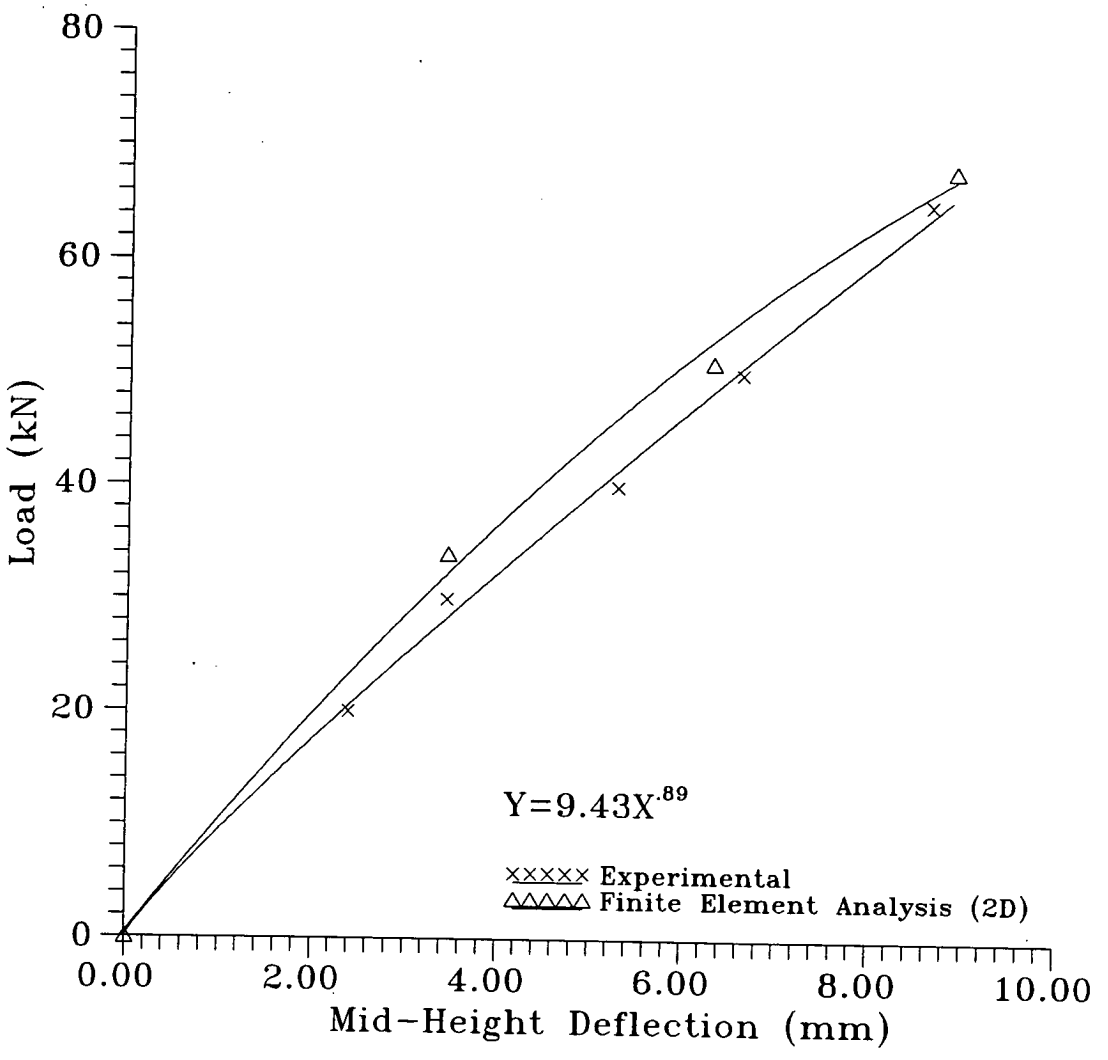


Fig. 6.80 Theoretical and experimental results for deflections at mid-height of column HCE_1 (8 mm)

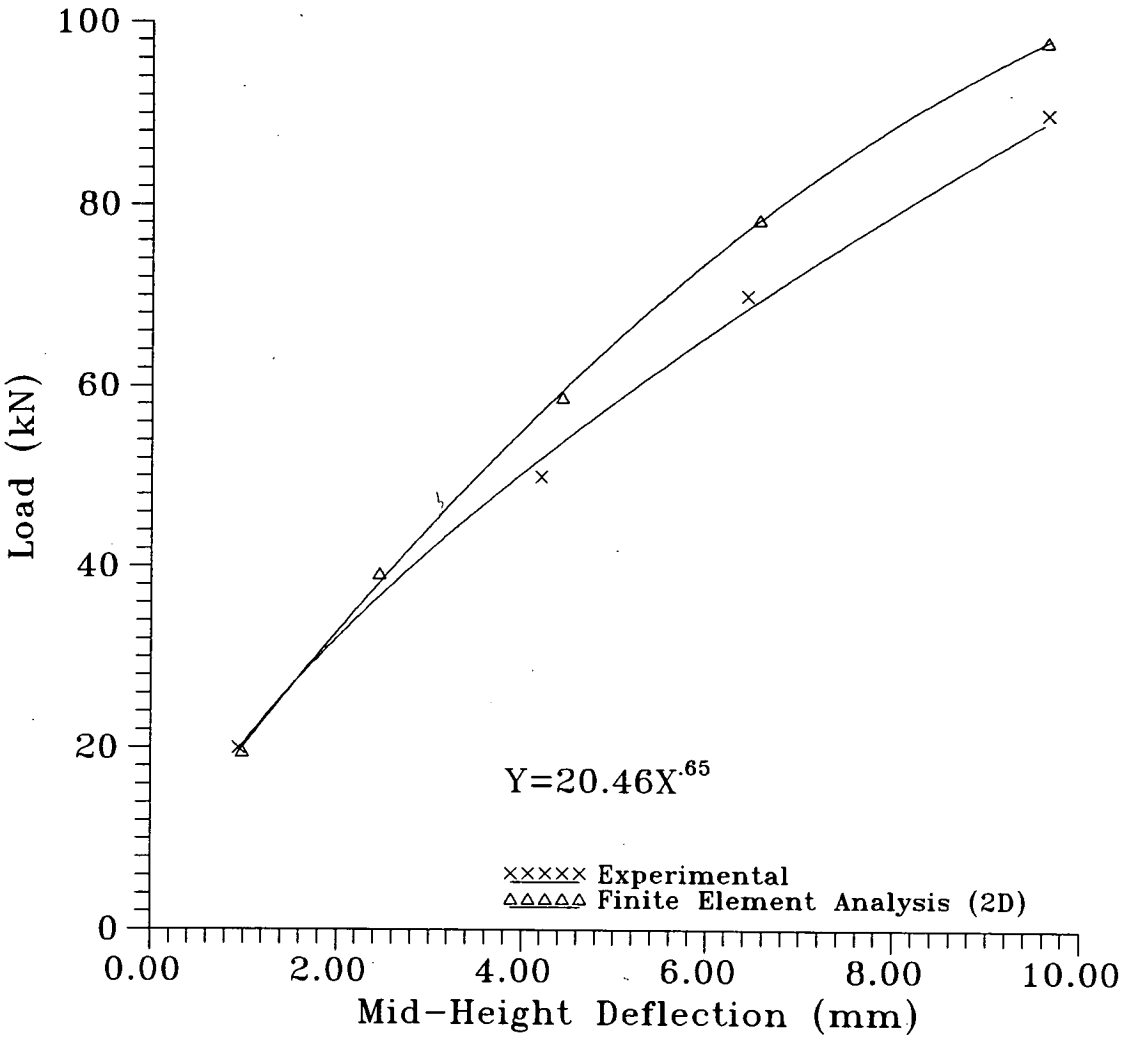


Fig. 6.81 Theoretical and experimental result for deflections at mid-height of column HCE_1 (20 mm)

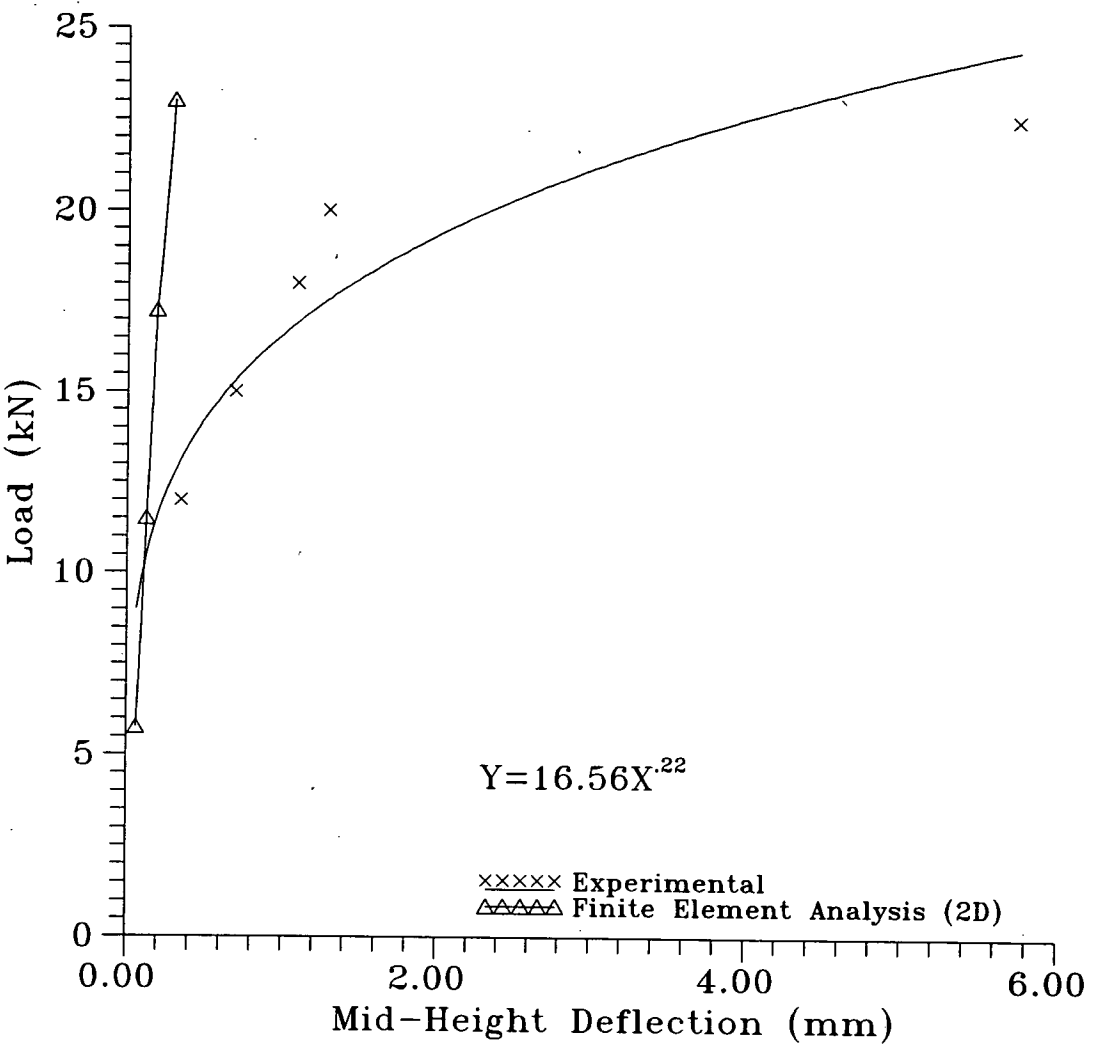


Fig. 6.82 Theoretical and experimental result for deflections at mid-height of column FCE_2 (No Steel)

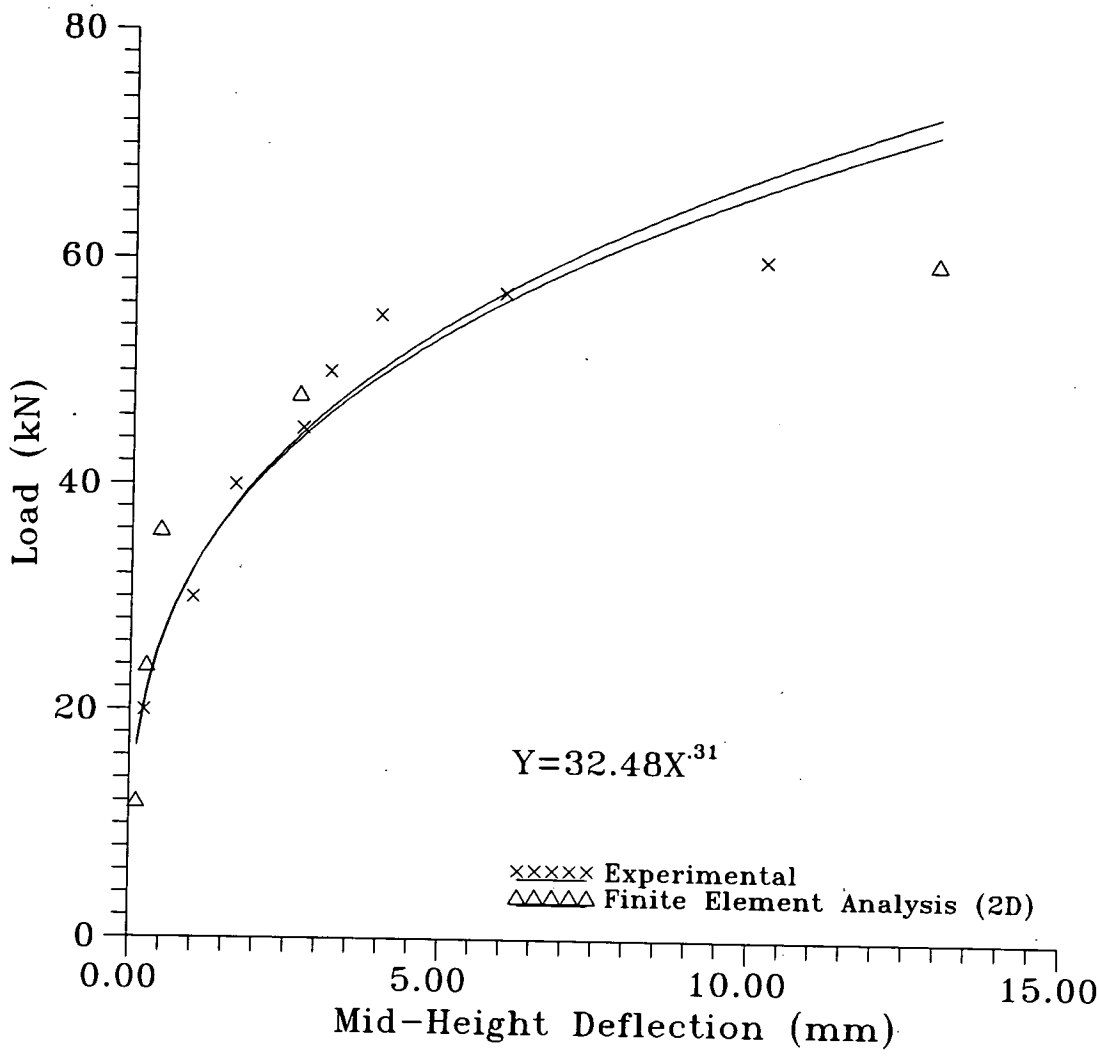


Fig. 6.83 Theoretical and experimental result for deflections at mid-height of column FCE_2 (10 mm)

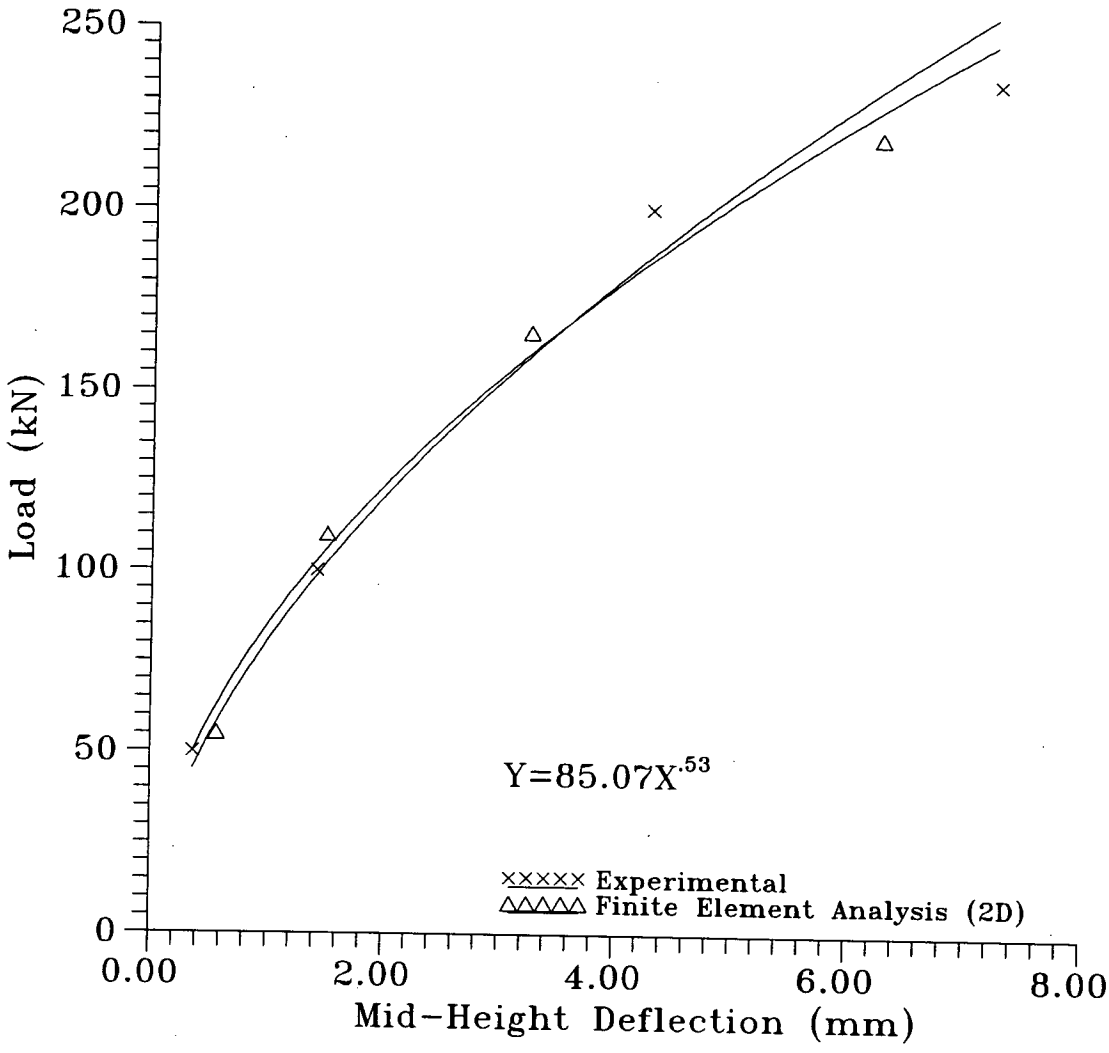


Fig. 6.84 Theoretical and experimental result for deflections at mid-height of column FCE_2 (20 mm)

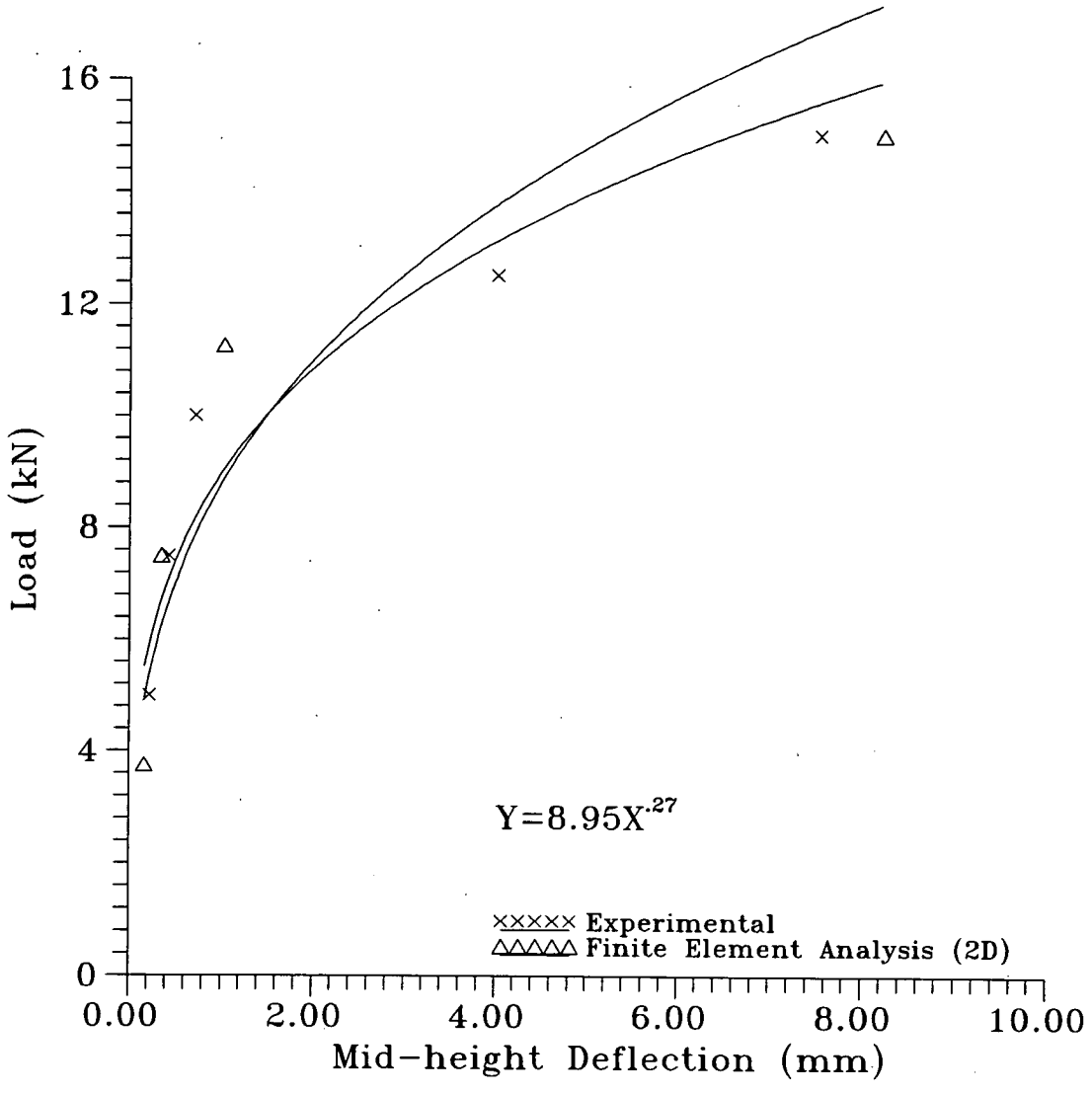


Fig. 6.85 Theoretical and experimental reults for deflections at mid-height of column HCE_1 (No Steel)

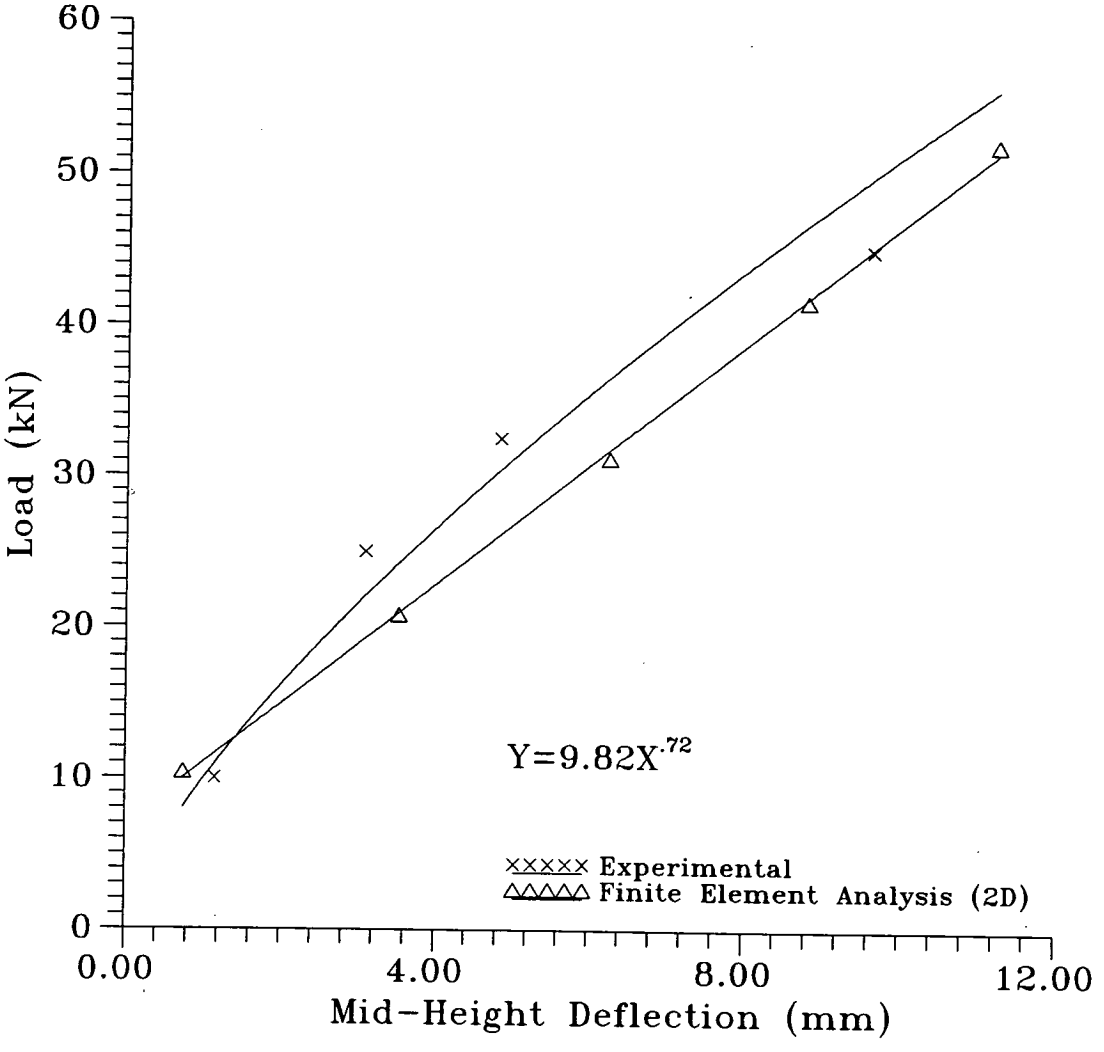


Fig. 6.86 Theoretical and experimental results for deflections at mid-height column HCE_2 (8 mm)

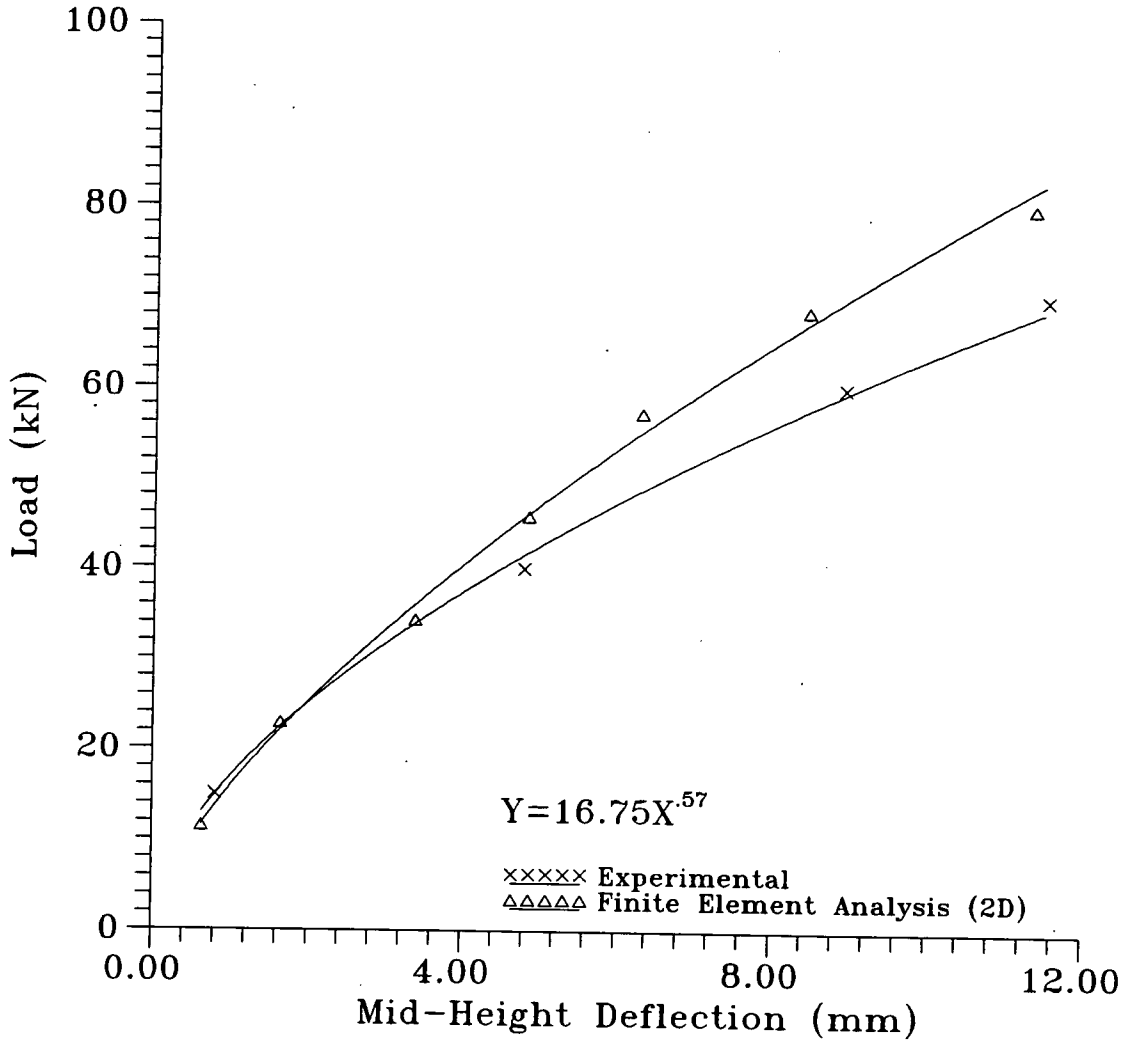


Fig. 6.87 Theoretical and experimental result for deflections at mid-height of column HCE_2 (20 mm)

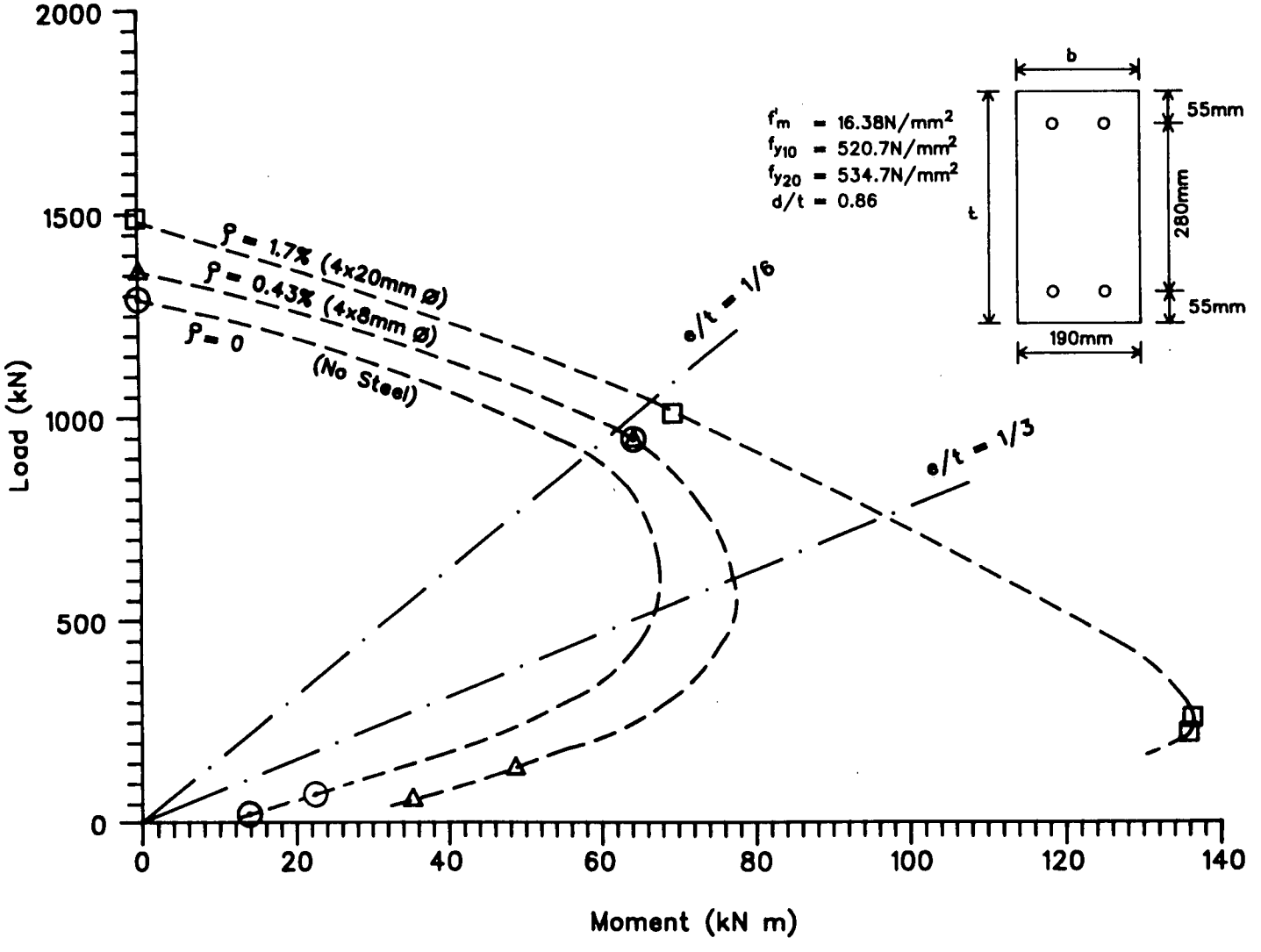


Fig. 6.88 Load–moment interaction diagrams for full–block masonry columns

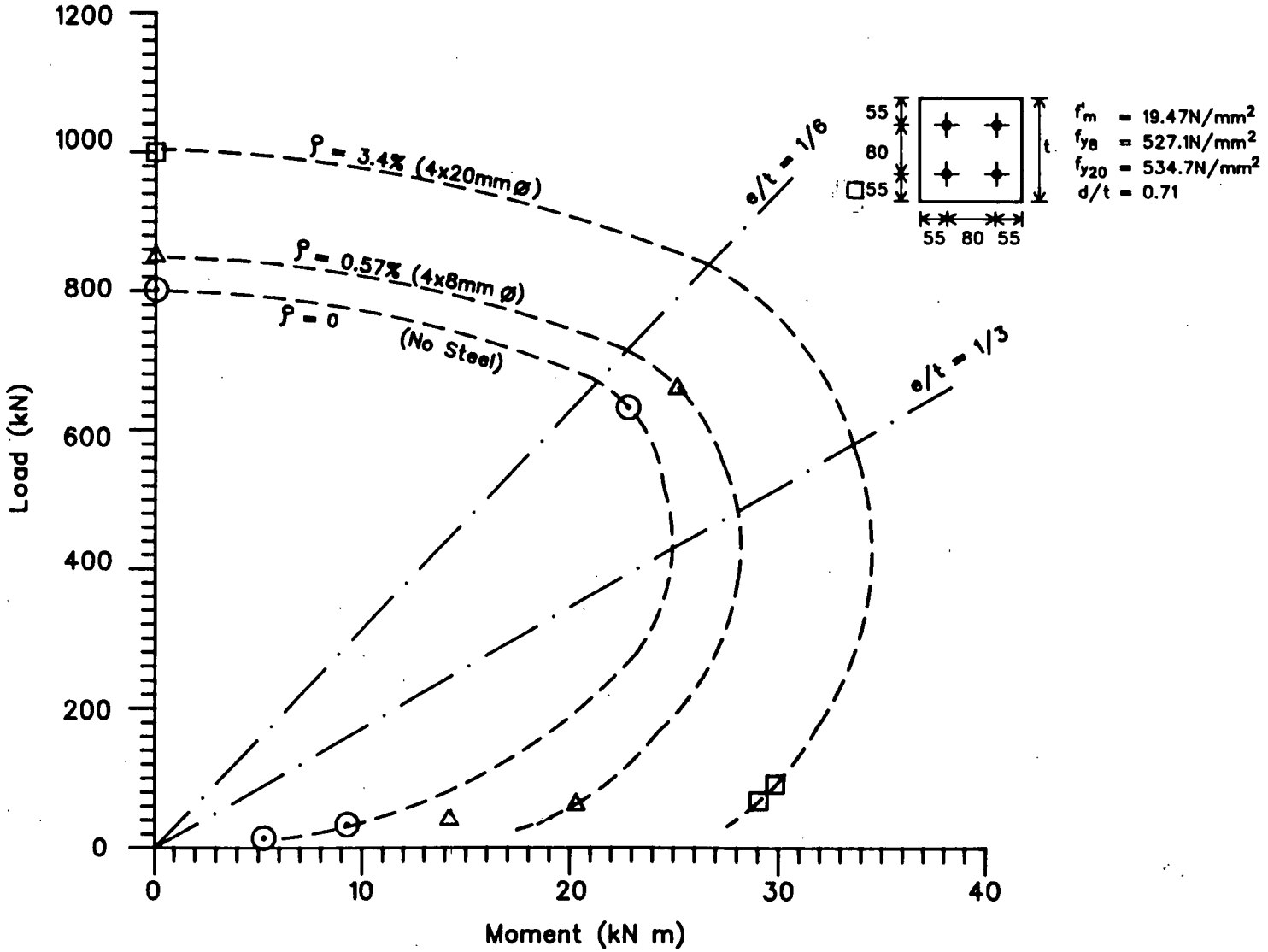


Fig. 6.89 Load–moment interaction diagrams for half–block masonry columns

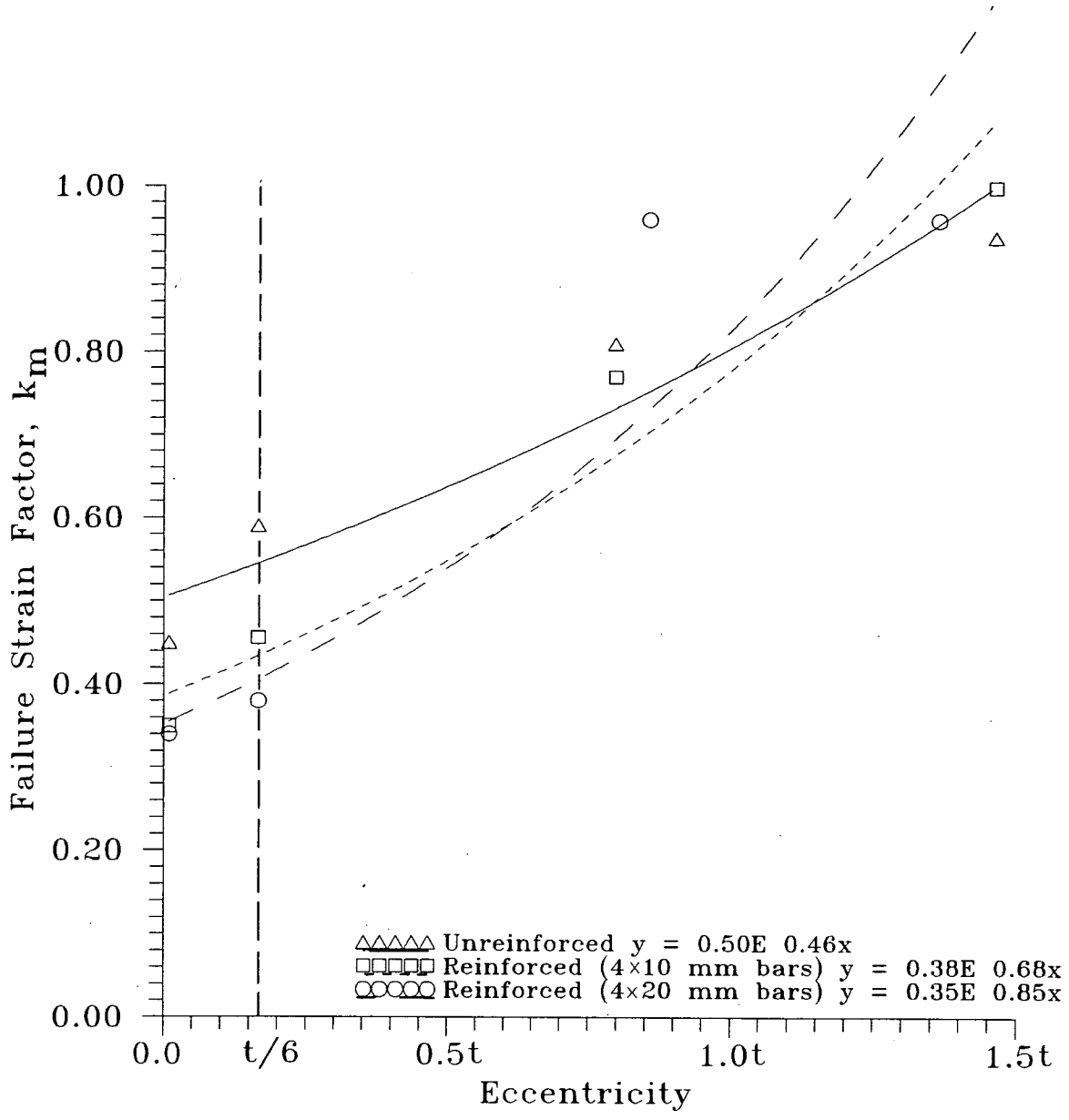


Fig. 6.90 Relationship between failure strain and load eccentricity for full-block masonry columns
($k_m = k_s$ in the case of concentric loading)

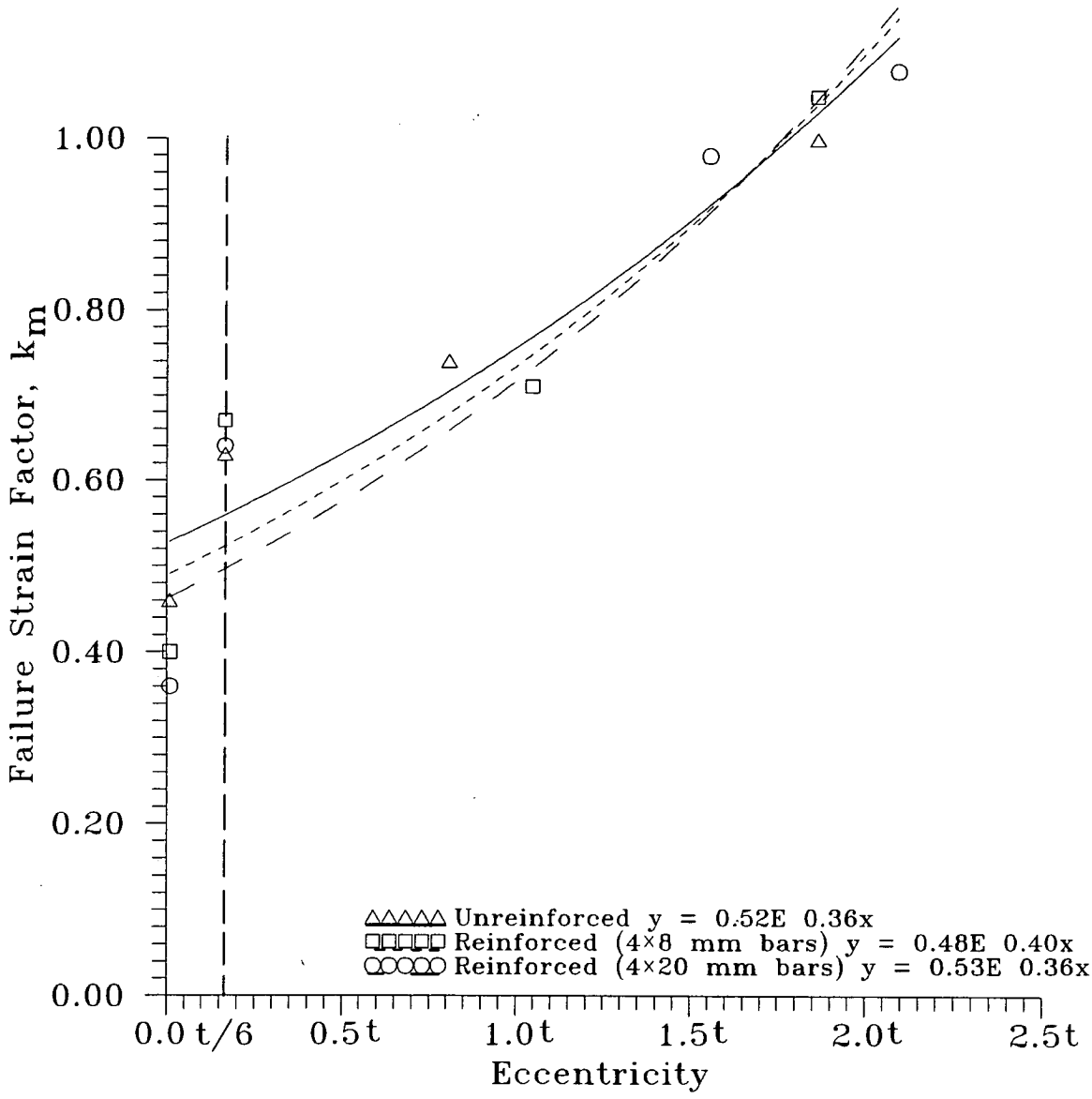


Fig. 6.91 Relationship between failure strain and load eccentricity for half-block masonry columns
($k_m = k_s$ in the case of concentric loading)

CHAPTER 7
GENERAL SUMMARY, CONCLUSIONS AND SUGGESTIONS FOR FURTHER WORK

7.1 GENERAL SUMMARY

This thesis presents the results of a study which has been carried out on blockwork masonry prisms compressed under axial concentric compression and eccentric load applied normal to unit bed face by two different eccentricities t/6 and t/3 in order to study the behaviour and effect of the strain gradient on enhancing the compressive strength of blockwork masonry f'_m.

A total of thirty five four block high prisms were investigated in this study, the variables were: the load eccentricity, the prism cross-sectional area (full or half-block) and whether the prisms were built with or without concrete infill.

To get a better picture of the prism deformation, stress distribution on different materials of the prism components, and crack formation, the prisms were analysed using the finite element technique.

The thesis also presents the results of experimental and theoretical investigations which were carried out to study the strength and behaviour of reinforced blockwork masonry columns subjected to axial concentric compression, and combined bending and axial load.

A total of twenty four blockwork masonry short columns were built with different percentages of vertical reinforcement and were tested up to failure

under different eccentricities in order to establish the load-moment strength interaction diagrams.

On the basis of assumptions used in the design of reinforced concrete columns using ultimate limit states design principles and the test results gathered from this study, a theoretical method was suggested to predict the ultimate strength of short blockwork columns compressed under different load eccentricities.

7.2 CONCLUSIONS

On the basis of the experimental and theoretical investigations, the overall conclusions drawn are:

(1) Compared with concentrically loaded prisms, the effect of the strain gradient on enhancing the ultimate extreme fibre stress of eccentrically loaded blockwork prisms was found to be significant. The ultimate extreme fibre stress for prisms loaded under an eccentric loading of t/6 increased by 51% and 45% for unfilled and filled full-block respectively, and by 62% and 50% for unfilled and filled half-block prisms respectively. The ultimate extreme fibre stress for prisms loaded under an eccentric loading of t/3 increased by 78% and 58% for unfilled and filled full-block prisms respectively, and by 153% and 83% for unfilled and filled half-block prisms respectively.

(2) The ultimate extreme fibre stress, f'_m, for eccentrically loaded prisms (or columns) could be determined by using an approximate linear method or by using either the trapezoidal or the trapezoidal centre methods which are based on the stress-strain relationship of a

confined 10 mm mortar joint[39]. The trapezoidal centre method proved to be more accurate in estimating f'_m. The depth of the neutral axis was also estimated using the trapezoidal centre method.

(3) The finite element analysis results gave a clear view of the prism's behaviour during the experimental part of this study. It gave adequate information on the prism's deformation and stress distribution for each material of the prism components.

(4) Columns provided with reinforced caps at both ends were found to be good in preventing crushing from occurring in areas near to the machine platens, when either concentric or eccentric loads were applied.

(5) Using finite element techniques, it was found that if blocks provided with cut-outs or openings were used in the lower block for the purpose of removing drops of mortar and welding material from inside, the dimensions of the opening should kept to a minimum size. Large openings in the block shells create concentrated high tensile stresses in the area on top of the opening. Therefore blocks or bond beam blocks provided with large openings are not recommended.

(6) Stirrups at the level of the upper side of a rectangular opening were found to be beneficial in reducing the harmful lateral tensile stresses.

(7) Columns tested with reinforced concrete caps at both ends have a similarity to site construction where the wall or column could be built

on a plain or reinforced footing and might carry one or more reinforced concrete or steel beams.

From the results of a finite element analysis survey carried out on columns with different strength of concrete in the caps, it was concluded that when the cap is filled with a concrete mix having a compressive strength higher than the concrete infill, the tensile stresses were reduced in the adjacent block shells. Therefore it is recommended that concrete with higher strength than the infill concrete and the block concrete should be used in the caps or joints.

(8) A new formula (equation 6.11) based on the test results is suggested to determine the short term static modulus of elasticity for reinforced blockwork short columns.

(9) The effect of strain gradient on enhancing the ultimate extreme fibre stress of unreinforced and reinforced full and half-block columns compressed under t/6 eccentric loads is significant. Compared to the concentrically loaded columns the ultimate extreme fibre stress increased by 51%, 44% and 40% for unreinforced and reinforced full-block columns (10 mm and 20 mm ϕ vertical bars) respectively. The ultimate extreme fibre stress also increased by 66%, 61% and 74% for unreinforced and reinforced half-block columns (8 mm and 20 mm ϕ vertical bars).

The explanation of the increase in the extreme fibre stress which occurs under eccentric loading is related to the high lateral tensile stresses in the blocks, caused by a high confinement stress in the

stresses in the blocks, caused by a high confinement stress in the mortar taking place on the compression side of the eccentrically loaded columns (or prisms), where the lateral tensile stresses in the block webs are small. This is different to the case of concentrically loaded columns (or prisms) where the mortar is under high confinement stresses causing high lateral tensile stresses in the block face shells as well as the webs.

(10) Based on ultimate limit state principles a new method of predicting the load capacity of blockwork masonry columns has been developed. The compressive strength of blockwork masonry could be determined from testing prisms having h/t ratio between 3 and 5 and built from blocks similar to the ones used in building the columns and with the same mortar and concrete infill mixes.

(11) Buckling of the longitudinal bars throughout the length of two lateral ties was the dominant mode of failure for all the axially loaded reinforced blockwork columns.

7.3 SUGGESTIONS FOR FURTHER WORK

The following topics are suggested as an extension to this study:

(1) More work is needed to study the effect of the strain gradient on enhancing the compressive strength of the prism, f'_m, by testing prisms with different types of hollow blocks, thickness, strength, percentage of infilled area to solid area. Other variables should also include different strengths of mortar and concrete infills.

(2) More work is needed to study the strength and behaviour of blockwork masonry prisms under concentric and eccentric loads in directions different than normal to the bed face unit, such as parallel to the bed face.

(3) It has been concluded from the current study that buckling of the longitudinal bars throughout the length of two lateral ties was the dominant mode of failure for all axially loaded columns. Therefore more work is needed to study the effect of reducing the spacing between two lateral ties for reinforced blockwork masonry columns.

(4) In this study all the columns tested in order to establish the load-moment strength interaction diagrams, were built from hollow blocks having the same compressive strength, dimensions, the same core taper and shell thickness. Also one type of mortar, concrete infill and steel reinforcement were used throughout, therefore more investigations should be carried out to study the effect of each of these factors as well as the effect of different reinforcement detailing on the strength and behaviour of the blockwork masonry columns.

REFERENCES

(1) BAKER, L.R., "The Flexural Action of Masonry Structures under Lateral Load", PhD Thesis, Deakin University, Australia, 1981.

(2) STANLEY, C.C., "Highlights in the History of Concrete", Cement and Concrete Association, Slough, 1979.

(3) ROBERTS, J.J, TOVEY, A.K., CRANSTON, W.B. and BEEBY, A.W. , "Concrete Masonry Designer's Handbook", Viewpoint Publ., Eyre and Spottiswoode Publ. Ltd., Leatherhead, 1983.

(4) ROBERTS, J.J., "Concrete Masonry", Cement and Concrete Association, Slough, 1983.

(5) ROBERTS, J.J., "Reinforced Concrete Masonry", Cement and Concrete Association, Slough, 1985.

(6) ROBERTS, J.J.,"Reinforced and Prestressed Masonry", Cement and Concrete Association, Slough, 1987.

(7) BEALL, C., "Masonry Design and Detailing", Prentice-Hall Inc., London.

(8) CANADIAN STANDARDS ASSOCIATION, "Masonry Design and Construction for Buildings", CSA-CAN3-S304, 1978.

(9) AMERICAN CONCRETE INSTITUTE, "Building Code Requirement for Concrete Masonry Structures", ACI 531R-79, Revised 1981.

(10) BRITISH STANDARDS INSTITUTION, "Use of Masonry", BS 5628: Part 1: 1978, Parts 2 and 3: 1985.

(11) LYSE, I., "Tests of Reinforced Brick Columns", Journal of Amer. Cera. Soc., Vol. 26, Nov. 1933, pp 584-497.

(12) BREBNER, A., "Notes on Reinforced Brickwork", Tech. Pap. 38, Vols 1 and 2, Government of India, 1923.

(13) WITHEY, M.O., "Tests on Reinforced Brick Masonry Columns", Proc. Amer. Soc. Test. Mate., ASTM, Vol. 34, Part II, 1934, pp 387-405.

(14) DAVEY, N. and THOMAS, F.G., "The Structural Use of Brickwork", The Inst. of Civil Eng., Stru. and Buil. Paper No. 24, Feb. 1950, pp 3-66.

(15) ANDERSON, D.E. and HOFFMAN, E.S., "Design of Brick Masonry Columns", Int. Conf. on Masonry Stru. Syst., Univ. of Texas, Austin, 1967, pp 94-100.

(16) BRETTLE, H.J., "Ultimate strength Design of Reinforced Brickwork Piers in Compression and Biaxial Bending", Civil Eng. Tran. Inst., Eng. Australia, CE 12, (1), No. 49, 1970.

(17) ARMSTRONG, A.C. and HENDRY, A.W., "The Compressive Strength of Brickwork with Reinforced Bed Joints", Brit. Cera. Res. Assoc., Tech. Note 209, 1973.

(18) OHLER, A. and GOPFERT, N., "The Effect of Lateral Joint Reinforcement on the Strength and Deformation of Brickwork Piers", Proc. 6th IBMAC, Rome, 1982, pp 677-688.

(19) ELTRAIFY, E.A., "Uni-axial and Bi-axial Bending of Reinforced Brick Masonry Columns", PhD Thesis, University of Edinburgh, Edinburgh, 1983.

(20) EDGELL, G.J. and TEMPLENTON, W., "Reinforced Brickwork Columns", Proc. 7th IBMAC, Melbourne, Australia, 1985, pp 1065-1073.

(21) SHANK, J.R. and FOSTER, H.D., "Strength of Concrete Block Pilasters under Varied Eccentric Loading", Ohio State Univ. Exper. Station Bulletin No. 60, 1931.

(22) FEEG, C., LONGWORTH, J. and WARWARUK, J., "Effects of Reinforcement Detailing for Concrete Masonry Columns", Structural Engineering Report No. 76, Civil Engineering Department, University of Alberta, Edmonton, 1979.

(23) SALIM, A.H., "The Effect of Confinement Reinforcement on Load Carrying Capacity of Masonry Prisms", Proc. 2nd Canadian Masonry Symp., Ottawa, Canada, pp 65-72.

(24) STURGEON, G.R., LONGWORTH, J. and WARWARUK, J., "An Investigation of Reinforced Concrete Block Masonry Columns", Structural Engineering Report No. 91, University of Alberta, Edmonton, 1980.

(25) AL-SARRAF, S.Z., FAIYADH, F.I. and KHALAF, F.M., "A Study of the Capacity and the Behaviour of Reinforced Short Columns Subjected to Axial Load", Masonry Inter., No. 7, 1986, pp 3-7.

(26) KHALAF, F.M., "A Study of the Compressive Strength and Behaviour of Concrete Blockwork Masonry with Special Reference to Reinforced Columns", PhD Thesis, University of Edinburgh, Edinburgh, 1991.

(27) DRYSDALE R.G. and HAMID, A.A., "Capacity of Concrete Block Masonry Prisms Under Eccentric Compressive Loading", ACI Journal, Vol. 80, No. 2, 1983, pp 102-108.

(28) KHALAF, F.M. and HENDRY, A.W., "Effect of Bed-Face Preparation in Compressive Testing of Masonry Units", Proc. 2nd Int. Masonry Conf., British Masonry Soc., No. 4, 1990, pp 129-130.

(29) BRITISH STANDARDS INSTITUTION, "Bending Dimensions and Scheduling of Bars for the Reinforcement of Concrete", BS 4466: 1981.

(30) NEVILLE, A.M., "Properties of Concrete", 3rd Edn., London, Pitman Books, 1981.

(31) BRITISH STANDARDS INSTITUTION, "Sampling and Testing of Mineral Aggregates, Sands and Fillers", BS 812: Part 1: 1975.

(32) BRITISH STANDARDS INSTITUTION, "Aggregates from Natural Sources for Concrete", BS 882: 1982.

(33) BRITISH STANDARDS INSTITUTION, "Sands for Mortar for Plain and Reinforced Brickwork Blockwalling and Masonry", BS 1200: 1976.

(34) BRITISH STANDARDS INSTITUTION, "Specification for Hot Rolled Steel Bars for the Reinforcement of Concrete", BS 4449: 1978.

(35) BRITISH STANDARDS INSTITUTION, "Testing Concrete", BS1881: Part 121: 1983.

(36) BRITISH STANDARDS INSTITUTION, "Precast Concrete Masonry Units", BS 6073: Parts 1 and 2: 1981.

(37) BRITISH STANDARDS INSTITUTION, "Structural Use of Concrete: Code of Practice for Special Circumstances", BS 8110: Part 2: 1985.

(38) AMERICAN CONCRETE INSTITUTE, "Building Code Requirements for Reinforced Concrete", ACI 318-83, 1983.

(39) KHALAF, F.M., "An Investigation into the Capacity and Behaviour of Concrete Block Specimens Loaded Parallel to the Bed Face", Proc. 8th IBMAC, Ireland 1988 pp 752-763.

(40) KHALAF, F.M., HENDRY, A.W. and FAIRBAIRN, D.R., "Compressive Strength of Concrete Block Masonry Prisms Tested Concentrically and Eccentrically Normal and Parallel to Bed Face", Proc. 3rd Int. Sem. on Struct. Masonry for the Developing Countries, Mauritius, 1990, pp 123-135.

(41) MAHER, A. and DAVID, D., "Mortar Constituent of Concrete in Compression", ACI Journal. Vol. 79, No. 2, 1982, pp 100 -109.

(42) HATZINIKOLAS, M., LONGWORTH, J. and WARWARUK, J., "Failure Modes for Eccentrically Loaded Concrete Block Masonry Walls", ACI Journ., Vol. 77, No. 3, 1980.

(43) PAGE, A.W., "Finite Element for Masonry", Journ. of Stru. Div., ASCE, Vol. 104, St.8, 1978, pp 1267-1285.

(44) WALKER, P.J., "A Study of the Behaviour of Partially Prestressed Brickwork Beams", PhD Thesis, University of Edinburgh, Edinburgh, 1987.

(45) TURNSEK, V. and CACOVIC, F., "Some Experimental Results on the Strength of Brick Masonry Walls", Proc. 2nd IBMAC, Edited by H.W.H. West and K. Speed, BCRA, Stoke-on-Trent, 1971, pp 149-156.

(46) LUSAS, "Finite Element Stress Analysis System", Finite Element Analysis Ltd., Forge House, Kingston upon Thames, Surrey.

(47) HAMID, A.A. and CHUKWUNEYE, A.O., "Compression Behaviour of Concrete Masonry Prisms", Journal of Struct. Eng., ASCE, Vol. 112, No. 3, 1983, pp 605-613.

(48) HATZINIKOLAS, M., LONGWORTH J. and WARWARUK, J., "Concrete Masonry Walls", Struct. Eng. Report No. 70, Civil Engineering Department, University of Alberta, Alberta, 1978.

(49) AFSHARI, F. A., "Analytical Modelling of Masonry Prisms", phD Thesis, University of Michigan, Ann Arbor, 1987.

(50) BOULT, B. F., " Concrete Masonry Prism Testing", ACI journal, Vol. 76, No. 4, 1979, pp 513-535.

(51) DRYSDLE, R. G. and HAMID, A. A., "Behaviour of Concrete Masonry under Axial Compression", ACI Journal, Vol. 76, No. 6 ,1979, pp 707-721.

(52) HAMID, A. A. and DRYSDALE, R. G., "Suggested Failure Criteria for Grouted Masonry Under Axial Compression", ACI journal, Vol.76, No. 10, 1979, pp 1047-1061.

(53) AFSHARI, F. A. and KALDJIAN, M. J., " Finite Element Analysis of Concrete Masonry Prisms", ACI Journal, Vol. 86, No. 5, 1989, pp 525-530.

(54) AMRHEIN, J.E., "Reinforced Masonry Engineering Handbook", 3rd Edition, Masonry Institute of America, Los Angeles, 1978.

(55) SAHLIN, S., "Structural Masonry", Printice-Hall Inc., Englewood Cliffs, N. J., 1971.

(56) ORTON, A., "Structural Design of Masonry", Longman Inc., New York, 1986.

(57) CHEEMA, T. S. and KLINGNER, R. E., "Compressive Strength of Concrete Masonry Prisms", ACI Journal, Vol. 83, No. 2, 1986, pp 88-97.

(58) KHALAF, F.M., HENDRY, A.W. and FAIRBAIRN, D.R., "Mechanical Properties of Materials Used in Concrete Blockwork Construction", Magazine of Concrete Research, Vol. 44, No. 158, Mar. 1992, pp 1-14.

(59) KHALAF, F.M., HENDRY, A.W. and FAIRBAIRN, D.R., "Elastic Modulus and Strength of Hollow Concrete Block Masonry with Reference to the Effect of Lateral Ties", Magazine of Concrete Research, Vol.44, No. 160, Sep. 1992, pp 185-194.

(60) KHALAF, F. M., HENDRY, A. W. and FAIRBAIRN, D. R., "Reinforced Blockwork Masonry Columns", ACI Journal, Vol. 90, No. 5, Sep-Oct. 1993, pp 496-504.

(61) DAVIES, S. R.,"Design of Short Reinforced Masonry Columns Under Uniaxial Bending", Proc. of the 3rd Inter. Seminar on Struc. Masonry for the Developing Countries, Mauritius, July 1990, pp. 213-222.

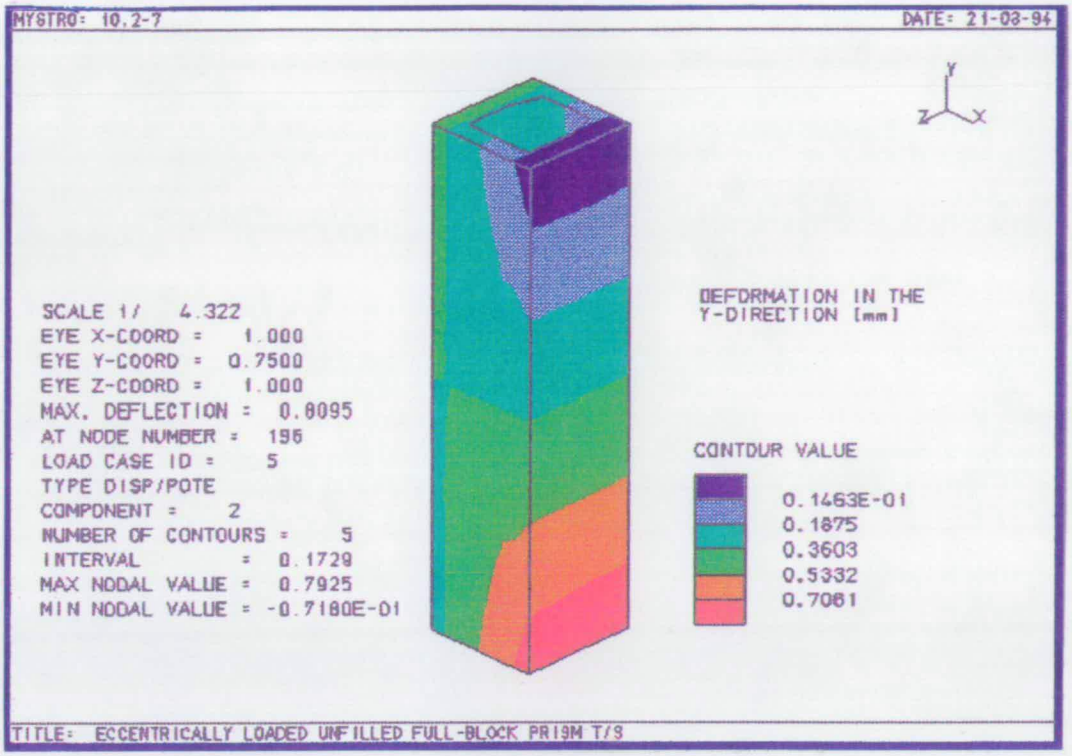


Fig. A.1 Deformation in the Y-direction of unfilled full-block prism compressed under eccentric load for e = t/3

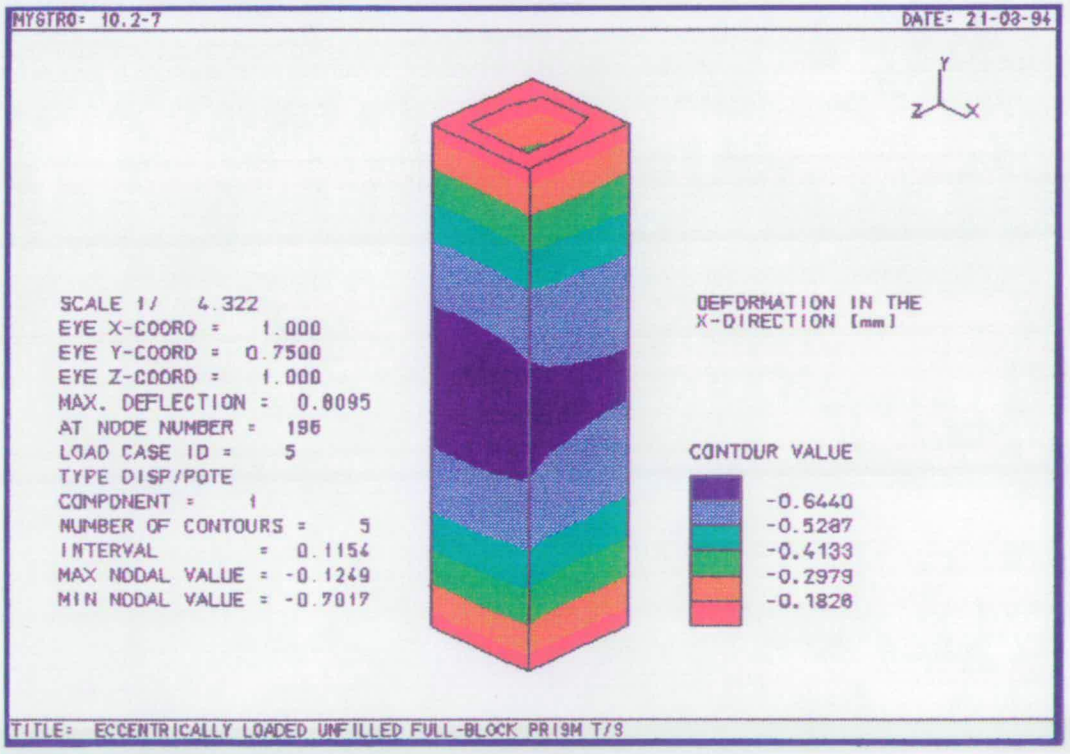


Fig. A.2 Deformation in the X-direction of unfilled full-block prism compressed under eccentric load for e = t/3

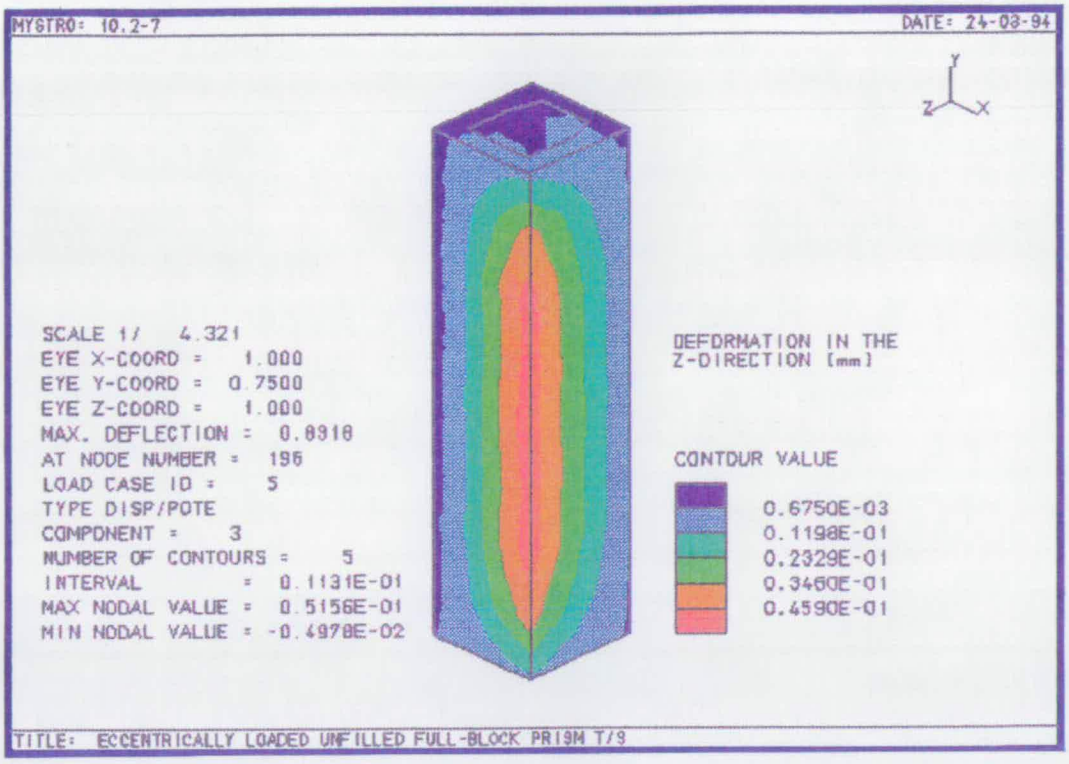


Fig. A.3 Deformation in the Z-direction of unfilled full-block prism compressed under eccentric load for e = t/3

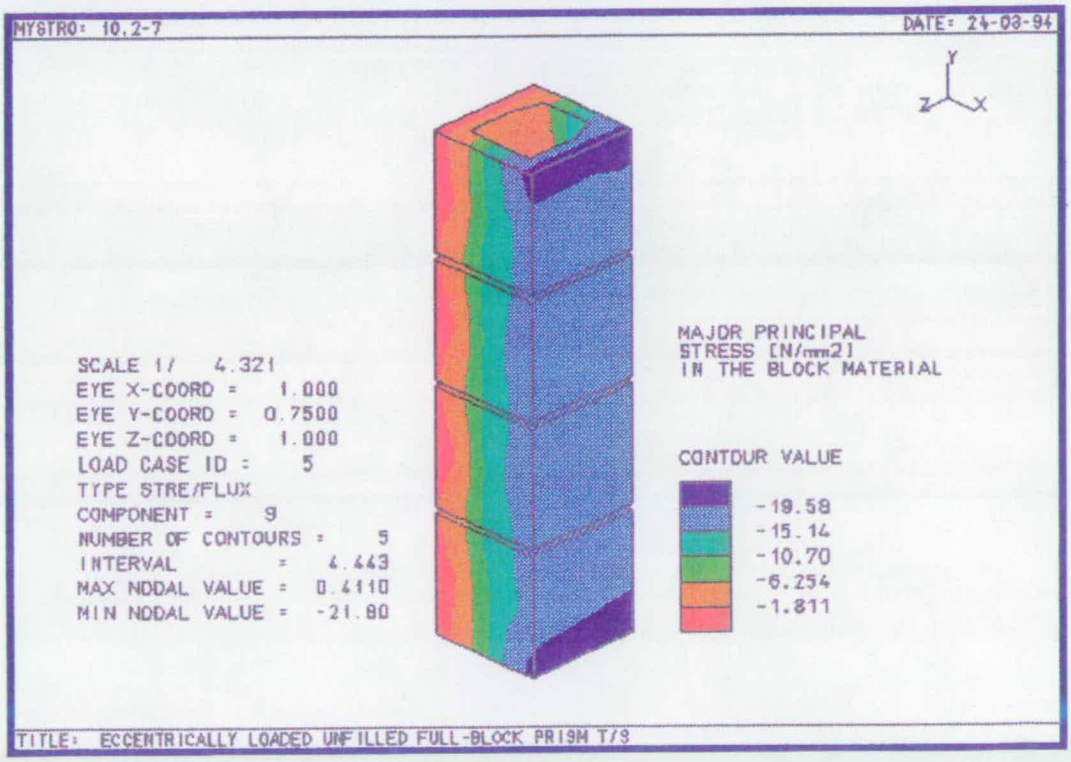


Fig. A.4 Major principal stress in the block material of unfilled full-block prism compressed under eccentric load for e = t/3

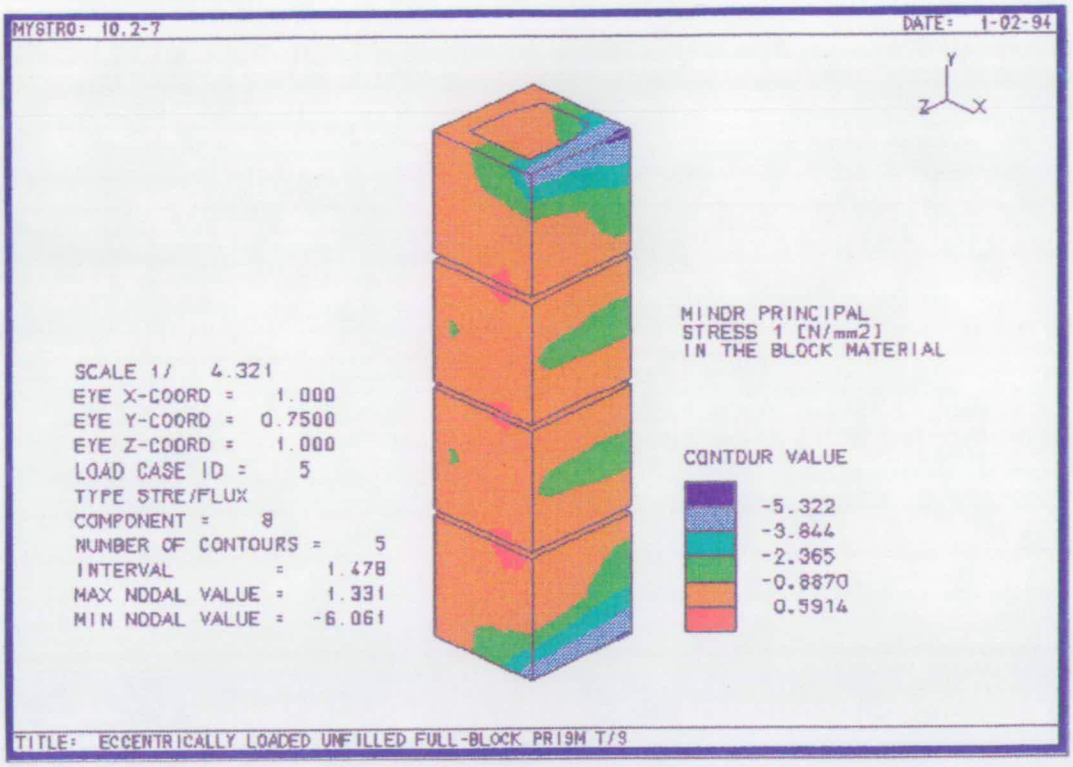


Fig. A.5 Minor principal stress 1 in the block material of unfilled full-block prism compressed under eccentric load for e = t/3

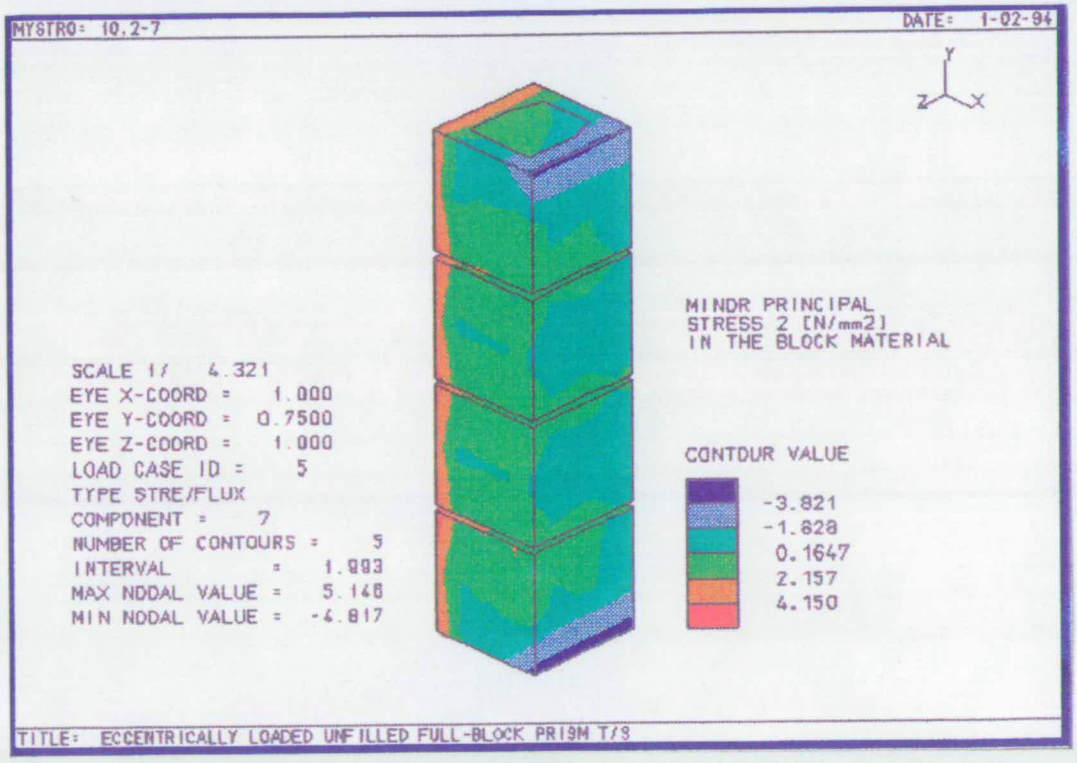


Fig. A.6 Minor principal stress 2 in the block material of unfilled full-block prism compressed under eccentric load for e = t/3

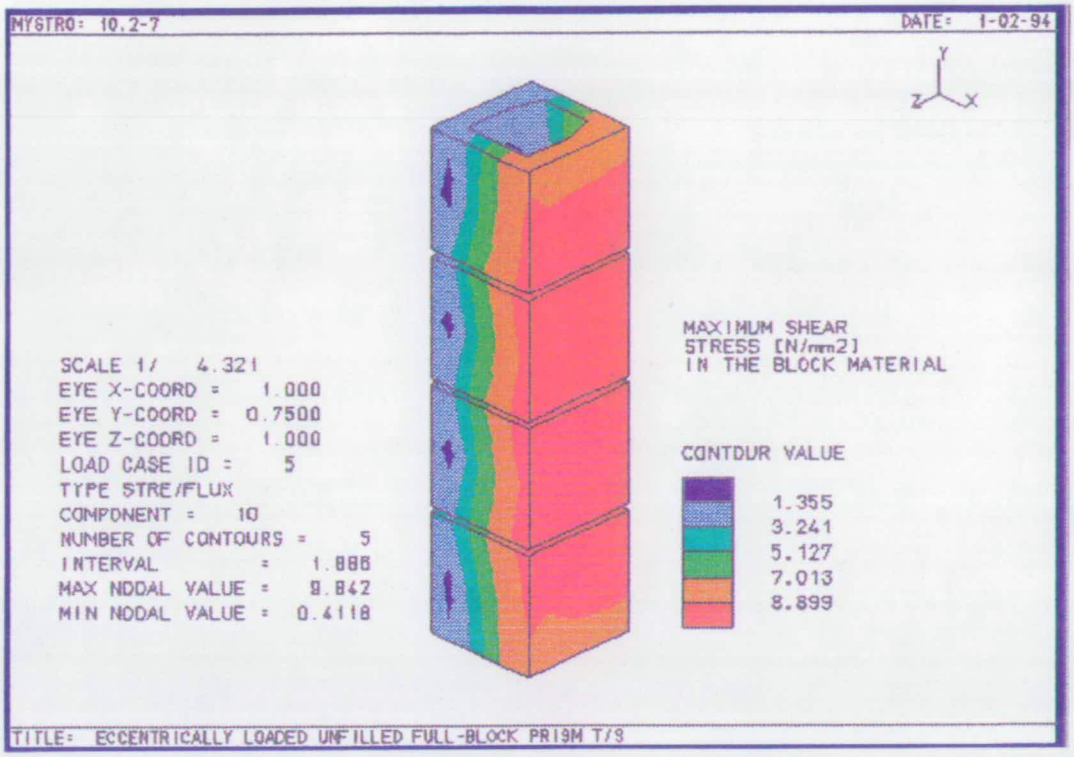


Fig. A.7 Shear stress in the block material of unfilled full-block prism compressed under eccentric load for e = t/3

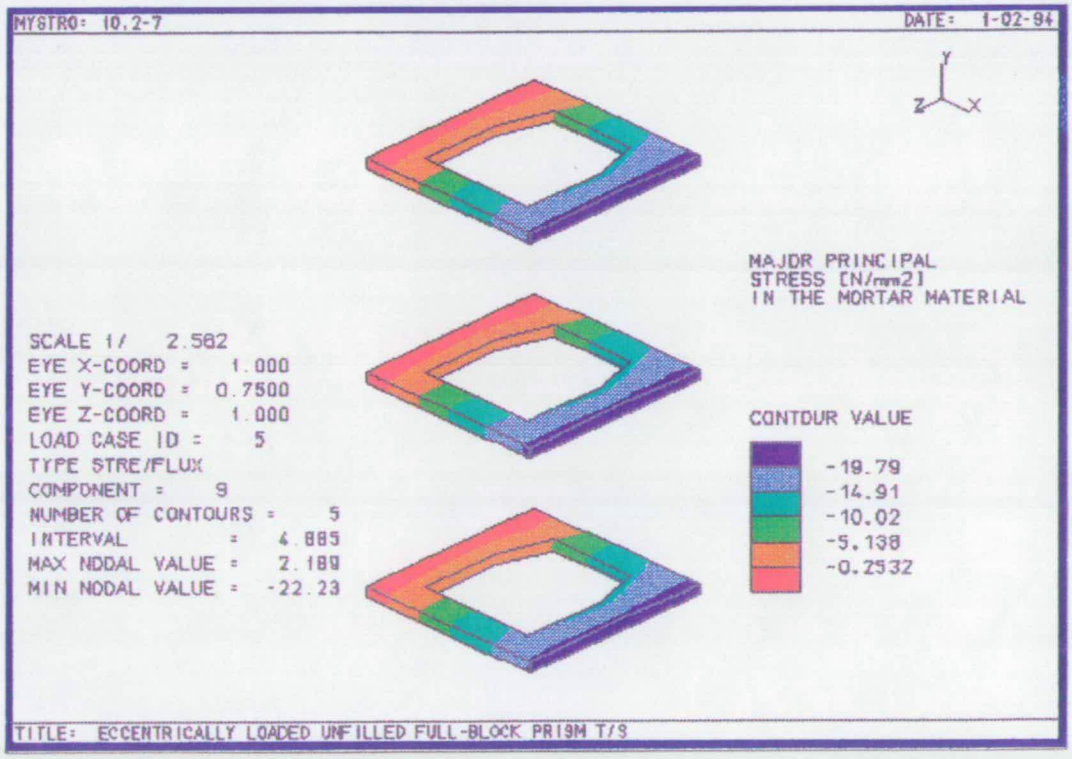


Fig. A.8 Major principal stress in the mortar material of unfilled full-block prism compressed under eccentric load for e = t/3

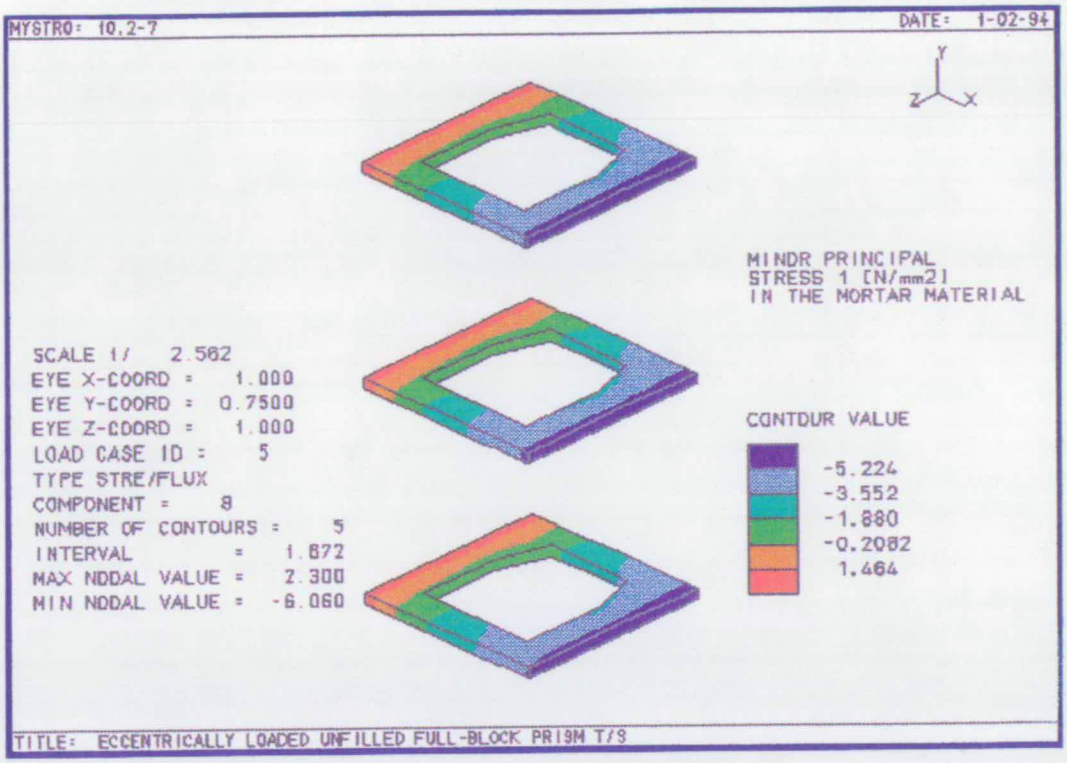


Fig. A.9 Minor principal stress 1 in the mortar material of unfilled full-block prism compressed under eccentric load for e = t/3

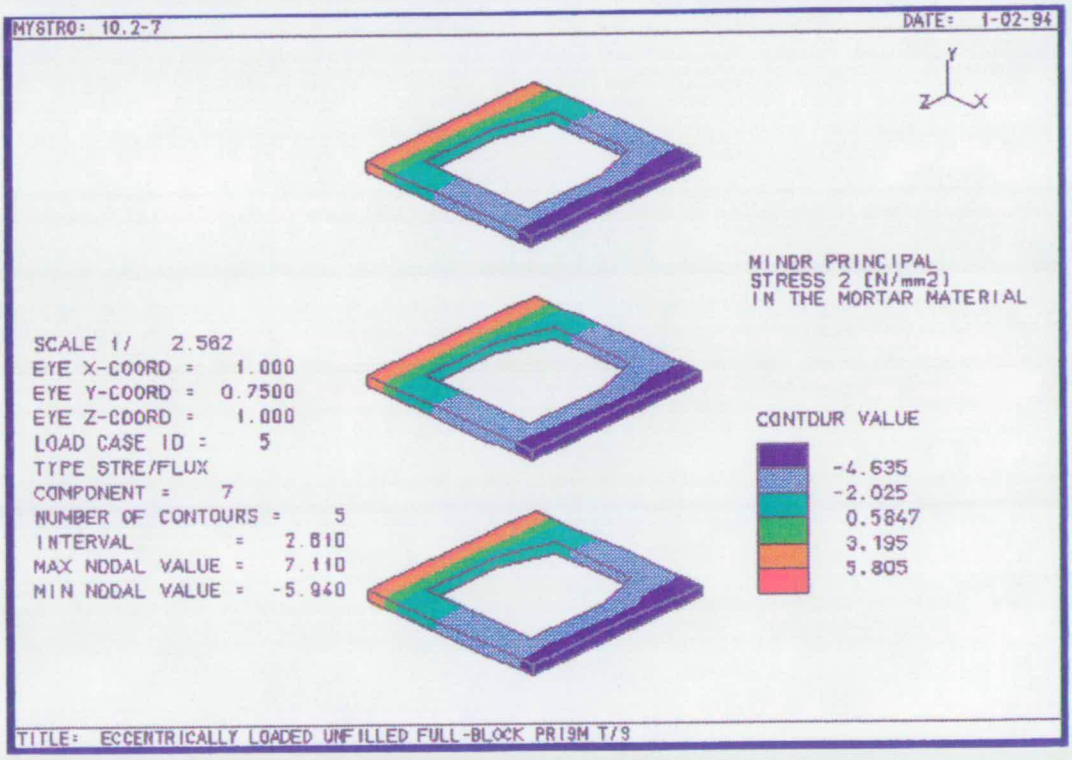


Fig. A.10 Minor principal stress 2 in the mortar material of unfilled full-block prism compressed under eccentric load for e = t/3

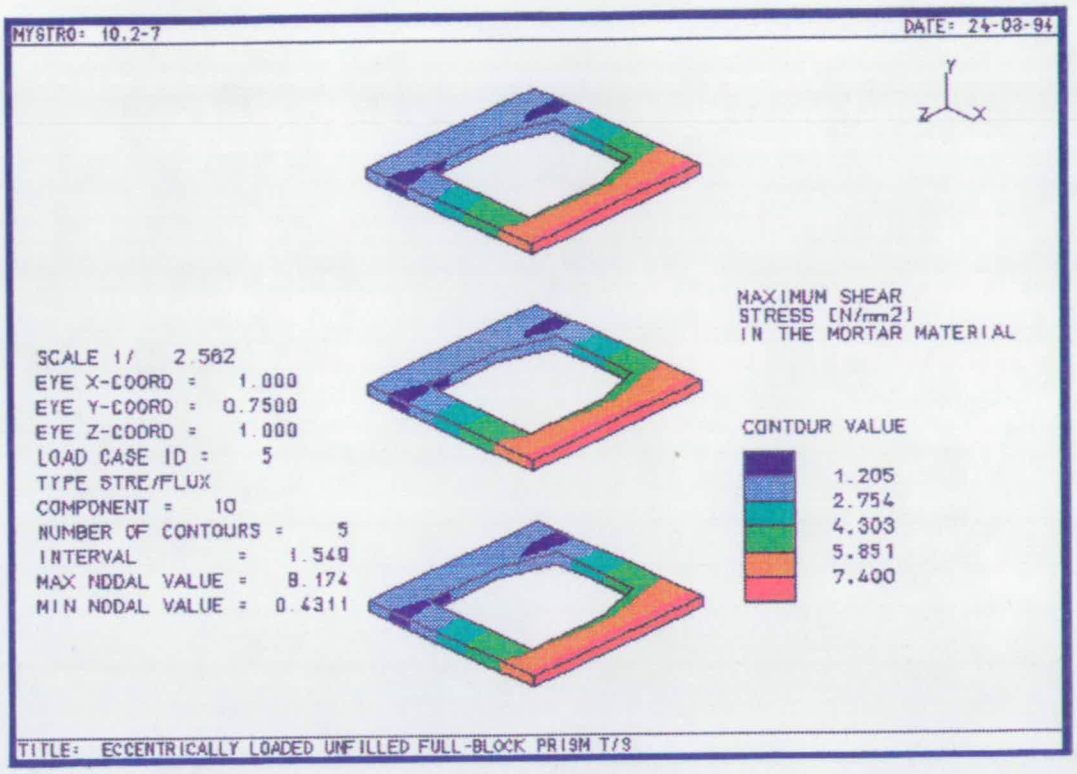


Fig. A.11 Shear stress in the mortar material of unfilled full-block prism compressed under eccentric load for e = t/3

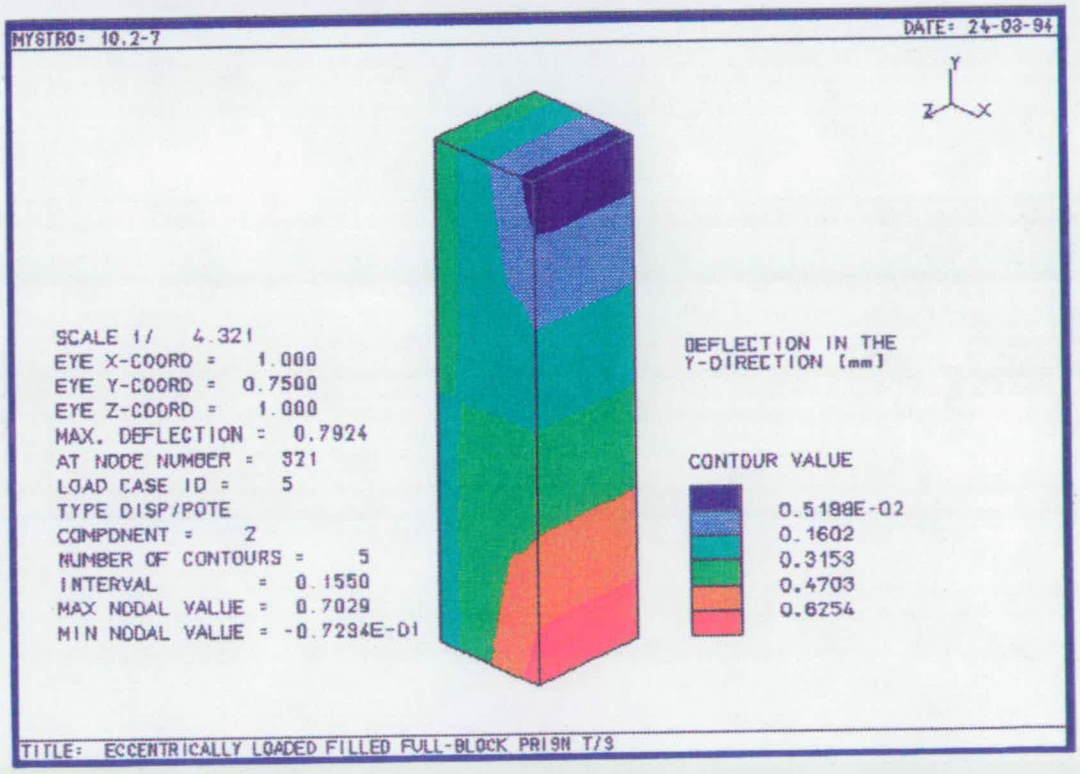


Fig. A.12 Deformation in the Y-direction of filled full-block prism compressed under eccentric load for e = t/3

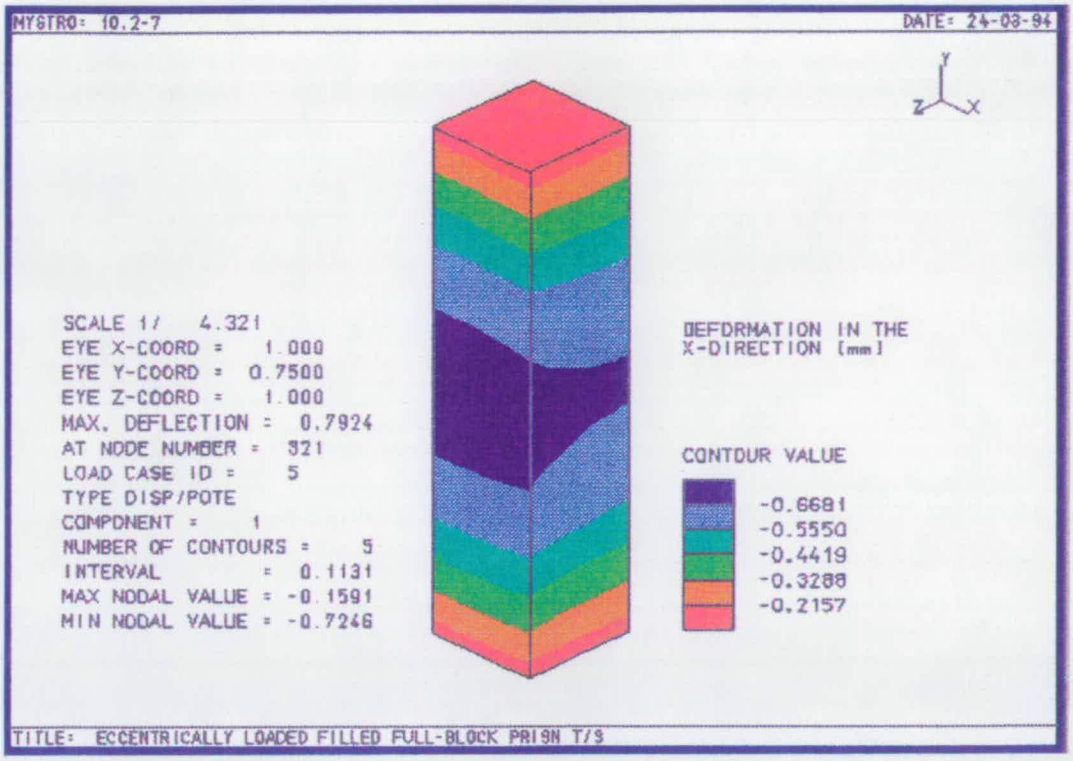


Fig. A.13 Deformation in the X-direction of filled full-block prism compressed under eccentric load for e = t/3

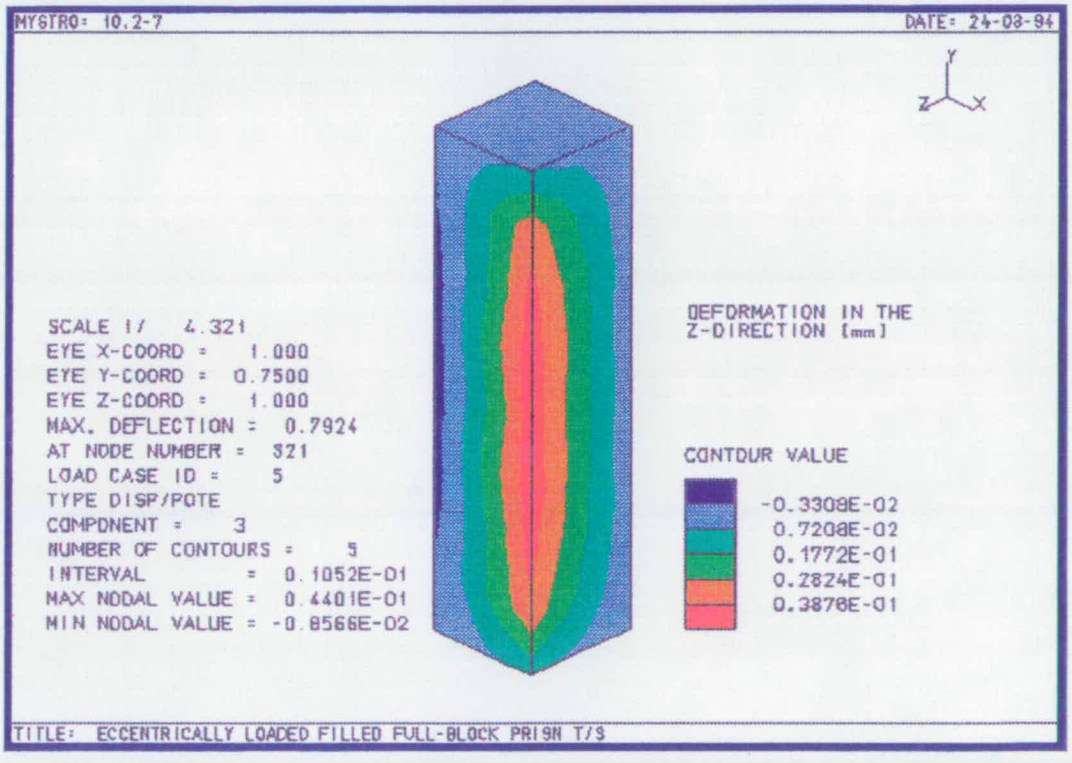


Fig. A.14 Deformation in the Z-direction of filled full-block prism compressed under eccentric load for e = t/3

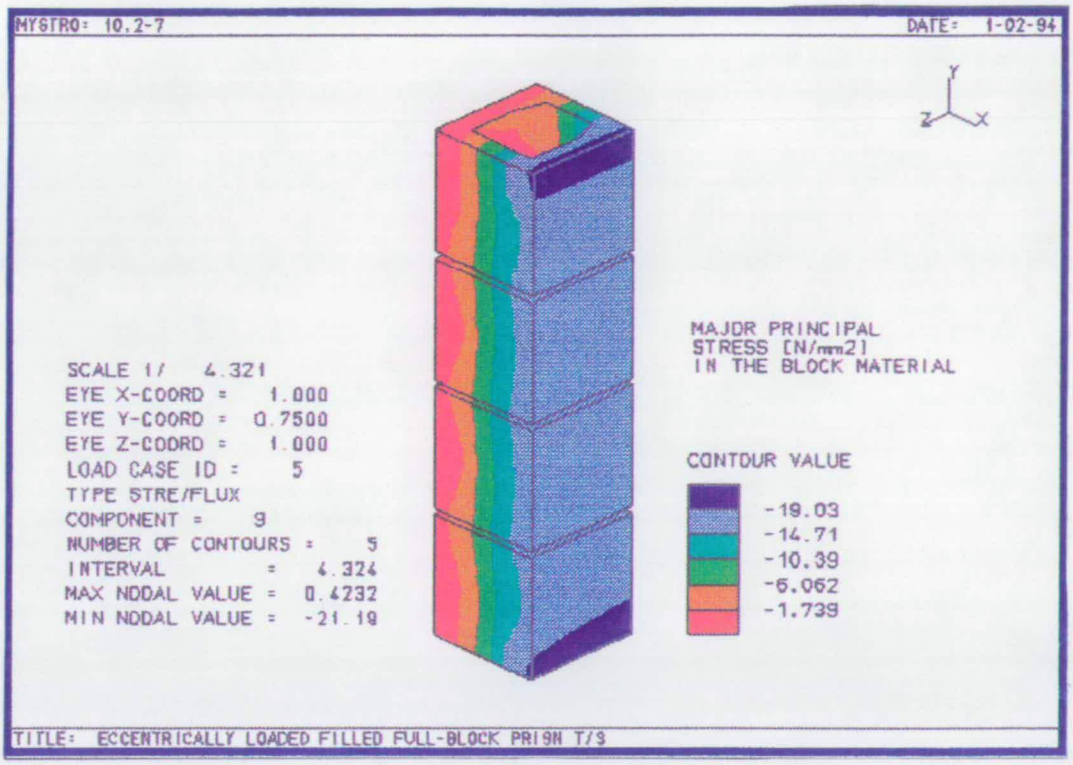


Fig. A.15 Major principal stress in the block material of filled full-block prism compressed under eccentric load for e = t/3

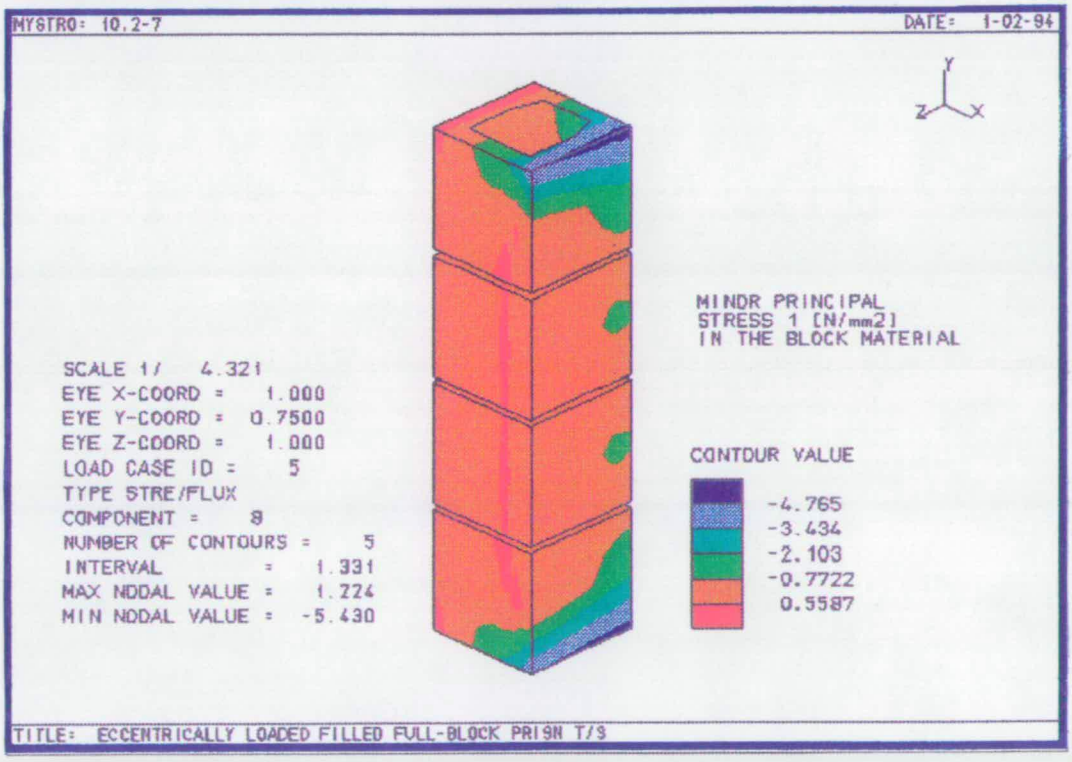


Fig. A.16 Minor principal stress 1 in the block material of filled full-block prism compressed under eccentric load for e = t/3

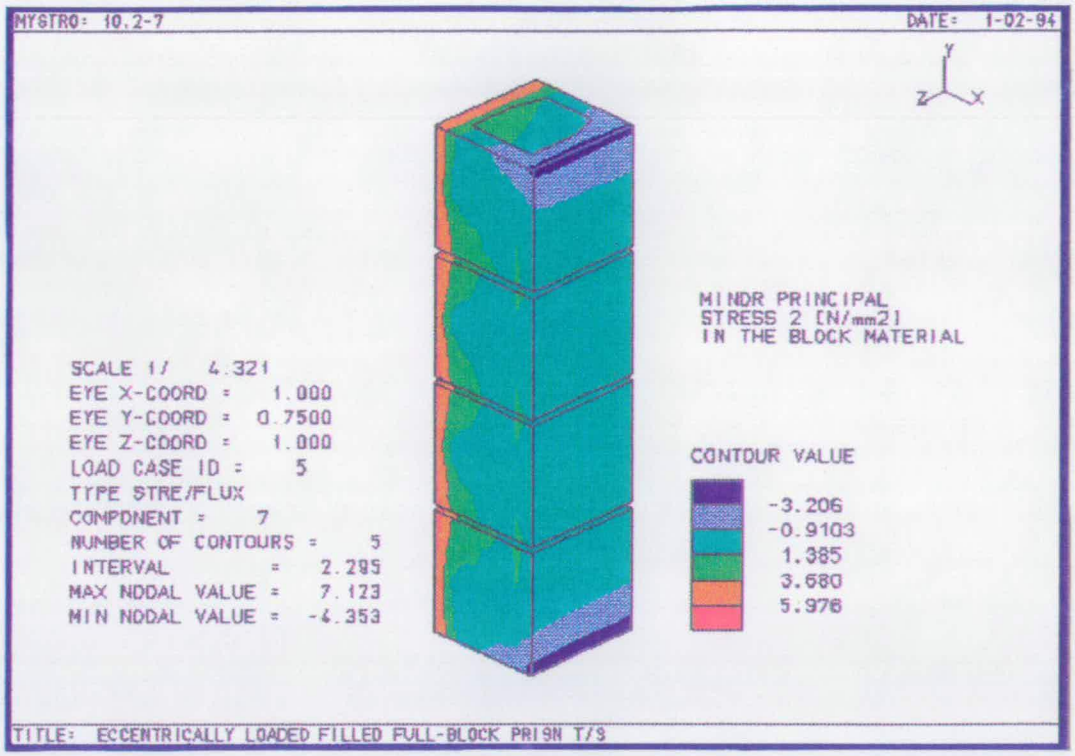


Fig. A.17 Minor principal stress 2 in the block material of filled full-block prism compressed under eccentric load for e = t/3

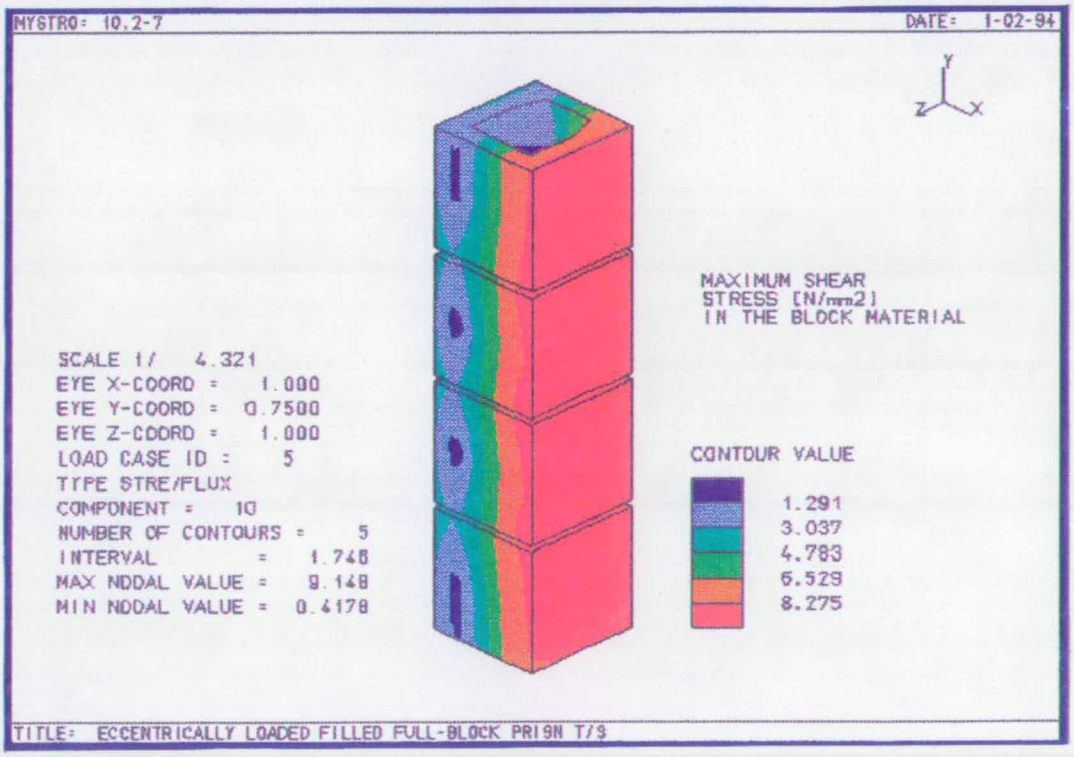


Fig. A.18 Shear stress in the block material of filled full-block prism compressed under eccentric load for e = t/3

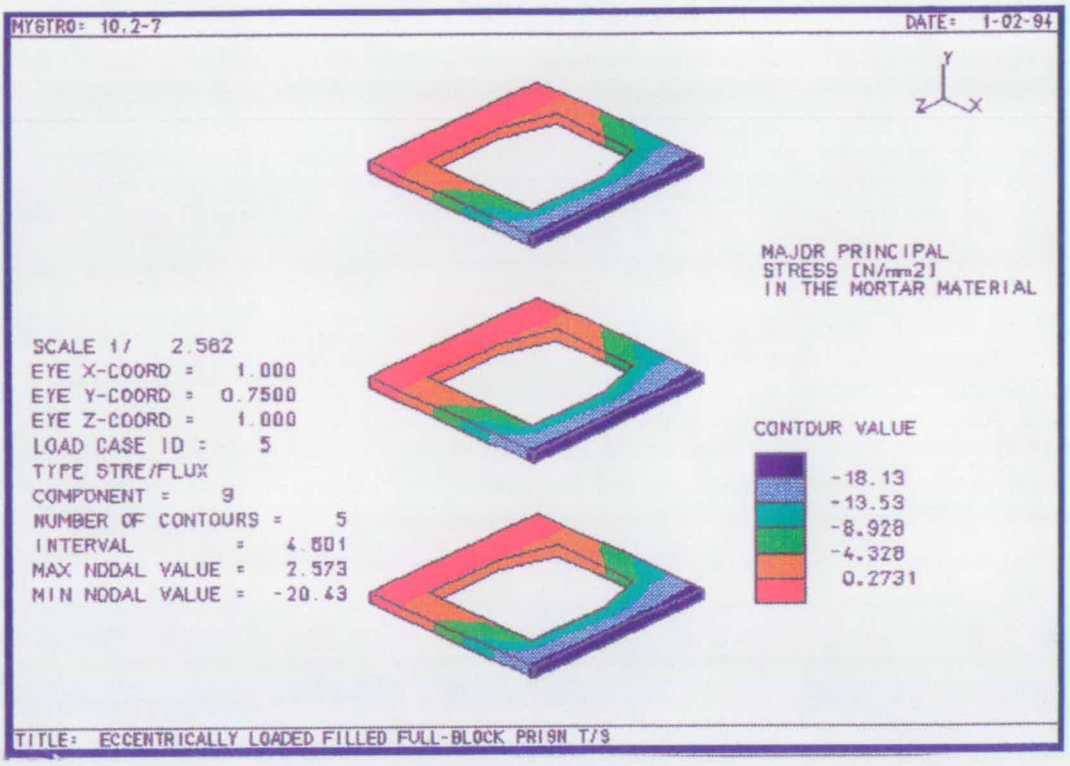


Fig. A.19 Major principal stress in the mortar material of filled full-block prism compressed under eccentric load for e = t/3

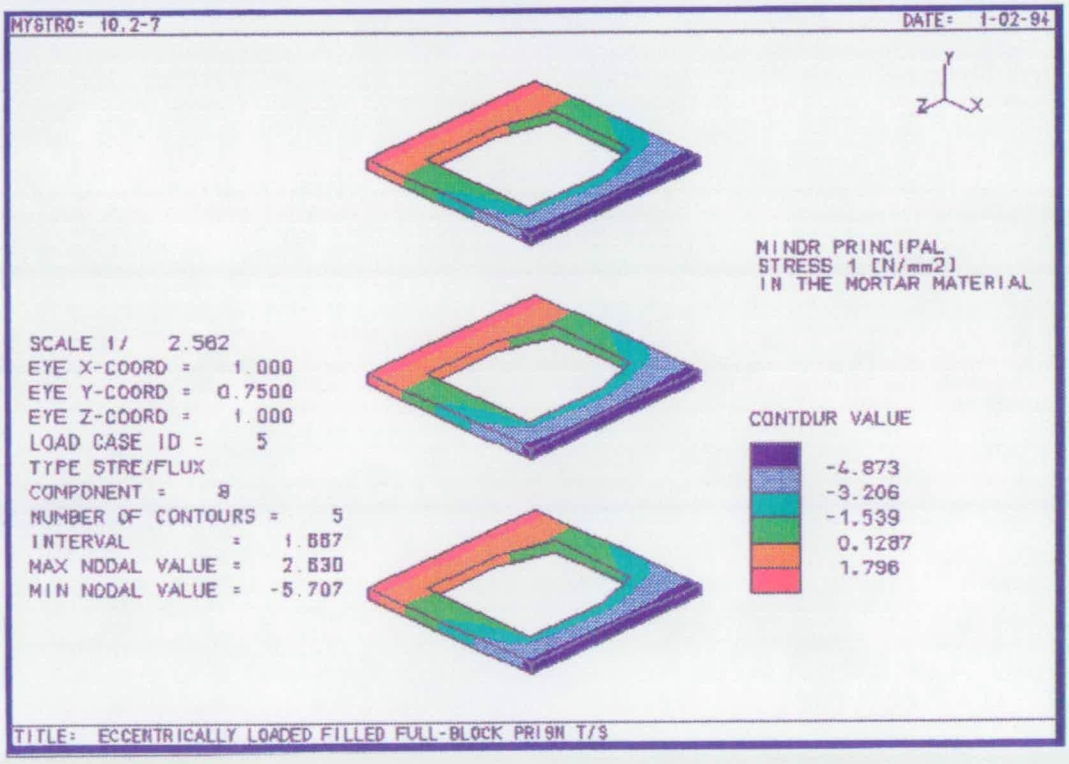


Fig. A.20 Minor principal stress 1 in the block material of filled full-block prism compressed under eccentric load for e = t/3

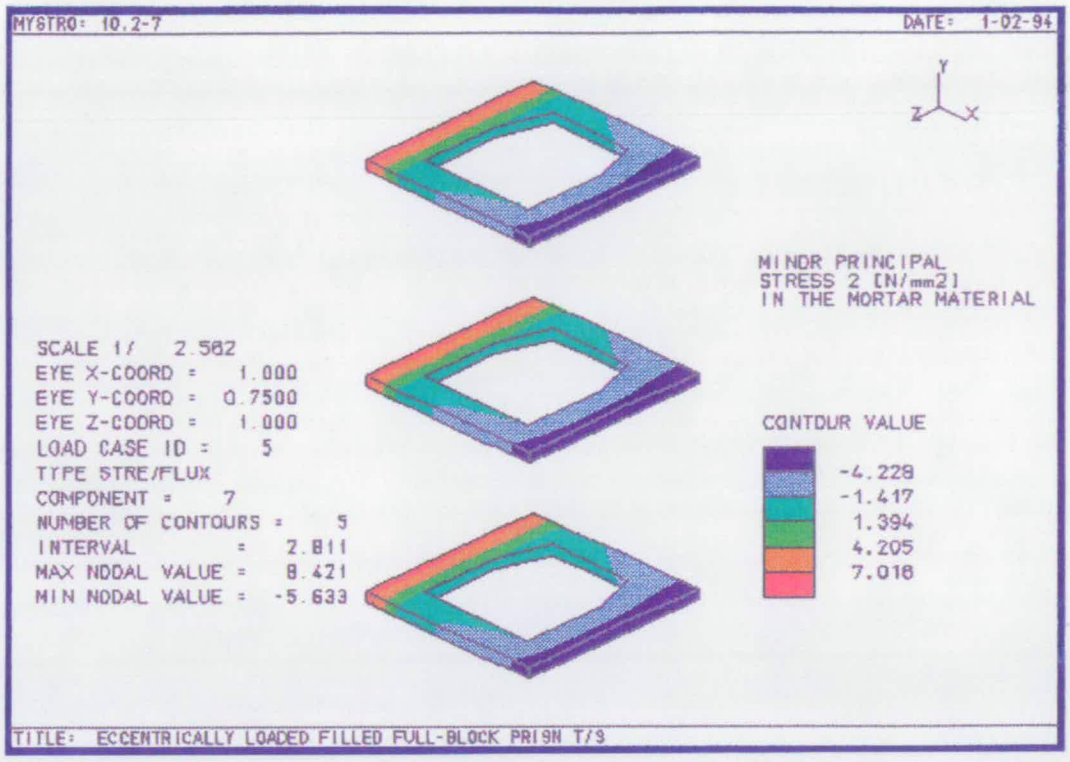


Fig. A.21 Minor principal stress 2 in the block material of filled full-block prism compressed under eccentric load for e = t/3

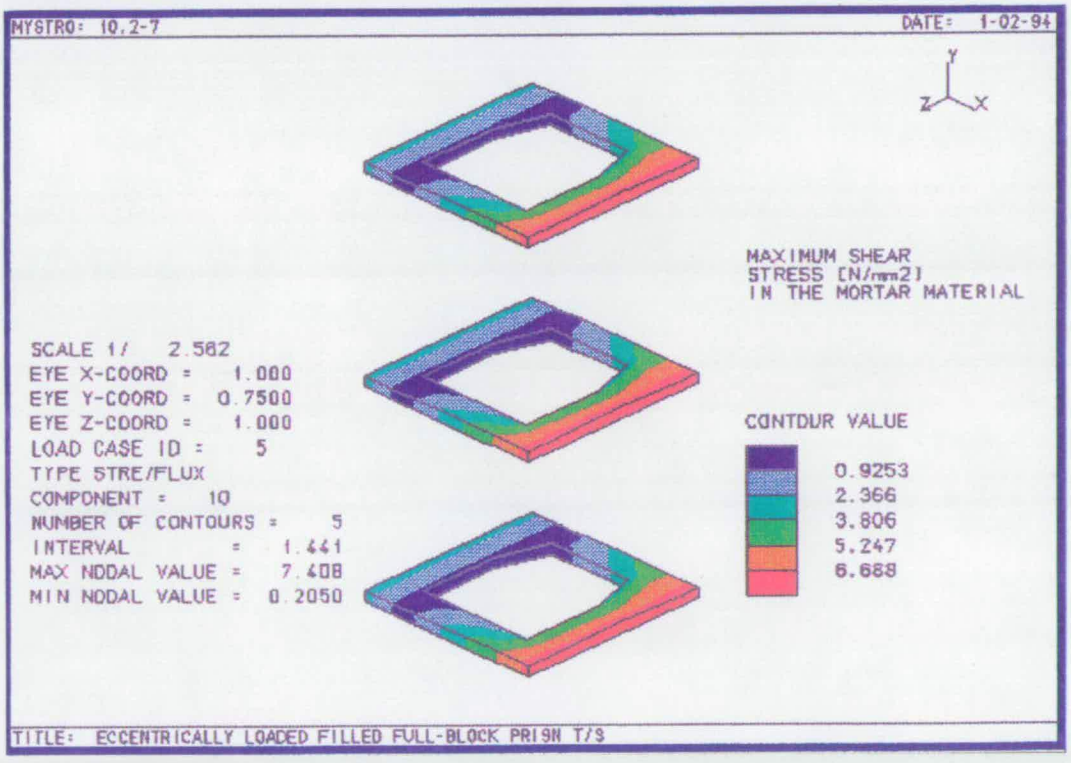


Fig. A.22 Shear stress in the mortar material of filled full-block prism compressed under eccentric load for e = t/3

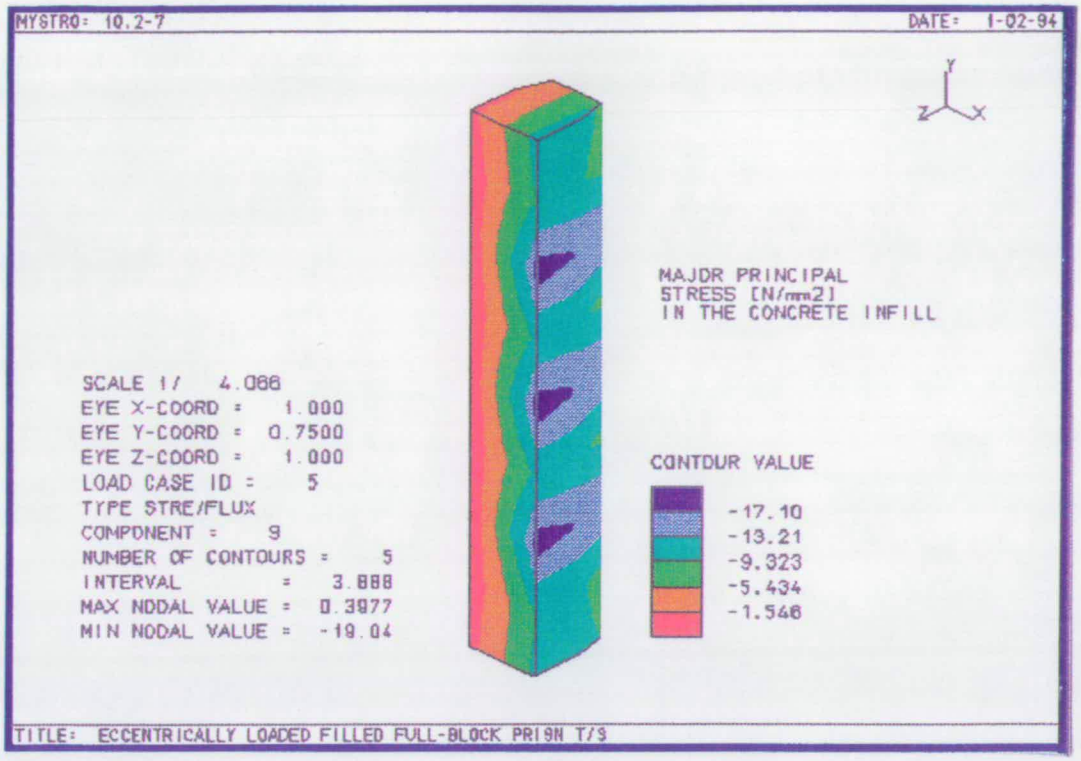


Fig. A.23 Major principal stress in the concrete infill of filled full-block prism compressed under eccentric load for e = t/3

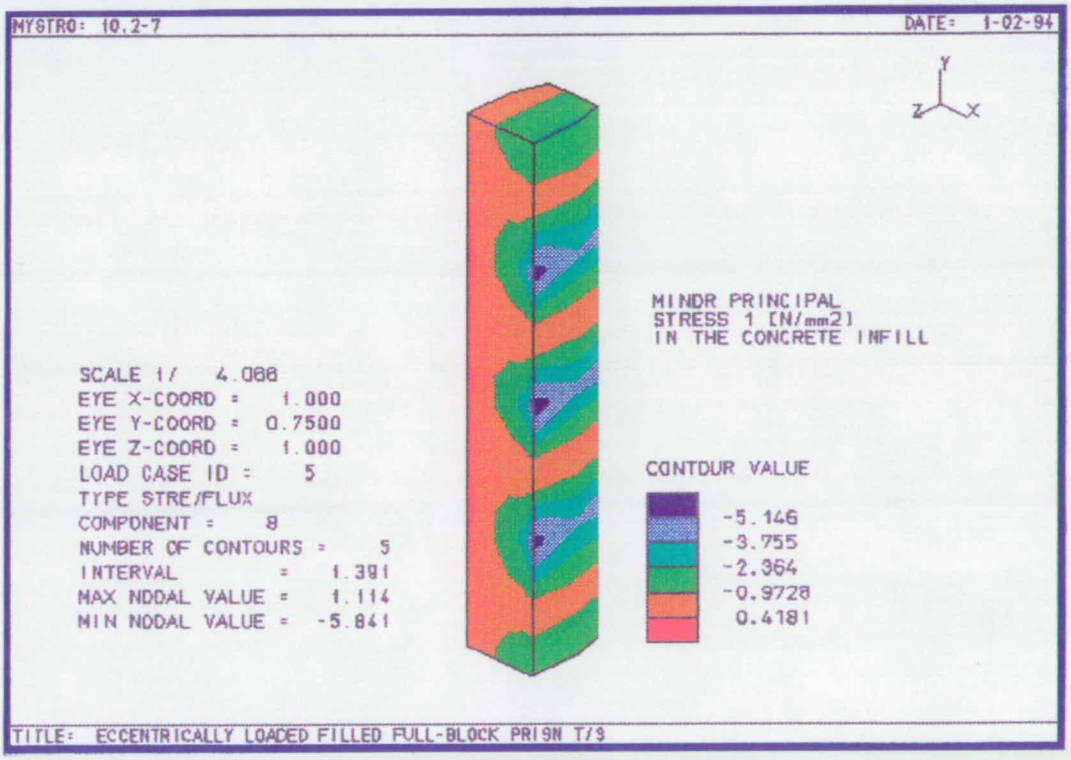


Fig. A.24 Minor principal stress 1 in the concrete infill of filled full-block prism compressed under eccentric load for e = t/3

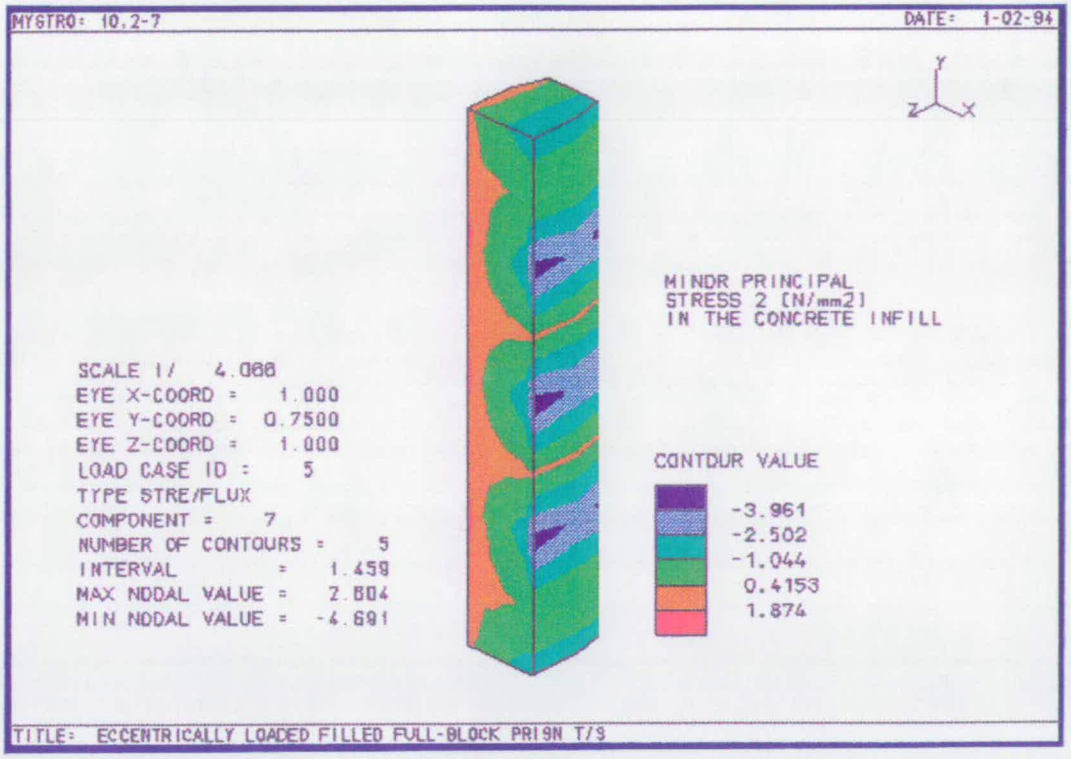


Fig. A.25 Minor principal stress 2 in the concrete infill of filled full-block prism compressed under eccentric load for e = t/3

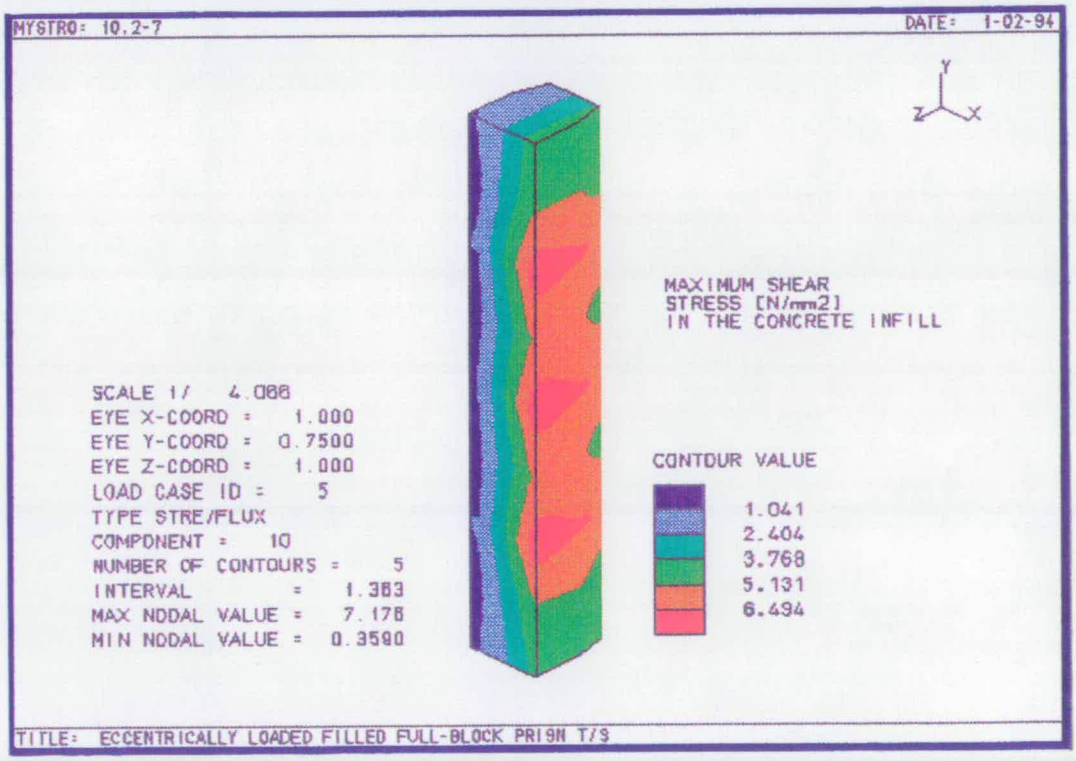


Fig. A.26 Shear stress in the concrete infill of filled full-block prism compressed under eccentric load for e = t/3

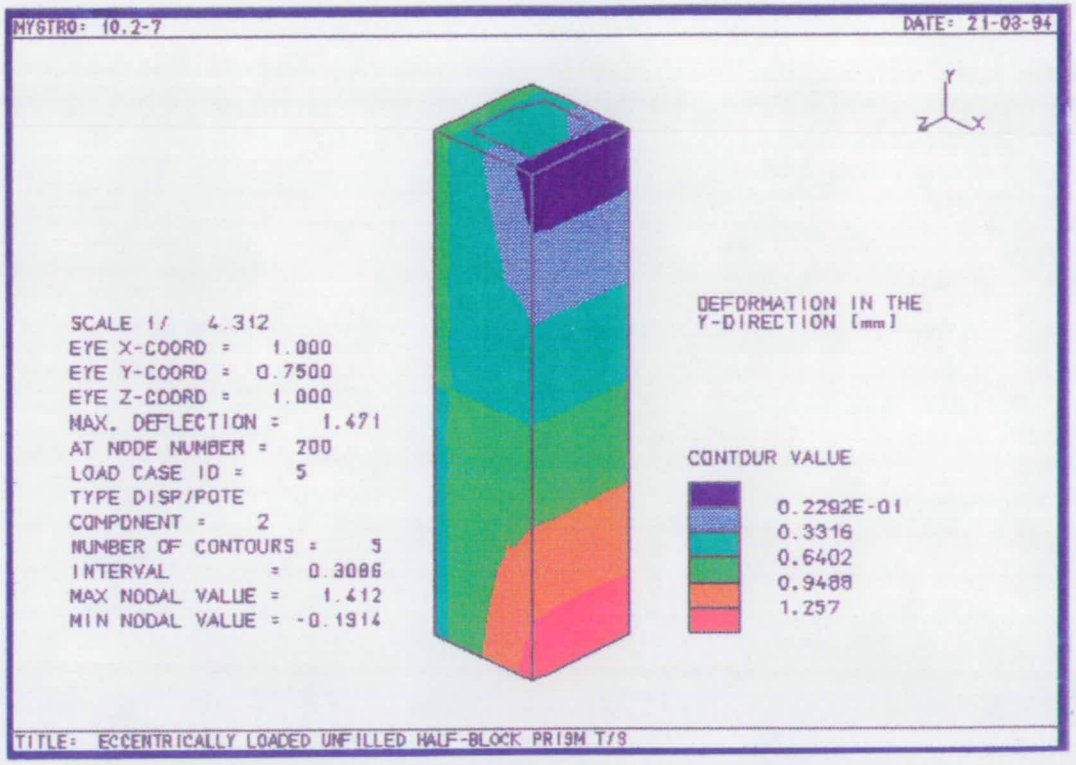


Fig. A.27 Deformation in the Y-direction of unfilled half-block prism compressed under eccentric load for e = t/3

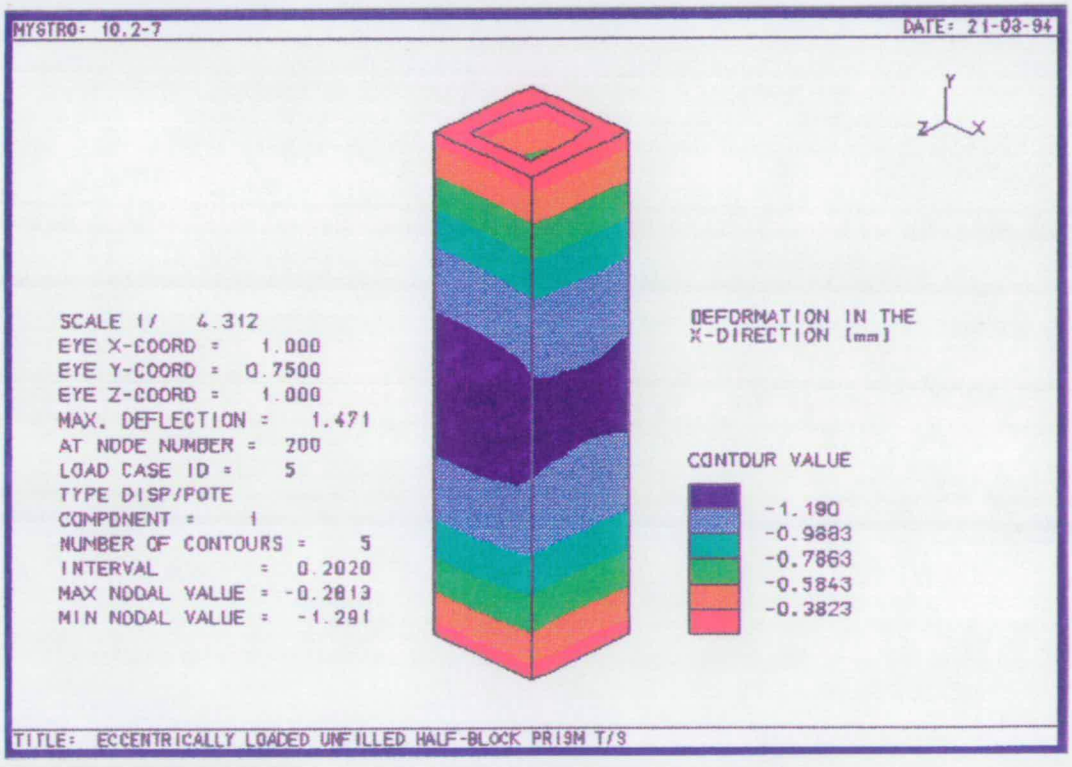


Fig. A.28 Deformation in the X-direction of unfilled half-block prism compressed under eccentric load for e = t/3

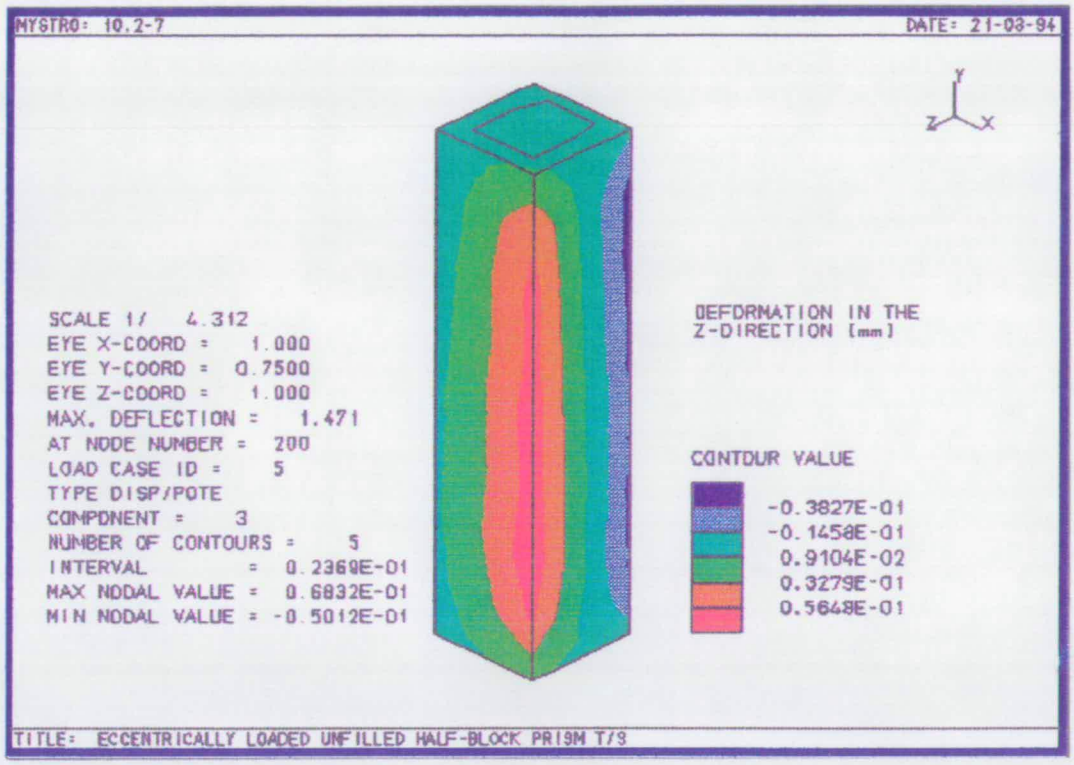


Fig. A.29 Deformation in the Z-direction of unfilled half-block prism compressed under eccentric load for t/3

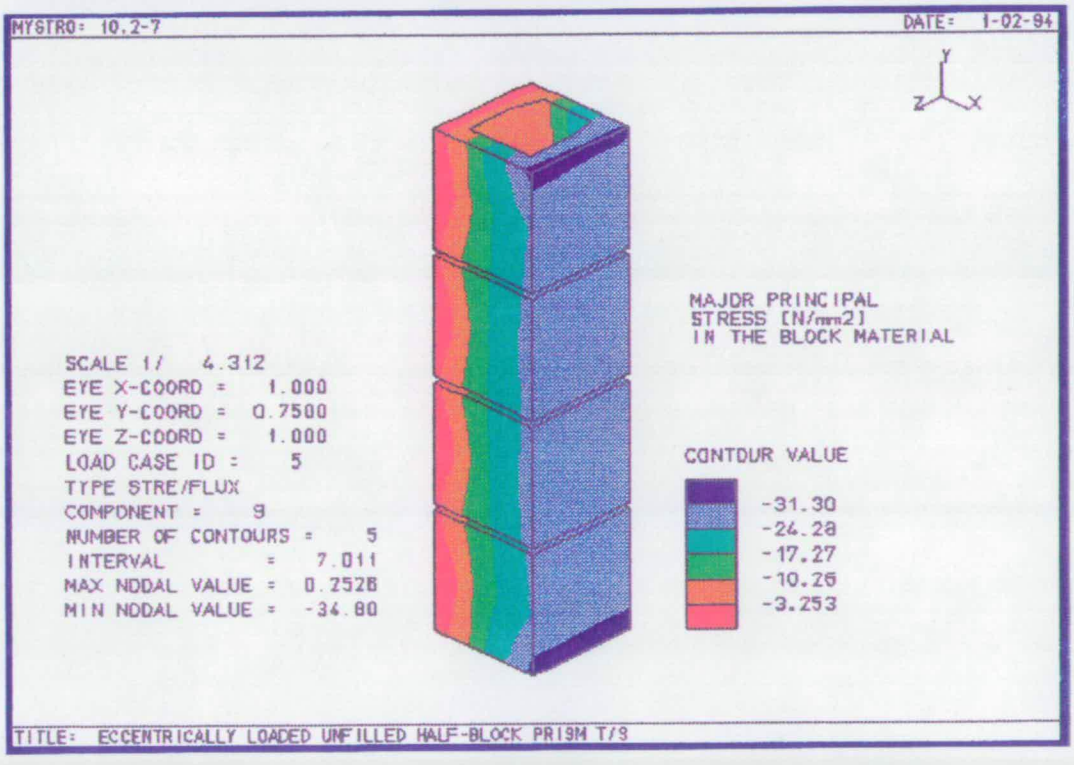


Fig. A.30 Major principal stress in the block material of unfilled half-block prism compressed under eccentric load for e = t/3

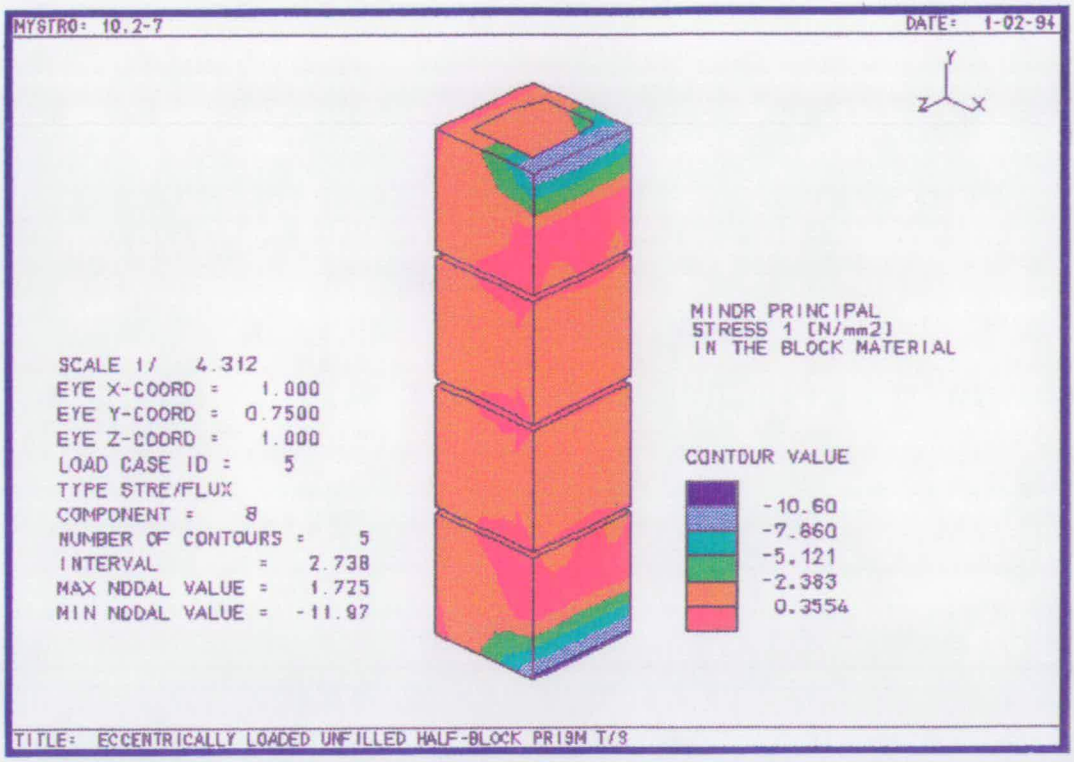


Fig. A.31 Minor principal stress 1 in the block material of unfilled half-block prism compressed under eccentric load for e = t/3

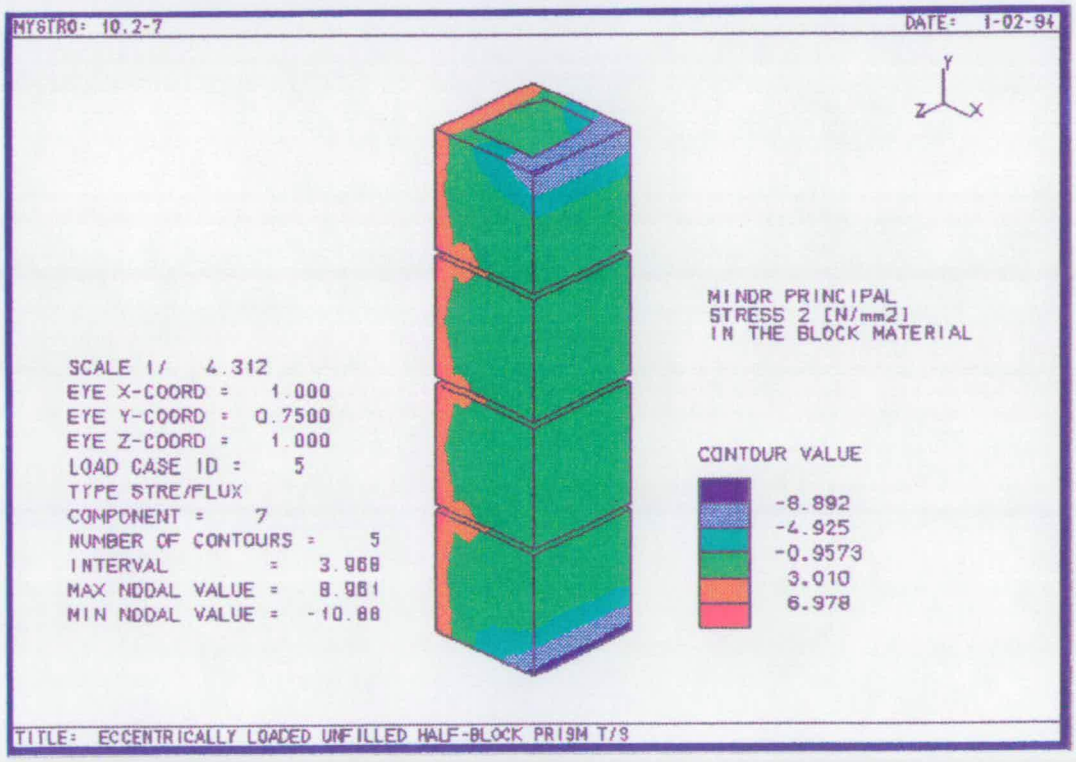


Fig. A.32 Minor principal stress 2 in the block material of unfilled half-block prism compressed under eccentric load for e = t/3

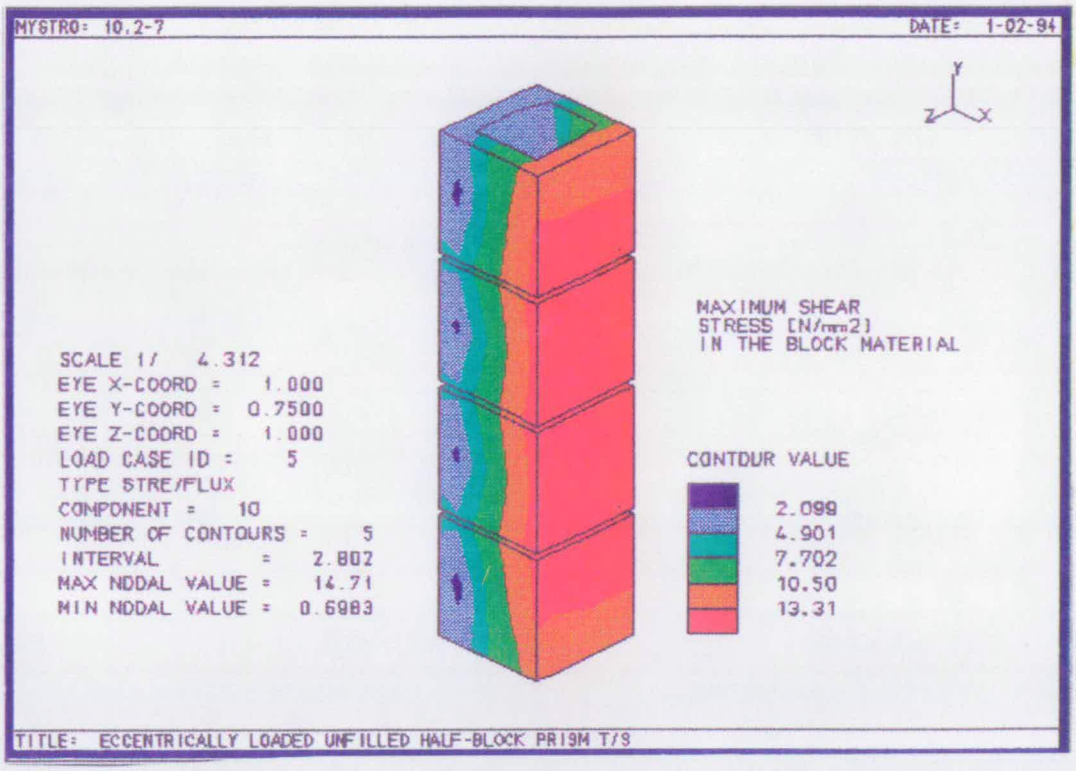


Fig. A.33 Shear stress in the block material of unfilled half-block prism compressed under eccentric load for e = t/3

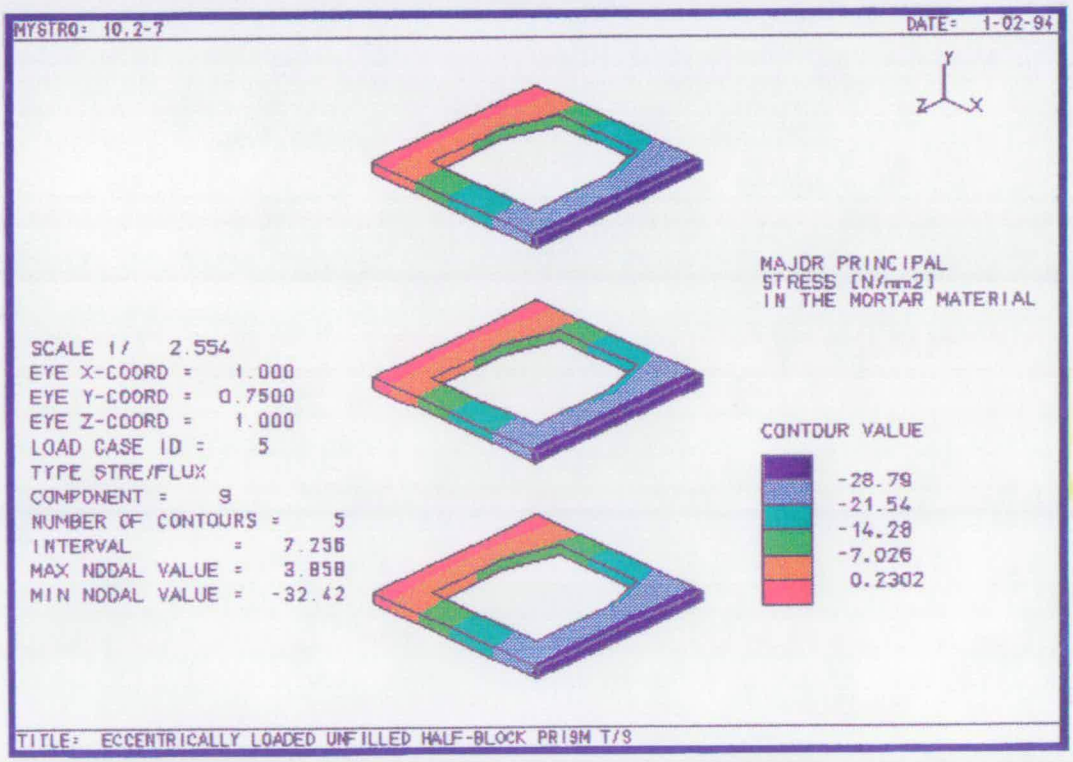


Fig. A.34 Major principal stress in the mortar material of unfilled half-block prism compressed under eccentric load for e = t/3

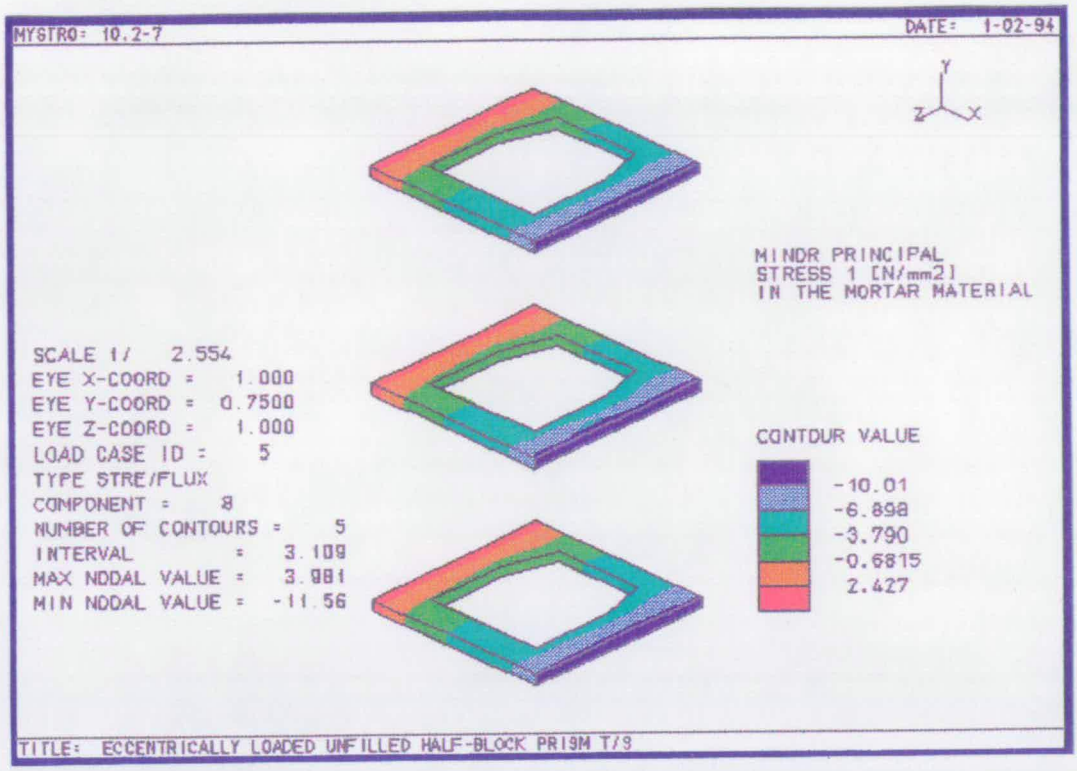


Fig. A.35 Minor principal stress 1 in the block material of unfilled half-block prism compressed under eccentric load for e = t/3

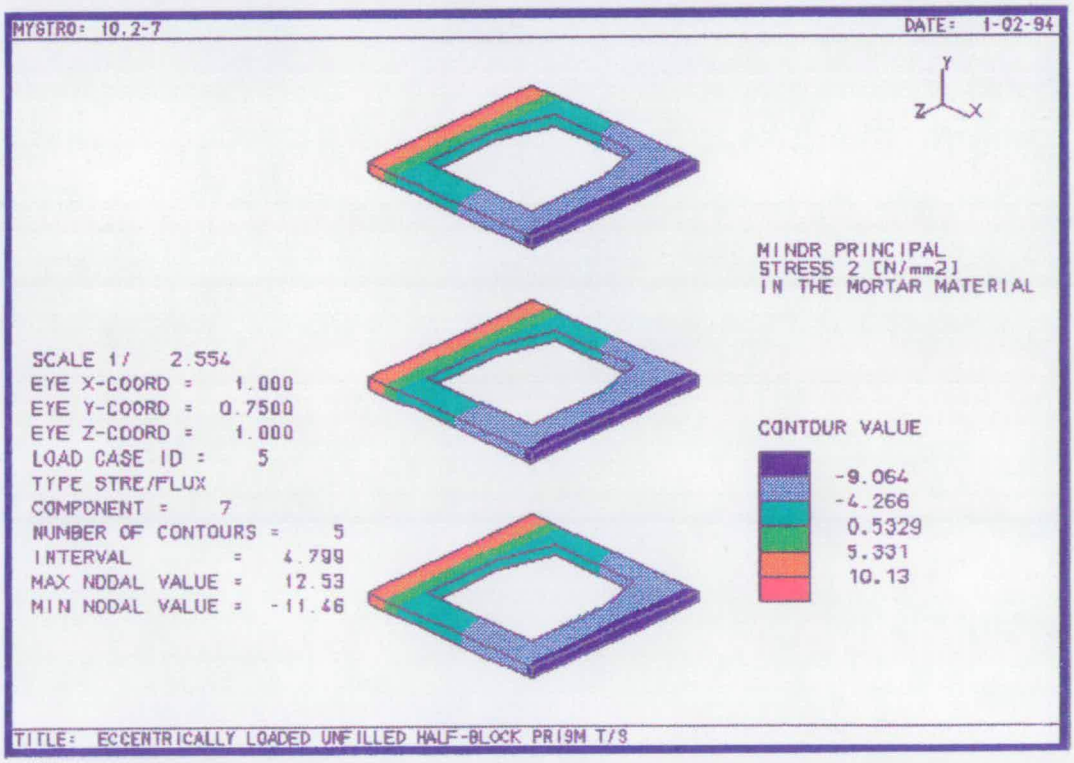


Fig. A.36 Minor principal stress 2 in the block material of unfilled half-block prism compressed under eccentric load for e = t/3

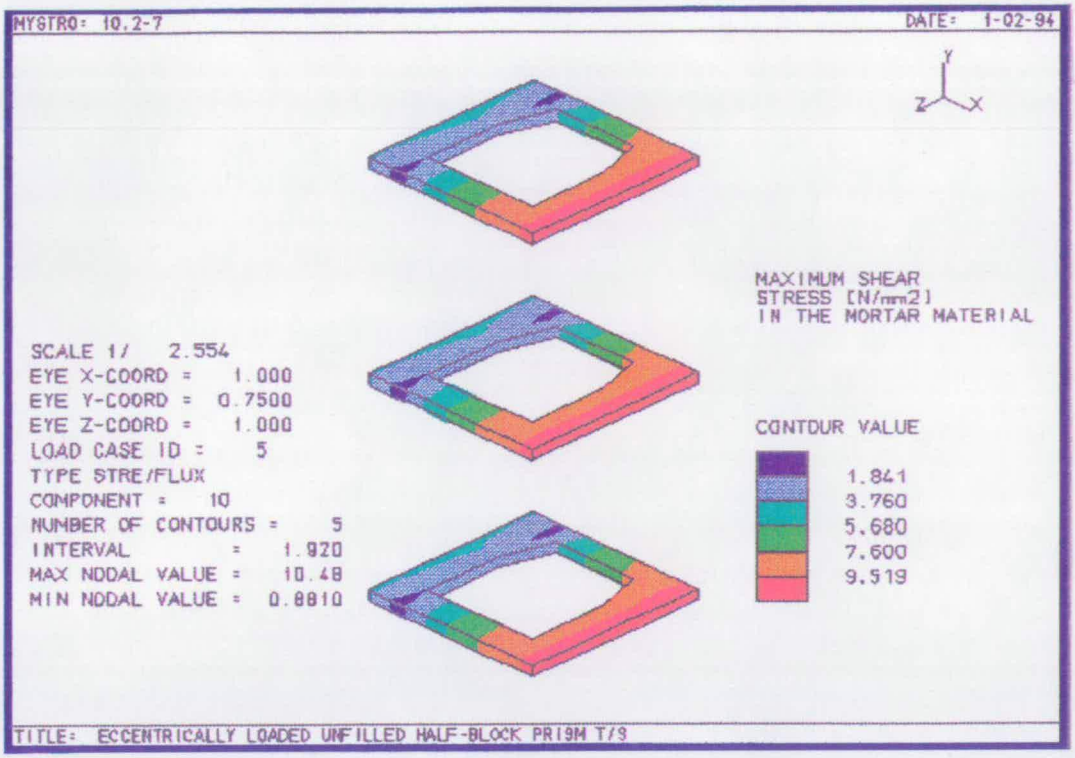


Fig. A.37 Shear stress in the mortar material of unfilled half-block prism compressed under eccentric load for e = t/3

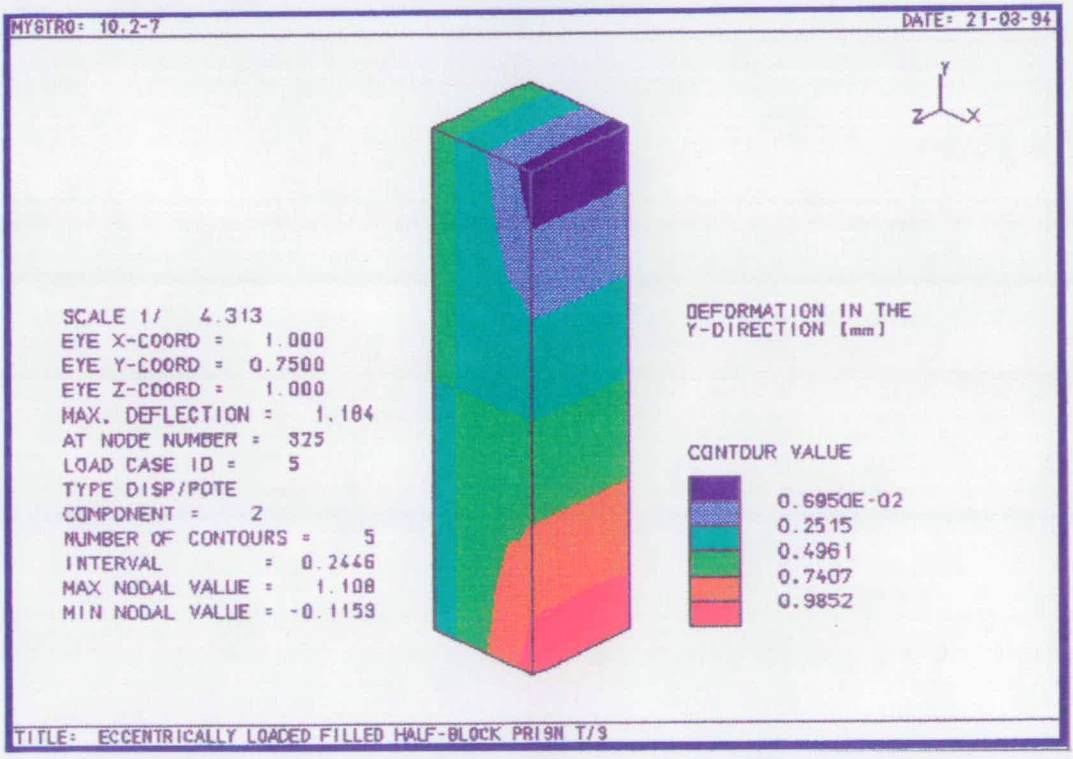


Fig. A.38 Deformation in the Y-direction of filled half-block prism compressed under eccentric load for e = t/3

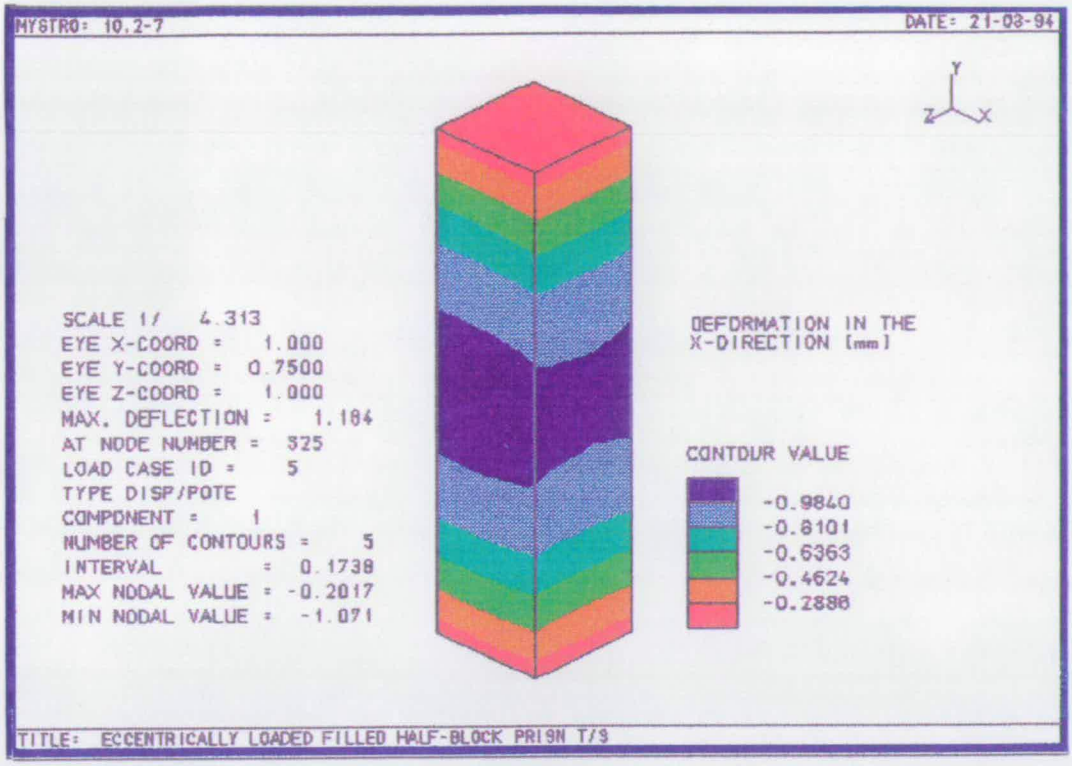


Fig. A.39 Deformation in the X-direction of filled half-block prism compressed under eccentric load for t/3

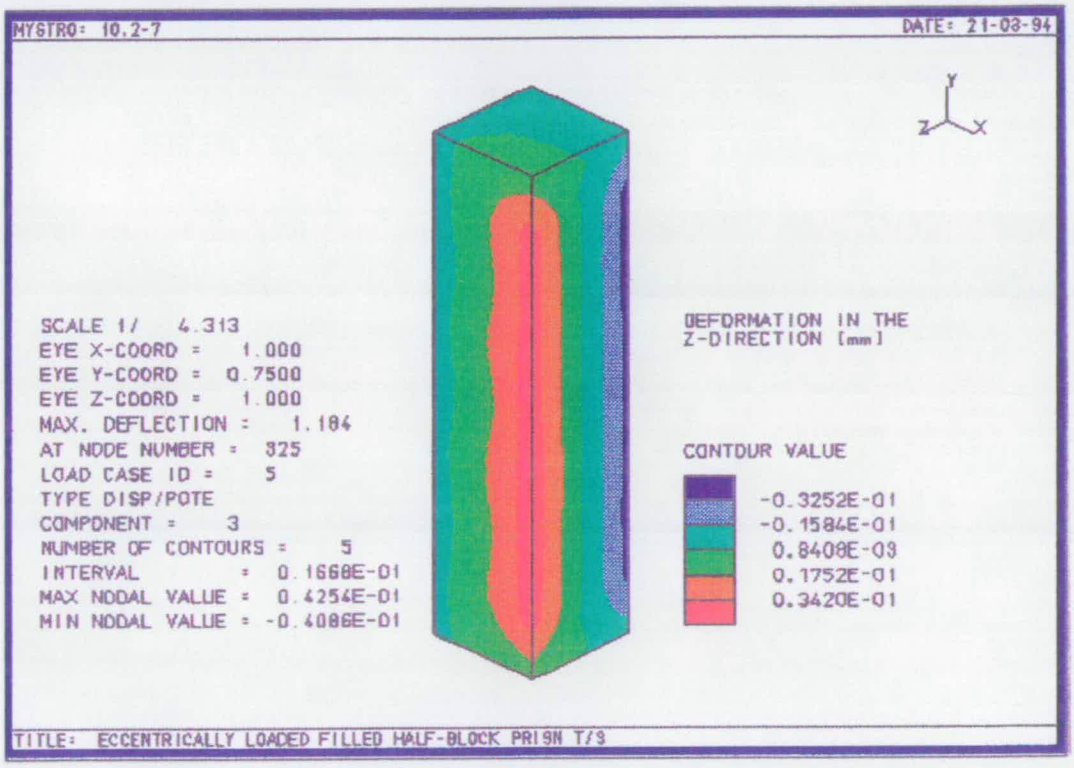


Fig. A.40 Deformation in the Z-direction of filled half-block prism compressed under eccentric load for e = t/3

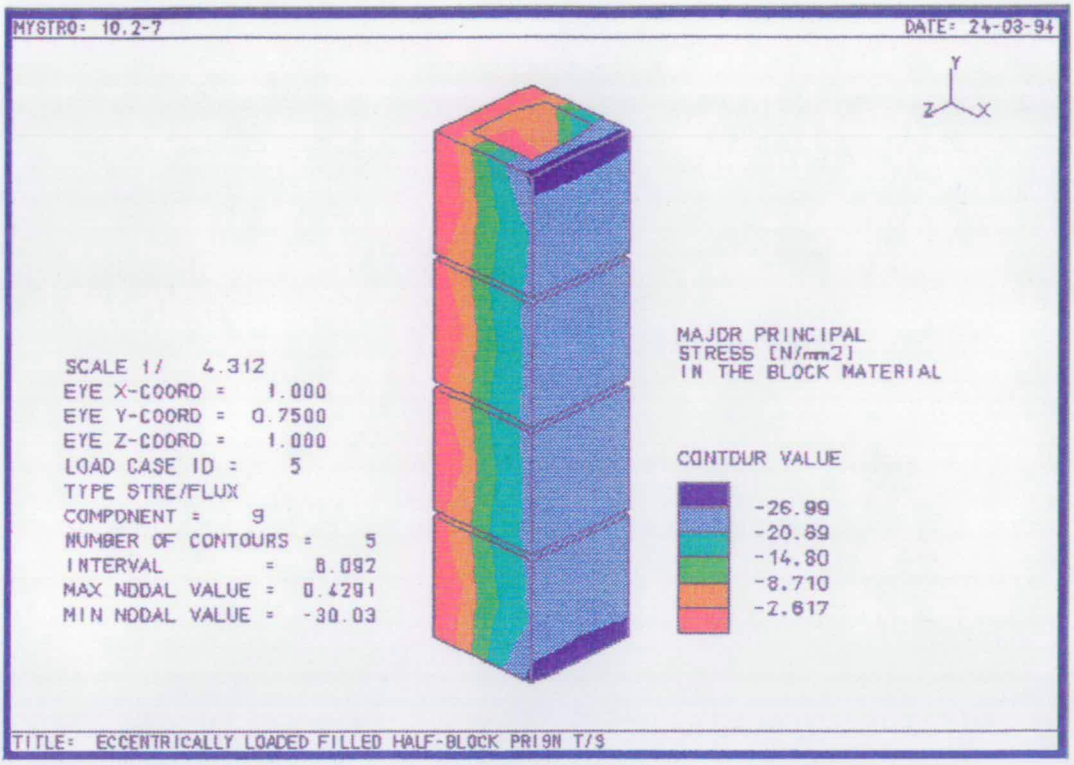


Fig. A.41 Major principal stress in the block material of filled half-block prism compressed under eccentric load for e = t/3

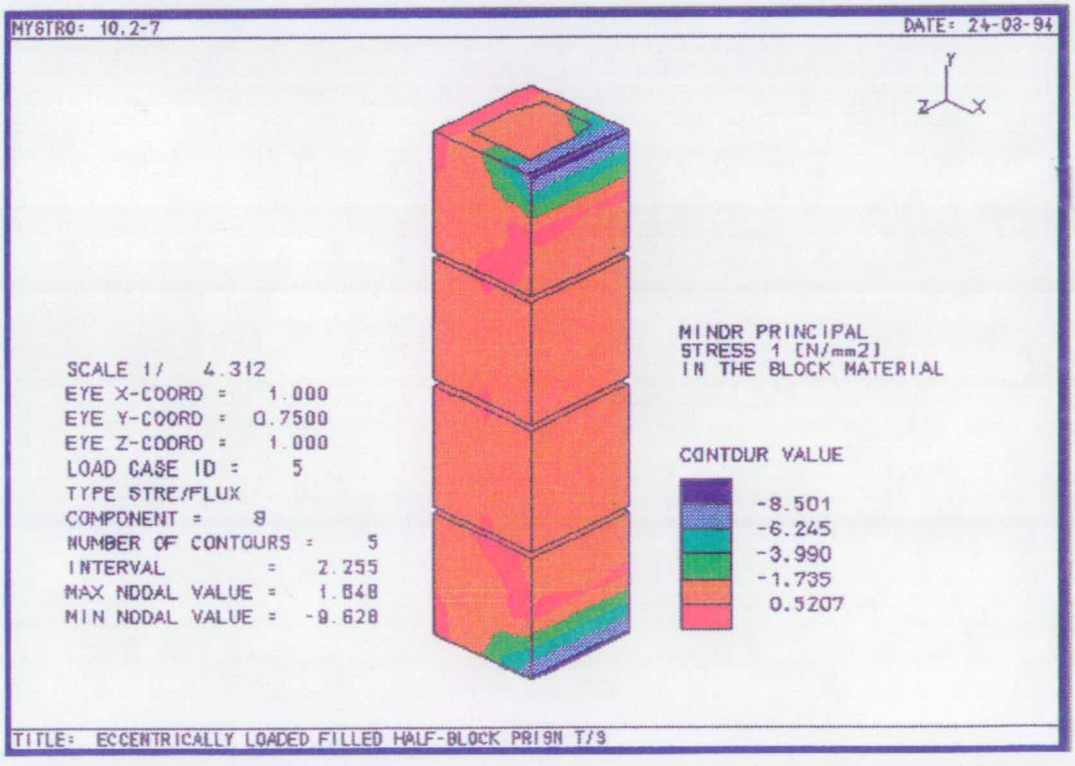


Fig. A.42 Minor principal stress 1 in the block material of filled half-block prism compressed under eccentric load for e = t/3

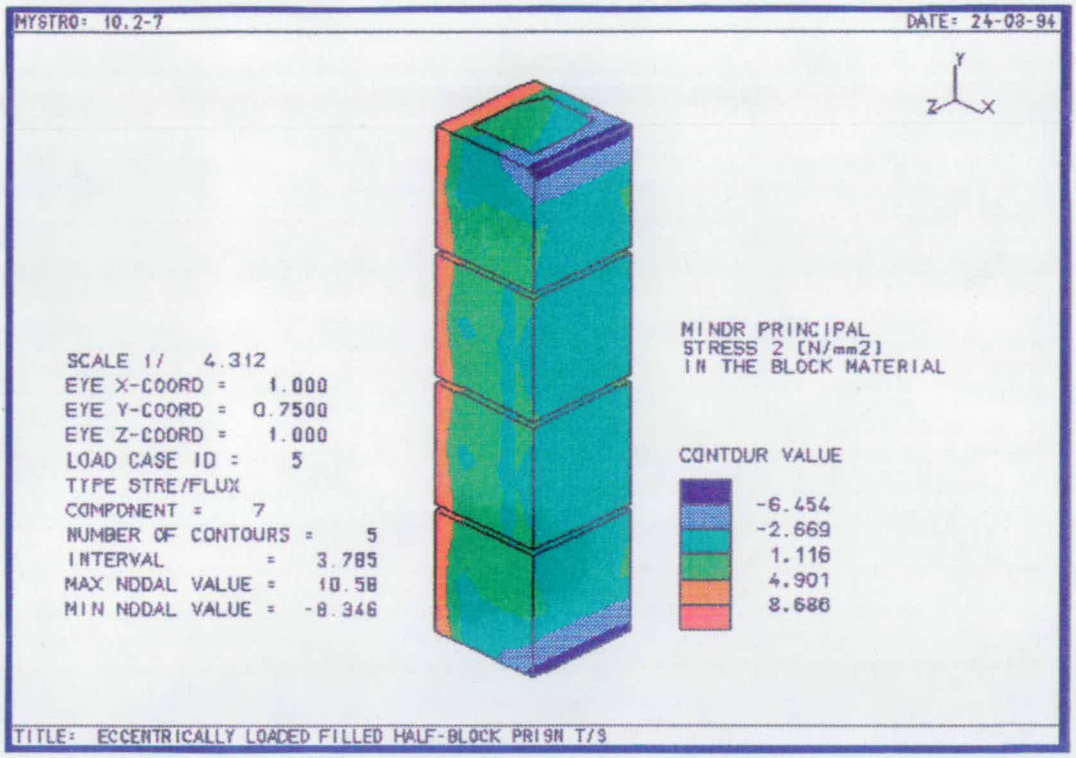


Fig. A.43 Minor principal stress 2 in the block material of filled half-block prism compressed under eccentric load for e = t/3

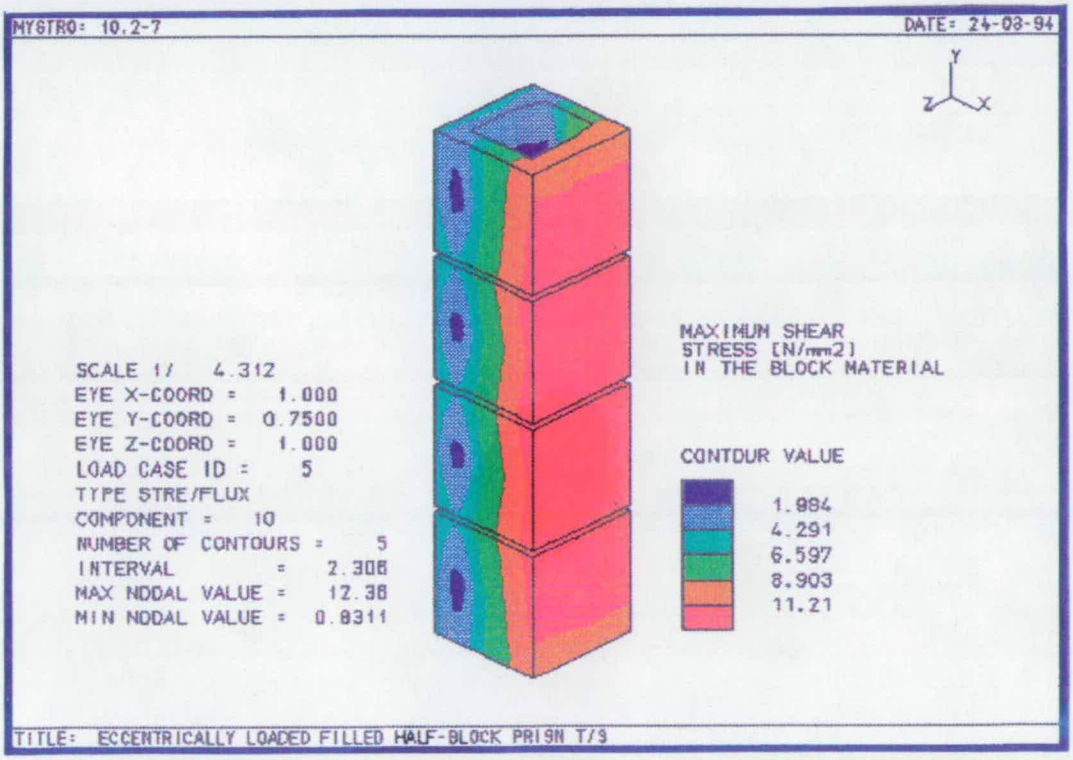


Fig. A.44 Shear stress in the block material of filled half-block prism compressed under eccentric load for e = t/3

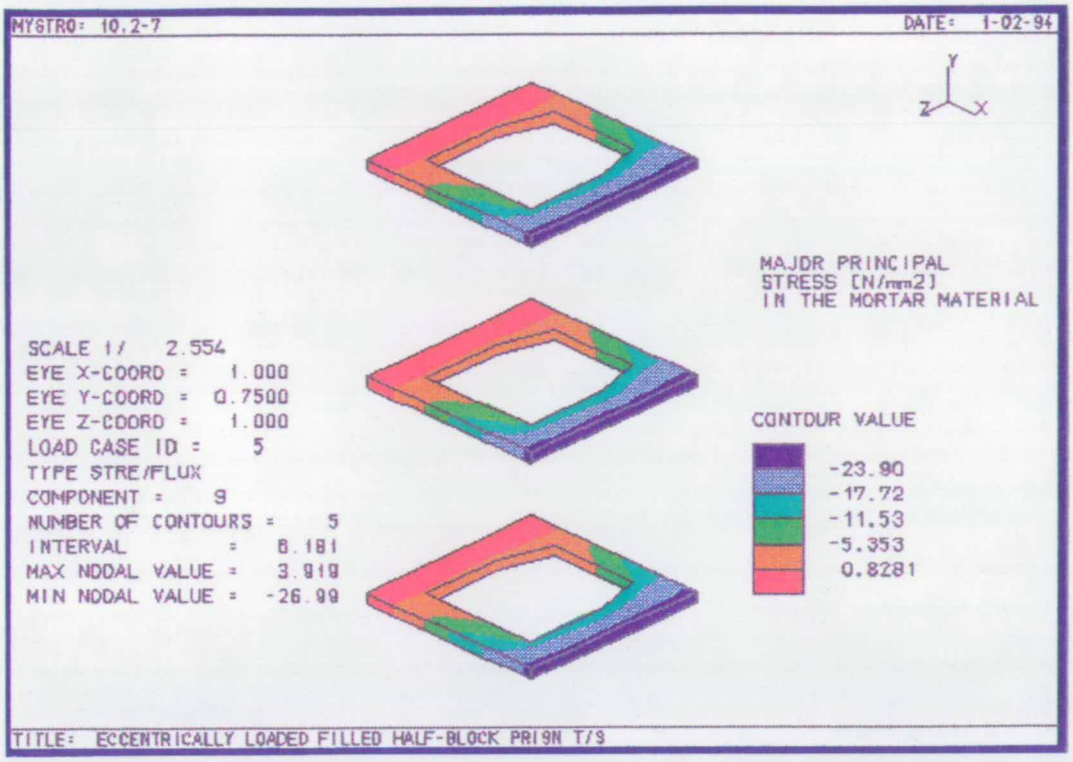


Fig. A.45 Major principal stress in the mortar material of filled half-block prism compressed under eccentric load for e = t/3

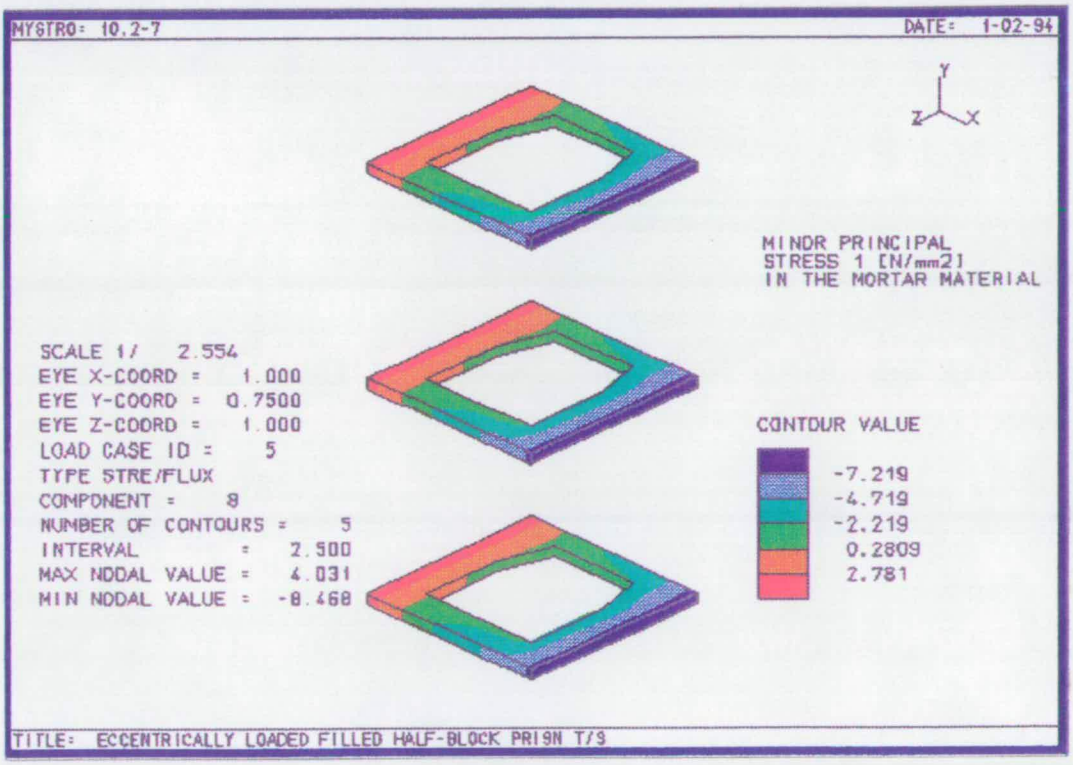


Fig. A.46 Minor principal stress 1 in the mortar material of filled half-block prism compressed under eccentric load for e = t/3

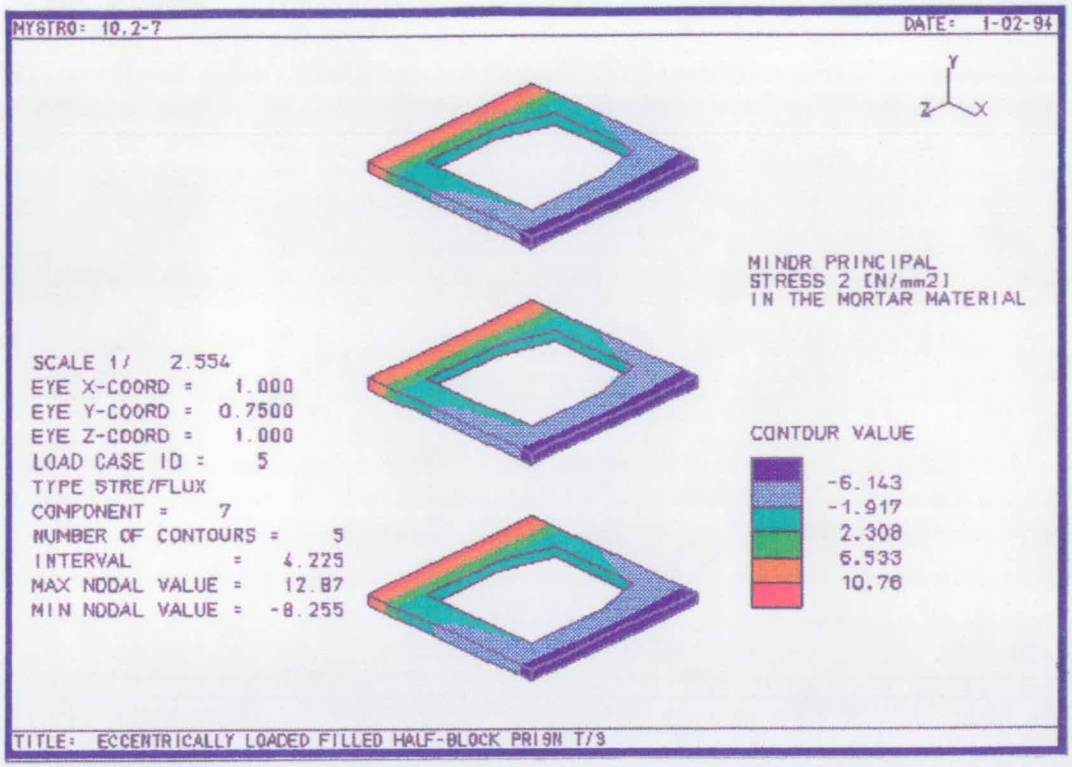


Fig. A.47 Minor principal stress 2 in the mortar material of filled half-block prism compressed under eccentric load for e = t/3

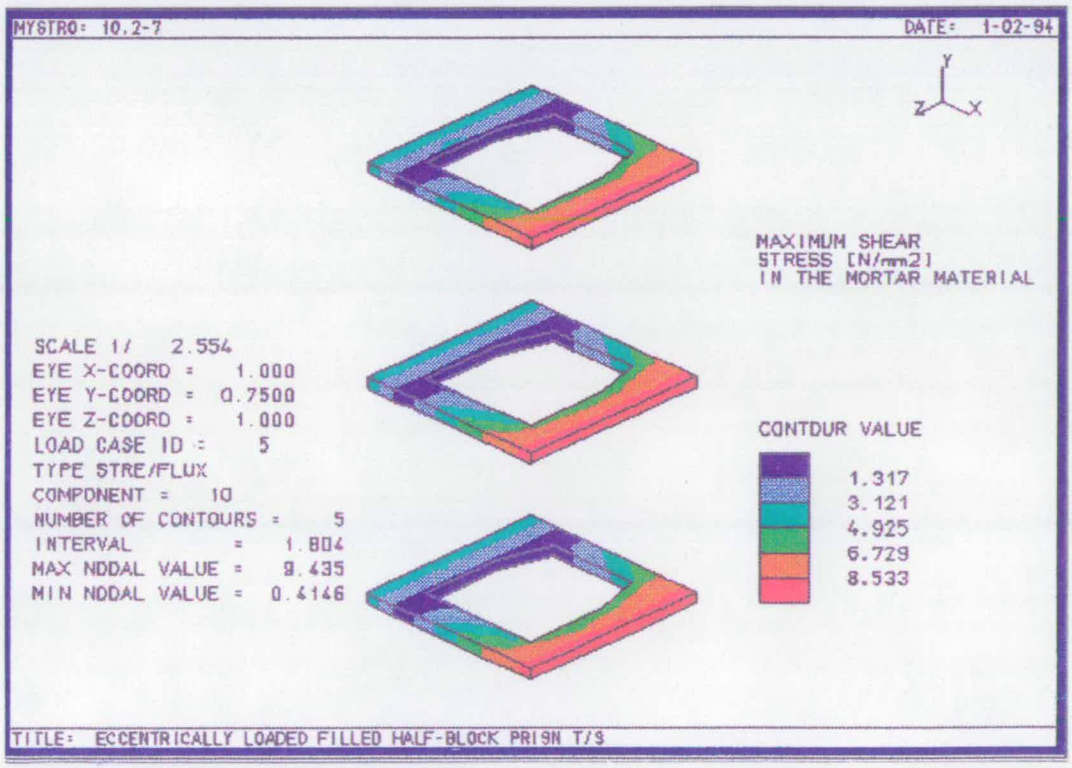


Fig. A.48 Shear stress in the mortar material of filled half-block prism compressed under eccentric load for e = t/3

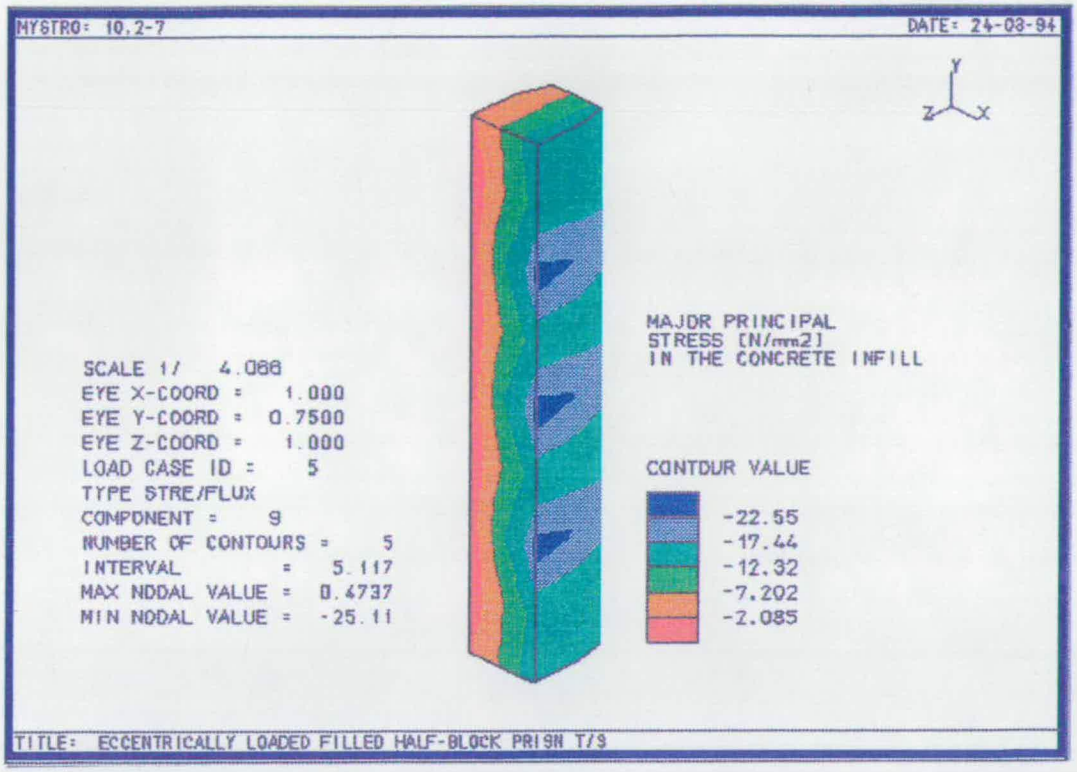


Fig. A.49 Major principal stress in the concrete infill of filled half-block prism compressed under eccentric load for t/3

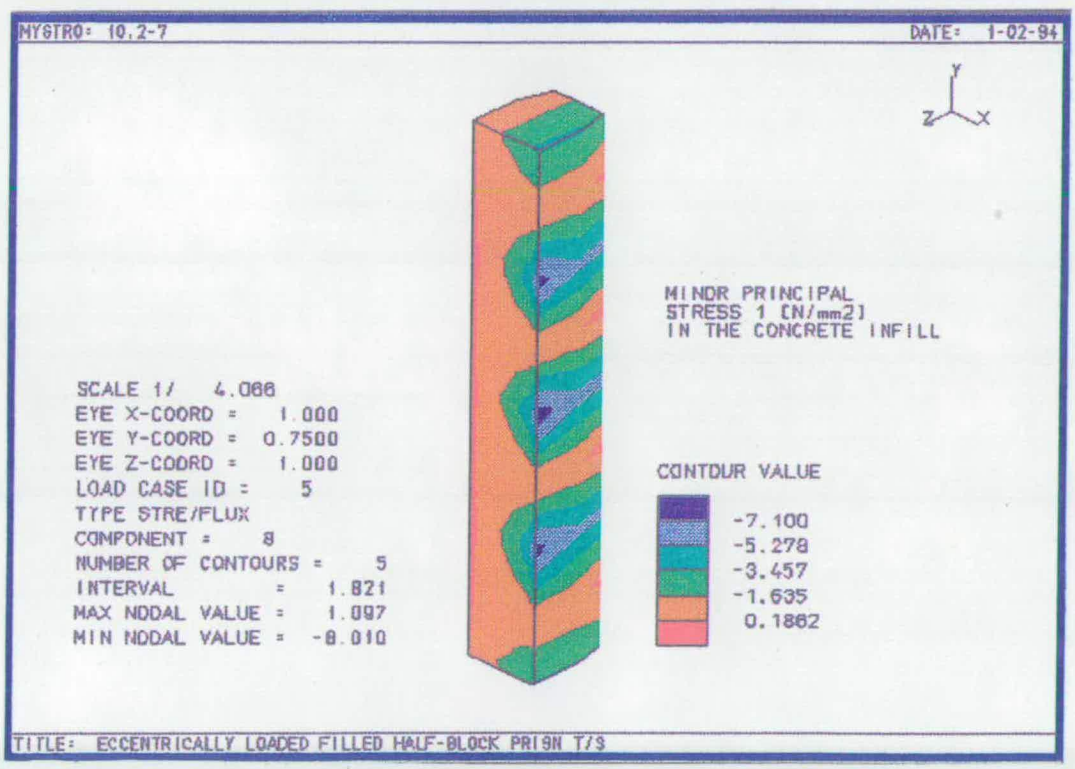


Fig. A.50 Minor principal stress 1 in the concrete infill of filled half-block prism compressed under eccentric load for t/3

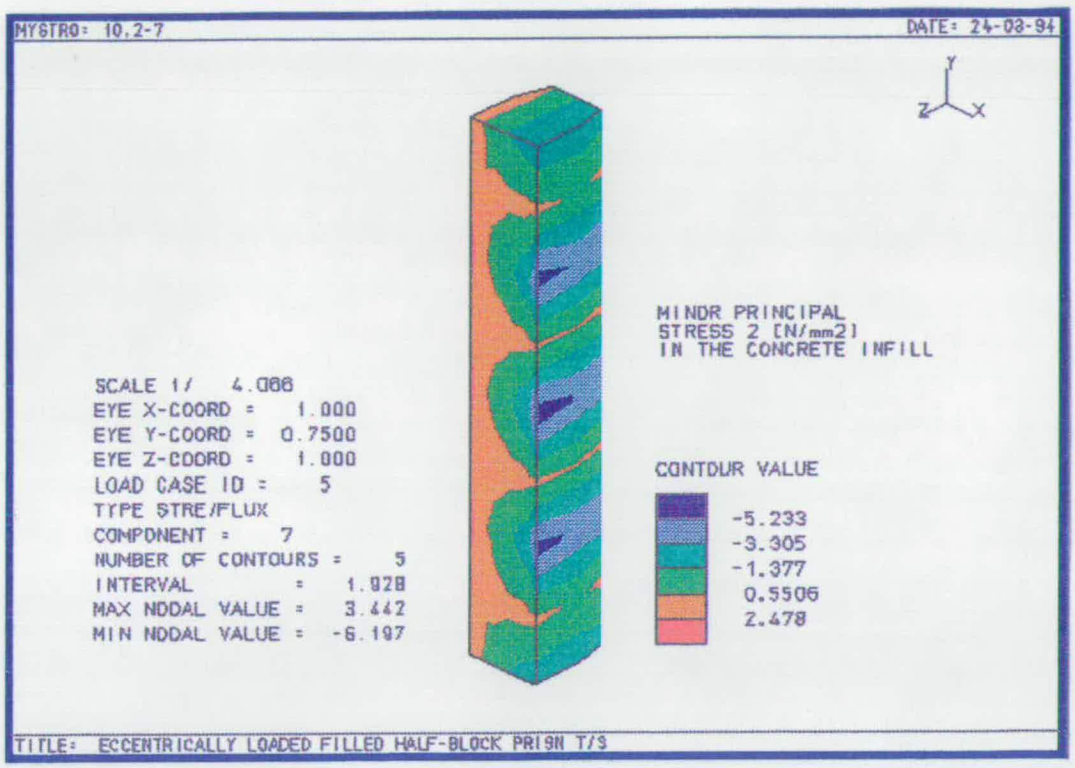


Fig. A.51 Minor principal stress 2 in the concrete infill of filled half-block prism compressed under eccentric load for e = t/3

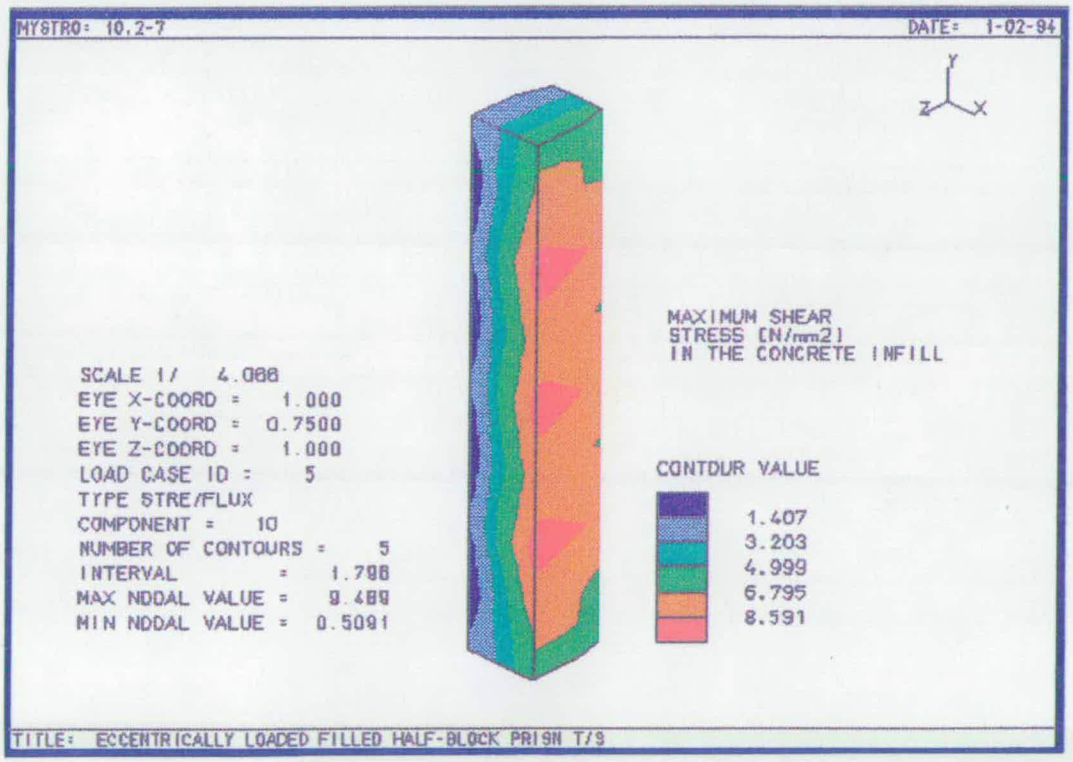


Fig. A.52 Shear stress in the concrete infill of filled half-block prism compressed under eccentric load for e = t/3

APPENDIX B

To determine the parabolic stress-block factors k_1, k_2 and k_3, assume the stress in masonry is given by:

$$f = f'_m \{2\frac{\varepsilon}{\varepsilon_m} - (\frac{\varepsilon}{\varepsilon_m})^2\} \qquad .....(B.1)$$

where

f = Compressive stress

f'_m = Compressive strength of Masonry

ε = Strain

ε_m = The strain at maximum stress

let $f = y$ $\quad f'_m = A$ $\quad \frac{\varepsilon}{\varepsilon_m} = x$ $\quad \frac{\varepsilon_u}{\varepsilon_m} = x_1$

hence the equation of the parabolic curve is given by:

$$y = A(2x - x^2) \qquad .....(B.2)$$

Area under curve $= \int_0^{X_1} y\,dx = k_1.A.X_1$

$$= \int_0^{X_1} A(2x-x^2)dx$$

$$= A\left(2\frac{X_1^2}{2} - \frac{X_1^3}{3}\right)$$

$$\therefore \quad k_1 = \left(x_1 - \frac{x_1^2}{3}\right)$$

$$k_1 = \frac{\varepsilon_\mu}{\varepsilon_m} - \frac{1}{3}\left(\frac{\varepsilon_\mu}{\varepsilon_m}\right)^2 \qquad \text{.....(B.3)}$$

To find k_2 take moment about y-axis

$$(1-k_2).x_1.\ \text{area under curve} = \int_0^{x_1} yx\,dx$$

$$= A\int_0^{x_1}(2x^2 - x^3)dx$$

$$= A\left(\frac{2X_1^3}{3} - \frac{X_1^4}{4}\right)$$

$$(1 - k_2)X_1 = \frac{\frac{2X_1^3}{3} - \frac{X_1^4}{4}}{(X_1^2 - \frac{X_1^3}{3})}$$

$$(1 - k_2) = \frac{\frac{2}{3} - \frac{X_1}{4}}{(1 - \frac{X_1}{3})}$$

$$\therefore \quad k_2 = \frac{(1 - \frac{X_1}{3} - \frac{2}{3} + \frac{X_1}{4})}{(1 - \frac{X_1}{3})}$$

$$= \frac{(\frac{1}{3} - \frac{1}{12}X_1)}{(1 - \frac{X_1}{3})}$$

$$= \frac{(4 - X_1)}{(12 - 4X_1)}$$

$$k_2 = \frac{(4 - \frac{\varepsilon_u}{\varepsilon_m})}{(12 - 4\frac{\varepsilon_u}{\varepsilon_m})} \qquad \text{.....(B.4)}$$

To find k_3

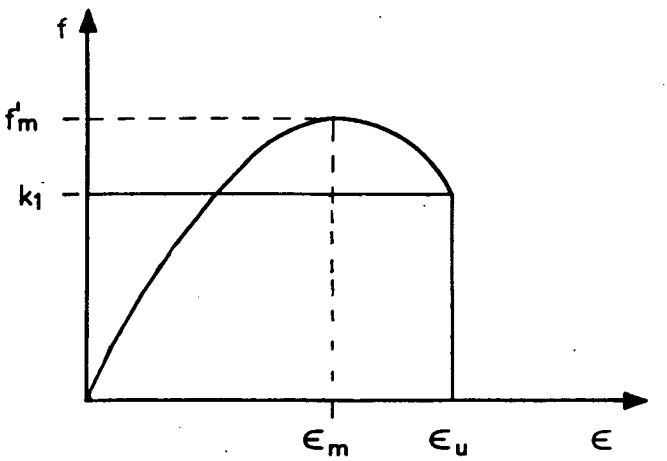
from equation B.2

$$k_3.A = A(2X_1 - X_1^2)$$

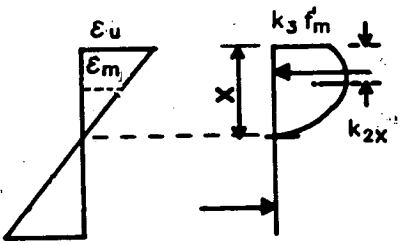
where $k_3.A$ is the value of y at $x = X_1$

$$k_3 = 2X_1 - X_1^2$$

$$= \frac{2\varepsilon_u}{\varepsilon_m} - \left(\frac{\varepsilon_u}{\varepsilon_m}\right)^2 \qquad \text{....(B.5)}$$



(a) Stress-strain relationship for masonry



(b) Strain profile (c) Stress-block

Fig. B.1 Parabolic stress-block
(a) Stress-strain relationship
(b) Strain profile
(c) Stress-block

APPENDIX C

TABLE C.1

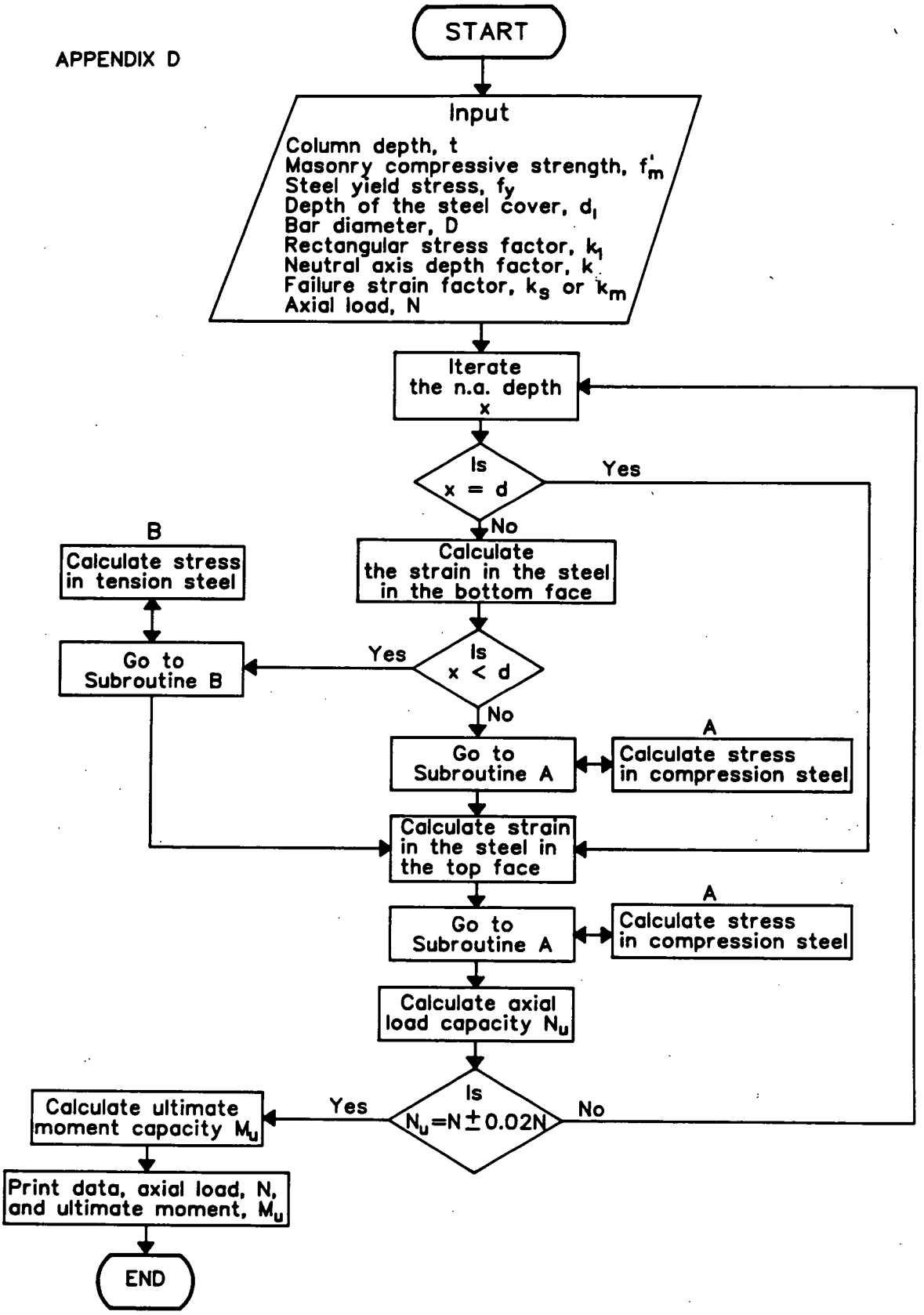
DESIGNATION OF THE BLOCKWORK COLUMNS

Type	Description
FCA (No Steel)	Full-block axially loaded unreinforced masonry column.
FCA (10 mm)	Full-block axially loaded masonry column reinforced with four 10 mm ϕ vertical bars and 8 mm ϕ lateral ties.
FCA (20 mm)	Full-block axially loaded masonry column reinforced with four 20 mm ϕ vertical bars and 8 mm ϕ lateral ties.
$FCE_{t/6}$ (No Steel)	Full-block unreinforced masonry column compressed under eccentric load at e = t/6.
$FCE_{t/6}$ (10 mm)	Full-block masonry column reinforced with four 10 mm ϕ vertical bars and 8 mm ϕ compressed under eccentric load at e = t/6.
$FCE_{t/6}$ (20 mm)	Full-block masonry column reinforced with four 20 mm ϕ vertical bars and 8 mm ϕ lateral ties compressed under eccentric load at e = t/6.
FCE_1 (No Steel)	Full-block masonry unreinforced column compressed under eccentric load at e > t/6 (e = 312 mm).
FCE_1 (10 mm)	Full-block masonry column reinforced with four 10 mm ϕ vertical bars and 8 mm ϕ lateral ties compressed under eccentric load at e > t/6 (e = 338 mm).
FCE_1 (20 mm)	Full-block masonry column reinforced with four 20 mm ϕ vertical bars and 8 mm ϕ lateral ties compressed under eccentric load at e > t/6 (e = 536 mm).

FCE_2 (No Steel)	Full-block masonry unreinforced column compressed under eccentric load at e > the eccentricity of type E_1 column (e = 575 mm).
FCE_2 (10 mm)	Full-block masonry column reinforced with four 10 mm ϕ vertical bars and 8 mm ϕ lateral ties compressed under eccentric load at e > the eccentricity of type E_1 column (e = 575 mm).
FCE_2 (20 mm)	Full-block masonry column reinforced with four 20 mm ϕ vertical bars and 8 mm ϕ lateral ties compressed under eccentric load at e > the eccentricity of type E_1 column (e = 580 mm).
HCA (No Steel)	Half-block axially loaded unreinforced masonry column.
HCA (8 mm)	Half-block axially loaded masonry column reinforced with four 8 mm ϕ vertical bars and 8 mm ϕ lateral ties.
HCA (20 mm)	Half-block axially loaded masonry column reinforced with four 20 mm ϕ vertical bars and 8 mm ϕ lateral ties.
$HCE_{t/6}$ (No Steel)	Half-block unreinforced masonry column compressed under eccentric load at e = t/6.
$HCE_{t/6}$ (8 mm)	Half-block masonry column reinforced with four 8 mm ϕ vertical bars and 8 mm ϕ lateral ties compressed under eccentric load at e = t/6.
$HCE_{t/6}$ (20 mm)	Half-block masonry column reinforced with four 20 mm ϕ vertical bars and 8 mm ϕ lateral ties compressed under eccentric load at e = t/6.
HCE_1 (No Steel)	Half-block masonry unreinforced column compressed under eccentric load at e > t/6 (e = 155 mm).

HCE_1 (8 mm)	Half-block masonry column reinforced with four 8 mm ϕ vertical bars and 8 mm ϕ lateral ties compressed under eccentric load at e > t/6 (e = 200 mm).
HCE_1 (20 mm)	Half-block masonry column reinforced with four 20 mm ϕ vertical bars and 8 mm ϕ lateral ties compressed under eccentric load at e > t/6 (e = 297 mm).
HCE_2 (No Steel)	Half-block masonry unreinforced column compressed under eccentric load at e > the eccentricity of type E_1 column (e = 355 mm).
HCE_2 (8 mm)	Half-block masonry column reinforced with four 8 mm ϕ vertical bars and 8 mm ϕ lateral ties compressed under eccentric load at e > the eccentricity of type E_1 column (e = 355 mm).
HCE_2 (20 mm)	Half-block masonry column reinforced with four 20 mm ϕ vertical bars and 8 mm ϕ lateral ties compressed under eccentric load at e > the eccentricity of type E_1 column (e = 400 mm).

APPENDIX D



Flow diagram for the reinforced blockwork masonry column program